

## N O T I C E

THIS DOCUMENT HAS BEEN REPRODUCED FROM  
MICROFICHE. ALTHOUGH IT IS RECOGNIZED THAT  
CERTAIN PORTIONS ARE ILLEGIBLE, IT IS BEING RELEASED  
IN THE INTEREST OF MAKING AVAILABLE AS MUCH  
INFORMATION AS POSSIBLE



National Aeronautics and  
Space Administration

SCG 810339R  
NASA CR-165409

## 30/20 GHZ FLIGHT EXPERIMENT SYSTEM PHASE II FINAL REPORT

by L. Bronstein, Y. Kawamoto, J. J. Ribarich,  
J. R. Swope, B. J. Forman, S. G. Bergman,  
S. Reisenfeld

### VOLUME 2. EXPERIMENT SYSTEM DESCRIPTION

(NASA-CR-165409-Vol-2) THE 30/20 GHZ FLIGHT  
EXPERIMENT SYSTEM, PHASE 2. VOLUME 2:  
EXPERIMENT SYSTEM DESCRIPTION Final Report,  
Apr. 1980 - Mar. 1981 (Hughes Aircraft Co.)  
NASA S469 p HC A20/MF A01  
ACCESS DEPT.

N82-20363

Unclass  
15420

CSC 17B G3/32

**HUGHES AIRCRAFT COMPANY**

prepared for  
**NATIONAL AERONAUTICS AND SPACE ADMINISTRATION**

NASA Lewis Research Center  
Contract NAS 3-22340



TECHNICAL REPORT STANDARD TITLE PAGE

1. Report No.	2. Government Accession No.	3. Recipient's Catalog No. <b>NASA CR-165409</b>	
30/20 GHz Flight Experiment System Phase II Final Report Volume 2. Experiment System Description		5. Report Date <b>July 1981</b>	6. Performing Organization Code <b>44-10-00</b>
		8. Performing Organization Report No. <b>810339R</b>	
7. Author(s) <b>L. Bronstein, Y. Kawamoto, J.J. Ribarich, J.R. Scope, B.J. Forman, S.G. Bergman, S. Reisenfeld</b>		10. Work Unit No.	
9. Performing Organization Name and Address <b>Hughes Aircraft Company Space and Communications Group El Segundo, California</b>		11. Contract or Grant No. <b>NAS 3-22340</b>	
		13. Type of Report and Period Covered <b>Phase II Final Report April 1980-March 1981</b>	
12. Sponsoring Agency Name and Address <b>NASA Lewis Research Center 21000 Brookpark Road Cleveland, Ohio 44135</b>		14. Sponsoring Agency Code	
15. Supplementary Notes <b>Project Manager: J.L. Fiala NASA-Lewis Research Center Cleveland, Ohio 44135</b>			
16. Abstract  A detailed technical description of the 30/20 GHz flight experiment system is presented in this volume. The overall communication system is described with performance analyses, communication operations, and experiment plans. Hardware descriptions of the payload are given with the tradeoff studies that led to the final design. The spacecraft bus which carries the payload is discussed and its interface with the launch vehicle system is described. Finally, the hardwares and the operations of the terrestrial segment are presented.			
17. Key Words (Selected by Author(s))		18. Distribution Statement	
19. Security Classif. (of this report) <b>Unclassified</b>	20. Security Classif. (of this page) <b>Unclassified</b>	21. No. of Pages <b>469</b>	22. Price*

## CONTENTS

	<u>Page</u>
1. INTRODUCTION AND SUMMARY	1-1
2. COMMUNICATION SYSTEM DESIGN	
2.1 Communications	2-1
2.1.1 Requirements	2-1
2.1.2 Spacecraft Payload Block Diagram	2-7
2.1.3 Satellite Antenna Pointing	2-8
2.1.4 Antenna Configuration Trades	2-9
2.1.5 Terrestrial Segment	2-9
2.1.6 Communication Link Performance	2-13
2.1.7 Propagation Reliability	2-19
2.1.8 Telemetry Tracking and Command	2-26
2.1.9 Payload Weight and Power	2-28
2.1.10 Options	2-29
2.2 Communication System Control	2-34
2.2.1 Channel Access	2-34
2.2.2 System Synchronization	2-37
2.2.3 Link Control	2-49
2.2.4 Payload Control	2-49
2.2.5 Station Control	2-52
2.3 Experiments	2-53
2.3.1 Experiment Plan	2-53
3. COMMUNICATION PAYLOAD	
3.1 Satellite Antenna	3-1
3.1.1 Requirements	3-1
3.1.2 Design Issues	3-3
3.1.3 Cluster Feed Approach	3-21
3.1.4 Selected Antenna Subsystem Configuration	3-24
3.1.5 Option 1 Subsystem	3-27
3.1.6 Antenna Subsystem Weight and Power	3-27
3.1.7 Electrical Performance	3-29
3.1.8 Antenna Technology Assessment	3-31
3.1.9 19 GHz Beacon Antenna	3-32
3.2 Microwave Subsystem	3-35
3.2.1 Requirements	3-35
3.2.2 Subsystem Design	3-35
3.2.3 Weight and Power	3-37
3.2.4 Performance	3-51
3.2.5 Options	3-51
3.2.6 Technology Assessment	3-55
3.3 Baseband Processor	3-57
3.3.1 BBP Requirements	3-57
3.3.2 System Description	3-59
3.3.3 Functional Elements	3-67
3.3.4 Weight and Power Estimates for the Baseband Processor	3-86



3.3.5	Performance	3-88
3.3.6	Impact of the Reduced Capacity (Option 1) Processor	3-95
3.3.7	Technology Assessment	3-99
3.3.8	Telemetry and Command List for the Digital Subsystem	3-99
4.	SPACECRAFT BUS	
4.1	Spacecraft Bus	4-1
4.1.1	Spacecraft Design	4-1
4.1.2	Trade Studies	4-12
4.1.3	Spacecraft Subsystems	4-13
4.1.4	LEASAT Modifications for 30/20 GHz System	4-79
4.2	Launch Vehicle System	4-105
4.2.1	Introduction	4-105
4.2.2	Launch Configuration	4-105
4.2.3	Launch Operations Description	4-110
4.3	Space Segment Reliability	4-118
5.	TERRESTRIAL SEGMENT	
5.1	Implementation of Communications Links	5-3
5.1.1	Antennas	5-3
5.1.2	TWT Power Amplifiers	5-11
5.1.3	Downconverter	5-11
5.1.4	Upconverters	5-11
5.1.5	Low Noise Amplifiers	5-12
5.2	Implementation of Communications Operations	5-13
5.2.1	Requirements and Design Approach	5-13
5.2.2	Central Control Station	5-14
5.2.3	Trunk Station	5-37
5.2.4	Customer Premise Service Stations	5-52
5.3	Implementation of Mission Operations	5-57
5.3.1	Launch Operations	5-59
5.3.2	Flight Control Subsystem	5-63
5.3.3	Mission Planning Subsystem	5-71
5.3.4	MOS Data Processing Subsystem	5-73
5.4	Implementation of Experiment Operations	5-86
5.4.1	Experiment Operations Requirements	5-86
5.4.2	Experiment Operations Design Approach	5-87
5.4.3	Experiment Operations Description	5-87

## ILLUSTRATIONS

	<u>Page</u>
1-1 Spacecraft Isometric	1-2
1-2 LEASAT Spacecraft Stowed Configuration	1-3
1-3 Launch Configuration	1-5
1-4 Typical Cradle Shuttle Bay Installation	1-6
2-1 30/20 GHz Flight Experiment System	2-2
2-2 Typical Antenna Coverage	2-2
2-3 Trunking Service Frequency Plan	2-4
2-4 CPS Frequency Plan	2-4
2-5 Spacecraft Functional Block Diagram	2-6
2-6 Antenna Configuration Selection	2-10
2-7 Terrestrial System	2-10
2-8 Master Control Terminal	2-11
2-9 TDMA Trunk Station	2-12
2-10 TDMA CPS Station	2-12
2-11 Reduced Area Coverage	2-14
2-12 Link Reliability	2-21
2-13 Diversity Gain Versus Separation Distance	2-23
2-14 Diversity Reception and Transmission Affect on Trunk Line Rain Outage	2-24
2-15 CPS Links Expected Rain Outage	2-25
2-16 Satellite TT&C Configuration	2-26
2-17 Option 1 Spacecraft Functional Block Diagram	2-30
2-18 Option 2 Spacecraft Functional Block Diagram	2-32
2-19 Option 2 Frequency Plan	2-33
2.2-1 Trunking Channel Assignment	2-35
2.2-2 Trunk Frame Format	2-35
2.2-3 CPS Channel Assignment	2-37
2.2-4 CPS Frame Format	2-38
2.2-5 Trunk Synchronization Initial Acquisition	2-39
2.2-6 Metric Code	2-40
2.2-7 Typical Circuit for Frequency and Timing Synchronization	2-42
2.2-8 Trunk Synchronization	2-42
2.2-9 Trunk System Guard Time Estimate	2-42
2.2-10 CPS Synchronization	2-46
2.2-11 CPS Synchronization, Error Measurement	2-46
2.2-12 Trunking Site Link Control	2-50
2.2-13 CPS Link Control	2-50
2.2-14 Payload Control	2-51
2.2-15 Subsystem Monitor and Control	2-53
2.3-1 Flow Chart Showing Permissible Order of Plan Segments	2-57
2.3-2 LNR at 30 GHz Indirect Measurement of Noise Figure	2-63
2.3-3 30/20 Precipitation Effects	2-72

3. 1-1	Antenna Coverage Requirements	3-2
3. 1-2	CPS Antenna Coverage Model	3-2
3. 1-3	Antenna Configuration Selection	3-5
3. 1-4	Polarization Selective Surface Subreflectors Create Two Focal Areas for Two Orthogonal Linear Polarizations	3-6
3. 1-5	Prime Fed Shared Grid Aperture Configuration	3-7
3. 1-6	Folded Optics and Prime Fed Configurations Combined	3-7
3. 1-7	Frequency Selective Surface Creates Two Focal Areas for Two Separate Frequency Bands	3-8
3. 1-8	Dual Reflector Configuration with FSS Feed Technique	3-9
3. 1-9	Receive Scanning Feed Networks	3-9
3. 1-10	Transmit Scanning Feed Networks	3-10
3. 1-11	Section 1 Trunk/CPS Coverage	3-11
3. 1-12	Offset Cassegrain Directive Gain Contours	3-12
3. 1-13	Reduced Area Coverage	3-13
3. 1-14	CPS Beam Scanning with Feed Horn/Beam Doublets	3-13
3. 1-15	Variable Power Divider Block Diagram and Relative Power Outputs	3-14
3. 1-16	Offset Cassegrain Directive Gain Contours	3-16
3. 1-17	CPS Spot Beam Gain Pointing Loss Reduction	3-17
3. 1-18	Scanning Feed Networks	3-18
3. 1-19	Cassegrain Antenna Contour Gain at 28.8 GHz	3-18
3. 1-20	Prime Fed Reflector Contour Gain at 28.8 GHz	3-20
3. 1-21	Cassegrain Antenna Contour Gain at 19 GHz	3-20
3. 1-22	Prime Fed Reflector Contour Gain at 19 GHz	3-23
3. 1-23	Comparison of Single and Cluster Feed Approaches	3-23
3. 1-24	Antenna Subsystem Configuration	3-24
3. 1-25	Baseline Communications Antenna Block Diagram	3-26
3. 1-26	Tracking Feed Array and Comparator	3-27
3. 1-27	Option 1 Communications Antenna Block Diagram	3-28
3. 1-28	Option 1 Scanning Feed Networks	3-29
3. 1-29	Beacon Antenna Pattern	3-33
3. 1-30	19 GHz Beacon Antenna Schematic Diagram	3-33
3. 2-1	Baseline Microwave Subsystem Block Diagram	3-36
3. 2-2	Frequency Conversion Plan	3-38
3. 2-3	CPS Gain Distribution and Levels	3-38
3. 2-4	Trunk Gain Distribution and Levels	3-38
3. 2-5	System Noise Figure	3-40
3. 2-6	Two Stage Amplifier Configuration	3-40
3. 2-7	Baseline Receiver	3-40
3. 2-8	Mixer Configuration	3-42
3. 2-9	IF Switch Matrix Concept	3-42
3. 2-10	Crossbar Coupler Switchpoint Detail	3-44
3. 2-11	Mask Set for Multiple FET Chip Switch Element	3-44
3. 2-12	Upconverter Design	3-46
3. 2-13	7 Watt GaAs FET SSPA	3-46
3. 2-14	FET Submodule Configuration	3-46
3. 2-15	Telemetry Transmitter	3-48
3. 2-16	Local Oscillator Source Design	3-48
3. 2-17	Monopulse Tracking Microwave Circuits	3-50
3. 2-18	Option 2 Microwave Subsystem Block Diagram	3-54
3. 2-19	Option 2 Receiver	3-56

3.3-1	Baseband Processor Functions	3-58
3.3-2	Baseband Processor Simplified Functional Block Diagram	3-60
3.3-3	Baseband Processor Block Diagram, Input Section	3-60
3.3-4	Baseband Processor Block Diagram, Store and Forward Section	3-62
3.3-5	Baseband Processor Block Diagram, Output Section	3-66
3.3-6	Baseband Processor Timing	3-66
3.3-7	IF Downconverter and FDM Demultiplexer	3-68
3.3-8	32 Mbps Soft (Hard) Decision QPSK Demodulator	3-69
3.3-9	128 Mbps Soft (Hard) Decision QPSK Demodulator	3-70
3.3-10	FEC Decoder Block Diagram	3-74
3.3-11	Metric Accumulator Gate Array	3-74
3.3-12	Weight and Power Versus Reliability for 64 by 64 Switch Matrix and Controller	3-76
3.3-13	256 Mbps QPSK Modulator and IF Converter	3-80
3.3-14	Convolutional Encoder Block Diagram	3-80
3.3-15	BFN Controller Block Diagram	3-83
3.3-16	IF Switching Matrix Controller Block Diagram	3-84
3.3-17	Spacecraft Oscillator Frequency Update Technique	3-84
3.3-18	Bit Error Rate Versus $E_b/N_0$ for Rate 1/2 Viterbi Decoding. Eight Level Quantized Simulations with 32 Bit Paths, and Infinitely Finely Quantized Transfer Function Bound	3-92
3.3-19	Performance Comparison of Viterbi Decoding Using Rate 1/2, Code with 2-, 4-, and 8 Level Quantization, Path Length = 32 Bits	3-94
3.3-20	Option 1 Reduced Capacity Baseband Processor Block Diagram, Input Section	3-96
3.3-21	Option 1 Baseband Processor Block Diagram, Store and Forward Section	3-96
3.3-22	Option 1 Baseband Processor Block Diagram, Output Section	3-96
3.3-23	Propagation Delay Versus Power Dissipation per Gate for Digital Technologies	3-98
4-1	Design Confidence Results From Uncomplicated Spinning Configuration, High Flight Content Subsystems Assure Performance Margins	4-3
4-2	LEASAT External Configuration	4-5
4-3	LEASAT Internal Configuration	4-6
4-4	Despun Platform Equipment Layout	4-7
4-5	Spacecraft System Functional Block Diagram	4-15
4-6	ACS Component Layout	4-18
4-7	Simple Attitude Control Subsystem Uses Ground Command for all Controls Except Autonomous Despin	4-20
4-8	ACS Uses Single Servo Loop for Steady State Control	4-22
4-9	Intelsat IV BAPTA (Photo A25566)	4-29
4-10	LEASAT BAPTA Cross Section	4-30
4-11	Hughes Extensive and Successful BAPTA Experience Summary	4-30
4-12	Flight Qualified Earth Sensor (Photo A31858)	4-31
4-13	Flight Qualified Sun Sensor Assembly (Photo 74-26828)	4-32
4-14	LEASAT Electrical Power Subsystem Block Diagram	4-36

4-15	Power Subsystem Component Locations	4-38
4-16	Solar Array Power Availability Exceeds Requirements With Ample Margin	4-39
4-17	Cycle Life Versus Depth of Discharge	4-42
4-18	Solid Propulsion Subsystem Motor for LEASAT (Modified Stage III Minuteman Motor)	4-48
4-19	Stage III Minuteman Performance	4-50
4-20	Liquid Bipropellant Subsystem Schematic	4-52
4-21	Flight Proven Marquardt R40 Thruster Assembly Used in LBS	4-54
4-22	Reaction Control Subsystem Schematic	4-56
4-23	Flight Proven HE-54 Thruster Performance Easily Satisfies LEASAT Requirements	4-58
4-24	Highly Reliable RCS Flow Control Valve	4-58
4-25	Thermal Control Elements	4-64
4-26	Bulk Thermal Mathematical Model	4-66
4-27	Reasonable Design Range Achieved for all Seasons with LEASAT Passive Design	4-66
4-28	STS Environment Used to Determine Thermal Control Requirements	4-68
4-29	LEASAT Structural Arrangement	4-70
4-30	Spacecraft Cradle Assembly	4-72
4-31	Solar Panel and Battery Support	4-74
4-32	30/20 GHz TT&C Subsystem	4-78
4-33	NASA Standard Near Earth Transponder and Interfaces	4-78
4-34	Antenna Positioner Electronics Block Diagram	4-84
4-35	Antenna Positioner Electronics	4-84
4-36	30/20 GHz Payload Layout	4-87
4-37	Side View of Shelf with Associated Despun and Spinning Thermal Barriers	4-91
4-38	Reflector Axis View of Shelf	4-92
4-39	LEASAT Spacecraft Isometric	4-92
4-40	Lateral g's Limit LEASAT Distance from Despun Shelf	4-92
4-41	Launch Configuration	4-106
4-42	Typical Cradle Shuttle Bay Installation	4-107
4-43	Spacecraft Launch Configuration	4-108
4-44	Ascent Operations Overview	4-111
4-45	Spacecraft Ejection	4-112
4.3-1	30/20 GHz Payload Reliability Block Diagram	4-120
4.3-2	Microwave Subsystem Reliability Block Diagram	4-120
4.3-3	Communication Antenna Subsystem Reliability Block Diagram	4-121
4.3-4	Digital Electronics Reliability Block Diagram	4-122
4.3-5	Analog Electronics Reliability Block Diagram	4-123
5-1	Terrestrial System	5-2
5-2	Master Control Terminal	5-2
5-3	Standard Trunk Station Hardware Configuration	5-5
5-4	Master Control Terminal Trunk Station Baseband Processing	5-7

5-5	MCT Antenna Site	5-8
5-6	Customer Premise Service Station	5-9
5-7	MM Wave HPA Block Diagram	5-10
5-8	Downconverters	5-10
5-9	Upconverters	5-12
5-10	Central Control Station	5-17
5-11	Central Control Station	5-19
5-12	Data Processing Subsystem Organization	5-22
5-13	Central Data Processing Subsystem Configuration	5-23
5-14	Basic Software Structure	5-24
5-15	Display Processor Data Paths	5-25
5-16	Communications Management Software, CCS Real Time Processing	5-26
5-17	Communications Management Software, CCS Off-Line Processing	5-26
5-18	Channel Allocation	5-28
5-19	Channel Allocation Routing	5-29
5-20	IF Switch Control	5-30
5-21	Scan Beam Control Matrix	5-30
5-22	Baseband Processing Control	5-32
5-23	Input Memory Control Programming	5-33
5-24	BBP Routing Switch Interconnects	5-33
5-25	Routing Switch Control Memory Programming	5-34
5-26	Output Memory Control Programming	5-34
5-27	Link Control Software	5-36
5-28	Station Status and Control Software	5-38
5-29	TDMA Multiplexer/Demultiplexer	5-40
5-30	Option 2, FDMA System	5-42
5-31	Trunk Interface	5-42
5-32	ESS 4 Switching System	5-44
5-33	Time Division Switching Network	5-45
5-34	Burst Synchronizer Functional Diagram	5-46
5-35	Typical Circuit for Unique Word Processing	5-46
5-36	Diversity Switch Implementation	5-47
5-37	Propagation Delay Difference	5-48
5-38	Remote Site Clock Recovery and Modulator ON/OFF Signal Generation	5-50
5-39	Trunk Station Software	5-50
5-40	CPS Station Interface	5-54
5-41	Bell System No. 101 Electronic Switching System	5-54
5-42	CPS TDMA Multiplexer/Demultiplexer	5-55
5-43	Mission Operation System Organization	5-56
5-44	Timeline	5-58
5-45	Launch Operations Flow Chart	5-60
5-46	Ascent Operations Ground Control System Block Diagram	5-62
5-47	TACS Simplified Block Diagram	5-64
5-48	Mission Control Center Functional Block Diagram	5-65
5-49	Flight Operations Control Subsystem	5-68
5-50	Ranging System	5-70
5-51	Attitude Determination Function	5-70
5-52	Orbit Determination Function	5-72

5-53	East-West Stationkeeping Profile	5-74
5-54	ANIK Stationkeeping Experience	5-74
5-55	Mission Operations Software Real Time Processing	5-75
5-56	Telemetry Data Processing Logic	5-76
5-57	Command Processing Logic	5-76
5-58	Ranging Task Data Flow	5-78
5-59	Antenna Control Logic	5-80
5-60	Mission Operations Software Off-Line Processing	5-80
5-61	Experiment Operations Interfaces	5-88
5-62	Experiment Operation Functional Flow	5-91
5-63	Experiment Support Software Off-Line Processing	5-91

TABLES

	<u>Page</u>
1-1 Spacecraft Weight Summary	1-4
1-2 Power Summary (Watts)	1-6
1-3 Space Segment Reliability	1-7
2-1 Service Requirements Summary	2-5
2-2 Technology Requirements	2-5
2-3 Spacecraft RF Performance	2-15
2-4 Terrestrial RF Performance	2-16
2-5 Trunk Link Budget (dB)	2-17
2-6 CPS Uplink Budget	2-18
2-7 CPS Downlink Budget (256 Mbps)	2-18
2-8 20 GHz Telemetry Link Budget (dB)	2-27
2-9 30 GHz Command Link Budget (dB)	2-28
2-10a Spacecraft Payload Weight	2-28
2-10b Spacecraft Payload Power Requirement	2-29
2-10c Payload Power Dissipation	2-29
2-10d Weight Comparison	2-31
2-10e Power Requirements Comparison	2-31
2.2-1 Trunk System Synchronization Methods	2-43
2.2-2 Trunk System Error Contributions to Guard Time Systematic Errors	2-44
2.2-3 Trunk System Error Contributions to Guard Time Random Errors	2-44
2.2-4 Trunk TDMA Overhead	2-45
2.2-5 CPS Preamble Symbol Allocation	2-48
2.3-1 Service Experiments	2-54
2.3-2 Service and Technology Experiments	2-55
2.3-3 Technology Experiments	2-56
3.1-1 Performance Requirements for Multiple Beam Antenna	3-3
3.1-2 Antenna Requirements for Baseline System	3-4
3.1-3 Electronically Controlled Switching Circulator Characteristics	3-10
3.1-4 Electronically Controlled Variable Power Divider Characteristics	3-15
3.1-5 Electronically Controlled Variable Power Combiner Characteristics	3-15
3.1-6 Comparison of Gain and Feed Complexity Single and Cluster Feeds	3-22
3.1-7 Antenna Subsystem Weight and Power	3-30
3.1-8 Baseline CPS/TS Antenna Performance Estimates	3-31
3.1-9 Antenna Technology Assessment	3-32
3.2-1 SOW Requirements on Microwave Subsystem Design	3-35
3.2-2 TWTA Characteristics	3-45
3.2-3 SSPA Comparison	3-47
3.2-4 Microwave Subsystem Weight and Power	3-51
3.2-5 Microwave Subsystem Command Requirements	3-52
3.2-6 Microwave Subsystem Telemetry Requirements	3-52



3.2-7	Circuit Losses and Power Delivered to Antenna Feed	3-53
3.2-8	Microwave Subsystem Gain Flatness and Phase Linearity	3-53
3.3-1	64 MBPS Data Serial Lines Entering Baseband Switch	3-63
3.3-2	64 MBPS Data Serial Lines Leaving Baseband Switch	3-64
3.3-3	Required Baseband Switch Matrix Size	3-77
3.3-4	Analog Electronics Power, Size, and Weight Estimates	3-86
3.3-5	Digital Electronics Power, Size and Weight Estimates	3-87
3.3-6	Trunk Mode Digital Electronics Power Estimate	3-87
3.3-7	Baseband Processor Power	3-88
3.3-8	Phase Jitter Degradation	3-89
3.3-9	Timing Jitter Degradation	3-91
3.3-10	Burst Demodulator Performance Estimate	3-91
3.3-11	Coding Gains of Rate 1/2 Convolutional Codes Using the Viterbi Decoding Algorithm	3-93
3.3-12	Coding Improvement	3-95
3.3-13	Option 1 Processor Analog Electronics Power, Size, and Weight Estimates	3-95
3.3-14	Option 1 Processor Digital Electronics Power, Size, and Weight Estimates	3-97
3.3-15	Baseband Processor Power and Weight Summary	3-97
3.3-16	Gate Array Devices Used in the Baseband Processor Design	3-100
3.3-17	Baseband Processor Digital Electronics Complexity Estimate	3-100
3.3-18	Analog Electronics Technology	3-101
3.3-19	Baseline Physical Design Approach	3-101
3.3-20	Telemetry and Command List for Digital Subsystem	3-101
4-1	Weight Summary	4-8
4-2	Power Source Sizing	4-9
4-3	Command and Telemetry Allocation	4-10
4-4	Electromagnetic Effects Control Requirements	4-11
4-5	Trade Studies	4-12
4-6	Alternative Orbit Injection Cost Trade	4-13
4-7	ACS Design and Performance Summary	4-25
4-8	SPS Thrust Vector Error Budget (Degrees)	4-25
4-9	Antenna Pointing Performance	4-27
4-10	Attitude Control System Hardware Summary	4-28
4-11	BAPTA Physical Characteristics	4-28
4-12	Earth Sensor Characteristics	4-31
4-13	Sun Sensor Characteristics	4-32
4-14	Power Subsystem Performance	4-35
4-15	Power Source Sizing	4-37
4-16	LEASAT Solar Array Design Factors	4-40
4-17	Qualified Production Solar Cell Types Comparison	4-40
4-18	Power Electronic Components - Physical Characteristics	4-43
4-19	LEASAT Battery Cell Characteristics	4-44
4-20	LEASAT Bulk Spacecraft Temperature Predictions Used to Evaluate Unit Temperatures	4-68
4-21	LEASAT Computer Predicted Unit Temperatures to Allow Reasonable Unit Design Temperatures on Orbit	4-69
4-22	Ultimate Design Load Factors, g's	4-76
4-23	Structural Design Criteria	4-76
4-24	NASA Standard Near Earth Transponder Characteristics	4-80

4-25	System Command Link (S Band)	4-81
4-26	System Telemetry Link (S Band)	4-81
4-27	System Ranging Link (S Band)	4-82
4-28	EIRP, G/T, and Antenna Gain Values Used in Link Calculations	4-82
4-29	East-West Beam Pointing Error Budget	4-86
4-30	North-South Beam Pointing Error Budget	4-89
4-31	Beam Rotation Error Budget	4-90
4-32	Antenna Positioner Mechanism Characteristics	4-90
4-33	LEASAT Maximum Limit Component "G" Levels	4-93
4-34	Comparison of LEASAT and 30/20 GHz Despun Shelf Weights	4-100
4-35	Spacecraft Weight Summary	4-101
4-36	Bus Subsystem Weights (LB)	4-102
4-37	Power Summary (Watts)	4-103
4-38	Eclipse Power Summary (Watts)	4-104
4-39	Bus Subsystem Power	4-104
4-40	Prelaunch Through Shuttle Ejection Sequence of Events	4-113
4-41	Post Ejection Sequencer Activities (Coast Phase)	4-114
4-42	Transfer Orbit Operations	4-116
4-43	Early On-Orbit Operations	4-117
4-44	30/20 GHz Reliability for Various Success Criteria Mission Duration: 2 Years	4-118
4-45	30/20 GHz Reliability for Various Success Criteria Mission Duration: 4 Years	4-118
5-1	Terrestrial Segment Functions	5-1
5-2	Antenna Performance	5-4
5-3	Design Parameters	5-12
5-4	Terrestrial Segment Requirements Allocation	5-14
5-5	Terrestrial Segment - Summary of Key Features	5-15
5-6	Central Control Station Requirements	5-16
5-7	Computer and Peripheral Parts List for DEC PDP 11/44 (11 Total)	5-22
5-8	Trunk Station Requirements	5-38
5-9	CPS Station Requirements	5-53
5-10	Mission Operations System Requirements Allocation	5-57
5-11	Flight Control Functions	5-64

## 1. INTRODUCTION AND SUMMARY

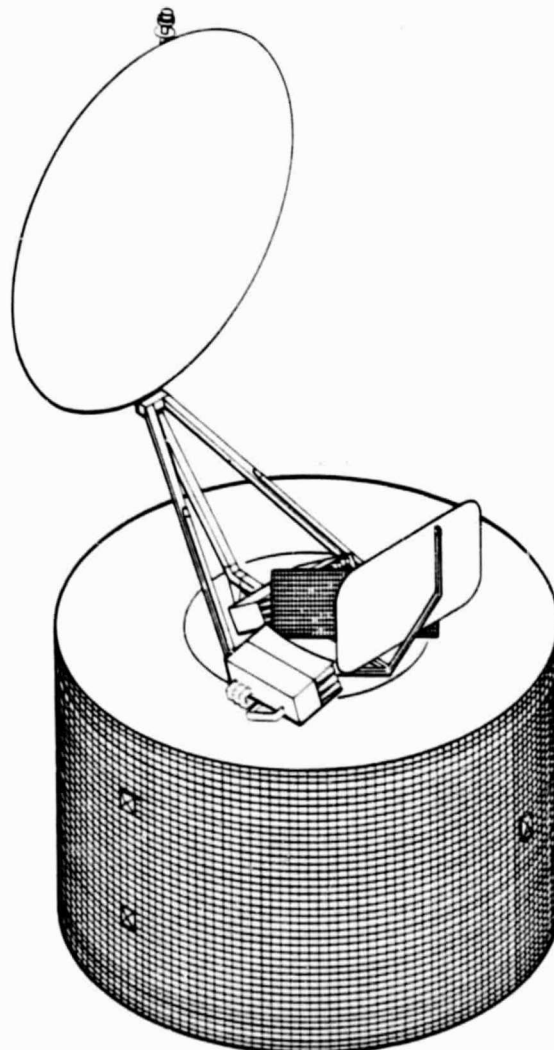
The objective of this study was to provide the information which NASA requires to select a concept for a 30/20 GHz flight experiment and to procure the major system elements of the 30/20 GHz communications system. The study, which began in April 1980, first examined a baseline concept provided by NASA; then several alternate concepts suggested by the contractor and approved by NASA. Evaluations were made of the cost, schedule, risk, and technology development requirements associated with these concepts. A final concept was defined by NASA in March 1981. This report is devoted entirely to that final concept. The analyses of the previous concepts were presented to NASA as they were developed and were documented in task completion reports.

The design for the communication subsystem components is presented in Section 3. Although NASA is funding technology development studies, which will result in proof of concept models for most of these components, the design presented in this report is a Hughes design. This approach is taken for two reasons. First, the technology studies were still in an early stage at the time the design was made; and second, Hughes considers that it will be more competent to reach correct make or buy decisions and to effectively procure components if it has been through the preliminary design process. At this time no decisions have been made regarding the source of any of the communication components. Make or buy decisions will be made early in the system definition phase (Phase B).

The final concept was selected by NASA because it was considered to provide as comprehensive an experiment as could be performed within realistic funding constraints. The communication concept is described in the next section. It consists of trunking service (TS) and customer premise service (CPS) experiments. The trunking system serves four spot beams which are interconnected in a satellite switched time division multiple access (SS-TDMA) mode by an IF switch matrix. The CPS system covers two large areas in the eastern half of the United States with a pair of scanning beams. The individual spots which comprise these CPS areas are interconnected through a baseband processor (BBP) onboard the satellite. Both trunk and CPS systems use an antenna with a 10 foot main reflector. The downlink data rate of 256 Mbps (for both trunk and CPS) are supported by 40 watt TWTAs being developed for NASA by Hughes Electron Dynamics Division. Since the trunk and CPS services are not simultaneous, the trunk TWTAs are also used for the CPS. The CPS total uplink data rate is broken into 32 Mbps uplink channels so that low cost earth stations can be employed.

The NASA 30/20 GHz flight experiment has a 2 year duration, however, the satellite is to be designed for a 4 year lifetime so that additional use of the satellite can be made by industry if there is a need. The spacecraft propulsion system must have fuel for 4 years of stationkeeping in both inclination, longitude, and spacecraft attitude.

It is a NASA requirement that the communication payload be installed on an existing spacecraft bus. A 4 year lifetime is required. The bus employed by Hughes is the LEASAT spacecraft. Figure 1-1 shows the 30/20 GHz flight experiment installed on the LEASAT bus. The antenna employs a Cassegrain configuration. The planar surface is a frequency selective screen which separates the transmit and receive signals. The trunk feeds are part of the scanning beam feed arrays which are shown. The



810339-223

FIGURE 1-1. SPACECRAFT ISOMETRIC

20 GHz beacon antenna is also visible. The beacon signal is available on propagation measurements anywhere in the contiguous United States (CONUS). It also carries the telemetry and ranging data.

The LEASAT spacecraft configuration is shown in Figure 1-2. It is the first communication satellite designed to be launched only by the Space Shuttle and to take full advantage of the Shuttle's considerable launch cost savings. In its launch configuration, LEASAT is 422 cm in diameter and 430 cm in height. The spacecraft is a dual spin configuration, with a rate of 30 rpm on station. The spinning section contains the propulsion, attitude control, and power subsystems. The despun section contains the telemetry, command, and communication subsystems and the spacecraft's earth pointing antennas. The antennas and the equipment on the despun platform are replaced by the 30/20 GHz payload. The spinning section is virtually unchanged.

The LEASAT propulsion system incorporates the perigee and apogee stages needed to lift the spacecraft from low Shuttle orbit into synchronous orbit. A liquid propellant system will be used for perigee augmentation and the complete apogee impulse. Four years of on-orbit station keeping and attitude control will be provided by a standard monopropellant hydrazine system.

The 30/20 GHz flight experiment vehicle will weigh 17,071 pounds in the Shuttle bay and 3,095 pounds when it reaches synchronous orbit. Its weight

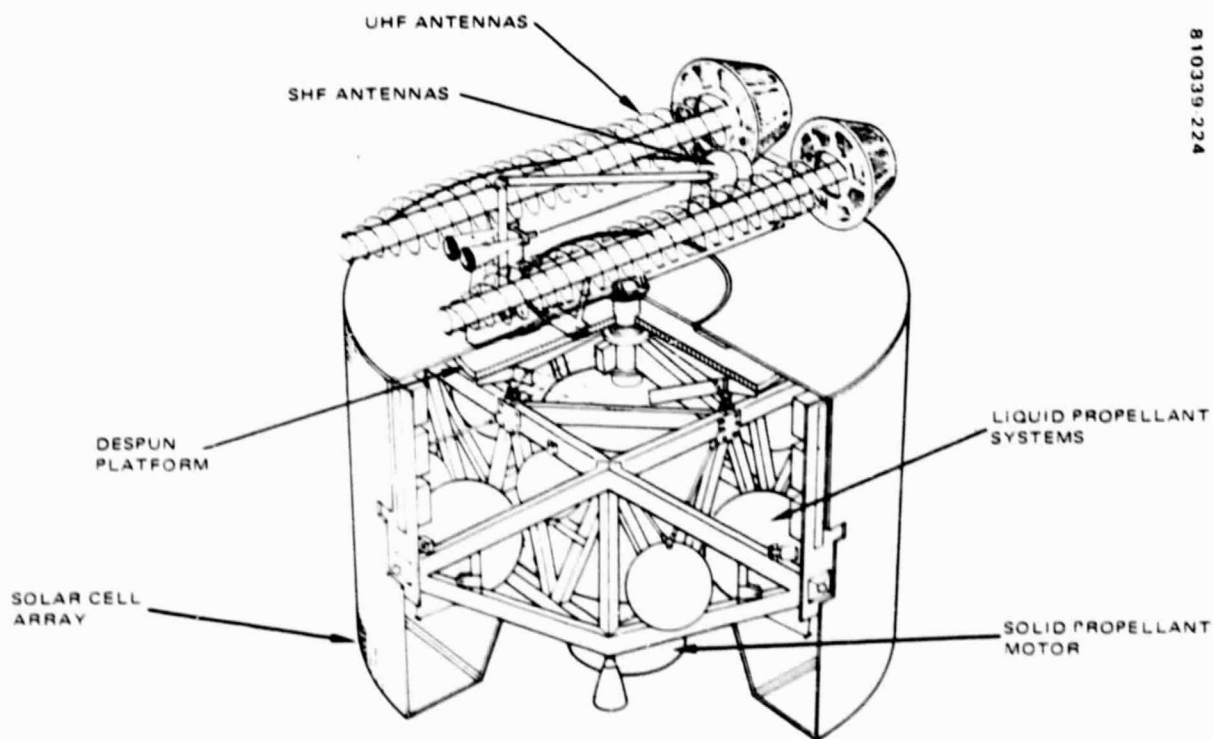


FIGURE 1-2. LEASAT SPACECRAFT STOWED CONFIGURATION

at the end of 4 years will be 2,750 pounds. A weight summary is given in Table 1-1. The total spacecraft weight margin provided by excess propulsion capability is 156 pounds. A 10 percent payload weight margin of 42 pounds was allocated to the payload leaving 114 pounds as rotor weight margin. The ultimate limit in payload weight is the stability requirement that the spin to transverse inertia ( $I_s/I_t$ ) ratio be greater than 1.05. As much as half of the 114 pound rotor margin could be reallocated to the payload if the remainder of the rotor margin were positioned near the perimeter of the rotor. The actual fraction of the 114 pounds which is available for the payload depends on whether the payload weight growth was above the despun platform (e. g., antenna) or in the despun platform which is near the center of gravity. If the first of two options which were studied at NASA's direction were implemented, the payload weight would be reduced by 49 pounds by eliminating one of the scanning beams and reducing the BBP throughput. The additional margin provided by option 1 does not appear necessary. The second option, which added an FDMA capability to the payload, added 16 pounds to the payload. Adoption

TABLE 1-1. SPACECRAFT WEIGHT SUMMARY

Item	Payload Weight, lb	
Payload		465
Antenna	189	
Microwave	123	
Digital	111	
Margin (10%)	42	
Bus		2,285
TT&C	123	
Controls	75	
Power	541	
Propulsion	323	
Structure	1,100	
Margin (rotor)	114	
Spacecraft (dry)		2,750
Propellant (BOL)		345
RCS (4 <sup>+</sup> yr)	324	
LAM residual	21	
Spacecraft (BOL)		3,095
Transfer orbit expendables		12,191
Shuttle deployment		15,286
Cradle and ASE		1,785
Shuttle payload		17,071

of option 2 would appear to leave adequate margin. Also, option 2 could be removed if necessary without any significant effect on the remainder of the payload.

Table 1-2 is a power summary of the 30/20 GHz spacecraft. The major portion of the trunking service payload power is for the four 40 watt TWTAs. In the CPS mode, only two of the TWTAs are used but the BBP, which is used primarily for the CPS mode, replaces these TWTAs as a power user. The effect in power demand of the two options is insignificant compared to the very large power margin.

The 30/20 GHz flight experiment spacecraft will be carried in the Space Shuttle as shown in Figures 1-3 and 1-4. It will be held in the Shuttle bay by a reusable cradle, which attached to the mainframe of the Shuttle at five points. While the Shuttle is orbiting at an altitude of 160 n.mi., the

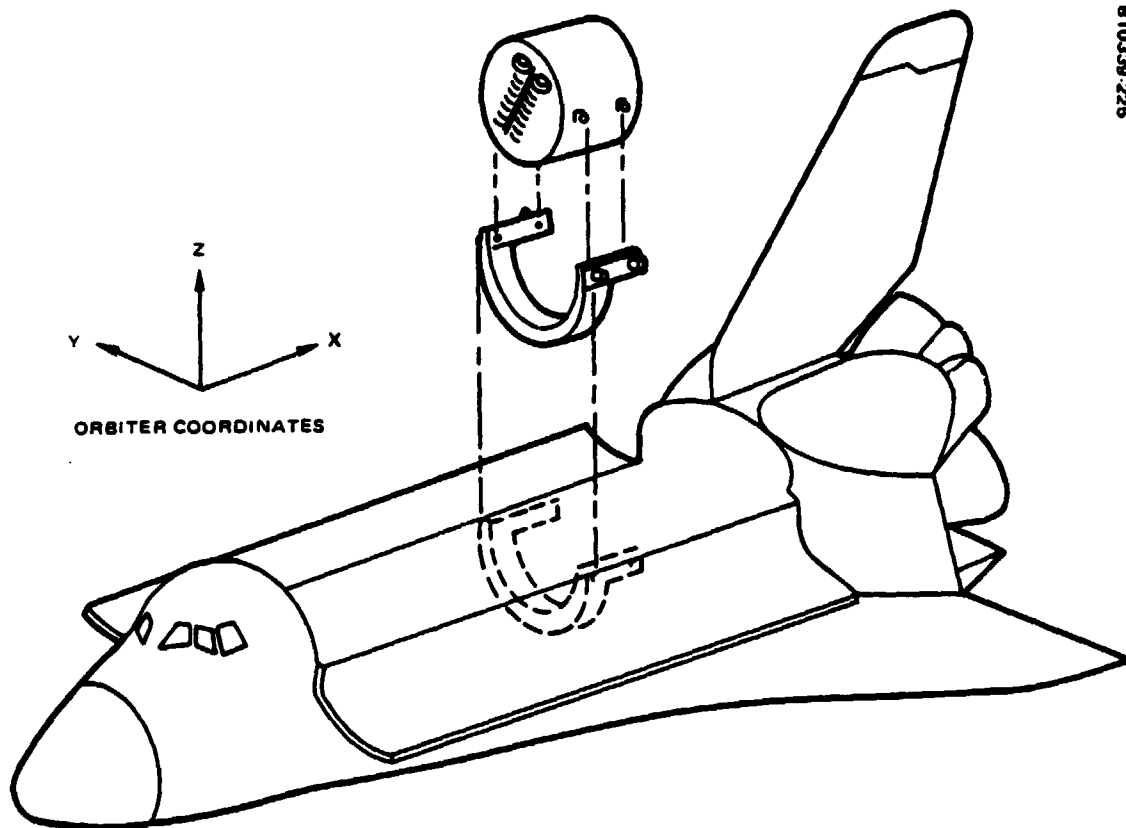


FIGURE 1-3. LAUNCH CONFIGURATION

TABLE 1-2. POWER SUMMARY (WATTS)

Item	Baseline	
	TS	CPS
Payload		
Antenna	1.8	9.8
Microwave	515.6	285.6
Digital	41	223.2
Bus	228	228
TT&C (48)		
Controls (37)		
Power (92)		
Thermal (51)		
Spacecraft	786.4	746.6
Capability (4 yr)	1,090	1,090
Margin	303.6	343.3

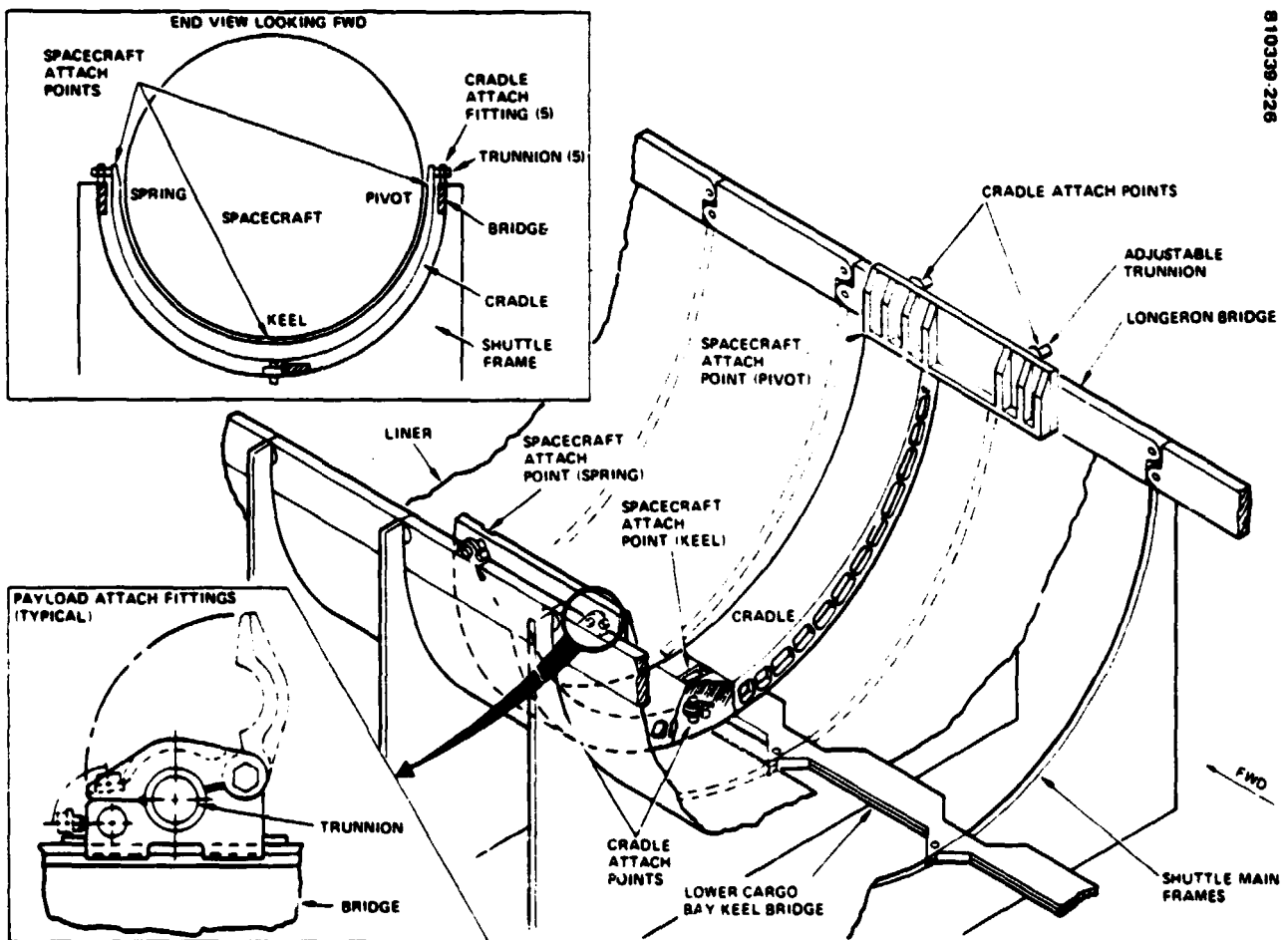


FIGURE 1-4. TYPICAL CRADLE SHUTTLE BAY INSTALLATION



spacecraft will be ejected by two springs which supply a separation of 160 n.mi., the spacecraft will be ejected by two springs which supply a separation velocity of 40 cm/sec and a rotational speed of 1.8 rpm. Spinup rockets will increase the satellite's rate to 30 rpm approximately 300 seconds after release. The solid propellant perigee motor will be fired 45 minutes after release. The empty motor case and its supporting structure will then be dropped. The liquid propellant motors will supply the additional velocity needed to put the spacecraft in elliptic transfer orbit. On reaching synchronous orbit, the communications antenna will be deployed and operational service will begin.

A summary estimate of the reliability of the space segment is given in Table 1-3. The reliability of the launch and orbit insertion is included in the estimates. The estimate uses an existing reliability estimate for the LEASAT bus and the number and type of parts used in the payload. The assumptions and model used are described in 4.3, Space Vehicle Reliability.

TABLE 1-3. SPACE SEGMENT RELIABILITY

Item	2 years	4 years
1) Complete communication capability	0.80	0.62
2) Complete trunk capability	0.94	0.81
3) Complete CPS capability	0.81	0.65
4) Loss of no more than 1 of 4 trunk beams and no more than 1 spot from each scanning beam	0.92	0.79

The reliability shown is quite adequate to meet mission objectives, particularly since the partial failures of case 4 will not seriously interfere with these objectives. The scanning beams each have a total of 16 spots in the uplink and 10 spots in the downlink so the loss of one spot from each of the two areas can be tolerated. The reason for the lower reliability of the CPS relative to the trunking service is the complexity of the beam forming networks of the scanning beams.

The terrestrial segment of the 30/20 GHz flight experiment consists of trunk terminals, CPS terminals, and a master control terminal (MCT). The trunk terminals have 5 meter antennas and employ site diversity to improve propagation reliability. The CPS stations are of two types: 1) small stations which transmit at a 32 Mbps burst rate and use a 3 meter antenna, and 2) large stations which transmit at 128 Mbps and use 5 meter antennas. All terminals receive at 256 Mbps. The MCT consists of a trunk terminal and a central control station which controls both the communication network and the spacecraft operation. NASA will procure the MCT and a small CPS terminal; experimenters will procure other terminals.

## 2. COMMUNICATION SYSTEM DESIGN

The design of the 30/20 GHz flight experiment communication system has the following three aspects:

- 1) Design of the communication links which satisfy the specified service requirements
- 2) Design of the communications operations system which controls the communication links and enables the multiplicity of users to access the system in an orderly and efficient manner
- 3) Design of the experiments which make use of the communication system

### 2.1 COMMUNICATIONS

#### 2.1.1 Requirements

The flight experiment must address the service capabilities of an operational system of the 1990's and the technologies required to provide these capabilities. This flight experiment, as defined by NASA, is illustrated in Figure 2-1. The experiment has two parts: a trunk service (TS) and a customer premise service (CPS). The TS provides high data rate bulk communications to a limited number of nodes. In an operational system as many as 20 or more nodes might be served. The flight experiment is specified to comprise a six node network with four nodes active simultaneously. The six nodes are shown in Figure 2-2. Los Angeles and Cleveland are always part of the network. Tampa and Houston are alternates to New York and Washington, respectively. The specified access method is satellite switched time division multiple access (SS-TDMA). Each node transmits sequential bursts of data to the other nodes. Each station transmits at least one burst per a frame to each node with which it communicates. The bursts are in synchronism with a switch matrix onboard the satellite. This switch matrix, which operates at IF, connects each uplink beam at any instant in time with the downlink beam for which its data is intended. The means by which the use of the SS-TDMA is controlled and synchronized is discussed in 2.2. The earth terminals for the TS are specified to have

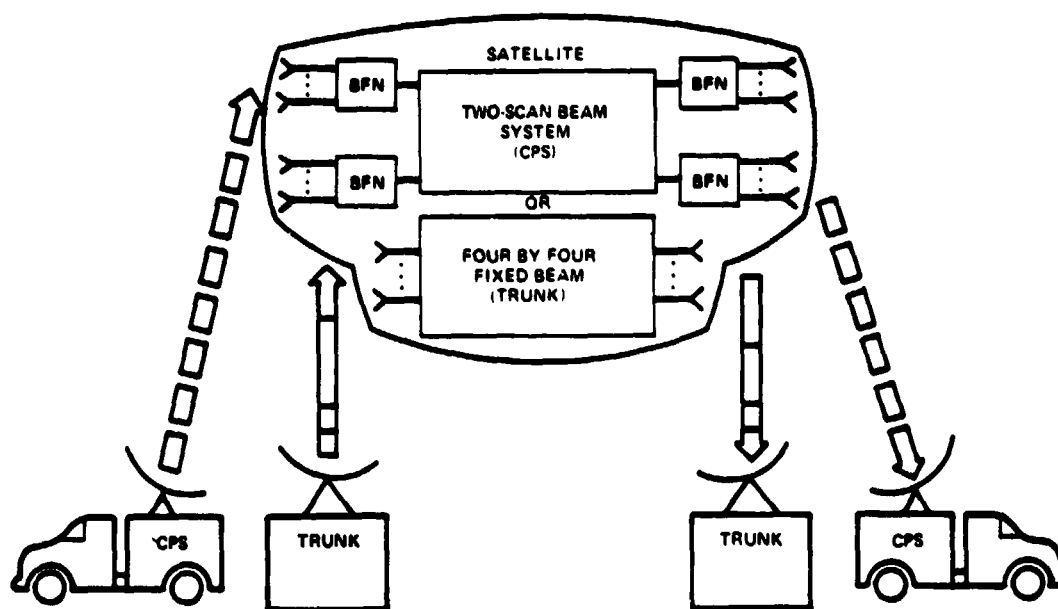


FIGURE 2-1. 30/20 GHZ FLIGHT EXPERIMENT SYSTEM

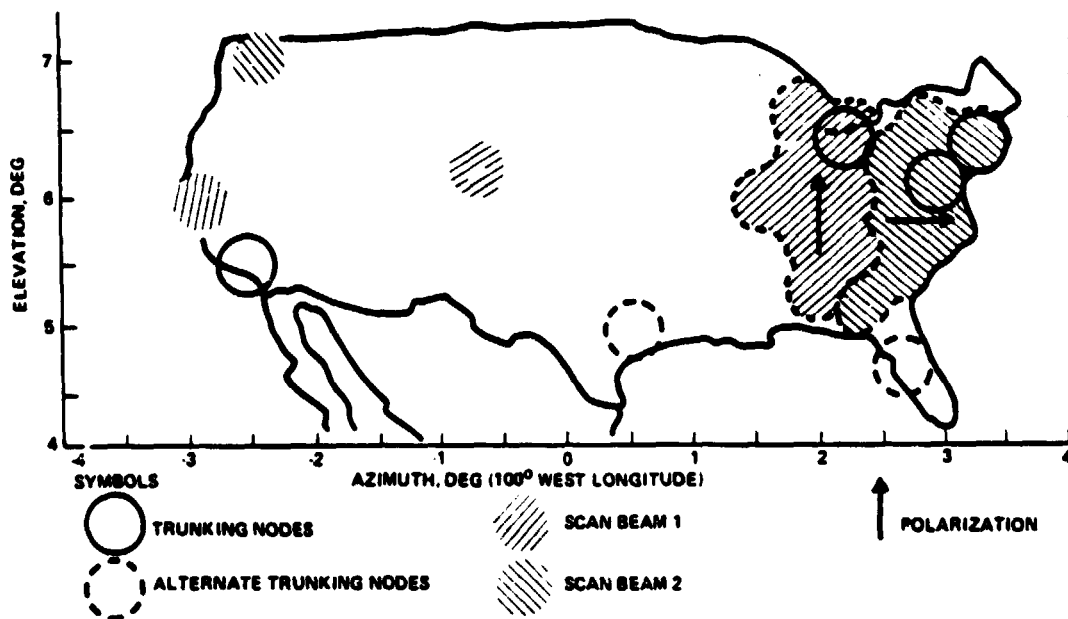


FIGURE 2-2. TYPICAL ANTENNA COVERAGE

5 meter antenna diameters and to employ site diversity to minimize the effect of rain attenuation. The burst rate is specified to be 256 Mbps. The average data rate will be somewhat less because of the overhead resulting from guard time and preambles (3.2). The bit error rate (BER) requirement is 10<sup>-6</sup>. The required rain margins are 18 dB on the uplink and 8 dB on the downlink. The resulting propagation reliability is discussed later in this section.

An operational CPS serves many small and medium users scattered about the country. The CPS requires two scanning beams. The required coverage of these beams is illustrated in Figure 2-2. Each beam covers a contiguous area in the eastern United States plus one or two isolated beams in the west. The scanning beam covers its area by moving a spot beam about the area. This antenna configuration imposes SS-TDMA operation because users in different spots have access to the satellite at different times. The fraction of the satellite capacity assigned to each spot is adjusted to match the traffic requirements by varying the fraction of the TDMA frame spent by the beam at each spot. A baseband processor (BBP) is required to store data received from each spot in the uplink beams until a downlink beam is pointed at the spot for which the uplink data is intended. Without this store and forward capability the up and downlink beams would be constrained to point simultaneously at each pair of spots which had a traffic interconnection. This would require a very large number of antenna steps. The time consumed by these stepping operations would reduce the system efficiency to an inadequate level. The store and forward capability allows each beam to address each spot in its area once per frame. During this dwell it would receive and transmit all data associated with that spot. The requirement to provide forward error correction capability also imposes a need for a BBP to demodulate and decode uplink coded data and encode data for attenuated downlinks.

Two types of CPS terminals are required. Terminals which transmit a 32 Mbps burst rate require 3 meter antennas and terminals which transmit 128 Mbps require 5 meter antennas. All CPS terminals receive at 256 Mbps. The CPS is required to maintain performance in the presence of 15 dB of uplink attenuation and 6 dB of downlink attenuation. As mentioned above, forward error correction (FEC) is specified as an aid to meeting this requirement.

Simultaneous operation of the TS and CPS systems is not required.

One of the objectives of the flight experiment is to improve frequency reuse by means of the multispot beam antenna. Figure 2-3 and 2-4 show the NASA frequency plan. This plan requires all trunk modes to reuse the same frequency band except for Washington which can be frequency isolated from New York. Likewise, the two scanning beams occupy the same channels. The two CPS beams are polarization isolated. The total uplink burst rate is 128 Mbps. This can be composed of either four 32 Mbps channels or a single

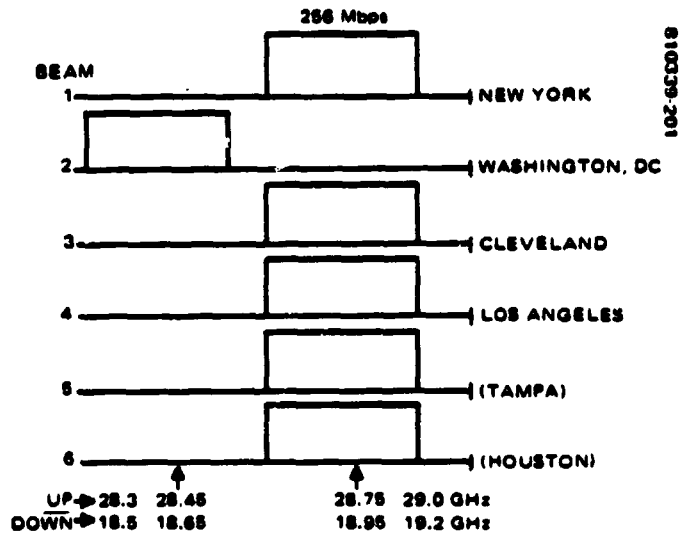


FIGURE 2-3. TRUNKING SERVICE FREQUENCY PLAN

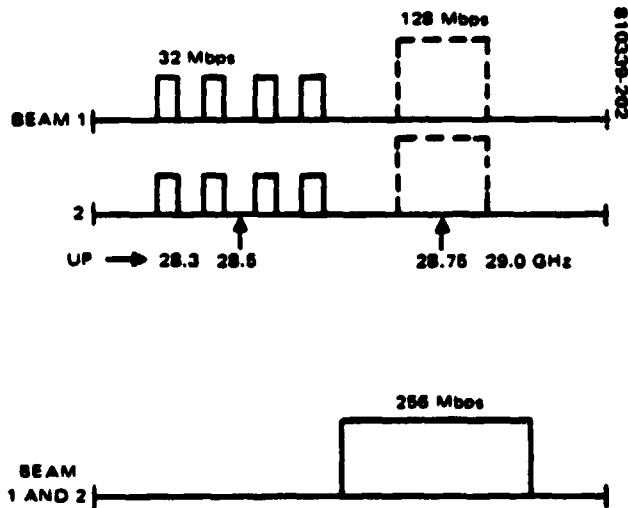


FIGURE 2-4. CPS FREQUENCY PLAN

128 Mbps channel. A single downlink channel at 256 Mbps is required on each beam. Because the uplink throughput on this experiment is only half the downlink throughput, at most one-half of the uplink frame is occupied.

The service requirements discussed above are summarized in Table 2-1.

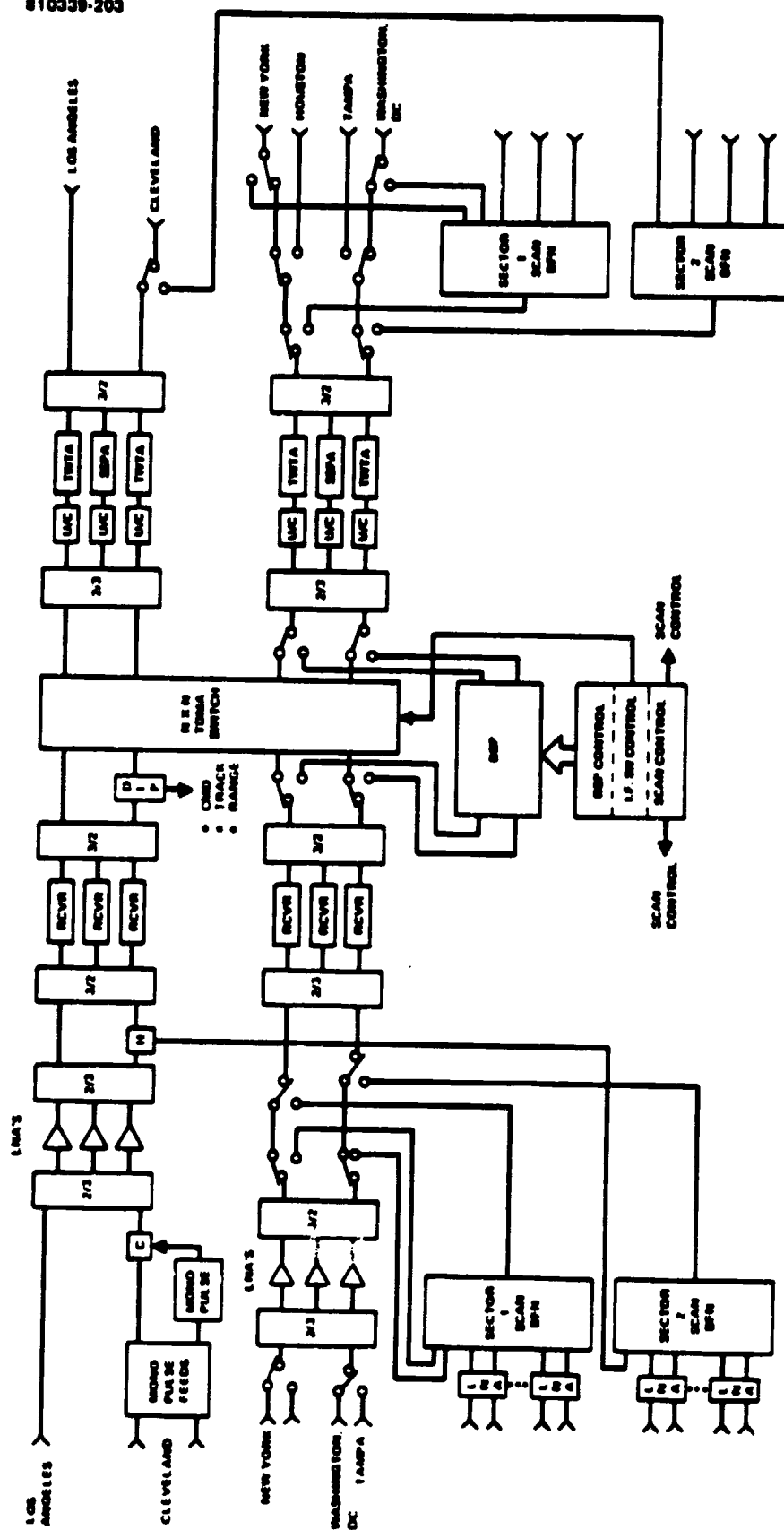
In addition to the service requirements NASA has specified a number of technology requirements which are required by potential operational systems of the 1990's but which are not needed to satisfy the service requirements of this flight experiment. These technology requirements are summarized in Table 2-2.

TABLE 2-1. SERVICE REQUIREMENTS SUMMARY

Service Requirements	Service	
	Trunk Service	Customer Premise Service
Coverage	Four-by-four with two alternate nodes (Los Angeles, Cleveland, New York, Washington, Tampa, Houston)	Two adjacent sectors in the earth, United States plus isolated spots in western United States
Burst data rates	256 Mbps, nominal	Uplink: H - 32 Mbps or 1 - 128 Mbps, nominal  Downlink: 1 - 256 Mbps
Interconnectivity	Four-by-four SS-TDMA	Baseband processor and beam forming network
Ground station antenna size	5 m (site diversity)	5 m for 128 Mbps 3 m for 32 Mbps
Rain margin (uplink/downlink)	18/8 dB (power)	15/6 dB (power + FEC)

TABLE 2-2. TECHNOLOGY REQUIREMENTS

Satellite transmit antenna	Diameter = 3 m Peak gain $> 51$ dB ( $3^\circ$ from boresight)
Satellite receive antenna	Halfpower beamwidth equal to transmit HPBW
Baseband processor	Scalable to throughputs of 480 Mbps/beam and 4 Gbps total
Satellite high power amplifier	Primary HPAs: 40 W TWTA with efficiency greater than 40% Backup HPAs: solid state
IF switch matrix	Scalable to 20 beams interconnect



**FIGURE 2-5. SPACECRAFT FUNCTIONAL BLOCK DIAGRAM**

NASA required that the receive antenna beamwidth equal the transmit beamwidth in order to minimize the number of receive feeds; however, although the use of a single reflector for both transmit and receive doubles the number of receive feeds required to cover the assigned area, this approach has two important advantages for both the satellite and earth terminals. The earth terminal transmitter power can be reduced by over 3 dB because of the increased satellite receive gain. The satellite benefits in two ways. First, the weight of a second reflector (2 meter diameter), its support structure and deployment mechanism, is eliminated. Second, the transmit antenna can be pointed more accurately since it includes the uplink beacon tracking feeds. A single reflector for both frequencies is made possible by the use of a planar frequency selective surface (FSS) which creates separate focal regions for transmit and receive feeds. Thus no duplexers are required and both receive and transmit feeds can be independently optimized. This FSS technology is considered by Hughes to be important for multispot beam antennas because it provides two antennas without requiring a second reflector. Consequently, with NASA's permission, Hughes has designed the satellite antenna with a 3 meter aperture for both transmit and receive.

#### 2.1.2 Spacecraft Payload Block Diagram

The spacecraft payload shown in Figure 2-5 implements the requirements described previously. Section 3 presents detailed descriptions of the antenna, microwave and digital portions of the payload. The operation of the overall payload is summarized below.

The upper portion of the diagram represents the trunk service components and the lower half the CPS components. The switches are shown in the TS mode configuration. Low noise amplifiers (LNA) are installed at the feeds in order to establish the spacecraft noise figure before the losses imposed by the beam forming network of the CPS scanning beam antenna are incurred. At the time this configuration was developed the beam forming networks (BFN) loss was estimated to be over 3 dB. Recent data from Electromagnetic Sciences indicates that the loss will be less than 1 dB. Consequently, the use of LNA at the feeds will be reevaluated in the next phase of this program. The use of an LNA at each feed imposes a significant weight penalty especially when redundancy is provided. The weight penalty for using distributed LNAs is about 6 pounds. If the CPS LNAs were redundant the weight penalty (including the redundancy switches) for distributed LNAs would be about 15 pounds. The trunk feeds are also provided LNAs because several of them are also used for the scanning beams. Also, at 30 GHz, the losses in waveguide runs are appreciable. The TS LNAs are 3 for 2 redundant because of the importance of each of the small number of beams. CPS LNAs are single string to avoid the weight penalty associated with providing additional LNAs and the associated switching for the large number of receive scan beam feeds. There are 29 feeds for the receive scan beams. Individual receivers with 3 for 2 redundancy are provided for the four active trunk feeds because all trunk modes except Washington use the same frequency. The receivers downconvert the signals to 6 GHz which has been selected as the operating frequency of the IF switch matrix. The



switch matrix interconnects the four active uplinks with four active downlinks to provide SS-TDMA. A 6 by 4 matrix is used to provide redundancy as described in 3.2. A 1 ms frame is divided into subframes. During each subframe, each uplink is connected to a single downlink. Over the course of the frame each uplink is connected to each of the downlinks. The synchronization of the earth terminals' transmissions and the IF switch are discussed in 2.2.

The four trunk transmitters use 40 watt TWTAs as high power amplifiers as required by NASA. The redundant transmitters are required to be solid state. Hughes has chosen GaAs FET HPAs over IMPATTs because of the greater potential of the GaAs FET. This trade is discussed in 3.2. A saturated output power of 7.5 watts is anticipated to be available with these backup transmitters. The impact of this low power is discussed in 2.1.5.

The receive beam forming networks scan the antenna beams over the coverage area by switching the receiver input from feed to feed. Switching is also provided to allow the New York and Washington receivers to be used for the CPS when the system is in the CPS mode. The baseband processor receives the 6 GHz output of the receivers. Each of these signals contains either four 32 Mbps frequency multiplexed QPSK signals or a single 128 Mbps signal. The signals are demodulated and the data stored until a downlink scanning beam is pointed at the spot for which the data is intended, at which time it is read out to the appropriate transmitter at a rate of 256 Mbps.

### 2.1.3 Satellite Antenna Pointing

A requirement to point the satellite antenna to within  $\pm 0.05$  degrees ( $3\sigma$ ) of the designated target has been imposed to limit pointing loss to less than 0.5 dB on the uplink. Because the spacecraft attitude cannot be maintained to this accuracy the antenna points independently of the spacecraft attitude by tracking an earth based beacon. The antenna has two degrees of freedom. Elevation tracking is provided by a mechanical drive which is also used to rotate the reflector from its launch position stowed against the top of the spacecraft cylinder to its deployed position. Azimuth tracking is provided by the spacecraft despin system which despins the entire payload equipment platform to point the antenna at its azimuth position. The error signal for both the elevation and despin control systems is derived from a two axis monopulse tracker. This monopulse tracker uses four auxiliary feeds surrounding the Cleveland feed to measure the elevation and azimuth errors relative to the beacon transmitted from the MCT at Cleveland. This beacon could be located at a location less susceptible to rain attenuation with the tracking feeds suitably relocated; however, the beacon which is modulated by the command signal is narrowband and has a large rain margin. Earth sensors, which are required for spacecraft attitude control as well as for despin during transfer orbit operations, provide a less accurate backup pointing capability in case of beacon outage.

The satellite antenna and microwave monopulse hardware are described in 3.1 and 3.2.3. The overall antenna pointing system is discussed in 4.1.

#### 2.1.4 Antenna Configuration Trades

Figure 2-6 illustrates the effect of scan loss on the gain of large antennas operating at high frequencies. The curves apply to a beam which is directed to Boston, 3 degrees from the antenna boresight. Because the beam defocussing increases with the number of beamwidths by which the beam is displaced from boresight, the off axis scan loss is particularly severe at 30 GHz. This defocussing can be reduced by increasing the ratio of focal length to antenna diameter (F/D).

The practical focal length of a prime fed antenna is limited by the satellite dimensions to about 12 feet. A Cassegrain configuration allows this limit to be overcome. The focal length which can be obtained with a Cassegrain configuration depends on the eccentricity of the hyperloldal subreflector. An eccentricity of 3 provides a 24 foot focal length. The diameter of the parent parabolic antenna is also 24 feet. (The 10 foot antenna is an offset section of the parent parabola.) The Cassegrain antenna then has an F/D = 1 compared to 0.5 for the prime fed configuration.

The original specification was for a 10 foot (3 meter) diameter for the transmit antenna and a receive beamwidth equal to the transmit beamwidth. At 20 GHz, a 6 foot (1.8 meter) diameter provides the required beamwidth. It can be seen that at the specified diameters, there is little advantage to the Cassegrain configuration; however, for Shuttle diameter antennas which NASA considers appropriate to operational systems, the improvement provided by the Cassegrain configuration is significant. Consequently, the Cassegrain configuration was selected. Also, since a 10 foot receive diameter has been adapted, as discussed in 2.1.1 the Cassegrain configuration, in conjunction with this increase in diameter provides a substantial increase in receive gain.

#### 2.1.5 Terrestrial Segment

The terrestrial segment of the 30/20 GHz Flight Experiment system, Figure 2-7, consists of the master control terminal (MCT) and a CPS station provided by NASA and trunk and CPS stations provided by experimenters. The NASA CPS station will be mobile.

The MCT shown in Figure 2-8 located in Cleveland is a trunk station with the central control station (CCS) attached. The trunk station is composed of a trunk terminal and two antenna sites. The antenna sites include the burst modems and all of the RF equipment. The trunk terminal includes the equipment which interfaces with the user, buffers continuous user data to convert this data to TDMA burst data and synchronizes the transmission of the data bursts. The diversity switch connects the trunk terminal with one or the other 5 meter antenna sites depending on the severity of rain attenuation at each site. At the MCT one of the antenna sites is colocated with the trunk terminal and the other is connected by a microwave link. The MCT has, in addition to its trunk capability, a CPS capability with a 128 Mbps uplink. This capability eliminates the need for a NASA CPS terminal with a 5 meter antenna in addition to the 3 meter CPS terminal.

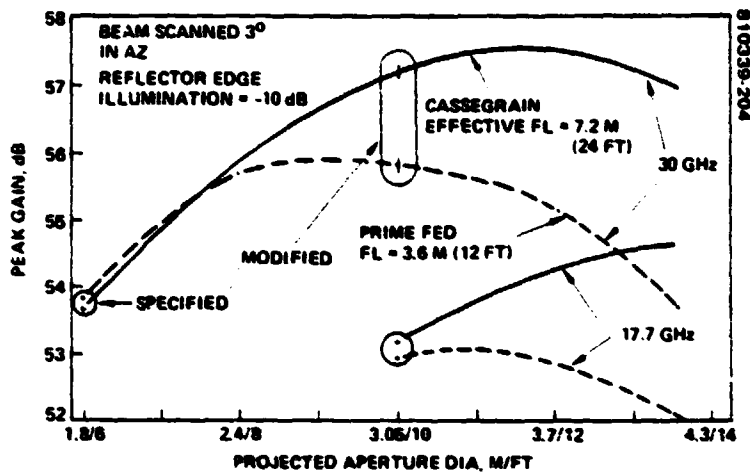


FIGURE 2-6. ANTENNA CONFIGURATION SELECTION

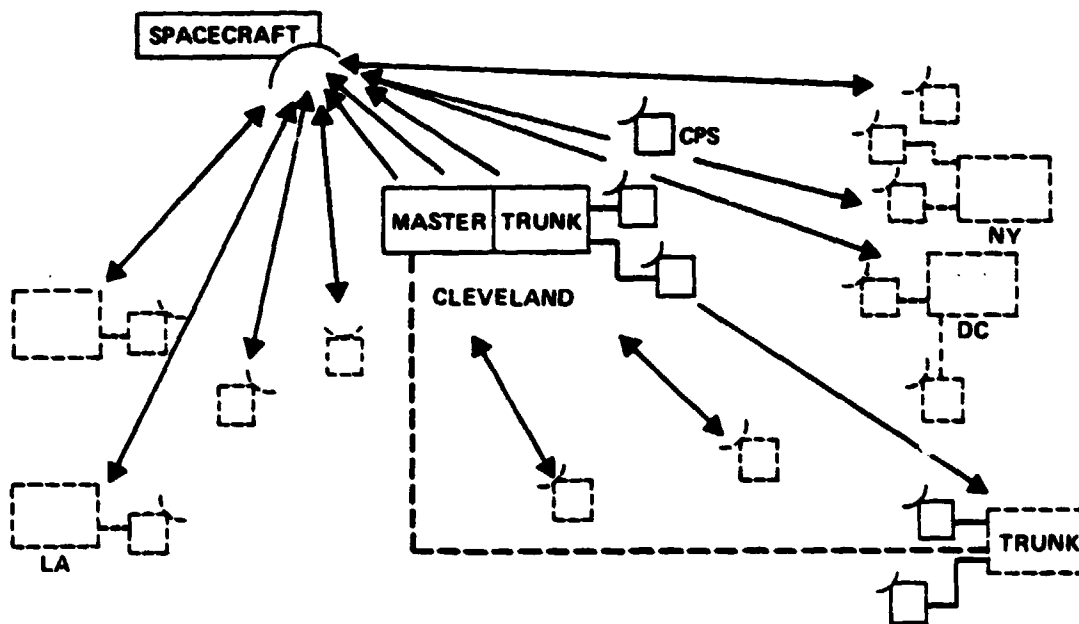


FIGURE 2-7. TERRESTRIAL SYSTEM

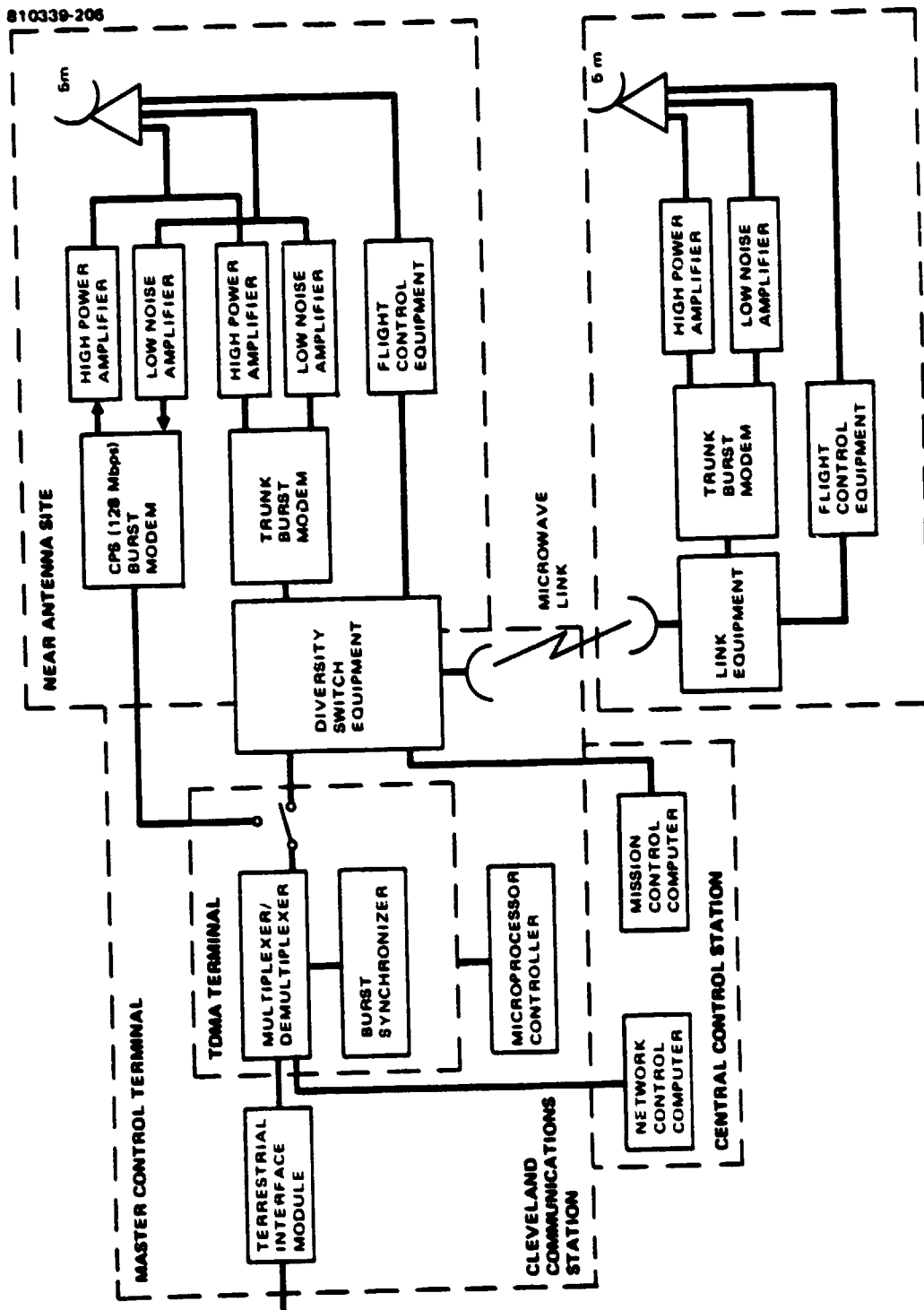


FIGURE 2.8. MASTER CONTROL TERMINAL

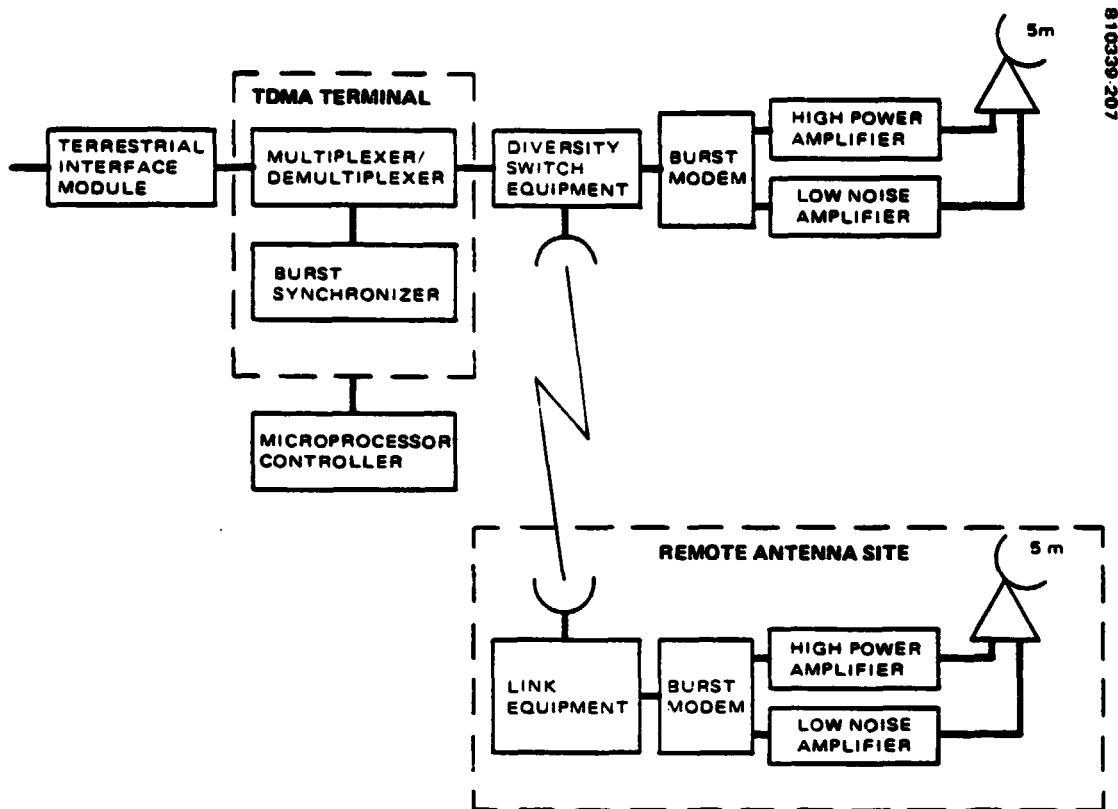


FIGURE 2-9. TDMA TRUNK STATION

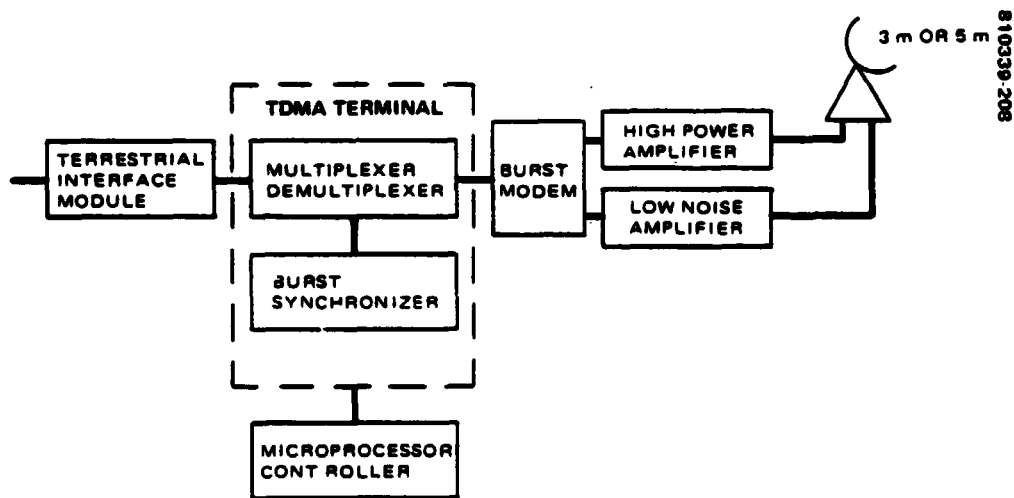


FIGURE 2-10. TDMA CPS STATION

The CCS controls the mission operations, the communication operations, and the experiment operations. The mission operations which included the operation of the spacecraft during launch and transfer orbit and the maintenance of the spacecraft bus attitude, orbit and health throughout the mission are supported by the mission operations computer. The communication operations include the activities which coordinate earth terminals and payload. These activities which include TDMA burst synchronization, demand assignment, link control and payload control are supported by the network control computer.

A typical TDMA trunk station shown in Figure 2-9 is identical to the trunk service portions of the MCT. It includes the TIM, microprocessor controlled TDMA terminal, and diversity switch. One of the two antenna sites is colocated with the station and the remote antenna site is connected by a microwave link.

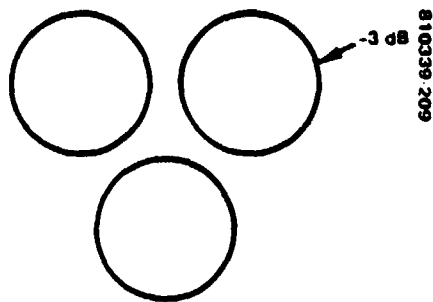
There are two types of CPS stations considered for this system (Figure 2-10). One is a 5 meter antenna station which handles the 128 Mbps uplink burst rate and the other is a 3 meter antenna station with a 32 Mbps uplink burst rate. The downlink burst rate is 256 Mbps for both stations. TDMA synchronization is accomplished with burst synchronizer and formatting, and decommutation is handled by microprocessor.

The RF parameters of the earth terminals are given in the next section.

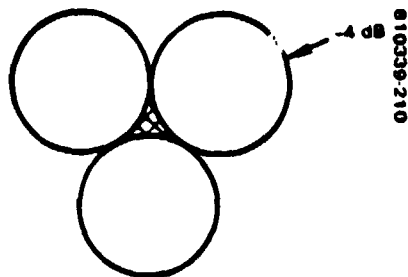
#### 2.1.6 Communication Link Performance

##### 2.1.6.1 Spacecraft RF Performance

The spacecraft RF performance is summarized in Table 2-3. The antenna performance is for a beam pointed at the vicinity of New York. This beam is approximately 3 degrees from the antenna boresight. Consequently, it suffers a loss of 1.6 dB on receive and 1 dB on transmit due to off axis defocussing. The trunk pointing loss is based on a total pointing error of  $\pm 0.05^\circ$  ( $3\sigma$ ). The contour level loss suffered by the antenna in the CPS mode results from the requirement for contiguous coverage. The stated loss is for a feed system in which each spot beam is associated with a single feed. This loss can be reduced by more complex feed structures as discussed in 3.1; however, except for an experiment involving two feeds, the performance of the simpler arrangement was accepted. Also, a higher gain is available over most of the coverage area. As shown in Figures 2-11(a) and (b) the loss can be reduced from 8 dB in transmit to about 4 dB by giving up 14 percent of the area and to 3 dB by sacrificing 35 percent of the area.



a) 35 PERCENT TOTAL COVERAGE AREA LOSS



b) 14 PERCENT TOTAL COVERAGE AREA LOSS

FIGURE 2-11. REDUCED AREA COVERAGE

TABLE 2-3. SPACECRAFT RF PERFORMANCE

Antenna	19.0 GHz		28.8 GHz	
	Trunk	CPS	Trunk	CPS
Diameter, m	3	3	3	3
Peak gain (3° from boresight), dB	53.1	53.1	56.1	56.1
Contour level, dB	-	8.1	-	7.1
Feed loss, dB	1.6	1.9	0.9	0.9
Net gain, dB	51.5	43	55.2	48.1
Transmit (19 GHz)	TWTA		SSPA	
	Trunk	CPS	Trunk	CPS
Power out, dBW	16 (40 W)	16 (40 W)	8.5 (7 W)	8.5 (7 W)
Circuit loss, dB	-0.45	-0.45	-0.45	-0.45
Power to antenna (dBW)	15.5 (36 W)	15.5 (36 W)	8 (6.4 W)	8 (6.4 W)
EIRP, dBW	67	58.5	59.5	51
Receive (28.8 GHz)		CPS	Trunk	
Antenna temperature, °K		290	290	
Receiver noise figure, dB		5 (627°K)	5 (627°K)	
Circuit loss, dB		-0.4	-0.7	
System noise temperature, dB-°K		30	30.3	
G/T, dB		18.1	24.9	

The transmit circuit loss for both TS and CPS includes 0.15 dB for the circulator switches used to select the power amplifier, 0.3 dB for five feet of WR51 waveguide from the output circuits to the antenna feed.

The satellite receiver noise figure is for a four stage GaAs FET amplifier with a 4.9 dB noise figure and about 20 dB of gain followed by a receiver with a 7.5 dB noise figure. The circuit loss is made small by the placement of the LNAs near the feeds. The trunk loss is slightly higher because of the associated redundancy and configuration switches.

#### 2.1.6.2 Earth Terminal Performance

The performance of the earth station RF is shown in Table 2-4. The antenna diameter was specified by NASA. The 5 meter CPS stations are capable of a 128 Mbps uplink. The 3 meter stations are limited to 32 Mbps. The antenna efficiency is 60 percent before accounting for surface tolerance losses of 2.0 dB at 30 GHz and 1.0 dB at 20 GHz. These losses are based on a tolerance of 0.64 mm rms and an F/D of 0.5. The maximum transmitter



TABLE 2-4. TERRESTRIAL RF PERFORMANCE

Antenna Diameter, m	Trunk	CPS	
	5	5	3
28.8 GHz			
Transmit gain, dB	59.7	59.7	55.3
Transmit loss, dB	-1.3	-1.3	-1.3
Transmitter power, dBW	21 (125 W)	13 (20 W)	13 (20 W)
EIRP, dBW	79.4	71.4	67
19 GHz			
Receive gain, dB	57.2	57.2	52.7
Receive loss, dB	-0.5	-0.5	-0.5
Sky noise temperature, °K	260	260	260
Receiver noise figure, dB	1.9	1.9	1.9
System noise temperature, dB °K	26.8 (479°K)	26.8	26.8
G/T	30.4	30.4	25.9

power for the trunk service is 125 watts. In clear weather the transmitter is backed off by 18 dB to 2.0 watts. The power is continuously adjusted to match the rain attenuation. The 5 meter CPS terminal transmitter has a saturated output of 20 watts for the 128 Mbps signal. The 3 meter CPS terminal uses the same transmitter for the 32 Mbps signal.

The sky noise temperature in clear weather is only 60°K but a sky temperature of 260°K is used to compute the system temperature because of the increase in sky temperature when the rain attenuation is at the trunk maximum of 8 dB. The CPS downlink rain margin requirement is only 6 dB but, because of the use of FEC, an actual margin of 9.4 dB is achieved. Consequently, 260°K was used for all links. This high sky temperature reduces the benefit obtained by cooling the low noise amplifier. A GaAs FET noise figure of 1.9 dB is expected to be achievable at room temperature for this mission. Cooling would improve G/T less than 1 dB.

### 2.1.6.3 Trunk Link Budget

The trunk link budget is shown in Table 2-5. The basis for the EIRP and G/T were given in the previous sections.

The atmospheric and path losses were based on a terminal elevation angle of 37° which would apply to a terminal in New York operating through a satellite at 100° west longitude. The earth station antenna pointing error includes ±0.02° for spacecraft orbital motion. The remainder of the ±0.05°

TABLE 2-5. TRUNK LINK BUDGET (dB)

Component	Uplink, 28.8 GHz	Downlink TWTAs, 19 GHz	Downlink SSPA, 19 GHz
EIRP, dBW	79.3	67	59.5
Pointing loss (transmit)	1.5	0.2	0.2
Path loss	213.1	209.5	209.5
Rain attenuation	18	8	0.5
Atmospheric loss	0.7	1	1
Pointing loss (receive)	0.6	0.7	0.7
G/T (dB/°K)	24.9	30.4	30.4
Boltzmann's Constant, dBW/°K	-228.6	-228.6	-228.6
C/N <sub>0</sub>	98.9	106.6	106.6
C/N <sub>0</sub> , end-to-end		98.2	98.2
Data rate (256 Kbps)		84.1	84.1
E <sub>b</sub> /N <sub>0</sub>		14.1	14.1
E <sub>b</sub> /N <sub>0</sub> , required		14.1	14.1

error is due to antenna setup errors and environmentally induced errors. This error could be reduced to a negligible value by autotracking or, perhaps, steptracking and might be reducible by more elaborate setup procedures and a more expensive structure. The potential reduction of the downlink pointing loss of 0.7 dB does not justify the additional expense and, although the uplink loss of 1.5 dB is considerable it appears less costly to compensate with increased transmitter power. Improvements in antenna technology could alter this conclusion. The polarization loss due to depolarization by rain is considered part of the rain attenuation.

The link requirement that  $E_b/N_0 = 14.1$  dB includes 3.5 dB for implementation, interference, and nonlinearity degradations and 10.6 dB to achieve a  $10^{-6}$  BER.

The 40 watt TWTAs, required by NASA for reasons of technology development, allows the trunk link requirement to be satisfied with a 120 watt earth terminal transmitter. When the 7 watt SSPA is used the link requirements can only be met with a 0.5 dB downlink rain margin rather than the required 8 dB. The 8 dB margin could be restored by increasing the earth terminal transmitter output to 550 watts.

#### 2.1.6.4 CPS Link Budgets

The CPS uplink budget is shown in Table 2-6. The downlink budget is shown in Table 2-7. Because of the regeneration of the digital signals by the BBP the up and downlinks are independent and each is allocated one-half

TABLE 2-6. CPS UPLINK BUDGET

Component	5 m (128 Mbps)	3 m (32 Mbps)
EIRP, dBW	71.4	67.0
Pointing loss	1.5	1.5
Atmospheric loss	0.7	0.7
Path loss	213.1	213.1
Rain attenuation prior to use of FEC	7.6	7.6
G/T	18.1	18.1
Boltzmann's Constant (dBW/°K)	<u>-228.6</u>	<u>-228.6</u>
C/N <sub>0</sub>	95.2	90.8
Data rate	<u>81.1</u>	<u>75.1</u>
E <sub>b</sub> /N <sub>0</sub>	14.1	15.7
Rate change gain	3	3
Coding gain	4.4	4.4
Additional rain attenuation when FEC applied	7.4	7.4
Equivalent E <sub>b</sub> /N <sub>0</sub> at maximum attenuation	14.1	15.7
Required E <sub>b</sub> /N <sub>0</sub>	<u>14.1</u>	<u>14.1</u>
Margin	0	1.6

TABLE 2-7. CPS DOWNLINK BUDGET (256 Mbps)

Component	5 m		3 m	
	TWTA	SSPA	TWTA	SSPA
EIRP, dBW	58.5	51.	58.5	51.
Path loss	209.5	209.5	209.5	209.5
Rain attenuation prior to FEC	2.	1.1	2.	0
Atmospheric loss	1.	1.	1.	1.
Pointing loss	0.7	0.7	0.7	0.7
G/T	30.4	30.4	25.9	25.9
Boltzmann's Constant (dBW/°K)	<u>-228.6</u>	<u>-228.6</u>	<u>-228.6</u>	<u>-228.6</u>
C/N <sub>0</sub>	104.3	98.2	99.8	94.3
Data rate	<u>84.1</u>	<u>84.1</u>	<u>84.1</u>	<u>84.1</u>
E <sub>b</sub> /N <sub>0</sub>	20.2	14.1	15.7	10.2
Rate change gain	3	3	3	3
Coding gain	4.4	4.4	4.4	4.4
Additional rain attenuation when FEC applied	7.4	7.4	7.4	3.5
Equivalent E <sub>b</sub> /N <sub>0</sub> at max. rain attenuation	20.2	14.1	15.7	14.1
Required E <sub>b</sub> /N <sub>0</sub>	14.1	14.1	14.1	14.1
Total rain margin	15.5	8.5	11	3.5*

\*If FEC used on all channels

of the  $10^{-6}$  bit error rates. The theoretical requirement for a  $BER = 0.5 \times 10^{-6}$  is  $E_b/N_0 = 11.1$ . Three dB is added for impairments and interference for a total of 14.1 dB.

The uplink losses are the same as for the trunk link discussed above. The rain attenuation, however, is handled differently because of the use of FEC. The total uplink rain margin is required to be 15 dB. FEC provides a gain of 7.4 dB of which 3 dB is due to a 2 to 1 reduction of the bit rate when the rate 1/2 coding, is applied and the burst rate is unchanged. Thus, a 7.6 dB power margin is required to complete the 15 dB rain margin. All rain attenuation up to 7.6 dB is accommodated by boosting the terminal transmitter power. The FEC is only applied when the attenuation exceeds 7.6 dB because a coded channel requires twice as much of the TDMA frame as an uncoded channel. The received  $E_b/N_0$  remains at the clear weather values of 14.1 dB and 15.7 dB for the 5 and 3 meter stations respectively until the attenuation exceeds 7.6 dB at which time FEC is applied and  $E_b/N_0$  increases. As the attenuation increases to 15 dB the effective  $E_b/N_0$  drops to the clear weather value. Note that the ratio of symbol energy to noise density,  $E_b/N_0$ , never drops below 9.6 dB so the coding gain does not fall below 4.4 dB.

The downlink data rate is 256 Mbps for all cases. The normal mode is to use the TWTA. A 2 dB power rain margin is provided so that FEC will not be required for low rain rates which occur frequently. When the attenuation exceeds the power margin, the FEC is applied. Again the 40 watt TWTA is oversized so that a high  $E_b/N_0$  is obtained when 6 dB of rain attenuation is experienced. Thus, a total rain margin of 16 dB is available for the 5 meter earth terminal. Another way of presenting the link budget would allot a 8.6 dB power margin so that FEC would only be required when the attenuation exceeded that value. The total rain margin is still 16 dB. A similar situation obtains for the 3 meter earth terminal with a total margin of 12.2 dB. Of course if the downlink rain attenuation reached these values the uplink would not be available because the attenuation at 30 GHz would exceed the available margin.

When the SSPA is used with the 5 meter terminal the rain margin still exceeds the required 6 dB; however, the combination of SSPA with 3 meter terminal requires FEC even in clear weather. Thus, if a TWTA failed and were replaced by an SSPA only coded signals could be successfully transmitted to the 3 meter terminals.

### 2.1.7 Propagation Reliability

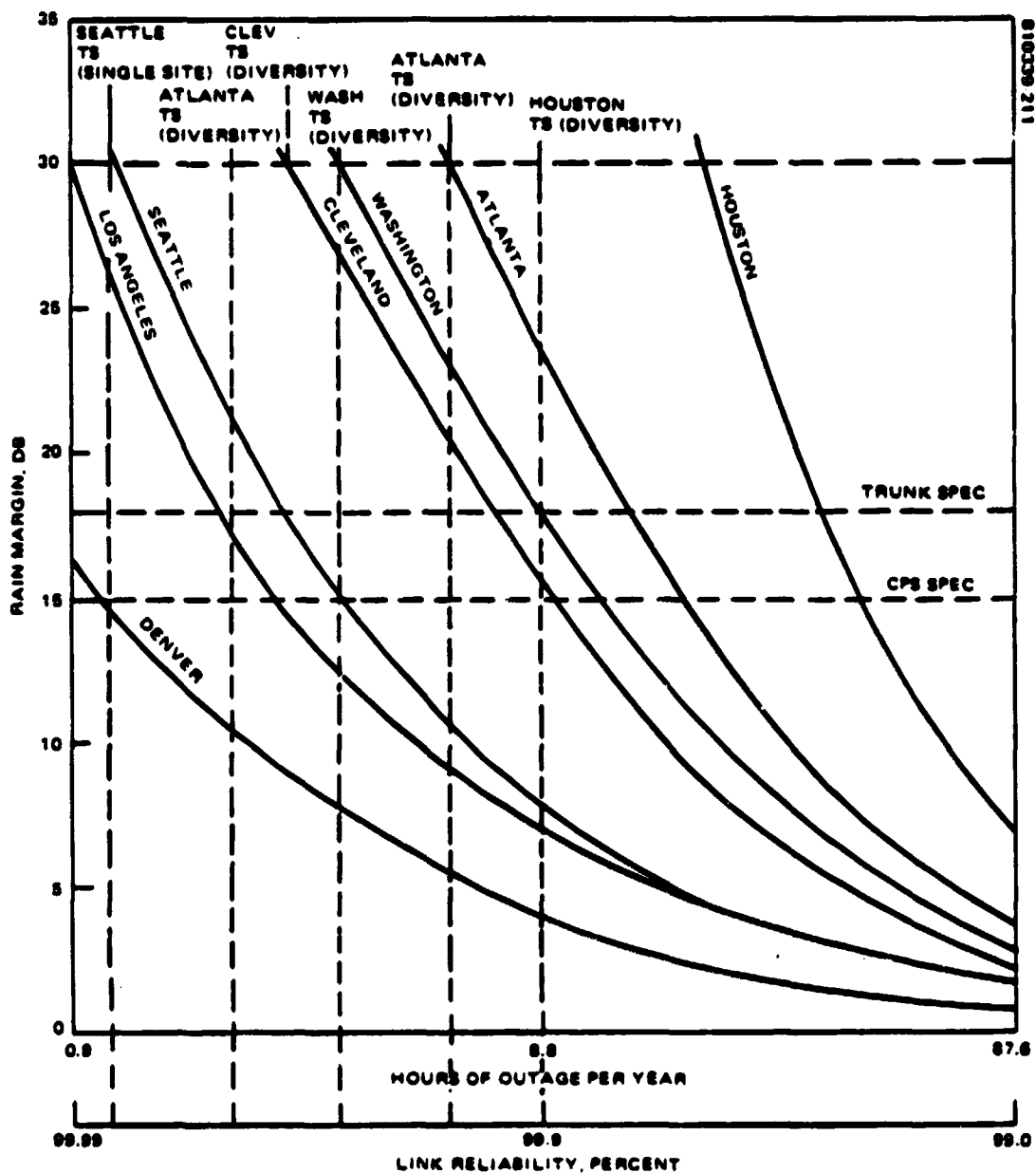
The performance of the communication system and the resulting rain margins were discussed in the previous section. An estimate of the propagation reliability associated with these margins is given in this section.

The relation between rain margin and the percentage of the time that links are out of service because of rain is not generally established. Experimental data exists for a very limited number of locations in the United States and for very limited periods (1 or 2 years). Because of the great variations in rain rate characteristics between even areas in the same rain zone and from year to year it is difficult to extrapolate this data to predict rain outage in a particular location for any year or to predict rain outage averaged over a long period of time (e.g., 10 years). Another approach to estimating rain outage is to use one of the models which has been developed for this purpose. The model divides the world into rain zones. Each zone is associated with a frequency distribution of rain rate. The model combines this data with the physics of rain attenuation and a model of rain height to determine the frequency distribution of rain outage.

The modified Global Prediction Model (Cruse and Blood, 1979) presented in the NASA Communications Division Publication "A Propagation Effects Handbook for Satellite Systems Design" pages 6-18 to 6-26 was used to develop the propagation reliability estimates presented below.

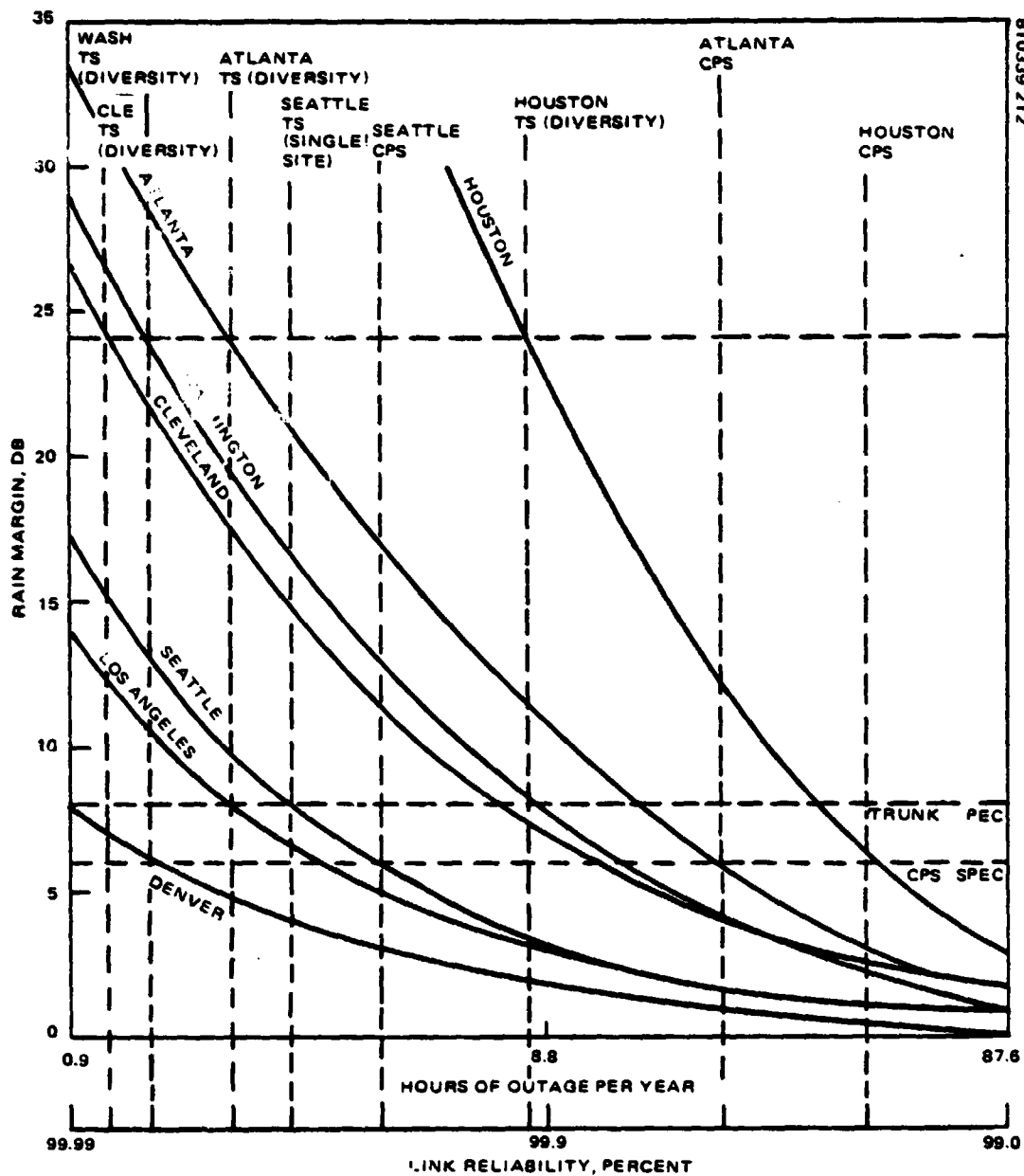
For each selected location ground station latitude, longitude and altitude, and satellite elevation angle are entered into the model. Results are shown in Figure 2-12(a) for the 20 GHz downlink and in Figure 2-12(b) for the 30 GHz uplink. Results are given in terms of the propagation reliability or hours per year of outage as a function of the rain margin provided. The specified rain margins are shown. For the 20 GHz downlink the specified rain margins are 8 dB for the trunk and 6 dB for the CPS. The lowest propagation reliability in the system is, as expected, the Houston CPS link which has a reliability of 99.5 percent. This reliability is also achieved on the 30 GHz uplink indicating a good balance of rain margins. The single site trunk reliability is only slightly better; however, site diversity is available for trunk sites. The diversity improvement was estimated using the technique of Goldhirsch (1975) and Rohrsik which is abstracted in the NASA handbook referenced above, pages 6-69 and 6-70. Figure 2-13, which is reproduced from that report, shows that for diversity reception the diversity gain depends on both site separation and the single site attenuation. The parameter in the figure is single site attenuation. Assuming a 14 km site separation it can be seen that a single site attenuation of 24 dB is associated with a diversity gain of 16 dB. Thus, when an 8 dB rain margin is provided at each of two redundant sites the resulting propagation reliability is the same as would be achieved by providing a 24 dB rain margin at a single site. The resulting reliabilities are shown for several downlinks.

The Goldhirsch data does not cover 30 GHz; however, it is possible to make a reasonable estimate of the propagation reliability achievable through diversity on the uplink. The data in Figures 2-12(a) and (b) indicate that the single site propagation reliability provided by the 18 dB uplink margin and by the 8 dB downlink margin are nearly equal. Since attenuation at 30 GHz is a little more than twice that at 20 GHz for the same rain rate this implies that the rain rates at which these attenuations occur are nearly the same. The probability of outage at a terminal with site redundancy is the



a) 30 GHZ UPLINK

FIGURE 2-12. LINK RELIABILITY



b) 20 GHZ DOWNLINK

FIGURE 2-12 (CONTINUED). LINK RELIABILITY

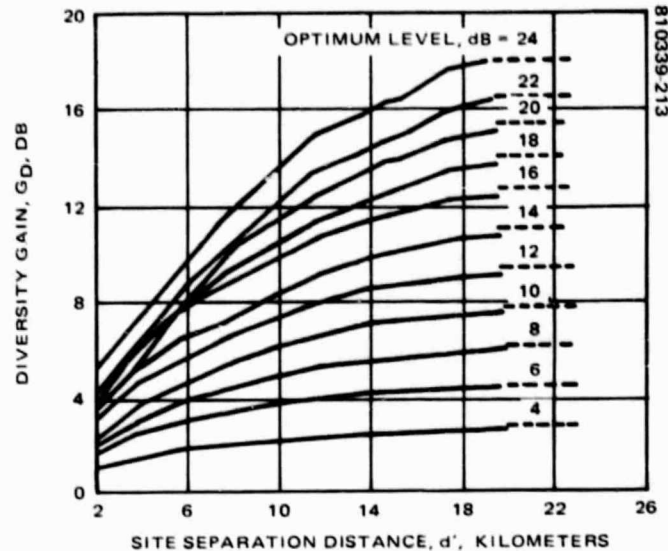


FIGURE 2-13. DIVERSITY GAIN VERSUS SEPARATION DISTANCE

probability that this common rain rate will be exceeded at both sites. This probability is independent of radio frequency. Thus, the same reliability can be expected at 30 GHz with an 18 dB margin as was calculated at 20 GHz for an 8 dB margin.

For a link to be useful in most applications it is necessary that the link be available in both directions. The probability that at least one of the two halves of the duplex link is out is given by:

$$P = 1 - (1 - P_A)(1 - P_B)$$

where

$P_A$  = probability that the terminal A to terminal B link is out

$P_B$  = probability that the terminal B to terminal A link is out

Some results of these calculations are given for trunk links in Figure 2-14 and for CPS links in Figure 2-15. The use of diversity saves about 24 hours per year on the Houston-Washington circuit and about 11 hours on the LA-Washington circuit. Almost all of the gain on the LA-Washington circuit is due to the diversity at Washington. In general, it does not appear cost effective to apply diversity to terminals in the arid West since the single site reliability of these stations is higher than the reliability with diversity in the rainy areas of the country. The reliability of the CPS circuits which terminate at an Eastern city run between 99.5 percent and 99.9 percent for the specified rain margins.



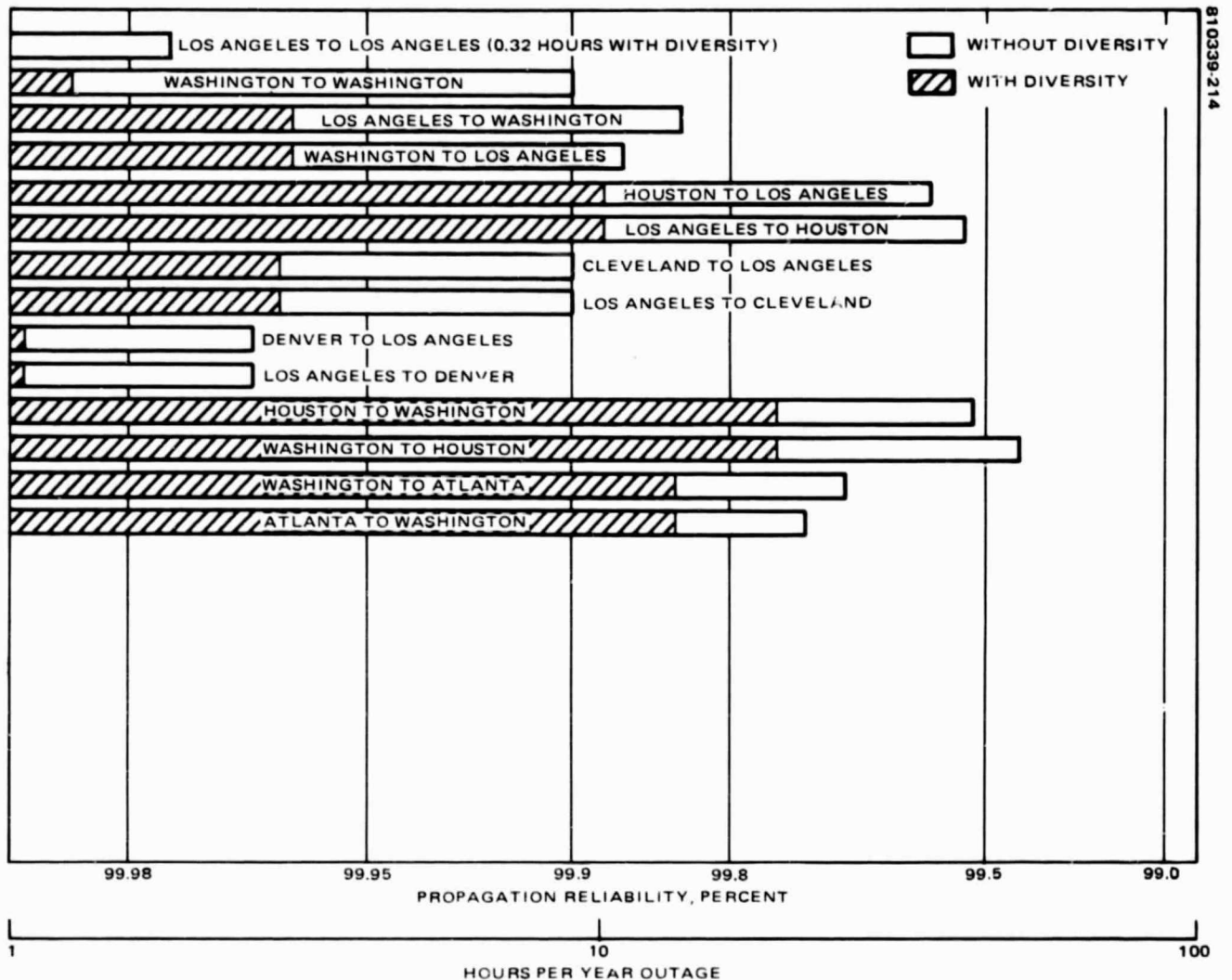


FIGURE 2 14. DIVERSITY RECEPTION AND TRANSMISSION EFFECT ON TRUNK LINE RAIN OUTAGE

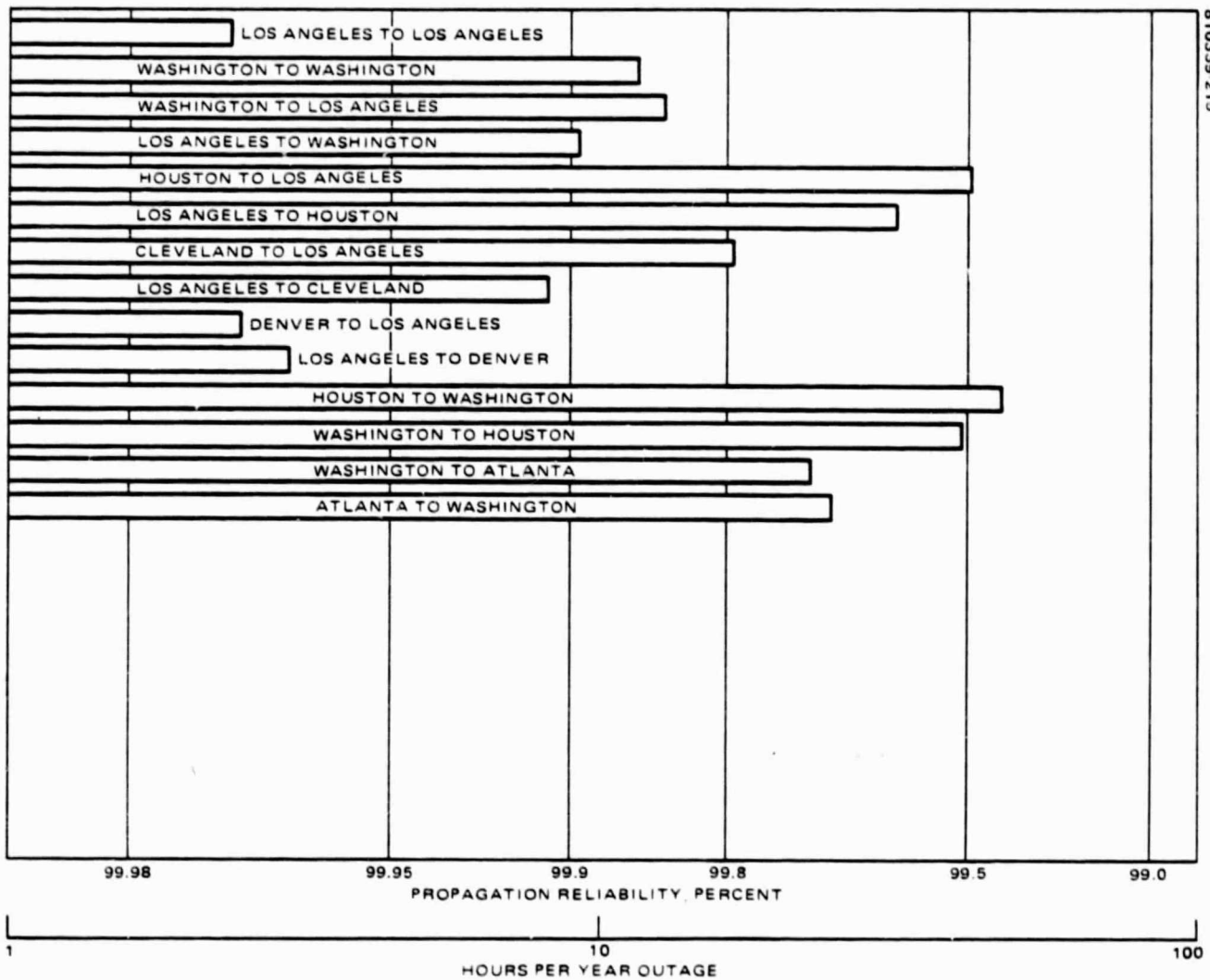


FIGURE 2-15. CPS LINKS EXPECTED RAIN OUTAGE

### 2.1.8 Telemetry Tracking and Command

The telemetry tracking and command (TT&C) system will operate on two frequency bands. During transfer orbit, the TT&C system will operate at S band in conjunction with the NASA STDN network. Once the satellite is at its orbital station, the TT&C function will operate through the 30/20 GHz payload as discussed below. If the 30/20 GHz TT&C link should become unavailable because of an anomaly or severe rain attenuation the on-station TT&C function can return to the S band mode. The S band TT&C links operate through the NASA standard near earth transponder (NASA/SNET). Since this transponder is installed on the bus, S band TT&C operation is discussed in 4.2 Spacecraft Bus Modification.

The satellite TT&C configuration is shown in Figure 2-16. When the satellite is in its normal on-station mode it receives the 30 GHz carrier containing the command and ranging information on the Cleveland beam of the multibeam antenna. As shown previously in the payload block diagram, the uplink TT&C signals are always continuously available whether the Cleveland beam is being used as a fixed beam in the trunk mode or as a scanning beam in the CPS mode. The TT&C signal is separated from the communication uplink by a frequency diplexer and downconverted to the NASA/SNET frequency.

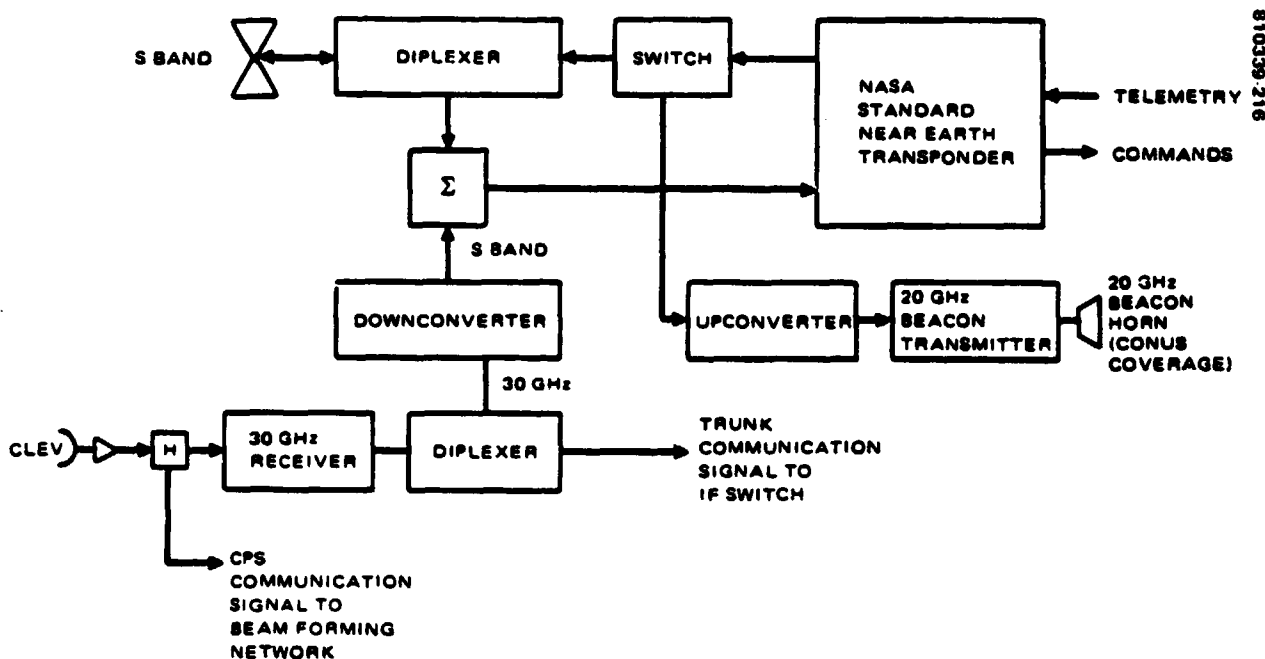


FIGURE 2-16. SATELLITE TT&C CONFIGURATION

The input signal to the NASA/SNET is identical to that received on the STDN uplink. The operation of the NASA/SNET is discussed in 4.2. The S band telemetry and ranging signal generated by the NASA/SNET can be switched between the S band antenna and the 20 GHz upconverter. The upconverted signal is transmitted over the 20 GHz beacon which also serves the experiment plan discussed in the next section. The beacon transmitter is an 0.5 watt GaAs FET amplifier. The beacon antenna is a horn with half power beamwidth of approximately 3 by 6 degrees which covers all of the contiguous United States.

The telemetry link budget is given in Table 2-8. The signal modulating the beacon is the same as the one which modulates the S band carrier. The telemetry signal is a 2 Kbps Bi oL (Manchester encoded) data stream modulated directly on the carrier. The carrier, at times, is also modulated by the command subcarrier which is allowed to leak through the NASA/SNET, and the 125 Kz square wave ranging signal. Except for the satellite antenna, the gains and losses are identical to those for the trunk downlink. The telemetry signal suffers a 3.4 dB modulation loss. The available rain margin relative to a bit error rate of  $10^{-5}$  is 25.5 dB, which, when coupled with the site diversity at the MCT, provides nearly perfect propagation reliability.

The command link budget is shown in Table 2-9. Gains and losses here are identical to those of the trunk uplink. The modulation loss shown does not account for simultaneous ranging which would increase the modulation loss by 8 dB. The resulting rain margin coupled with site diversity provides extremely high propagation reliability. It is not necessary to perform ranging if the extra rain margin is needed for command.

TABLE 2-8. 20 GHz TELEMETRY LINK BUDGET (dB)

Transmitter power (dBW)	-3 (0.5 W)
Circuit loss	0.3
Antenna gain	27
EIRP	23.7
Path loss	209.5
Atmospheric loss	1
Receive pointing loss	0.7
G/T (dBW/°K) <sup>-1</sup>	30.4
Boltzmann's Constant (dBW/°K)	-228.6
C/N <sub>0</sub>	71.5
Modulation loss	3.4
Data rate	33 (2 Kbps)
E <sub>b</sub> /N <sub>0</sub>	35.1
Required E <sub>b</sub> /N <sub>0</sub>	9.6
Rain margin	25.5

TABLE 2-9. 30 GHz COMMAND LINK BUDGET (dB)

Transmitter power, dBW	0 (1 W)
Circuit loss	1.3
Antenna gain	<u>59.7</u>
EIRP, dBW	
Transmit pointing loss	1.5
Atmospheric loss	0.7
Receive pointing loss	0.6
Antenna gain	<u>55.2</u>
Received signal power, dBW	-102.3
Modulation loss (no simultaneous ranging)	4.8
Command signal strength, dBW	-107.1
Command threshold, dBW	<u>-140.1</u>
Rain margin	33.0

#### 2.1.9 Payload Weight and Power

Table 2-10(a) summarizes the weight of the spacecraft payload. This weight is well within the capability of the LEASAT bus. Table 2-10(b) gives the prime power requirement imposed by the payload. In the trunk mode, which sizes the solar panels, the largest user is the transmitter whose 4 TWTAs consume 460 watts. When a 7 watt SSPA replaces a 40 watt TWTAs, the power requirement drops by 43 watts. In the CPS mode only two transmitters are used. This power savings offsets the requirement of the BBP.

Another power related spacecraft problem is that of dissipating heat generated on the payload platform. Table 2-10(c) summarizes this dissipation. Again, the power dissipated by the BBP in the CPS mode is offset by the reduction of TWTAs dissipation.

TABLE 2-10(a). SPACECRAFT  
PAYLOAD WEIGHT

<u>Item</u>	<u>Weight, lb</u>
Antenna	189
Microwave	127.4
Baseband processor	<u>111.2</u>
Total	427.6

**TABLE 2-10(b). SPACECRAFT PAYLOAD POWER REQUIREMENT**

<u>Item</u>	<u>Trunk Mode, W</u>	<u>CPS Mode, W</u>
Antenna	2	10
Microwave	521	268
Baseband processor	<u>41</u>	<u>225</u>
Total	<u>564</u>	<u>503</u>

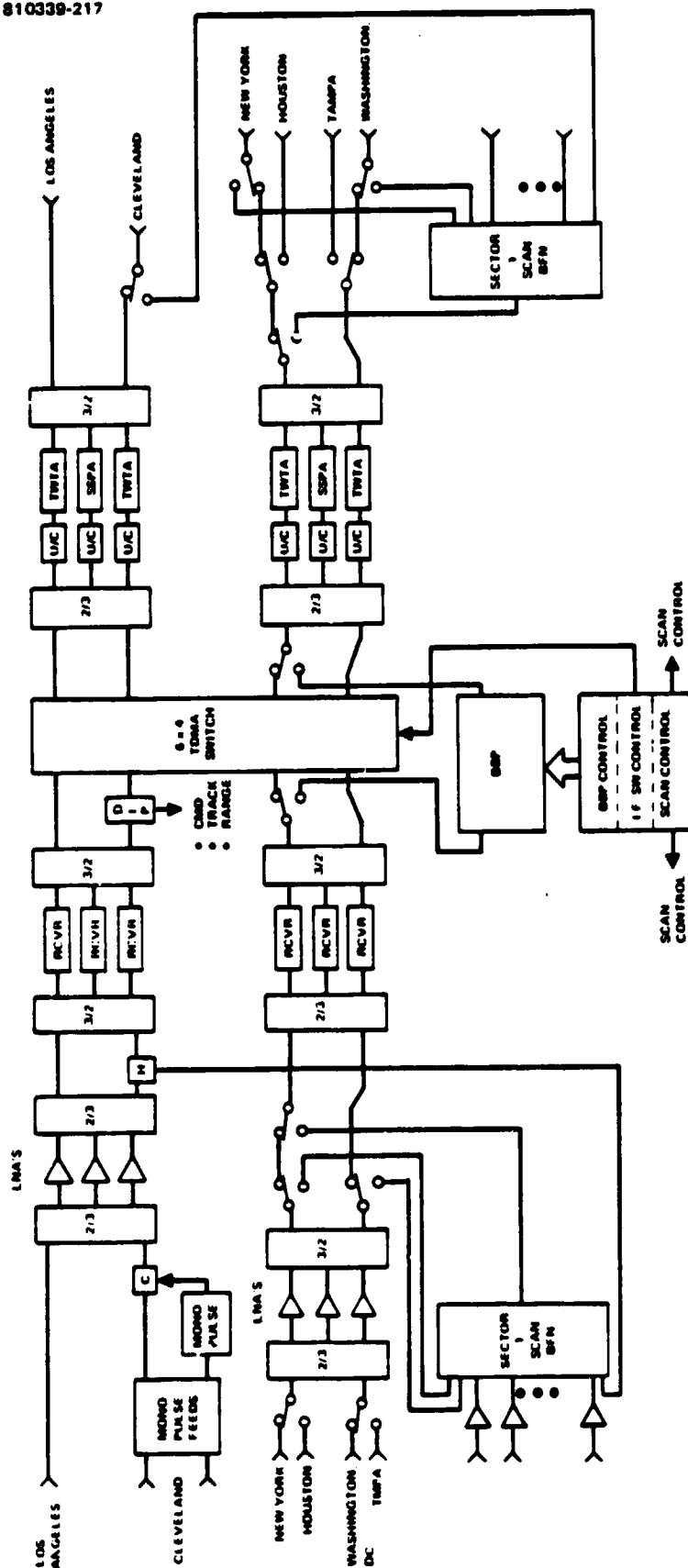
**TABLE 2-10(c). PAYLOAD POWER DISSIPATION**

<u>Item</u>	<u>Trunk</u>		<u>CPS</u>	
	<u>4 TWTAs</u>	<u>2 TWTAs/2 SSPA</u>	<u>2 TWTAs</u>	<u>1 TWTAs/1 SSPA</u>
Antenna	31	17	20	12
Equipment platform				
Microwave	377	348	196	181
BBP	<u>41</u>	<u>41</u>	<u>225</u>	<u>225</u>
Equipment platform				
Total	<u>418</u>	<u>387</u>	<u>421</u>	<u>408</u>
Payload total	<u>449</u>	<u>404</u>	<u>441</u>	<u>418</u>

#### 2.1.10 Options

Two options, specified by NASA, were examined to determine their impact on spacecraft weight, power, and cost. Option 1 is to eliminate one of the two CPS scanning beams and to reduce the throughput of the remaining beams from four 32 Mbps and one 128 Mbps uplink channels to a pair of 32 Mbps channels. The downlink burst rate is reduced from 256 Mbps to 128 Mbps. Figure 2-17 shows the resulting configuration. A contiguous coverage sector is provided in the east, including New York and Washington D.C. Isolated spots are Cleveland, Seattle, Denver, and San Francisco.

The purpose of considering Option 1 was to reduce payload weight and cost and increase the spacecraft weight margin. The cost saving is discussed in Volume 4. The weight saving (see Table 2-10(d)) in the antenna is only 16 pounds because the reflector system, antenna support structure, and telemetry are unaffected. The BBP weight reduction of 33 pounds is more significant. The BBP power requirement in the CPS mode is reduced from 225 watts to 89 watts but the solar power requirements are driven by the trunk mode (Table 2-10(e)). In any case, neither weight nor power differences impact the choice of spacecraft bus.



**FIGURE 2-17. OPTION 1 SPACECRAFT FUNCTIONAL BLOCK DIAGRAM**

TABLE 2-10(d). WEIGHT COMPARISON

Item	Baseline	Option 1	Option 2
Antenna	189.2	173	189.2
Microwave	127.4	127.4	143.4
BBP	<u>111.2</u>	<u>78.6</u>	<u>111.2</u>
Total	427.8	379	443.8

TABLE 2-10(e). POWER REQUIREMENTS COMPARISON

Item	Baseline		Option 1		Option 2	
	Trunk	CPS	Trunk	CPS	Trunk	CPS
Antenna	2	10	2	6	2	10
Microwave	521	268	521	268	524	271
BBP	<u>41</u>	<u>225</u>	<u>41</u>	<u>89</u>	<u>41</u>	<u>225</u>
Total	564	503	564	363	567	506

Option 2 adds a four beam by four beam FDMA routing experiment to the baseline communication system as shown in Figure 2-18. The nodes selected for the FDMA experiments are the same as the fixed trunk beams in the baseline. The receiver design is modified from the baseline to provide an RF (20 GHz) output in addition to the IF (6 GHz) output. By demultiplexing and multiplexing at RF rather than IF, the payload weight is minimized. Full interconnectivity is provided by the waveguide connections. Additional RF switches are required so that the outputs of FDMA multiplexer can be routed directly to power amplifier bypassing the upconverters required for the IF switch outputs.

The frequency plan for the FDMA mode is shown in Figure 2-19. The New York and Washington D. C. beams have a common polarization and require frequency isolation. The Los Angeles beam uses the same polarization as New York and Washington D. C. but is spatially isolated from these beams. The Cleveland beam is isolated by cross polarization relative to the other three beams. Total available bandwidth per beam is 400 MHz and the channel bandwidth per link is 100 MHz.

Option 2 does not significantly affect power and only increases payload weight by 16 pounds. Since payload weight margin is more than adequate it appears that this experiment would be accommodated.



810339-218

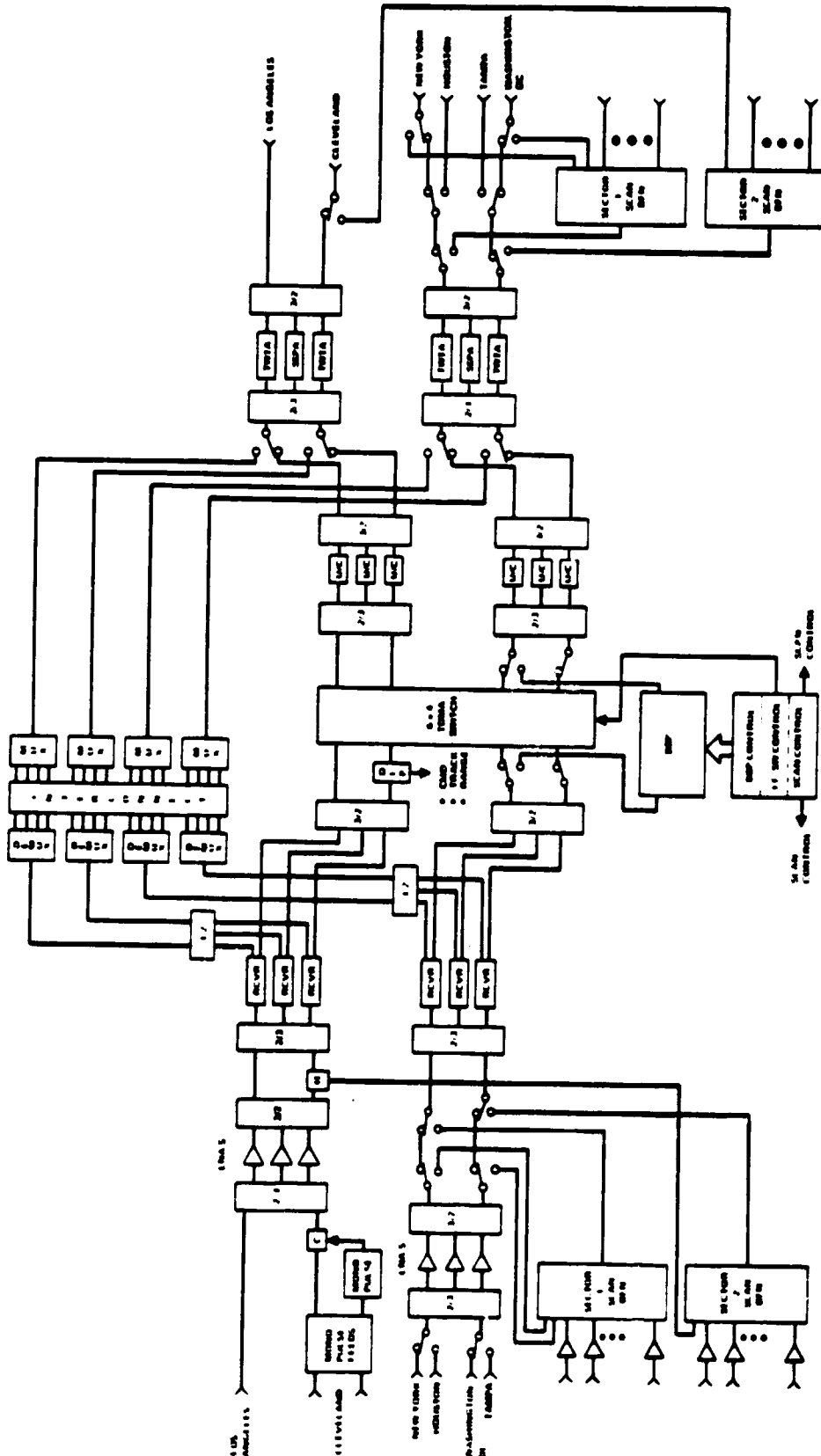


FIGURE 2-18. OPTION 2 SPACECRAFT FUNCTIONAL BLOCK DIAGRAM

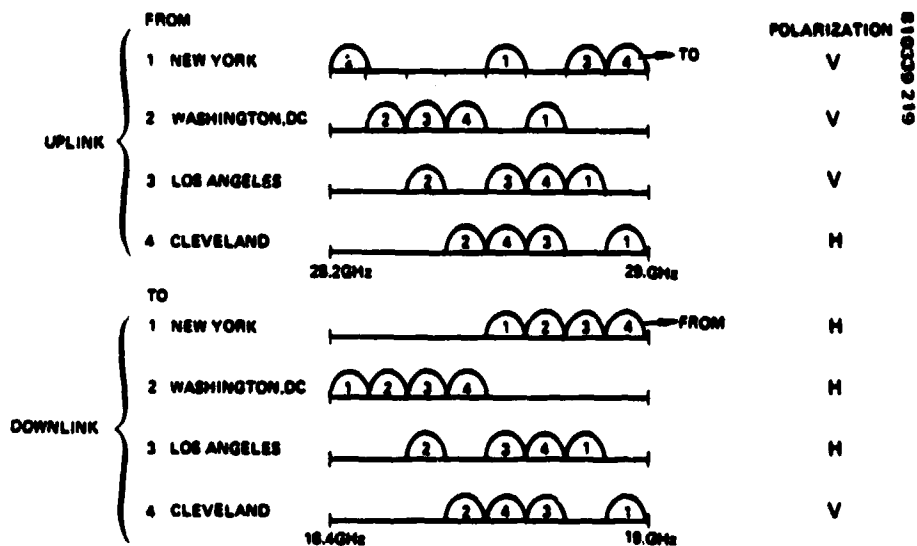


FIGURE 2-19. OPTION 2 FREQUENCY PLAN

## 2.2 COMMUNICATION SYSTEM CONTROL

The design and performance of the communication links have been summarized in Section 2.1. This section describes the functions of the system which controls the operation of these links. Several aspects of the communications system and its use must be controlled.

- 1) Channel access. In an operational system with many users whose traffic requirements vary over time and location it is necessary for efficient operation to assign time and frequency channels to users as they are needed and in a way that avoids interference between users. The problem of controlling channel access is discussed in 2.2.1.
- 2) System synchronization. In order to implement the control of channel access it is necessary to synchronize earth station transmissions with each other and with the spacecraft switching functions. The method for doing this is described in 2.2.2.
- 3) Link control. Rain margins for a 30/20 GHz system will be considerably larger than those provided at C and Ku Band. In order to maintain uplink carrier to interference ratio it is necessary to control earth station transmitter power so that the carrier power density of all signals received at the spacecraft are approximately equal. This requires that the transmitter power vary with rain attenuation. This problem is discussed in 2.2.3.
- 4) Payload control. The spacecraft payload has an IF switch matrix for trunk service, a baseband switch for customer premise service and a scanning beam antenna which uses a beam switching arrangement. Another set of switches controls the flow of coded

signals to the baseband processor decoders. Subsection 2.2.4 describes the method of controlling the format and sequence of these switching operations.

- 5) Station control. The operation of the stations is monitored and controlled (in part for manned stations) by the central control station. This task is discussed in 2.2.5.

### 2.2.1 Channel Access

In the 30/20 GHz flight experiment channel access is primarily a CPS problem. In the trunk system the spacecraft routing between uplink and downlink beams is preassigned. The user facility has the responsibility of multiplexing data from its individual sources into sets of data. Each set is composed of data for a particular downlink beam. The user facility informs the earth terminal of the composition of the data stream. The earth terminal has the responsibility of transmitting each of these sets of data at a time such that the spacecraft IF switch routes it to the proper downlink.

The routing provided by the BBP to CPS data is not preset. When an individual source initiates a call the earth terminal will forward the channel request to the master control terminal (MCT) which will assign a time slot for the data and notify the BBP when in the frame the signal will be received and where it is to be routed.

#### 2.2.1.1 Trunk Station Channel Access

Trunk system multiple access is implemented with fixed spot beam antennas and the satellite IF switch. A trunk station operating through one of the spot beams is assigned a specific time in which it will be connected to a specific destination. A short time later the IF switch will change configuration and the transmitting station will be connected to a different destination. The IF switch thus cycles through all the destination stations for which the transmitting station has been allocated time on the channel. Concurrently, each of the trunk stations in the other spot beams is cycled by the IF switch. Since the IF switch has no memory and cannot rearrange the timing of transmissions, only one uplink at a time sends data destined for a particular downlink. The trunk stations must synchronize their transmissions with the IF switch destination changeovers so that the signals are connected by the IF switch to the appropriate downlink beams.

To illustrate, consider the channel allocation for the four spot beams in the flight experiment system as presented in Figure 2.2-1. Each of the four cities shown operates on a separate spot beam antenna, thus each may transmit simultaneously; however, each is interconnected to a different destination. A loopback connection at the beginning of the frame is provided for synchronization purposes. Burst allocations for the different cities are of different lengths depending on traffic requirements.

In the flight experiment the IF switch sequence is not changed automatically to respond to changes in traffic. It can be changed manually to accommodate gross changes in traffic or to accommodate particular experiments. Thus, a terminal will normally have a predetermined uplink burst

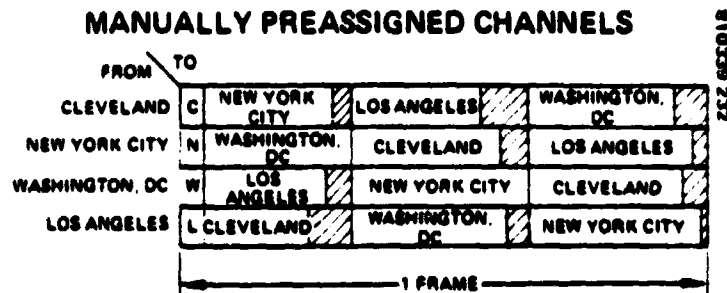


FIGURE 2.2-1. TRUNKING CHANNEL ASSIGNMENT

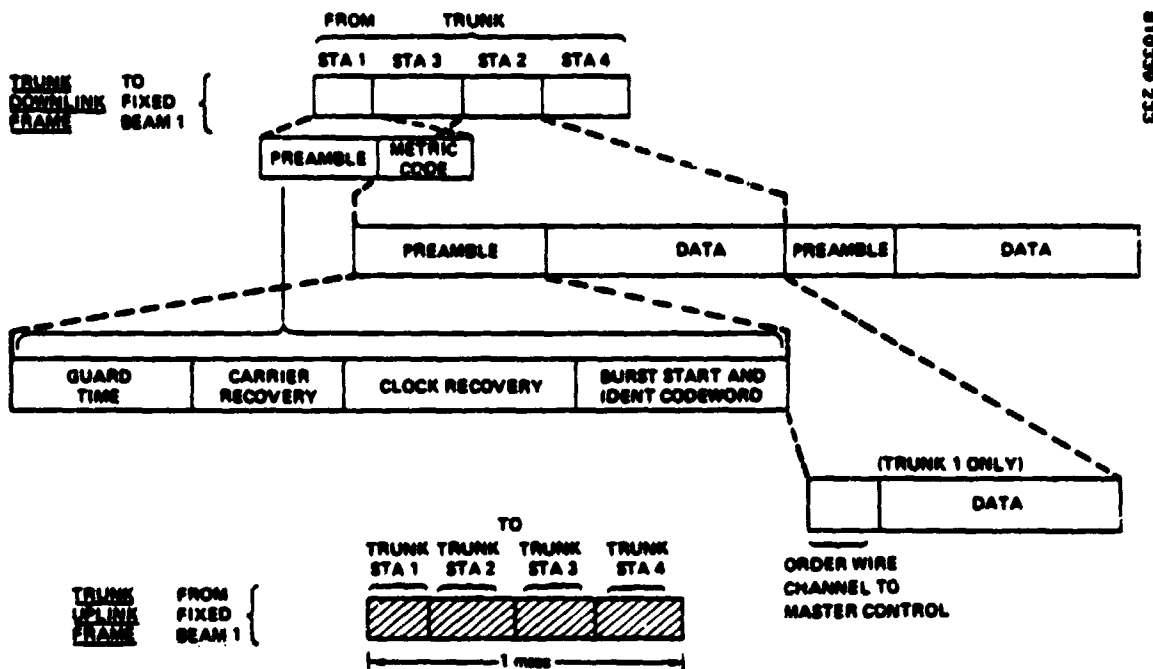


FIGURE 2.2-2. TRUNK FRAME FORMAT

period for each destination. Individual message sources are then assigned space in the appropriate burst by the user facility and no action is required of the satellite communication system.

A further expansion of the channels for the data in a single beam (1) is shown in Figure 2.2-2. The top portion of the figure shows data, with format details, flowing in the downlink of a spot beam to station 1 from each of the four stations. The bottom portion of the figure shows the uplink from station 1 to each of the four stations. A frame period of 1 millisecond has been selected as a reasonable compromise between system efficiency and high speed buffer memory size needed to store each transmittal burst at the ground station.

The burst for each station consists of a preamble and a data block. As mentioned previously, the first channel of the frame is looped back to the transmitting station and its data block contains synchronization

information (metric code). The preamble consists of guard, carrier and clock recovery, burst start, and synchronization identification code word times. The guard time is inserted to ensure that the burst lies within the allotted IF switch time in the presence of system time uncertainties (see 2.2.2). The carrier and clock recovery data enables the ground receiving station demodulator to lock on to the incoming signal. The burst start and code word are used by the station to sense data start and for frame counting. The preamble is defined as system "overhead" for efficiency calculations.

The data block of each burst varies according to the traffic to each station. The message format for the data bursts is determined by their associated user with the TDMA channels passing whatever format that is delivered at the terminal interface. Traffic to or from the master control terminal, here assumed to be in beam 1, is allocated time for the orderwire channel that is used to exchange network control data.

#### 2.2.1.2 CPS Station Channel Access

The multiple access interconnectivity problem is much more complex for a CPS system than for a trunk system. The problems are compounded by the larger number of spots which must be interconnected and by the large number of stations which must access the system. Also, many, if not most, of the stations will be small stations with light traffic loads making it necessary to form satellites to earth station links on demand. In this concept, channel capacity is allocated in real time in response to requests for service. To fully optimize the use of the system resources for CPS service, all traffic would be assigned on demand. This would involve reprogramming the scanning beam antenna controller and the baseband processor in real time. Optimum channel assignment algorithms are available for application to the CPS channel allocation problems.

For the experiment program, a combination of preassignment and a form of demand assignment will be used for the baseline system. The onboard baseband processor associated with the CPS nodes will be configured to accommodate channel allocation for individual 64 Kbps CPS to CPS circuits. The beam scanning pattern and beam dwell time for each CPS area will be preassigned on the basis of average, long term traffic demand. Within the beam dwell period each CPS station will have a number of individual circuit channels. These channels will be used on a simulated demand assignment basis. That is, various channel use routings will be selected from precomputed data and transmitted to the spacecraft as though it were computed in real time. Figure 2.2-3 illustrates this concept with N scan beam dwell areas and times, and for a particular area/time (beam 2) shows two CPS stations accessing the beam. The individual users, A and B (station 1) or C and D (station 2), access the system on a demand assignment basis. This mechanization satisfies the requirements of the experiment program and will provide data for development of effective processors, switching, and efficiency of channel use for potential operational systems while reducing the cost of the experiment program. The ability to effectively assign satellite capacity to fit demand can be evaluated by experimenters.

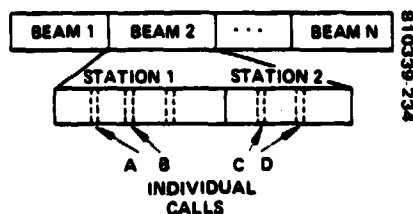


FIGURE 2.2-3. CPS CHANNEL ASSIGNMENT

The frame format details are shown on Figures 2.2-4(a) for the CPS downlink and 2.2-4(b) for the uplink. As in the trunk system a 1 millisecond frame period has been selected. An additional factor in choosing a CPS frame period is the desire to limit the size of the baseband processor storage. The downlink frame is divided into subframes for each CPS dwell area according to traffic requirements. Each subframe, as in the case of the TS system, contains a preamble and data block. Since terminals can be in the receive mode continuously, no guard time is required. The stations are always ready to receive a subframe burst. The preamble is used by all stations in a beam area to lock up their demodulators. Each station then counts from the code word time by an MCT specified value to gate in its particular station data (i. e., 21, 22, or 2i). Within each station data is found orderwire information from the MCT and data from other CPS stations.

The uplink frame format has a preamble and data burst for each station in the beam area. Since each station must transmit its bursts at the proper time with respect to other stations in the beam area, guard times are necessary to prevent transmission overlap. Data bursts contain orderwire information for the MCT and data going to other CPS stations.

A superframe is defined as M frames. Once every superframe a downlink burst consisting of a carrier acquisition signal, a clock acquisition signal, a unique word, and transmit burst timing information on the orderwire channel will be sent to each scan region containing one or more CPS stations which are not currently active in the network. To enter the network, a CPS transmits a response word on the uplink control channel.

### 2.2.2 System Synchronization

Each earth station transmission in this SS TDMA system must be synchronized so that the burst reaches the satellite coincident with the satellite window for that burst. In the trunk system the window is established by the IF switch matrix which sets up a connection to route the burst to the intended downlink. In the CPS system the window is established by the BBP which assigns a destination to each received burst according to the time it is received. If CPS terminals are synchronized with their BBP windows they will automatically avoid interference with uplinks from other terminals in the same beam. Trunk terminals do not share beams in this system; however, if there was more than one trunk station in a beam the same principle would apply.

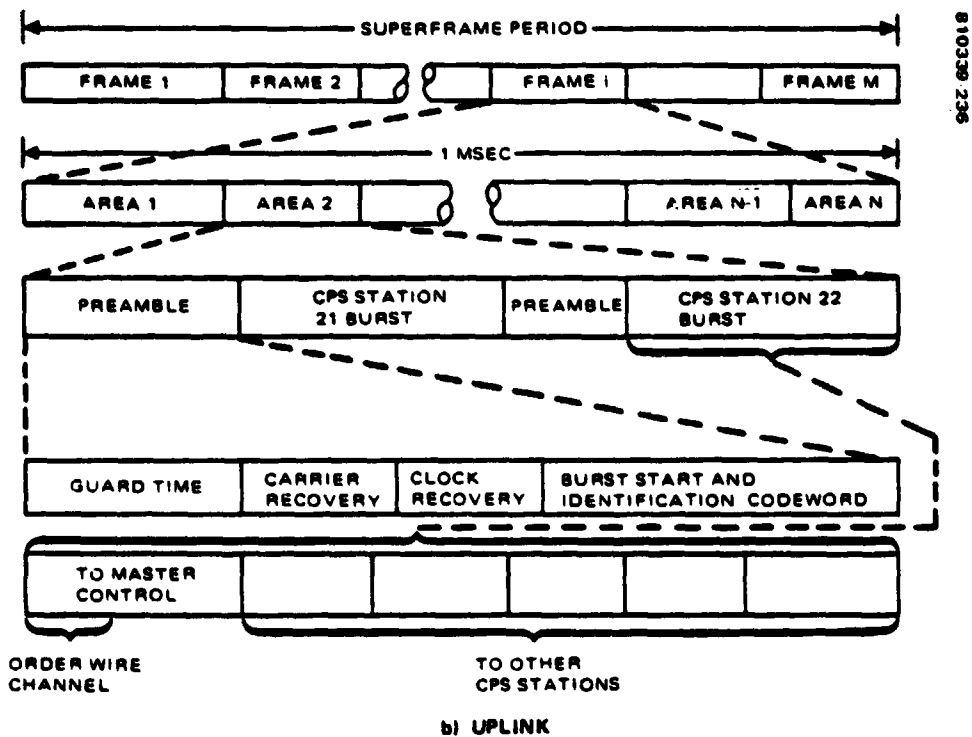
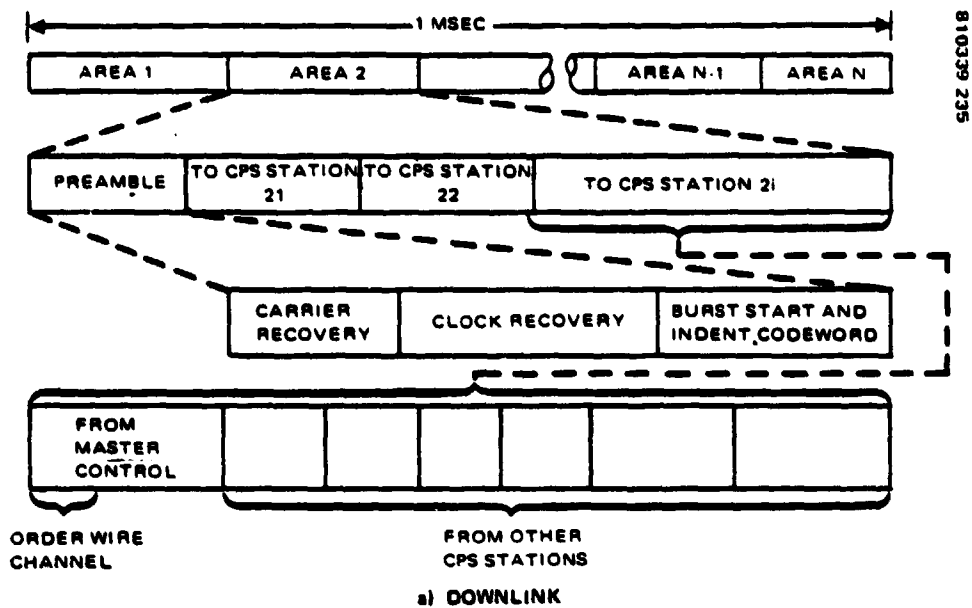


FIGURE 2.2.4. CPS FRAME FORMAT

The NASA specification requires closed loop synchronization for both trunk and CPS systems. Hughes has conceived closed loop synchronization schemes which make use of the spacecraft switching to minimize the earth terminal hardware requirements and the dependence of earth terminals on the MCT. These schemes are described in the following sections.

### 2.2.2.1 Trunk Synchronization

Trunk synchronization involves timing the uplink burst transmissions so that they arrive at the spacecraft when the IF switch is in the proper state to route the signals to the desired destination. Initial acquisition of synchronization is a two step process. It is performed by the CCS via the MCT to initiate network communications. In the first step, the CCS obtains a system timing reference; in the second step the CCS determines the burst transmission times. Figure 2.2-5 is a timing diagram that illustrates trunk station initial acquisition.

The system reference oscillator is located in the spacecraft. The first step of initial acquisition is to obtain this clock reference at the MCT. It is initiated by commanding the IF switch into a switching sequence which includes a loopback window to the MCT in each frame. The MCT then transmits a continuous wave signal to the spacecraft. The portion of the signal that goes through the loopback window is received by the MCT. The received signal has a pulse each 1 ms frame time. The clock generator in the MCT is phase locked to this received signal. This provides the synchronization reference pulse.

Once the clock reference is obtained, the burst transmission time,  $T_B$ , is determined.  $T_B$  is measured from the time the synchronization reference pulse is received and is estimated by calculating the path delay to

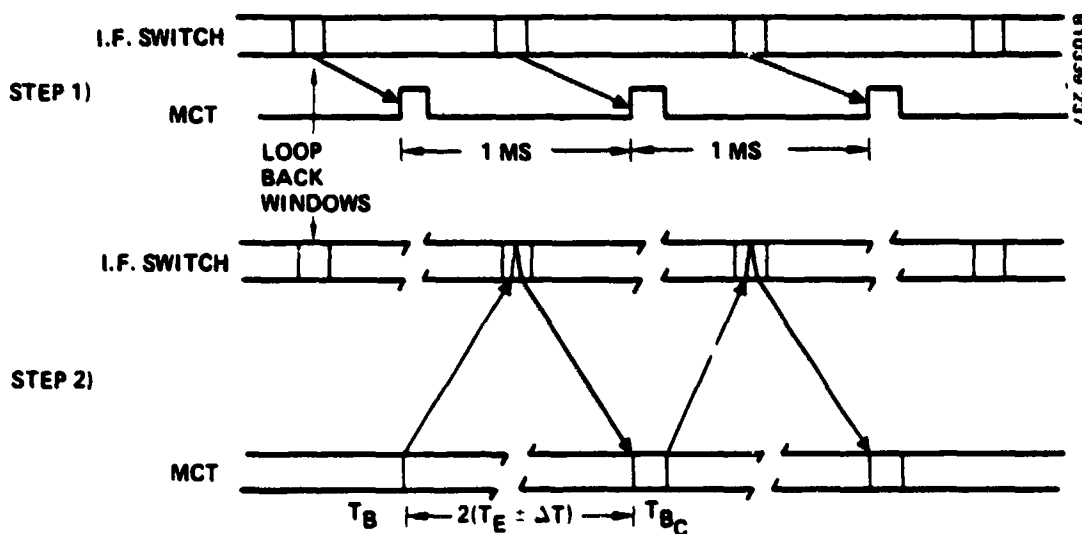


FIGURE 2.2-5. TRUNK SYNCHRONIZATION INITIAL ACQUISITION





ORIGINAL PAGE IS  
OF POOR QUALITY

is shown in Figure 2.2-7. The alternate approach, reference oscillator in the MCT, would require locking up the spacecraft oscillators and tracking the MCT reference via the uplink frame rate, clearly requiring additional hardware.

Synchronization of other trunk stations is accomplished by the same technique used by the MCT; however, the MCT helps them achieve initial synchronization. The IF switch is programmed to provide an interconnect between the MCT and the trunk station and a loopback window to the trunk station. The MCT transmits a synchronization reference burst and order-wire information to the trunk station in each frame. The trunk station phase locks its clock generator to the receipt of the sync reference burst. The CCS calculates an estimated time of burst transmission,  $T_B$ , using the spacecraft ephemeris and the trunk station location. This estimated burst transmission time is sent to the trunk station via the order wire channel. The trunk station uses the estimate to transmit a burst to the loopback window. A metric code is truncated by closure of the IF switch at the end of the loopback window. The trunk station examines the contents of the received metric word, determines the error, and corrects subsequent transmissions.

Continuous synchronization updates are needed to accommodate the slowly varying slant range between the ground terminal and the satellite and the clock instabilities. This is accomplished by continuously transmitting loopback synchronization bursts, monitoring the burst position within the assigned slot, and incrementing or decrementing the burst timer  $\pm 1$  symbol when the position differs from the prescribed value. Trunk station synchronization is illustrated in Figure 2.2-8.

Fast re-entry acquisition is used when the ground terminal has lost sync for a short time (<5 minutes). Synchronization time measurements are made from a regenerated clock that is phase locked to the spacecraft oscillator. The clock will free wheel through sync loss periods and continue to produce timing signals, see Figure 2.2-7. The longer the loss of sync period the larger the sync timing error that results from the free wheeling clock.

The use of a closed loop synchronization technique has been specified for the flight experiment system. Embedded in this technique is the use of an open loop and distributed type of system that can be readily tested during the program to study effects on communications efficiency and system costs. Table 2.2-1 summarizes pertinent descriptions and comments relative to each of the techniques.

The TS frame format guard time potentially can be reduced to its smallest value through the use of a closed loop technique. This in turn maximizes communications or frame efficiency. Tables 2.2-2 and 2.2-3 list systematic and random errors that contribute to guard time. The oscillator drift error accumulates during the 0.5 second between ground station clock updates. Figure 2.2-9 illustrates the guard time errors and gives

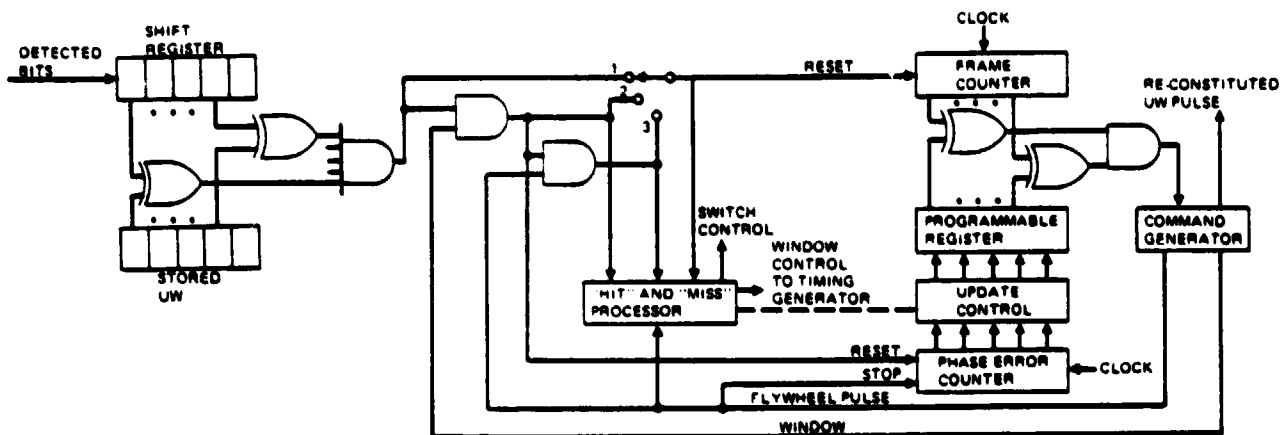


FIGURE 2.2-7. TYPICAL CIRCUIT FOR FREQUENCY AND TIMING SYNCHRONIZATION

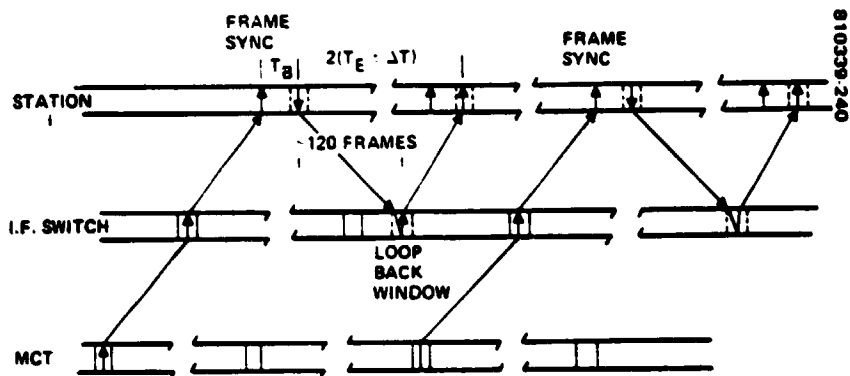
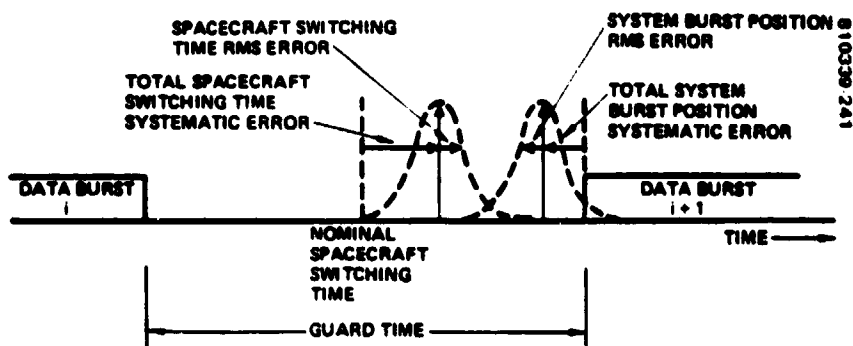


FIGURE 2.2-8. TRUNK SYNCHRONIZATION



$$\text{GUARD TIME} \geq 2 (\text{SYSTEMATIC ERROR}) + 5 (\text{RANDOM RMS ERROR})$$

$$\text{GUARD TIME} = 2 (44.2 \text{ NS}) + 5 (5.3 \text{ NS})$$

$$\text{GUARD TIME} \geq 115 \text{ NS}; +10\% \text{ CONTINGENCY} \geq 125 \text{ NS}$$

FIGURE 2.2-9. TRUNK SYSTEM GUARD TIME ESTIMATE

TABLE 2.2-1. TRUNK SYSTEM SYNCHRONIZATION METHODS

System Type	Description	Comments
Distributed synchronization	Each trunk station separately acquires its own frame timing. In this closed loop technique, the trunk station transmits a sync pulse which passes through the spacecraft switch and is routed back to the originating ground station. If the arrival time of the sync pulse is in error, it will be truncated by the window formed by the spacecraft switch closure. The truncation is a timing error signal which can be used by the trunk station for uplink start of frame correction.	<ul style="list-style-type: none"> <li>• The control channel is not used, and therefore a very small amount of spacecraft capacity is used for synchronization.</li> <li>• The control equipment is not complex for inclusion in a trunk station.</li> <li>• The synchronization does not depend upon precision trunk station location information.</li> <li>• The trunk channels may be maintained even with a short dropout of the central control station.</li> <li>• A closed loop system maintains high synchronization precision.</li> </ul>
Centralized open loop synchronization	The central control station, through path delay measurements, determines satellite position and velocity vectors. This information is called ephemeris. From the ephemeris and the exact positions of the ground stations, the slant delay and delay rate to each ground station are computed. This information is distributed from the central control station to the trunk stations on the control channel. The information defines the uplink frame start time relative to the downlink frame start time.	<ul style="list-style-type: none"> <li>• The system is a strong candidate for CPS use.</li> <li>• Most of the computing is done by a central control station centralized computing facility.</li> <li>• Precision ephemeris must be maintained at the central control station.</li> <li>• Synchronization depends upon precision position information of the trunk stations and the central control station.</li> </ul>
Centralized closed loop synchronization	The central control station transmits synchronization pulses which pass through the satellite switch to each trunk station, are detected and retransmitted on the uplink, pass through the spacecraft switch, and are transmitted on the downlink back to the central control station. The trunk station delay is adjusted by the central control station through the control channel until the returned synchronization pulse is returned without truncation through the window formed by the satellite switch closure. The sync pulse truncation forms an error signal at the central control station which may be driven to zero by timing adjustment.	<ul style="list-style-type: none"> <li>• A relatively small amount of computing is required.</li> <li>• A moderate amount of satellite overhead is required for timing correction over the control channel.</li> <li>• The synchronization does not depend upon precision trunk station position information.</li> <li>• The sync pulse truncation equipment is localized in the central control station.</li> <li>• High precision is maintained in the closed loop system.</li> </ul>

**TABLE 2.2-2. TRUNK SYSTEM ERROR CONTRIBUTIONS  
TO GUARD TIME SYSTEMATIC ERRORS**

<u>Source</u>	<u>Error, NS, Max</u>
IF switching matrix	
Switching time uncertainty	1
Settling time	1
Path length variation	0.5
IF switching matrix controller	
Switching time uncertainty	14
Rise/fall time	10
Oscillator drift (0.5 sec)	0.3
Total spacecraft switching time uncertainty	26.8
Spacecraft	
Radial velocity (5 ft/sec, max)	1.5
Ground	
Timing resolution (128 MHz clock)	7.8
Oscillator drift (0.5 sec)	0.3
Sync burst resolution (128 Mbps)	7.8
Total system burst position uncertainty	<u>17.4</u>
Total	44.2

**TABLE 2.2-3. TRUNK SYSTEM ERROR CONTRIBUTIONS  
TO GUARD TIME RANDOM ERRORS**

<u>Error Source</u>	<u>Error, NS, RMS</u>
IF switching matrix	
Switching time jitter	1
IF switching matrix controller	
Oscillator jitter	1
Logic jitter	0.5
Total spacecraft switching time uncertainty	1.5
Spacecraft	
Path length jitter due to turbulence	0.5
Ground	
Sync measurement jitter	5.0
Oscillator jitter	0.1
Logic jitter	0.5
Total system burst position uncertainty	<u>5.05</u>
Total	5.3

the computation formula. The total overhead can then be calculated, see Table 2.2-4, and from this produces the frame efficiency. The frame efficiency is determined by the number of information bits transmitted in relation to the total number of bits transmitted. Calculated in terms of times it is given by:

$$\eta = \frac{T_F N_{SF} T_{OH}}{T_F} \times 100 \text{ percent}$$

where

$T_F$  = Frame duration

$N_{SH}$  = Number of subframes

$T_{OH}$  = Overhead time per subframe

$N_{SF} = 4$

$$\eta = \frac{1 \text{ msec} - 4(0.441 \mu\text{sec})}{1 \text{ msec}} \times 100 \text{ percent} = 99.8 \text{ percent}$$

It should be noted that this high efficiency results from the small number of nodes in the system. In an operational system with 20 nodes the efficiency would be much lower. Because the traffic level varies between the links it is not possible to avoid conflicts where more than one node talks to the same node in the same subframe without leaving gaps in the frame structure. To avoid the inefficiency associated with these gaps the subframes must be further subdivided into subframes which are distributed

TABLE 2.2-4. TRUNK TDMA OVERHEAD

Overhead/Trunk Subframe		
Overhead Contributor	Time, $\mu\text{sec}$	Duration, No. Symbols
Guard time	0.125	16
Carrier recovery time	0.073	10
Clock recovery time	0.157	20
Burst start and ID code word	0.086	11
Total	0.441	57

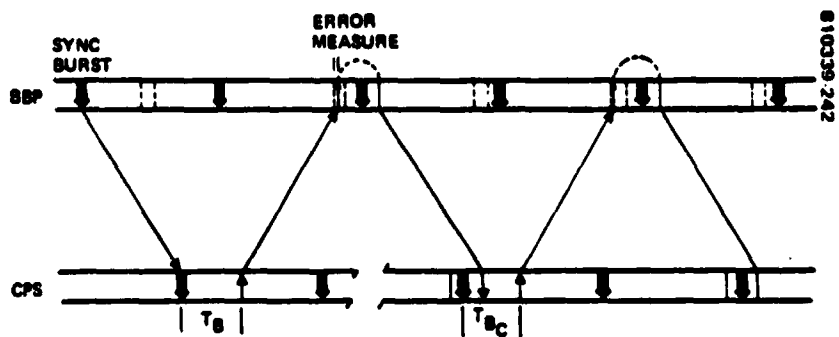


FIGURE 2.2-10. CPS SYNCHRONIZATION

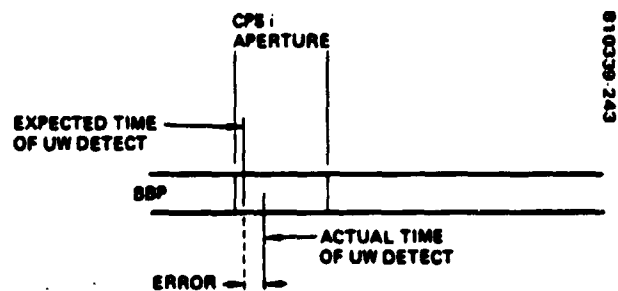


FIGURE 2.2-11. CPS SYNCHRONIZATION, ERROR MEASUREMENT

through the frame according to an optimal allocation algorithm such as the Greedy algorithm. This procedure results in as many as  $n^2 - n$  switch operations per frame. The resulting efficiency for  $n = 20$  modes is 70 percent.

The trunk system guard time estimate is composed of spacecraft switching time errors and system burst position errors as shown in Figure 2.2-9. Each of these components is composed of systematic error and random error contributors. These error sources are shown in Table 2.2-1, and 2.2-2, respectively. The total guard time is estimated to be 115 nanoseconds.

Table 2.2-3 shows the contribution of each of the preamble elements to the trunk frame overhead.

#### 2.2.2.2 CPS Synchronization

Similar to TS synchronization, there are various CPS synchronization problems that need resolution. One task is to cause transmission of the uplink burst to arrive at the spacecraft when the scanning beam antenna is servicing the area containing the CPS station. Figure 2.2-10 is a timing diagram illustrating the CPS synchronization process. The CCS programs the baseband processor to provide a synchronization reference burst to the CPS station on each frame. The CPS station receives the sync reference bursts and phase locks the local clock generator to these bursts. The CCS calculates an estimated burst transmission time,  $T_B$ , measured from the time of receipt of the sync reference burst, from the spacecraft ephemeris and station location. This time is sent to the CPS station via the orderwire. The CPS uses the estimated burst transmission time to transmit to the baseband processor.

The baseband processor receives the transmission and makes a burst timing error measurement. The CCS determines the time the baseband processor should detect the unique word contained in the CPS uplink burst. This information is stored in the baseband processor, and is compared to the actual time of unique word detection (see Figure 2.2-11). The difference between the two times is the burst timing error. The error is sent to the CPS station on the orderwire of the next downlink frame. Burst errors are averaged over 1/2 second and used to correct burst transmission time,  $T_{BC}$ . This procedure is performed continuously to maintain synchronization. As in the trunk system, once synchronization is established the reference bursts from the baseband processor are no longer needed. Burst transmissions are measured from the time of receipt of the downlink burst.

The above closed loop synchronization technique will result in a system efficiency that is equal to and most likely better than an open loop system. The CPS TDMA efficiency is determined as for the trunk station.



The beam forming network controller constrains the maximum number of subframes per frame to 64. The system efficiency at worst case is thus:

$$\eta = \frac{T_F - N_{SF} T_{OH}}{T_F} \times 100 \text{ percent}$$

$$= \frac{1 \text{ ms} - 64 (3.8125 \mu\text{sec})}{1 \text{ ms}} \times 100 \text{ percent}$$

$$= 76 \text{ percent}$$

The CPS TDMA overhead is shown in Table 2.2-5. The guard time is estimated to be 1.25  $\mu\text{sec}$  due to a 1  $\mu\text{sec}$  switch time. The downlink carrier and clock recovery times are significantly shorter than the corresponding uplink times. This is because timing estimates may be updated on a single downlink burst for all stations, while on the uplink, carrier and clock must be reacquired on each burst for each station. Greater carrier and clock recovery times must be allocated in the encoded mode because of the reduced signal to noise ratio at the demodulator input.

TABLE 2.2-5. CPS PREAMBLE SYMBOL ALLOCATION

Preamble								
Guard Time		Carrier Recovery		Clock Recovery		Burst Start and Identification Codeword		
Link	Guard Time, Symbol Periods		Carrier Recovery Time, Symbol Periods		Clock Recovery Time, Symbol Periods		Burst Start and Identification Codeword, Symbol Periods	
	Syncs	Time, $\mu\text{sec}$						
32 Mbps uplink	20	1.25 $\mu$	10 (50 for coding)	312 nsec (1.56 $\mu$ )	20 (100 for coding)	624 nsec (3.125 $\mu$ )	11 (88 for coding)	344 nsec (2.75 $\mu$ )
128 Mbps uplink	80	1.25 $\mu$	10 (50 for coding)	78 nsec (390 nsec)	20 (100 for coding)	145 nsec (780 nsec)	11 (88 for coding)	85.8 nsec (656 nsec)
256 Mbps	160	1.25 $\mu$	3 (15 for coding)	11.7 nsec (58.5)	6 (30 for coding)	23.4 nsec (117 nsec)	11 (88 for coding)	42.9 nsec (343 nsec)

### **2.2.3 Link Control**

An important characteristic of any operational system at 30/20 GHz is its approach to maintaining high propagation reliability despite the severe degradation associated with realistic rain rates. Because of the uncertainties in the statistics of this degradation and the novelty of the techniques which are appropriate to this band, the demonstration of these techniques is an important objective of the 30/20 GHz experiment program. The techniques applied in the experiment programs are uplink power control at both the trunk and CPS stations, site diversity at the trunk stations, and forward error correction coding in the CPS subsystem.

#### **2.2.3.1 Trunk Station Link Control**

Control of the trunk station link margin is illustrated in Figure 2.2-12. The trunk station measures the signal to noise ratio of the 20 GHz spacecraft beacon signal. These measurements are either relayed to the CCS for analysis or processed by the local microprocessor computer. As the S/N decreases due to rain, the station begins to increase its transmitter power (1). When the transmitter power limit is reached, the CCS or trunk station initiates diversity switching (2). In addition to the beacon signal, the CCS receives rain gauge, BER, and spacecraft received signal strength measurements which can be used for link margin control decisions. The implementation of site diversity is discussed in the Terrestrial Segment, Trunk Station Section.

#### **2.2.3.2 CPS Station Link Control**

Control of the CPS station link margin is illustrated in Figure 2.2-13. The CPS station measures the signal to noise ratio of the 20 GHz spacecraft beacon signal. These measurements are either passed to the CCS for analysis or processed in the local microprocessor computer. The uplink transmitted power is adjusted to match rain attenuation. When the transmitter power limit is reached, coding is invoked by the CCS. Bit error rate, rain gauge data and satellite received signal strength measurements are also available for link control decisions.

### **2.2.4 Payload Control**

The most flexible satellite processor design concept is to use programmable random access memory (RAM) sequence controllers for each of the multiple access switching modes: trunking IF switch, CPS store and forward processor, and scanning beam controller. A circuit assignment change is made by the central control station reloading the appropriate RAMs via the command or data channel. For instantaneous frame change-over, a ping-pong set of RAMs is used, updating a memory at a slow control

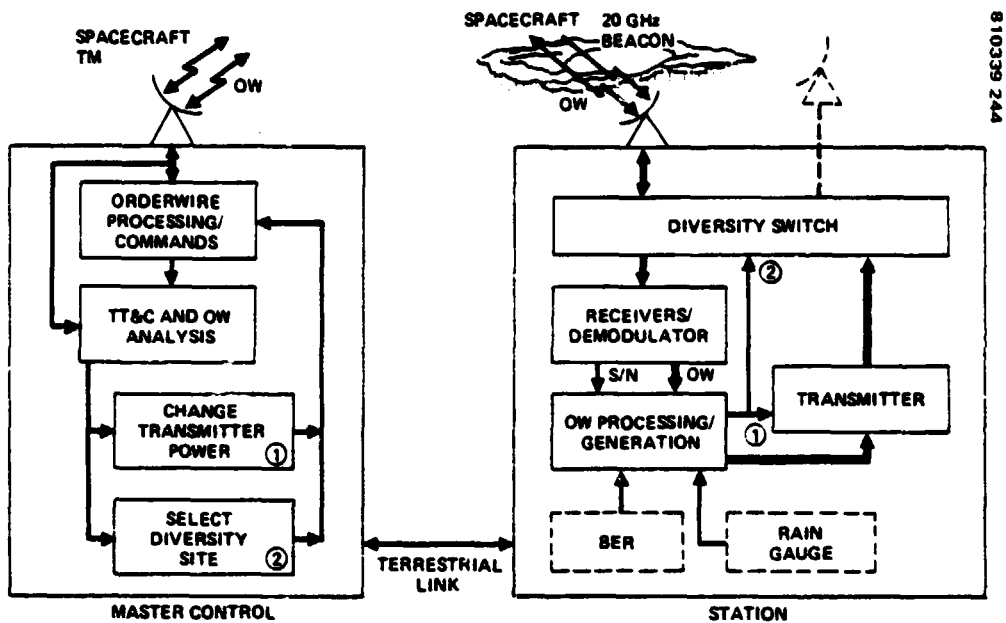


FIGURE 2.2-12. TRUNKING SITE LINK CONTROL

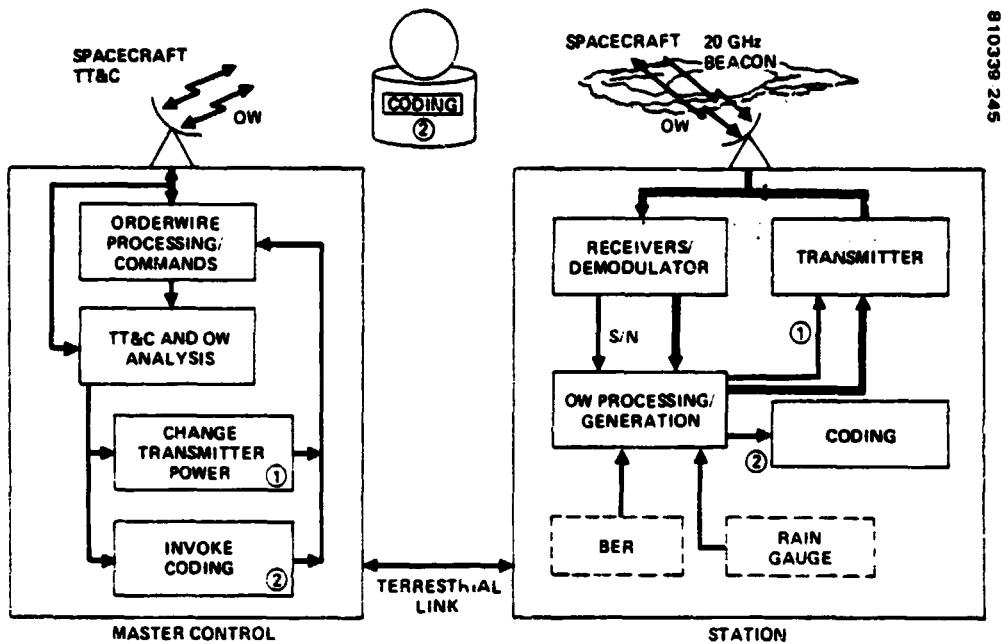


FIGURE 2.2-13. CPS LINK CONTROL

channel rate. The master station accumulates assignment changes and implements total system frame changeover at pre-established sync times. The payload control requirements were developed for this design concept implementation.

The key issues for payload control are control channel implementation, control channel data rate, frame changeover synchronization method, and master station processing requirements. The control channel is implemented through the spacecraft bus telemetry and command channel. This channel operates at a slow 1 to 8 Kbps data rate. This rate is adequate for the IF switch controller and scanning beam controller which are updated in response to changes in average traffic demand. The baseband processor store and forward control memories must be updated in response to individual 64 Kbps circuit demands and for FEC coding to provide rain margin. This may require fairly frequent updates needing rapid response so the store and forward control channel is implemented through the communications data stream. It operates at the 128 Mbps burst rate provided by the master control terminal. The frame changeover synchronization method is discussed in 2.2.2, synchronization and CCS processing requirements are discussed in 3.3.2. The payload control function is diagrammed in Figure 2.2-14.

The IF switch control matrix is manually prepared from allocation of trunk frame time slots. The duration of time for each trunk station pair interconnect is allocated from traffic model. Any excess capacity is equitably distributed among interconnects to simplify accommodation of additional traffic. The IF switch control matrix is transmitted to the IF switch controller via the spacecraft command link.

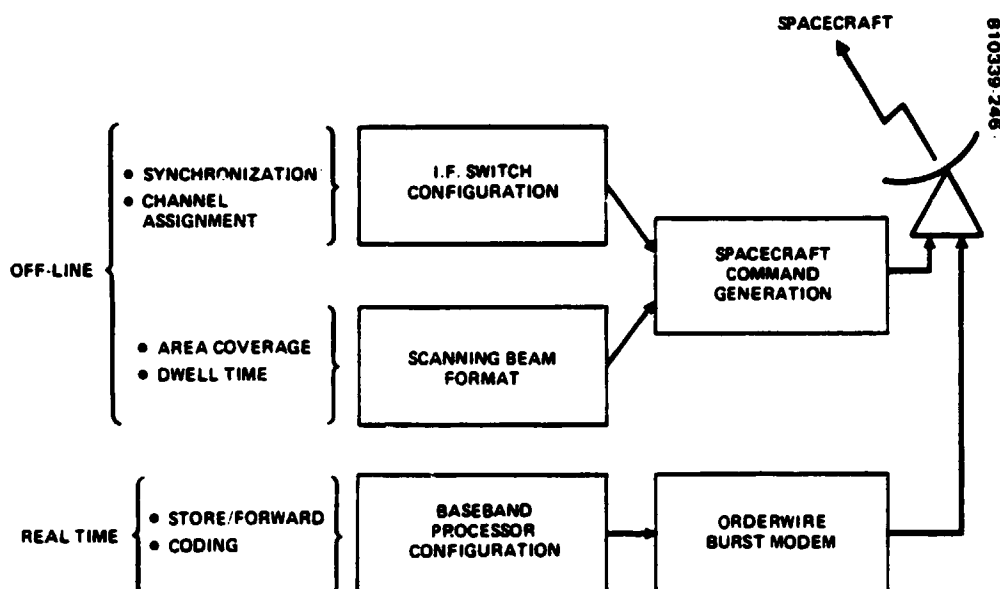


FIGURE 2.2-14. PAYLOAD CONTROL

The scanning beam antenna control matrix is manually prepared from the dwell time allocated for each area. Dwell times are allocated by using a traffic model. The scanning beam antenna control matrix is transmitted to the scanning beam antenna controller via the spacecraft command link.

Control memories in the baseband processor route message traffic through the store and forward buffers so that station interconnects can be completed. The store and forward routing may be dynamic to accommodate forward error correction coding which is used for rain margin control. The control memory contents are determined in real time by software. These control memory address vectors are transmitted to the baseband processor controller via the orderwire channel.

The procedures and software for preparing payload control memories are discussed in 3.3.2. Command data flow is given in Section 5.3.

#### 2.2.5 Station Control

All remote trunk and CPS stations are under control of the CCS. The remote stations send station status and configuration messages to the CCS via the orderwire or a terrestrial link. The CCS in turn sends experiment directives, and reconfiguration commands to the remote stations. These messages are in addition to the normal exchange of channel assignments, link control, and synchronization messages required for normal operation.

In a manual system, the remote stations would have to be manned when they were operating. The station operator would monitor the station equipment, prepare status messages for the CCS and manually enter these messages into the orderwire channel. Instructions for the remote station operator would be received via the orderwire. Voice communication on a terrestrial link could be used as a backup station control link.

The remote stations could be unmanned if the station control function were automated. An operational system would probably use unmanned stations. The remote station would be instrumented to collect status data from all operating components for relay to the CCS in much the same way telemetry is collected on a spacecraft. Software at the CCS monitors the station status messages for system performance and equipment outages. Spare equipment units are remotely switched into service and maintenance personnel are dispatched from a repair depot to repair the failed equipment. The remote station monitor equipment is shown in Figure 2.2-15. The station monitor equipment could also be used to sample experiment data and relay the data samples to the CCS for analysis. The features of the spacecraft telemetry analysis software could be used to monitor the experiment data to detect opportunities for special experiments, such as rain conditions, and to provide real time control of the experiment operation.

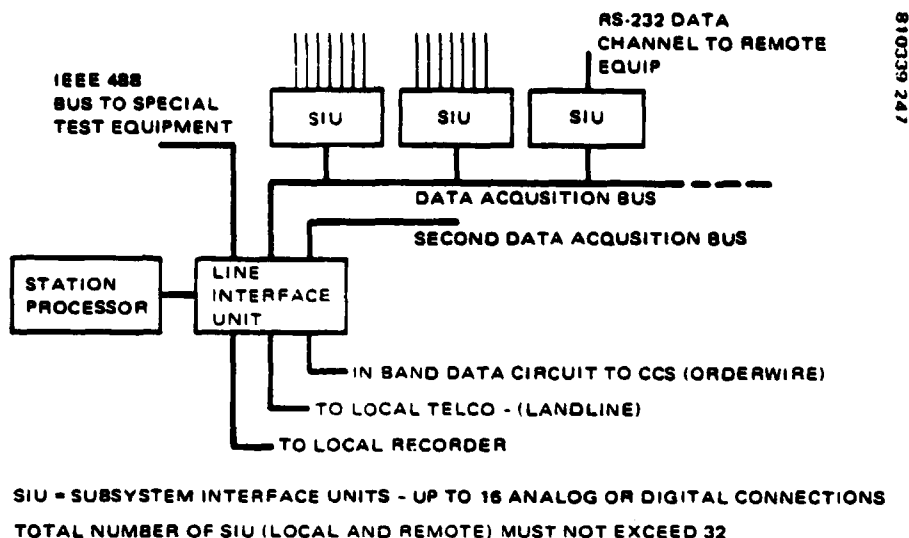


FIGURE 2.2-15. SUBSYSTEM MONITOR AND CONTROL

## 2.3 EXPERIMENTS

Experiments are the primary objective of the 30/20 GHz flight experiment system. In this section, a detailed experiment plan is described and then the experiment operations are discussed.

### 2.3.1 Experiment Plan

#### 2.3.1.1 Experiments Summary

The overall experiment plan has two primary objectives: 1) to evaluate and demonstrate the quality of communication service to be achieved in an operational system in the 30/20 GHz frequency band, and 2) to evaluate newly developed technologies whose performance is critical to successful operation in this band. Although the actual experiments to be conducted during the mission will be determined from the responses to the announcement of opportunities to experiment this plan is based on the NSAS LeRC "Experiment Planning Document," June 1980.

Experiments are broken into three categories: 1) service experiments (Table 2.3-1), 2) service and technology experiments (Table 2.3-2), and 3) technology experiments (Table 2.3-3). The ID numbers in the tables' left columns are the codes used in NASA's document; the right columns indicate the corresponding experiments in this plan with the first numbers indicating the segments and the category of experiments. The latter is described in a flow chart shown in Figure 2.3-1. This overview is not strictly chronological because periods of clear weather naturally are interspersed with periods of precipitation. After part 3 of the plan, "Initial Testing During Clear Weather," has been completed, parts 5, 6, and 8 will be implemented during periods of precipitation with intervening continued clear weather tests

TABLE 2.3-1. SERVICE EXPERIMENTS

Experiment as Designated in NASA LeRC "Experiments Planning Document," June 1980		Experiments in This Plan
ID No.	Title	
PS-1	30/20 GHz Propagation Measurements	5.2, 6.5
PS-2	Prop Constraints on Digital Systems	6.3, 8.2
PS-3	Prop Constraints on Scanning MBA Systems	8.2
PS-4	Above 40 GHz Propagation	Equipment not available in baseline system
PS-5		
PS-6		
PS-7		
PS-8	Demon of Voice, Video and Data Services	Carrier experiment
PS-9	FDMA/TDMA Operational Comparison	Carrier experiment, Option 2
PS-10	Bit Stability During Switching	6.2
PS-11	Customer Premise Station	
PS-12	Demand Assignment Control for CPS	7.2
PS-13	Narrowband FDMA System	Carrier experiment
PS-14	System Synchronization Evaluation	4.3, 6.4, 7.1, 8.2
PS-15	Heavy Route Trunking Applications	Carrier experiment; see PS-8
PS-16	Long Haul Spacecraft Compatibility Experiment	Carrier experiment
PS-17	Long Haul Space Diversity Experiment	Carrier experiment
PS-18	Service Demand Experiments - Non-Diversity	Carrier experiment
PS-19	Service Demand Experiments - Diversity	Carrier experiment
PS-20	Dynamic Traffic Model - Trunking	Carrier experiment
PS-21	Dynamic Traffic Model - CPS	Carrier experiment
PS-22	Dynamic Traffic Model - Combined	Carrier experiment
PS-23	C-Band and Ku-Band Experiments	Equipment not available in baseline system
PS-24	Synchronization Parameterization	4.3, 7.1
PS-25	Diversity Operation	6.2
PS-26	Link Power Control	6.1
PS-27	Propagation Availability	5.2, 5.3, 6.3, 6.5, 8.2
PS-28	Market Development Experiment	Carrier experiment; see PS-8
PS-29	Propagation Experiment	5.2, 5.3, 6.2, 6.3, 6.5
PS-30	User Acceptance	Carrier experiment
PS-31	30/20 GHz Propagation Phenomena	5.2, 5.3, 6.3, 6.5, 8.2
PS-32	Systems Impact of 30/20 GHz Propagation	3.1, 5.1, 6.1, 6.2
PS-33	30/20 GHz Propagation Experiment	5.2, 5.3, 6.3, 6.5, 8.2
PS-34	Test Market Experiment	Carrier experiment

TABLE 2.3-2. SERVICE AND TECHNOLOGY EXPERIMENTS

Experiment as Designated in NASA LeRC "Experiments Planning Document," June 1980		Experiments in This Plan
ID No.	Title	
PSAT-1	Air-to-Ground Communications	CPS user experiment
PSAT-2	Spread Spectrum Feasibility	Emergency service user experiment
PSAT-3	Multilevel TWT Control	Equipment not available
PSAT-4	Cophasing Parameterization	Equipment not available in baseline system
PSAT-5	Cophasing Stability Measurements	Equipment not available in baseline system
PSAT-6	Low Bit Rate FDMA/TDM	Carrier experiment; see PS-13
PSAT-7	Variable Bit Rate SS-TDMA	8.1
PSAT-8	Trunking and CPS Experiments	4.3, 6.1, 6.4, 7.1, 8.1, 8.2
PSAT-9	Space Diversity Experiment	6.2
PSAT-10	Adaptive Fade Compensation	6.1, 6.2, 8.1
PSAT-11	Adaptive Polarization	3.1, 5.1, 5.2, 6.5

of part 4 and 7. Implementation of the plan must provide sufficient flexibility to accommodate the (frequent) condition of precipitation in some geographic regions and clear weather in others. When this condition exists, the demonstration system will usually be configured toward the precipitation region.

2.3.1.2 is a summary of the experiments included in this plan and is grouped in the categories consistent with the flow chart. Of 68 experiments in the Experiment Planning Document 58 are accommodated by the Hughes design.

#### 2.3.1.2 Experiments in This Plan, Summary

##### Part 1: Prelaunch Tests

- 1.1 Determine spacecraft transponder performance, prior to launch
  - 1.2 Determine spacecraft antenna performance, prior to launch
- (These two experiments are combined in the detailed pages)



TABLE 2.3-3. TECHNOLOGY EXPERIMENTS

Experiment as Designated in NASA LeRC "Experiments Planning Document," June 1980		
ID No.	Title	Experiments in This Plan
PT-1	Transponder Performance Evaluation	3.2, 4.1
PT-2	20 GHz TWT Transmitter Experiments	3.2.3, 4.1
PT-3	Multiple Spot and Scanning Beam Antenna Evaluation	3.1, 4.2, 7.2
PT-4A	Impatt Solid-State Transmitter	Equipment not available
PT-4B	GaAs FET Solid-State Transmitter	3.2.2, 4.1
PT-5		
PT-6	Intersatellite Relay	Equipment not available in baseline system
PT-7	IF Switch Matrix Performance Test	3.2.4, 4.1
PT-8		
PT-9	Baseband Processor Evaluation	3.2.5, 4.1
PT-10		
PT-11	Channel Interference Experiment	3.2.3, 4.1, 4.4
PT-12	Baseband Processor Error Detection and Correction	8.1
PT-13	Small Earth Station Dual Feed Experiment	Carrier experiment
PT-14	Intersatellite Link	Equipment not available in baseline system
PT-15	30/20 GHz Multiple Scanning Spot Beam Antenna	Equipment not available in baseline system
PT-16	Synchronization	4.3, 7.1
PT-17	Intersatellite Link Capability	Equipment not available in baseline system
PT-18	Fade Control Techniques	6.1, 6.2, 8.1
PT-19	Ground Terminal Technology	7.2
PT-20	Antenna Pointing Accuracy	4.2, 7.2
PT-21	Interference Assessment	4.4
PT-22	Intersatellite Link	Equipment not available in baseline system
PT-23	Network Link System Monitoring	6.1, 6.2, 8.1
PT-24	Multiple Carriers Per Amplifier	3.2.3, 4.1
PT-25	Beam Acquisition and Tracking	2.1, 3.3
PT-26	Prelaunch Simulation and Tests	1.1, 1.2
PT-27	Fundamental Flight System Tests	2.1
PT-28	Technology Experiments	3.2, 4.1, 7.2

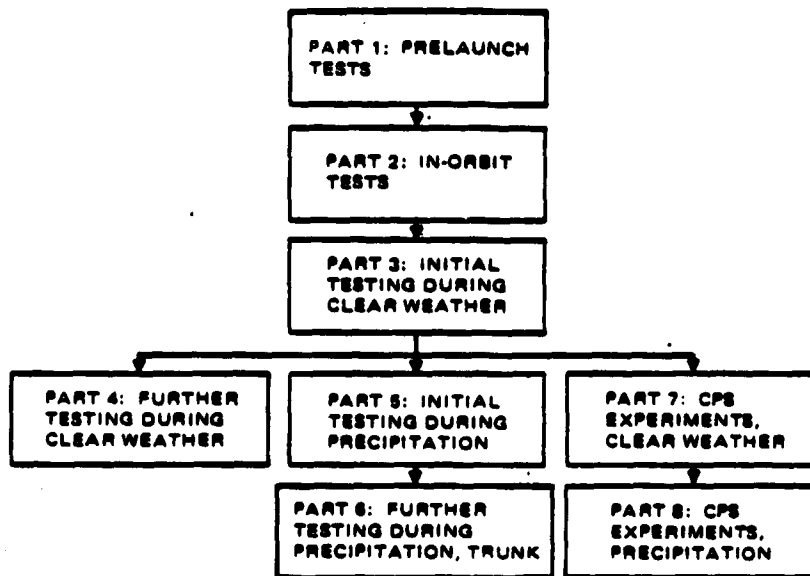


FIGURE 2-3-1. FLOW CHART SHOWING PERMISSIBLE ORDER OF PLAN SEGMENTS

**Part 2: In-orbit Tests**

- 2.1 Verify operational status of communication system

**Part 3: Initial Testing During Clear Weather**

- 3.1 Determine polarization purity of downlink beam, Cleveland and Los Angeles
  - 3.2.1 Low noise amplifier
  - 3.2.2 Solid-state high power amplifiers
  - 3.2.3 Traveling-wave tube amplifier
  - 3.2.4 IF switch
  - 3.2.5 Baseband processor
- 3.3 Evaluation of synchronization technique
- 3.4 Open loop synchronization

**Part 4: Further Testing During Clear Weather**

- 4.1 Monitor performance of critical technologies in spacecraft
- 4.2 Antenna patterns of the trunk beams
- 4.3 Limits on system timing
- 4.4 Interference assessment

**Part 5: Initial Testing During Precipitation**

- 5.1 Cross-polarization due to precipitation
- 5.2 Data collection from beacons
- 5.3 Data collection from rain gauges

## Part 6: Further Testing During Precipitation, Trunk System

- 6.1 Optimize algorithms for power control
- 6.2 Demonstrate and optimize power control and diversity
- 6.3 Precipitation effects on trunk stations
- 6.4 Recovery from precipitation - produced outages  
(Experiments 6.3 and 6.4 are combined in the detailed pages)
- 6.5 Continued data collection from beacons

## Part 7: CPS Experiments, Clear Weather

- 7.1 Limits on CPS system timing
- 7.2 In-orbit patterns of CPS antenna beam

## Part 8: CPS Experiments, Precipitation

- 8.1 FEC control algorithms
- 8.2 Effects of precipitation on CPS timing

### 2.3.1.3 Experiments Description

In this section each experiment is described in detail including objectives, variables, desired results and evaluation techniques, and methods, means, and equipment to be used in performing the experiments.

### EXPERIMENTS 1.1 AND 1.2

Components of Experiment Plan  
Part 1: Prelaunch Tests

Determine spacecraft transponder and antenna performances, prior to launch

Primary Category: Technology

Objectives: To verify satisfactory performance of the spacecraft transponder and spacecraft antenna, prior to launch; to compile a data base of selected transponder and antenna performance parameters, for later comparison with initial in-orbit tests and continuing mission experiments.

NOTE: The following "standard" transponder and antenna tests will be performed in accordance with usual HAC procedures, and details of these tests (variables, results, methods and equipment, etc) are omitted from this plan, in the interests of a concise presentation. These tests are usually computer controlled but it may be necessary to perform them by hand if suitable computer controlled test equipment is unavailable in the 20 GHz

and 30 GHz bands. Antenna pattern measurements require a range of suitable length (approximately 12,000 feet for far-field measurements).

#### Transponder

- 1) Noise figure
- 2) Gain (minimum RF input power to produce saturated output)
- 3) Linearity and gain transfer
- 4) Power output at saturation
- 5) In band frequency response and gain slope for:
  - a) Saturated output
  - b) 6 dB overdrive
  - c) 6 dB backoff
- 6) Group delay versus frequency at saturated output
- 7) Image and spurious rejection
- 8) DC power input versus RF power output (6 dB above saturation to 24 dB below saturation)

The following nonstandard transponder and antenna tests will also be performed:

#### EXPERIMENT 1.1: Transponder Tests

Transponder Tests	Variables	Results and Evaluation	Methods, Means, and Equipment
Reconfiguration rate and switching time (IF switch)	Use command system to vary reconfiguration rate up to and beyond maximum specified rate (approximately 500,000 reconfigurations per second)	Monitor all output ports and verify proper reconfiguration. Measure delay and jitter as function of rate. Measure dc power required. Monitor possible EMI from switching pulses.	Requires timing generators, oscilloscopes, etc, with resolution of the order of 1 ns (hp 8082A, hp 1722B are representative)

### Antenna "Standard" Tests

- 1) Patterns in azimuth and elevation, each trunk beam
- 2) Polarization purity (co-polarized/cross-polarized ratio), each trunk beam
- 3) Gain at boresight, relative to isotropic, trunk beams
- 4) Direction of boresight relative to monopulse tracker
- 5) Input impedance, each trunk beam
- 6) Polarization purity, beacons

### EXPERIMENT 1.2: Antenna Tests

Antenna Tests	Variables	Results and Evaluation	Methods, Means, and Equipment
Antenna patterns, scanning beam; polarization purity, scanning beam	Energize each feedhorn in turn	Take (far field) antenna patterns in azimuth and elevation; measure polarization purity, each beam position. Satisfactory performance requires that beam width and polarization purity meet or exceed specification over entire sector.	Requires circuitry to position beam on command
Beam position precision, scanning beam (pointing loss reduction)	Vary beam position control to achieve one beam, two contiguous beams, and three contiguous beams; repeat at four extreme scan positions and at midscan.	Take detailed pattern in vicinity at beam crossover; pointing loss should not exceed 0.4 dB any direction.	Same as above
Power handling capacity	Use maximum power, all four trunk beams	<ol style="list-style-type: none"> <li>1) Far field strength should be proportional to RF power (no nonlinearities)</li> <li>2) No spurious signals produced in receiver pass band</li> <li>3) Any structural heating (polarizer, FSS) is within specifications.</li> </ol>	Requires complete spacecraft (antenna and transponder)

**ORIGINAL PAGE IS  
OF POOR QUALITY**

**EXPERIMENT 2.1**

**Component of Experiment Plan**  
**Part 2: In-orbit Tests**

**Verify operational status of communication system, trunks, beacons, or CPS system**

**Primary Category:** Technology

**Objectives:** To verify satisfactory performance of the spacecraft communication systems following launch and orbit-insertion maneuvers; to verify proper operation of ground stations with spacecraft

**NOTE:** The following "standard" tests will be performed; results may be partially qualitative rather than quantitative, since purpose of this experiment is limited to verification of normal operation under unstressed conditions. Later experiments will measure performance limits of communication system.

- 1) Minimum transmitter (ground) RF power to saturate spacecraft downlink output power amplifier
  - a) Each trunk beam
  - b) CPS system
- 2) Bit error rate at 256 Mbps, each trunk station to/from the master control terminal (MCT)
- 3) Received signal strength at various geographic locations from spacecraft beacons
- 4) TDMA connectivity, trunk stations to trunk station and CPS station to CPS station

**EXPERIMENT 3.1**

**A Component of Experiment Plan**  
**Part 3: Initial Testing During**  
**Clear Weather**

**Determine polarization purity of downlink beam**

**Primary Category:** Service

**Objectives:** To determine the cross-polarized component of trunk beams, as a necessary calibration procedure prior to measuring the depolarizing effects of precipitation (Experiment 5.1), to verify antenna performance in orbit, by comparing results with prelaunch measurements (Experiment 1.2)

Variables:	None (polarization on downlink fixed by spacecraft antenna)
Results and Evaluation:	Results are cross-polarization ratios at sites. Should check within $\pm 1$ dB to prelaunch measurements
Method, Means, and Equipment:	Requires equipment to receive either of two orthogonal polarizations at each of four trunk antennas. Baseline system includes full receiving capability at the main site (dual polarized feeds and dual receivers) and limited receiving capability at diversity site (dual feeds, single receiver, occasional use switch to connect receiver to desired feed). Receivers are calibrated so receiver output proportional to polarized energy received.

#### EXPERIMENT 3.2.1

A Component of Experiment Plan Part 3: Initial Testing During Clear Weather	Performance of low noise amplifier in spacecraft
---	---

Primary Category:	Technology
Objective:	To verify satisfactory performance of spacecraft low noise amplifiers (at 30 GHz), and monitor this performance over time; to evaluate the suitability of the LNR for use in operational spacecraft with a 30 GHz uplink
Variables:	Vary uplink power. See text below and attached viewgraph.
Results and Evaluation:	Receiver noise figure is determined at MCT from knowledge of normal signal level/bit (telemetered to MCT) and of uplink power reduction ("A"). Satisfactory performance requires that noise figure be within specification (less than approximately 5 dB) during mission lifetime.
Methods, Means, and Equipment:	See text below and Figure 2.3-2. Requires signal strength monitor on each receiver channel, with output telemetered to MCT (signal strength monitor is also required by spacecraft digital electronics). Requires means to vary and monitor ground station transmitter power.

#### LNR at 30 GHz; Indirect Measurement of Noise Figure

The noise performance of the "front end" of the 30 GHz spacecraft receiver will be monitored from the ground, independently of the overall performance of the trunk uplink-downlink system.

- **CONDITION 1 (NORMAL):**  
MEASURE SIGNAL LEVEL/BIT @  
30 GHz ON SPACECRAFT; CALL  
THIS  $EB_1$

- **TRANSITION:**  
REDUCE UPLINK POWER UNTIL  
LINK BER =  $10^{-1}$ ; POWER  
REDUCTION ( $A$ , dB) KNOWN AT  
GROUND STATION

- **CONDITION 2:**  
 $BER = 10^{-1}; \frac{EB_2}{NOR} = -1dB$   
THEREFORE:  $NOR = \text{RECEIVER NOISE} = (EB_2 + 1)dBM$   
 $= (EB_1 - A + 1)dBM$

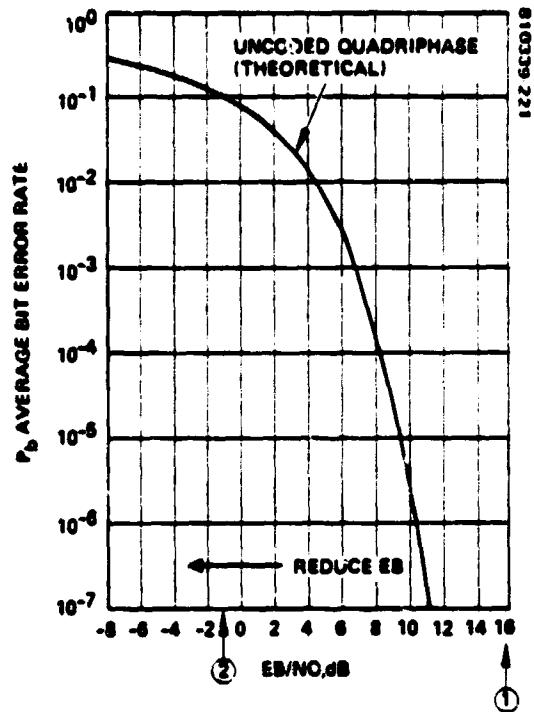


FIGURE 2.3-2. LNR AT 30 GHz INDIRECT MEASUREMENT OF NOISE FIGURE

Bit error rate (BER) is a sensitive indicator of system noise. The concept of this experiment is to operate the system with reduced uplink power, so that the noise contributed by the uplink receiver is the dominating factor in producing an artificially high BER. With knowledge of BER under normal conditions, the uplink power reduction, the resulting BER, and the demodulator characteristic, the experimenter may determine the uplink receiver noise.

### EXPERIMENT 3.2.2

A Component of Experiment Plan  
Part 3: Initial Testing During  
Clear Weather

Performance of solid state high power  
amplifiers in spacecraft

Primary Category: Technology

Objective: To verify satisfactory performance of spacecraft solid state high-power amplifiers, and monitor this performance over time; to evaluate the suitability of the SS-HPA designs for use in operational spacecraft with a 20 GHz downlink

**NOTE:** The tests to be performed on the solid state high-power amplifiers are essentially the same as those to be performed on the traveling wave tube amplifiers (although the expected performance specifications may be different). Details of variables, results, equipment, etc, are the same as on Experiment 3.2.3.



### EXPERIMENT 3.2.3

A Component of Experiment Plan  
Part 3: Initial Testing During  
Clear Weather

Performance of traveling wave tube  
amplifiers in spacecraft

Primary Category: Technology

Objectives: To determine the performance of the spacecraft TWTAs and monitor this performance over time; to evaluate the suitability of the TWT A design for use in operational spacecraft with a 20 GHz downlink.

### EXPERIMENT 3.2.3

Tests	Variables	Results and Evaluation	Methods, Means, and Equipment
Power output, gain, gain compression, efficiency, overdrive	Using one CW trunk carrier per amplifier, vary drive power by varying uplink power	Output power, gain, gain compression, and efficiency should meet or exceed specification; amplifier should recover from input overdrive without degraded performance	Input power monitored at input to each amplifier; output power monitored at output redundancy switch (requires three monitors on each spacecraft); monitor dc bus current to each amplifier; telemeter to MCT
Intermod products	Using two CW trunk carriers per amplifier, vary uplink power on both carriers simultaneously. Carrier frequencies must be known accurately	Monitor downlink signal for third-order intermod products (at known frequency); satisfactory performance requires that these products be below specification	Since the two carriers must originate at different ground stations (to avoid intermod products in the ground TWT A), this experiment requires joint control of the ground stations.

### EXPERIMENT 3.2.4

A Component of Experiment Plan  
Part 3: Initial Testing During  
Clear Weather

Performance of IF switch in  
spacecraft

Primary Category: Technology

Objectives: To determine the performance of the spacecraft IF switch, and monitor this performance over time; to evaluate the suitability of the IF switch design for use in operational spacecraft

### EXPERIMENT 3.2.4

Test	Variables	Results and Evaluation	Methods, Means, and Equipment
Reconfiguration rate and switching time	Using order-wire command, vary reconfiguration rate to a maximum greater than 500,000 reconfigurations per second	Under direction of the MCS, monitor received signals at two or more trunk ground stations operating in SS TDMA mode. Compare timing of switching commands with timing of switchovers as received at ground stations. Measure delay and jitter as function of reconfiguration rate.	Requires precise timing at MCT, digital recording, and analysis of results. Record timing pulses and received signal at each participating trunk station during experiment, transmit to MCT for analysis in "off line" mode.

### EXPERIMENT 3.2.5

A Component of Experiment Plan  
Part 3: Initial Testing During  
Clear Weather

Performance of baseband processor in  
spacecraft

Primary Category: Technology

Objectives: To verify satisfactory performance of the spacecraft baseband processor and monitor this performance over time; to evaluate the suitability of the BBP for use in operational spacecraft

### EXPERIMENT 3.2.5

Tests	Variables	Results and Evaluation	Methods, Means, and Equipment
Demodulators/modulators	Use CPS ground stations to send uplink signal at variable power levels.	Monitor downlink signal for BER; determine BER as function of $E_b/N_0$	Requires 256 Mbps BER test equipment
Connectivity, channel crosstalk	Under command of MCT, gradually increase system load on TDMA system through BBP, simulating many CPS users.	Monitor downlink signals (at MCT) for proper routing; examine typical channels for crosstalk at high data rates.	Requires suitable software at MCT to determine proper routings; requires precise timing references.
FEC performance	Under ground command, use FEC on CPS downlink to improve "rain margin" (this initial test is done in clear weather). Under ground command, with FEC used on uplink, properly decode uplink signal on spacecraft and route to noncoded downlink.	Monitor downlink signals for proper response to ground commands (should be done at MCT).	Requires suitable software at MCT

### EXPERIMENT 3.3

A Component of Experiment Plan      Evaluation of synchronization technique  
Part 3: Initial Testing During  
Clear Weather

Primary Category:      Service

Objective:      To evaluate the efficiency of baseline synchronization technique

Variables:      Guard times

Results and Evaluation:      Determine minimum guard times required to allow reliable acquisition and avoid interference

Methods, Means, and Equipment:      Requires MCT to modify channel assignment information to terminals. Manual operation is adequate.

### EXPERIMENT 3.4

A Component of Experiment Plan      Evaluation of open loop synchronization  
Part 3: Initial Testing During  
Clear Weather

Primary Category:      Service

Objective:      To evaluate the efficiency of open loop synchronization techniques and compare them to baseline closed loop synchronization method

Variables:      Orbit determination configurations (trilateralization, range rate and angle, range and range rate); vary guard times

Results and Evaluation:      Compare relative size of guard times required to allow reliable acquisition and avoid interference

Methods, Means, and Equipment:      Requires ranging transponders at two additional terminals for trilateralization. Requires terminal microprocessors to convert timing instructions from MCT.

### EXPERIMENT 4.1

A Component of Experiment Plan      Monitor performance of critical technologies in spacecraft  
Part 4: Further Testing During  
Clear Weather

Primary Category: Technology

NOTE: This experiment is a continuation of Experiment 3.2; the sub-experiments listed in that experiment will be repeated at approximately 30 day intervals, with provision for more frequent testing if evidence of premature performance degradation occurs on any of the critical technological components.

#### EXPERIMENT 4.2

A Component of Experiment Plan      Antenna patterns of the trunk beams  
Part 4: Further Testing During  
Clear Weather

Primary Category: Technology

Objectives: To verify proper operation of trunk beam antenna subsystem and to monitor this performance over time

Variables: Antenna attitude is varied by ground commands so each trunk beam is "swept through" direction toward its trunk ground station (spacecraft-ground station comprise pattern range, with spacecraft mechanisms serving as antenna positioner). Repeat at 6 month intervals to detect any performance degradation with time.

Results and Evaluation: Compare patterns with ground based measurements (Experiment 1.2) antenna

Methods, Means, and Equipment: Requires accurate and precise control of antenna main reflector and antenna azimuth (as normally provided)

#### EXPERIMENT 4.3

A Component of Experiment Plan      Limits on system timing  
Part 4: Further Testing in  
Clear Weather

Primary Category: Service

Objectives: To determine the limits on system timing and synchronization due to orbit uncertainties, digital control circuitry, switch performance, and base-band processor; extends results of Experiments 3.2.4, 3.2.5, and 3.3.

<b>Variables:</b>	Under command of the MCT, increase system load (number of stations transmitting) and data rate at each station until synchronization failure occurs and/or BER becomes excessive. Repeat for various system configurations.
<b>Results and Evaluation:</b>	Note conditions at onset of timing failures and compare with rated system capacities. Measure time to restore system synchronization after loss of sync, as function of system load and of data traffic.
<b>Methods, Means, and Equipment:</b>	Same as Experiment 3.3, with additional software at MCT necessary

#### EXPERIMENT 4.4

A Component of Experiment Plan	Interference assessment
Part 4: Further Testing in Clear Weather	

<b>Primary Category:</b>	Technology
<b>Objectives:</b>	To measure susceptibility of trunk system to interference from geographically adjacent trunk stations
<b>Variables:</b>	Under command of the MCT, increase uplink power from trunk station A (using power normally available for rain margin) to decrease carrier/interference ratio at spacecraft antenna for trunk B.
<b>Results and Evaluation:</b>	Monitor BER for trunk B as function of C/I ratio. Suggested stations: 1) New York and Boston alternate as trunks A and B (includes polarization isolation); 2) Washington, D.C. and Boston (no polarization isolation, increased geographic separation)
<b>Methods, Means, and Equipment:</b>	No special equipment needed. Uses "rain margin" power in clear weather conditions to create artificially high level of interference.

#### EXPERIMENT 5.1

A Component of Experiment Plan	Cross-polarization due to precipitation
Part 5: Initial Testing During Precipitation	

<b>Primary Category:</b>	Service
<b>Objective:</b>	To determine cross-polarization due to precipitation on the Cleveland trunk beam (Experiment 3.1 must precede this experiment).
<b>Variables:</b>	Precipitation rate varies naturally
<b>Results and Evaluation:</b>	Compile data on cross-polarization versus precipitation conditions; use results of path rain gauge instrumentation (Experiments 5.3 and 6.4) to construct improved models of depolarization effects of precipitation
<b>Method, Means, and Equipment:</b>	Requires equipment to receive either of two orthogonal polarization; same equipment used in Experiment 3.1

#### EXPERIMENT 5.2

A Component of Experiment Plan  
Part 5: Initial Testing During  
Precipitation

Begin data collection from stations  
acquiring beacon signals

<b>Primary Category:</b>	Service
<b>Objective:</b>	Use spacecraft beacon and low cost ground equipment to establish numerous monitoring stations throughout CONUS; develop a comprehensive data base on propagation.
<b>Variables:</b>	Primary variable is precipitation; location of ground sites is secondary variable, but dependence on "volunteer" ground stations limits control of this variable
<b>Results and Evaluation:</b>	Record attenuation, depolarization, and phase dispersion to maximum extents economically feasible at each location. Record local precipitation as function of time. Analyze locally if possible, and send results to Cleveland for development of CONUS propagation models.
<b>Method, Means, and Equipment:</b>	Desirable to have six calibrated receivers at each location (see BSTJ, May to June 1978, p. 1241; omit off-axis beams), but single receiver site usable.

### EXPERIMENT 5.3

A Component of Experiment Plan  
Part 5: Initial Testing During  
Precipitation

Data collection from rain gauges along  
line of sight paths

Primary Category: Service

Objective: Improved path models for precipitation effects  
along earth-to-satellite paths

Variables: Precipitation rate, varies naturally

Results and  
Evaluation: Results will consist of precipitation information  
along line of sight paths, averaged over relatively  
short time (a few minutes, maximum), with time  
code for correlation with propagation events as  
monitored by communication system. Should pro-  
vide improvement over existing precipitation data  
along propagation paths, particularly for low  
elevation angles.

Methods, Means,  
and Equipment: Requires five or six rain gauges, spaced approxi-  
mately 4 km apart, along line of sight at each  
instrumented trunk station. Requires telemetry  
system (dedicated phone line) to transmit informa-  
tion to trunk station, with provision for off-line  
transmission to MCT.

### EXPERIMENT 6.1

A Component of Experiment Plan  
Part 6: Further Testing During  
Precipitation, Trunk  
System

Optimize algorithms for power control

Primary Category: Service

Objective: To compile data relating the major parameters of  
a power control algorithm (clear weather margin,  
amount of hysteresis) to the resulting rates and  
duration of power level switching, and to the resul-  
tant BER; to formulate algorithms that provide  
satisfactory BER with minimum switching

Variables: Precipitation; power control algorithms

Results and  
Evaluation:

Minimal desired results are optimum power control algorithms for the particular sites employed; desirable result is a general procedure for formulating an optimum power control algorithm, given ground station and spacecraft locations and precipitation data along line of sight.

Methods, Means,  
and Equipment:

Requires power control capability as provided in system, and appropriate software at MCT. May require data compiled from path modeling instrumentation (Experiments 5.3 and 6.4).

## EXPERIMENT 6.2

A Component of Experiment Plan  
Part 6: Further Testing During  
Precipitation, Trunk  
System

Demonstrate and optimize power  
control and diversity

Primary Category:

Service

Objectives:

To compile data relating the major parameters of a diversity switching algorithm (level of fade producing site switchover, amount of hysteresis) to the resulting rates and duration of site switching and the effect, if any, on data integrity; to evaluate and demonstrate techniques to maximize data integrity during switchover; to evaluate algorithms that utilize both power control and site diversity to minimize outages while providing satisfactory BER; to monitor performance of power control subsystem and diversity switchover subsystem during the mission lifetime

Variables:

Precipitation; power and diversity control algorithms

Results and  
Evaluation:

(This experiment is an extension of Experiment 6.1 for sites that employ both power control and diversity). Minimal desired results are optimum algorithms for joint use of power control and site diversity at Cleveland, desirable results are general procedures for: 1) choosing diversity sites, 2) formulating optimum algorithms for joint control/diversity given ground station and spacecraft locations and precipitation data along line of sight paths.

Methods, Means,  
and Equipment:

Diversity stations as provided in system; otherwise, same as Experiment 6.1



## EXPERIMENTS 6.3 and 6.4

A Component of Experiment Plan  
Part 6: Further Testing During  
Precipitation, Trunk  
System

Precipitation effects on trunk station,  
including outages. See Figure 2.3-3.

Primary Category: Service

Objectives: To determine effects of precipitation on service provided through trunk station, at maximum data rates, with optimum power control and diversity strategies; to determine duration of outages during mission; to evaluate and demonstrate ability of system to reacquire trunk station after passage of precipitation event causing outage.

Variables: Precipitation; power control and diversity algorithm (from Experiment 6.2); data rate to trunk station experiencing precipitation

Results and Evaluation: Results will consist of compilation of information on downlink signal (signal level, timing jitter, resultant BER) to be correlated with data on precipitation along line of sight path from Experiment 5.3, to be used to predict reliability of service in operational system.

Methods, Means, and Equipment: Same as Experiments 5.3 and 6.2

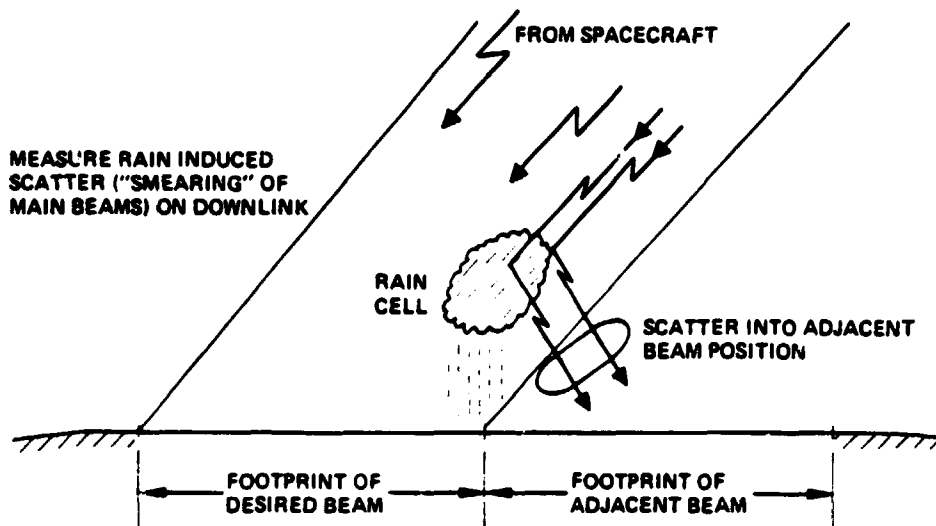


FIGURE 2.3-3. 30/20 PRECIPITATION EFFECTS

## EXPERIMENT 6.5

A Component of Experiment Plan  
Part 6: Further Testing During  
Precipitation, Trunk  
System

Continue data collection from stations  
acquiring beacon signals

Primary Category: Service

Continuation of Experiment 5.2; see that  
experiment for objectives; variables; results and  
evaluation; and methods, means, and equipment.

## EXPERIMENT 7.1

A Component of Experiment Plan  
Part 7: CPS Experiments, Clear  
Weather

Limits on CPS system timing

Primary Category: Service

Objectives: To extend the results of Experiment 4.3, to  
determine limits on system timing due to reposi-  
tioning time of scanning beam; to determine time  
necessary to acquire a CPS ground station from  
ground station "cold start," and from MCT "cold  
start"

Variables: Under command of MCT, increase CPS system load  
(number of stations, data rates) until synchroniza-  
tion failure occurs and/or BER becomes excessive.  
Simulate outage of CPS station, simulate outage at  
MCT. Vary scan rate of CPS beam.

Results and  
Evaluation: Note conditions at onset of timing failures and  
compare with rated system capacities. Measure  
time to restore synchronization after CPS or MCT  
outage. Measure effect of increasing scan rate on  
timing uncertainties, CPS system.

Methods, Means,  
and Equipment: Requires CPS station with equipment to determine  
BER at 256 Mbps burst rate, and with precise  
timing capability

## EXPERIMENT 7.2

A Component of Experiment Plan      In-orbit patterns of CPS antenna beam  
Part 7: CPS Experiments, Clear  
Weather

Primary Category:      Technology

Objective:      To determine in-orbit antenna patterns of scanning beam

Variables:      (This experiment is similar to Experiment 4.2.)  
Antenna attitude is varied by ground command so that CPS beam (in fixed position relative to the spacecraft) is "swept through" direction toward New York trunk station (spacecraft - NY trunk station comprise pattern range, with spacecraft serving as antenna positioner; NY station is used because it is copolarized with CPS system.) Repeat with CPS beam repositioned (relative to spacecraft) at its scanning extremes. Repeat at 6 month intervals.

Results and Evaluation:      Compare patterns with ground-based measurements (Experiment 1.2)

Methods, Means, and Equipment:      Same as Experiment 4.2

## EXPERIMENT 8.1

A Component of Experiment Plan      Demonstrate and evaluate FEC control algorithms  
Part 8: CPS Experiments,  
Precipitation

Primary Category:      Technology

Objectives:      To demonstrate and optimize algorithms for uplink and downlink forward-error-correction; to demonstrate and evaluate techniques for insuring data integrity when switching to and from coded mode; to evaluate cost effectiveness of FEC at CPS ground station

Variables:      Precipitation; FEC control algorithms

Results and Evaluation:      Record data rate and BER as function of precipitation and of attenuation level at which FEC is used; optimize algorithm by finding maximum fade that

can be tolerated with specified BER and no coding; repeat for various precipitation conditions and geographic locations.

Methods, Means,  
and Equipment:

Transportable CPS ground station with rain gauge instrumentation, and equipment to determine BER at 256 Mbps burst rate

## EXPERIMENT 8.2

A Component of Experiment Plan  
Part 8: CPS Experiments,  
Precipitation

Effects of precipitation on CPS timing

Primary Category:

Service

Objective:

To determine effects of precipitation on CPS timing and synchronization

Variables:

Precipitation; traffic on CPS system

Results and  
Evaluation:

Measure time to acquire CPS station, from "cold start", as function of precipitation attenuation (and possibly dispersion), and of CPS system load

Methods, Means,  
and Equipment:

Same as Experiment 8.1

### 3. COMMUNICATION PAYLOAD

The design for the communication subsystem components is presented in this section. Although NASA is funding technology development studies, which will result in proof of concept models for most of these components, the design presented in this report is a Hughes design. This approach is taken for two reasons. First, the technology studies were still in an early stage at the time the design was made; and second, Hughes considers that it will be more competent to reach correct make or buy decisions and to effectively procure components if it has been through the preliminary design process. At this time no decisions have been made regarding the source of any of the communication components. Make or buy decisions will be made early in the system definition phase (Phase B).

#### 3.1 SATELLITE ANTENNA

##### 3.1.1 Requirements

The functional requirements on the antenna are illustrated in Figure 3.1-1. For trunk service (TS) the antenna is to provide six fixed beams as shown by the solid and dashed circles. Both receive (27.5 to 30 GHz) and transmit (17.7 to 20.2 GHz) operation are required. For customer premise service (CPS) the antenna is to provide two scanning beams, each of which covers a contiguous area in the eastern United States. In addition to the contiguous areas, the scanning beams are to address three spots in the western United States, as shown in the shaded circles. As in the TS, both uplink and downlink coverage are required.

In addition to the above requirements which are imposed by the mission requirements there are a number of technology requirements. The technology used in the experiment system is required to be extrapolatable to that required by an operational system of the 1990's. An operational system hypothesized by NASA is illustrated in Figure 3.1-2. This system would have six independent scanning beams for CPS. These beams would each reuse the frequency spectrum. There would also be perhaps twenty or more fixed beams for TS with considerable frequency reuse between these beams. This operational system would allow participation by low cost CPS earth stations.

Based on these operational system requirements, NASA has specified several characteristics of the flight experiment antenna. The diameter of the transmit antenna is specified at 23M. It is to have a peak gain at a point

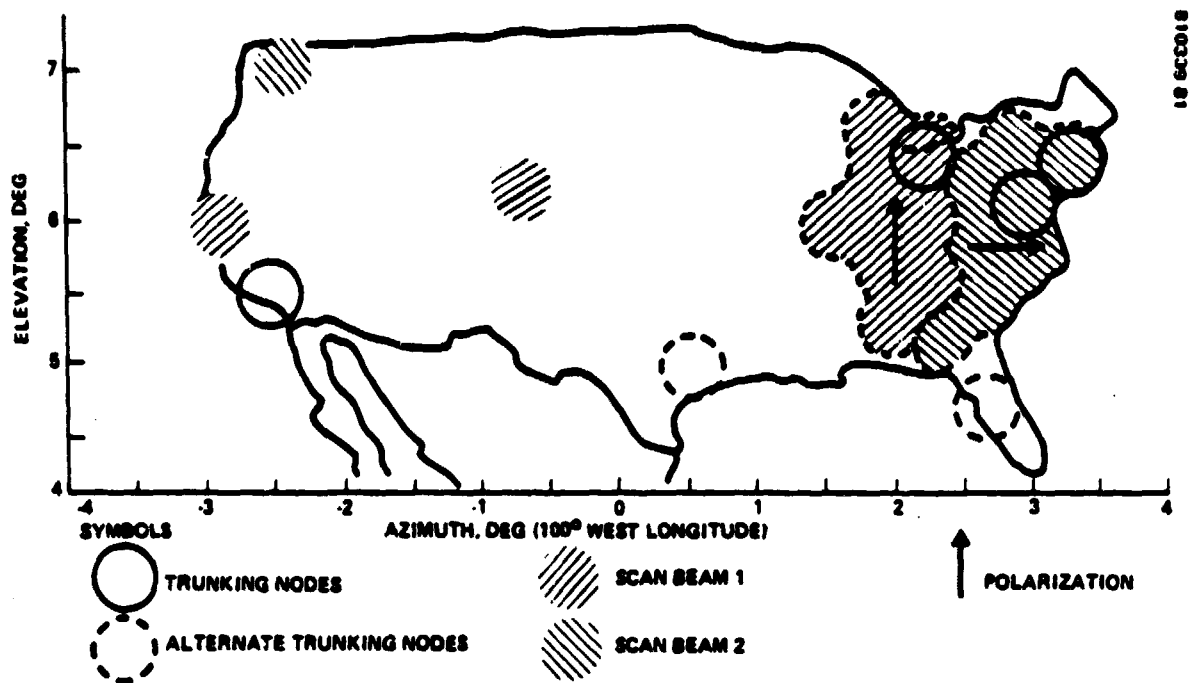


FIGURE 3.1-1. ANTENNA COVERAGE REQUIREMENTS

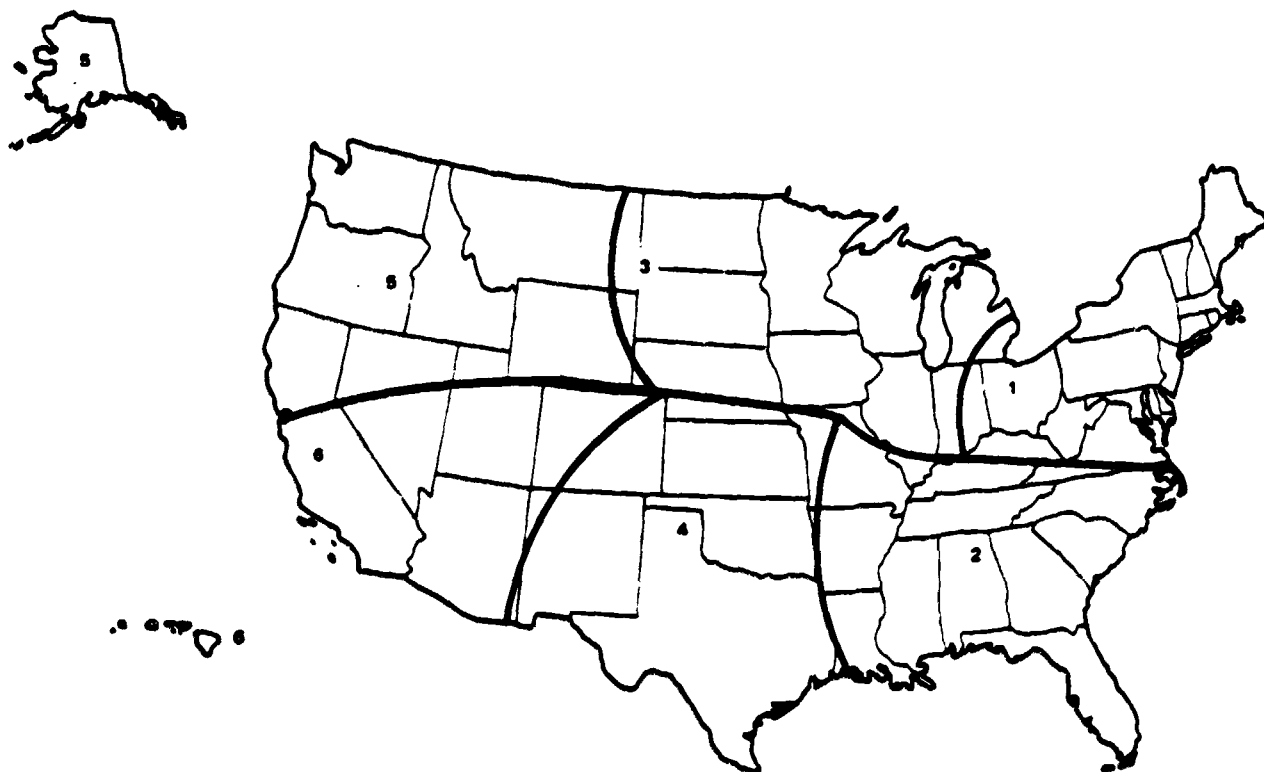


FIGURE 3.1-2. CPS ANTENNA COVERAGE MODEL

about 3° from antenna boresight of ≥51 dB. The receive antenna was specified to have a half power beamwidth equal to that of the transmit antenna because the receive scanning beams must cover the same area as the transmit scanning beams; however, with NASA's concurrence Hughes has elected to use the same 3M diameter for the receive function as well as the transmit. Although this choice results in a combination of more CPS feeds and reduced CPS coverage it also results in some advantages. The receive gain is higher; consequently lower power earth station transmitters can be used. Also, it allows use of a single reflector without a frequency selective annulus.

The requirements on the antenna are summarized in Table 3.1-1. The isolation and pointing accuracy requirements were generated in section 2.1. Although the bandwidth capability was not specified and the communication links require a bandwidth of only a few hundred MHz, a requirement has been imposed on the antenna design that it be compatible with an operational system using the entire allocated bandwidth.


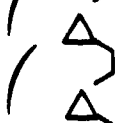


### 3.1.2 Design Issues

The number of separate functions performed by the antenna is illustrated in Table 3.1-2. In addition to transmit and receive functions for both CPS and TS it should be noted that for each CPS function there are two beams. It is desirable, in order to minimize antenna cost and spacecraft weight and complexity, to reduce the number of physical antennas in operational systems as well as for the flight experiment system. As shown below, Hughes has configured the antenna system with only one main reflector. This configuration provides separate transmit and receive feed systems. Other

TABLE 3.1-1. PERFORMANCE REQUIREMENTS FOR MULTIPLE BEAM ANTENNA

Service	Link	Trunking Fixed Beam	Customer Premise Scanning Beam
Half power beamwidth, (deg)	Up Down	0.27 recommended 0.4 specified	0.27 recommended 0.4 specified
Operational freq range (GHz)	Up Down	27.5 to 30.0 17.7 to 20.2	27.5 to 30.0 17.7 to 20.2
Bandwidth, GHz	Up Down	2.5 2.5	2.5 2.5
Number of beams	Up  Down	4 simultaneously active (6 nodes) 4 simultaneously active (6 nodes)	2 simultaneously active 2 simultaneously active
Minimum peak gain 3 deg off boresight, dB	Down	51	51
Isolation between beams, dB	Up Down	≥26 ≥26	≥26 ≥26
Power handling capability, W	Down	40	40
Pointing accuracy (degrees)		0.04 (3σ)	0.04
Polarization	Both	Linear	Linear

TABLE 3.1-2. ANTENNA REQUIREMENTS FOR BASELINE SYSTEM

<u>Four Antenna Functions</u>		
1) Transmit TS signals		Six fixed spot beams $\sim 0.4^\circ$ HPBW
2) Receive TS signals		Six fixed spot beams $\sim 0.3^\circ$ HPBW
3) Transmit CPS signals		Two scanning spot beams two sectors $\sim 0.4^\circ$ HPBW
4) Receive CPS signals		Two scanning spot beams two sectors $\sim 0.3^\circ$ HPBW

major issues are the optical configuration of the antenna and the technique for scanning the CPS beam.

### 3.1.2.1 Optical Configuration

The selection of optical configuration was discussed in section 2.1. The performance of prime fed and Cassegrain configurations was compared (Figure 3.1-3), and although the off axis scan loss is not significant at the specified transmit and receive diameters, there will be a large improvement for off boresight beams in the gain of the Shuttle diameter antennas which NASA expects to be used in operational systems of the 1990's. Also, because the flight experiment receive diameter was selected to be the same as the transmit diameter (3M), a considerable increase in receive gain is achieved by use of a Cassegrain configuration. The selected offset Cassegrain configuration for the experimental system is a good choice with all engineering design goals considered. For an operational system with a larger diameter, about 4 meters (13.1 feet) for example, shaped dual reflector configurations other than the classical paraboloidal main reflector and hyperboloidal subreflector need to be considered since better scan performance with these systems in the offset geometry has been reported.\*,\*\*

### 3.1.2.2 Scanning Technique

Given a dual reflector configuration with a spherical wave source there are two methods of scanning independent multiple CPS beams. One

---

\*D. C. D. Chang and K. C. Lang, "A Scan-Corrected Offset Dual Reflector Antenna System," 1980 International Symposium Digest - Antennas and propagation, Vol 2, pp. 557-559.

\*\*30/20 GHz Spacecraft Multi-Beam Antenna System, Status Review, Contract No. NAS 3-22498 Prepared for NASA/Lewis Research Center, Cleveland, Ohio by Ford Aerospace & Communications Corp., May 1981.



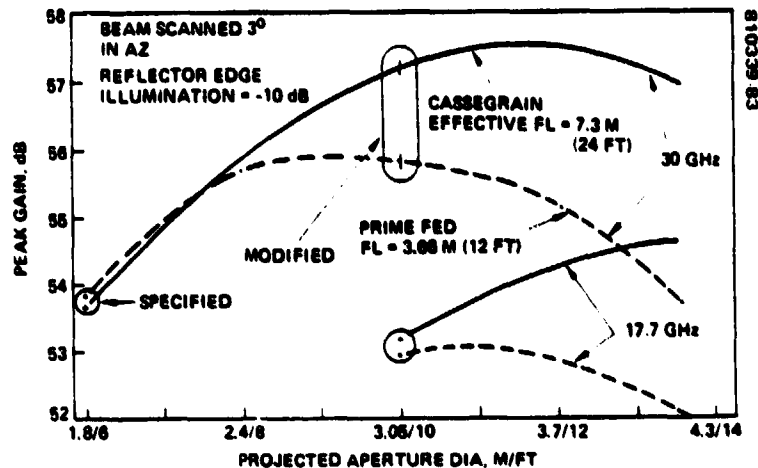


FIGURE 3.1-3. ANTENNA CONFIGURATION SELECTION

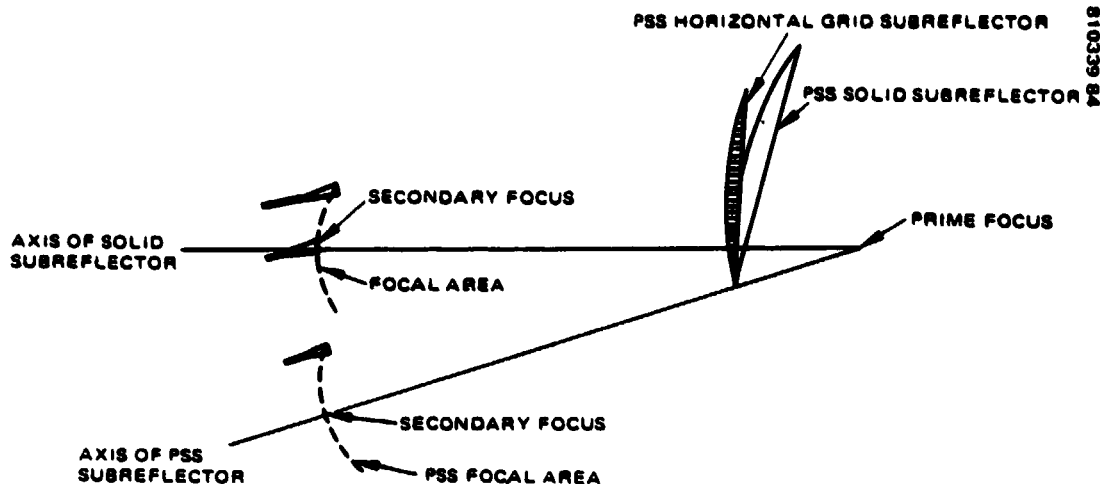
method uses a small linear phased array which is imaged onto a large main reflector by a suitably designed pillbox feed system.\* This technique, which would distribute the high power amplification among the feed elements, is in too early a stage of development to consider for this flight experiment. Also, a single 40 watt power source for each beam has been specified. The other method uses an array of fixed feeds. A switching beam forming network routes receive and transmit power to or from a particular feed element or small group of feed elements. The beam is scanned by varying the switch connections in time. The latter technique has been adapted for the flight experiment. The problems associated with successful use of this technique are discussed later in this section.

### 3.1.2.3 Integration of Antenna Functions in a Single Physical Aperture

Because of the use of fixed feeds as the basis of the scanning beam, scanning beam feeds which point at trunk terminals can be used as the trunk feeds. Thus the trunk and GPS feed arrays can be combined. The two GPS beam feed arrays are essentially a single large feed array with separate switching networks. Thus they readily share the same antenna. The only problem, then, in satisfying all the antenna requirements with a single reflector is to separate transmit and receive feeds. It is undesirable to use common feeds for transmit and receive because it is difficult if not impossible to achieve adequate performance in a close packed feed array for both bands. Also, waveguide duplexers are lossy. Consequently, a means was sought to provide separate feed regions for transmit and receive.

One method for creating two focal regions is explained with the aid of Figure 3.1-4. A Cassegrain configuration with two subreflectors was chosen

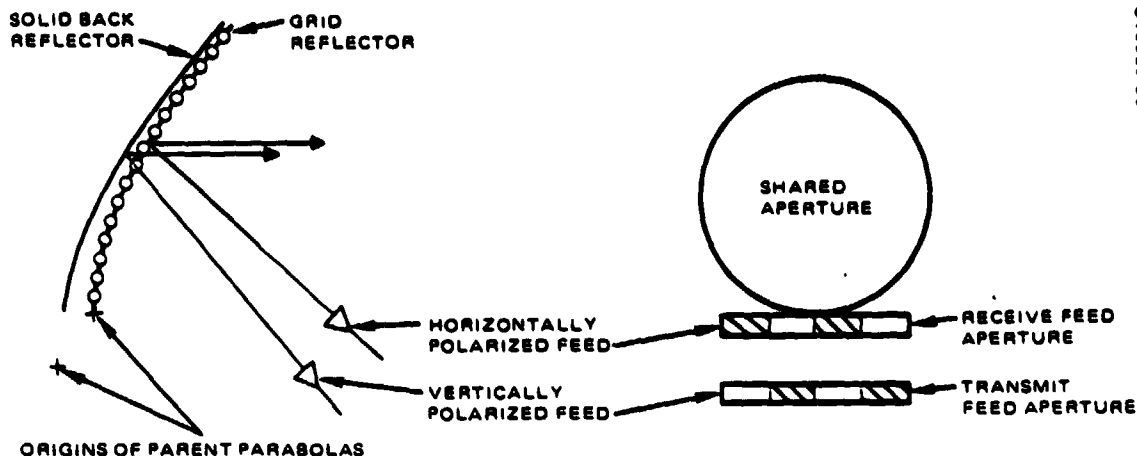
\*A. S. Acampora, C. Dragone, and D. O. Reudink, "A Satellite System with Limited-Scan Spot Beams," IEEE Trans, on Comm., October 1979, pp. 1406-1415.



**FIGURE 3.1-4. POLARIZATION SELECTIVE SURFACE SUBREFLECTORS CREATE TWO FOCAL AREAS FOR TWO ORTHOGONAL LINEAR POLARIZATIONS**

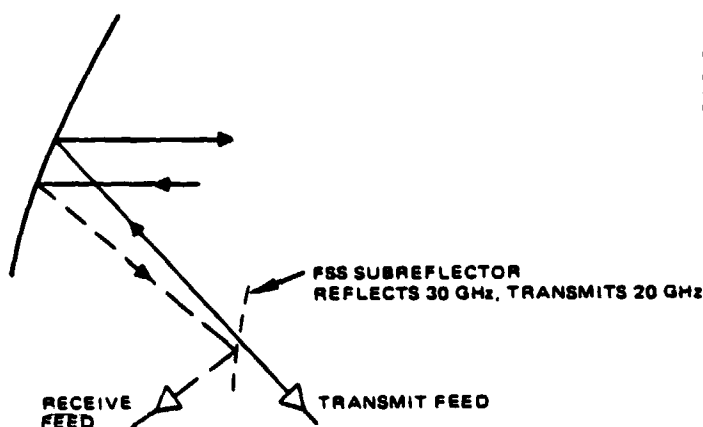
as the first candidate for consideration. Two subreflectors with a common focus (prime focus of the main reflector) have horizontal and tilted axes and secondary foci displaced as shown. The top focal area has a vertically polarized feed. This transmits or receives vertically polarized waves that propagate unimpeded through the polarization selective surface (PSS) horizontally gridded front and reflect off the back solid subreflector. The horizontally polarized feed at the focal area located below the vertically polarized feed reflects from the PSS since horizontally polarized waves must reflect from a horizontal grid. This vertical arrangement of feeds is not conducive to a satisfactory mechanical layout on the satellite primarily because of unfavorable mass properties of the overall satellite system. An alternative arrangement is with the two subreflector axes horizontally displaced from the main reflector axis. However, radiation pattern analysis showed the latter scheme to have significantly inferior gain performance compared to that achieved by a feed system with its axis coincident with the main reflector axis. For these reasons, the PSS approach was rejected. A variation of this approach using two overlapping subreflectors with a common prime focal point and nonparallel axes is to use a frequency selective surface (FSS) for the front subreflector in place of the PSS, and to have 20 GHz reflect off the FSS subreflector and 30 GHz pass through the FSS to reflect off the back subreflector. However, this concept has the same gain performance limitations as the PSS technique and was also rejected.

A second technique for creating two focal regions is the shared aperture used, for example, on the Hughes SBS satellite antenna. This configuration as depicted in Figure 3.1-5 has two prime fed gridded paraboloidal reflector antennas occupying nearly the same volume. A horizontally gridded parabola reflects horizontally polarized radiation but transmits vertically polarized radiation. Because the offsets of the two reflectors from the origins of their parent parabolas are different, the focal regions of the two parabolas are separated as shown. The transmit and receive frequency band signals



810339 85

FIGURE 3.1-5. PRIME FED SHARED GRID APERTURE CONFIGURATION



810339 86

FIGURE 3.1-6. FOLDED OPTICS AND PRIME FED CONFIGURATIONS COMBINED

are fed by partitioning each feed array into a contiguous sequence of sub-arrays with alternating transmit/receive functions. Thus, a geographical area is served by one polarization on transmit and by the other on receive. This technique was rejected because it is suitable only to a prime fed configuration.

A third technique for creating two focal regions is the dual reflector configuration with an FSS subreflector that is prime fed by 20 GHz and Cassegrain fed by a 30 GHz feed (Figure 3.1-6). Here, advantage is taken of the magnification designed into the Cassegrain system to correct somewhat for scan loss at the higher frequency band where the receive beam scans 1 - 1/2 as many bandwidths as the transmit beam. The disadvantage of this approach is that of satellite imposed physical constraint of the prime focal length and subsequent limitation on controlling scan loss.

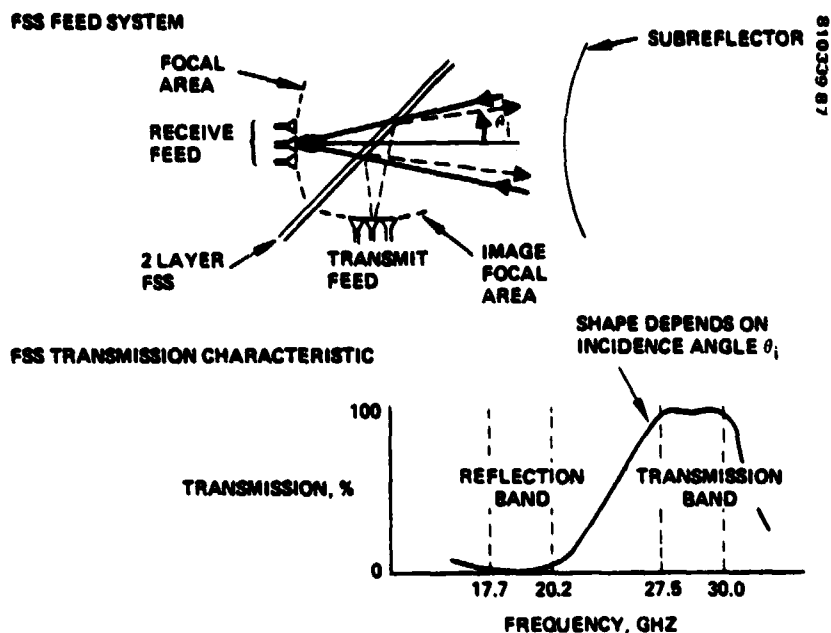


FIGURE 3.1-7. FREQUENCY SELECTIVE SURFACE CREATES TWO FOCAL AREAS FOR TWO SEPARATE FREQUENCY BANDS

The method selected is depicted in Figure 3.1-7. Two focal regions are created with a common aperture by utilizing a planar FSS. In this example, the common aperture is a subreflector of a dual reflector antenna system. The FSS spatially isolates the receive feed from the transmit feed with the receive feed located about the secondary focus of the subreflector and the transmit feed located about the mirror image of that focus. A two-layer FSS structure designed as a two-section transverse electromagnetic wave filter with the transmission characteristic depicted performs this desirable function. This approach was selected for use in the dual reflector configuration shown in Figure 3.1-8.

#### 3.1.2.4 Beam Forming Networks

Figures 3.1-9 and 3.1-10 illustrate the method of scanning a beam using a beam forming network (BFN). In the receive network the feeds are connected to the receiver through a switching network which, under control of the scan controller, connects one feed at a time to the receiver. The switches are high speed ferrite circulators with semiconductor driver circuits. The transmit BFN operates the same way to sequence the high power amplifier output to each of the transmit feeds. Electromagnetic Sciences Corporation is presently developing electronically controlled magnetic circulators, phase shifters and VPDs which would lead to hardware for proof of concept model MBAs to be built by the two MBA technology contractors for

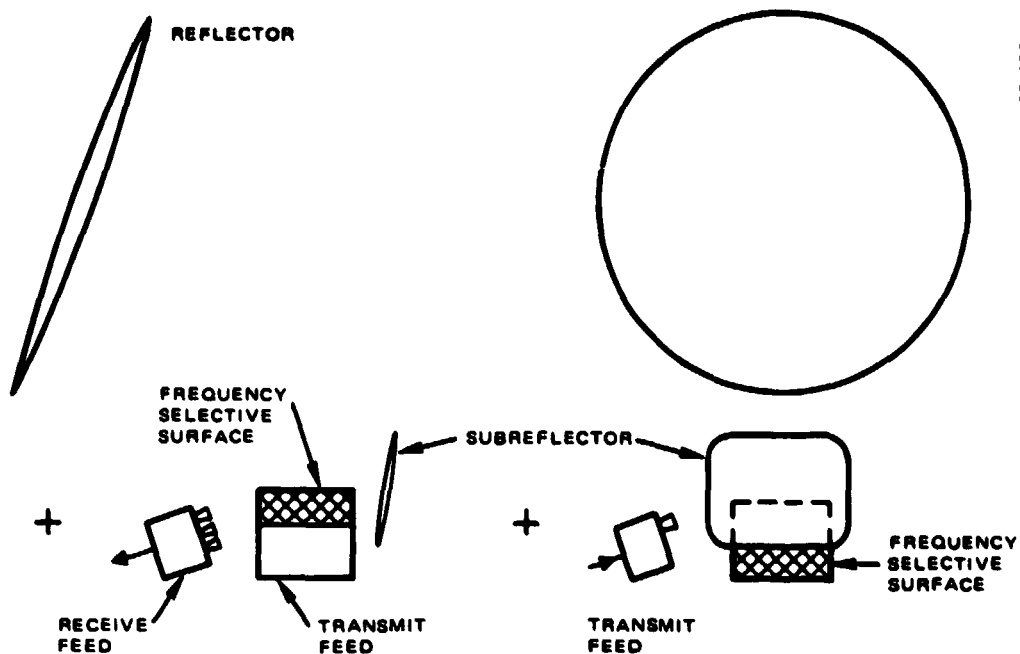


FIGURE 3.1-8. DUAL REFLECTOR CONFIGURATION WITH FSS FEED TECHNIQUE

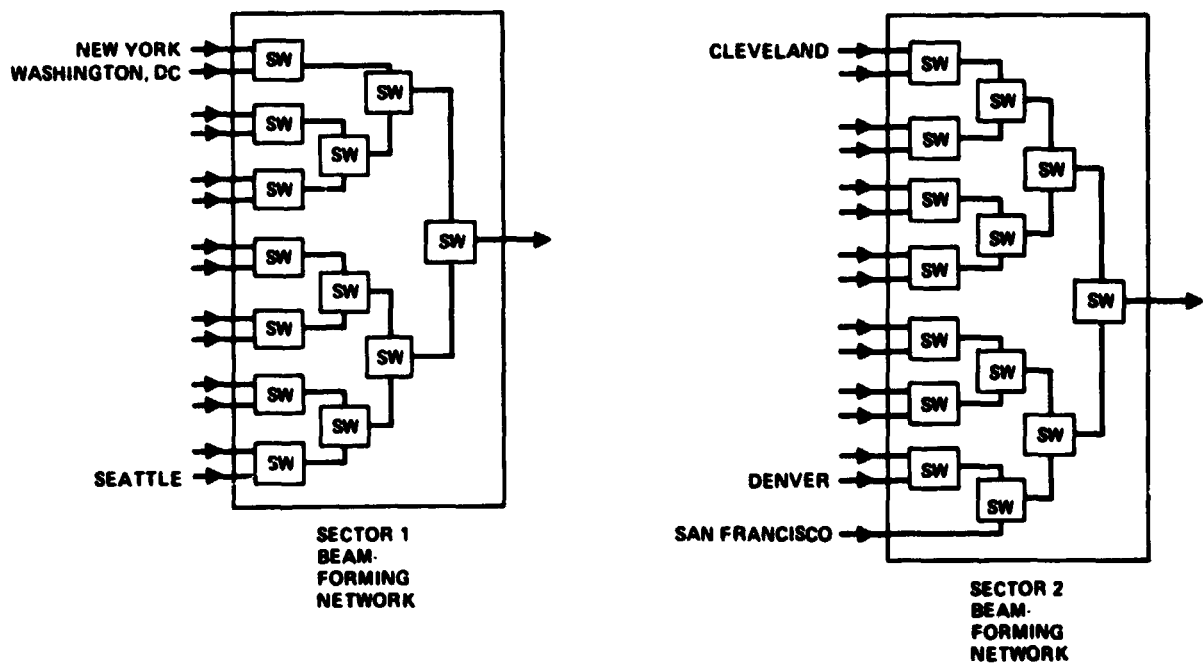


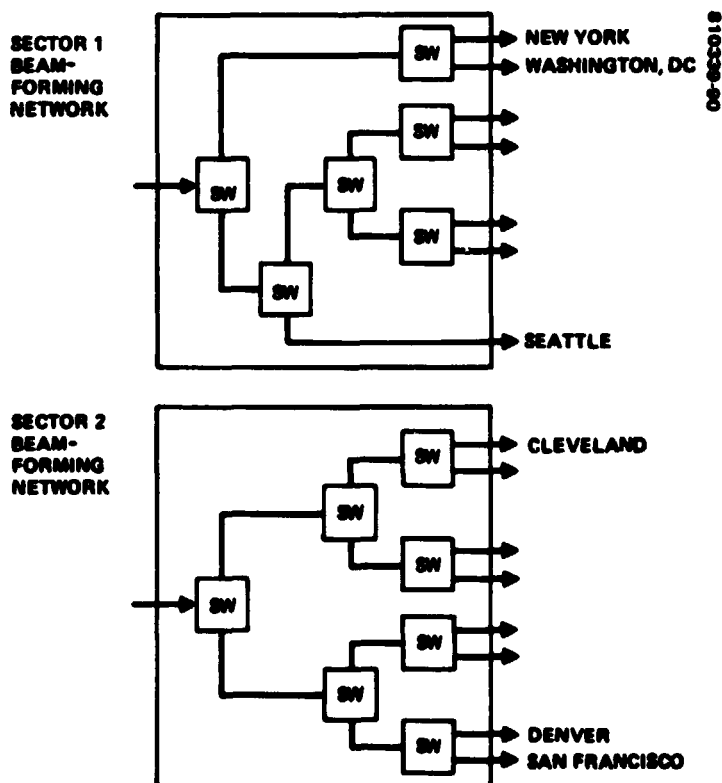
FIGURE 3.1-9. RECEIVE SCANNING FEED NETWORKS

**TABLE 3.1-3. ELECTRONICALLY CONTROLLED SWITCHING CIRCULATOR CHARACTERISTICS\***

<u>Parameter</u>	<u>Performance</u>
Freq range GHz	18.35 to 19.35
Insertion loss, dB	0.15 measured
Isolation to third port	23 dB measured
VSWR	1.15:1 measured
Shape	Triangular X-sect
Size (excl driver, max)	1 in./face x 0.312 in. high
Weight (excl driver)	0.42 oz predicted
Switching energy, $\mu$ J max**	40 measured
Switching time, $\mu$ sec	0.4 measured
Switching rate (max), Hz	25,000
Power handling, WATTS CW	30 predicted
Temperature range, °C	0 to 50 predicted

\*Table provided by Electromagnetic Sciences Corp.

\*\*Includes losses in Drivers.



**FIGURE 3.1-10. TRANSMIT SCANNING FEED NETWORKS**

NASA: Ford and TRW. The design characteristics of the transmit switching circulator, some measured and the rest predicted, are given in Table 3.1-3. The receive switching circulator would be scaled down by wavelength from the transmit design except for the driver whose weight and size would be same as for transmit. Insertion loss, isolation and VSWR would be about the same at 30 GHz as at 20 GHz. Coverage of the east coast sector by this technique is shown in Figure 3.1-11. The limitations of this approach are illustrated in Figure 3.1-12. Because of the finite size of the feeds (approximately two wavelengths in diameter) the coverage overlap is limited as shown. A terminal at the intersection of three spots would experience an uplink gain which is almost 7 dB below peak gain and a downlink gain over 8 dB below peak gain. If the coverage shown in Figure 3.1-13(a) can be accepted the gain loss reduces to about 4 dB and about 14 percent of the total coverage area is lost. If the coverage loss is limited to 3 dB, as shown in Figure 3.1-13(b), then 65 percent of the area is covered. In addition to the loss incurred by CPS terminals located near the spot intersection a small loss is incurred on the downlink to the New York and Washington trunk terminals because the beam peaks cannot be pointed at both cities.

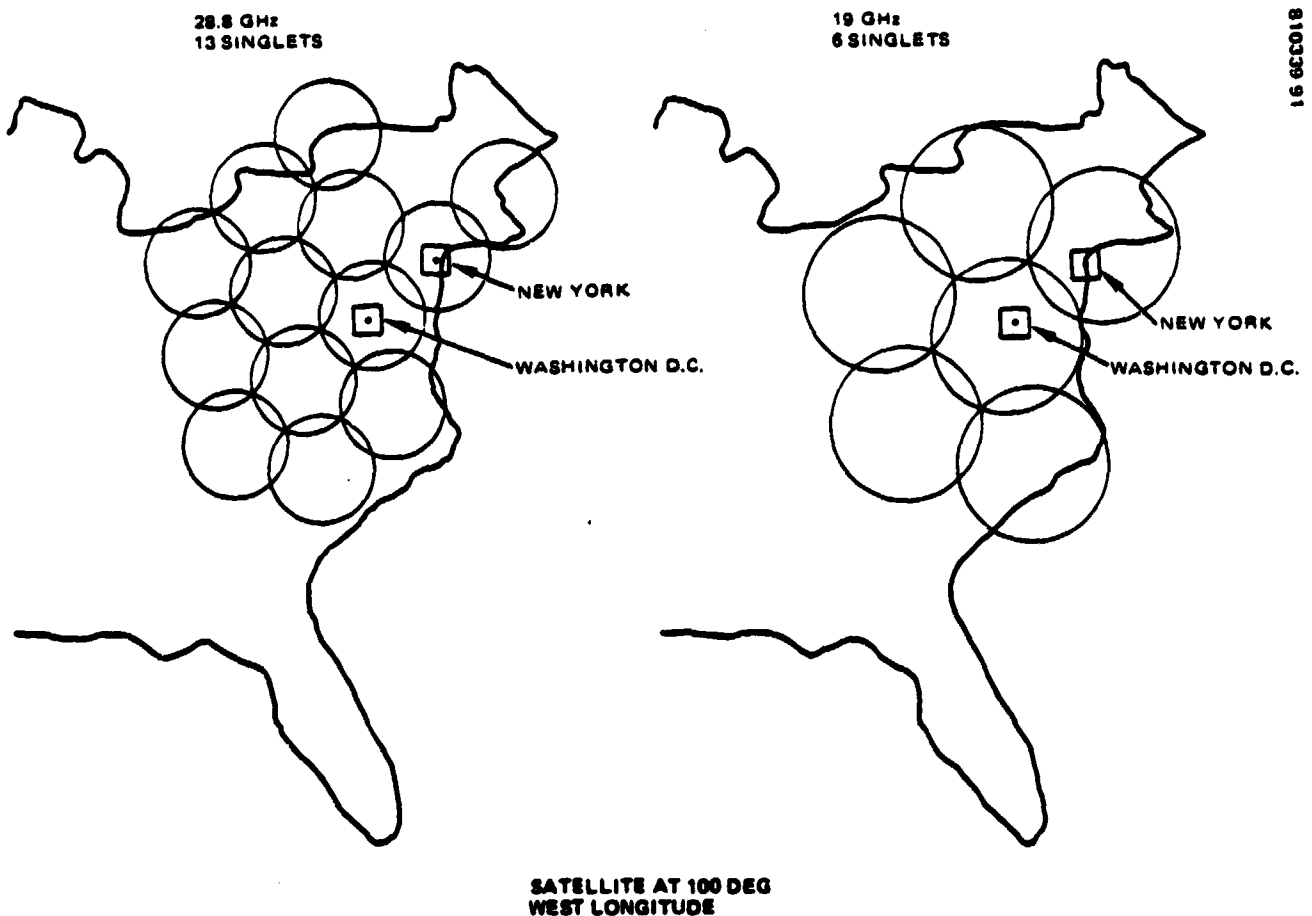


FIGURE 3.1-11. SECTOR 1 TRUNK/CPS COVERAGE

REFLECTOR DIAMETER = 3 m (10 ft)  
EFFECTIVE FOCAL LENGTH = 7.3 m (24 ft)

FREQUENCY = 28.8 GHz

FREQUENCY = 19 GHz

810309 92

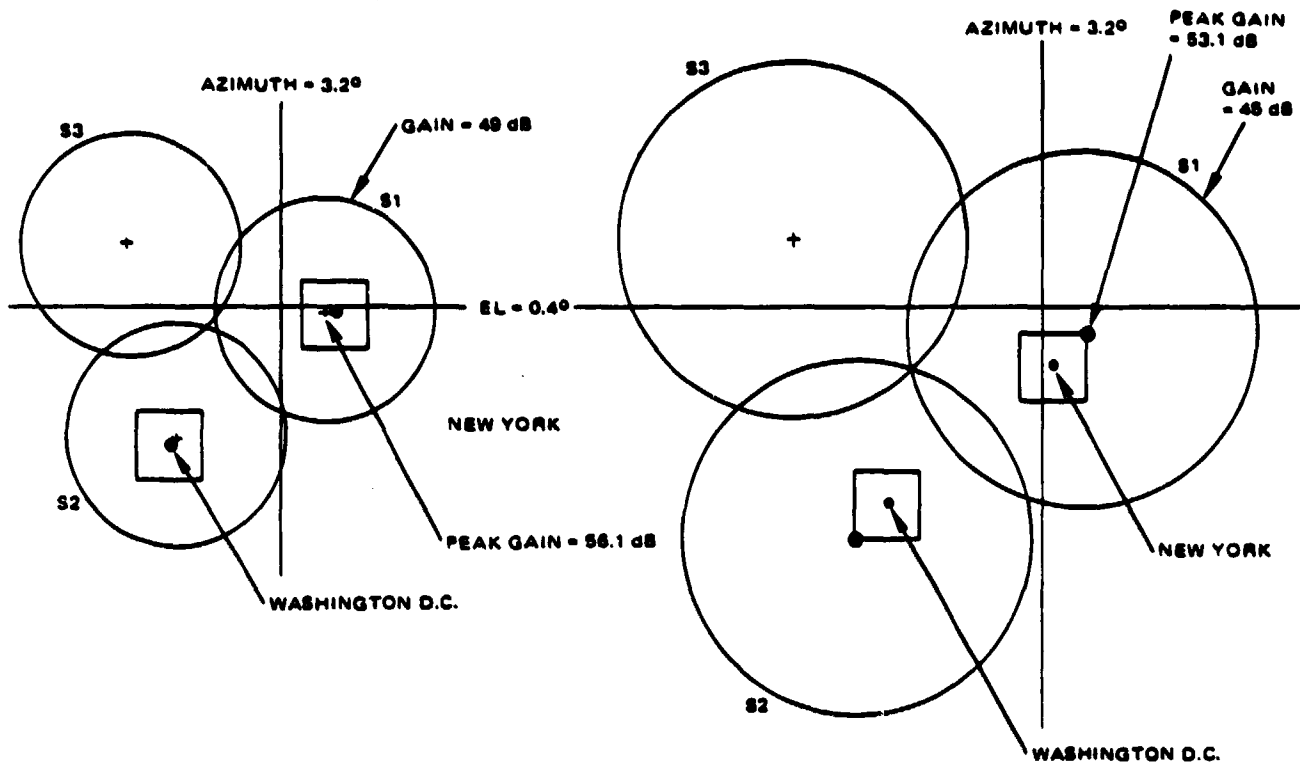
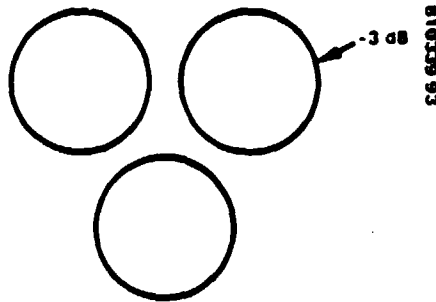


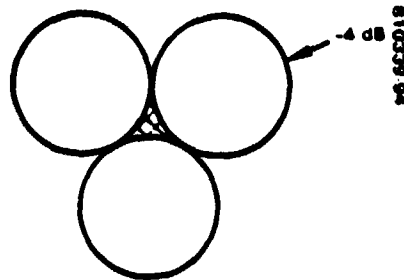
FIGURE 3.1-12. OFFSET CASSEGRAIN DIRECTIVE GAIN CONTOURS

The BFN design described above provides adequate performance for the flight experiment because the links can be closed using the specified 40 watt satellite HPA and modest earth terminal transmitters. The required link margins are achieved even with the area losses of 7 and 8 dB; however, for operational systems better performance over an area covered by spot beams is desirable. One means of improving this performance is illustrated in Figure 3.1-14. Beams can be formed between the primary spots by sharing power between contiguous feed elements to form doublets. Horns A and B are contiguous and connected by a VPD with five controllable states. The chart relates division of power among horns A and B to doublet beam peak scan angle ( $\theta$ ) measured relative to beam peak A when all power is in horn A ( $P_A = 1$ ,  $P_B = 0$ ) and approximate doublet peak gain for four other power splits including the equal power split condition when the singlet beams are assumed to cross over 4 dB below their peaks. In order to generate these doublets it is necessary to replace the switches of Figure 3.1-9 and Figure 3.1-10 by variable power dividers.





a) 35 PERCENT TOTAL COVERAGE AREA LOSS



b) 14 PERCENT TOTAL COVERAGE AREA LOSS

FIGURE 3.1-13. REDUCED AREA COVERAGE

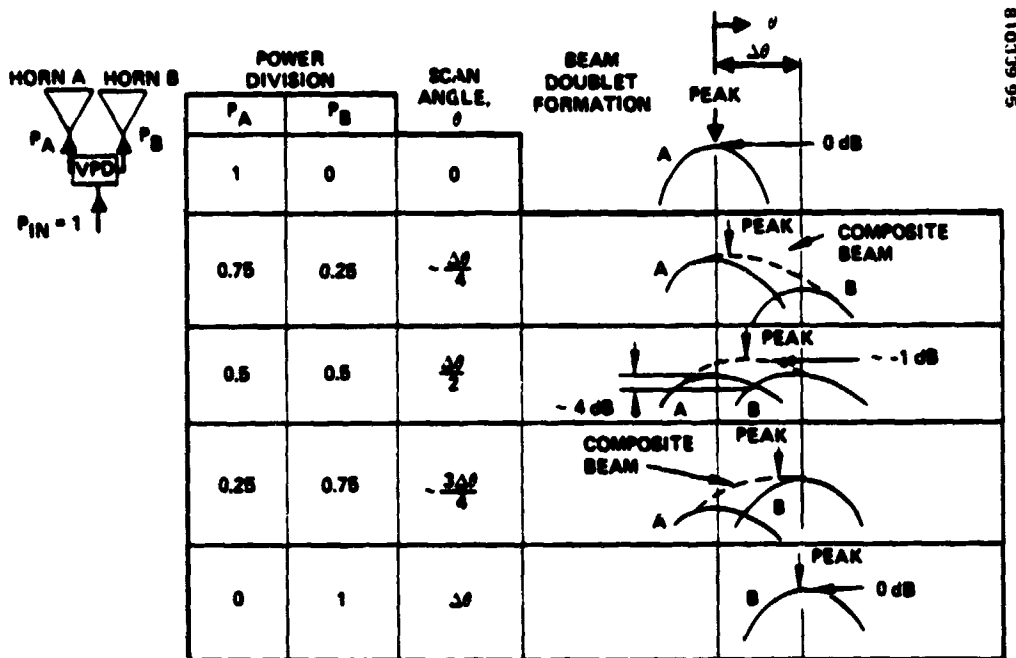


FIGURE 3.1-14. CPS BEAM SCANNING WITH FEED HORN/BEAM DOUBLETS

The number of states needed to maximize gain over a coverage area depends on the specified area, and the crossover level of the adjacent beams generated by the adjacent feed elements. For this illustrative example, the coverage area is simply a line connecting the beam peaks. With five controllable beam positions it can be shown that the use of only three, the two singlets and equal power division doublet, give near optimum gain along the coverage line. This is because the doublet and either singlet cross over about three or four tenths of a dB below the doublet peak. There might be more advantage to multiple VPD state control if the singlets crossover at a lower level. In the two wavelength diameter feed element design corresponding to Figure 3.1-8 where the adjacent elements are at their closest possible spacing of two wavelengths adjacent singlets crossover about 6 dB below the peaks and the doublet peak gains are down about 3 dB from the singlet peaks.

A three bit VPD design that could provide the power divisions in the above 5 control state example is described in Figure 3.1-15. A flux drive type phase shifter is assumed in the design having the characteristics listed in Table 3.1-4 for 20 GHz operation and in Table 3.1-5 for 30 GHz operation. These values for the transmit device have been reported by Electromagnetic Sciences Inc. at the NASA Industry Briefing in Washington, D. C., 7 May 1981.

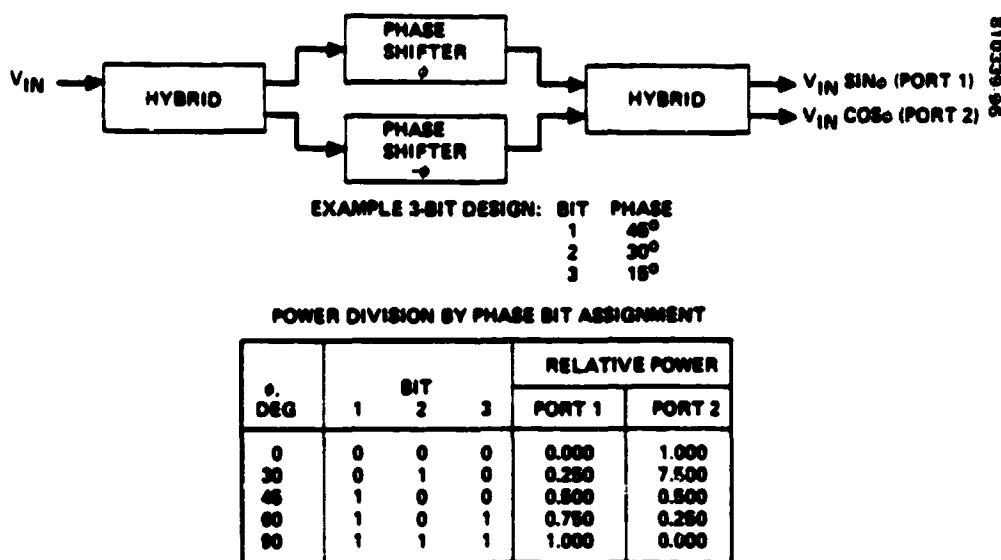


FIGURE 3.1-15. VARIABLE POWER DIVIDER BLOCK DIAGRAM AND RELATIVE POWER OUTPUTS

**TABLE 3.1-4. ELECTRONICALLY CONTROLLED  
VARIABLE POWER DIVIDER CHARACTERISTICS\***

<u>Parameter</u>	<u>Predicted Performance</u>
Frequency range (GHz)	18.85 to 19.35
Power ratio range, dB	0 to $\pm 20$
Insertion loss, dB any setting	0.4
VSWR, max	1.2:1
Output-to-output isolation, dB	20
Phase shift/power division accuracy	Per table
Size (excl drivers), in. max	1.25 x 0.75 x 3.3
Weight (excl drivers), oz max	1.8
Power handling, W CW ***	60
Switching energy, $\mu$ j max**	75
Switching rate, Hz Max	25,000
Temperature range, $^{\circ}$ C	0 to 50 $^{\circ}$
Switching time, $\mu$ sec max	0.4

\* Table provided by Electromagnetic Sciences Corporation.

\*\* Measured values.

\*\*\* Includes losses in drivers.

**TABLE 3.1-5. ELECTRONICALLY CONTROLLED VARIABLE POWER  
COMBINER CHARACTERISTICS\***

Parameter	Performance Goal	Comments
Frequency range	27.5 to 30.0 GHz	
Bandwidth	1.5 GHz	27.85 to 29.35 GHz for breadboard
Switching rate	100,000 operations per sec instantaneous max 20,000 average	Average rate depends on position in BFN and switching scenario
Switching time	0.5 $\mu$ sec max	Most significant design parameter (0.5 $\mu$ sec interpreted as total switching time)
Switching energy	40 $\mu$ joule per operation max	Strong function of switching time
Insertion loss	0.42 dB max	
VSWR	1.25:1 max 1.1 goal	Strongly influenced by Tee/hybrid design
Min attenuation and range	20 dB min	0 to 20 dB attenuation range $\pm 3^{\circ}$ differential phase error
Number of bits	6	
Temperature range	0 to 50 $^{\circ}$ C	

\*Table provided by Electromagnetic Sciences Corporation.

REFLECTOR DIAMETER - 3m (10 ft)  
EFFECTIVE FOCAL LENGTH - 7.3 m (24 ft)

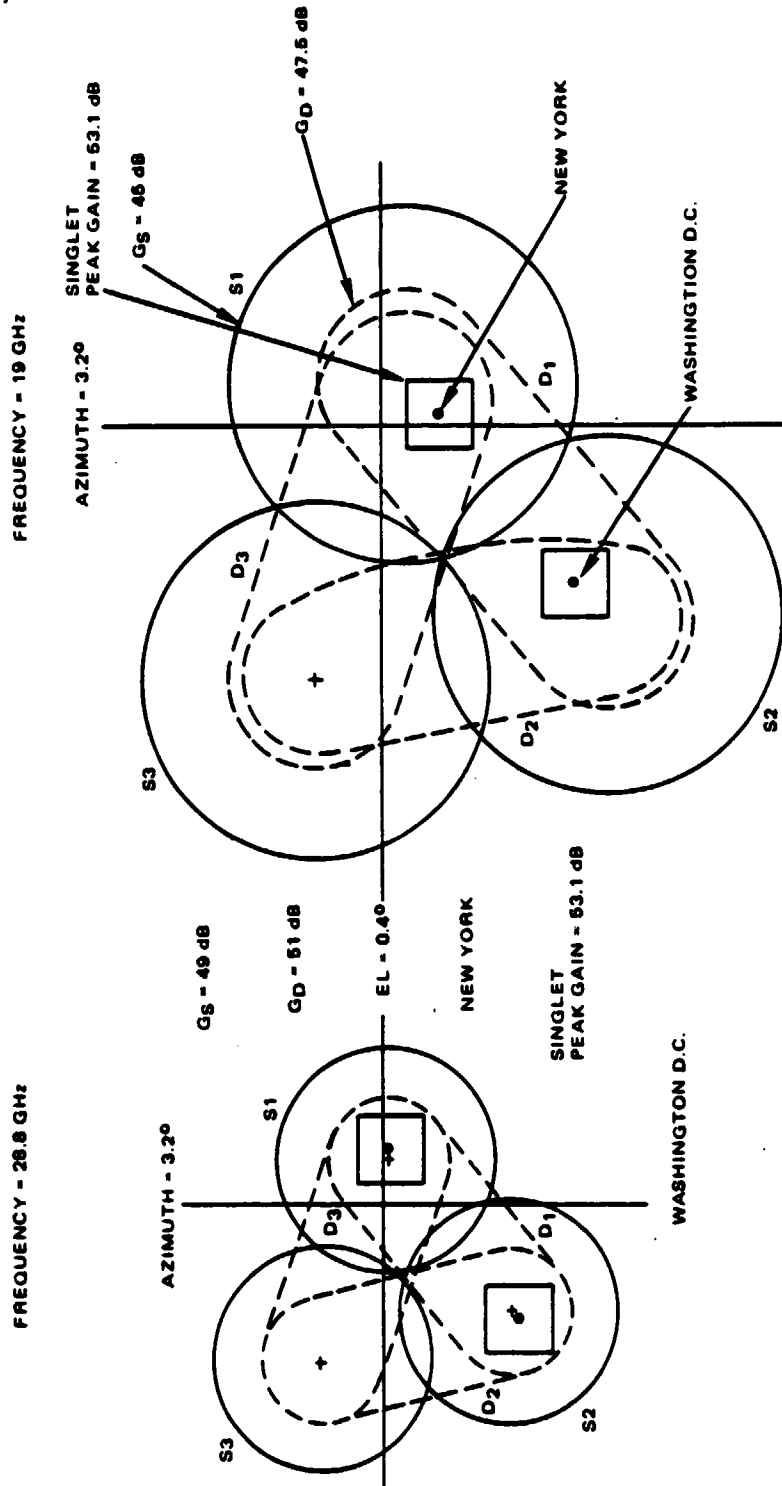


FIGURE 3.1-15. OFFSET CASSEGRAIN DIRECTIVE GAIN CONTOURS

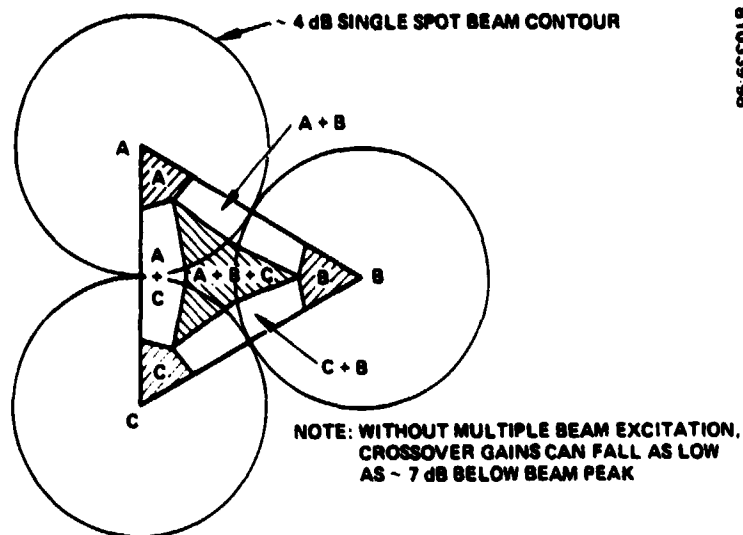


FIGURE 3.1-17. CPS SPOT BEAM GAIN POINTING LOSS REDUCTION

The performance improvement using doublets generated by splitting power equally between adjacent feeds is shown in Figure 3.1-16. A total area gain coverage improvement of 2 dB on the uplink and 2.5 dB on the downlink results. In general, it would be possible to use the other combinations shown in Figure 3.1-15 to break the area into smaller subareas with slightly higher gain. Also it is possible to share the power between three feeds and create the pattern shown in Figure 3.1-17. The complexity of the feed network is increased and the beam must make more steps each frame thus reducing the system efficiency.

In order to provide an experiment with doublet technology, the sector 1 BFN has been modified by replacing the switch for the New York and Washington feeds with a VPD so that a doublet can be generated between these two spots. The resulting BFN is shown in Figure 3.1-18.

### 3.1.2.5 Contiguous Coverage Feed Optimization

The problem of covering a contiguous area with an array of fixed feeds was discussed in the previous section. The reduction of satellite antenna gain for terminals which are distant from the beam peaks can be minimized by careful selection of feed size. The gain reduction is due to the separation of adjacent beams imposed by the physical size of the feeds. If the feed diameter is reduced the feeds can be moved closer together, and the beam peaks can be moved closer together so that antenna gain at points between beam peaks is nearer to the peak gain; however, as the feed diameter is reduced beyond some value the peak gain is reduced. The optimum feed

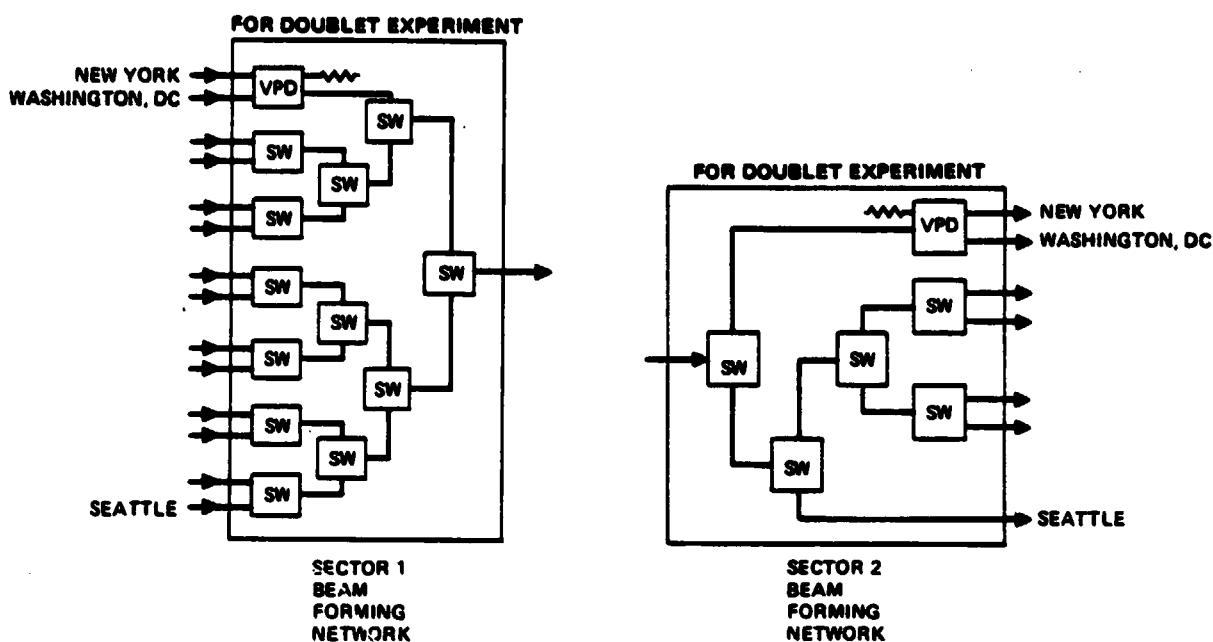


FIGURE 3.1-18. SCANNING FEED NETWORKS

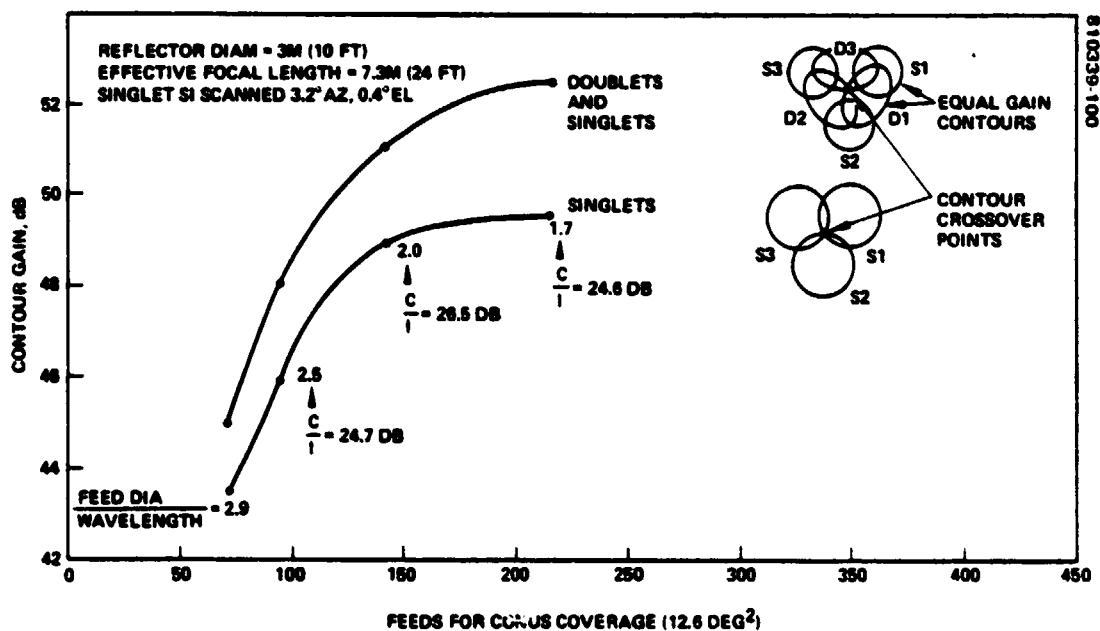


FIGURE 3.1-19. CASSEGRAIN ANTENNA CONTOUR GAIN AT 28.8 GHZ

size in terms of gain is one which maximizes the minimum gain over the coverage area. Another consideration however, is that the number of feeds required to cover a specified area increases as the diameter of the feeds is decreased and the feed separation increases.

An analysis of the antenna performance in terms of minimum gain coverage over all CONUS and beam-to-beam isolation was performed using a dual reflector computer program that predicts accurately the secondary radiation pattern of an offset circular aperture feed horn. The feed design parameter was the horn diameter. The results of this analysis for the receive frequency of 28.8 GHz are given in Figure 3.1-19 which gives the relationship between minimum receive gain coverage provided by a step-scanned CPS beam in the New York region and the number of feeds required for full CONUS coverage. Both singlet and doublet mechanizations were studied. In the singlet mechanization, one singlet beam is formed for each feed excited. All feeds are identical circular aperture horns, close-packed in a triangular lattice array so that all scanning spot beam constant gain contours overlayed on CONUS would produce a corresponding beam array. Three such singlet beam contours overlapping at a common crossover point are sketched alongside the curve labeled singlets. For a specific feed design, the gain value plotted is for the minimum gain value of the three contours that intersect at a common point. This value represents the minimum gain that would be achieved over all CONUS. Each feed has a diameter (in wavelengths) whose value is shown by a data point on the curve. As the diameter decreases, the feed spacing decreases, causing the number of feeds required for CONUS coverage to increase. The curve indicates that feed diameters larger than about two wavelengths cause excessive separation between beam peaks with correspondingly lower crossover gains and large area gain coverage loss at points between peaks. As the diameter is decreased below two wavelengths, the minimum gain increases slowly at the expense of an increased number of feeds to cover CONUS. This occurs because crossover gain is increasing as the beam crossover level gets closer to the beam peak. Also a feed diameter of two wavelengths appears to maximize the beam-to-beam isolation. C/I in Figure 3.1-19 is the ratio of the carrier measured at a point equidistant between three beam peaks to an interfering signal generated by a beam that is three spots distant. This value of C/I is reduced from the conventionally defined value because C is measured at a point several dB below peak gain (-8 dB at 19 GHz and -7 dB at 28.8 GHz for a two wavelength diameter feed). Also the sidelobe envelope was used to estimate I which gives a worst case value since an interfering signal is unlikely to typically arrive at the peak of a sidelobe. Design consideration of this problem can help reduce this likelihood. A second curve in the figure shows that if doublets are created to fill in the areas between the singlets, a gain benefit of about 2.5 dB is realized; however, this configuration adds significantly to the complexity, weight, and cost of the beam forming network because all switches would be replaced by VPDs. If a prime fed reflector were used rather than a Cassegrain configuration the results of the above tradeoff for the receive case change to those shown in Figure 3.1-20. The gain performance for a comparable number of feeds covering CONUS is about the same as for the Cassegrain configuration but the C/I is significantly lower.

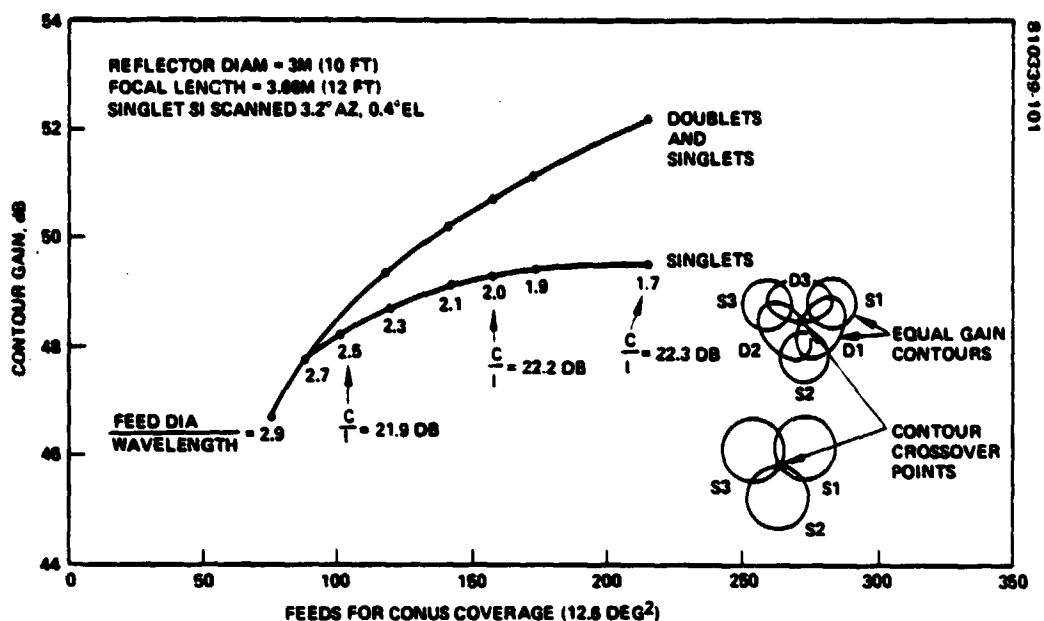


FIGURE 3.1-20. PRIME FED REFLECTOR CONTOUR GAIN AT 28.8 GHZ

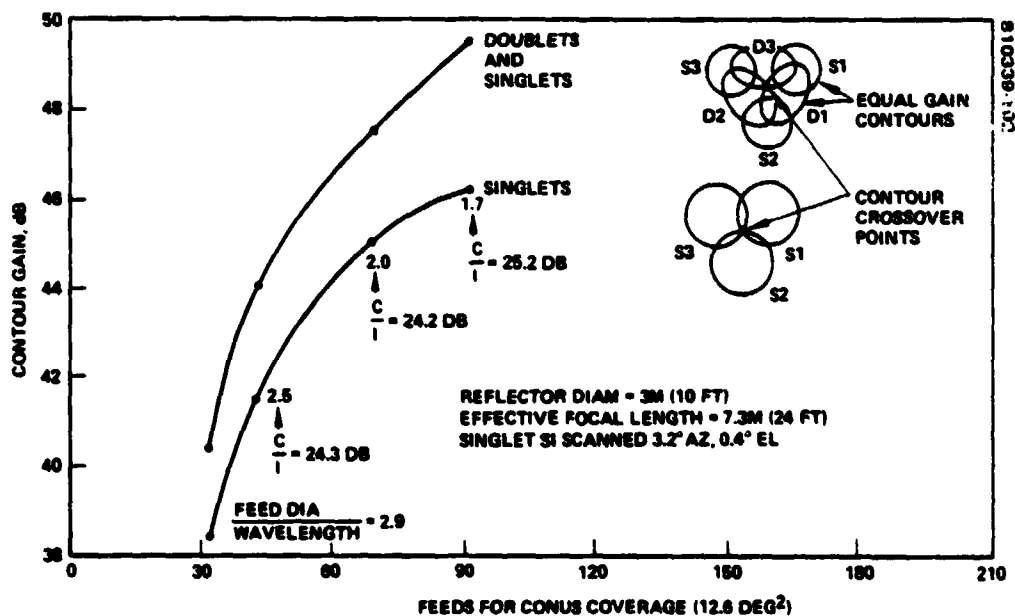


FIGURE 3.1-21. CASSEGRAIN ANTENNA CONTOUR GAIN AT 19 GHZ



For the Cassegrain configuration at 19 GHz the relationship between coverage gain and number of feeds for coverage of CONUS is given in Figure 3.1-21 and is based on the same assumptions used for 28.8 GHz coverage performance. Again, the use of doublets gives about 2 dB more gain than singlets. Transmit and receive feeds can be independently designed due to their physical isolation by the FSS. The optimum feed diameter at transmit is also about two wavelengths. This design results in a total of about 70 transmit feeds.

Figure 3.1-22 addresses the prime fed configuration at 19 GHz. The optimum feed design is about two wavelengths, giving 70 feeds covering CONUS. Doublets and singlets together yield more than 2 dB gain than singlets alone, as with the Cassegrain design. A comparison of the 19 GHz performance of the prime fed and Cassegrain configurations shows gain and C/I for the 70 feed design to be about the same. As expected, the increased F/D provided by the Cassegrain configuration is less important at 20 GHz where the 3° scan angle represents fewer beamwidths. Generally, it is seen that the Cassegrain design does not give much different coverage gain than the prime fed design. This is because the Cassegrain beams with less scan loss and beam broadening cross over at lower levels than the prime fed reflector beams.

### 3.1.3 Cluster Feed Approach

Another means of improving area coverage is the use of a cluster feed in place of each single feed and the use of a beam forming network like that proposed by Ford.\* The network permits switching of one cluster to another with reuse of some constituent feeds in the clusters the corresponding singlet beams will crossover at higher levels. This approach as depicted in Figure 3.1-23 will result in higher gain performance, as the crossover level of the adjacent beams comes closer to the peak gain. As shown, for example, cluster 1 and cluster 4 which are nonoverlapping are spaced  $2.646 d_1$  apart while clusters 3 and 4 are only  $d_1$  apart and overlapped with 4 reused constituent feeds. This ratio of feed cluster separations 1:2.646 corresponds directly to the ratio of beam separations achievable so that if we start with nonoverlapping cluster feed produced beams with about 1.3 half power beam separation those beams produced by the overlapping feeds may be only 0.5 half power beamwidths apart. Thus, with this approach the peak gain of a scanned beam from a Cassegrain design is higher than from a prime fed design. Continuing with the Cassegrain a comparison of the single and cluster feed approaches in terms of gain and feed complexity is made in Table 3.1-6. The cluster feeds give significantly more net gain than the single feeds, at least 2.2 dB at 19 GHz and at least 2.6 dB at 28.8 GHz. However, about ten times more components in the BFNs are required in the cluster feeds.

---

\*30/20 GHz Spacecraft Multi-Beam Antenna System, Review 1, Contract No. NAS 3-22498 October to November 1980; presented to NASA/Lewis Research Center, Cleveland, Ohio by Ford Aerospace & Communications Corp., Western Development Laboratory Division.

TABLE 3.1-6. COMPARISON OF GAIN AND FEED COMPLEXITY SINGLE AND CLUSTER FEEDS

Frequency GHz		Performance, dB					Feed Complexity			Power/Sector, ** W	
		Single Feeds (Feed Diam = 2λ)		Cluster Feeds (Feed Diam = 0.667λ)			No. Components for Conus Coverage			Single Feeds	Cluster Feeds
		Doublets	Singlets	Spacing = d <sub>1</sub>		Spacing = 1.732 d <sub>1</sub>	Single Feeds (Feed diam = 2λ)	Cluster Feeds			
				Feed Diam = 0.667λ	Feed Diam = λ						
19	Contour Gain	47.5	45	53	51	70 horn	630 horn 561 SW	280 horn 245 SW	13	>78	
	Feed Loss, max	2.2	1.9	3.5	3.5	66 VPD	69 VPD 79 Phase shifters	31 VPD 35 Phase shifters	(9 beams)		
	Net gain	45.3	43.1	49.5	47.5		79 LNAs	35 LNAs			
28.8	Contour Gain	51	49	55	54	140 horn	1260 horn 1102 SW	560 horn 490 SW	28 (20 beams)	>189	
	Feed* Loss	0.9	0.9	1.3	1.3	132 VPD	138 VPD 158 Phase shifters	62 VPD 70 Phase shifters			
	Net gain	50.1	48.1	53.7	52.7		158 LNAs	70 LNAs			

\* Receive LNA after each single feed horn and between switch matrix and phase shifter in cluster feed.

\*\* 1 ms frame time.

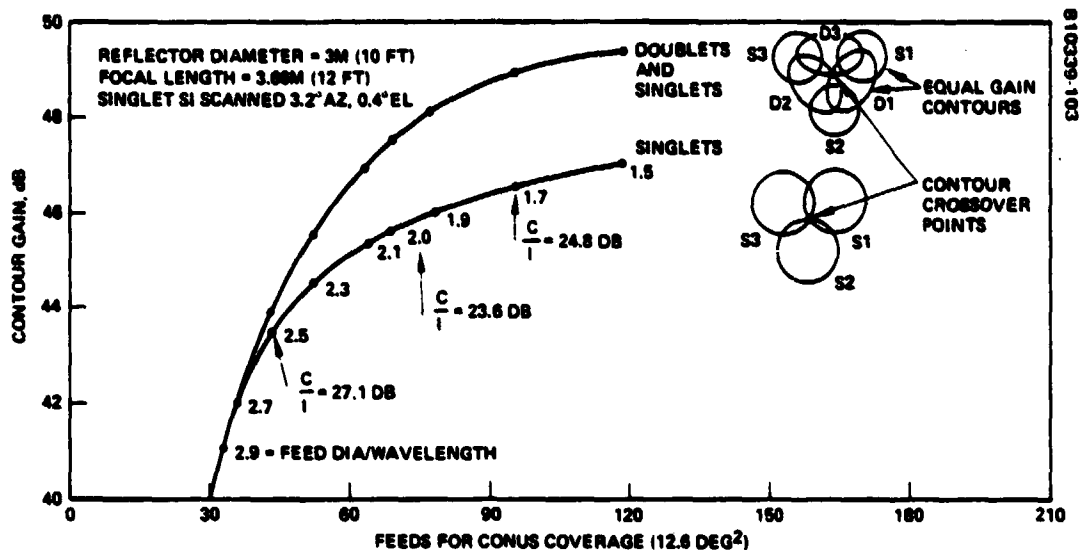


FIGURE 3.1-22. PRIME FED REFLECTOR CONTOUR GAIN AT 19 GHZ

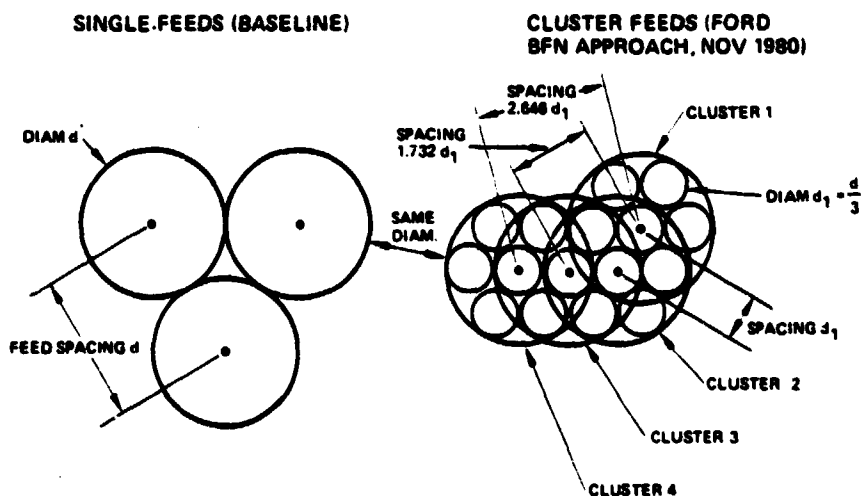


FIGURE 3.1-23. COMPARISON OF SINGLE AND CLUSTER FEED APPROACHES

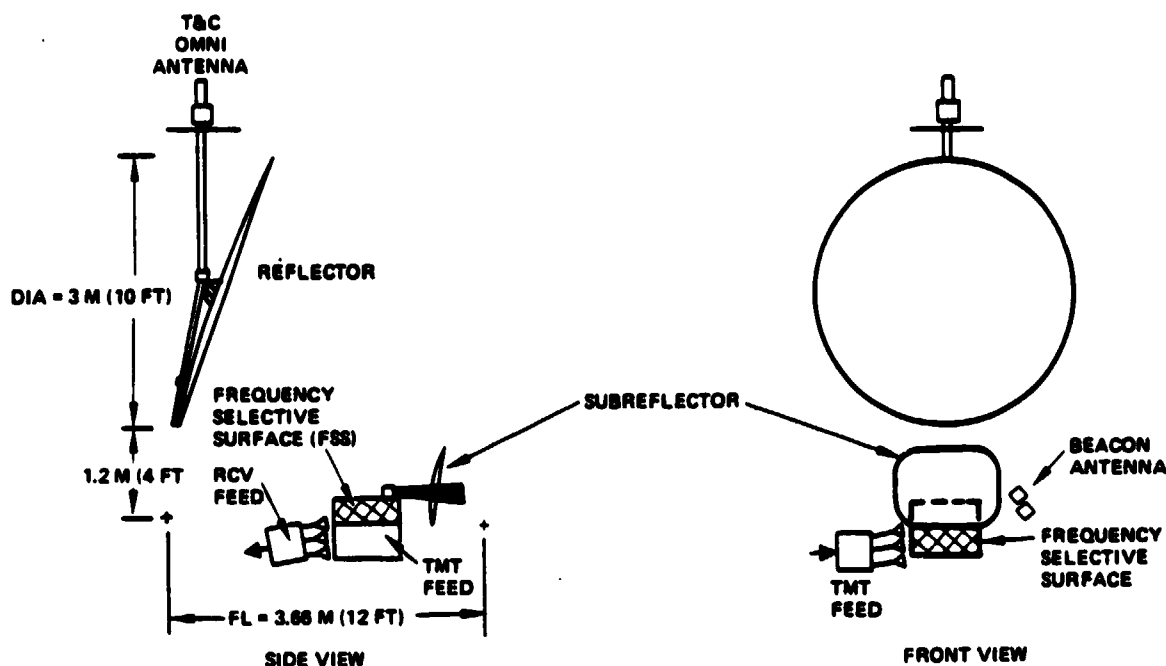


FIGURE 3.1-24. ANTENNA SUBSYSTEM CONFIGURATION

#### 3.1.4 Selected Antenna Subsystem Configuration

The selected antenna subsystem configuration is shown in side and front views in Figure 3.1-24. Three antennas comprise the subsystem: 1) communications; 2) tracking and command (T&C); and 3) beacon.

The communications antenna is an offset Cassegrain with a reflector diameter of 3 meters (10 feet) and a prime focal length of 3.66 meters (12 feet). Offset, subreflector aperture, and focal length dimensions are adjusted to allow use of a planar FSS between the subreflector and the secondary focus at which the receive feed is located. The FSS is inclined approximately  $45^\circ$  to the boresight symmetry plane of the reflector and designed for low transmission loss at receive frequencies and low reflection loss at transmit frequencies. The transmit feed is positioned at the mirror image of the secondary focus which is at the side of the FSS in the front view. This configuration spatially isolates the transmit and receive feeds and allows independent design optimization.

The T&C omni antenna uses a support structure similar to that of the SBS omni antenna. Antenna stowage and deployment will be similar to that of the SBS satellite.

The beacon antenna is an array of two pyramidal horns and is identical to the beacon antenna used on COMSTAR except perhaps for its structural support brackets.

The communications antenna performs a number of functions as described previously and the basic circuit block diagram that is used to describe how they are accomplished is given in Figure 3.1-25. There are a total of 29 receive feed horns and 15 transmit feed horns associated with the same diameter reflector and geographical coverage areas. The allocation of these feeds for accomplishing the four basic functional requirements for trunk and CPS signal routing internal and external to the subsystem is explained in the subsequent paragraphs. Low noise amplifiers (LNA) are provided at the feeds to improve system noise temperature. The LNAs are described in section 3.2 (Microwave Subsystem).

The trunking portion of the antenna has six feeds on both transmit and receive. Only one feed horn is used to generate a beam at a trunk node. Four of the six beams can be used at any time. Low speed latching switches connect either New York or Houston and either Washington, D. C. or Tampa to the transponder. Three LNAs are provided for each pair of feeds to help ensure that all trunk beams are usable with three for two redundancy.

There are two scanning beams for transmit and two for receive. Because the receive beamwidth is two-thirds that of transmit about nine-fourths as many receive horns are needed as for transmit to scan a beam over the same sector. On receive, one scanning beam serves the east coast sector with 13 spots plus an additional spot for Seattle. Two of the beam 1 spots are generated for New York and Washington, D. C. for sharing trunk feeds as shown. Low speed latching switches switch these feeds from the trunk waveguide to the CPS beam forming network. The other 11 spots have dedicated feeds. A total of fourteen horns is used therefore in the sector 1 receive beam forming network (BFN). The second scanning spot beam serves sector 2, adjacent to sector 1, also with 13 spots. One of the beam 2 spots is created by a shared Cleveland trunk feed and the remaining spots by 12 dedicated feeds. Two additional feeds for covering Denver and San Francisco are connected to the sector 2 receive BFN giving it a total of 15 feeds. The LNAs for the CPS feeds are nonredundant except for spots using trunk feeds.

Each transmit scanning beam serves six spots per sector. The sector 1 BFN shares two trunk feeds for New York and Washington D. C. and uses four dedicated feeds for the rest of the sector. Seven feeds in all are needed since an additional feed is dedicated to Seattle. The sector 2 BFN has a total of eight feeds with one trunk feed shared for Cleveland, five dedicated feeds for the rest of the sector and two dedicated feeds for Denver and San Francisco.

Four auxiliary tracking feeds are included in the receive feed clustered about the Cleveland horn to provide signals for the monopulse tracking system. As shown in Figure 3.1-26, the tracking feed array includes a sum channel horn and four auxiliary feeds which surround the sum horn. Other horns identical to the sum horn are added where necessary to ensure a uniform mutual coupling environment to all four auxiliary tracking feeds. These additional like horns can be those used for communications if the beacon is completely within one of the scanning beam contiguous areas. If the beacon

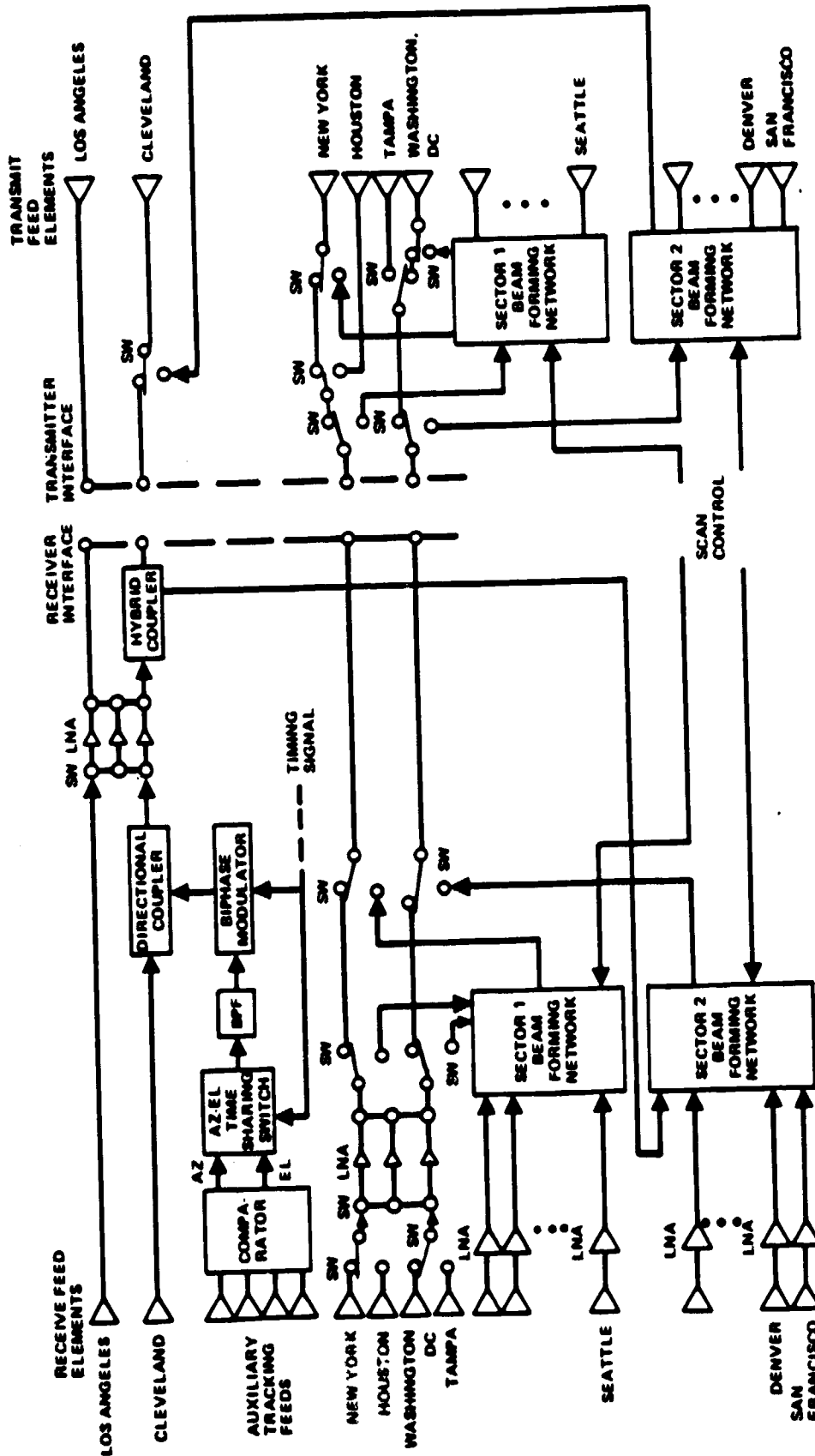


FIGURE 3.1-25. BASELINE COMMUNICATIONS ANTENNA BLOCK DIAGRAM

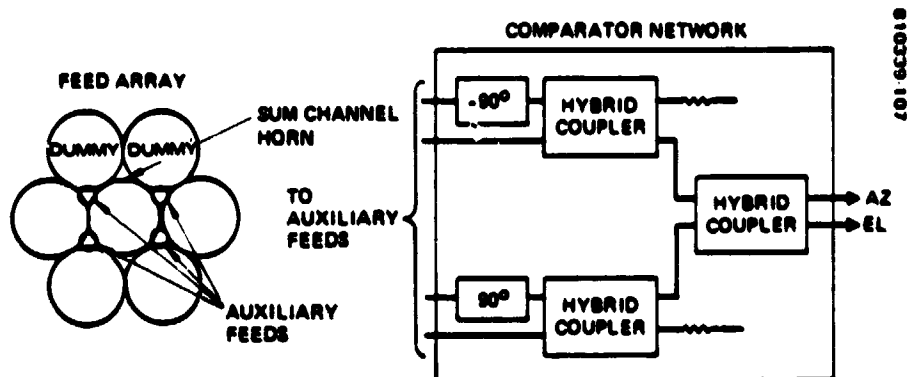


FIGURE 3.1-26. TRACKING FEED ARRAY AND COMPARATOR

is in an isolated beam, the dummy horns are not required. The three hybrid coupler comparator network with two  $90^\circ$  fixed phase shifters produces two signal pair differences, i.e., azimuth and elevation signal outputs and connects the four horn array to the remainder of the receive tracking network shown in Figure 3.1-25. This technique is being implemented in the Space Shuttle Ku band radar communications antenna system.

### 3.1.5 Option 1 Subsystem

As shown in Figure 3.1-27, the option 1 antenna subsystem uses one scanning beam feed network for receive and one for transmit with the same coverage. On receive, 16 spots can be scanned with 12 of the spots covering the baseline sector 1 area and the other four covering Cleveland, Seattle, Denver, and San Francisco. The 15 circulator switches are electronically controlled to route power from only one feed horn (see Figure 3.1-28) at a time to the sum port.

The transmit feed operates the same way as the receive feed. However, there are only 10 feed horns and nine switches.

### 3.1.6 Antenna Subsystem Weight and Power

Weight and power estimates for antenna subsystem components are given in Table 3.1-7. Major weight contributions are from the reflector and support structures. The baseline transmit and receive feed weights, including the tracking circuit, total 48 pounds or 25 percent of the total subsystem weight. For option 1 the total feed weight is 34 pounds, or 19.6 percent of the subsystem weight. Feed horns are conical and of aluminum construction. T&C omni antenna and beacon antenna weights are known quantities, since existing designs are assumed. Note that the weight of the LNAs are included in the total weight of 189 pounds for the antenna. Without the LNAs the total weight is estimated at 182.6 pounds. In section 2.1 a tradeoff between the baseline system approach with LNAs behind the receive CPS feed elements and an alternative design with fewer LNAs placed behind the CPS beam forming network at the receiver input was described. This trade will be reviewed in the next phase of the 30/20 GHz communications study program.

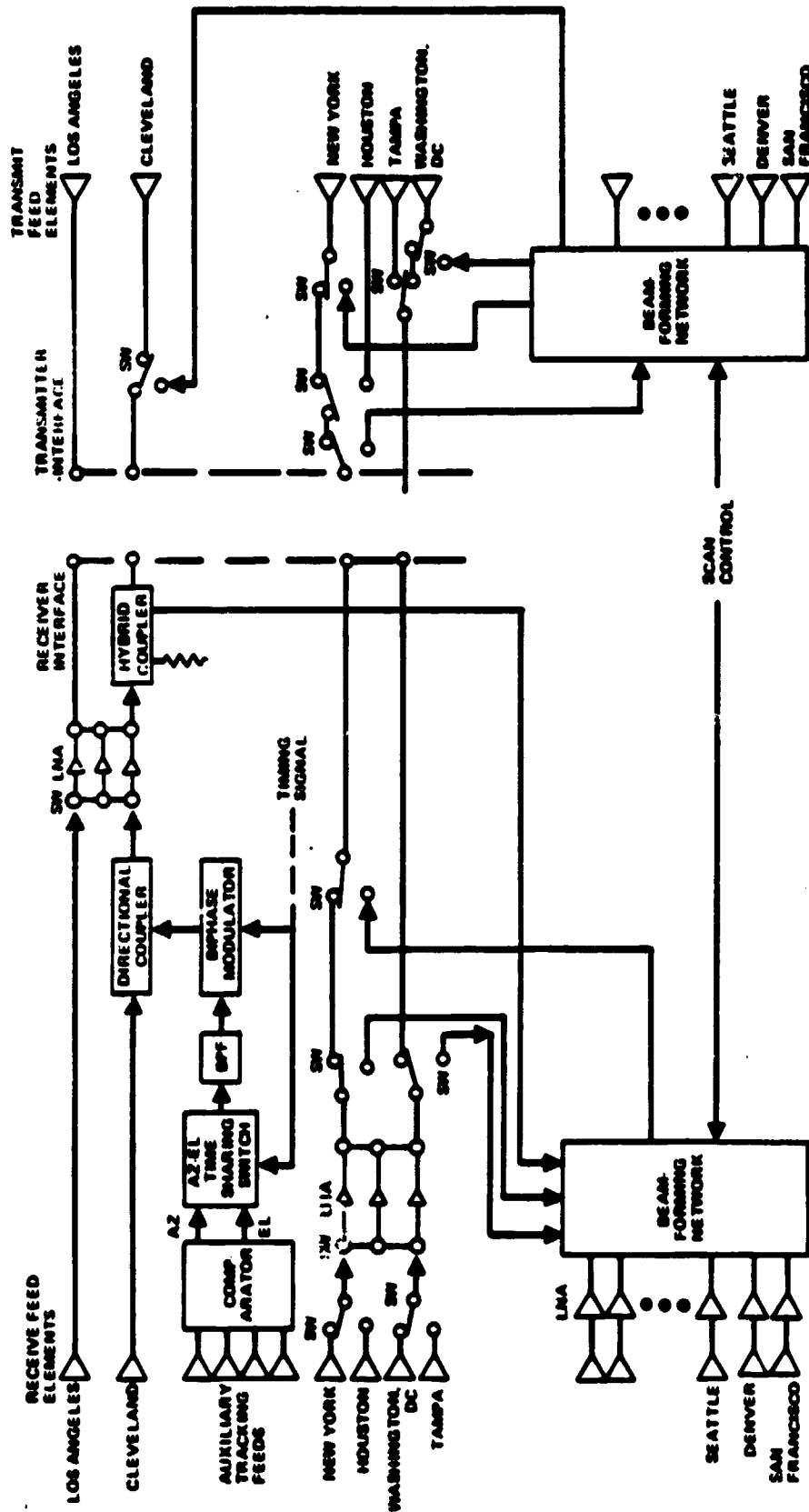


FIGURE 3.1-27. OPTION 1 COMMUNICATIONS ANTENNA BLOCK DIAGRAM



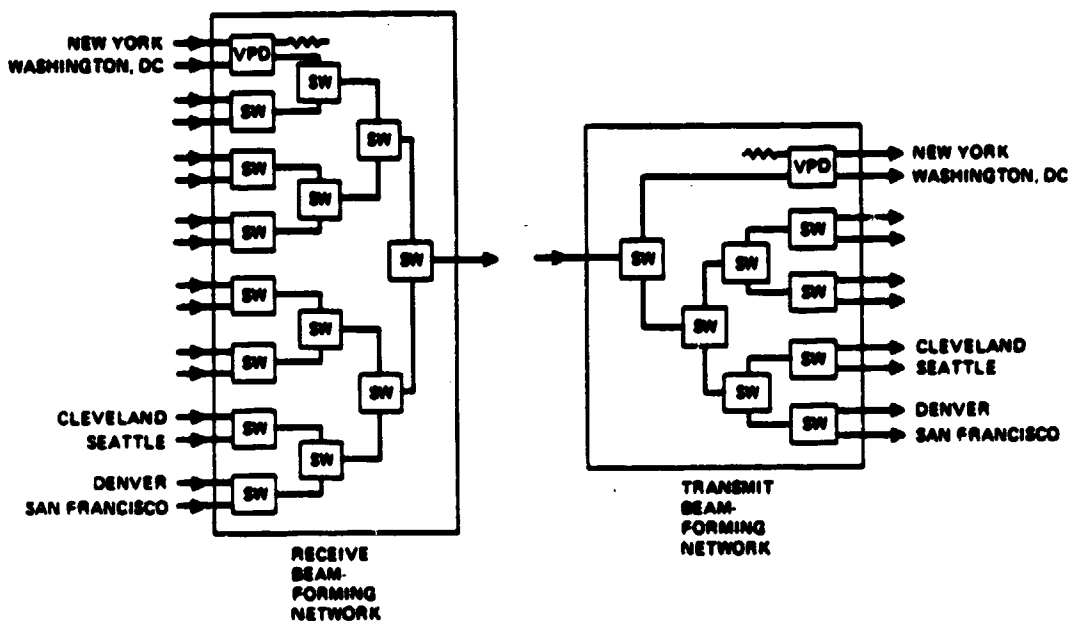


FIGURE 3.1-28. OPTION 1 SCANNING FEED NETWORKS

Also, included in Table 3.1-7 are estimates of total power consumption for the switches and VPDs in the baseline and optional subsystems for a typical uplink/downlink interconnectivity plan for which a TDMA frame time of 1 ms is divided into as many subframes as there are CPS feeds. The baseline CPS feed power consumption is nearly halved in relation to the option 1 CPS feeds. This is due to the reduction of scanning beams from two to one, which thereby reduces the number of control switches from 26 to 14 in the option 1 receive CPS feed, and from 12 to 8 in the option 1 transmit CPS feed. LNA power consumption is based on all LNAs being active except for the two redundant LNAs (baseline and option 1).

### 3.1.7 Electrical Performance

The performance estimates for the TS and CPS antenna functions for both uplink and downlink are given in Table 3.1-8. First, the calculated half-power beamwidth is given. Next, the maximum possible theoretical gains for a uniformly excited aperture (100 percent aperture efficiency) are given for reference: 55.7 dB for transmit 19 GHz and 59.3 dB receive 28.8 GHz. Below this row, the directive gains of singlets scanned 3° off boresight are given and it's these values that the link calculations and overall communications system performance are based. These gains were calculated with the aid of an offset dual reflector computer program based on scalar geometrical optics and include losses due to spillover, scan off boresight and illumination taper plus an additional area gain loss of 8.1 dB at 19 GHz and 7.1 dB at 28.8 GHz for CPS operation. These losses are listed below the resulting net directive gain since they are deduced from the net directive gain figures. The computations are based on the assumptions of a circular aperture feed horn offset from the axis onto a focal surface

TABLE 3.1-7. ANTENNA SUBSYSTEM WEIGHT AND POWER

Component	Quantity		Total Weight, lb		Total Power, W			
					Baseline		Option 1	
	Baseline	Option 1	Baseline	Option 1	CPS	Trunk	CPS	Trunk
Reflector	1	1	50	50				
Subreflector	1	1	6	6				
30/20 GHz FSS	1	1	5	5				
Receive feed								
Horn	32	19	12.8	7.6				
LNA	32	19	6.4	3.8	5.2	0.8	3.2	0.8
Low speed circulator switch	18	17	1.6	1.5	Nil	Nil	Nil	Nil
High speed circulator switch	27	15	2.4	1.4	2.4		1.4	
Transmit feed								
Horn	18	13	12.6	9.1				
Low speed circulator switch	7	6	0.7	0.6	Nil	Nil	Nil	Nil
High speed circulator switch	13	9	1.3	0.9	1.2		0.7	
Waveguide interconnection, TX and RX	1 set	1 set	6	5				
Receive tracking circuit	1	1	4	4	1	1	1	1
T&C Omni antenna	1 assembly	1 assembly	0.6	0.6				
Telemetry beacon antenna	1 assembly	1 assembly	7.8	7.8				
Support structures	1 set	1 set	61.8	60				
Miscellaneous			10	10				
Totals			189	173	9.8	1.8	6.3	1.8

\*As of 25 June 1981.

such that a singlet beam is scanned to the edge of CONUS at about  $3.2^\circ$  azimuth,  $0.4^\circ$  elevation. To obtain net directive gain the losses due to depolarization by the reflector curvature and by beam pointing error are estimated in the table below area gain loss and would have to be subtracted from the directive gains given above that row. Worst case feed losses, through the New York CPS line, are also tabulated according to major component contribution and totaled. It should be noted that the FSS losses of 0.5 dB include variation in angle of incidence of a feed produced wave over a substantially large range and over a 500 MHz bandwidth.

Finally, net gains are given based on the subtraction of estimated feed losses, beam pointing losses and polarization losses from the calculated directive gains. EIRP is simply determined by adding 16.0 dBW power to the net transmit gains in dB. Power dissipation is the conversion of feed loss to attenuation of the 40 watt input.

TABLE 3.1-8. BASELINE CPS/TS ANTENNA PERFORMANCE ESTIMATES

Cassegrain Configuration Main Reflector Dia: 3 M (10 ft)

Parameter	Service			
	Trunking		Customer Premise	
Frequency, GHz	19	28.8	19	28.8
Half power beamwidth, Deg	0.4	0.27	0.4	0.27
Directive gain of singlet on boresight, 100% aperture efficiency, dB	55.7	59.3	55.7	59.3
Losses due to illumination taper spillover and scan	2.6	3.2	2.6	3.2
Directive gain of singlet scanned 3.2° Az and 0.4° El, dB	53.1 peak	56.1 peak	53.1 peak	56.1 peak
Area gain loss due to operation off beam peak	Negligible	Negligible	8.1	7.1
Polarization loss, dB	0.1	0.1	0.1	0.1
Feed losses, dB				
Frequency selective surface (FSS)	0.5	0.5	0.5	0.5
Switching circulator, high speed	—	—	0.6	—
Switching circulator, low speed	0.5	0.2	0.3	0.2
Waveguide and horn	0.5	0.1	0.5	0.1
Net loss	1.5	0.8	1.9	0.8
Net gain, dB	51.5	55.1	43.0	48.1

### 3.1.8 Antenna Technology Assessment

Key component technology status is summarized in Table 3.1-9. New technologies are in the reflector with its large surface area and small surface tolerance, the 30 GHz LNA with a desired 5 dB noise figure and the integration of all components with a steadfast accurate alignment after reflector deployment. The reflector will be made with graphite structure that must be mechanically and temperature stable. The subreflector will also be made of graphite. For the subreflector size envisioned, experience with the Ku band Shuttle center fed reflector should extend to the hyperboloidal design without difficulty.

LNA technology status is discussed with the microwave subsystem. The integration and alignment of an offset Cassegrain antenna system with two reflectors, an FSS plate for separating transmit/receive feeds, a 30 GHz tracking feed and high speed beam forming networks using 30/20 GHz circulator switches represents a new satellite subsystem technology. The use of 30/20 GHz frequency components will place emphasis on their accurate alignment by specifying fine tolerances throughout the subsystem that significantly exceed those encountered at lower satellite communications bands.

TABLE 3.1-9. ANTENNA TECHNOLOGY ASSESSMENT

<u>Component/Activity</u>	<u>Technology Status</u>
Reflector, paraboloidal	New technology (graphite) large accurate surface
Subreflector, hyperboloidal	Ku band shuttle (graphite paraboloid)
30/20 GHz FSS	Design technique exists
Feed horn	Designs scaled from lower RF
LNA	Device expected to achieve 5.0 dB NF
High speed switch	Designs exist at other frequencies
VPD and driver	Receive: Scaled version of transmit Transmit: Existing technology
Tracking feed	Several approaches related to existing technology, e.g., Ku band shuttle radar/communications antenna
T&C omni antenna	GOES/GMS design
20 GHz beacon antenna	Existing technology
Integration	New technology

### 3. 1. 9 19 GHz BEACON ANTENNA

The 19 GHz beacon antenna which Hughes built for the COMSTAR satellites is a two horn array with two input feed ports. The ports are used to generate two spatially orthogonal linearly polarized radiation patterns for CONUS coverage. The pattern is shown in Figure 3.1-29 and is seen to have an elliptically shaped gain contour. This shape is achieved by designing the array horn elements to individually provide an azimuthal beamwidth equal to the east-west dimension of CONUS and setting the vertical array spacing and horn orientation to reduce the elevation beamwidth to the north-south dimension of CONUS. Gain coverage is about the same for both polarizations. This design provides an edge gain that is optimum.

Key design features of the antenna are that the two horns are identical pyramidal types 3 feet in length with a 5.5 inch square aperture and these are fed by a pair of both orthomode tee junctions and magic tees. Referring to the network schematic in Figure 3.1-30, an orthomode tee is connected to the throat of each horn to enable the feeding of two polarizations at the two orthomode tee isolated ports. For one polarization the two orthomode tees connect to a magic tee with the input port for the associated polarization and the fourth unused port terminated with an absorbing load. The orthogonally polarized signal is fed through the second magic tee that connects to the orthomode tees.

ORIGINAL PAGE IS  
OF POOR QUALITY

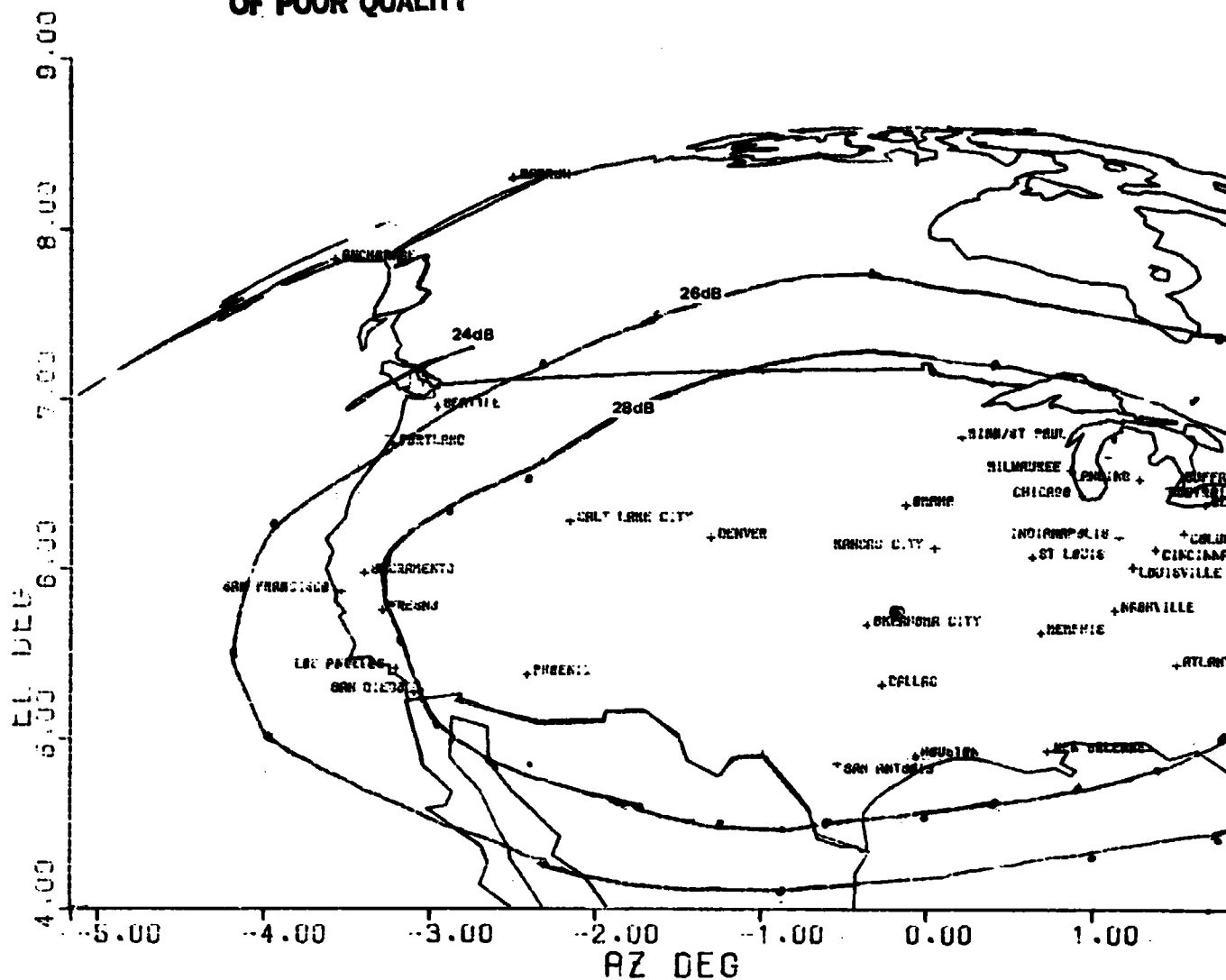


FIGURE 3.1-29. BEACON ANTENNA PATTERN

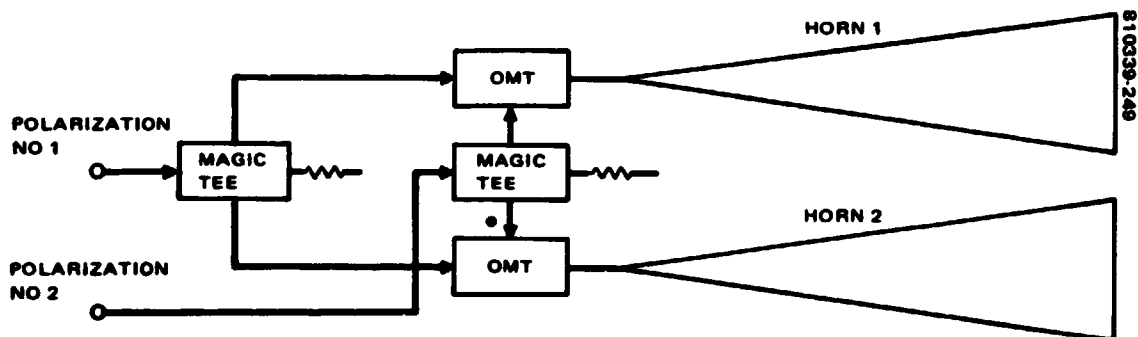
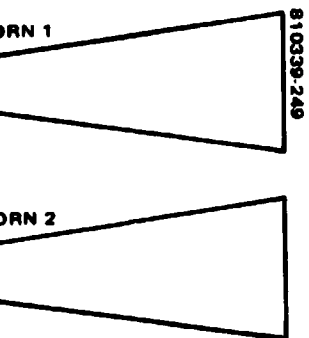
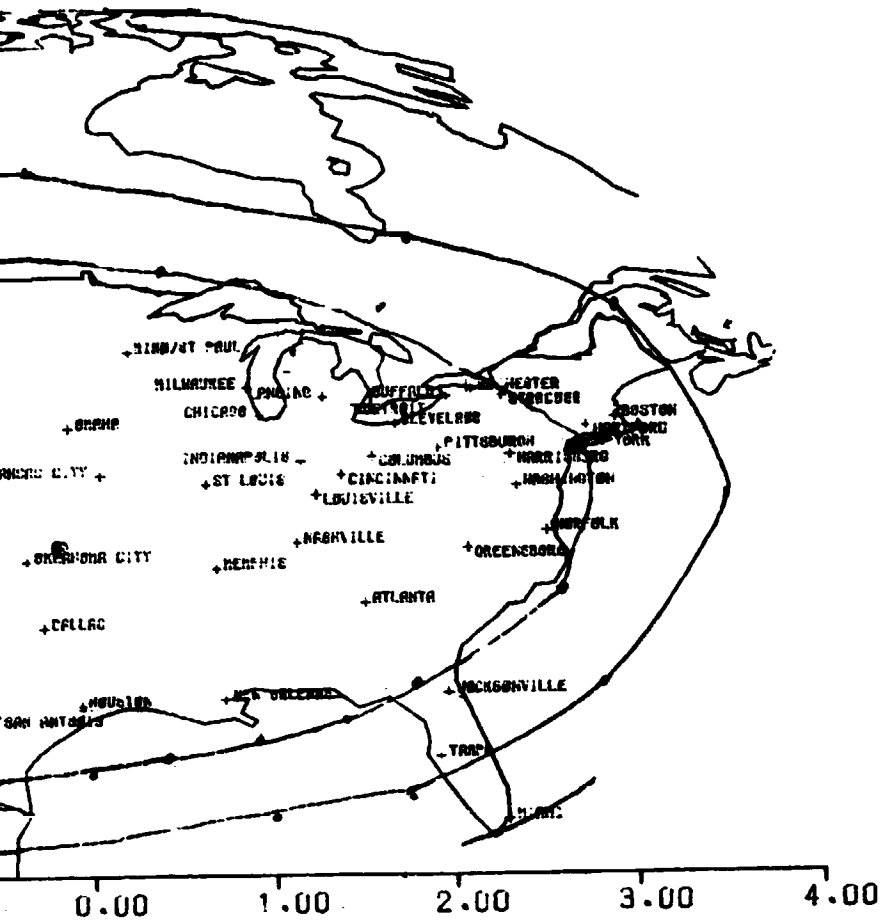


FIGURE 3.1-30. 19 GHZ BEACON ANTENNA SCHEMATIC DIAGRAM

810339-249

ORIGINAL PAGE IS  
OF POOR QUALITY



DIAGRAM

2  
BOLDOUT FRAME

## 3.2 MICROWAVE SUBSYSTEM

### 3.2.1 Requirements

The requirements are shown in the block diagram (see Figure 3.2-1) and in Table 3.2-1. In the trunk mode the microwave subsystem receives four 30 GHz inputs from the antenna. It amplifies and downconverts these inputs to IF (6 GHz) for an IF matrix which routes each input to one of four downlink transmitters. The transmitters must upconvert the signals to the 20 GHz transmit band. The high power amplifiers are specified to be 40 watt TWTAs with an efficiency of at least 40 percent. Redundancy for each pair of TWTAs is specified to be by solid state high power amplifiers (SSPA). The type of SSPA and its performance are not specified. Hughes has selected a 7.5 watt GaAs FET amplifier for this redundancy function. The rationale for selection of a GaAs FET over an IMPATT is given in Section 3.2.2.8. The 7.5 watt level was chosen as being a practical limit for this mission as well as matching the capability expected of the proof of concept models being developed for NASA by Texas Instruments and TRW. This level is adequate to close the links but with minimal rain margin.

In the CPS mode the output of two of the receivers are switched to the baseband processor. Likewise, two of the transmitters are switched to the output of the BBP. The transmitters for the CPS mode are two of the four used in the trunk mode.

TABLE 3.2-1. SOW REQUIREMENTS ON MICROWAVE SUBSYSTEM DESIGN

<u>Item</u>	<u>Requirements</u>
Trunk service	Four simultaneously active 256 Mbps trunk channels with satellite switched time division multiple access (SS TDMA)
Customer premise service (CPS)	Two uplink channels consisting of either four 32 Mbps or one 128 Mbps nominal data rate and two downlink channels with 256 Mbps transmission capability
Trunk/CPS connectivity	Provide capability for connecting two uplink channels to the baseband processor (BBP) and two outputs from BBP to two downlink channels
TWT power output and efficiency	40 watt single mode TWT, dc to RF efficiency $\geq 40\%$
Solid state power amplifier	Provide solid state power amplifiers as backup for TWTs. Power and efficiency unspecified.
IF switch matrix	The switch design shall be capable of expansion to provide 20 x 20 switching capability

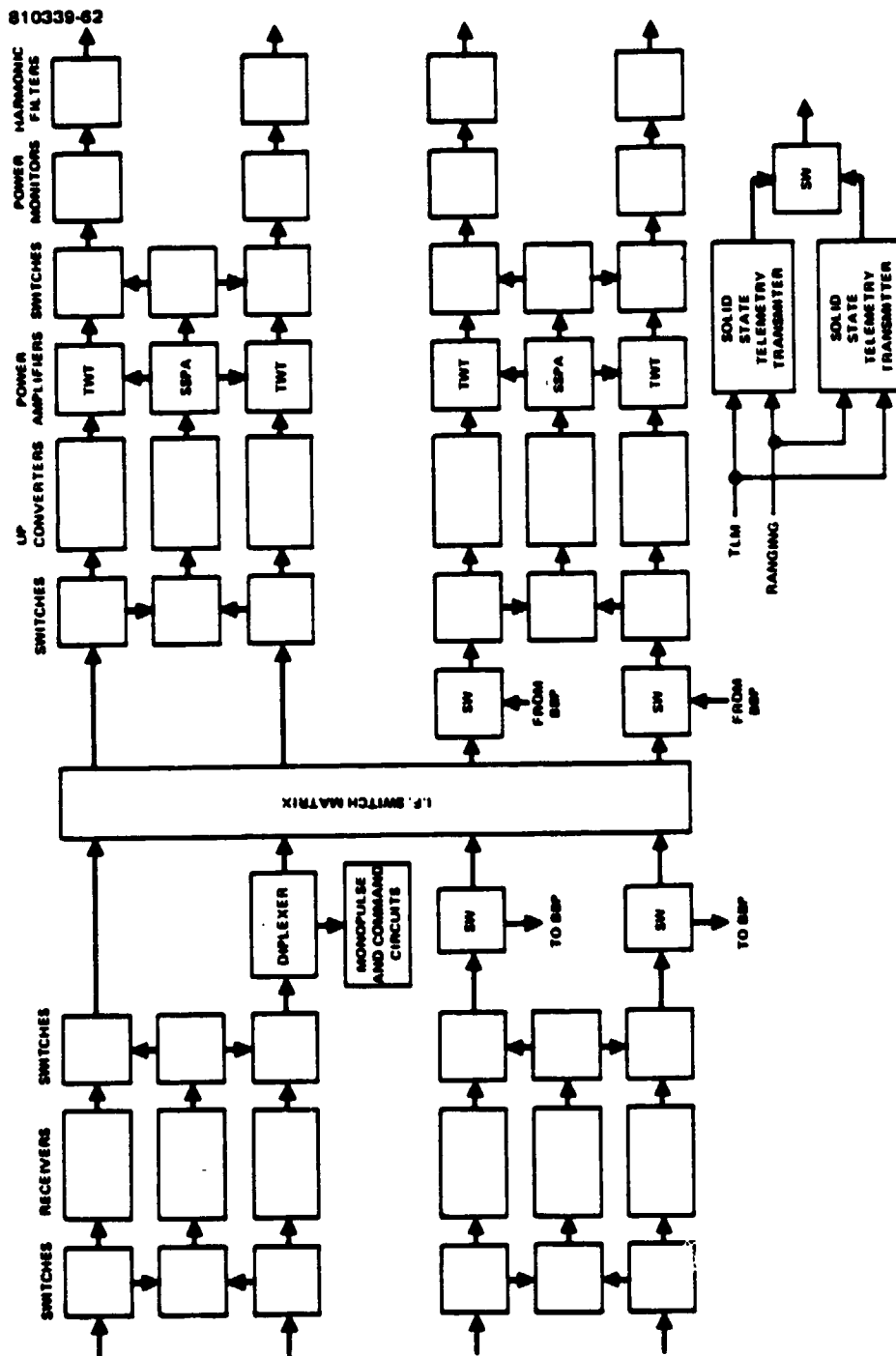


FIGURE 3.2.1. BASELINE MICROWAVE SUBSYSTEM BLOCK DIAGRAM



### 3.2.2 Subsystem Design

The subsystem configuration is, in large part, defined by the system requirements imposed by NASA. The design of the components of this configuration is discussed in section 3.2.2.5. Before turning to the subsystem components it is necessary to define a number of subsystem characteristics.

#### 3.2.2.1 Frequency Plan

The microwave subsystem frequency plan selection is based upon the considerations listed below:

- 1) Compatibility with the entire available frequency band
- 2) Spurious responses
- 3) Simplicity of local oscillator design
- 4) Compatibility with IF TDMA switch matrix
- 5) Avoidance of spectral inversion

The frequency plan chosen should meet the criteria listed in items 2 through 5 over the entire band available for use i. e., 27.5 to 30 GHz for the uplink and 17.7 to 20.2 GHz for the downlink. The requirement to use a SS TDMA switch dictates that a dual conversion frequency plan be used since implementation of this switch at the output frequency range is very difficult and costly. Ease of local oscillator implementation and the desire to avoid spectral inversion leads to the use of low side downconversion and upconversion to avoid the generation of very high local oscillator frequencies.

Figure 3.2-2 shows the frequency plan selected for downconversion to the IF and upconversion to the output frequency bands.

#### 3.2.2.2. Gain Distribution and Level Control

Figure 3.2-3 and 3.2-4 show the gain distribution and signal levels for the CPS and trunk service links. The level associated with each stage is the level at the input of the stage above the level number given in each block. The signal level at the antenna output is calculated from the system noise density, data rate, and uplink  $E_b/N_0$  data as given in the link budgets of section 2.1 of this report.

The solid state power amplifiers are not shown in Figures 3.2-3 and 3.2-4, however the SSPA gain is approximately 7.5 dB less than the TWT and is consistent with the SSPA power output of 7 watts. Automatic gain control (AGC) is implemented in the IF amplifier section of the upconverter. The AGC is placed in this unit so that it can compensate for gain variations of all components prior to the upconverter. The AGC dynamic range requirement is determined by the minimum input level for the CPS application and

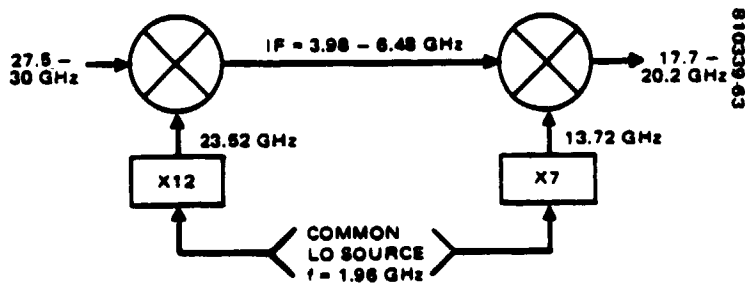


FIGURE 3.2-2. FREQUENCY CONVERSION PLAN

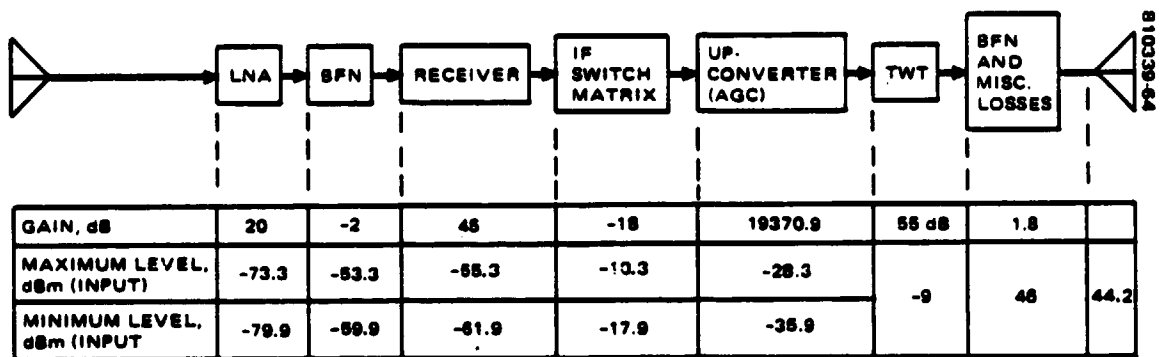


FIGURE 3.2-3. CPS GAIN DISTRIBUTION AND LEVELS

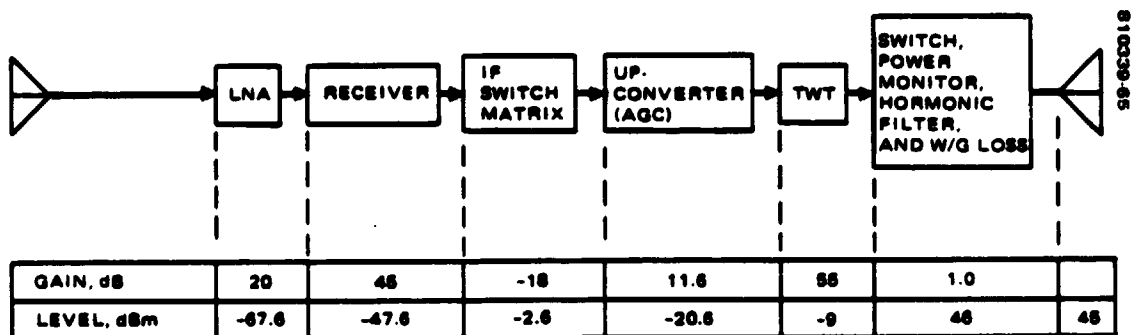


FIGURE 3.2-4. TRUNK GAIN DISTRIBUTION AND LEVELS

the maximum upconverter input level associated with the higher data rate trunk service. This level range is 15.3 dB; the actual design requirement of 20 dB includes margin for gain drift of all components preceding the upconverter.

### 3.2.2.3 Telemetry, Tracking, and Command

The system design includes a TT&C function in the 30/20 GHz band. This capability is backed up by an S band system discussed in Section 4.1. The 30 GHz command and ranging carrier is also modulated with the monopulse tracking error modulators. A diplexer following one of the receivers separates this carrier from the communication signal. The monopulse and command circuits demodulate command and ranging to baseband signals and convert the monopulse tracking modulators to dc error signals. The telemetry transmitter combines the telemetry and ranging signals and modulates the resulting signal on the telemetry carrier.

### 3.2.2.4 Receiver Design

As discussed in Section 2.1 the satellite payload has been configured with LNAs at the antenna receive feeds. The total receiver function is then divided between the LNAs and the receiver.

#### 3.2.2.4.1 Low Noise Amplifier Design

The LNA provides low noise amplification with sufficient gain to establish the communications repeater noise figure. A low noise amplifier based upon GaAs FET devices has been chosen for its combination of low noise figure and its weight and power. A four or five stage GaAs FET low noise amplifier will weigh less than 0.25 lb, require approximately 0.2 watts of regulated power and enable a system design based upon a 5 dB uplink receiving subsystem noise figure. If a 0.1 dB post-LNA contribution is allowed which is consistent with an LNA gain of 20 dB and a receiver noise figure of 7.5 dB then the LNA noise figure should be 4.9 dB and the gain should be at least 20 dB.

Figure 3.2-5 is a family of curves which show system noise figure as a function of the number of stages with device gain and noise figure as parameters. The data given in the figure include a loss of 0.15 dB for the loss of the waveguide junction circulator at the amplifier input. The loss in the waveguide which connects the antenna feed to the amplifier is part of the antenna gain budget. To achieve the desired system noise figure it is apparent that a device noise figure of about 3.5 dB with an associated low noise gain of 4.5 to 5.0 dB is required.

The low noise amplifier using such a device is a four stage amplifier consisting of a waveguide circulator at the input and two waveguide mounted microwave integrated circuit (MIC) amplifiers each having two GaAs FET low noise devices. An additional waveguide circulator is used between the two sections of the amplifier. Figure 3.2-6 shows the configuration of a two stage waveguide mounted amplifier.

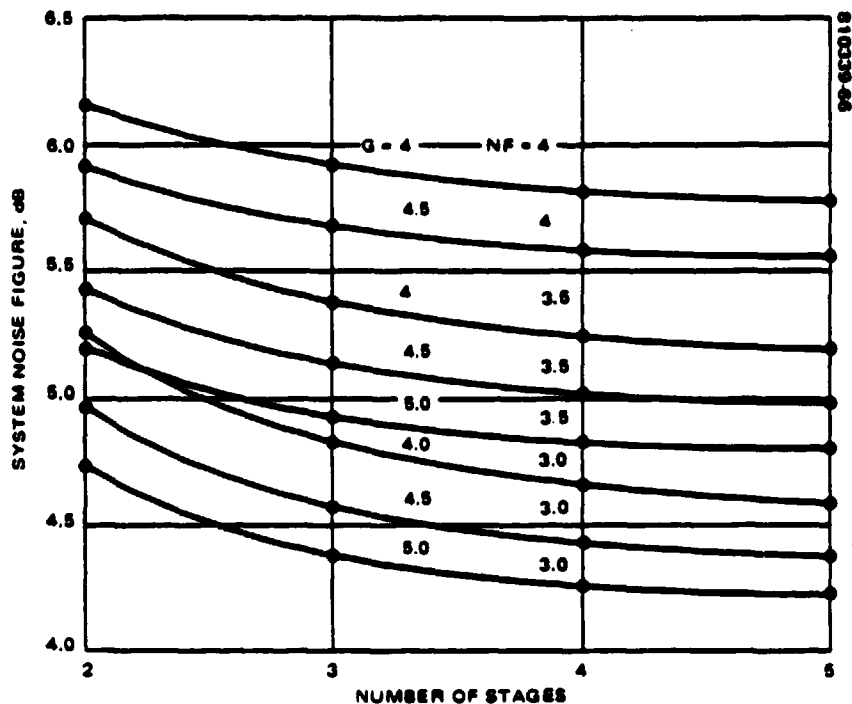


FIGURE 3.2-5. SYSTEM NOISE FIGURE

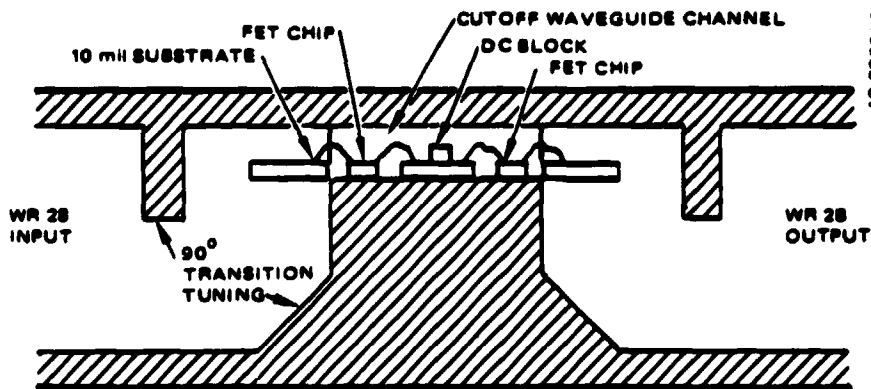


FIGURE 3.2-6. TWO STAGE AMPLIFIER CONFIGURATION

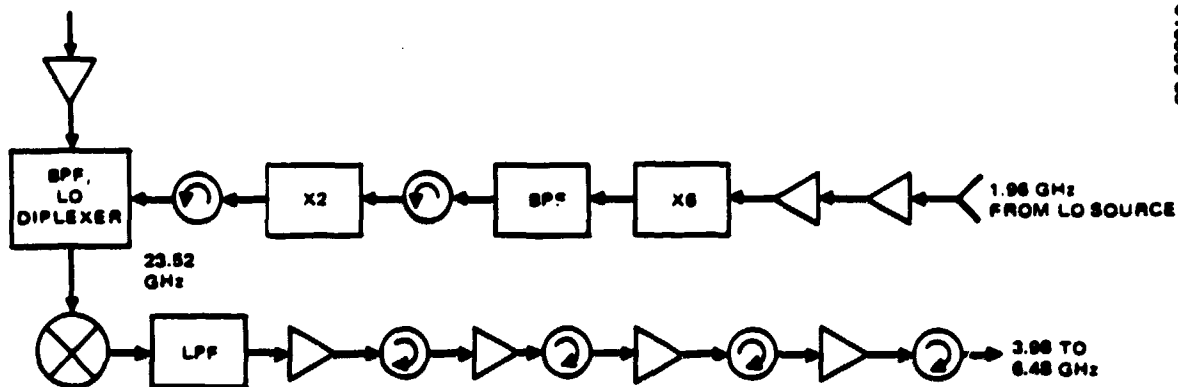


FIGURE 3.2-7. BASELINE RECEIVER

### **3.2.2.4.2 Receiver Design**

Figure 3.2-7 is a block diagram of the system receiver. The receiver includes one low noise RF amplification stage, a single ended waveguide first mixer, the first local oscillator times 12 frequency multiplier, and a four stage IF amplifier.

The low noise RF stage is used to reduce overall receiver noise figure to permit the use of a simple first mixer rather than resorting to an image enhancement mixer. Receiver noise figure is 7.5 dB which adds only 0.1 dB to the noise figure of the low noise amplifier. The receiver noise figure is based on an RF amplifier noise figure of 5 dB and gain of 5 dB, a mixer conversion loss of 6 dB, and an IF noise figure of 3 dB.

The first local oscillator and the input signal are summed in a common junction diplexer consisting of a bandpass filter centered at the signal frequency and a bandpass filter centered at the local oscillator frequency. The signal bandpass filter is a three pole, iris coupled, 0.1 dB ripple Chebyshev type and establishes the communications channel noise bandwidth. Equal ripple bandwidth of the filter is 600 MHz since the receiver must accommodate a data rate of 256 Mbps QPSK data and either one of two channel frequencies separated by 300 MHz. Figure 3.2-8 shows the construction of the mixer and diplexer.

A low pass filter which has a cutoff frequency of approximately 7 GHz is used following the mixer to reject signal and local oscillator frequencies.

The four stage IF amplifier uses high gain (12 dB per stage), low noise GaAs FET amplifiers. Circulators are used between each stage to reduce amplitude and phase ripple caused by amplifier mismatch.

Construction of the receiver is in MICs except for the first mixer and the final times two frequency multiplier of the local oscillator chain.

### **3.2.2.5 IF Switch Matrix Design**

There are three primary areas of design trades in the design of the IF switch matrix: 1) architecture; 2) device selection; and 3) method of implementing redundancy. The most important consideration in the first, architecture, is the requirement that the switch design be capable of expansion to a 20 by 20 switch. Hughes has conducted trade studies in-house which lead to the conclusion that the coupled crossbar design is the favored approach. For this configuration can be easily packaged, made internally redundant, used in a broadcast mode, and it is smaller in size and weight especially in high order matrix switches.

The second tradeoff to be made in switch matrix design is device selection. Again previous trade studies clearly favor the use of GaAs FET switching devices because of superior performance in power consumption and

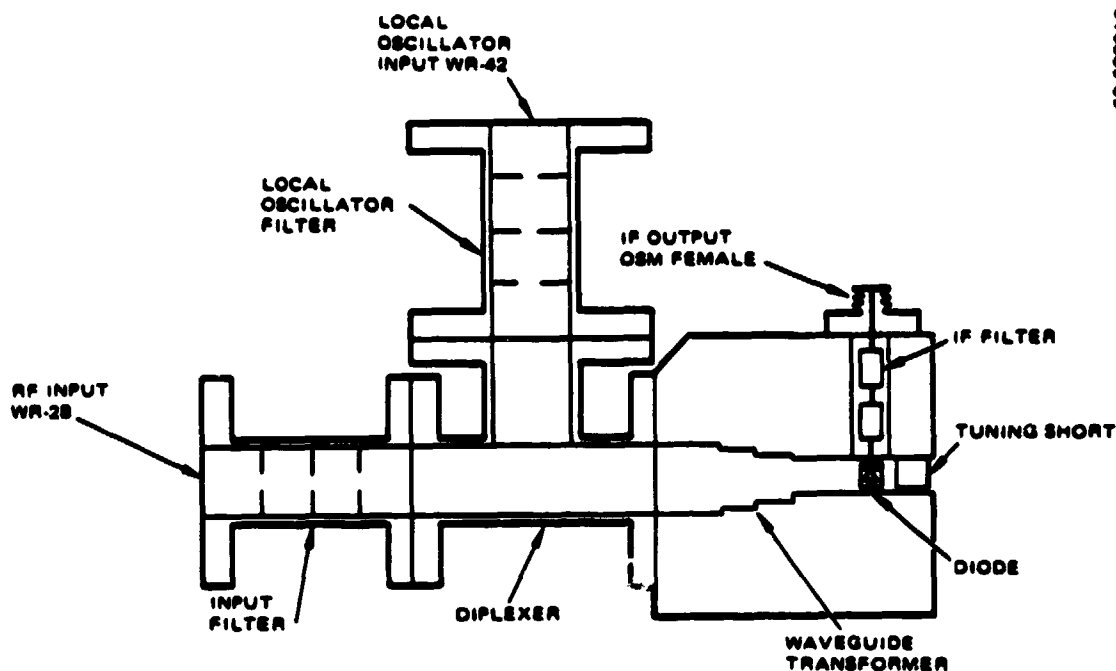


FIGURE 3.2-8. MIXER CONFIGURATION

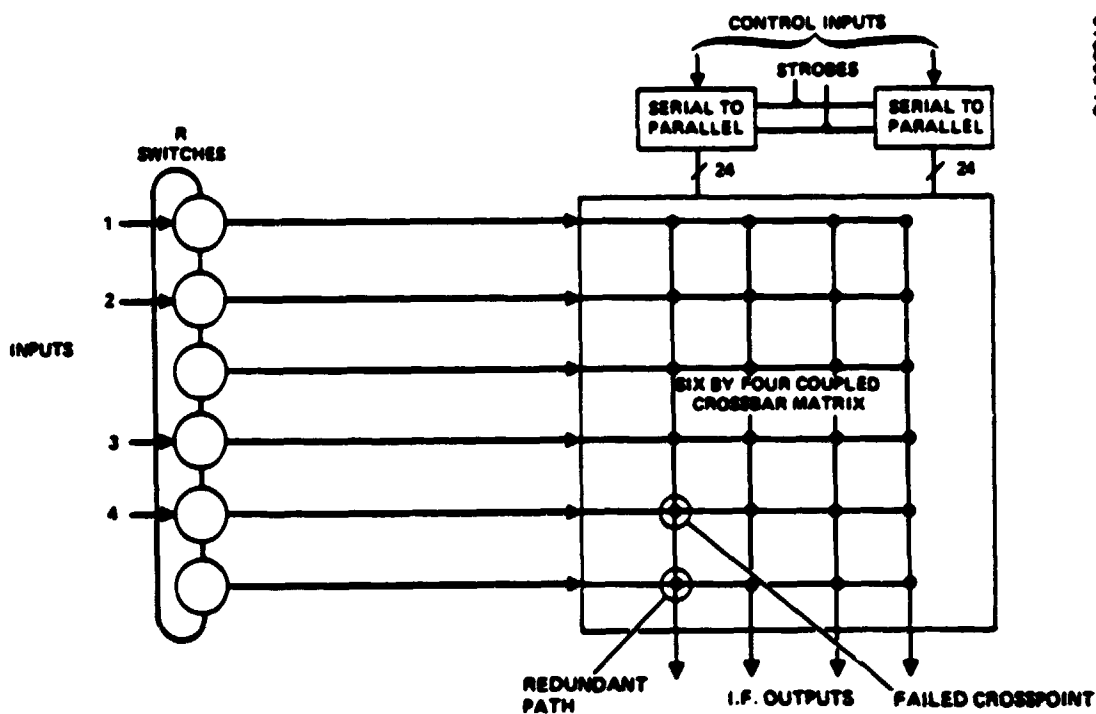


FIGURE 3.2-9. IF SWITCH MATRIX CONCEPT

switching speed. A secondary tradeoff concerns the choice between the use of passive FET switches or active amplifier switches. The passive FET switch is somewhat more reliable, and is easily implemented in monolithic MIC, but has the disadvantage that gain must be provided to make up for switch loss. The switched amplifier is more difficult to implement in monolithic MIC form, but has the advantage of reducing overall insertion loss by virtue of its gain in the ON-state, and also provides greater ON/OFF isolation per FET device. The loss associated with the use of passive switches can be made up by IF amplification. If the order of the matrix is high enough to cause very high loss (>50 dB) it might not be possible to avoid degradation of system temperature without driving amplifiers into saturation. In this case an active amplifier switch would be adopted. For this design study the passive FET switch has been selected for its greater reliability and its ability to be implemented in a monolithic MIC circuit. This choice appears to still result in a design which can be extrapolated to the higher order matrices of an operational system; however the device selection will be reconsidered in the next phase.

The third design trade concerns the method of implementing redundancy. Again previous in-house trade studies clearly favor the use of the wraparound internal redundancy technique over other possible approaches.

The basic concept of the IF switch matrix is shown in Figure 3.2-9. Redundant serial to parallel converters are used to convert the serial command data from the switch matrix digital control unit to parallel on/off signals routed to each crosspoint of the coupled crossbar switch matrix. The redundant on/off crosspoint control signals are combined in a diode "or" circuit contained in the switch driver circuit used with each crosspoint.

The six "R" switches at the inputs are used to select redundant paths by routing the appropriate input signal to a redundant path. This is accomplished by changing the digital control unit program memory when a failure is detected.

Figure 3.2-10 shows the detail of the switch crosspoint. Each crosspoint consists of a coupler and dual FET passive switch mounted on the input module, the same circuits mounted on the output module, and the feed through which couples between the two modules. In the concept illustrated in Figure 3.2-10, the power coupling ratios are graduated to achieve minimum loss and equal coupling losses independent of the path selected.

The dual FET switch consists of two switched FETs in series on a monolithic MIC chip. These chips have been developed, built, and tested at Hughes. The mask set for these chips is shown in Figure 3.2-11.

Ongoing trade studies may result in changes in three areas: 1) to change the redundancy concept by eliminating the coaxial "R" switches and using a 6 by 6 matrix with a full wraparound redundancy concept; 2) use of a single active switched FET amplifier in place of the dual FET passive

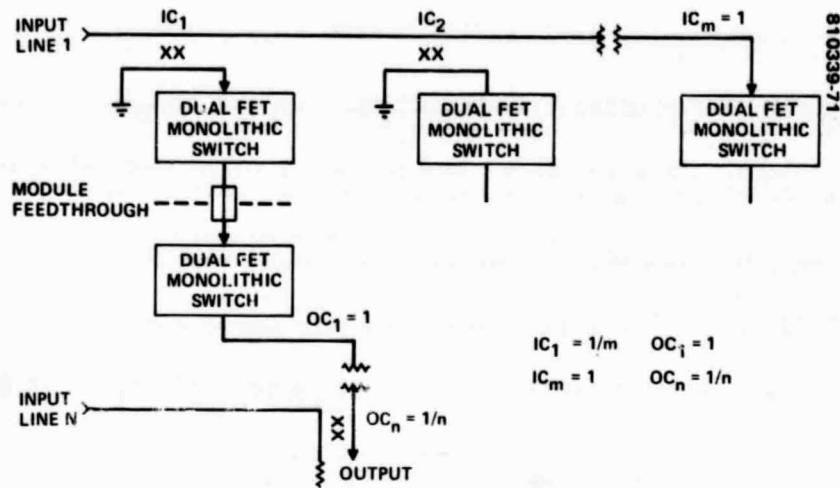


FIGURE 3.2-10. CROSSBAR COUPLER SWITCHPOINT DETAIL

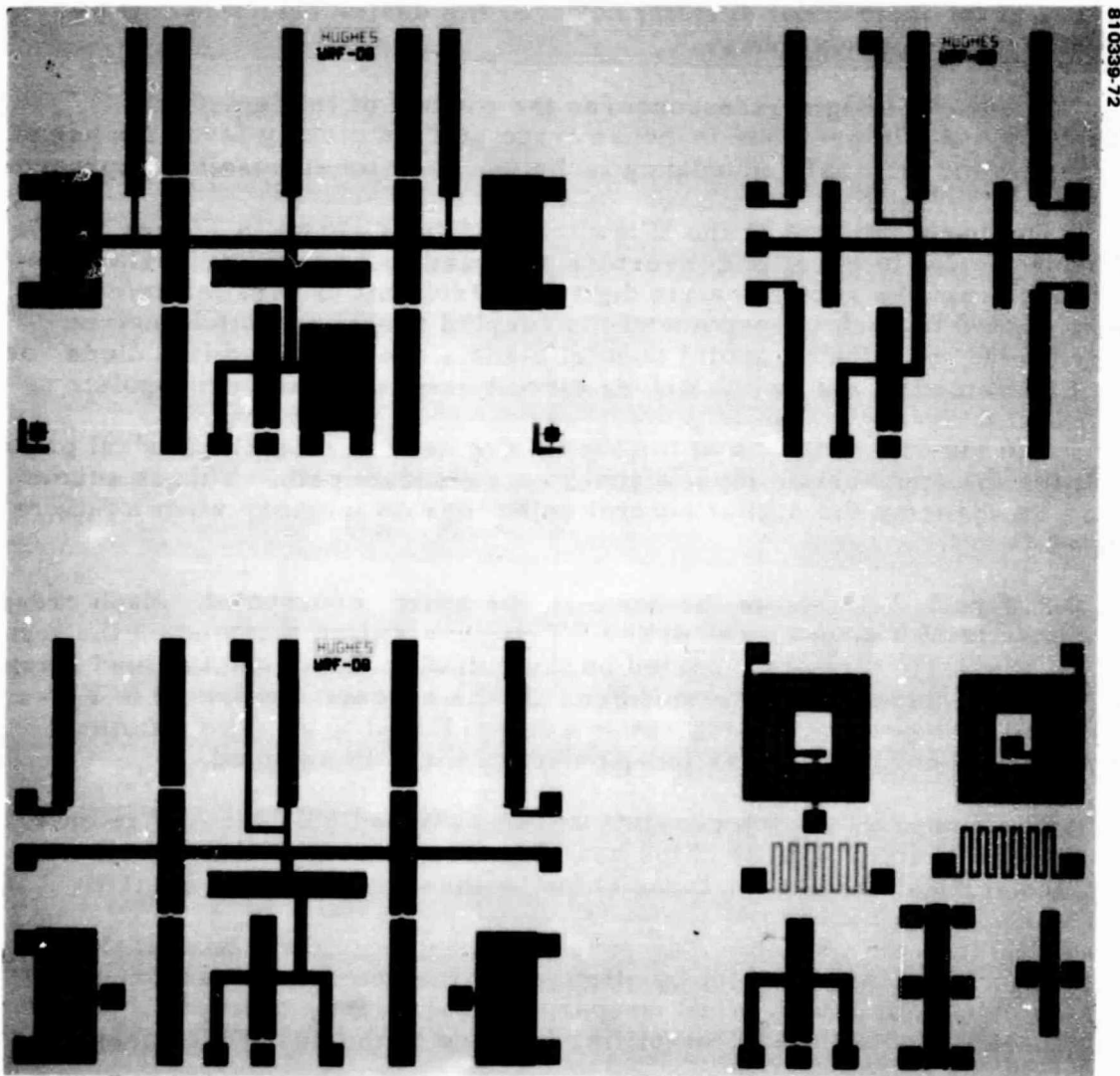


FIGURE 3.2-11. MASK SET FOR MULTIPLE FET CHIP SWITCH ELEMENT



switch as discussed above; and 3) use of uniform loose coupling instead of graduated minimum loss coupling.

### 3.2.2.6 Upconverter Design

Figure 3.2-12 is a block diagram of the upconverter. A three stage IF amplifier amplifies the signal prior to upconversion. The output of the third stage is sampled, detected, amplified, filtered, and used to control a current controlled diode AGC attenuator to maintain a constant signal level at the input to the upconverter mixer. The mixer is a balanced two diode MIC mixer since conversion loss is not critical. The bandpass filter following the mixer is a three pole, 0.1 dB ripple. Chebyshev filter constructed in waveguide. This filter has an equal ripple bandwidth of 2 GHz. Net gain of the upconverter from IF input to RF output is 30 dB when the AGC attenuation is minimum. AGC control range is 20 dB. All circuits except the output bandpass filter are constructed in MIC.

### 3.2.2.7 TWT Characteristics

Table 3.2-2 gives the TWT and the TWT power supply characteristics. These characteristics are based upon a recent proposal made by Hughes Electron Dynamics Division for a 36 watt TWT at the same frequency.

### 3.2.2.8 Solid State High Power Amplifier Design

Table 3.2-3 is a comparison of the two design approaches considered for the SSPA. At this point in time IMPATT is capable of higher device power capability and higher efficiency; however, the GaAs FET power technology is rapidly changing. The comparison in one year could change in favor of the GaAs FET as device power capability and efficiency can be expected to improve and the GaAs FET approach has significant advantages in several other respects.

TABLE 3.2-2. TWTA CHARACTERISTICS

• Helix type	
• Three collectors for high efficiency	
• Frequency range	17.7 to 30.2 GHz
• Saturated gain	55 dB
• Saturated power output	40 W
• Efficiency	40% TWT 90% high voltage supply* 36% overall
• Weight, lb	
TWT	3
Power supply	7

\*Constant current linear regulator, efficiency at min or EOL bus voltage = 90%.

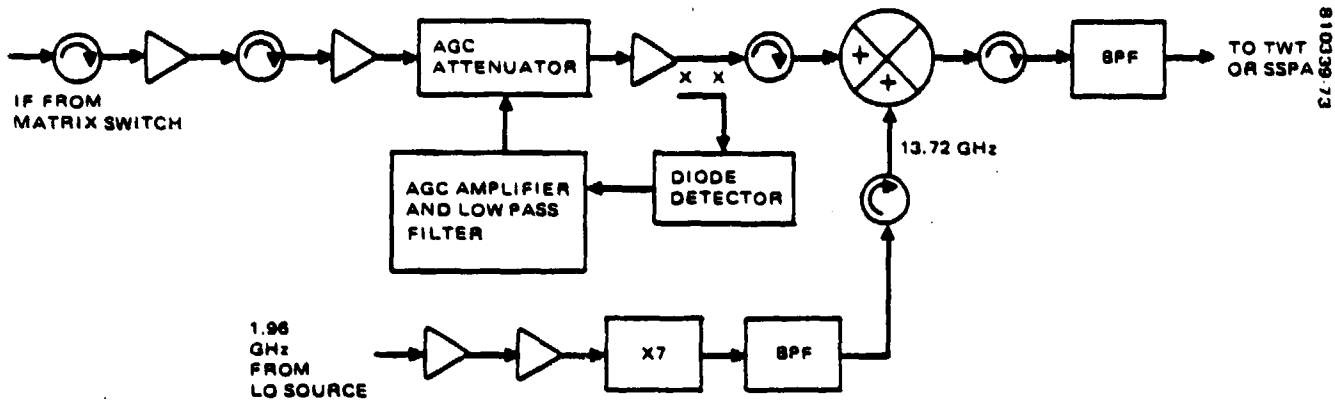


FIGURE 3.2-12. UPCONVERTER DESIGN

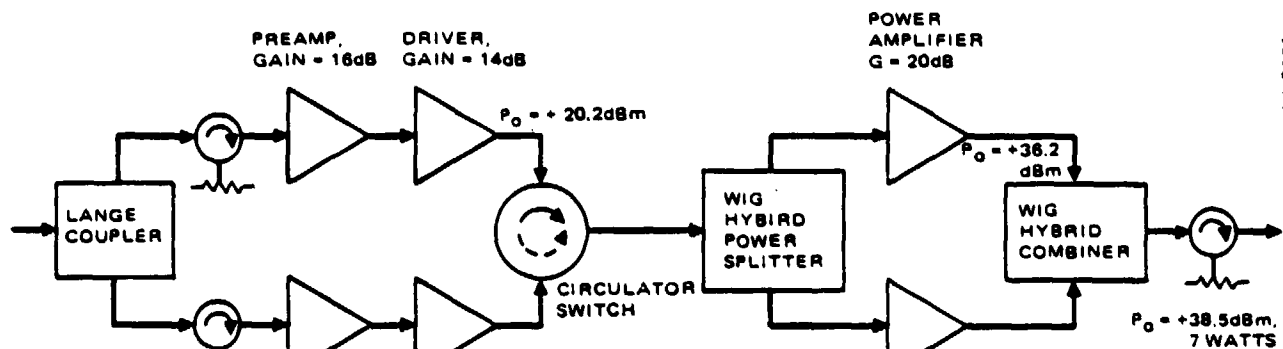
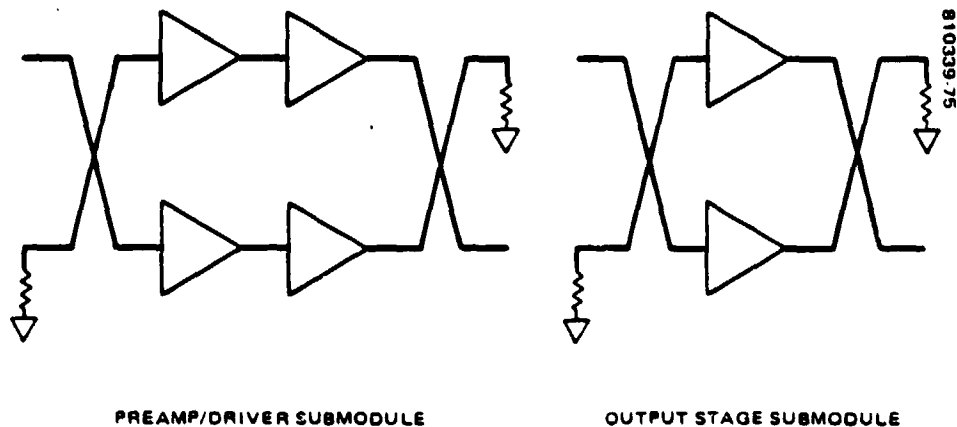


FIGURE 3.2-13. 7 WATT GaAs FET SSPA



PREAMP/DRIVER SUBMODULE

OUTPUT STAGE SUBMODULE

FIGURE 3.2-14. FET SUBMODULE CONFIGURATION

TABLE 3.2-3. SSPA COMPARISON

Parameter	GaAs FET Design	Impatt Design
Efficiency, % (including power supply)	10	15
RF power output, W	7	7
Total number of GaAs FET preamp devices	12	18
Total number of high power devices	36	6 (2 watt), 3 (4.5 to 5 watt diodes)
Bandwidth	>1 GHz easily achievable	Gain/bandwidth tradeoff
Stability	Unconditionally stable	Negative resistance device
Effects on modulated signal fidelity	Negligible	Potential problem area for injection locked design
Power device junction, temperature, °C	≤100	200 to 250
Supply voltages, volt	8 to 15	70 to 80; tight regulation required
Growth capability	Greater potential	Mature technology

A block diagram of the SSPA is shown in Figure 3.2-13. Overall transmitter gain is 48 dB. The chain consists of modularized building blocks with two 4 watt output stage modules combined with a short slot waveguide hybrid combiner to achieve the final output power. The short slot 90° waveguide hybrid has the advantages of compact dimensions, waveguide bandwidth, and low loss. The system includes redundancy in the preamp/driver chain with a circulator switch at the output. The driver power output will be on the order of 130 mW, operating at or near Class A operation. The driver output is split, again by a short slot waveguide hybrid splitter. The final amplification/power stage of the 4 watt module will consist of four 1 watt balanced amplifier submodules combined with a planar MIC combiner. A planar four way MIC combiner has been used at 15 GHz and provides the greatest flexibility in terms of size and ease of integration.

Each of the two 4 watt output modules as well as the preamp and driver units will use balanced submodules as building blocks. A balanced amplifier approach allows for direct series cascading of submodules while maintaining bandwidth and minimizing VSWR ripple without the need for interstage isolators. A balanced amplifier configuration in the power submodules enables use of higher gain devices with lower power levels. Broader bandwidths can be achieved by matching to the higher impedance levels of the lower power devices; also improved heat dissipation can be achieved. The block diagrams for the submodules are shown in Figure 3.2-14.

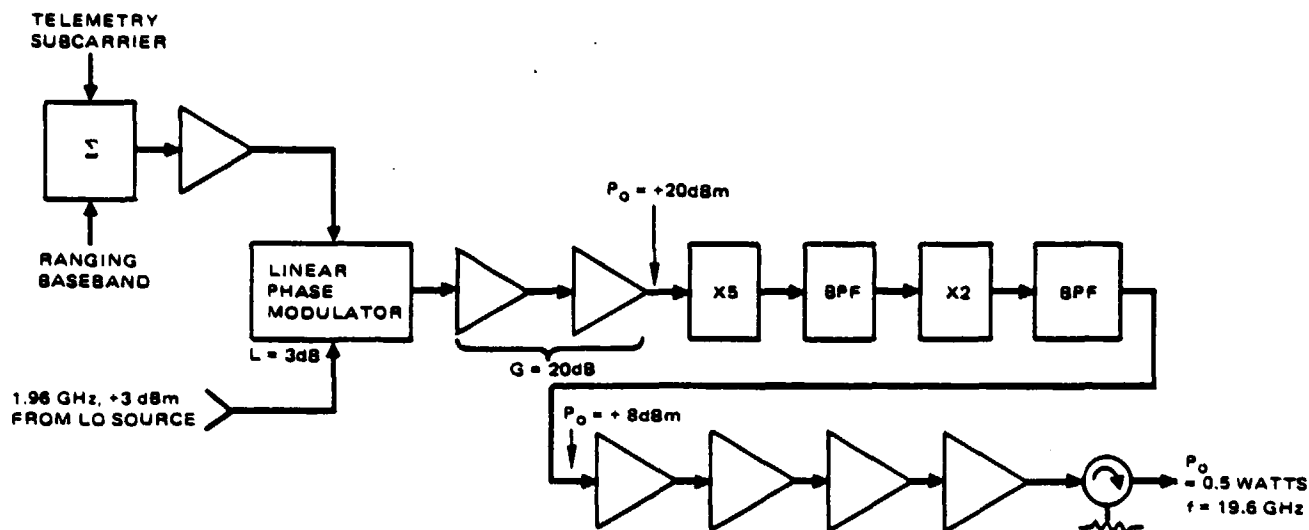


FIGURE 3.2-15. TELEMETRY TRANSMITTER

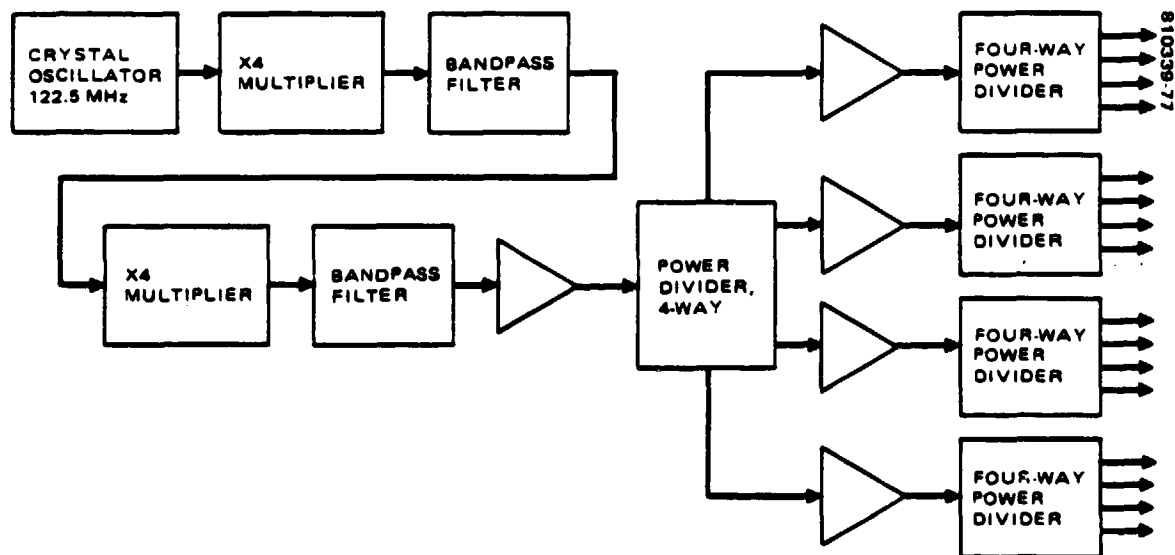


FIGURE 3.2-16. LOCAL OSCILLATOR SOURCE DESIGN

### 3.2.2.9 Telemetry Transmitter

The telemetry transmitter block diagram is shown in Figure 3.2-15. The telemetry subcarrier and the ranging baseband from the uplink command receiver circuits are combined and used to linearly phase modulate a 1.96 GHz carrier from the local oscillator source. A times ten frequency multiplier multiplies the 1.96 GHz carrier to 19.6 GHz. A four stage GaAs FET power amplifier provides a one-half watt power output.

### 3.2.2.10 Local Oscillator Source Design

Figure 3.2-16 is a block diagram of the local oscillator source. The crystal oscillator frequency is set relatively high to reduce the frequency multiplication ratio. This also reduces the phase noise generated in the local oscillator frequency multiplier chain. The crystal oscillator is housed in a temperature controlled enclosure to ensure good frequency stability.

The crystal oscillator is frequency multiplied by 16 in two cascaded X4 frequency multipliers. Each X4 multiplier stage is followed by a bandpass filter which attenuates undesired harmonics generated in the multipliers.

The output of the X16 multiplier is then amplified and power split in a four way power divider consisting of three 3 dB hybrids. Each output of the four way divider is amplified and again divided in a four way power divider to provide the capability of 16 outputs, 14 of which are required by the microwave subsystem. The two unused outputs are terminated.

Two identical local oscillator sources are used in the microwave subsystem and both have power on so that individual outputs can be selected in the event of a failure.

### 3.2.2.11 Monopulse Tracking Microwave Circuits

The implementation of the antenna monopulse angle tracking function is shown in Figure 3.2-17. A single channel monopulse technique used successfully in previous space programs provides angle tracking. The antenna uses four different feeds symmetrically spaced about the sum channel feed horn and a comparator network of three waveguide magic tees to generate azimuth and elevation error signals. These error signals are time-shared by a circulator switch which alternately selects one or the other. The time-shared signal then goes through a bandpass filter which passes the command carrier but rejects data carriers. The error signal is processed in a line length modulator with two circulator switches. The resulting biphasemodulated error signal is summed in a directional coupler with the sum signal and the relative phase adjusted to produce amplitude modulation of the received uplink command carrier. The combined signal is then amplified and converted to IF by the LNA and the receiver. The diplexer following the receiver separates the receiver IF output into data and command carrier outputs. The command carrier, amplitude modulated with error signal

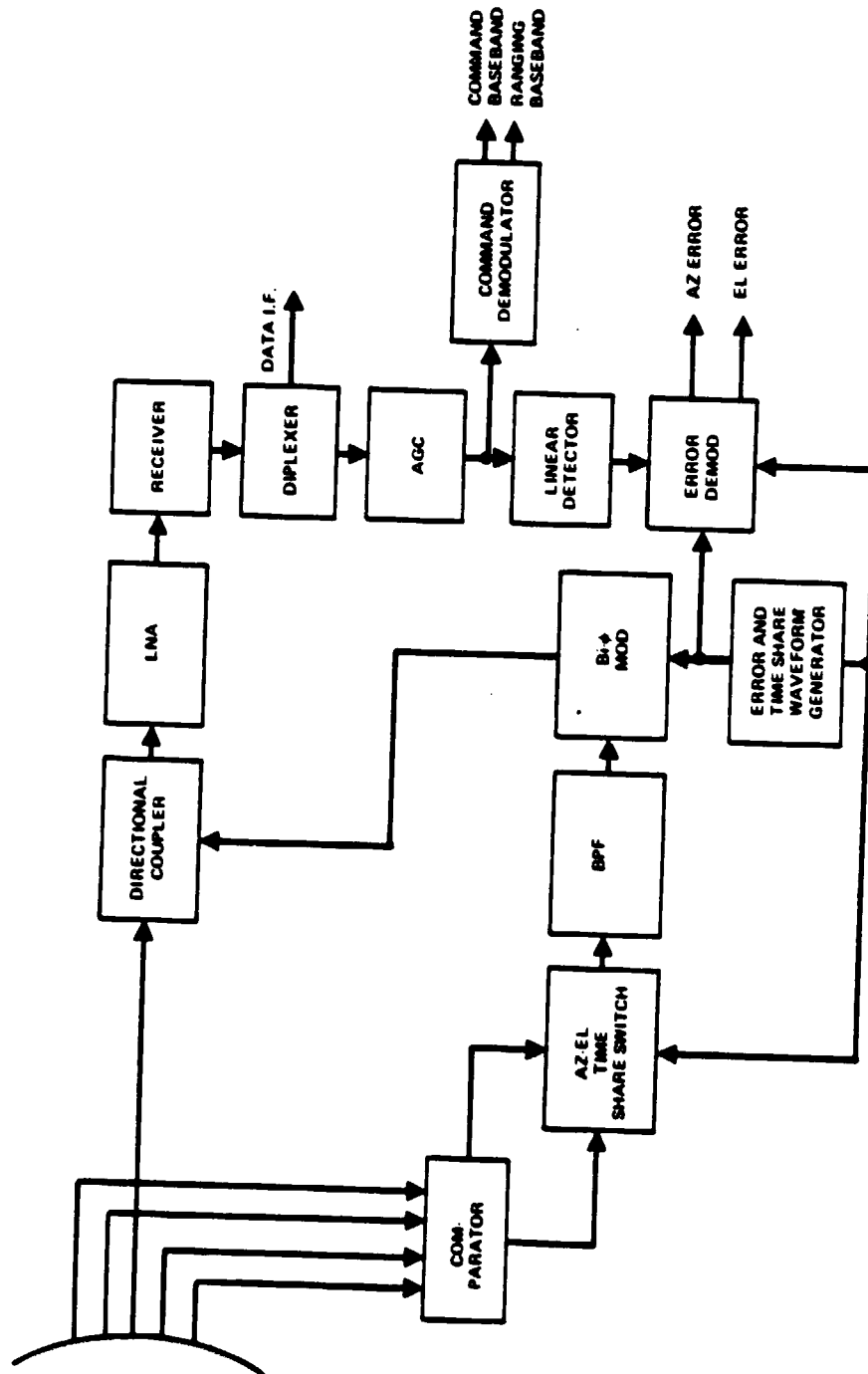


FIGURE 3.2-17. MONOPULSE TRACKING MICROWAVE CIRCUITS

information, is then passed through an AGC circuit to ensure that the antenna/receiver error transfer function remains nearly constant and independent of command signal level variation. The AGC circuit output is then detected, synchronously demodulated, and separated into dc error signals whose amplitude is a function of angle error magnitude and whose polarity is a function of error direction. A separate command and ranging demodulator is used to demodulate the frequency modulated command and ranging signals.

The time-sharing signal and error modulation are generated by digital circuits and are low rate ( $\leq 200$  Hz) for compatibility with the low speed circulator switch in the antenna subsystem. The time-sharing signal period is both synchronous with and twice that of the error signal.

### 3.2.2.12 Telemetry and Command Requirements

The microwave subsystem's command requirements are shown in Table 3.2-4 and its telemetry requirements are shown in Table 3.2-5.

### 3.2.3 Weight and Power

The component weights and power are listed in Table 3.2-6. The upper portion of the chart lists components for the baseline system. The lower portion lists additional components required for option 2. The option 2 receiver weight is increased by 0.5 lb and power is increased by 0.5 watt because of the addition of an upconverter, additional local oscillator, multiplier, and RF output amplifier stages. The weight and power of the LNAs is accounted for in the antenna subsystem.

### 3.2.4 Performance

#### 3.2.4.1 Output Circuit Losses and Power Delivered to Antenna

Table 3.2-7 gives the circuit losses, amplifier power, and the power delivered to the antenna feed for the four possible cases. The circuit losses given in the table include 0.15 dB for the circulator switches used to select the power amplifier and 0.3 dB for the power monitor and harmonic filter. The loss of 0.55 dB for five feet of WR 51 waveguide from the output circuits to the antenna feed is accounted for in the antenna gain budget as is the loss in the high speed beam forming network switches and the low speed antenna configuration switches.

TABLE 3.2-4. MICROWAVE SUBSYSTEM  
COMMAND REQUIREMENTS

<u>Command Function</u>	<u>Number of Commands</u>
Receiver select	12
CPS/trunk mode select	4
Telemetry transmitter select	1
Transmitter select	12
Local oscillator source selection	14

**TABLE 3.2-5. MICROWAVE SUBSYSTEM  
TELEMETRY REQUIREMENTS**

Function	Signal Type	Number Required
Power amplifier drive level	Analog	6
Transmitter power monitor	Analog	4
Subsystem status bits	Discrete	43
TWTA parameters	Analog	12
Temperature monitor	Analog	10

**TABLE 3.2-6. MICROWAVE SUBSYSTEM WEIGHT AND POWER**

Component	Quantity*	Weight, lb	Power, W Trunk Mode	Power, W CPS Mode
Receiver	4 + 2	18	30	15
IF diplexer	1	0.3		
IF switch matrix	1	4	3	
30 GHz circulator switches	6	1.8		
Upconverters and IF amplifiers	4 + 2	9	9	4.5
TWTA	4	40	460	230.0
Solid state power amplifier (SSPA)	2	14	**	**
20 GHz circulator switches	7	2.1		
Monopulse and command electronics	1 + 1	6	3	3
IF coaxial switches	30	9		
LO source	2	8	8	8
Telemetry transmitter	1 + 1	4	6	6
Output power monitor	4	2	1.6	1.6
Output harmonic filters	4	1.2		
Interconnections		8		
Totals (baseline)		127.4	520.6	268.1
20 GHz circulator switches	22	6.6		
Additional for receiver	4 + 2	3	3	3
Demultiplexer	4	4.8		
Summer	4	1.6		
Additional for option 2		16.0	3	3

\*Operating plus redundant.  
 \*\*SSPA is used in place of a TWTA.



TABLE 3.2-7. CIRCUIT LOSSES AND POWER DELIVERED TO ANTENNA FEED

Power Amplifier Type and Power Output	Service	Circuit Losses	Power Delivered to Antenna Feed
TWT-40	Trunk	0.45 dB	36.1
TWT-40	CPS	0.45 dB	36.1
SSPA-7	Trunk	0.45 dB	6.3
SSPA-7	CPS	0.45 dB	6.3

#### 3.2.4.2 Channel Bandpass Characteristics

The channel bandpass characteristics of primary interest are gain flatness and phase linearity over the data bandwidth. The two principal contributors to these parameters are the bandpass filter in the upconverter and the bandpass filter preceding the downconverter mixer in the receiver. The upconverter filter is deliberately made very wide in bandwidth so that its contribution is small. The receiver bandpass filter must be more narrow in bandwidth since it precedes the AGC circuit of the upconverter in the case of the trunk service and it is desirable to minimize transmitter noise power sharing due to uplink receiver noise. Other contributors to gain flatness and phase linearity performance are the receiver active circuits, the switch matrix, the upconverter circuit, and the power amplifier. These circuits contribute primarily phase and gain ripple due to intercomponent impedance mismatches.

Table 3.2-8 gives phase linearity and gain flatness estimates for the microwave subsystem for both trunk service and CPS service. The filter data of Table 3.2-8 are based upon theoretical filter response characteristics. The component phase ripple and amplitude ripple data are estimated based upon similar subsystems.

TABLE 3.2-8. MICROWAVE SUBSYSTEM GAIN FLATNESS AND PHASE LINEARITY

Mode	BPF Phase Variation, deg	BPF Filter Gain Variation, dB	Component Phase Ripple, deg	Component Gain Ripple, dB	Total Phase Variation, deg	Total Gain Variation, dB
CPS	±0.02	±0.05	±5	±0.4	±5	±0.45
Trunk	±1.91	±0.05	±7	±0.55	±8.9	±0.6

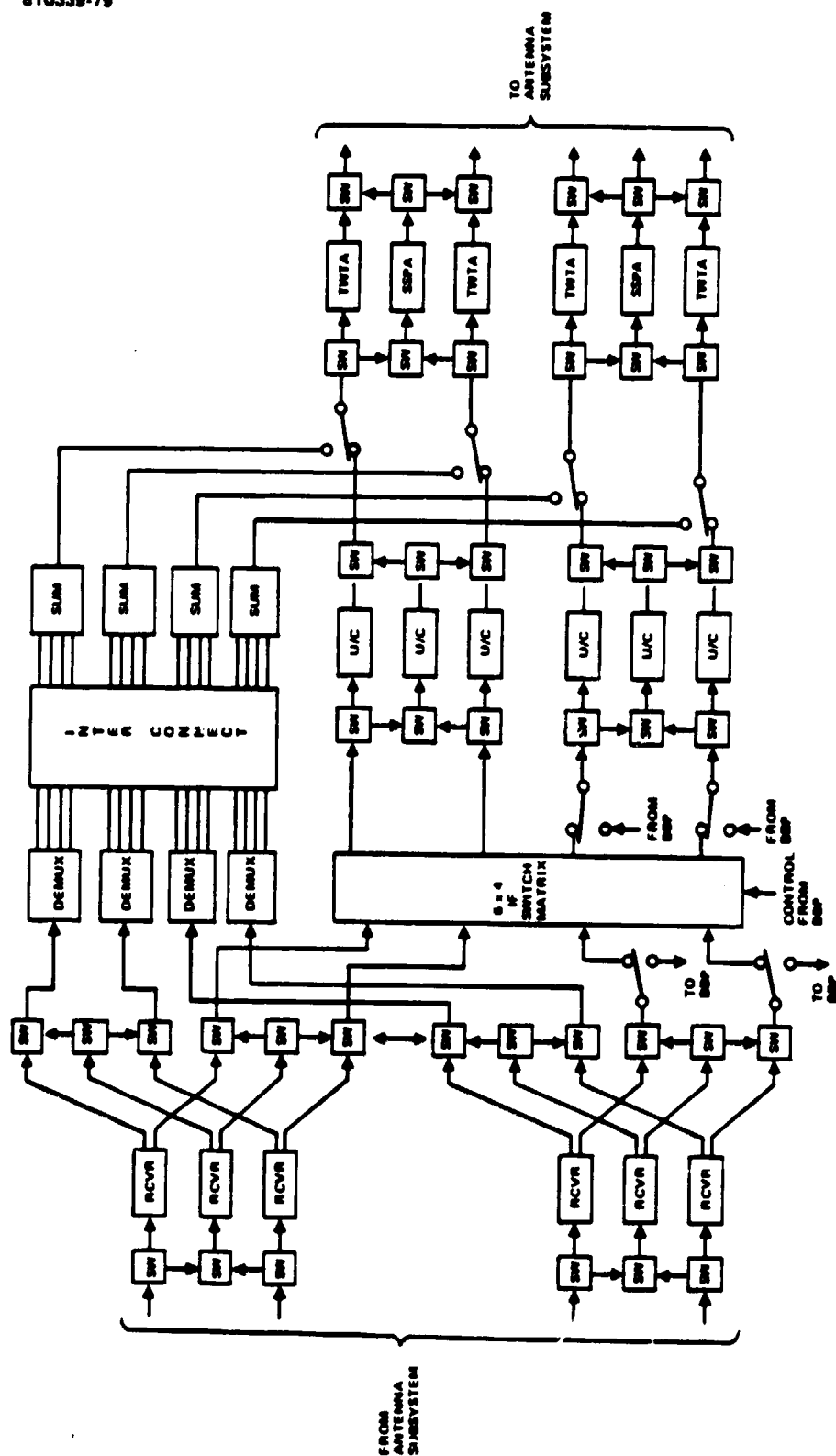


FIGURE 3.2-18. OPTION 2 MICROWAVE SUBSYSTEM BLOCK DIAGRAM

### 3.2.5 Options

#### 3.2.5.1 Option 2 Modifications to Microwave Subsystem

Figure 3.2-18 shows the configuration of the microwave subsystem for option 2 which provides the capability of either SS TDMA or FDMA operation for the trunk service.

The configuration has several additions to the baseline system. The receivers provide an RF output for FDMA operation of the trunk service. Additional redundancy switches are required to select the receiver RF outputs. Four 4 channel demultiplexing filters, interconnections, and four 4 way summers are added to provide the FDMA capability. Additional mode switches are required to select FDMA or TDMA inputs to the power amplifiers.

#### 3.2.5.2 Receiver Modifications

Figure 3.2-19 shows the receiver design for the option 2 microwave subsystem. The design has several additions with respect to the baseline receiver design. An upconverter mixer and bandpass filter are added to upconvert the receiver IF to the output frequency range. Two output RF stages and an AGC function are added to provide a constant drive RF signal at the proper level for FDMA operation. An amplifier, a times seven frequency multiplier, and a bandpass filter are added to provide the local oscillator frequency required for upconversion. An IF hybrid power divider is added to provide a separate IF output and IF input to the upconverter mixer. An RF hybrid power divider is added to provide local oscillator source drive to the added frequency multiplier.

#### 3.2.6 Technology Assessment

The technology required for the microwave subsystem is considered to be within the state of the art with the exception of the low noise amplifier used in the antenna subsystem. The noise figure and associated low noise gain required to meet the system noise figure goal of 5 dB requires a modest improvement in GaAs low noise device performance at the uplink frequency.

The Hughes Electron Dynamics Division has a contract from the NASA Goddard Space Flight Center to develop a low noise receiver consisting of a five stage preamplifier, mixer, and local oscillator with an overall noise figure design goal of 4 dB. Results to date indicate that 5 dB should be achievable within the next year. Device noise figures as low as 3.6 dB with an associated low noise gain of 4 dB have been measured on devices having a gate length of 0.5 microns. Work is being done to improve device manufacturing processes to permit reduction of device gate length in order to obtain improved noise figure and associated gain.

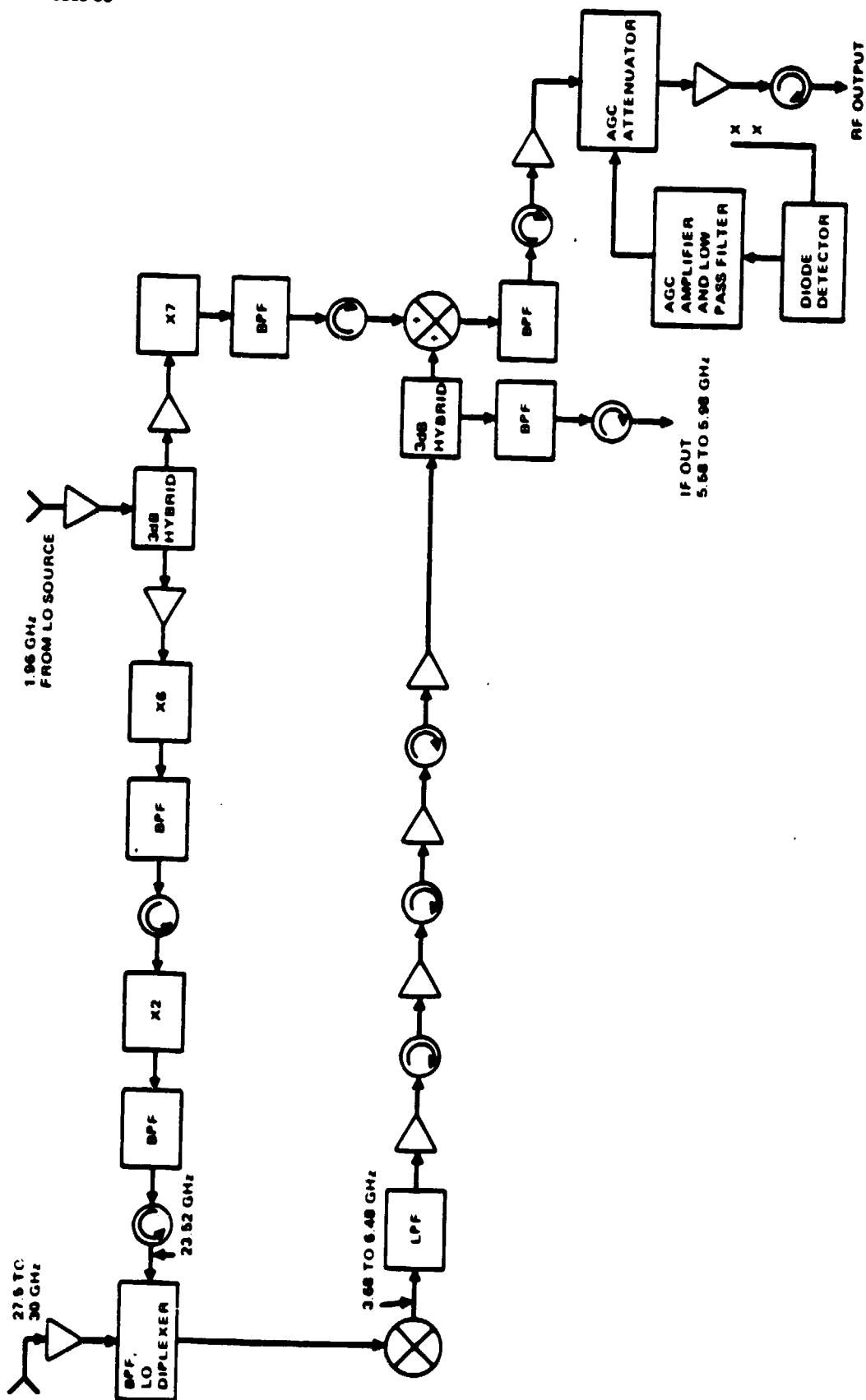


FIGURE 3.2-19. OPTION 2 RECEIVER

### 3.3 BASEBAND PROCESSOR

#### 3.3.1 BBP Requirements

The functional requirements on the baseband processor (BBP) are illustrated by Figure 3.3-1. The BBP performs complex baseband data routing functions in the CPS mode. The single trunk function is that of sequencing the IF switch matrix. This switch sequence is reprogrammable in the BBP via the command link.

The primary function of the BBP is the routing of CPS data. A pair of scanning beams collect this data from earth terminals on a TDMA basis. The microwave receiver downconverts the data from the 30 GHz uplink to a 6 GHz IF frequency. The receiver output contains frequency multiplexed channels. At any time, there are either four 32 Mbps quadrature phase shift keying (QPSK) channels or a single 128 Mbps channel. The BBP must demultiplex and demodulate these signals and store the data until one of the downlink scanning beams is pointed at the terminal for which each message is intended, at which time it reads out that data to the transmitter serving that scanning beam. The output data is a single channel for each beam at 256 Mbps QPSK. The routing format can be modified via the orderwire in response to changes in the CPS traffic pattern. Because the output rate on each beam is twice the total input rate, the downlink outputs will be active for at most half the TDMA frame.

As much as 25 percent of the received CPS data can be FEC encoded. The BBP must separate this data from the uncoded data and decode it before processing it through the store and forward operation described above. Similarly, the BBP may be required to FEC encode up to 25 percent of the transmitted CPS data.

In addition to the store and forward and FEC functions, the BBP controls the operation of the scanning beam antenna as well as the IF switch matrix, takes part in the system synchronization and orderwire functions and provides the master clock for the system.

The BBP stores and executes the sequences for each of the four independently scanning CPS beams. The sequences can be read out over the orderwire on demand and can be reprogrammed via the orderwire or the command link.

The system synchronization scheme is described in Section 2.2. The BBP supports synchronization by the following functions:

- 1) Transmits a frame synch from which the trunk and CPS terminals can time their uplink bursts
- 2) Measures the errors in time of receipt of CPS uplink bursts
- 3) Transmits these error measurements to the CPS terminals via the orderwire so that the terminals can correct their burst times; trunk synchronization is handled by the master control terminal (MCT).

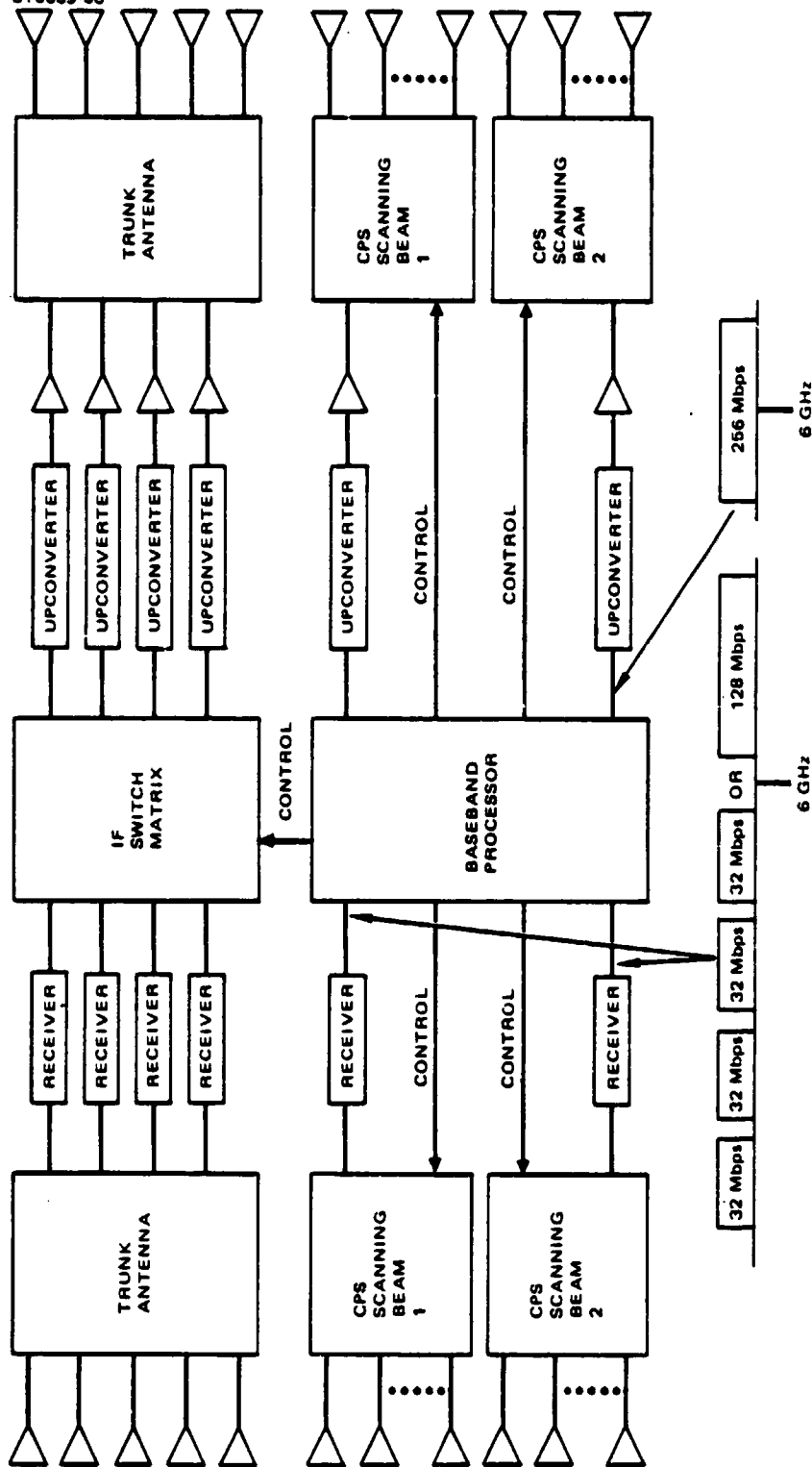


FIGURE 3.3-1. BASEBAND PROCESSOR FUNCTIONS

The BBP extracts orderwire data from the CPS uplink data streams for transmission to the MCT.

The BBP derives the system master clock from the onboard oscillator. The operation of this clock is monitored at the MCT and its frequency is periodically corrected. The MCT also corrects the system for the effects of residual frequency errors as described in Section 2. 2.

### 3.3.2 System Description

#### 3.3.2.1 Baseband Processor Architecture

The baseband architecture drivers are the functional requirements, low power consumption, low weight, high reliability, radiation hardness, and the speed limitations and design limitation of available digital logic technologies. Large advantages in weight reductions and reliability improvement may be realized with LSI. Large reductions in power consumptions may be realized by using advanced logic technologies in the LSI design, such as Hughes Newport Beach SOS-CMOS, Fairchild FAST, Signetics ISL (Integrated Schottky Logic), Fairchild 9480 I<sup>3</sup>L, or Fairchild Isoplanar ECL. An important factor in serial bit rate versus number of parallel line design decisions is the maximum clocking speed consistent with the logic family in the design. A power efficient design will be characterized by extensive use of digital technologies characterized by low delay power products.

##### 3.3.2.1.1 Input Sections

Figure 3.3-2 is a block diagram of the BBP. The input section (see Figure 3.3-3) receives the two CPS receiver outputs at 6 GHz.

Each line contains frequency division multiplexed signals. At a given time, each line may contain four 32 Mbps FDM signals or one 128 Mbps signal. The BBP downconverts these signals from the 6 GHz IF and frequency demultiplexes them. The demultiplexed signals are then routed by analog switches to either hard decision demodulators for nonencoded bursts, or soft decision demodulators for encoded bursts. The output of the soft decision demodulators is a 3 bit word for each received symbol. At the demodulator outputs, the demodulated bit stream goes through a unique word detector for frame synchronization and for I-Q ambiguity resolution. The timing error of uplink burst from each earth station is periodically measured by the sync interface unit. The measurements are passed to the orderwire interface unit for insertion in the downlink orderwire channels. In this manner the timing error is reported back to each earth station for transmit time correction.

The demodulators have the capability to measure the carrier level of uplink bursts. The carrier level of the received signal from each earth station is periodically measured by the signal strength measurement unit. These signal strength measurements are transferred to the orderwire interface unit for insertion into the downlink orderwire data.

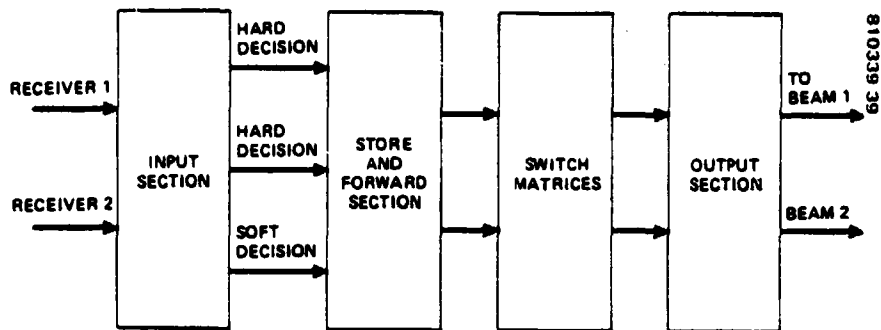


FIGURE 3.3-2. BASEBAND PROCESSOR SIMPLIFIED FUNCTIONAL BLOCK DIAGRAM

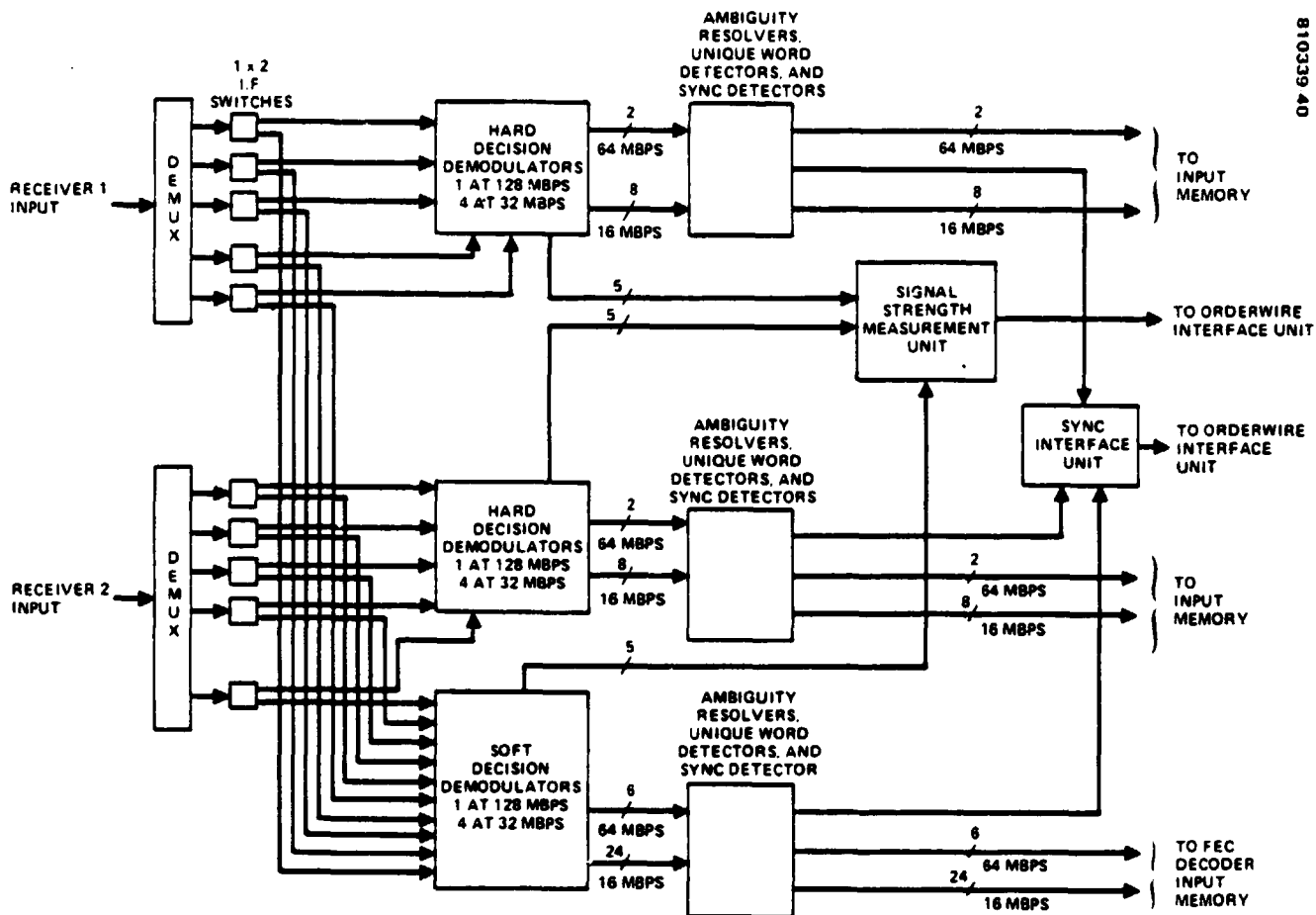


FIGURE 3.3-3. BASEBAND PROCESSOR BLOCK DIAGRAM, INPUT SECTION



### 3.3.2.1.2 Store and Forward Section

Figure 3.3-4 is the store and forward section of the baseband processor. The demodulated data enters double buffered input memories. For uncoded hard decision data, the input memory size for each half of each of two double buffered memories is 2K by 64 bits which is one frame, 1 msec, of storage. The 3 bit soft decision demodulated data enters a decoder input memory which is double buffered with each half having a capacity of 2K by 3 by 64 bits.

The store and forward section of the baseband processor which does data routing individually routes 64 bit words. Since the frame time is 1 msec, the average data rates of individual TDMA channels are multiples of 64 Kbps, i. e.,  $N \times 64$  Kbps, where  $N = 1, 2, 3, \dots$ . The memory control sequences stored in the memory controllers determine the TDMA channelization in the spacecraft. The earth terminals provide TDMA channelization by transmitting uplink bursts and receiving downlink bursts at the proper time in the frame.

The outputs of the input memories are dynamically cross-connected to the output memories by the baseband switch. An orderwire interface unit has an input and an output connected to the baseband switch for interleaving downlink orderwire data originated in the BBP and for extracting uplink orderwire data which is transmitted to the BBP. The baseband switch has an output for each of the two downlink scanning beam antennas. Each baseband switch output enters a output memory for rate buffering.

The routing sequence may be modified under master control station command. A new control sequence may be sent to the spacecraft either on the orderwire channel or on the command link. A changeover in time slot assignment and store and forward timing and control may be made on a single frame without interruption of service or loss of data.

The routing sequence in spacecraft memory may be monitored either on the downlink orderwire channel or on the telemetry link.

The convolutional decoders are used on rain attenuated encoded bursts. The coding gain makes up for link loss due to rain attenuation. Rate  $1/2$ , constraint length 5, 3 bit soft decision convolutional decoders are used. The decoders implement the Viterbi Algorithm. The coding gain is 4.4 dB. Since the burst rate is fixed, a rate  $1/2$  encoding of the data implies that twice as much energy per information bit will be used in transmission. The result is a rate gain of 3 dB. The overall improvement due to decoding is the sum of the coding gain and the rate gain which is 7.4 dB.

The maximum read or write rate of the CMOS memories in the baseband processor design is 2 MHz. The 64 Mbps demodulator outputs (from 128 Mbps demodulators) are serial to parallel converted with 32 bit gate array LSI devices implemented with Fairchild FAST (FGA 750) logic. The parallel converted data is read into a CMOS memory at 2M words/sec. The

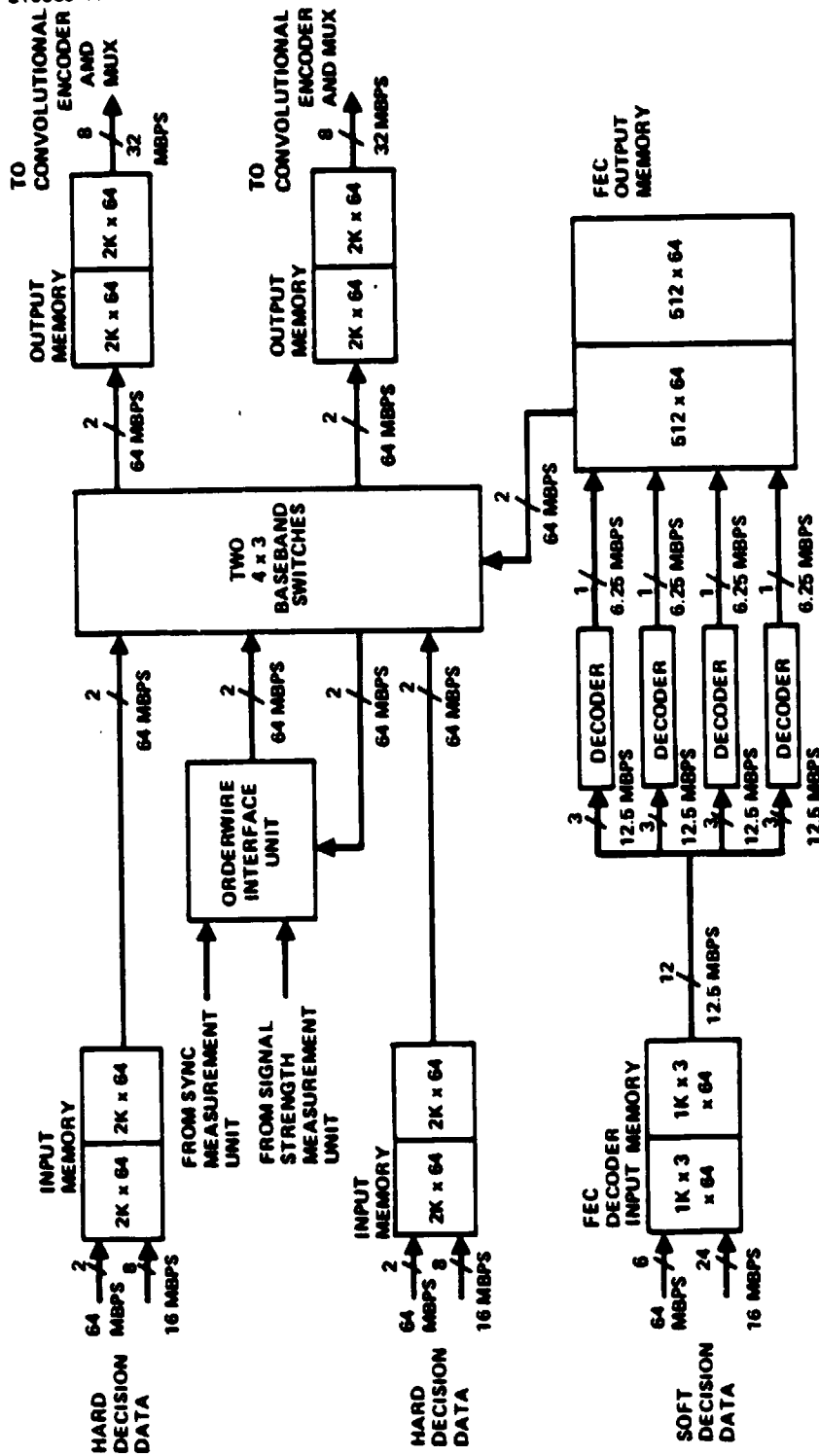


FIGURE 3.3-4. BASEBAND PROCESSOR BLOCK DIAGRAM, STORE AND FORWARD SECTION

16 Mbps demodulator outputs (from 32 Mbps demodulators) are serial to parallel converted with 32 bit gate array LSI devices implemented with Hughes 5  $\mu$ M SOS-CMOS. This parallel converted data is read into memory at 1/2M word/sec.

The input memories are read using the spacecraft clock. The CMOS input memories are read in 32 bit parallel words at 2M words/sec. These words are parallel to serial converted to 64 Mbps serial bit streams using Fairchild FAST (FGA 750) gate array LSI devices. The converted output of each of the two input memories is two 64 Mbps bit streams.

The FEC decoder input memory is read at 390.62K words/sec in 32 bit parallel words. These parallel words are parallel to serial converted using 32 bit Hughes 5  $\mu$ M SOS-CMOS gate array LSI devices. The output of the FEC decoder input memory is 12.5 Mbps serial bit streams. Three of these bit streams corresponding to 3 bit parallel soft decision words are routed to the input of each of four convolutional decoder units.

The convolutional decoders are rate 1/2, constraint length 5, 3 bit soft decision decoders which implement the Viterbi Algorithm. The convolutional decoders are composed of Fairchild 9480 I<sup>3</sup>L gate array LSI devices. The output of each of the four decoders is a 6.25 Mbps serial bit stream. These bit streams are serial to parallel converted and enter a FEC output memory which is CMOS and is double buffered with each half being of size 512 by 64 bits. The 6.25 Mbps bit streams at the decoder outputs are serial to parallel converted to 32 bit parallel words 195.31K words/sec, using Hughes 5  $\mu$ M SOS-CMOS gate array LSI devices. These 32 bit words are written into the FEC output memory. The data is read out of the FEC output memory at 2M words/sec for each of two 32 bit parallel words. Each of the 32 bit words is parallel to serial converted by a Fairchild FAST (FGA 750) gate array. The result is two 64 Mbps serial bit streams.

Two lines at 64 Mbps are generated by an orderwire interface unit to transfer baseband processor originated data to downlink orderwire channels. Serial bit stream data generated from units listed in Table 3.3-1 must be dynamically cross-connected

TABLE 3.3-1. 64 MBPS DATA SERIAL LINES ENTERING  
BASEBAND SWITCH

<u>Unit Originating 64 Mbps Data</u>	<u>Number of Lines</u>
Input memory (unit 1)	2
Input memory (unit 2)	2
Orderwire interface	2
FEC decoder output memory	2

A dual 4 by 3 baseband switch cross connects the 64 Mbps serial data lines. This switch is constructed using off the shelf Fairchild FAST (54FXXX) logic. The switch output lines are summarized in Table 3.3-2. Two lines go to the orderwire interface unit so that uplink orderwire data can be transferred to the baseband processor.

Two lines go to each of two output memories. The 64 Mbps serial lines are serial to parallel converted at 2M words/sec by 32 bit Fairchild FAST (FGA750) gate array LSI circuits. The two output memories are double buffered CMOS memories with each half having size 2K by 64 bits. Data is read from the output memories at 1M word/sec in 32 bit words. The memory output is parallel to serial converted using 32 bit Fairchild FAST (FGA750) gate array LSI circuits. Each of the two output memories has a serial converted output of eight lines at 32 Mbps each.

### 3.3.2.1.3 Output Section

Referring to the output section of the baseband processor shown in Figure 3.3-5, the output of each of the two output memories goes to a convolutional encoder and a mux. For data which will not be convolutionally encoded, all eight lines contain 32 Mbps serial bit stream data. For data which will be convolutionally encoded only four of the eight 32 Mbps lines contain data because the encoder will double the data rate. The convolutional encoder outputs are eight lines at 32 Mbps. The convolutional encoders are Fairchild Isoplanar ECL gate array LSI devices. The nonencoded or encoded eight lines at 32 Mbps are multiplexed together and converted into two 128 Mbps serial bit streams for each of two multiplexers, on the same gate array as the encoder. The two 128 Mbps bit streams are input into each of two 256 Mbps QPSK modulators. The modulators use ECL digital circuits, thin film RF amplifiers, and RF hybrids. The two modulator outputs are upconverted to 6 GHz and are output to the two upconverters which correspond to the two scanning beam downlink antennas.

### 3.3.2.1.4 Control Functions

In addition to the functions shown in the previous block diagrams there are a large number of control functions required for operation of the BBP as well as for control of the IF switch matrix and the scanning beam.

TABLE 3.3-2. 64 MBPS DATA SERIAL LINES LEAVING  
BASEBAND SWITCH

<u>Unit At Switch Output Terminating 64 Mbps Lines</u>	<u>Number of Lines</u>
Output memory (unit 1)	2
Output memory (unit 2)	2
Orderwire interface unit	2

In order to route data in the BBP, a digital routing controller provided the requiring timing and control signals to the following:

- 1) IF hard/soft demodulator routing switches
- 2) Input memories
- 3) FEC decoder input memory
- 4) Convolutional decoders
- 5) FED decoder output memory
- 6) Orderwire interface unit
- 7) Baseband switch
- 8) Output memories
- 9) Convolutional encoders
- 10) MUXs
- 11) Modulators
- 12) Sync detectors
- 13) Sync interface unit
- 14) Signal strength measurement unit
- 15) Demodulators

As shown in Figure 3.3-6, the baseband processor contains an onboard oscillator which is the master oscillator for the TDMA system. This oscillator may be frequency corrected from the ground either by the command link or through the uplink orderwire channel. The baseband processor contains a beam forming network controller which controls the scanning sequences of the uplink and downlink scanning beam antennas. The digital routing controller controls the data memory write and read sequences, the analog routing switch sequences, the baseband switch sequences, the decoder timing, the encoder timing, and the Mux timing to implement the store and forward, decode, and encode functions. New data routing sequences may be loaded into the controller memory via the uplink orderwire channel or via the command link. For trunk operation, which cannot occur simultaneously with CPS operation, the IF switch controller controls the IF switch sequence.

New IF switch sequences may be entered via the command link. The contents of the IF switch controller sequence memory may be monitored via the telemetry link. The contents of the BFN controller sequence memory

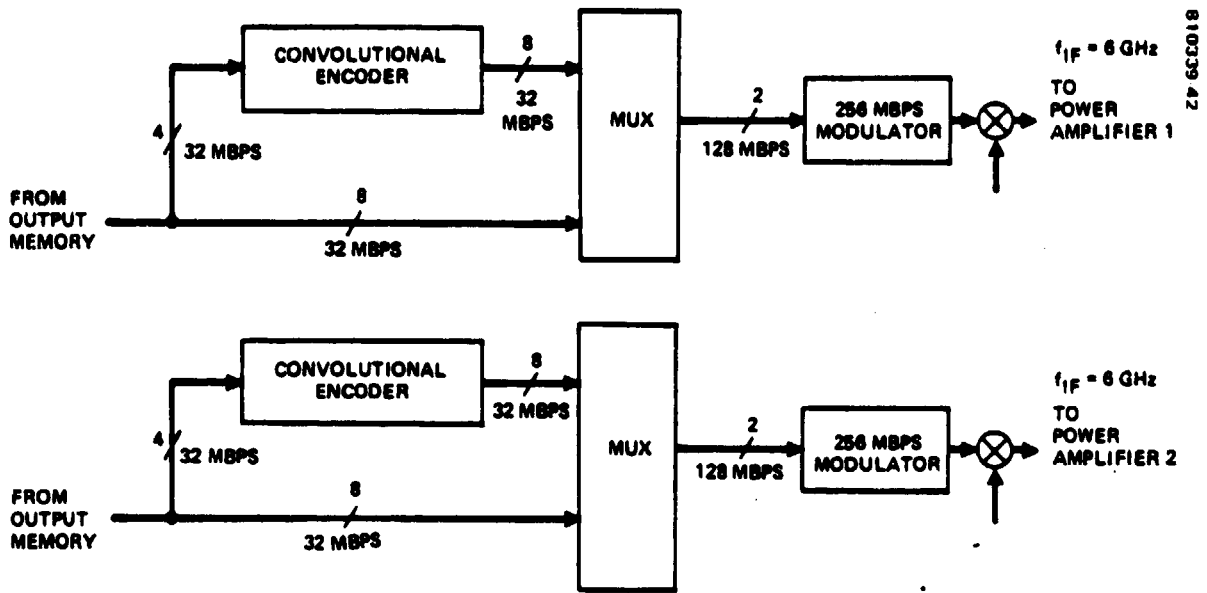


FIGURE 3.3-5. BASEBAND PROCESSOR BLOCK DIAGRAM, OUTPUT SECTION

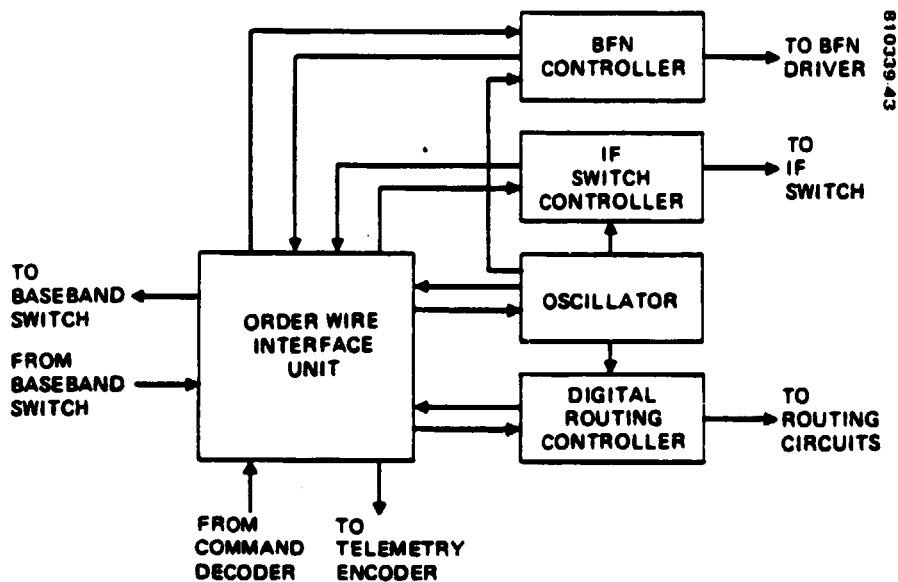


FIGURE 3.3-6. BASEBAND PROCESSOR TIMING

or the digital routing controller sequence memory may be monitored either on the downlink orderwire channel or on telemetry.

### 3.3.3 Functional Elements

The functional elements shown in the block diagrams of the previous section are described below.

#### 3.3.3.1 Demultiplexers

The IF downconverters and frequency division demultiplexers are shown in Figure 3.3-7. The receiver IF output with center frequency 6137.448 MHz enters a bandpass filter which has a bandwidth of 800 MHz. The signal is mixed with a local oscillator frequency of 5612.448 MHz which converts the band containing the signals to the range of 225 MHz to 825 MHz. The signals are 1:2 power split. One arm of the power splitter output is 1:4 power split. Each output of this power splitter is amplified with 25 dB gain and is bandpass filtered to demultiplex the four 32 Mbps frequency channels. The demultiplexer filters have a 32 MHz bandwidth and have center frequencies of 250 MHz, 325 MHz, 400 MHz, and 425 MHz. After passing through the bandpass filters, the signals are downconverted to a common IF frequency of 20 MHz, amplified with 30 dB gain, and lowpass filtered to eliminate undesired mixer outputs.

The 128 Mbps channel is extracted from the other output of the 1:2 power splitter by a bandpass filter with a 635 MHz center frequency and 128 MHz bandwidth. After filtering, the signal is amplified with 14 dB of gain and is downconverted to a 125 MHz IF frequency. The signal is then amplified with 25 dB of gain and is lowpass filtered to remove undesired mixer outputs.

#### 3.3.3.2 Demodulators

The block diagram of the 32 Mbps demodulator is given in Figure 3.3-8, and the block diagram of the 128 Mbps demodulator is given in Figure 3.3-9. The modulation is QPSK. The demodulators acquire a phase reference from an uplink signal, extract clock timing from the signal, and demodulate inphase (I) and quadrature (Q) serial bit streams. The demodulators also measure carrier level of the input signal. Nonencoded bursts are routed to hard decision analog to digital converters which make a data "0" or data "1" decision on each demodulated bit. Encoded bursts are routed to soft decision A/D converters which make an eight level (3 bit) decision on each demodulated bit. The soft decision A/D converters provide qualitative information on whether a decision is strongly or weakly in the decision region of the decided bit. The convolutional decoder can use this information to enhance coding gain.

The demodulators have carrier and clock acquisition circuits which are specially designed for burst mode operation. The incoming signal is input into a  $X^4$  nonlinearity in the carrier recovery circuit in order to produce

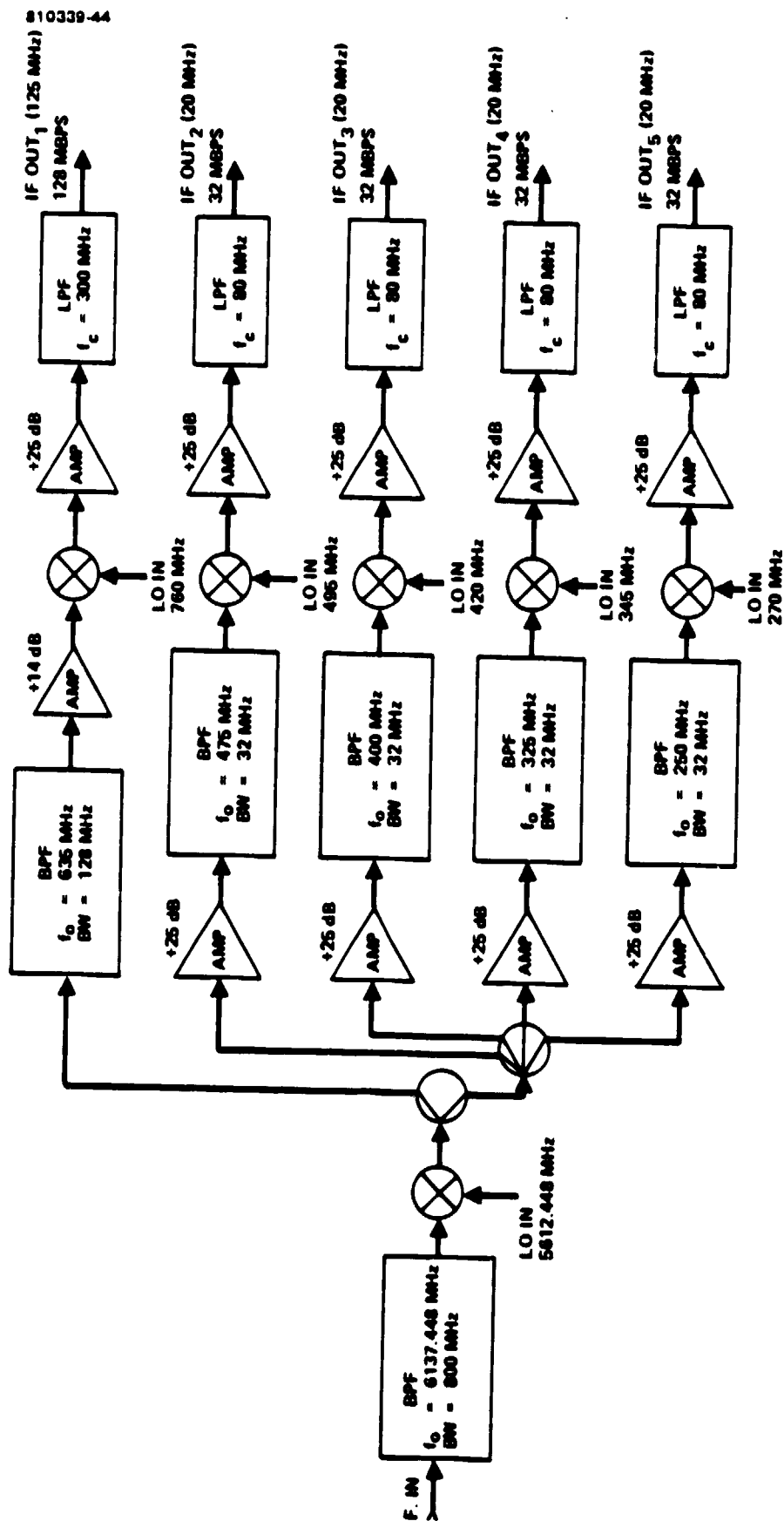


FIGURE 3.3-7. IF DOWNCONVERTER AND FDM DEMULTIPLEXER



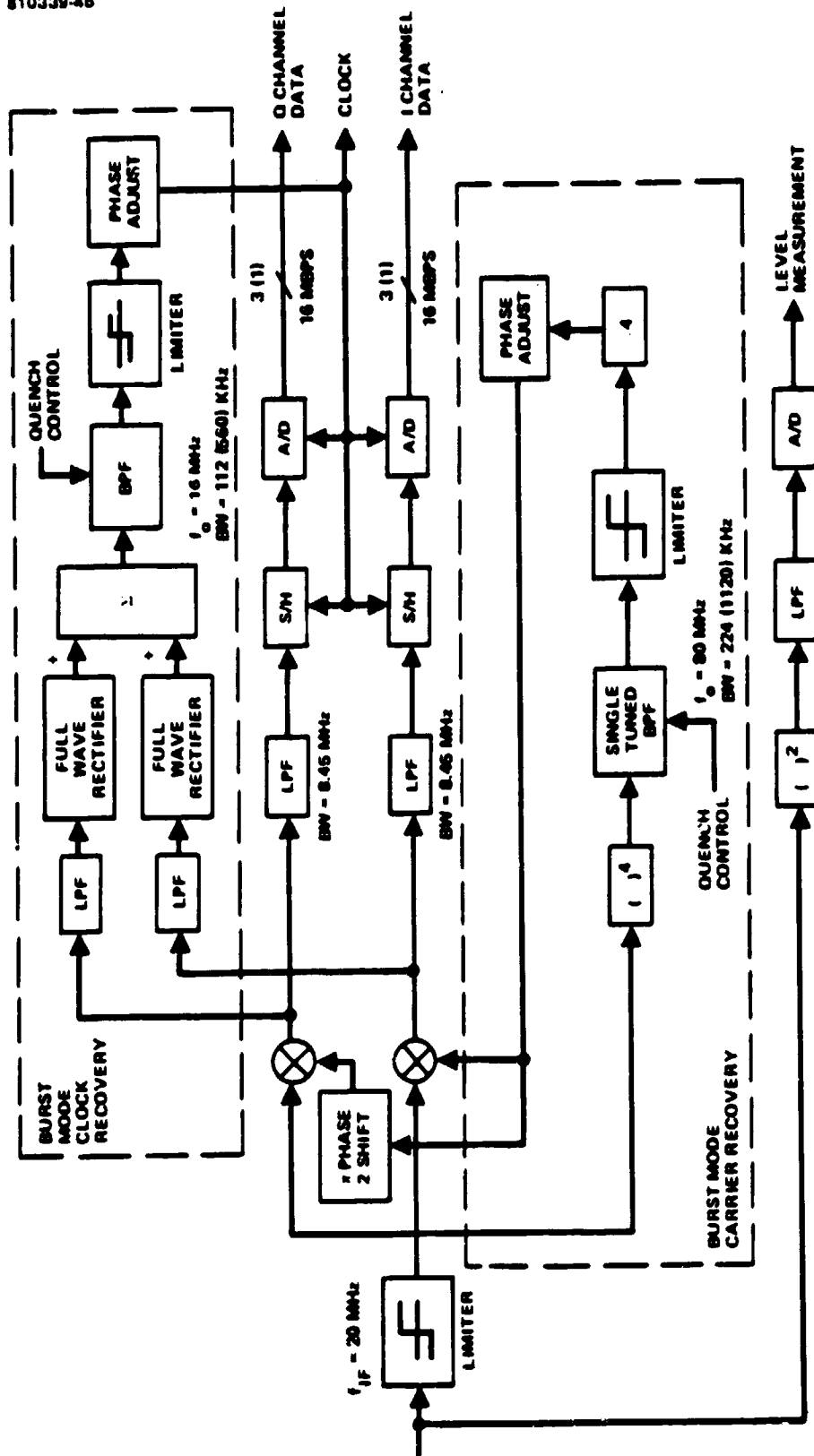
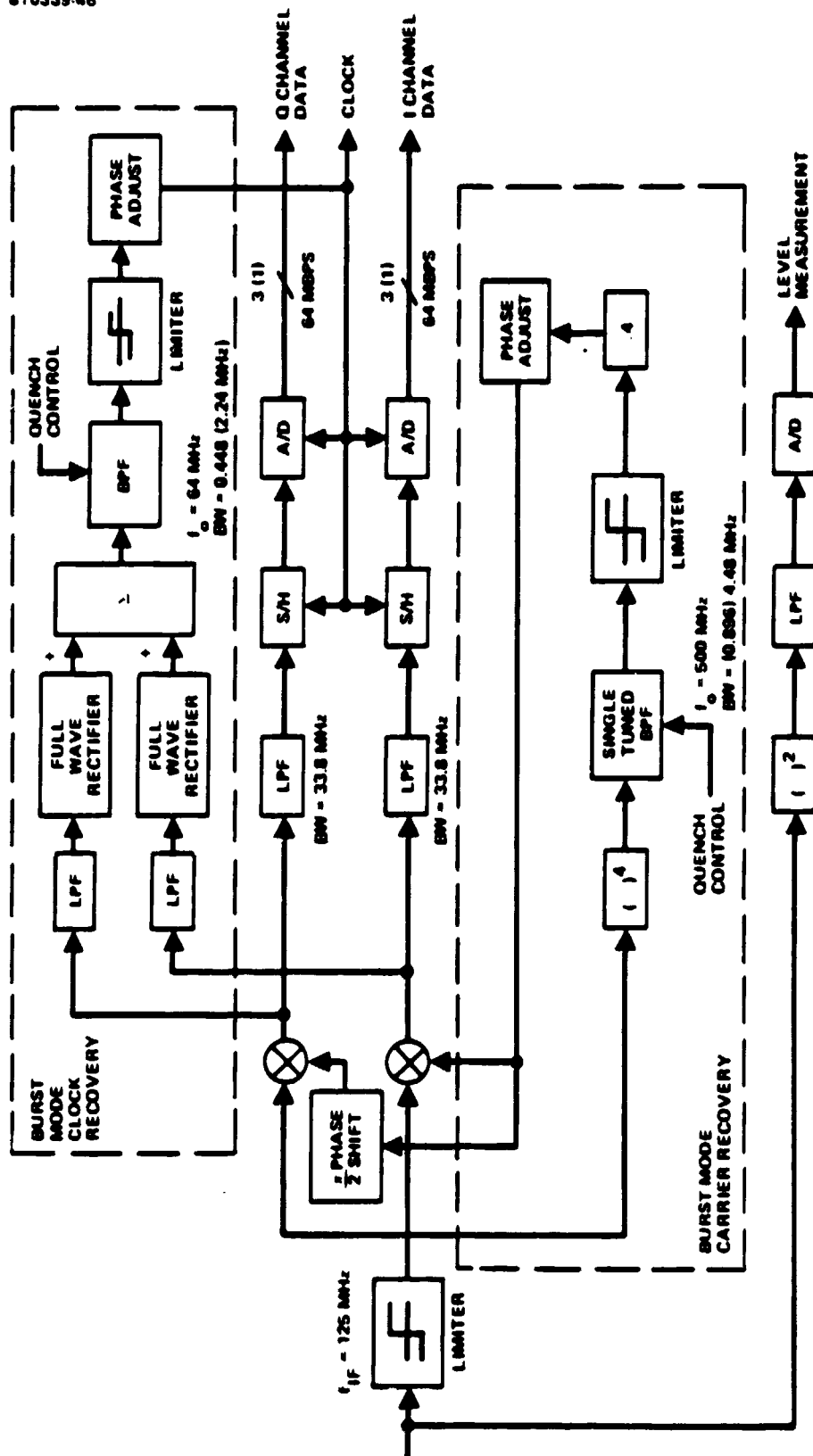


FIGURE 3.3.8. 32 MBPS SOFT (HARD) DECISION QPSK DEMODULATOR



**FIGURE 3.3.9. 128 MBPS SOFT (HARD) DECISION QPSK DEMODULATOR**

a frequency component without modulation at four times the IF frequency. This component is extracted using a bandpass filter. The filter output is hardlimited and divided by four to produce a carrier reference signal. This reference signal is phase adjusted for differential propagation delay. The reference signal is applied as an input to the inphase mixer, is phase shifted by 90°, and applied as an input to the quadrature mixer to coherently mix the inphase and quadrature signal component to baseband.

The clock recovery circuit inputs are the inphase and quadrature mixer outputs. The outputs are low pass filtered and full wave rectified. The rectifier outputs, having a discrete component at the clock frequency, are summed. The sum is input to a bandpass filter to extract the clock frequency component. The clock component is phase adjusted and is input to the data demodulator section. The recovered clock is also a demodulator output signal.

At the inphase and quadrature mixer outputs, the I and Q baseband signal components are input into passive detection filters which integrate the signal energy on a symbol by symbol basis. The filter outputs are sampled using the recovered clock signal for timing. The samples are then A/D converted. For hard decisions, the A/D converter is one bit or, a hard limiter. For soft decisions, a three bit A/D converter is used. The A/D converter outputs are the demodulated data.

The IF signal is limited at the demodulator input to bound the signal dynamic range at the input to the  $X^4$  nonlinearity. The carrier level measurement circuit receives the prelimited carrier signal.

The bandpass filters in the carrier and clock recovery circuits are quenched or reset to zero initial conditions at the end of each TDMA burst. This minimizes the worst case acquisition times in the carrier and clock circuits.

#### 3.3.3.2.1 Carrier Recovery

The carrier recovery circuit for the 32 Mbps demodulator is shown in Figure 3.3-8 and for the 128 Mbps demodulator is shown in Figure 3.3-9. The recovery circuit is the feedforward type, as opposed to a phase lock loop, in order to minimize the acquisition time while providing small steady state jitter in the recovered phase reference signal.

The input signal is amplitude limited to provide a constant amplitude into a fourth order nonlinearity. At the output of the nonlinearity, there will be a signal component at four times the IF frequency that is essentially free of modulation. This component is extracted with a bandpass filter with center frequency at four times the IF frequency (500 MHz for the 128 Mbps demodulators and 80 MHz for the 32 Mbps demodulators). The bandwidth of this filter determines the acquisition time and steady state performance of the carrier recovery circuit. In the nonencoded mode, the bandpass filter bandwidth

symbol duration product was chosen as,

$$BT = 0.07.$$

Therefore, for the 32 Mbps demodulators the bandpass filter bandwidth is 1120 KHz while for the 128 Mbps demodulators the bandpass filter bandwidth is 4.48 MHz.

In the encoded mode, the carrier recovery circuit input will be at a reduced signal to noise ratio. The signal to noise ratio loss in the fourth order nonlinearity will be greater than in the nonencoded mode. For the soft decision demodulators, the bandwidths of the bandpass filters are reduced from those in the hard decision demodulators in order to keep the recovered phase jitter at reasonable levels. For the soft decision demodulators,

$$BT = 0.014,$$

which results in a bandwidth of 896 KHz for the 128 Mbps demodulators and 224 KHz for the 32 Mbps demodulators.

The bandpass filters are quenched, or reset to zero initial condition, at the end of each TDMA burst. The timing for this reset is generated in the digital routing controller. The quenching limits the worst case acquisition time by eliminating the phase information from the previous TDMA burst in the filter memory.

For the 128 Mbps demodulators the bandpass filters are the helical resonator type, and for the 32 Mbps demodulators the filters are synthesized with discrete electronic components.

The BPF output is fed into a limiter and divide by four circuit (ECL for the 128 Mbps demodulators and ECL and Schottky TTL for the 32 Mbps demodulators). The divide by four circuit output is phase adjusted for propagation delay and is input into the inphase and quadrature mixer circuits.

#### 3.3.3.2.2 Clock Recovery

The clock recovery circuit for the 32 Mbps demodulator is shown in Figure 3.3-8 and for the 128 Mbps demodulator is shown in Figure 3.3-9. The I and Q mixer outputs of the demodulator enter lowpass filters which limit noise and remove double IF frequency components. The filter outputs are full wave rectified. The result of this nonlinear operation contains a discrete spectral component at the clock frequency. The full wave rectifier outputs are summed, since there is some energy at the clock frequency in each of the I and Q branches of the demodulator. The clock frequency component is recovered in a bandpass filter. The bandwidth of this filter establishes the acquisition time and steady state clock jitter performance of the circuit.

The center frequency of the bandpass filter is at the clock frequency (16 MHz for the 32 Mbps demodulators and 64 MHz for the 128 Mbps demodulators). For the hard decision demodulator, the bandwidth symbol duration product is set at,

$$BT = 0.035$$

and for the soft decision demodulators which operate at a reduced signal to noise ratio,

$$BT = 0.007.$$

The hard decision demodulator filter bandwidths are 2.24 MHz for the 128 Mbps demodulators and 560 KHz for the 32 Mbps demodulators.

The soft decision demodulator filter bandwidths are 448 KHz for the 128 Mbps demodulators and 112 KHz for the 32 Mbps demodulators.

The bandpass filter output is hard limited, phase adjusted, and sent to the demodulator sample, hold, and A/D converter circuits. The recovered clock is also output to the ambiguity resolver, unique word detector, sync detector, and input memory. The acquisition time of the clock recovery circuit with  $BT = 0.035$  is about 20 symbol duration periods after a carrier recovery has occurred.

#### 3.3.3.2.3 Data Demodulation

After carrier and clock have been recovered from the signal, the demodulator mixer output contains I and Q signals which have been mixed to baseband. The signals pass through passive detection filters which are three pole Butterworth filters with  $B_3 \Delta BT = 0.53$ , where  $B_3 \Delta B$  is the 3 dB cutoff frequency of the filter and T is the symbol duration. The filter outputs are sampled at the symbol rate. The samples are A/D converted (3 bit for soft decision demodulators and 1 bit for hard decision demodulators). The A/D converter outputs are the demodulated data.

#### 3.3.3.3 FEC Decoder

The FEC decoder must take a convolutionally encoded bit stream and encode it to produce a 6.3 Mbps data stream. Since the code has a constraint length of 5 and a rate of 1/2, 16 node calculations must be done for each input symbol (2 bits). Because of the speed requirements and the technologies available it was decided to use eight metric accumulator elements with each element performing 2 node calculations per symbol.

A block diagram for the FEC decoder is shown in Figure 3.3-10. The input data is supplied to the metric calculator which finds the inner product of the input symbol with each of the four possible code vectors.

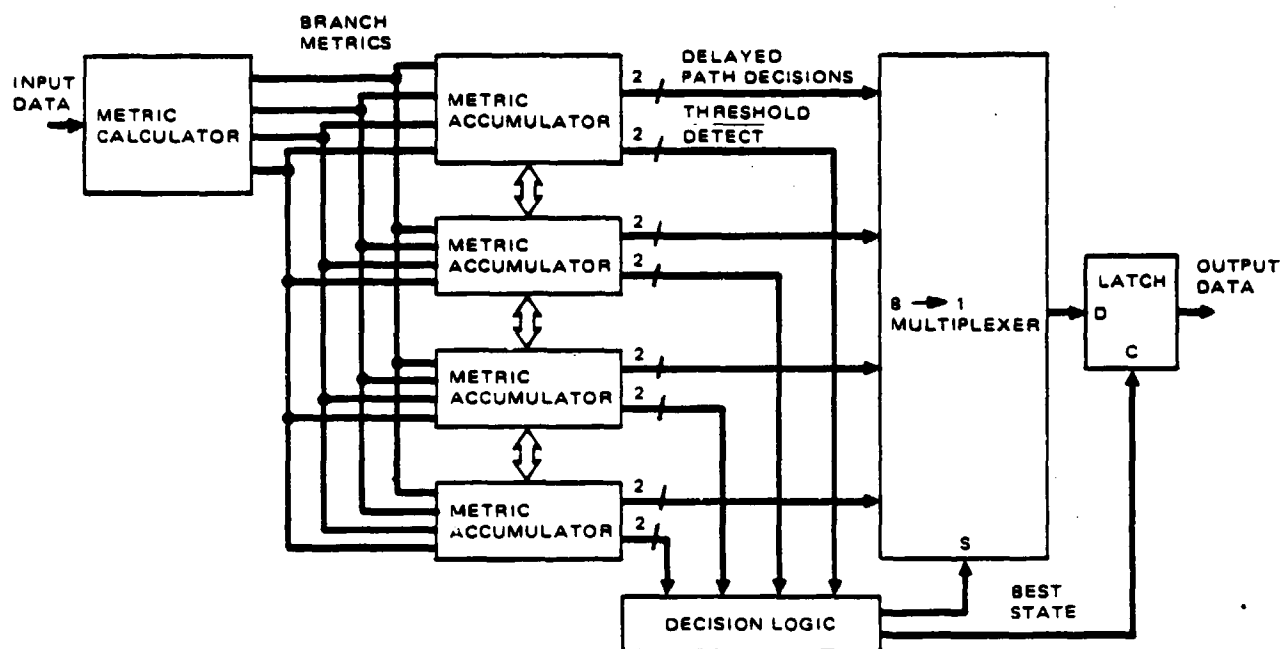


FIGURE 3.3-10. FEC DECODER BLOCK DIAGRAM

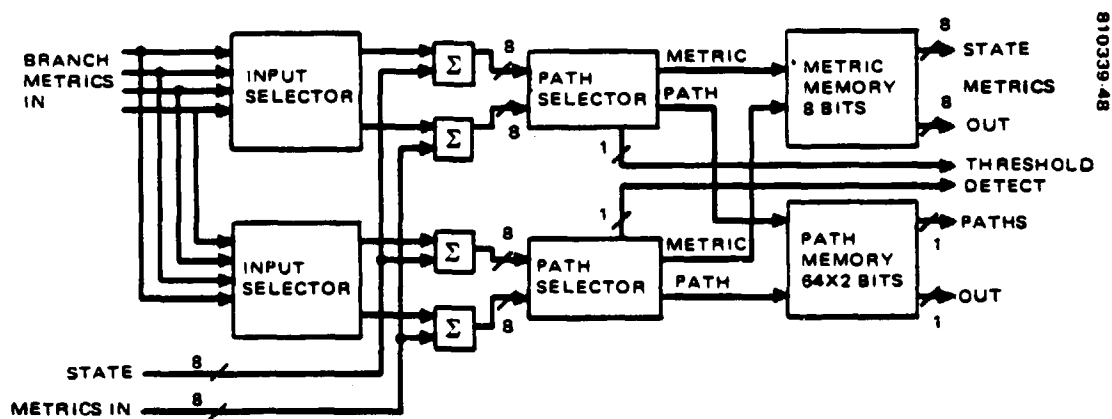


FIGURE 3.3-11. METRIC ACCUMULATOR GATE ARRAY

Since the input data is a quantized soft decision, the inner products, or branch metrics, are four bits each. These branch metrics are then accumulated in the appropriate way by the metric accumulator elements. When an accumulated metric is greater than a certain threshold value, the associated threshold detect output will become active. The decision logic will arbitrarily select a node from those whose metric is greater than the threshold. This decision will be passed to the output multiplexer and latch which will in turn select the data from the chosen path decision output. The optimum decision process consists of choosing the node with the greatest metric, but making a 16 way comparison at high speed requires a great deal of hardware. Simply choosing a path whose metric is above a threshold induces almost no degradation from the optimum and can be done at high speed with simple hardware.

Essential to the efficient implementation of this FEC decoder is a monolithic metric accumulator element. This element will be implemented using a Fairchild 9480 I<sup>3</sup>L gate array integrated circuit. This device has adequate speed (can cycle in 60 ns and 79 ns is available for cycle), uses less power than LS TTL and has a very high gate density (4000 gates/package).

A block diagram of the metric accumulator gate array is shown in Figure 3.3-11. The branch metrics are input to the input selectors which route the four metrics to the correct adders under off-chip control. The other inputs to the adders are two state metrics from other metric accumulator elements. The path selectors choose the greater metric sum and pass it through to the metric memory. The path is a one or a zero depending on whether the upper or lower metric was selected. The path memory is a pair of 64 bit long serial memories which have the effect of delaying the path data for 32 symbols (the path selector makes two decisions for each symbol). The path selector has the additional task of detecting when the sum exceeds the threshold level.

The entire decoder requires two clocks, a 12.6 MHz operation clock and a 6.3 MHz symbol clock. These would be supplied by the digital routing controller.

To prevent the metric accumulators from overflowing, there is a second threshold detect which is greater than the decision threshold. When any state metric exceeds this second value, a fixed amount is subtracted from every node. Since the same amount is subtracted from each, the relative values of the metrics remain unchanged.

#### 3.3.3.4 Store and Forward

The store and forward section of the BBP was shown in Figure 3.3-4. The hard decision data from the two sets of hard decision demodulators enters the two input memories. The soft decision demodulator data enters the FEC decoder input memory. This data is decoded and enters the convolutional decoder output memory. In order to route data to the two scanning beam downlink antennas, the outputs of the two input memories and FEC decoder

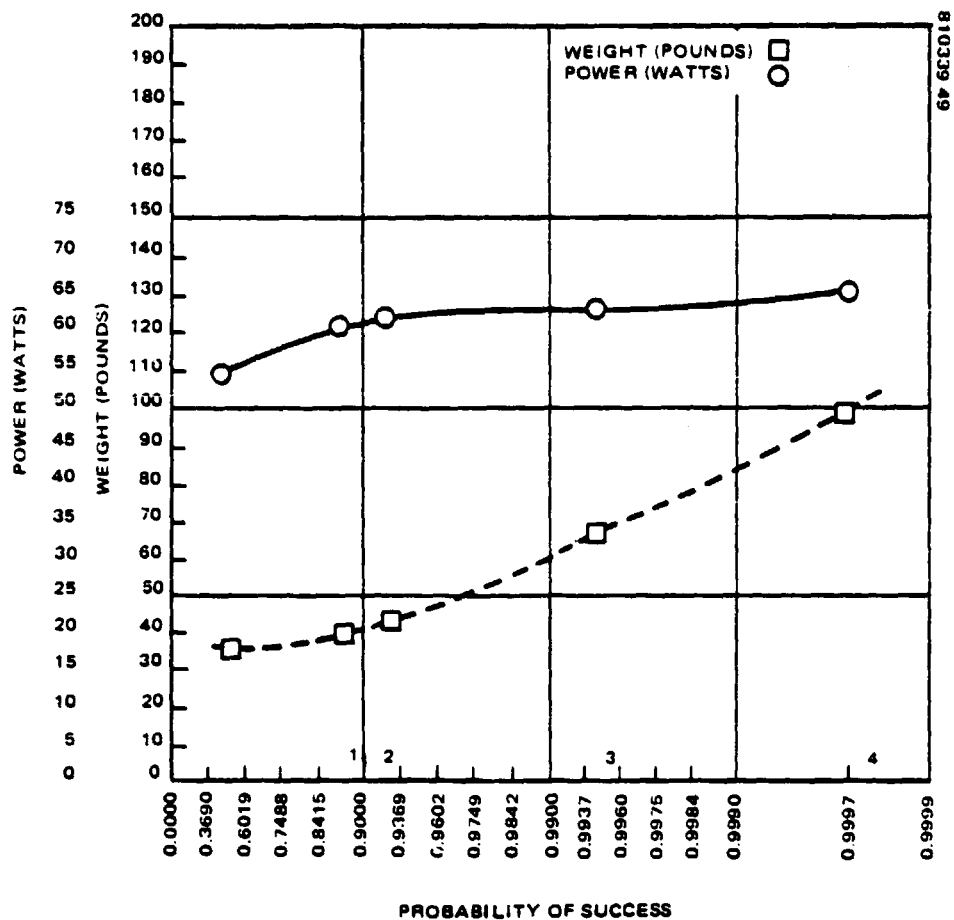


FIGURE 3.3-12. WEIGHT AND POWER VERSUS RELIABILITY FOR 64 BY 64 SWITCH MATRIX AND CONTROLLER



output memory must be dynamically interconnected. This interconnection is accomplished by means of a baseband switching matrix. The switching matrix output is routed to two output memories. Each output memory is dedicated to data which will go downlink on a particular scanning beam antenna.

The serial rate of data transferred between memories via the baseband switch is a design decision. Since a fixed data rate must flow between memories, a reduction in serial bit rate implies that the dimension and complexity of the baseband switch must increase.

The data rate chosen for the serial data transfer between memories is 64 Mbps. This data rate is consistent with the use of Fairchild FAST logic in the parallel to serial converters, in the serial to parallel converters, and in the switch. A faster serial data rate would require a technology change to more power consuming ECL logic.

The number of lines required for communication data at the IF switch input is four at 64 Mbps to handle a 256 Mbps throughput. Four output lines at 64 Mbps are also required. Two additional input lines at 64 Mbps each and output lines at 64 Mbps are provided to connect to the orderwire interface unit.

As the throughput capacity of the baseband processor is increased, the size of the baseband switch would have to be increased. The sizes of the switch for the experimental system and the operational system, including parts for the orderwire interface unit, assuming 64 Mbps serial bit streams, are shown in Table 3.3-3.

The baseband switch technology is extendable to the size required for the operational system, i. e., it is not necessary to run serial bit stream as ECL speeds in the order of 275 Mbps.

Figure 3.3-12 shows the trade between weight and power versus seven year reliability for a 64 by 64 switch and controller. Referring to this figure, the redundancy assumed in label points 1, 2, 3, 4 is as follows:

- 1) 1 redundant memory module; 1 extra feedback path in the switch
- 2) 2 redundant memory modules; 2 extra feedback paths in the switch

TABLE 3.3-3. REQUIRED BASEBAND SWITCH MATRIX SIZE

System	Data Throughput Capacity	Switch Size
Experimental	256 Mbps	Dual 4 by 3
Operational	4 Gbps	Dual 49 by 33

- 3) Same as 2 except for 2 for 1 redundancy
- 4) 3 for 1 redundancy on the controller and 3 feedback paths in the switch

The study shows that a high reliability switch and controller may be achieved with about 130 watts and 50 pounds. An operational system utilizing Fairchild FAST logic is feasible.

Although increasing the internal data rates would reduce the complexity of the baseband switch, the switch controller complexity remains essentially the same for either data rate. This is because the same number of interconnects must be made, and hence stored, for either arrangement. Since the switch controller consumes about 75 percent of the switch/controller weight budget, little would be gained by using a simpler, higher speed baseband switching matrix.

### 3.3.3.5 System Synchronization

The master timing source for the TDMA system is the spacecraft oscillator. The spacecraft oscillator frequency is finely adjusted as required by command from the master control station. Since onboard demodulation and modulation are functional only in the CPS mode, the method of system synchronization is different in the CPS and trunk modes.

#### 3.3.3.5.1 Trunk Mode

In the trunk mode, system synchronization is maintained by providing a loopback window, wherein a trunk station's uplink transmission is returned as a downlink transmission back to the originating station. The loopback window is created by providing the proper IF switch configuration at the beginning of each frame. At the beginning of each frame, a loopback window will be created for each beam.

Each trunk station will transmit a preamble which will pass, with time truncation, through the loopback window. The preamble for frame synchronization consists of a unique word followed by some metric bits. For perfect time synchronization, a fixed number of metric bits will be truncated by the end of the loopback window on the spacecraft. The required transmit timing adjustment may be determined by counting the actual number of metric bits that are returned through the spacecraft window. The downlink frame starts with the returned preamble. The returned unique word provides the ground terminal with downlink frame synchronization.

The provision for synchronization in the trunk mode consists of the capability to load the proper sequences into the IF switch controller memory to create the loopback window.

### 3.3.3.5.2 CPS Mode

In the CPS mode, the spacecraft may demodulate and modulate. On the downlink, the spacecraft generates and modulates a dwell start unique word at the beginning of every scan dwell. This unique word is demodulated by the CPS stations in the downlink antenna footprint. The unique word is generated and formatted on the spacecraft by the orderwire interface unit.

Uplink timing is maintained by the spacecraft reporting back uplink burst timing error to each CPS terminal. Each uplink burst transmission contains a preamble. The preamble contains a unique word which is detected through correlation on the spacecraft. Each burst has an expected arrival time. By taking the difference between the actual burst arrival time and the expected burst arrival time, the sync interface unit in the baseband processor computes the burst timing error. These measurements are periodically transferred to the orderwire interface unit where they are formatted for downlink orderwire transmission to the originating CPS stations. From this error measurement, the CPS station may correct its uplink burst timing.

### 3.3.3.6 Order Wire

Time slots, which establish order wire channels, are reserved for the communication of systems command, control, status, and request information between terminals or between a terminal and the spacecraft.

#### 3.3.3.6.1 Order Wire in the Trunk Mode

In the trunk mode, the orderwire channels are used for communication between the master control stations and the trunk stations. Typical uses of the orderwire channel include requests for more channel capacity, requests for less channel capacity, changeover to a new frame format, and changeover to a space diversity earth station. A frame reformat will require several uses of the orderwire channel to enable a smooth transition.

#### 3.3.3.6.2 Order Wire in the CPS Mode

In the CPS mode, the orderwire channels are used for communications between the CPS stations and the master control station and for communication between the stations and the baseband processor in the spacecraft. Typical uses of the orderwire channel include requests for more channel capacity, requests for less channel capacity, changeover to a new frame format, changeover to encoding or nonencoding on uplinks and downlinks and system synchronization, and carrier level report back from the satellite.

Requests for changes in time slots originate at the stations and are routed to the master control station. Changeover commands in frame format, frequency assignment, and encoded/nonencoded mode originate at the master control station and are distributed to the CPS stations in the network. The baseband processor transmits timing update and signal strength information to the CPS terminals via the downlink orderwire channel.

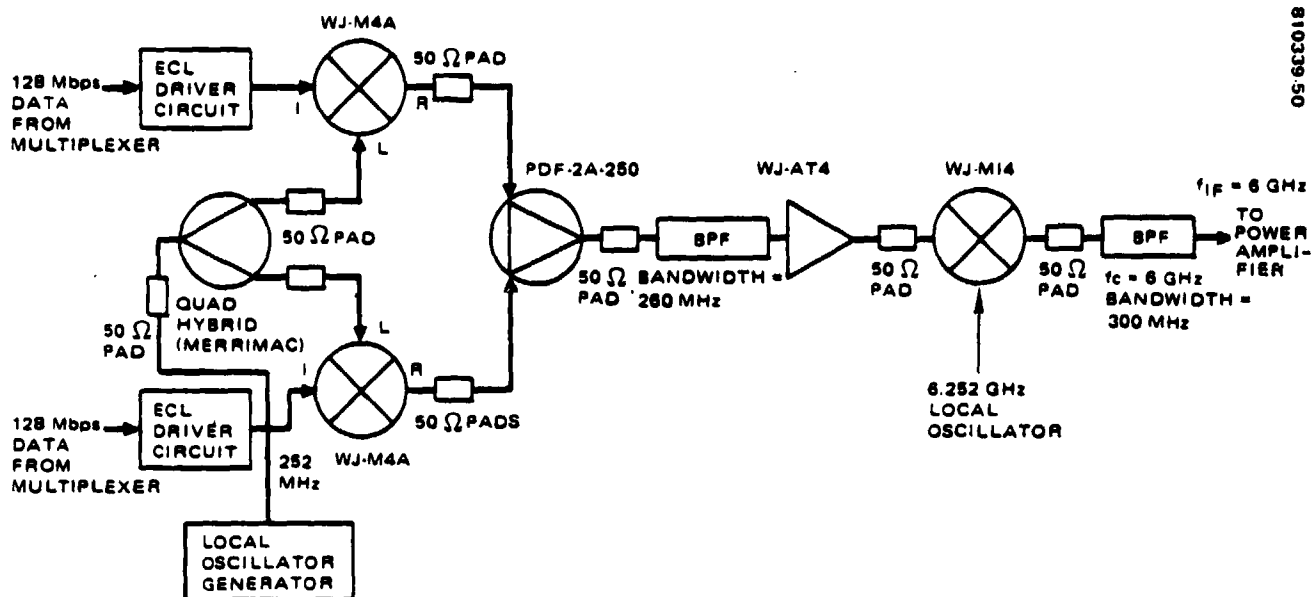


FIGURE 3.3-13. 256 MBPS QPSK MODULATOR AND IF UPCONVERTER

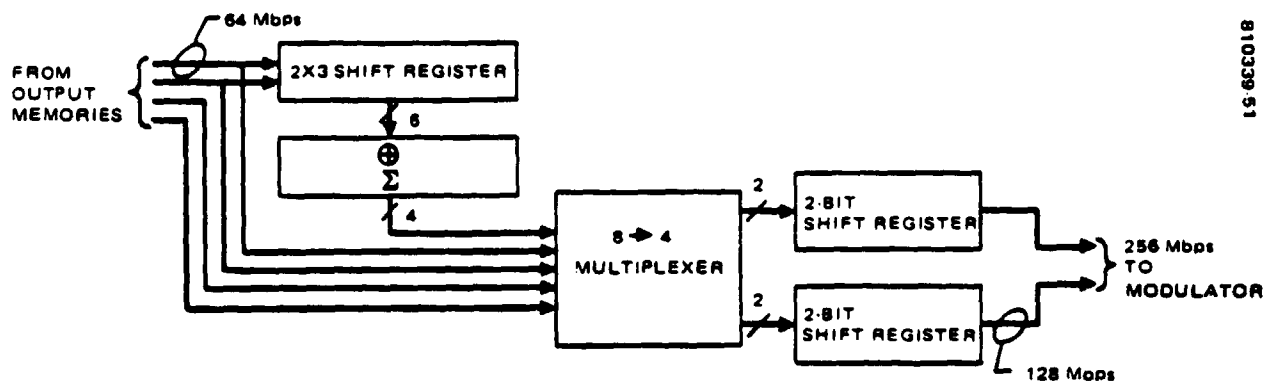


FIGURE 3.3-14. CONVOLUTIONAL ENCODER BLOCK DIAGRAM

### 3.3.3.7 Modulators

The spacecraft contains two identical 256 Mbps QPSK modulators. The modulators incorporate thin film RF amplifiers, RF hybrid packages, and currently available ECL logic circuits. A block diagram of one of the demodulators is shown in Figure 3.3-13.

The modulator places two parallel data streams of 128 Mbps rate onto a single carrier to form a 256 Mbps QPSK signal. In phase and quadrature phase versions of a local oscillator signal are created by dividing a 252 MHz signal in a quadrature hybrid device. Each data stream is biphase modulated onto one of the quadrature signals with a double balanced mixer. The two resulting signals are added together to form a QPSK signal.

The signal is then bandpass filtered so that the two sidebands created in the subsequent mixing process will not overlap. The signal is then mixed with another local oscillator to upconvert it to 6 GHz. A bandpass filter after the mixer selects the lower sideband at 6 GHz.

### 3.3.3.8 Convolutional Encoder

There are two rate  $1/2$ , constraint length 5 convolutional encoders on the spacecraft. A block diagram of a convolutional encoder is shown in Figure 3.3-14. A pair of 64 Mbps data lines enters a 2 bit wide by 3 bit long shift register which has all of its taps available to a mod-2 adder. This adder generates four linear combinations of its inputs. Next, a multiplexer selects between the mod-2 sums and the four input lines. This feature permits the encoder to be bypassed. Finally, the four outputs of the multiplexer are reduced to a pair of 128 Mbps lines by a pair of 2 bit parallel to serial registers.

This function will be fabricated as a Fairchild F300 type ECL gate array. The gate array has adequate speed and reduces the IC count to one for the entire encoder.

### 3.3.3.9 Digital Routing Controller

The digital routing controller serves as a buffer between the orderwire and T&C functions and the remainder of the baseband processor. The primary function of the controller is to program the memories which control the data paths through the communication subsystem (memory controllers, IF switching matrix controller, BFN controller, and the baseband switch).

The unit has command inputs from the command unit and the orderwire interface. The command unit is very low rate, so it is used for initialization purposes, with the orderwire channel being used for setting up complex routing functions quickly. It has internal inputs which are of a telemetry nature (signal strength, synchronization interface, switching controller memory contents, and the demodulator synchronization detectors).

Telemetry outputs are supplied to the telemetry unit and the orderwire interface. The orderwire telemetry link is the primary means for synchronizing the ground terminals. Internal outputs go to the controller memories to set up new switch configurations and scan beam patterns, and to the demodulators for signaling the ends of the bursts.

For a typical frame reformat operation, commands will be sent up the orderwire channel to the digital routing controller. There they will be decoded and sent to the appropriate controller. Once all the controllers have been loaded with the new configurations, a switchover command will be sent to them, causing the new configuration to take effect at the start of the next 1 ms frame.

When the subsystem is first powered up, it is not possible to send commands up the orderwire channel. However, the command link is operational continuously and the link can command the routing controller to set up a pre-established switching configuration. Once this pre-established configuration is operational, the orderwire channel may be used to update the configuration in accordance with traffic demands.

The digital routing controller will be built around a bit-slice type processor. The logic circuitry will be built using Schottky TTL and low power Schottky TTL. The memory will use low power TTL RAMs with error correction to prevent inadvertent reconfiguration in the event of a cosmic particle induced soft error.

#### 3.3.3.10 BFN Controller

The beam forming network (BFN) controller generates a repetitive sequence of control words to determine the position of a scanning antenna beam. Since the system has two uplink and two downlink scanning beam antennas, four BFN controllers are needed. Each 1 ms frame may be divided into as many as 64 beam positions of selectable duration.

A block diagram of the BFN controller is shown in Figure 3.3-15. Central to the unit are two identical memory units, A and B. In operation, one of the memories is on-line and supplies beam positions to the BFN. The other memory is off-line and may be loaded through the command interface unit to a different configuration. When it is desired to exchange the roles of memories A and B a command is sent, then at the start of the next 1 ms frame the memory roles will reverse. By switching at the frame boundary, the service is not interrupted. The memory mode control maintains the status of which memory is on-line and off-line, and which memory is to be verified by the telemetry interface unit.

A switchover time is stored with each scan beam position in memory. The timing unit compares these switchover times with the frame time, which it maintains. When they are equal, the memory address counter is incremented and the next switch state is read out.

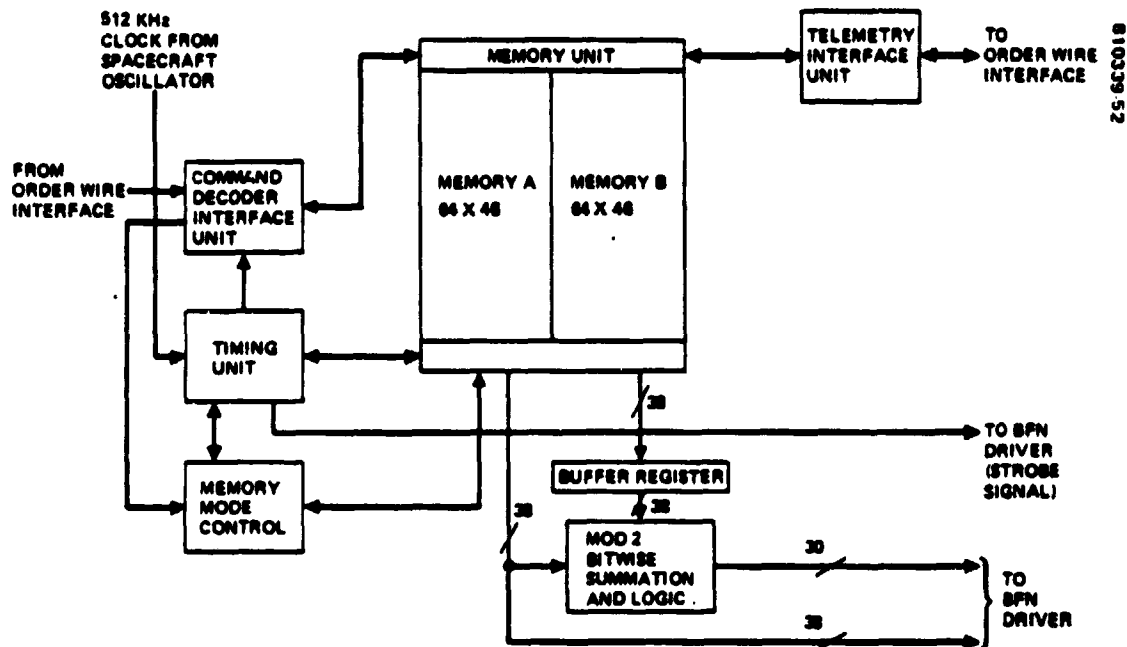


FIGURE 3.3-15. BFN CONTROLLER BLOCK DIAGRAM

The switching elements of the BFN only use power when they change state. For this reason, the BFN controller has two outputs, the beam position (38 bits) and the switch element strobes (30 bits). The mod-2 bitwise summation compares the previous beam position with the current and generates a strobe signal for each switch element setting that is different. In this way, only the switch elements which must change are strobed, thus greatly reducing the power consumption of the BFN.

The memories are radiation hard CMOS RAMs. This technology consumes very little power and is nearly completely immune to cosmic particle induced soft errors. Most of the logic circuitry is low power Schottky TTL, chosen because of its good speed power performance, ready availability, and proven space record. The remainder of the logic circuitry is made of standard Schottky TTL because of certain critical timing requirements.

### 3.3.3.11 IF Switch Controller

The IF switch controller generates a repetitive sequence of control words to determine the interconnection of trunk beams by the IF switch matrix. Each 1 ms frame may be divided into as many as 64 traffic bursts of selectable duration. In a traffic burst, each output of the switch matrix may have any one of the inputs routed to it.

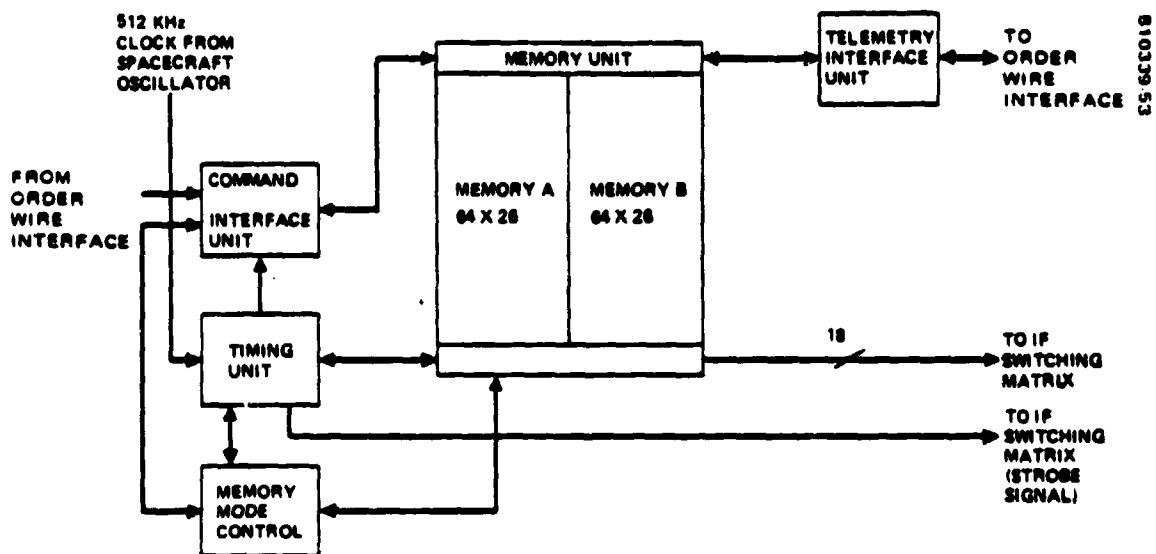


FIGURE 3.3-16. IF SWITCHING MATRIX CONTROLLER BLOCK DIAGRAM

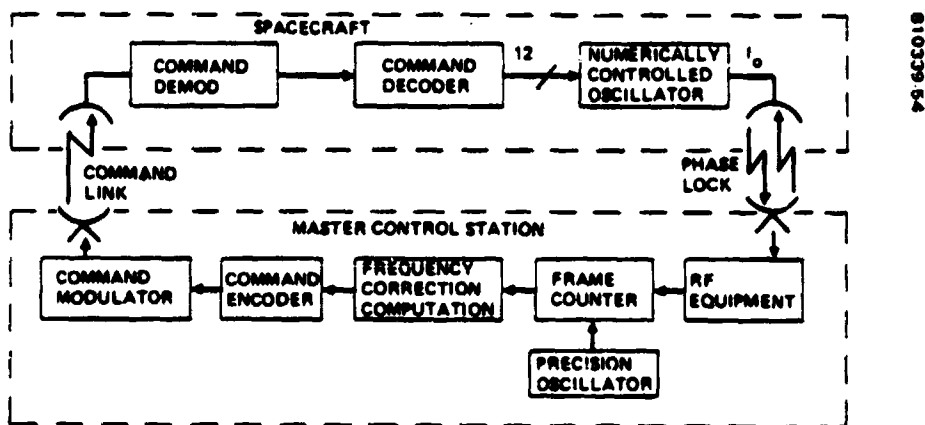


FIGURE 3.3-17. SPACECRAFT OSCILLATOR FREQUENCY UPDATE TECHNIQUE



A block diagram of the IF switching matrix controller is shown in Figure 3.3-16. Central to the unit are two identical memory units, A and B. In operation, one of the memories is on-line and supplies switch states to the switch matrix. The other memory is off-line and may be loaded via the orderwire channel (through the command interface unit) to a different configuration. When it is desired to exchange the roles of memories A and B a command is sent, then at the start of the next 1 ms frame the memory roles will reverse. By switching at the frame boundary, the service is not interrupted. The memory mode control maintains the status of which memory is on-line and off-line, and which memory is to be verified by the telemetry interface unit.

A switchover time is stored with each switch configuration in memory. The timing unit compares these switchover times with the frame time, which it maintains. When they are equal, the memory address counter is incremented and the next switch state is read out.

The memories are radiation hard CMOS RAMs. This technology consumes very little power and is nearly completely immune to cosmic particle induced soft errors. Most of the logic circuitry is low power Schottky TTL, chosen because of its good speed power performance, ready availability, and proven space record. The remainder of the logic circuitry is made of standard Schottky TTL because of certain critical timing paths.

#### 3.3.3.12 Spacecraft Oscillator Frequency Control

The frequency of the oscillator which determines the frame rate in the spacecraft is monitored by the master control station. The master control station is phaselocked to the spacecraft oscillator. Figure 3.3-17 shows a technique for spacecraft oscillator frequency correction. The number of received frames (and fractions of a frame) received over a period of time are compared to the expected number of received frames using the ground terminal oscillator as a reference. A frequency correction is computed from the error, and this error is transmitted to the spacecraft on the command link. The spacecraft oscillator achievable stability is  $\pm 9.2$  by  $10^{-11}$  per day. The earth terminal oscillator stabilities are  $\pm 1$  by  $10^{-11}$ .

A daily update in the spacecraft oscillator frequency is sufficient to limit the minor frame slippage at the spacecraft/terrestrial interface in the earth terminals (due to the combined effects of differential earth terminal clock drift and spacecraft oscillator drift) to one 125  $\mu$ sec minor frame slip every 70 days.

### 3.3.4 Weight and Power Estimates for the Baseband Processor

The weight and power estimates for the analog electronics are shown in Table 3.3-4 and for the digital electronics in Table 3.3-5. The numbers of active units of each type are given. For reliability, redundant units are provided and the total numbers of units are also listed. The weight of the analog electronics is 37 pounds and the weight of the digital electronics is 74.2 pounds. The total weight of the baseband processor is therefore 111.2 pounds.

The baseband processor may either operate in the CPS or trunk mode. In the CPS mode, the IF switch controller is not utilized, and the digital electronics power estimate in Table 3.3-6 reflects this. In the trunk mode, the digital electronics subunits, which are powered, are the IF switch controller, the orderwire interface unit, the digital routing controller, and the power supply (operating at a reduced power level). The digital electronics power estimate in the trunk mode is given in Table 3.3-6.

All of the elements of the processor are required in the CPS mode except the IF switch controller.

The total baseband processor powers in the CPS and trunk modes are summarized in Table 3.3-7.

If both CPS and trunk modes were operated simultaneously the total power would be 230.1 watts.

TABLE 3.3-4. ANALOG ELECTRONICS POWER, SIZE, AND WEIGHT ESTIMATES

Unit Type	No. of Active Units	Total No. of Units	Size Per Unit, in.	Total Power, W	Total Weight, lb
IF downconverter and routing switch	1	2	8-1/2 x 6 x 2	1.8	4
128 Mbps demodulator (soft decision)	1	2	5 x 6 x 2	4.5	3.6
128 Mbps demodulator (hard decision)	2	3	5 x 6 x 2	8.0	5.4
32 Mbps demodulator (soft decision)	4	4	5 x 6 x 1-1/2	13.6	6.0
32 Mbps demodulator (hard decision)	8	8	5 x 6 x 1-1/2	22.4	12.0
256 Mbps modulator and upconverter	2	3	5 x 6 x 2	6.0	6.00
Total				56.3	37.0

TABLE 3.3-5. DIGITAL ELECTRONICS POWER, SIZE, AND WEIGHT ESTIMATES

Subunit	No. of Active Units	No. of Units	Total Volume, in. <sup>3</sup>	Total Power, W	Total Weight, lb
Input memory	2	3	252	14.96	7.56
Output memory	2	3	240	12.32	7.20
FEC input memory	1	2	576	10.20	17.28
FEC output memory	1	2	104	1.94	3.12
FEC decoder	4	4	75.3	17.28	2.26
Memory control	6	7	105	3.18	3.15
Convolutional encoder	2	2	4	4.0	0.12
128 Mbps ambiguity resolver	3	3	6	3.75	0.18
32 Mbps ambiguity resolver	9	9	18	0.09	0.54
128 Mbps synch interface	3	3	6	3.75	0.18
32 Mbps synch interface	9	9	18	0.09	0.54
Signal strength interface	1	2	10	0.25	0.30
OW interface	1	2	104	1.94	3.12
Scan beam controller	4	5	334	34.56	10.0
IF switch controller	1	2	116.6	5.76	3.5
Digital routing controller	1	2	166.6	25.00	5.0
4 x 3 baseband switch (dual)	1	2	5.0	0.20	0.15
Power supply	1	2	480	34.68	10.0
Totals			2620		74.2
CPS				168.2	
Trunk				41	

TABLE 3.3-6. TRUNK MODE DIGITAL ELECTRONICS POWER ESTIMATE

<u>Subunit</u>	<u>Power, Watts</u>
IF switch controller	5.76
Orderwire interface unit	1.94
Digital routing controller	25.0
Power supply	8.2
Total	41

TABLE 3.3-7. BASEBAND PROCESSOR POWER

Component	CPS Mode Power, Watts	Trunk Mode Power, Watts
Analog electronics	56.3	0
Digital electronics	169.2	41
Total	224.5	41

### 3.3.5 Performance

#### 3.3.5.1 Carrier Jitter Degradation on BER

The QPSK demodulators and synchronization circuits are shown in Figures 3.3-8 and 3.3-9. Gardner\* has shown that for the carrier recovery circuit shown in Figures 3.3-8 and 3.3-9, with  $BT = 0.07$ , where  $B$  is the bandpass filter bandwidth and  $T$  is the symbol duration, the recovered carrier phase jitter less than 3.2 degrees at

$$\frac{E_b}{N_o} = 10.53 \text{ dB}$$

and the jitter is less than 2.3 degrees at

$$\frac{E_b}{N_o} = 15 \text{ dB}$$

The error rate with phase jitter may be evaluated assuming the phase error has approximately a Gaussian distribution and that  $\pi/\sigma \gg 1$  where  $\sigma$  is the rms phase error in radians. Under this assumption, the error probability,  $P_e$ , is given by

---

\*Floyd M. Gardner, "Carrier and Clock Synchronization for TDMA Digital Communications," European Space Agency Report, ESA TM-169, December 1976.

$$P_e = \frac{1}{2} \int_{-\pi/\sigma}^{\pi/\sigma} \operatorname{erfc} \left[ \sqrt{\frac{2E_b}{N_o}} (\cos(\sigma y) - \sin(\sigma y)) \right] \frac{1}{\sqrt{2\pi}} e^{-y^2/2} dy$$

$$+ \frac{1}{2} \int_{-\pi/\sigma}^{\pi/\sigma} \operatorname{erfc} \left[ \sqrt{\frac{2E_b}{N_o}} (\cos(\sigma y) + \sin(\sigma y)) \right] \frac{1}{\sqrt{2\pi}} e^{-y^2/2} dy$$

Where,

$$\operatorname{erfc}(x) = \frac{1}{\sqrt{2\pi}} \int_x^{\infty} e^{-y^2/2} dy$$

$E_b$  = the signal energy per bit

$\frac{N_o}{2}$  = the power spectral density of the additive Gaussian noise

The error rate degradation, D, in dB, due to recovered phase reference jitter is shown in Table 3.3-8.

The analysis does not include the effects of static phase offset of the recovered phase due to offset of the signal IF frequency and the bandpass filter center frequency.

The carrier acquisition time for the circuit is eight symbol intervals.

TABLE 3.3-8. PHASE JITTER DEGRADATION

$\frac{E_b}{N_o}$ , dB	Phase Jitter Deg, rms	D, Error Rate Degradation, in dB
10.53	3.2	0.33
15	2.3	0.46

### 3.3.5.2 Clock Jitter Degradation on Bit Error Rate

The QPSK demodulators and synchronization circuits are shown in Figures 3.3-8 and 3.3-9. Gardner has shown for the clock recovery circuits shown in these figures, with  $BT = 0.035$ , where  $B$  is the bandpass filter bandwidth in Hertz and  $T$  is the symbol duration in seconds,

$$\frac{\sigma_T}{T} = 0.013 \quad \text{at} \quad \frac{E_b}{N_o} = 10.53 \text{ dB},$$

and

$$\frac{\sigma_T}{T} = 0.010 \quad \text{at} \quad \frac{E_b}{N_o} = 15 \text{ dB},$$

where

$\sigma_T$  is the rms timing error, and

$T$  is the symbol period.

Assuming the timing error has approximately a Gaussian distribution and  $\sigma_T/T \ll 1$ , the error probability for QPSK may be expressed as,

$$P_e = \frac{1}{2} \operatorname{erfc} \left( \sqrt{\frac{2E_b}{N_o}} \right) + \frac{1}{2} \int_{-T}^T \operatorname{erfc} \left[ \sqrt{\frac{2E_b}{N_o}} \left( 1 - \frac{2|\tau|}{T} \right) \right] P(\tau) d\tau$$

where,

$$p(\tau) = \frac{1}{\sqrt{2\pi} \sigma_T} e^{-\frac{\tau^2}{2\sigma_T^2}}$$

and

$$\text{erfc}(x) = \frac{1}{\sqrt{2\pi}} \int_x^{\infty} e^{-y^2/2} dy$$

The bit error rate degradation due to timing jitter is shown in Table 3.3-9.

The analysis did not include the effect of static phase error in the recovered clock due to mismatch between the clock frequency and the center frequency of the bandpass filter in the synchronization circuit.

TABLE 3.3-9. TIMING JITTER DEGRADATION

$\frac{E_b}{N_o}$ , dB	$\frac{\sigma_r}{T}$	Error Rate Degradation, dB
10.53	0.013	0.12
15	0.010	0.12

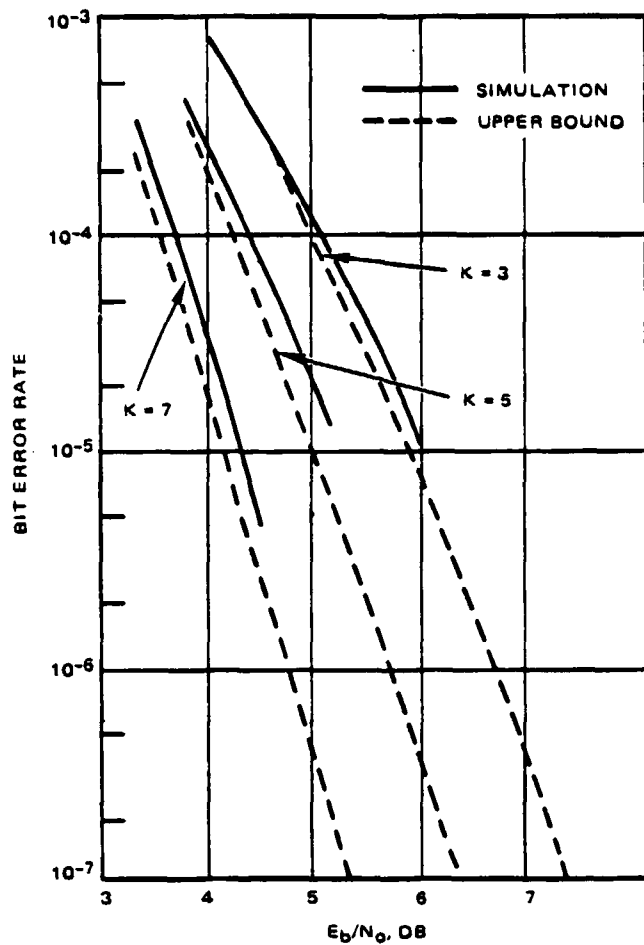
### 3.3.5.3 Demodulator Performance Summary

The demodulator performance summary is summarized in Table 3.3-10. The degradation factors included are carrier jitter, clock jitter, and non-ideal detection filtering.

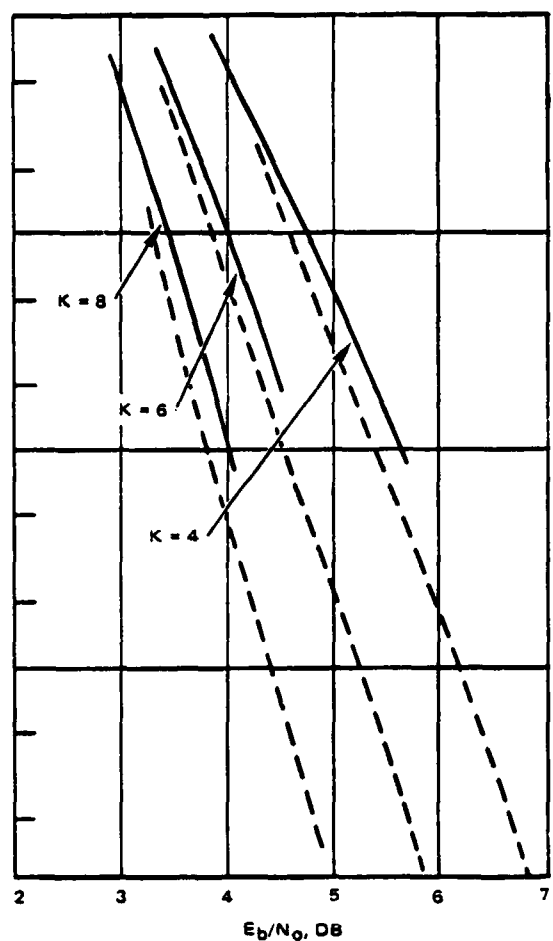
TABLE 3.3-10. BURST DEMODULATOR PERFORMANCE ESTIMATE

Degradation Component	dB		Comments
	Degradation at $E_b/N_o = 10.53$ dB	Degradation at $E_b/N_o = 15$ dB	
Filtering and limiting	0.3	0.3	$BT = 1.5$ $T =$ symbol period At $E_b/N_o = 10.53$ dB, $\sigma_\phi = 0.056$ radian At $E_b/N_o = 15.0$ dB, $\sigma_\phi = 0.040$ radian At $E_b/N_o = 10.53$ dB, $\sigma_r/T = 0.013$ At $E_b/N_o = 15.0$ dB, $\sigma_r/T = 0.010$ $B_N T = 0.07$ for carrier recovery $B_N T = 0.035$ for clock recovery
Carrier jitter	0.33	0.46	
Clock jitter	0.12	0.12	
Nonideal detection filters	0.7	0.7	
Totals*	1.5	1.6	

\*Does not include effects of static phase and clock timing offsets due to filter drift.



a) TRANSFER FUNCTION BOUND  $K = 3, 5, 7$



b) TRANSFER FUNCTION BOUND  $K = 4, 6, 8$

FIGURE 3.3-18. BIT ERROR RATE VERSUS  $E_b/N_0$  FOR RATE 1/2 VITERBI DECODING. EIGHT LEVEL QUANTIZED SIMULATIONS WITH 32 BIT PATHS, AND INFINITELY FINELY QUANTIZED TRANSFER FUNCTION BOUND.



#### 3.3.5.4 Coding Gain

A rate 1/2, constraint length 5, 3 bit soft decision Viterbi Algorithm decoder was chosen to provide a compromise between coding gain and onboard equipment complexity. For rate 1/2 codes, Figure 3.3-18 given by Jacobs and Heller,\* shows the comparison in error rate performance. Figure 3.3-18(a) shows a comparison between constraint length 3, 5, and 7, rate 1/2 convolutional codes; Figure 3.3-18(b) shows the error rate performance between constraint length between constraint length 4, 6, and 8 using the Viterbi decoding algorithms. The solid curve are simulation results for three bit soft decision decoding. The dashed lines are upper bounds for hard decision decoding. The coding gains for the K = 3, 5, and 7 codes are given in Table 3.3-11.

Since the decoder complexity increases exponentially with constraint length, the K = 5 decoder provides a good compromise between performance and complexity.

Figure 3.3-19 shows the error rate performance for a constraint length 5 decoder for one, two, and three bits of soft decisioning.\*\* The improvement in performance of a two bit soft decision decoder over a hard decision decoder is about 0.92 dB. The addition performance improvement of a three bit soft decision decoder over a two bit soft decision decoder is about 0.78 dB. The performance curve for nonencoded QPSK is provided as a reference.

Since the burst rate is fixed, twice as much energy per information bit is expended in transmission when rate 1/2 encoding. This is a 3 dB improvement due to rate. The total link improvement due to convolutional coding is given in Table 3.3-12.

TABLE 3.3-11. CODING GAINS OF RATE 1/2  
CONVOLUTIONAL CODES USING THE  
VITERBI DECODING ALGORITHM

<u>Constraint Length, K</u>	<u>Coding Gain, dB</u>
3	3.6 dB
5	4.4 dB
7	5.3 dB

\*I. M. Jacobs and J. A. Heller, "Performance Study of Viterbi Decoding as Related to Space Communications," Technical Report AD73821, The Linkabit Corporation, San Diego, CA, 31 August 1971.

\*\*J. Omura, "Convolutional Decoding; Theory and Practice," Lecture Notes, University of California, Los Angeles, University Extension for Continuing Education in Engineering and Mathematics, 26 to 28 June 1974.

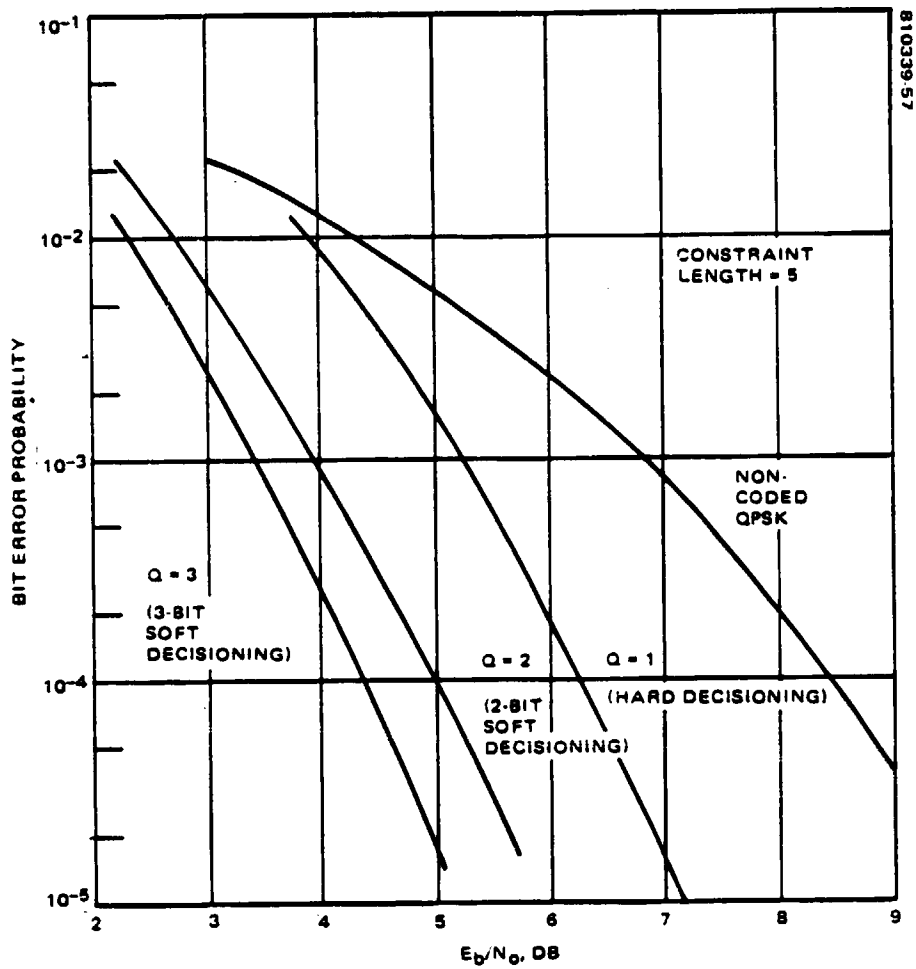


FIGURE 3.3-19. PERFORMANCE COMPARISON OF VITERBI DECODING USING RATE 1/2, CODE WITH 2-, 4-, AND 8 LEVEL QUANTIZATION, PATH LENGTH = 32 BITS

TABLE 3.3-12. CODING IMPROVEMENT

<u>Gain Type</u>	<u>Gain, dB</u>
R = 1/2 K = 5	4.4 dB
3 bit soft decision Viterbi decoder	
Rate gain	3.0 dB
Total improvement	7.4 dB

### 3.3.6 Impact of the Reduced Capacity (Option 1) Processor

A reduced throughput capacity (Option 1) baseband processor has been studied to obtain power and weight estimates. The functional block diagram of the Option 1 baseband processor is shown in Figures 3.3-20, 3.3-21, and 3.3-22. The reduced capacity system has two simultaneous 32 Mbps uplink TDMA channels. A single uplink and single downlink scanning beam antenna is incorporated into this system. The downlink consists of a single 128 Mbps TDMA channel. The analog electronics power and weight estimates for the Option 1 processor are shown in Table 3.3-13. The digital electronics power and weight estimates for the Option 1 processor are given in Table 3.3-14.

A comparison of the power and weight requirement of the full capacity processor and the reduced capacity (Option 1) processor is given in Table 3.3-15.

TABLE 3.3-13. OPTION 1 PROCESSOR ANALOG ELECTRONICS POWER, SIZE, AND WEIGHT ESTIMATES

Unit Type	No. of Active Units	No. of Units	Size Per Unit, in.	Total Power, W	Total Weight, lb
IF downconverter and routing switch	1	2	8-1/2 x 6 x 2	1.8	4
32 Mbps demodulator (soft decision)	1	2	5 x 6 x 1-1/2	3.4	3
32 Mbps demodulator (hard decision)	2	3	5 x 6 x 1-1/2	5.6	4.5
128 Mbps modulator and upconverter	1	2	5 x 6 x 2	3	4
Total	—	—	—	13.8	15.5

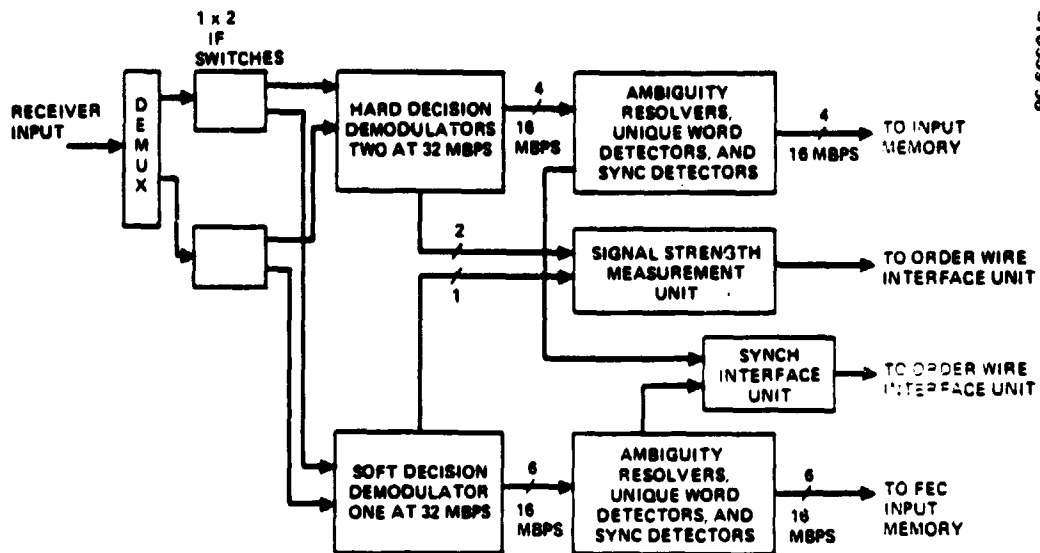


FIGURE 3.3-20. OPTION 1 REDUCED CAPACITY BASEBAND PROCESSOR BLOCK DIAGRAM, INPUT SECTION

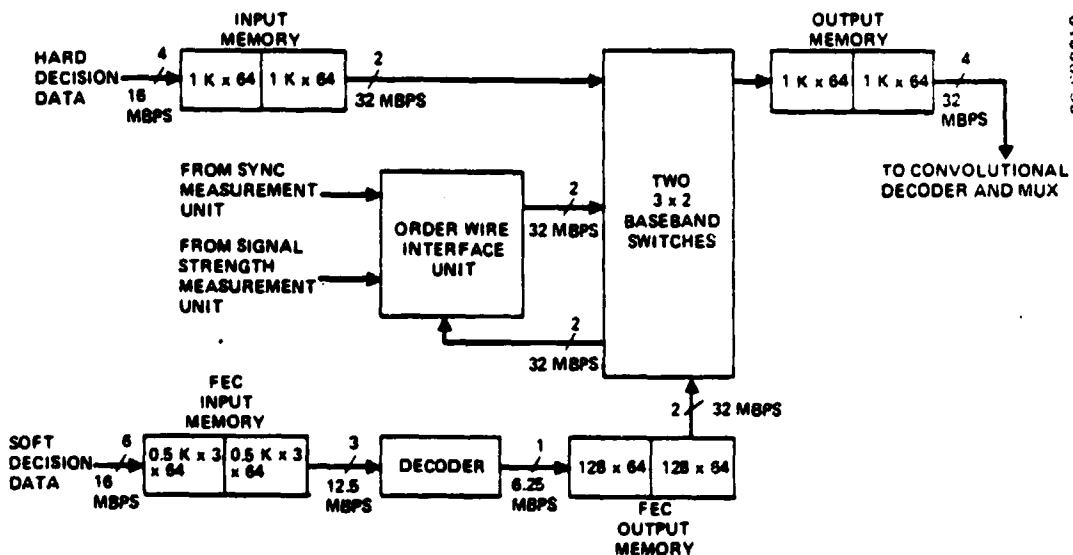


FIGURE 3.3-21. OPTION 1 BASEBAND PROCESSOR BLOCK DIAGRAM, STORE AND FORWARD SECTION

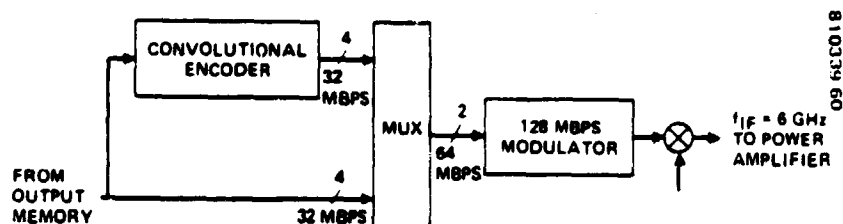


FIGURE 3.3-22. OPTION 1 BASEBAND PROCESSOR BLOCK DIAGRAM, OUTPUT SECTION

**TABLE 3.3-14. OPTION 1 PROCESSOR DIGITAL ELECTRONICS POWER, SIZE,  
AND WEIGHT ESTIMATES**

Subunit	No. of Active Units	No. of Units	Total Volume, in. <sup>3</sup>	Total Power, W	Total Weight, lb
Input memory	1	2	120	2.22	3.6
Output memory	1	2	108	2.00	3.26
FEC input memory	1	2	152	1.76	4.56
FEC output memory	1	2	108	1.88	3.26
FEC decoder	1	2	50	4.32	1.54
Memory control	4	4	81	2.12	2.45
Convolutional encoder	1	2	6	1.00	0.16
32 Mbps ambiguity resolver	2	2	5	0.02	0.16
32 Mbps sync interface	2	2	5	0.02	0.16
Signal strength interface	1	1	7	0.25	0.20
Order wire interface	1	2	140	1.94	4.24
Scan beam controller	2	3	270	17.28	8.16
IF switch controller	1	2	148	5.76	4.76
Digital routing controller	1	2	224	25.0	6.80
Baseband switch	1	2	6	0.16	0.20
Power supply	1	2	648	14.99	19.58
Total	—	—	2048	—	63.1
CPS mode				75 W	
Trunk mode				41 W	

**TABLE 3.3-15. BASEBAND PROCESSOR POWER AND WEIGHT SUMMARY**

Component	Full Capacity Processor			Reduced Capacity (Option 1) Processor		
	CPS Mode Power, W	Trunk Mode Power, W	Weight, lb	CPS Mode Power, W	Trunk Mode Power, W	Weight, lb
Analog electronics	56.3	0	37.0	13.8	0	15.5
Digital electronics	168.2	41	74.2	75	41	63.1
Total	224.5	41	111.2	88.8	41	78.6

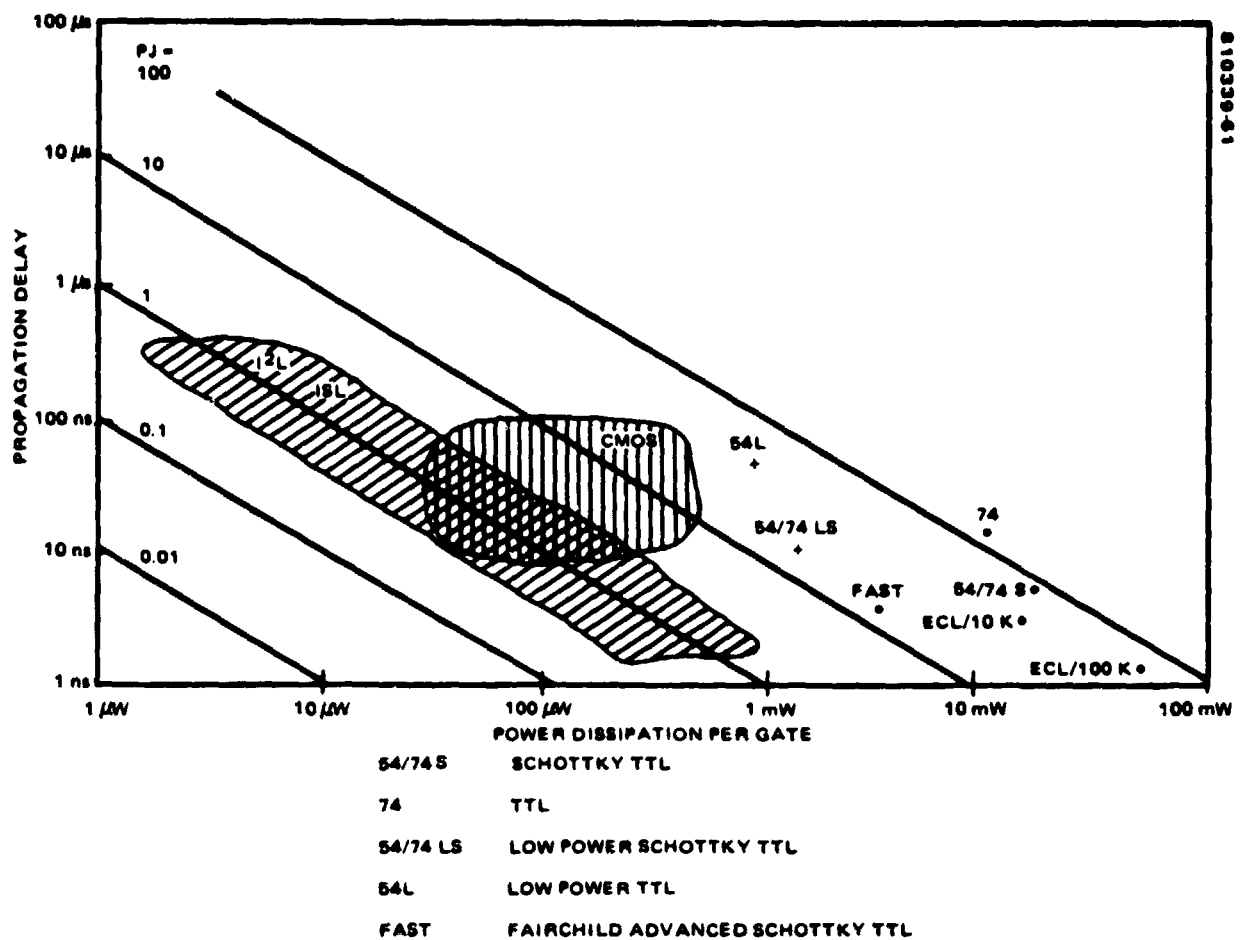


FIGURE 3.3-23. PROPAGATION DELAY VERSUS POWER DISSIPATION PER GATE FOR DIGITAL TECHNOLOGIES

The full capacity processor requires 224.5 watts in the CPS mode, 41 watts in the trunk mode, and weighs 111.2 pounds. The reduced capacity (Option 1) processor requires 88.8 watts in the CPS mode, 41 watts in the trunk mode, and weighs 78.6 pounds.

### 3.3.7 Technology Assessment

All of the technologies utilized in the baseband processor design will be available in 1982. The required LSI devices will be developed using gate array technology. Gate array devices have significant advantages over custom LSI devices:

- 1) Design time and cost of gate array development is far lower than full custom development.
- 2) Gate array device characteristics are better known than the characteristic of a newly developed custom LSI device.

Several device technologies are used for the gate array device types used in the design. The use of technology that meets the clock rate requirements of the logic design, and does not wastefully exceed the requirements, minimizes the overall power dissipation in the baseband processor. Figure 3.3-23 shows the propagation delay versus the power dissipation per gate for various digital technologies including ECL, Schottky TTL, TTL, low power Schottky TTL, low power TTL, CMOS, and I<sup>2</sup>L.

In the serial data transfer between memories which occur at a 64 Mbps clock rate, Fairchild FAST logic was chosen because of its speed capability at a low power dissipation level. While ECL is faster than FAST, it is considerably more power consuming and is on a poorer delay power product contour in Figure 3.3-23.

The gate array devices and technologies used in the baseband processor are listed in Table 3.3-16.

The numbers of devices and gate array technologies used in the digital electronics in the baseband processor design are listed in Table 3.3-17 and the analog electronics technologies are listed in Table 3.3-18. The physical design of the analog and digital electronics in the baseband processor is shown in Table 3.3-19.

### 3.3.8 Telemetry and Command List for the Digital Subsystem

The telemetry and command list is given in Table 3.3-20.

TABLE 3.3-16. GATE ARRAY DEVICES USED IN THE  
BASEBAND PROCESSOR DESIGN

<u>Function</u>	<u>Gate Array Technology</u>
Convolutional decoder	Fairchild 9480 1 <sup>3</sup> L
32 bit serial to parallel converter	Fairchild FAST
32 bit parallel to serial converter	Fairchild FAST
Ambiguity resolver	Fairchild FAST
Sync detector	Fairchild FAST
32 bit serial to parallel converter	Hughes 5 uM SOS-CMOS
32 bit parallel to serial converter	Hughes 5 uM SOS-CMOS
Convolutional encoder	Fairchild isoplanar ECL
High speed ambiguity resolver	Fairchild ECL
High speed sync interface	Fairchild ECL

TABLE 3.3-17. BASEBAND PROCESSOR DIGITAL ELECTRONICS COMPLEXITY ESTIMATE

Subunit	Disc	SSI	MSI	LSI	Gate Array Devices				
					SOS CMOS	Large 12L	Small 12L	ECL	Fast
Input memory			64		6				4
Output memory			64						8
FEC input memory			192		42				6
FEC output memory			32		8				2
FEC decoder			14			4			
Memory control		4	18						
Convolutional encoder		2						1	
128 Mbps ambiguity resolver		2						1	
32 Mbps ambiguity resolver		2					1		
128 Mbps synch interface		2						1	
32 Mbps synch interface		2					1		
Signal strength interface		1		1					
OW interface			32		8				2
Scan beam controller		12	38						
IF switch controller		10	30						
Digital routing controller			10	3					
Power supply	400	10							



TABLE 3.3-18. ANALOG ELECTRONICS TECHNOLOGY

<u>Component</u>	<u>Technology/Packaging</u>
IF downconverter and routing switch	<ul style="list-style-type: none"> <li>● Thin film RF amplifier chips, RF hybrid packages and GaAs FET solid state switches integrated into complex hybrid package</li> <li>● Discrete component filters</li> </ul>
128 Mbps demodulator	<ul style="list-style-type: none"> <li>● Thin film RF amplifiers and RF hybrids</li> <li>● ECL digital circuits</li> <li>● Discrete component filters</li> <li>● Quenchable BPFs are helical resonators</li> </ul>
32 Mbps demodulators	<ul style="list-style-type: none"> <li>● Thin film RF amplifiers and RF hybrids</li> <li>● Schotky TTL and ECL digital circuits</li> <li>● Discrete component filters</li> </ul>

TABLE 3.3-19. BASELINE PHYSICAL DESIGN APPROACH

Component Packaging	
RF analog	1 x 2 in. hybrids Multilayer PWBs
Digital	Multilayer PWBs
Power supply	3-D soldered/welded modules
Construction	
RF analog	PWBs bonded to honeycomb panel mounted in RF1 partitioned chassis
Digital	Multilayer PWBs bonded to honeycomb panel mounted in machined chassis
Power supply	Machined aluminum subassembly
Chassis	Milled out aluminum 60 mil lids

TABLE 3.3-20. TELEMETRY AND COMMAND LIST FOR DIGITAL SUBSYSTEM

Subunit	Command	Telemetry
IF switch controller	Load switch configuration sequence	Verify configuration sequence
	Sequence changeover	Verify changeover
BFN controller	Load scan sequence	Verify scan sequence
	Sequence changeover	Verify changeover
Digital routing controller	Load frame control sequence	Verify frame control sequence
	Sequence changeover	Verify sequence changeover
Oscillator	Set oscillator frequency	Verify digital word in oscillator controller
Convolutional decoder	Decode mode/test mode	Test data
Demodulators	Demodulate mode/test mode	Test data
Memories and baseband switch	Data routing mode/test mode	Test data

## 4. SPACE VEHICLE

### 4.1 SPACECRAFT BUS

The LEASAT bus has been chosen for the 30/20 GHz payload because it has ample payload capacity (>500 pounds, ~850 watts) and requires minimum modification but is inexpensive to launch. The LEASAT with the 30/20 GHz payload installed will require just over one-fourth of the payload bay length. Thus, the weight and length fractions of the shuttle payload will be nearly equal. This balance minimizes the shuttle launch cost and maximizes the opportunities for ride sharing. Also, the bus incorporates its own perigee stage so that a costly PAM is not needed. Other Hughes spacecraft were eliminated because either they had lower payload capability (SBS) or were most costly (HS 350). The LEASAT spacecraft will be flown and flight proven before the 30/20 GHz launch.

A description of the present LEASAT design will be presented first and then followed with a discussion of the modifications required for the 30/20 GHz program.

#### 4.1.1 Spacecraft Design

##### 4.1.1.1 Baseline Design

The LEASAT spacecraft is a dual spin configuration. The vehicle is spin stabilized and the communications payload is despun. It is inherently stable in all phases of the mission. The dual spin spacecraft is a well established, conservative design approach which has been used, and is now being used, for many satellites. Figure 4-1 provides an overview of the spacecraft system.

The spacecraft equipment is grouped into seven subsystems: communications; propulsion; telemetry, tracking, and command (TT&C); attitude control; power; thermal; and structure. The cylindrical, spinning section of the LEASAT spacecraft contains the solar cell arrays, power electronics, batteries, propulsion, and attitude control equipment. The despun section consists of an electronic equipment platform and the equipment of the communications and the telemetry, tracking, and command subsystem (including their antennas) which are mounted therein. The despun function is accomplished through a bearing and power transfer assembly (BAPTA).

#### 4. 1. 1. 2 Spinning Section

The external boundary of the spinning portion of the spacecraft illustrated by Figure 4-2 is the solar cell array cylinder. The cylinder, which is made up of four quarter cylinder sections, is supported by a truss structure at each of the four mating joints. The panels are removable to allow access to the spacecraft internal components. The four-sided truss structure is the primary load-carrying structure of the spacecraft. It supports the solar panel, all of the propulsion subsystem equipment, and eight platforms onto which are mounted the power control, attitude control, and TT&C spun electronics (see Figure 4-3). At its forward end, the truss also supports the BAPTA which, in turn, supports the despun section. The batteries are mounted on panels immediately adjacent to the solar panel mating joints.

The propulsion subsystems occupy most of the spinning section's volume. The solid propellant subsystem (SPS) is housed in the central cavity of the truss structure. The tanks of the liquid bipropellant subsystem (LBS) and the reaction control subsystem (RCS) are nestled between the members of the truss. These tanks include four 33 inch diameter propellant tanks and two helium tanks for the LBS, and four hydrazine tanks for the RCS. The SPS case is jettisoned from the spacecraft after its propellant has been expended.

#### 4. 1. 1. 3 Despun Section

The LEASAT satellite has all of the communications subsystem equipments, including the antennas, and most of the TT&C subsystem equipments in the despun section. Accordingly, no RF rotary joint is required and all RF signals travel unbroken paths between the multiplexers and the antennas, thereby eliminating a potential source of IM products and RF losses. The despun platform is located within the forward end of the spinning solar panel. High power transmitter equipments are mounted on the forward (antenna) side of the platform, and low signal level receiver and digital equipments are mounted to the aft side as shown in Figure 4-4.

The transmit and the receive UHF helical antennas are mounted on deployment mechanisms which are supported by the despun structure. The antennas deploy forward of the spacecraft body and away from each other, after being launched in a compact configuration that has them nestled close to each other and to the forward end of the spacecraft. A TT&C omnidirectional antenna is also deployed from its stowed launch position, to a position forward that of the deployed UHF antennas.

#### 4. 1. 1. 4 Design and Performance Characteristics

Large spacecraft bus performance margins support the prime mission objective of providing the specified communications service with a high probability of service continuity. This objective is achieved with an uncomplicated bus design incorporating key subsystem components which have been proven through wide use in long life synchronous orbit communications applications. Large margins are also provided for the communications subsystem performance.

A weight summary is shown in Table 4-1.

## SPACECRAFT SUBSYSTEMS

### • STRUCTURE

STS Cost-Geometry Optimized  
Conservatively Oversized  
In Current Flight Implementation  
Truss  
GRP Composite

Solar Panel Substrates  
Kevlar Construction from Current Flight Programs  
166" D x 108" L

Motor Adapter  
Permits Alternate Growth Motor

### • THERMAL

Predictable, Standard Spinner Design  
Benign (40° F to 71° F, 20° F Eclipse Min) Equipment Environment  
Spin Averaged Solar Load, Passive Design  
Simple Heater Augmentation on Propulsion, Batteries

### • POWER

Large Margins; Redundant  
Array Performance Backed by Over 80 Orbit Years Instrumented Flight Data  
Solar Cells, Power Control Electronics from Current Programs; Batteries, Discharge  
Regulator Scaled from Existing Designs  
1216 w. 5 year Equinox, Solar Flare Plus Trapped Radiation, 15% Array Margin  
Three 28.3 Ahr Batteries Including Redundancy; 42% DOD  
Constant Power, Current-Shared Battery Discharge  
Standard Passive Charge Control via Current-Limited Solar Cells; Continuous Trickle,  
Commandable High Rate

### • ATTITUDE CONTROL

Common Stable Spinner, Passive Nutation Damping, 50 RPM  
Motor/Bearing/Slipping Assembly: Intelsat IV/IVA, Comstar Design (over 50 orbit  
years on specific type)  
Existing Earth Sensors (14 flights), Sun Sensors (standard on all spinning Spacecraft)  
Earth Center Finding Despin Control - Simplification of Similar Flight Designs

### • PROPULSION SUBSYSTEMS

Proven Components  
System Proof Underway  
Provides 11% Mass Margin  
Solid Propellant Subsystem: Existing Minuteman Motor, over 600 Built; 7308 lb.  
Propellant, Fiberglass Case, CTPB 88% Solids  
Liquid Bipropulsion Subsystem: Regulated Bipropellant; Redundant Existing Design  
100 lb. Thrusters (Apollo) with 100:1 Nozzles; 3088 lb. Capacity, 4 Titanium Tanks,  
2 Helium Bottles, Welded Construction  
Reaction Control Subsystem: Flight Proven Tanks, Thrusters (Intelsat, Comstar, Others);  
Welded System, 352 lb. Capacity Accommodates 7 Years; 4 Lateral, 2 Axial 5 lb.  
Thrusters, Over 100 Flown

**BOLDOUT FRAME**

## COMMUNICATION SUBSYSTEM

### • ANTENNAS

#### UHF

- Design Based on Flight Experience/Test
  - MARISAT, SDS, TACSAT
  - Range Data On Modeled Spacecraft
- Intermodulation (IM) Product Control
  - Separate Transmit and Receive Antennas
  - Deployed Position Eliminates Spacecraft Coupling
  - Low-IM Construction
- Simple, Reliable Deployment
- Transmit and Receive
  - Type: Bifilar Helix
  - Polarization: RHCP

Axial Ratio: 0.8 dB  
Gain: 13.9 Tx/14.1 Rec

#### X-BAND HORNS

- Intelsat IVA Derived
- Earth Coverage, RHCP Transmit, LHCP Receive
- Gain 17.0 dB at  $\pm 9.0^\circ$
- Axial Ratio  $\leq 1.5$  dB

### • REPEATER

- Hardware Based on over 15 Orbit Years UHF Experience
  - MARISAT, SDS, TACSAT
- Extraordinarily High Reliability (0.937, 5 years)
  - Low Level Crosstrapping in Receiver
  - Ample Power and Mass Capability of Bus Used for Conservation
- IM Control
  - Low-IM Components in Transmit Line
  - No Common Transmit/Receive Path

CHANNEL	QTY	BW	G/T, dB/K
FB			
SHF Rcv		30 MHz	16.9
SHF Tx		50 MHz	-
UHF		25 KHz	-
25 KHz	6	25 KHz	13.9
500 KHz	1	500 KHz	13.9
5 KHz	5	5 KHz	13.9

### • COMMAND SUBSYSTEM

Reliable - Separate, Redundant Systems  
Clean Interface - Fully Compatible with Navy Equipment  
Capacity:  
Despun: 256 Pulsed, 8 Serial  
Spun: 128 Pulsed, 4 Serial

PARAMETER	FBP	OM
Link Margin	50 dB	19 dB
Coverage	Earth	40° T
Frequency		7980
Modulation	FSK	FM/FM
Rate	2/sec	≈ 1/sec

### • TELEMETRY SUBSYSTEM

Flexible Formatting, Reliable - Hughes Standardized Modular T  
Clean Interface - Fully Compatible with Navy Equipment  
Solid State Amplifier

Characteristics	
Frequency, MHz:	7245, 7275
EIRP, dBm:	28.3 over 40° Toroid in Transfer Orbit 37.4 over 13.4° Coverage On Orbit
Data Rate:	1000 bps
Modulation:	PCM/Biphase; 1.4 Rad max. Mod. Index
Despun Channels:	256
Spun Channels:	128
Dwell Mode:	1-7 CH.
Submultiplexing:	Battery Cell Voltages (96) Temperatures

FIGURE 4-1. DESIGN CONFIDENCE RESULTS FROM UNCOMPLICATED SPINNING CONFIGURATION, HIGH FLIGHT CONTENT SUBSYSTEMS ASSURE PERFORMANCE MARGINS

ance/Test  
Spacecraft  
Control  
ive Antennas  
es Spacecraft Coupling

Axial Ratio: 0.8 dB  
Gain: 13.9 Tx/14.1 Rec at  $\pm 9.3^\circ$

mit, LHCP Receive

Orbit Years UHF Experience  
ity (0.937, 5 years)  
In Receiver  
ability of Bus Used for Conservative Repeater Design

Transmit Line	Receive Path
BW	G/T, dB/K

EIRP, dBw
30 MHz
50 MHz
25 KHz
25 KHz
500 KHz
5 KHz

nt Systems  
patible with Navy Equipment

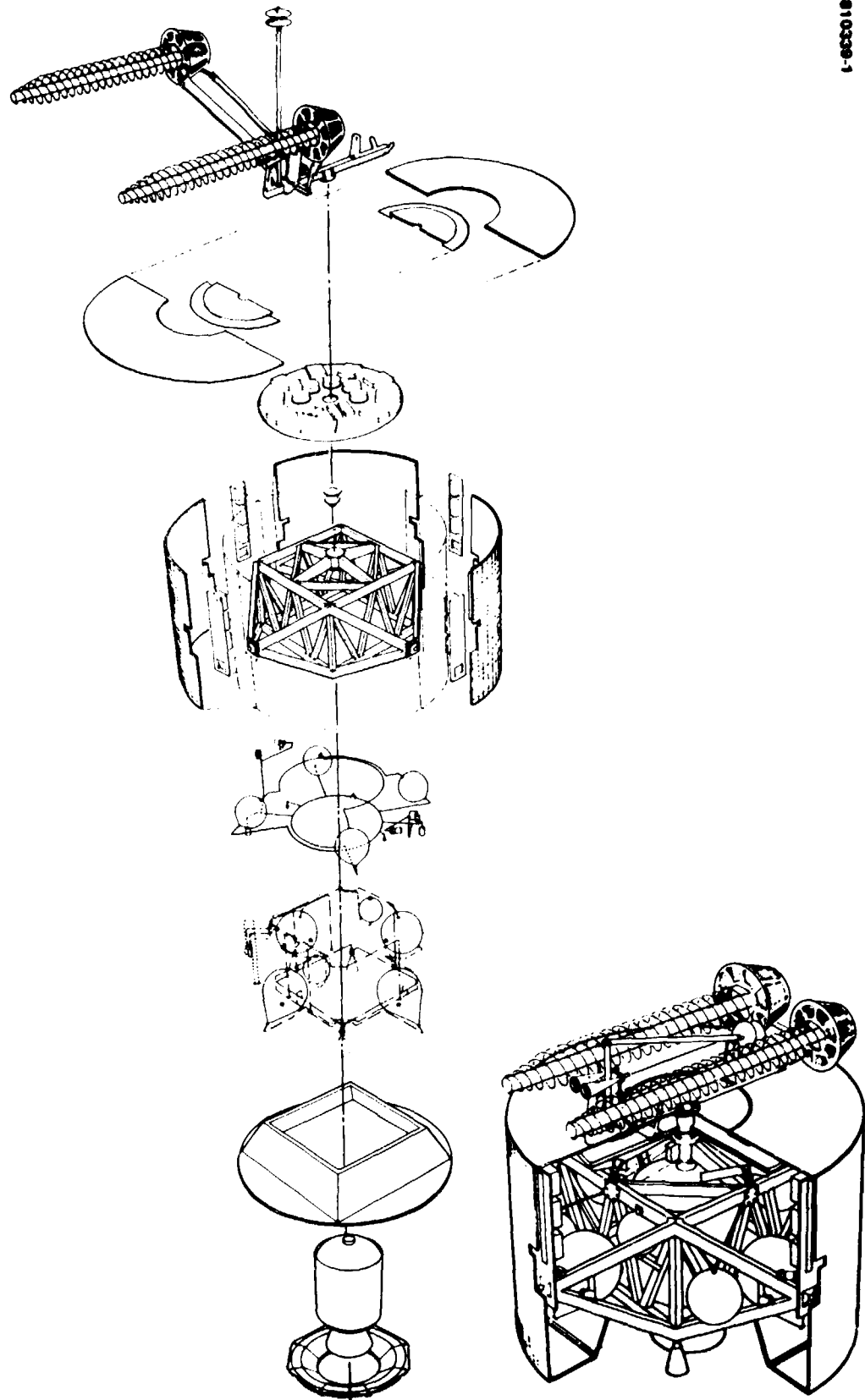
FBP	OMNI
60 dB	19 dB
Earth	40° Toroid
FSK	7980 MHz
2/sec	FM/FSK
	≈1/sec

— Hughes Standardized Modular T/M  
patible with Navy Equipment

7275  
over 40° Toroid in Transfer Orbit  
over 13.4° Coverage On Orbit  
bps  
Biphase; 1.4 Rad max. Mod. Index

ny Cell Voltages (96)  
atures

ING CONFIGUR-  
GINS



2  
FOLDOUT FRAME

PRECEDING PAGE BLANK NOT FILMED

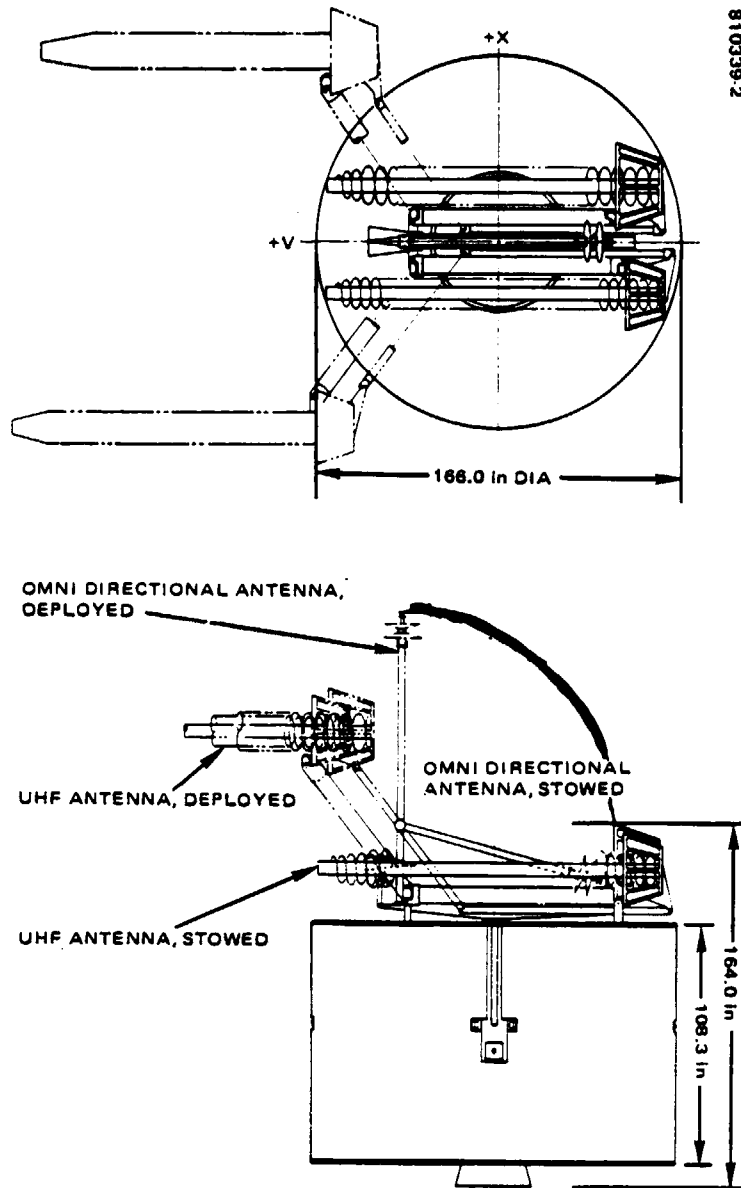


FIGURE 4-2. LEASAT EXTERNAL CONFIGURATION.

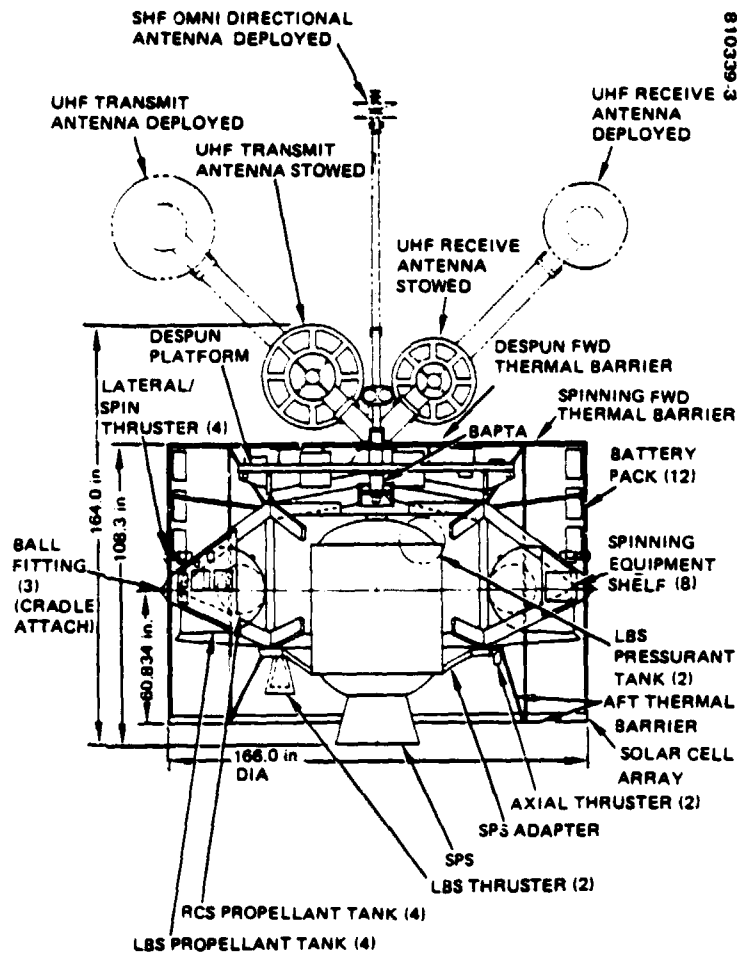
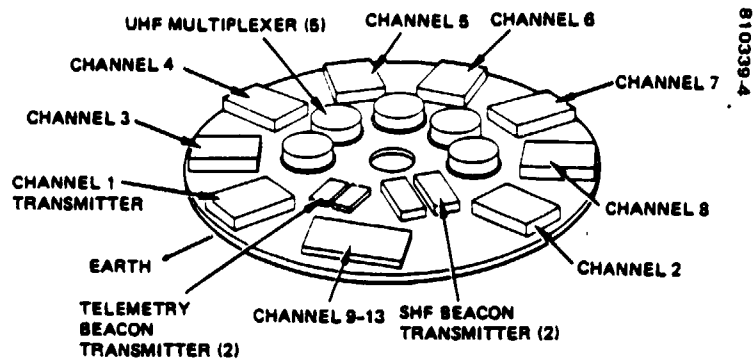
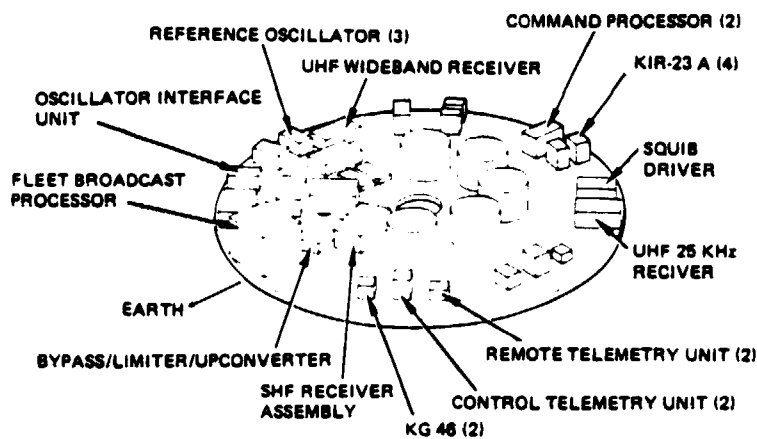


FIGURE 4-3. LEASAT INTERNAL CONFIGURATION

ORIGINAL PAGE IS  
OF POOR QUALITY



FORWARD



AFT

FIGURE 4-4. DESPUN PLATFORM EQUIPMENT LAYOUT



TABLE 4-1. WEIGHT SUMMARY

<u>Item</u>	<u>Weight, lb</u>
Communications	481
Telemetry and command	174
Attitude control	68
Reaction control (dry)	37
Electrical power	540
Thermal control	143
Structure	842
Wire harness	104
Liquid bipropellant subsystem (dry)	285
Balance weight	11
Margin	22
Spacecraft weight, end of 7 yr	2,729
Hydrazine used on station, 7 yr	137
Orbit acquisition hydrazine	122
Weight following apogee burn	2,989
Apogee burn	2,628
Preburn hydrazine	36
Attitude/orbit trim hydrazine	37
Weight following perigee burn	5,690
Perigee augmentation	1,381
SPS jettisoned mass	705
SPS expendables	7,387
Spinup hydrazine	20
Spacecraft at separation	15,181

The basic LEASAT spacecraft structure sizing has been based on a conservative 1.5 safety factor. Further, recent coupled loads analysis has shown that additional margin exists relative to current load levels. Owing to the large equipment shelf area which can be made available within the 166 inch diameter spacecraft body, ample installation volume exists for growth or the addition of experiments.

Power sources are sized with large margins for support of loads throughout 7 years as shown in Table 4-2. Multiple redundant batteries are sized for very low stress — 43 percent depth of discharge for the longest eclipse and full system load. This figure is in contrast to other 7 year synchronous orbit systems which are frequently designed to a more highly stressed 50 percent DOD. Redundancy provided by the three batteries permits full load support with loss of one of the batteries, increasing DOD to only 49 percent. Voltage sizing of the batteries permits loss of at least two of the 32 series cells in each battery.

TABLE 4-2. POWER SOURCE SIZING

Allocation	Power at 28 V		
	Summer Solstice	Equinox	Eclipse
Communications	739	739	739
Telemetry and command	71	71	71
Attitude control	34	34	34
Thermal control	51	96	51
Power control and distribution	61	66	177
Total	956	1006	1072
Battery charge	31	96	-
Main bus	987	1102	1072 (1254 Whr. 1.17 hr eclipse)
Available	7 yr: 1063	1194	3387 Whr.
Array margin, %	7 yr: 8	8	-
Battery depth of discharge, %	-	-	43

The solar panel output of 1194 watts at equinox is sized for an initial design margin of 15 percent, including full 7 year conservative solar flare and trapped radiation exposures. Over 80 orbit years of accurately telemetered spinning solar array performance on Hughes synchronous spacecraft shows predictability of array output to within  $\pm 2$  percent when the actual environment is taken into account. Thus, the excess panel allocation in the LEASAT design ensures that loads can be supported throughout the mission and that load increases for addition of experimental packages or for other purposes can be accommodated.

For assessment of communications payload and bus performance in orbit, a flexible telemetry subsystem has been provided. Table 4-3 lists the channel allocation to communications and bus subsystems. The total allocation includes 105 spare channels or 27 percent of the expected requirement. With the standardized modular telemetry system selected, increase or restructuring of this allocation is easily achieved. Commands are also summarized in the table. Sufficient capacity exists to support anticipated system needs, including specific payload requirements, serial digital commands for operations such as nonreal time thruster pulsing, and general purpose pulse commands. Spares include 66 pulse commands or 17 percent of the expected requirement, and 12 serial digital commands or 200 percent of the expected requirement.

TABLE 4-3. COMMAND AND TELEMETRY ALLOCATION

Subsystem	Command		Telemetry			
	Pulse	Serial	Analog	Bilevel	Conditioned	Serial-Digital
Communications	169	0	13	107	35	0
Attitude control	13	2	5	0	0	2
Power	79	0	14	7	22	0
Propulsion	20	0	0	9	31	0
TT&C	37	2	8	19	7	0
Total Required	318	4	40	142	95	2
Available	384	12	384 total channels			
Spares	66	8	105			

Thermal environments provided by the LEASAT dual spin bus design are a benign 40°F to 71°F for the payload over all seasonal conditions throughout the 7 year mission while in sun, and 20°F to 71°F including eclipses. These values are similar to or even more moderate than those for typical 7 year Hughes synchronous orbit spinning spacecraft, so that expected LEASAT electronic part performance can be predicted accurately by using established derating factors and on-orbit life history, thereby supporting LEASAT reliability computations.

Orbit control requirements are accommodated in the spacecraft design and fuel budgets. This provision includes fuel for the specified repositioning maneuvers and the inclination maneuver planned to maintain  $\pm 3^\circ$  latitude during the seventh year.

The system specification requires that the spacecraft parts and materials, including the solar array, meet performance requirements while taking into account the natural radiation exposures over the mission life. Because of the importance of geosynchronous orbit, the expected environment has been assessed over more than the past 10 years and the models upgraded continuously. The large number of geosynchronous spacecraft successfully operated have supported the adequacy of the environmental models and the suitability of the spacecraft designs. The LEASAT spacecraft achieves ample radiation hardening margins by use of circuits and components screened for environments in excess of those expected. Further, many components are hardened to the additional extremes of artificial exposures. Conservative trapped and solar flare environment models used for solar array sizing are those commonly used for Intelsat, COMSTAR, MARISAT, and others. Solar array flight data conclusively show the models are more severe than actual environments.

Principal components of the geosynchronous orbit environment include trapped electrons and protons, alpha particles, and hot plasmas. The low energy electrons, protons, and alpha particles deposit large ionizing surface doses ( $10^9$  rad) on exposed materials. Trapped electrons and flare particles which penetrate the solar cell covers are accounted for in solar cell

performance sizing. The more penetrating particles deposit energy in electronic circuits creating ionization doses in transistors of typically  $10^5$  rads (Si). The most significant effects from these are interactions with passivation layers in transistors and integrated circuits, and in gate insulation of MOSFETs. These exposures are routinely accommodated in Hughes designs through a combination of shielding, part selection, and circuit design, based on computer-modeled shielding analysis and use of an extensive base of test data for solar cells and all electronic parts used.

Proper LEASAT performance will be assured through electromagnetic control provisions based on existing Hughes spacecraft designs such as SDS. The LEASAT electromagnetic design will be implemented through a formal system level activity including design, analysis, and, as required, test.

Requirements specified or assumed for design purposes for control of electromagnetic effects are summarized in Table 4-4. Considerations first include control of EMI in the most conventional sense, addressing interaction between units and subsystems within the spacecraft, and interaction between the STS, ground sources, and the spacecraft during launch operations. Included is the usual consideration for safety with ordnance circuits in the electromagnetic environment. These EMI control requirements will be governed by MIL-STD-161 and MIL-STD-1541 which have routinely been applied to previous Hughes spacecraft.

Aspects of the LEASAT service require the recognition and implementation of TEMPEST provisions in the spacecraft electromagnetic design. Although actual TEMPEST testing is not required, the provisions of NACSEM 5100, as have been incorporated in prior Hughes spacecraft, are taken as a design basis for LEASAT.

Hughes design practices for control of electrostatic discharge (ESD) effects have been developed through an ongoing IR&D program involving geosynchronous spacecraft flight evaluation and tests including fullup spacecraft

TABLE 4-4. ELECTROMAGNETIC EFFECTS CONTROL REQUIREMENTS

Category	Requirement	Specified	Assumed Design Goal
EMI	MIL-STD-461/ MIL-STD-1541		X
TEMPEST	NACSEM 5100		X
Electrostatic discharge	Hughes design criteria		X
Intermodulation product control	Any 120 Hz BW: -23 dB Total, 5 kHz channel: -14 dB Any channel, at receive input: -30 dB above noise power density	X	
GFE unit power regulation		X	

exposure to discharge (Intelsat IV Y-1). Resulting design criteria have placed controls on static discharge sources (spacecraft external surface in particular) and also the potential receptors including the electrical distribution system and sensitive unit circuits. An additional benefit is enhanced protection of unit circuits to static discharge exposure during assembly and handling.

Portions of the intermodulation product control plan affect the design of the spacecraft chassis/external shell and electrical distribution system in a manner similar to that resulting from other electromagnetic effects.

The power regulation requirements specified for the GFE units will be accommodated in the spacecraft design. Where these are more severe than the general EMI requirements assumed, the GFE unit specification will prevail.

Although the electromagnetic effects control requirements are numerous and varied, a substantial amount of overlap exists. Similar sets of requirements, including TEMPEST, IM control, ESD, and EMP/SGEMP survivability as well as the usual EMI requirements, have been mutually incorporated in prior Hughes spacecraft such as SDS. Similarly, for an optimum LEASAT spacecraft design the requirements will be consolidated and implemented through a central, system level electromagnetic control activity consisting of design control, performance analysis, and testing as required.

#### 4.1.2 Trade Studies

Many design trade studies have been performed to establish the baseline spacecraft design. A summary of the key studies is provided in Table 4-5. Table 4-6 gives the alternative orbit injection cost trade.

TABLE 4-5. TRADE STUDIES

Subject	Alternative Designs	Characteristics Leading to Selection
Overall configuration	Integrated propulsion*	Lowest cost system, lowest Shuttle launch costs
	External propulsion (IUS or SSUS-A)	Larger Shuttle bay length required, heavier, high costs for both propulsion stage and Shuttle launch (see Table 4-6)
Attitude control	Spin stabilization*	Infrequent attitude command requirements, inherent thermal balance, inherent stability
	Three-axis control	Less solar cell cost, solar panel drive required, more complex attitude control equipment
Thermal control	Spinning forward barrier*	Inherent thermal averaging
	Despun barrier	Requires heat pipes imbedded in equipment platform
Structural load path	Semi-monocoque	Frequently used design with expendable launch vehicles
	Truss*	Lighter weight, simpler propulsion subsystem integration

\*Selected for implementation.

TABLE 4-6. ALTERNATIVE ORBIT INJECTION COST TRADE\*

Orbit Injection Approach	Internal Propulsion	SSUS-A and Apogee Motor	Inertial Upper Stage
STS payload, lb	16,967	16,544	30,000
Spacecraft length, in.	164	247	344
STS payload length, in.	170	253	350
STS launch cost	12.5	18.7	25.8
Propulsion stage cost	—	2.5	12.
Internal propulsion cost	1.2	0.4	—
Launch and injection cost	13.7	21.6	37.8
Cost increment with respect to baseline	—	7.9	24.1

\*Cost per launch in \$M.

#### 4. 1. 3 Spacecraft Subsystems

The spacecraft system functional block diagram is presented in Figure 4-5. The following paragraphs provide an introduction to each of the subsystems, including the subsystem functional summary.

The communications subsystem is an integrated design consisting of antennas, receivers, IF processors, and transmitters. It incorporates carefully planned redundancy and low level cross-strapping to achieve subsystem reliability matched to the high reliability of the total spacecraft. Large design margins and conservative performance predictions are incorporated to minimize program risk. Separate receive and transmit antennas, deployed away from the spacecraft body, are incorporated into the design to minimize intermodulation product interference.

The communications subsystem, including antennas, is mounted on the despun platform. The forward side of the platform carries only the RF transmitters, and the platform forms a shield between the transmitters and the remaining elements of the communications subsystem. All power, telemetry, and command signal lines passing from one side of the shelf to the other are filtered to prevent conducted RF interference from passing across the shelf boundary. Thermal control for the RF transmitters, the major power dissipation elements of the communications subsystem, is provided passively through simple radiative coupling to the end plane of the spacecraft facing the transmitters.

The wideband Fleet Broadcast signal is received on the earth coverage SHF receive antenna and down converted in the SHF receiver and routed to the processor. After processing, the resulting narrowband signal is routed to the Fleet Broadcast bypass/limiter and upconverter where it is filtered, limited, and frequency translated to UHF for transmission through the Channel 1 Fleet Broadcast UHF power amplifier. The Fleet Broadcast processor may be bypassed on command.

The three UHF channel groups are received through the common UHF receive helix antenna and preamplifier, split into the 500 KHz channel group (channel 2), the 25 KHz channel group (channels 3 to 8), and the 5 KHz channel group (channels 9 to 13). Each group is downconverted to IF in its receiver, and individual channels are split by channel filters and separately limited in the respective IF units. The 500 KHz channel and each of the 25 KHz channels are separately upconverted to UHF and transmitted through their own unique power amplifiers. The 5 KHz channels are combined after limiting, and upconverted and power amplified as a group. All UHF transmitter outputs are combined in the nine channel UHF multiplexer to form one output to the UHF transmit helix antenna.

The common equipment group contains the 5 MHz master oscillator which is the frequency reference for the total communications subsystem. This master oscillator is used as the reference for the Fleet Broadcast processor, the Fleet Broadcast beacon, and all local oscillators in the communications subsystem. The common group also contains the UHF transmit and receive antennas, the UHF preamplifier, and the UHF transmit multiplexer.

Virtually all elements of the communications subsystem are based upon existing Hughes designs. The SHF antennas are scaled from the Intelsat IVA earth coverage horn antennas and the UHF preamplifier is the SDS design. The UHF helical transmit and receive antennas, selected because of their low IM interactions and their deployment simplicity, are slightly lengthened versions of the SDS transmit helix. The receivers, IF processors, and upconverters are identical to existing Hughes designs or involve only minor modifications to these designs. The UHF power amplifiers are similar to the MARISAT design; however, they incorporate new ruggedized output devices to enhance the amplifier reliability. The 5 MHz master oscillator is the Frequency Electronics Incorporated (FEI) unit developed for the FLTSATCOM program.

#### 4.1.3.1 Telemetry, Tracking, and Command Subsystem

The LEASAT TT&C subsystem is a fully redundant all solid state implementation with extensive cross-strapping for improved reliability. Extensive use is made of existing designs in order to achieve a low risk subsystem. Signals are encrypted with a functionally redundant SHF omnicommand link, and the design is fully compatible with the FSC-79.

##### 4.1.3.1.1 Telemetry Group

The telemetry group has two operational configurations based upon ranging requirements. For normal on-station operation, when the tracking data are furnished by the OM-51, a single transmitter is required for the telemetry data. Simultaneous telemetry and tracking require that both transmitters be on. Each transmitter has a commandable telemetry mode and tracking mode.

LEASAT uses a data bus type of telemetry subsystem configuration. It is the same subsystem design that is being provided for the SBS and Anik C

ORIGINAL PAGE IS  
OF POOR QUALITY

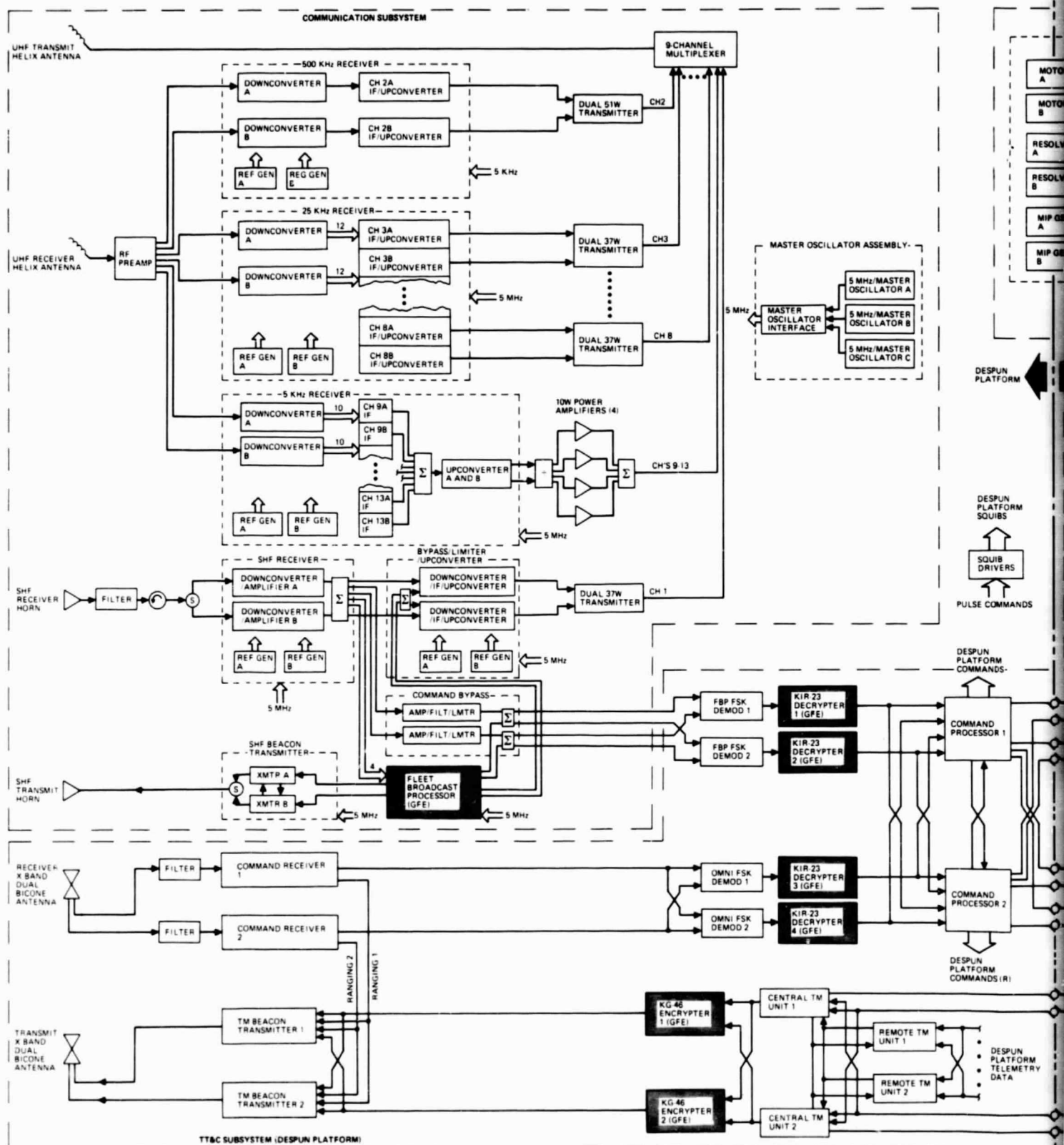
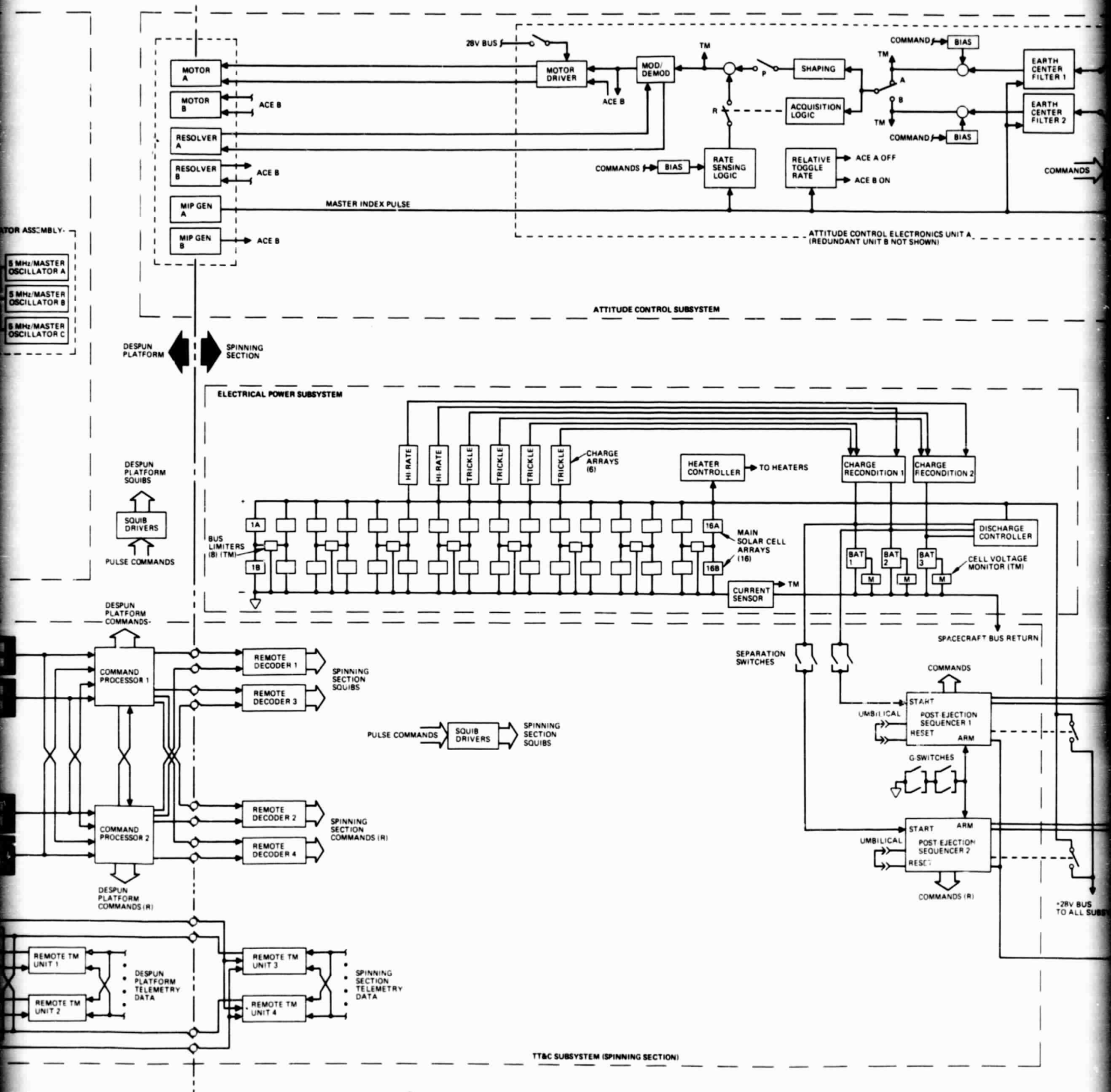


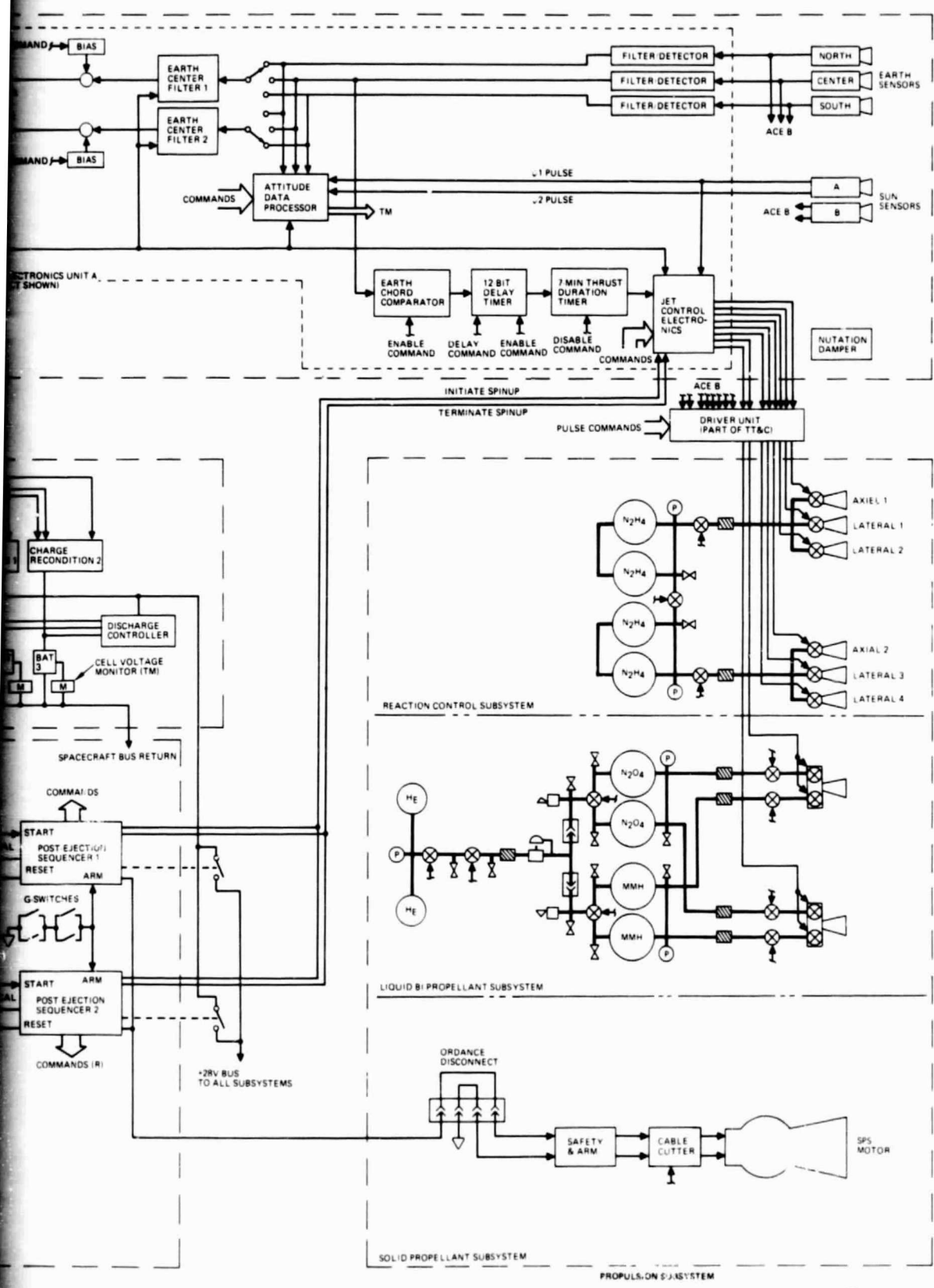
FIGURE 4-5. SPACECRAFT SYSTEM FUNCTIONAL BLOCK DIAGRAM





FOLDOUT FRAME 2

810339-5



3  
EOLDOUT FRAME

spacecraft. The remote telemetry unit (RTU) is the interface between spacecraft subsystems and the telemetry equipments. It gathers, formats and conditions user telemetry data and transmits these data to the central telemetry unit (CTU). The CTU is capable of dwelling on any telemetry parameters by command. In the dwell mode a large portion of the frame assignments are replaced by single or multiple selected parameters. Certain critical parameters, assessing the health of the satellite, are maintained

The telemetry RF equipment group contains two SHF solid state telemetry beacon transmitters and bicone transmit antenna. The beacon transmitters are derived from space-qualified hardware used on the SDS and Pioneer Venus programs, while the bicone antenna is a scaled SDS/Anik C dual mode bicone.

#### 4.1.3.1.2 Command Group

The command group is accessed via either the Fleet Broadcast processor or the SHF bicone antenna. It demodulates, decrypts, decodes, and distributes commands to all satellite subsystems, and provides the timed commands required for transfer orbit ejection. The two command links are cross-strapped after the decrypters to ensure that only KIR-23A authenticated commands are in parallel with the FBP command link. The command group has three primary modes of operation during the transition from the Shuttle parking orbit to transfer, during transfer orbit, and on-station operations. All commands required to achieve transfer orbit are automatically generated to a predetermined time line by redundant postejection sequencers. During transfer orbit the command group is accessed via an omni-bicone antenna that also serves as an on-station backup mode. For normal on-station operations, the command group is accessed via the FBP uplink.

Each command channel of the FBP has a dedicated external bypass. The FBP command channels and the external bypasses are cross-strapped to redundant FSK/NRZ demodulators. After detection in the modulator the NRZ data stream is converted to a KIR-23A compatible ternary format. The buffered data are then clocked to the decrypters. The command group uses the authentication characteristics of the KIR-23A to ensure that the omni-command link cannot compromise the FBP command link. Although it requires four decrypters, it is a straightforward implementation that does not suffer from the operational constraints imposed by timed switchover priority systems to control access to the decrypters.

#### 4.1.3.1.3 Tracking

Spacecraft tracking during normal on-station operations is performed using the ranging data from the OM-51 and the AN/FSC-79 azimuth and elevation data. During transfer orbit and as an on-station backup mode, spacecraft tracking is performed at SHF using the Hughes transportable ground stations. Tones at a baseband frequency different from those used as command tones modulate the command uplink at the TT&C ground station. The spacecraft receives the signal, demodulates it in the command receiver, then routes the baseband ranging tones to the telemetry transmitter. The standard telemetry

810339-6

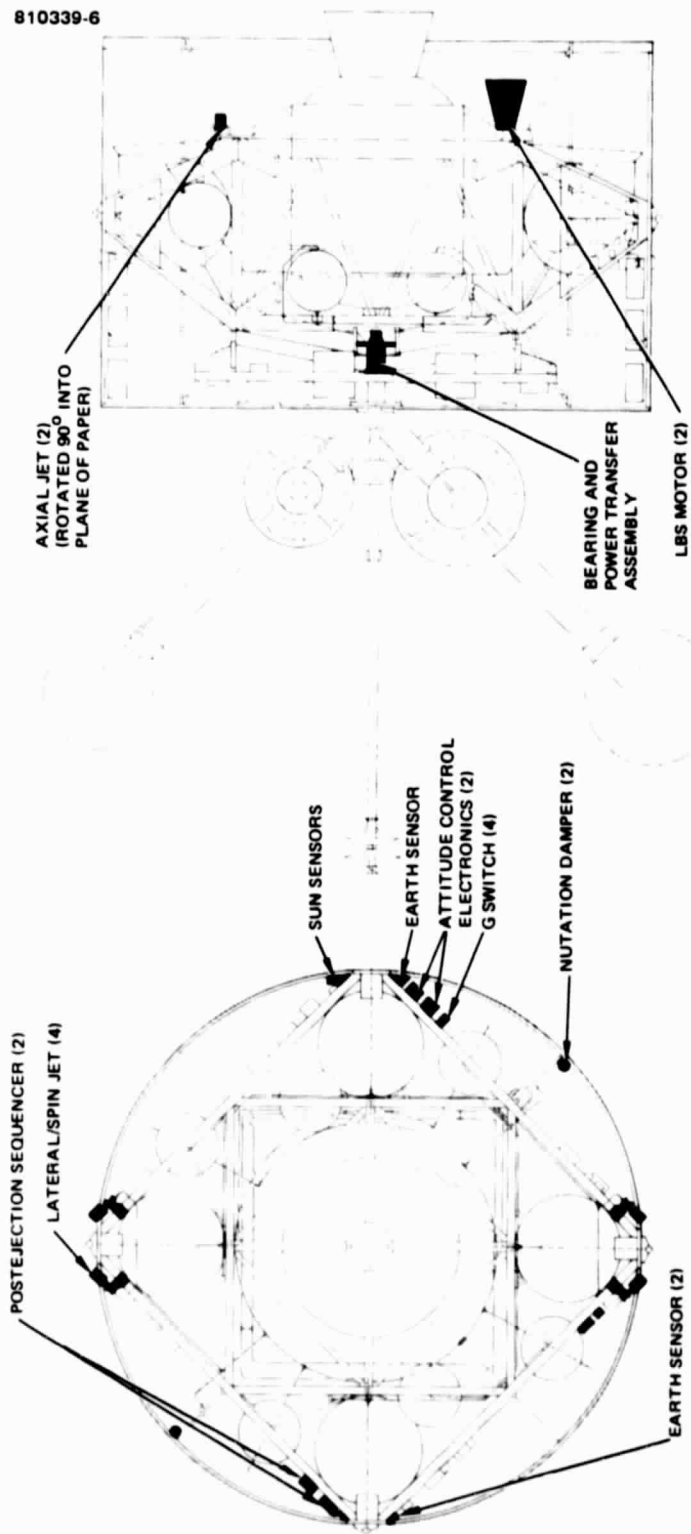


FIGURE 4-6. ACS COMPONENT LAYOUT

downlink is modulated by these ranging tones, received on the ground, and demodulated in the ground station telemetry receiver. The phase shift between the transmitted tone and received tone is then measured to determine the round trip time delay and, hence, the slant range to the spacecraft.

#### 4.1.3.2 Attitude Control Subsystem

The attitude control subsystem orients the antennas toward earth center and provides earth and sun sensor data to orient the spin axis normal to the orbital plane. The dual-spin configuration used for LEASAT employs the unusually simple attitude control subsystem (ACS) characteristic of passively stable spin-stabilized spacecraft. With a spin-to-transverse inertia ratio greater than unity during all phases of the mission, the vehicle is passively stable and requires only one active control loop in steady-state operation. The large angular momentum assures a low drift rate of the spin axis with attitude trim maneuvers required no more than once a month. A key element, the bearing and power transfer assembly (BAPTA), utilizes the well proven Intelsat IVA/COMSTAR design. Hughes' BAPTAs have accumulated more than 100 years of life in orbit without a failure.

The reference for the despun platform east-west pointing is provided by a spinning earth sensor whose output is filtered and threshold detected to generate leading and trailing edge earth pulses. These pulses are used together with the rotor/platform master index pulse in an earth center-finding circuit to generate an analog error signal. Offset pointing within the limits of the earth chord is provided. The attitude data processor generates the telemetry required for attitude determination. These data consist of ten different time interval measurements of 30  $\mu$ sec resolution. The jet control electronics processes commands for all jet firings. The spin synchronous reference for use in the pulsed mode may be selected from the sun sensor, earth sensor, or master index pulse generator. The jet control electronics are normally powered off when not being used.

The spacecraft sequence timer initiates the spinup maneuver. Termination of the spinup thrusting is controlled by a set of g-switches which sense when the spin rate reaches 30 rpm. The sequence timer also arms, fires, and jettisons the solid propellant rocket motor. The liquid bipropellant rocket motors are fired at succeeding perigee passes. Circuits for controlling the perigee firing of these motors are contained within the attitude control electronics.

This subsection presents the ACS design and performance, beginning with a description of ACS functions and their implementation. Next, performance characteristics and supporting analyses are presented. A description of ACS hardware follows, including photographs of qualified units.

##### 4.1.3.2.1 Description

ACS components and their location in the spacecraft are shown in Figure 4-6. The BAPTA provides the mechanical and electrical interface between the despun platform and rotor. It contains the motor and index pulse

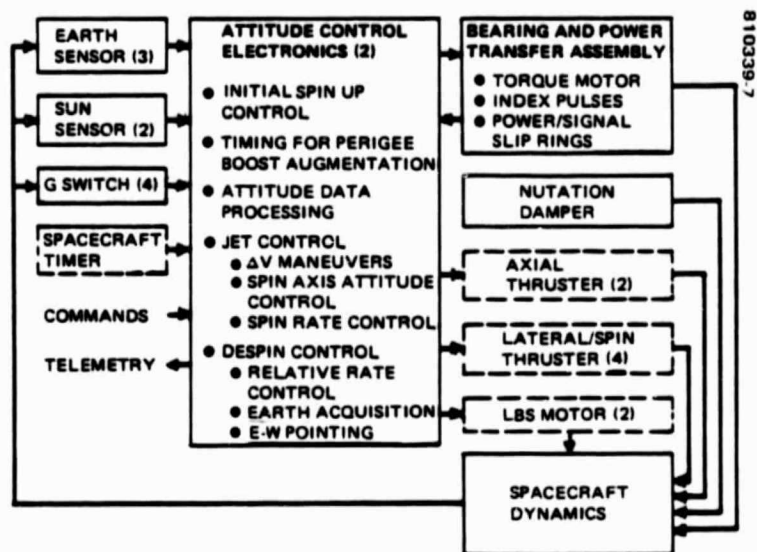


FIGURE 4-7. SIMPLE ATTITUDE CONTROL SUBSYSTEM  
USES GROUND COMMAND FOR ALL CONTROL EXCEPT  
AUTONOMOUS DESPIN

generator used for despin control. The remaining ACS components consisting of the earth sensors, sun sensors, nutation dampers, g-switches, and attitude control electronics (ACE) unit, are located on the rotor.

Propulsion subsystem thrusters, also located on the rotor, are controlled by the ACE. There are two 100 lbf liquid bipropellant subsystem (LBS) thrusters and six 5 lbf reaction control subsystem (RCS) jets. Two of the 5 lbf jets thrust axially and four thrust laterally. The lateral jets are canted 45° left and right in pairs to provide spinup and spindown torque components. When used for east-west stationkeeping, the lateral jets are fired in pairs to null spin torque.

ACS functions are shown in Figure 4-7 together with a schematic of data flow. Despin control is autonomous, using onboard equipment only. Initial spinup control and LSB thruster control for perigee boost augmentation are also autonomous. The other control functions, spin axis attitude control, spin rate control, and  $\Delta V$  maneuvers (all of which employ the propulsion subsystem thrusters), are performed infrequently and are operated via the telemetry and command (T&C) subsystem. Spacecraft attitude is computed at the contractor's operational control center (COCC) using telemetered sensor data. All of the onboard signal processing for the ACS is performed within the ACE, as shown in Figure 4-8 and described below.

#### 4.1.3.2.2 Attitude Determination and Control

The attitude data processor (ADP) section of the ACE generates the telemetry required for attitude determination. These data consist of 10 different time interval measurements of 30 microsecond resolution involving the  $\psi_1$  and  $\psi_2$  sun sensor pulses, leading and trailing edge earth sensor pulses, master index pulse (MIP), and minor frame synchronization. The complete set of ACS telemetry data consists of 148 bits of serial data plus 5 analog channels, each with an 8 bit resolution. Command of the ACS is accomplished using 13 pulse commands for selecting units and modes and 91 bits of serial data for setting biases and operating jets.

Each of the two ACEs is cross-strapped with redundant elements of the T&C subsystem. Since only one ACE can be turned on at a time, no ambiguity exists in the data transfer.

#### 4.1.3.2.3 East-West Error Signal Processing

The reference for platform east-west pointing is provided by a spinning earth sensor whose output is filtered and threshold detected to generate leading and trailing edge earth pulses. These pulses are used with the rotor/platform MIP in an earth center-finding circuit that generates an analog error signal. Offset pointing within the limits of the earth chord is accomplished by using a command bias. The resulting signal is appropriately shaped and used as the torque command to the motor driver.

Three earth sensors are provided, each with different north-south declinations (+6.2°, 0°, -6.2°). This ensures that at least one sensor will

810339 8

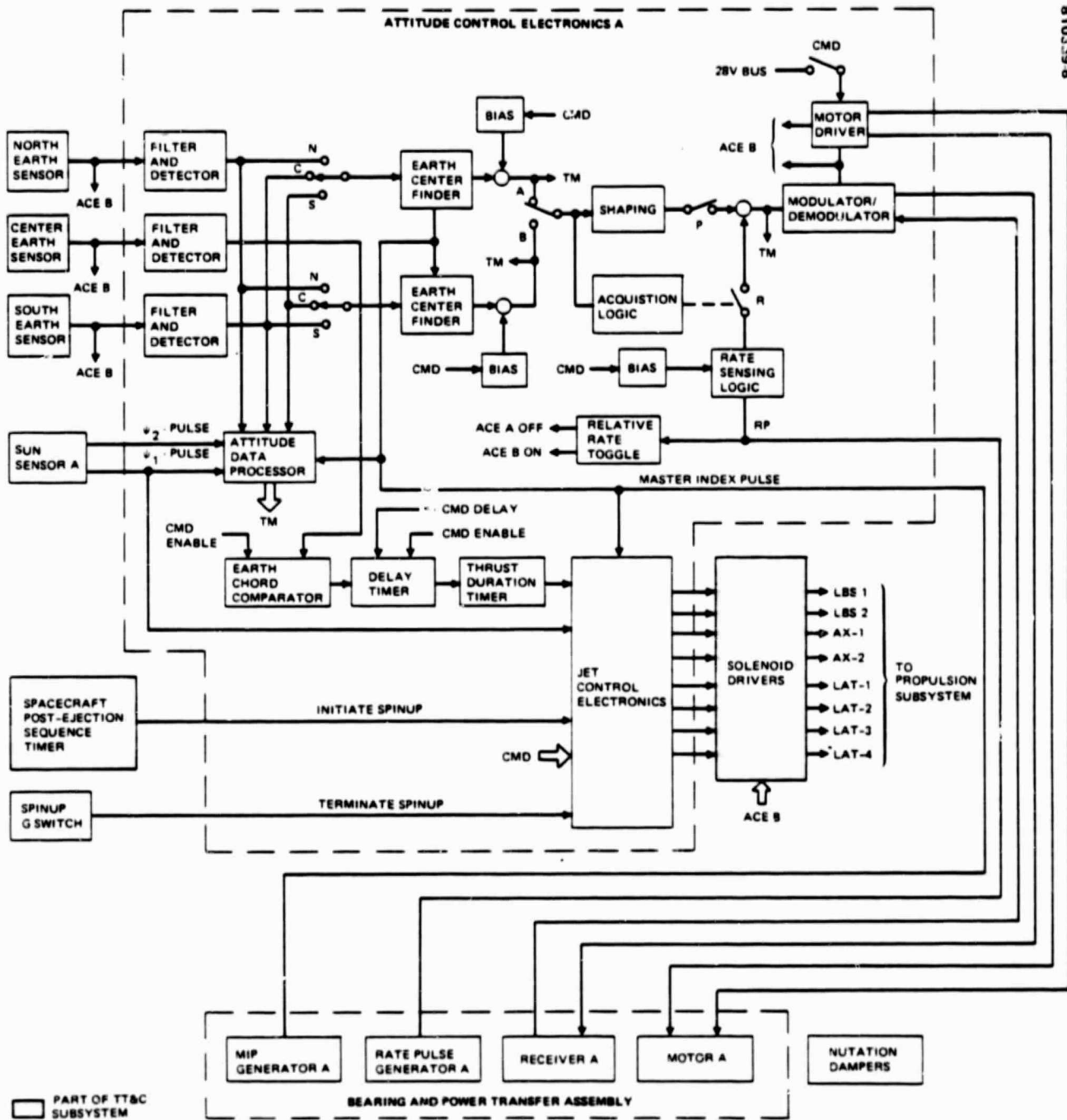


FIGURE 4-8. ACS USES SINGLE SERVO LOOP FOR STEADY STATE CONTROL



be usable in the event of failure of the second sensor and sun interference of the third. Moon discrimination logic is included to automatically prevent moon interference in the selected earth sensor. Switching between earth sensors is required four times a year (twice during each equinox season) to preclude sun interference. This switching can be accomplished without pointing transients by properly command biasing the standby earth center finder prior to transfer.

#### 4. 1. 3. 2. 4 Despin Control

Two modes of despin control accommodate all mission phases. The pointing mode is used in steady-state operation. The relative rate mode is used for initial platform despin and serves as a standby mode in case of temporary interruption of normal pointing control. Relative rate of the platform to the rotor is measured using the rate pulse generator (RPG) which outputs eight equally spaced pulses per shaft revolution. With the appropriate command bias, the platform can be despun inertially. When this is done and the pointing mode is enabled, earth acquisition occurs automatically from any initial platform azimuth angle. In the pointing mode, the relative rate loop is automatically enabled whenever pointing error exceeds earth chord limits. Thus, even in the event of a temporary loss of earth signal, the platform will return automatically to the earth pointing position.

The motor driver in each ACE is hardwired to its respective BAPTA motor. However, torque commands are cross-strapped into each driver so that either motor may be used with either ACE. The motor drivers are powered through separate line switches to permit this mode of operation. In addition, both line switches can be closed at the same time to operate both motors in parallel when increased control torque is desired, as for example during initial platform despin.

#### 4. 1. 3. 2. 5 Jet Firing Control

The jet control electronics (JCE) section of the ACE processes commands for all jet firings, including the LBS motors. These commands consist of jet selection, firing mode (continuous or pulsed), thrust duration in the continuous mode, and spin phase firing angle and number of pulses in the pulsed mode. The spin synchronous reference for use in the pulsed mode may be selected from the sun sensor, earth sensor, or MIP generator. The JCE is normally powered off when not in use.

Initial spinup after separation from the Shuttle is controlled by the ACE. The spacecraft postjection sequence timer initiates the spinup maneuver, which is performed by the RCS lateral spin jets. Termination of spinup thrusting is controlled by g-switches that sense when spin rate reaches 30 rpm. Four g-switches are used in a series-parallel circuit configuration for safety and reliability.

LBS motor burn at perigee of the transfer orbit is also controlled by the ACE. In the primary mode, the center earth sensor provides information

for initiating the sequence. As the spacecraft approaches perigee, earth chord length increases. When measured length exceeds a preset reference length, nominally 50°, a timer is started which initiates firing of the LBS motors. This signal in turn triggers a thrust duration timer. Delay time is adjustable by command. When used with the earth sensor, the delay is set for about 9 minutes. As a backup to the earth chord sensing technique, the delay timer may be started by command, and is designed for delay times of up to 12 hours.

#### 4.1.3.2.6 Redundancy Features

The ACS employs two fully redundant electronic channels plus cross-strapping of the sensors and torquers to provide high mission reliability. In addition, an automatic switching feature transfers control to the redundant ACE if the relative rate exceeds acceptable limits. This prevents platform spinup and simplifies recovery of normal pointing operation. The automatic transfer feature is enabled and disabled by command.

#### 4.1.3.2.7 Nutation Damping

Nutation damping is passive throughout the mission. Energy dissipation due to fluid propellant slosh has a stabilizing effect and contributes to damping. Two mercury damper tubes have been added to ensure adequate damping in all phases of the mission. These tubes are aligned parallel to the spin axis and are located near the outer periphery of the rotor.

#### 4.1.3.2.8 Trade Studies

An important reason for selecting the dual-spin configuration over a body-stabilized configuration is the simplicity and reliability of the ACS. Only one function, platform despin control, is required in steady-state operation. For a passively stable configuration such as LEASAT, this is performed by a single servo loop, using a simple IR earth sensor for the attitude reference. In contrast, the three-axis configuration requires a much more complex sensor and at least two active control loops. It also requires special sensing and control modes for stationkeeping maneuvers because of the disturbance torques induced by jet thrusting. The dual-spin configuration, with its large angular momentum, is virtually insensitive to such disturbances and requires no additional control modes.

An earth sensor was selected over a sun sensor for the LEASAT despin controller because it permits a simpler design and provides a more than adequate pointing accuracy. The earth sensor reference requires no time of day update or mode switching during eclipse. With analog error signal processing, the despin system is free of pointing transients sometimes encountered in sun-referenced digital controllers due to electric discharge effects or other interference sources.

#### 4.1.3.2.9 Performance Summary and Analysis

##### Dynamics

Table 4-7 lists the principal design and performance characteristics of the LEASAT ACS. The spacecraft will be separated from

TABLE 4-7. ACS DESIGN AND PERFORMANCE SUMMARY

<u>Spin Rate</u>		<u>Relative Rate Control</u>	
Initial rate at separation	2 rpm	Rate bias range	10 to 60 rpm
During SPS, transfer orbit, LBS	30 rpm	Rate bias quantization	0.2 rpm
On station (platform despun)	50 rpm	Relative rate toggle limits	50 $\pm$ 7 rpm
<u>Dynamics</u>		<u>Antenna Pointing</u>	
Inertia ratio		Earth acquisition	Automatic
In parking orbit	1.35	Acquisition range	$\pm 180^\circ$
In transfer orbit	1.59	Offset pointing range, E-W	Earth chord limits
On station	1.19	Pointing bias quantization	0.02 $^\circ$
Dry rotor moment of inertia	1873 slug-ft <sup>2</sup>	Pointing accuracy (UHF antennas)	
Nutation control	Passive	East-West	$\pm 0.54^\circ$
Nutation damping time constant	<240 sec	North-South	$\pm 0.46^\circ$
<u>Spin Axis Attitude Control</u>		Moon discrimination	Automatic
Normal spin axis orientation	Orbit normal		
Drift rate	0.1 deg/day		
Error range	$\pm 0.15^\circ$		
Minimum correction interval	28 days		

the Shuttle with its spin axis pointed along the solid propellant subsystem (SPS) motor fire attitude and a spin rate of 2.0 rpm. The platform and rotor will be locked together so that the vehicle will act as a single spinning body, except for fluids in the propulsion subsystem. To minimize fluid effects, the initial ullage volumes will be kept small (5 percent for LBS fuel and oxidizer and 17 percent for RCS hydrazine). Detailed analyses and simulations of the separation dynamics have been made to evaluate the effect of fluid motion and initial cg offset on the momentum vector. The results summarized in Table 4-8 indicate that errors associated with separation dynamics will be less than the NASA specified Shuttle attitude and alignment error, and that total SPS pointing error will be suitably small (<3.5 $^\circ$ ).

TABLE 4-8. SPS THRUST VECTOR ERROR BUDGET  
(DEGREES)

Source	Pitch	Yaw
Shuttle alignment error	2	2
Spacecraft cg offset from ejection plane (0.5 in.)	—	1.25
Ejection stroke misalignment (1.0 $^\circ$ )	0.5	—
Fuel slosh effect		
Hydrazine (344 lb, 83% FF)	1.70	—
LBS (3088 lb, 95% FF)	1.40	—
Precession during spinup	0.40	0.40
Maximum expected error	3.09	2.39

Closed valves in the gas manifolds of the LBS subsystem will prevent significant fluid transfer between tanks while in the Shuttle. These valves will be opened by command after SPS burn for use in transfer orbit maneuvers. In the case of the RCS, gas manifold valves are not used because the amount of fluid that can transfer is small (less than 15 pounds, limited by the small ullage volume). After separation and spinup to 30 rpm, the fluids will quickly equalize due to the 1.5 g centrifugal acceleration. Since the tanks are very close to the cg plane, dynamic unbalance due to unequal fluid levels is negligible. The spacecraft will therefore continue to spin about its nominal spin axis, except for the small ( $2^\circ$ ) initial nutation induced during separation.

At 30 rpm, the gyroscopic stiffness of the vehicle is adequate to maintain the momentum vector during SPS burn to within  $0.32^\circ$  of its initial value. This spin rate is also high enough to permit LBS burns with only one thruster, if necessary. Under such a condition, the coning angle will be less than  $1.5^\circ$ , which will have a negligible effect on orbit injection maneuver accuracy.

The platform is despun after final LBS burn in synchronous orbit and rotor speed is adjusted to its nominal rate of 50 rpm. With the antennas deployed, spin axis precession due to solar disturbance torque will be about  $0.01^\circ/\text{day}$ . Allocating  $\pm 0.15^\circ$  for spin axis attitude error permits trim maneuvers to be performed at 30 day intervals. It is reasonable, therefore, to compute and perform both the east-west stationkeeping and attitude trim maneuvers at the same time on 4 week centers.

In steady-state operation, the despin control loop keeps the platform despun and antennas pointed at the earth's center. Under normal conditions, the automatic switching feature, using relative rate sensing as described in 4.1.3.2.4, will prevent platform spinup. If the platform is allowed to spin up, the dynamic unbalance due to the deployed antennas ( $55 \text{ slug-ft}^2$ ) will result in a coning angle of about  $6^\circ$ . Despin torque needed to overcome the centrifugally induced load torque due to rotor transverse asymmetry of  $8 \text{ slug-ft}^2$  is 1.05 ft-lb. This is well within the capability of a single BAPTA motor that has a stall torque rating of more than 1.25 ft-lb. Thus, the platform with the antennas deployed cannot become trapped in an all-spun condition. It is possible, of course, to reduce dynamic load torque simply by removing momentum from the system. The spin jets allow this to be accomplished in a straightforward manner, and the relative rate loop is designed to operate at rates as low as 10 rpm.

On orbit, platform coning motion at spin frequency (0.83 Hz) due to rotor dynamic unbalance will not exceed  $0.025^\circ$ . This motion will induce some flexure of the UHF antennas, which have a first mode natural frequency of about 3 Hz. The flexure will be quite small, however, because of the frequency separation (3.6:1), which results in an amplification factor of only 1.04. The amplification factor at nutation frequency, which is 1.4 times spin frequency, will be slightly higher (1.09). The nutation amplitude itself, however, is small ( $< 0.02^\circ$ ) and lasts for only a short period after jet maneuvers.

TABLE 4-9. ANTENNA POINTING PERFORMANCE

Error Type	Pointing Error, deg				Comment
	East-West		North-South		
	UHF Antennas	X Band Horns	UHF Antennas	X Band Horns	
Static	0.25	0.05	0.25	0.05	Residual error in antenna calibration and alignment
Long term/ diurnal	0.11	0.06	0.21	0.16	Thermally induced errors and effect of attitude drift (28 day update)
Short term	0.09	0.09	0.06	0.06	Sensor and bearing noise and rotor wobble
Worst case transient	0.01	0.01	0.02	0.02	Nutation and pointing error induced by jet maneuvers
Pointing accuracy	0.46	0.21	0.54	0.29	Algebraic sum of four groups

### Performance

Factors affecting the antenna pointing accuracy are listed in Table 4-9. The principal errors are those associated with calibration, alignment, and thermally induced deformation of the UHF antennas, and the large allocation for spin axis drift. Other ACS error sources are small and easily met, as demonstrated in many other Hughes communication satellites. The predicted worst case error for UHF antenna pointing of  $0.54^\circ$  is well below the allocated total error of  $0.65^\circ$  used in computing communication link performance. For the X band antenna, the predicted worst case error is  $0.29^\circ$ , while link budgets use  $0.35^\circ$ .

#### 4.1.3.2.10 Equipment Description

### BAPTA

The ACS components for LEASAT are either the same as, or close derivatives of, existing designs, as shown in Table 4-10. The despun BAPTA is essentially identical to the design to be used on the satellite business system (SBS) spacecraft and is a slightly modified Intelsat IVA/COMSTAR BAPTA. A photograph of the latter is shown in Figure 4-9. For LEASAT, the mounting flange for the despun platform is modified, an RPG added for the relative rate control mode, and signal slip rings used in place of rotary transformers. Other features of the BAPTA remain unchanged, including the motor, bearings, preload mechanism, and lubrication. A cross section of the LEASAT BAPTA is shown in Figure 4-10 and design characteristics are shown in Table 4-11.

The main structural elements of the BAPTA are a beryllium housing (spun), a beryllium shaft (despun), a steel preload spring (despun), and two stainless steel angular contact ball bearings. The bulk of the launch loads are shunted past the BAPTA through pyrotechnically actuated pin pullers between the platform and rotor. The dual-flexure preload spring is stiff

TABLE 4-10. ATTITUDE CONTROL SYSTEM HARDWARE SUMMARY

Component	Number per Vehicle	Total Weight, lb	Average Power, W	Envelope Size, in.	Remarks
Earth sensor	3	1.80	0.75	5.1 x 2.1 x 3.1	Telesat, WESTAR, Palapa, SBS
Sun sensor	1	0.22	—	2.8 x 1.9 x 1.8	Used on all Hughes spacecraft (redundant)
BAPTA	1	21	2.8	12.5 x 8.75 diameter	Intelsat IVA (modified)
Nutation damper	2	3	—	24 x 0.8 diameter	Telesat
G switch	4	1.2	—	3.5 x 4 x 1	SDS
ACE	2	14	11.5	10.9 x 5.9 x 4.2	Design derived from Intelsat IV, SBS

TABLE 4-11. BAPTA PHYSICAL CHARACTERISTICS

<u>Parameter</u>	<u>Value</u>
Weight	21 lb
Dimensions	8.75 in. diam. x 13.9 in. long
Bearings	
Type	Angular contact, extra light
Size	90 mm bore
Class	AFBMA ABEC 9
Material	440C CEVM
Lubricant	Hughes lubricant per HMS 20-1727
Power slip rings	
Number of rings	4
Number of circuits	2
Circuit capacity	15 A each
Number of brushes per ring	4
Current density	79 A/in <sup>2</sup>
Ring material	Coin silver
Brush material	85% Ag, 3% C, 12% MoS <sub>2</sub>
Lubricant	MoS <sub>2</sub> , contained in brushes
Signal slip rings	
Number of rings	22
Brushes per ring	2
Pulse generators	
MIPG	2 redundant coils, each (1 pulse per revolution)
RPG	2 redundant coils, each (8 pulses per revolution)
Motor	
Type	Brushless dc resolver commutated
Number	2
Torque constant	0.85 ft-lb/A
Back EMF	1.15 V/rad/sec
Winding resistance	16.2Ω

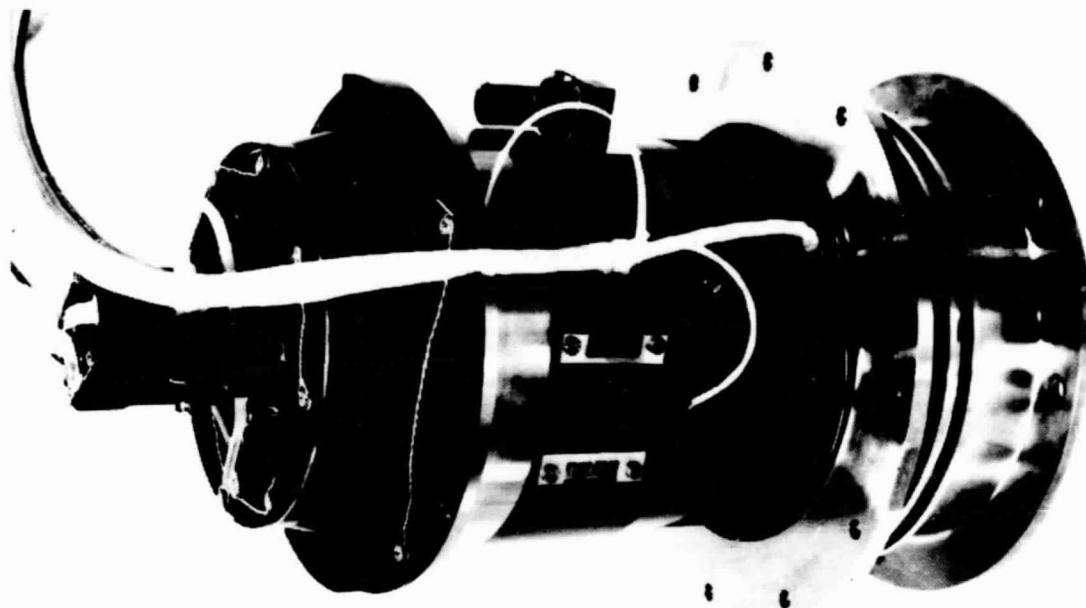


FIGURE 4-9. INTELSAT IV BAPTA (PHOTO A25566)

radially and soft axially, and it allows the unit to withstand large temperature excursions and gradients without large changes in the preload force and bearing torque. On-orbit torques range from 0.16 to 0.23 ft-lb early in life to 0.09 to 0.14 ft-lb after 4 years. At 50 rpm, each motor can deliver up to 0.94 ft-lb at 24 volts for a 4 to 1 margin over the maximum on orbit torque.

Electrical power transfer is accomplished with four spring-loaded cartridge brushes (dry lubricated) running on each of four separate coin rings to provide two separate power circuits with a rating of 15 amperes each. Signal transfer is provided by 22 individual coin silver rings, each with a pair of dry lubricated, leaf spring brushes. Extensive brush testing has been performed to establish wear rates and ensure ample design margins for wear life.

Several generations of BAPTAs have been designed and built at Hughes for communications spacecraft programs. Figure 4-11 presents the orbit history. The first unit launched early in 1969 on TACSAT lasted 4 years before the motor brushes wore out. All Hughes BAPTAs since then, except for OSO which required only a 2 year life, use brushless dc motors. The 25 BAPTAs in commercial communications spacecraft currently in orbit have accumulated 80 years of life without failure, with five operating over 5 years and one over 7 years. Hughes BAPTAs on military satellites have accumulated an additional 24 orbit years without failure.

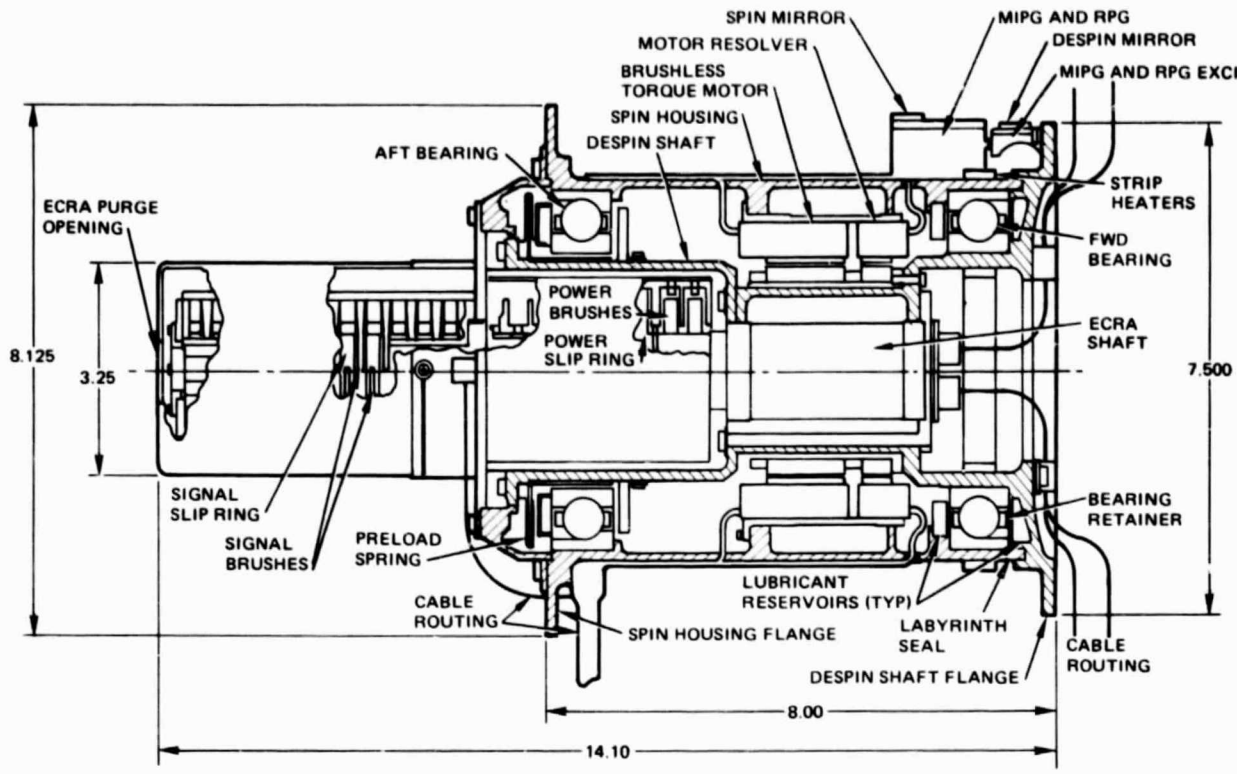


FIGURE 4-10. LEASAT BAPTA CROSS SECTION

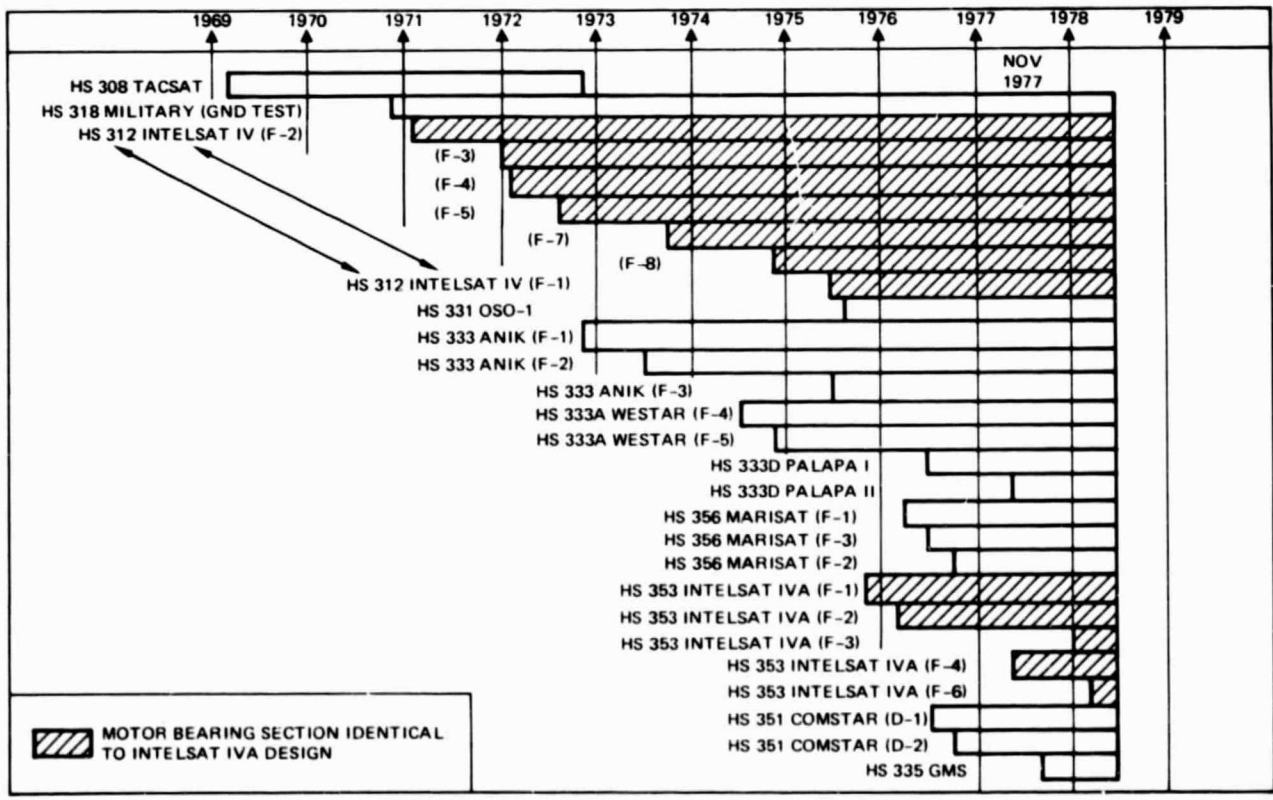


FIGURE 4-11. HUGHES EXTENSIVE AND SUCCESSFUL BAPTA EXPERIENCE SUMMARY



ORIGINAL PAGE  
BLACK AND WHITE PHOTOGRAPH

Earth Sensor

LEASAT will also use flight-qualified designs for the earth sensor, sun sensor, nutation damper, and g-switch. A photo of the earth sensor appears in Figure 4-12 and its design characteristics are listed in Table 4-12. The sensor is a narrow field of view (FOV) passive IR device that operated in the 14 to 16 micro CO<sub>2</sub> absorption band. As its FOV sweeps across the earth by the rotation of the spacecraft, earth radiance is converted into an electrical signal by a thermistor bolometer detector. Fourteen of these sensors have been launched and are operating successfully.

TABLE 4-12. EARTH SENSOR CHARACTERISTICS

<u>Parameter</u>	<u>Value</u>
Field of view	1.5° x 1.5°
Weight	0.6 lb
Spectral sensitivity	14 to 16 $\mu$ m
Size	2.2 x 1.8 x 5.1 in.
Input power requirements	$\pm$ 24 V, less than 0.25 W total power consumption
Type of output	Analog earth pulse, nominal amplitude: -3.8 V
Performance	
Bias shift in 24 hr	Less than 0.05°
Single edge angular jitter	Less than 0.15° (3 $\sigma$ )

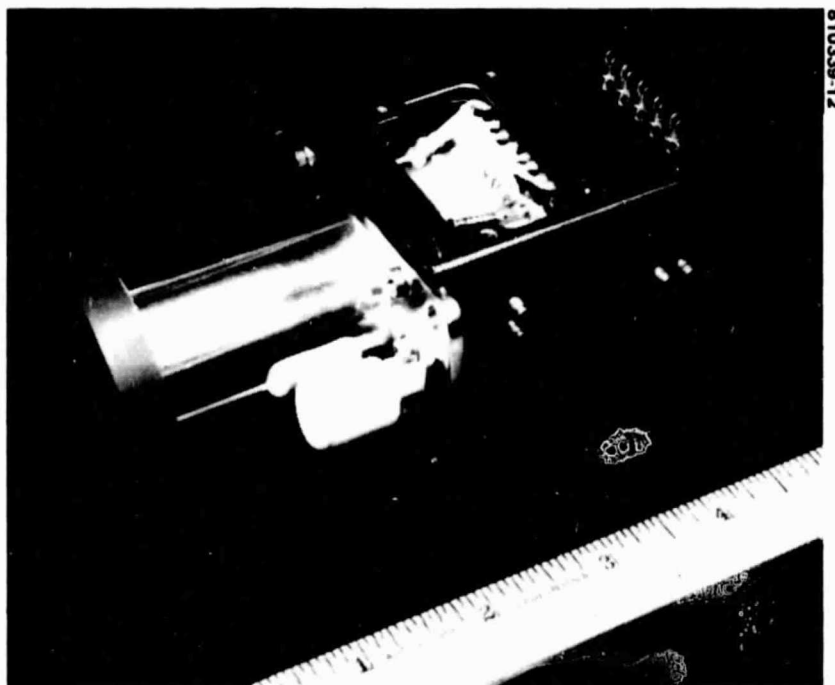


FIGURE 4-12. FLIGHT QUALIFIED EARTH SENSOR (PHOTO A31858)

### Sun Sensor

A photo of the sun sensor appears in Figure 4-13, and its design characteristics are listed in Table 4-13. The sun sensor consists of four shadow-masked silicon solar cell detectors mounted on a single bracket. Each detector has a narrow, fan-shaped FOV approximately  $0.85^\circ$  by  $90^\circ$ . Two of these units, the  $\psi_1$  sensors, are aligned with their fan planes parallel to the spin axis. The other two, the  $\psi_2$  sensors, have their fan planes inclined to the spin axis by  $35^\circ$  and are rotated about the spin axis from the two  $\psi_1$  sensors by  $35^\circ$ . This arrangement generates redundant  $\psi_1$  and  $\psi_2$  pulses and provides a spin synchronous reference as well as time interval data for determining the angle between the sun and spin axis. This technique has been used on all Hughes spinning spacecraft since the original Syncom in 1963.

TABLE 4-13. SUN SENSOR CHARACTERISTICS

<u>Parameter</u>	<u>Value</u>
Field of view (from spin axis)	$90^\circ \pm 35^\circ$
Weight	0.22 lb
Size	2 x 2 x 3 in.
Input power	None required
Type of output	Analog current, redundant $\psi_1$ and $\psi_2$ pulses
Performance	
Spin reference accuracy	$\pm 0.15^\circ$ (after calibration)
Sun elevation angle accuracy	$\pm 0.2^\circ$ (after calibration)

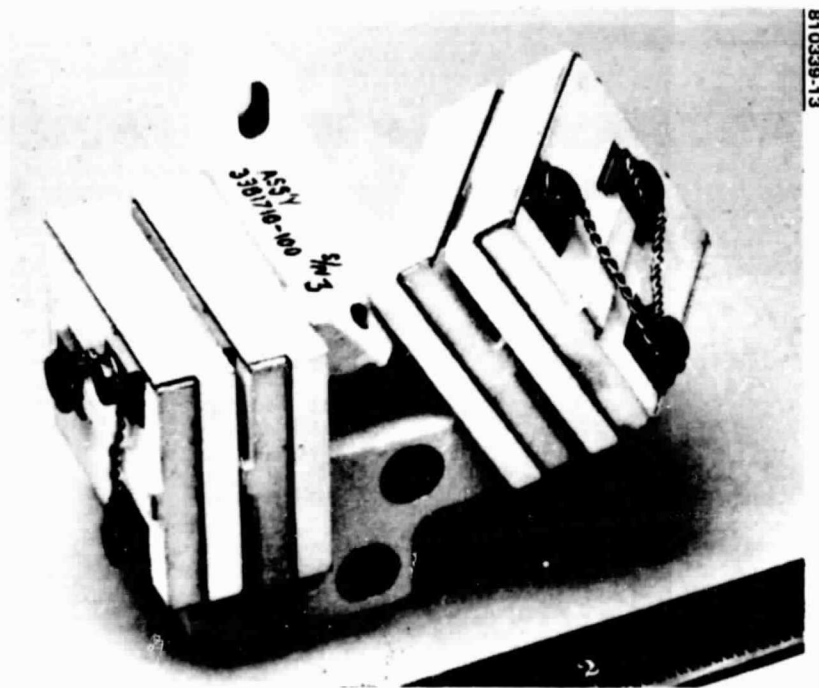


FIGURE 4-13. FLIGHT QUALIFIED SUN SENSOR ASSEMBLY (PHOTO 74-26828)

### Nutation Damper

The nutation damper consists of a straight tube, partially filled with mercury. The length (24 inches) and fraction fill (20 percent) are design parameters that depend on the nominal nutation frequency and the desired damping time constant. For LEASAT, the design is based on conditions near end of life when other sources of fluid damping, such as LBS and hydrazine propellants, are negligible. This mercury damper tube has been used on most of Hughes' passively stable spacecraft, such as Anik A, MARISAT, and ATS.

### G-Switches

The g-switches used for initial spinup thrust termination are mounted in two pairs on opposite sides of the rotor. They are actuated by the centrifugal acceleration and can be accurately adjusted for the desired spin speed. Units of this type are presently used on the SDS spacecraft.

### Attitude Control Electronics

The ACE unit consists of an assembly containing etched circuit card subassemblies and welded cordwood modules. Each unit is divided into three isolated compartments with appropriate interconnections. These separate the higher power circuits, such as the power supply and motor drivers, from the lower level circuits, which are subdivided into the despin controller section and the ADP/JCE section. Hughes designs and builds its own electric units to assure high quality control standards during all phases of fabrication, assembly, and test.

#### 4.1.3.2.11 Conclusion

The LEASAT ACS is a straightforward application of well proven techniques used in many Hughes satellites now in orbit. It is remarkably simple in design, requiring only one active control loop in steady-state operation. With the outstanding record of the despin bearing in orbit, and the redundancy and cross strapping provided, a very high mission reliability is assured. Flight-qualified designs already exist for most of the ACS components; therefore, development risk is negligible.

#### 4.1.3.3 Power Subsystem

The power subsystem is an efficient, fault-tolerant design which assures a 7 year mission life. Solar panel sizing provides a large margin well beyond 5 years. The full eclipse service requirement is met with conservative battery sizing which results in a benign 43 percent depth of discharge for the longest eclipse.

The solar cell array beginning of life (BOL) power has been sized to accommodate a radiation environment more severe than expected throughout the mission life. This radiation environment model has been used as the basis for Hughes solar array designs on Intelsat, COMSTAR, MARISAT, and

other geosynchronous programs. The solar cell array incorporates the most cost effective solar cell for the LEASAT configuration. The solar cell selected is the cell designated K 6.5. Compared with the prior K-6 output of 17.0 mW/cm<sup>2</sup>, the K6.5 cell output of 18.25 mW/cm<sup>2</sup> is 7 percent greater. The excess solar array voltage normally present due to reserve array capability is clamped at 30 Vdc by a set of eight pairs of modular solar panel tap shunt limiters.

The eclipse electrical load requirement of 1254 Whr is provided by a 3387 Whr battery capability resulting in the very benign 43 percent depth of discharge (DOD) during the longest eclipse. The capability is provided with three batteries each having 32 series cells. Each battery has a 28.8 A-hr capacity at an effective discharge voltage of 1.225 V/cell. With two of the three batteries, DOD increases to only 49 percent which still is below the typical 50 to 55 percent DOD design basis for present geosynchronous systems. The enhanced battery life resulting from this unusually low depth of discharge assures high confidence in the batteries' ability to support the LEASAT mission. Efficient stepdown discharge regulators accommodate a widely varying range of battery current-voltage characteristics to furnish 28 Vdc bus energy at minimum depth of discharge from the batteries. The dual redundant discharge regulators serve a load sharing function to control depth of discharge from the three batteries. Batteries are charged from dedicated boost sections of the solar array. These sections provide controlled battery charging through the passive current-limiting characteristic of the solar cells. This provision avoids the need for electronic control of charge current.

This subsection gives a summary functional description of the complete subsystem, showing the key elements integrated in an efficient, reliable design. Included is a discussion of the subsystem's predicted performance compared to the required performance, the main feature being the 8 percent power margin. Detailed descriptions of the subsystem elements are then presented, namely 1) the solar array, which features a high performance solar cell available from existing production, 2) the battery, which features a redundant design with heaters that provide a controlled thermal environment, 3) a battery discharge controller that can tolerate up to two battery cell failures per battery without adversely affecting the spacecraft operation, and 4) the power control electronics, which feature highly reliable, fault-tolerant designs.

#### 4.1.3.3.1 Subsystem Design and Performance Summary

The primary requirements for the power subsystem are summarized in Table 4-14. The specifications for GFE input power and regulation characteristics, mission period, and eclipse service are combined with the derived load requirements for the spacecraft subsystems and shown in detail in Table 4-15. These, together with requirements embodied in the Hughes LEASAT design philosophy such as redundancy, reliability, and elimination of critical single point failure modes, are combined to form the overall power subsystem requirements.

Solar cell array sizing provides a large power margin well beyond 5 years. Conservative battery sizing, which yields a benign 43 percent depth of discharge (DOD) for the longest eclipse, satisfies the full eclipse service requirement. The combined functions of the power sources, power control

TABLE 4-14. POWER SUBSYSTEM PERFORMANCE

<u>Parameter</u>	<u>Performance</u>
Total power/energy	
Sun, solstice	987 W 1093 W (5 yr)
Sun, equinox	1216 W (5 yr)
Eclipse	1254 W-hr (3387 W-hr, 43% DOD)
Eclipse service	Full
Bus voltage	28 to 30 Vdc
Fleet Broadcast processor (FBP)	
Power	33 W
Voltage	(above)
Ripple	<1.5 V p-p, 80 Hz to 100 kHz, square of sine wave; square wave rise and fall time >10 $\mu$ s
Narrow band CW interference conducted by bus to FBP	<1.5 V peak, 30 Hz to 15 kHz, linearly decreasing to 0.9 V peak at 150 kHz
Conducted transient from bus to FBP	Positive: 35 V peak; return to 10% of initial value within 100 $\mu$ s; 35 V/ $\mu$ s max leading edge; Negative: >0 V
Primary bus susceptibility to FBP power increase	Survive loading at 200% max rated power
Primary bus susceptibility to FBP short	Shorted processor may not be externally disconnected from bus in less than 50 $\mu$ s; spacecraft bus to survive processor short sustained for 50 $\mu$ s
Life	7 yr minimum spacecraft design life
Hardening	Solar array, electronics take into account natural environment
Reliability	Support system reliability requirement; avoid critical single point failure modes

electronics, and EMI provisions throughout the spacecraft equipment assure that power regulation characteristics required by the GFE units will be met. The 5 year LEASAT mission duration, including a conservative allowance for radiation exposure, is taken into account in all power subsystem equipment design.

Redundancy is provided throughout the power subsystem. A completely redundant battery is provided, and cell losses within a battery are accommodated. The modular solar array is inherently highly redundant. Electronic units are internally redundant, and critical single point failure modes are avoided. The spinning solar cell array requires no active positioners or sensor for sun orientation. The design results in a 5 year reliability of 0.99 for the subsystem.

The block diagram of the power subsystem is shown in Figure 4-14. Subsystem component locations in the spacecraft are shown in Figure 4-15. The basic subsystem design approach is nearly identical to that being incorporated on the SBS and Anik C spacecraft.

Power is furnished to the loads at 28 to 30 volts dc from a main regulated bus. During sunlight operation, power is obtained directly from

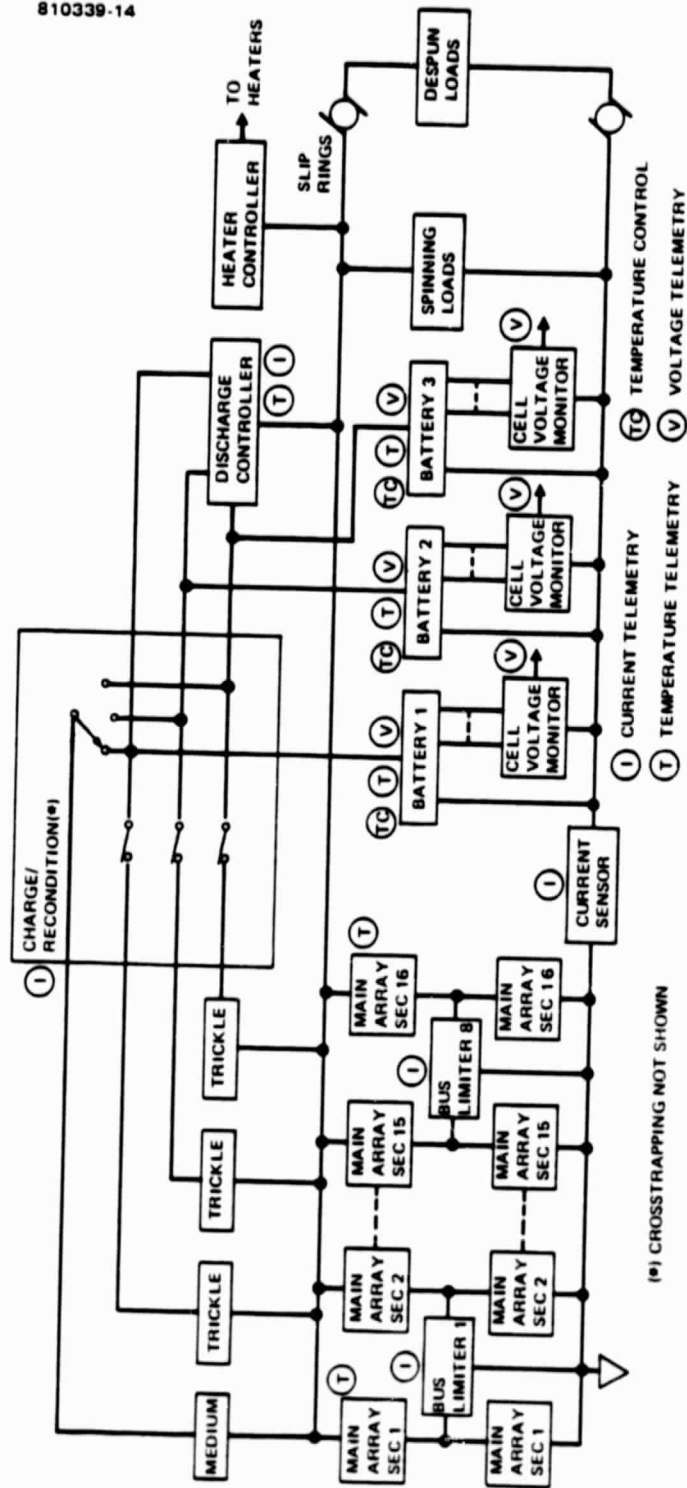


FIGURE 4-14. LEASAT ELECTRICAL POWER SUBSYSTEM BLOCK DIAGRAM

TABLE 4-15. POWER SOURCE SIZING

Subsystem/Unit	Power at 28 volts, W		
	Solstice	Equinox	Eclipse
Communications	739	739	739
Telemetry and Command	71	71	71
Command receivers (2)	7	7	7
Command processor (2)	11	11	11
Encrypter, KG-46 (1)	5	5	5
Remote telemetry multiplexer (9)	4	4	4
Central telemetry processor (2)	8	8	8
X band telemetry beacon	37	37	37
Attitude Control	34	34	34
Earth sensors (3)	1	1	1
Control electronics	31	31	31
Motor	2	2	2
Thermal Control	51	96	51
Battery heaters	—	45	—
Propulsion heaters	51	51	51
Power Control and Distribution	61	66	177
Bus limiters (3)	1	1	1
Battery discharge controller (2)	11	11	127
Charge/recondition	1	1	1
Current sensor (5)	1	1	1
Distribution loss	47	52	47
Battery Charge (main array)	31	96	—
Main Bus Requirement	987	1102	1072
Available			
7 yr	1063	1194	3387 W-hr
Array Margin, %			
7 yr	8	8	
Battery DOD (worst case, 1.17 hr eclipse, %)			43

the solar array. During eclipse, 90 percent efficient stepdown discharge regulators control load sharing and accommodate a wide range of battery current-voltage characteristics to furnish energy to the 28 volts dc bus. Batteries are charged from dedicated boost sections of the solar array. These provide 40 to 50 volt passively current limited battery charging without the need for electronic control of charge current. To reduce voltage stress and thermal load on subsystem regulators, the excess solar array voltage normally present due to reserve array capability and the post eclipse voltage transient is clamped at 30 volts dc by a set of eight pairs of modular shunt tap voltage limiters.

ORIGINAL PAGE IS  
OF POOR QUALITY

810339-15

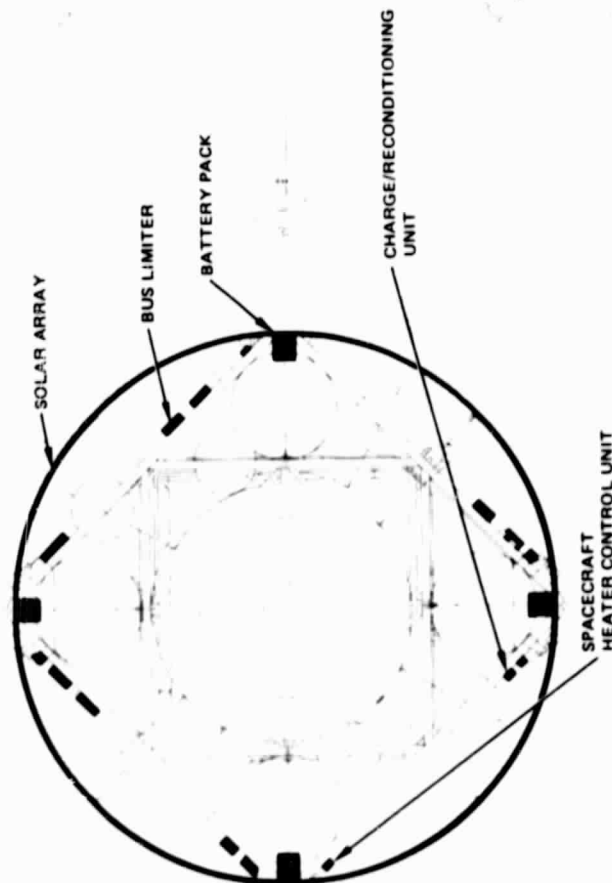
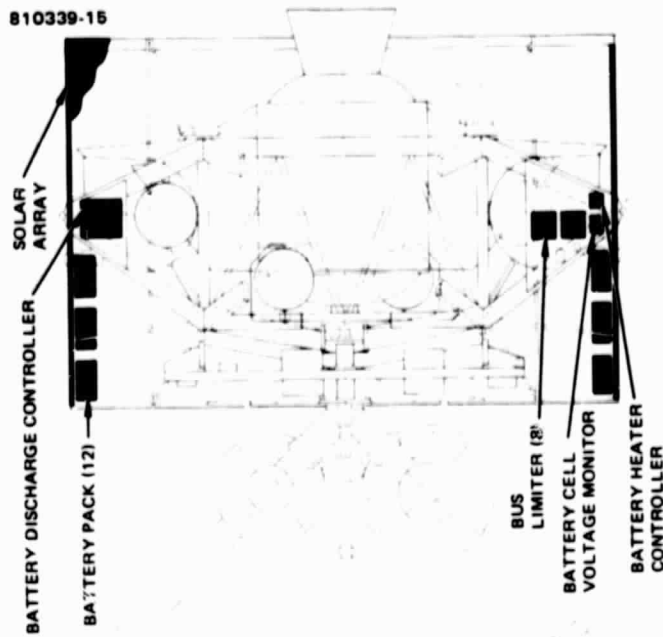


FIGURE 4-15. POWER SUBSYSTEM COMPONENT LOCATIONS



Except for ground commanded battery charge management following solar eclipses, the power subsystem functions automatically without need for ground control. In sunlight, the batteries are normally in an unloaded standby condition, but they automatically pick up the load should the bus approach the 28 volt lower limit due to an unexpected transient or load fault. Upon eclipse entry, a smooth transition automatically occurs from solar panel to battery operation. Following eclipse, the battery charge rate is selected by ground command, which connects dedicated portions of the solar array to the batteries. For replenishment charging following eclipse, batteries are sequentially charged at a high rate by combining trickle and medium rate arrays as shown in the block diagram. The charge arrays available permit high rate charging one battery at a time while the other two remain on trickle charge. Trickle charging for charge maintenance takes place at all times during the year.

#### 4.1.3.3.2 Performance

##### Solar Cell Array Performance

Solar array power output capability to the main bus during the mission is shown in Figure 4-16. The 5 year margins are 15 percent at the constraining (autumnal equinox) season and 14 percent at 7 years, based on a conservative allowance for the radiation environment. Compared with the  $\pm 2$  percent predictability of in-flight performance of the tested solar array, a large power reserve exists for design conservatism and, if desired, payload growth. Solar cell array output is based on the design factors summarized in Table 4-16. The overall solar array performance and modeling techniques used for LEASAT have been proven by flight data from over 80 orbit years of performance. Solar cell array sizing accommodates a radiation environment more severe than is expected throughout the mission life. This radiation environment model has been the basis for Hughes' solar array design on Intelsat, COMSTAR, MARISAT, and other geosynchronous programs.

Two existing production solar cell types shown in Table 4-17 were compared for LEASAT. The K 6.5 type solar cell was selected for both the LEASAT main array and charge arrays because it incorporates state of the art technology, is qualified, is available from existing production, and is more

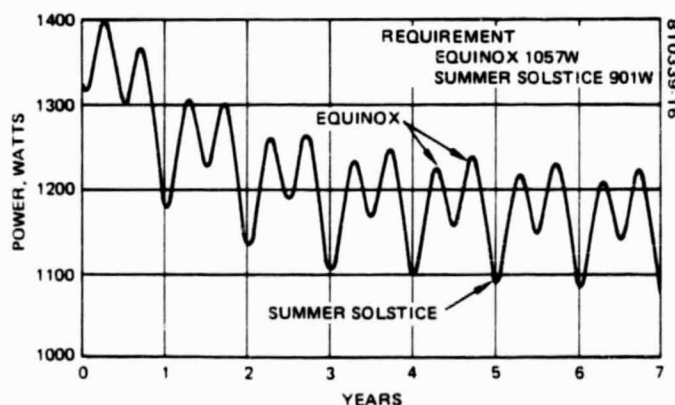


FIGURE 4-16. SOLAR ARRAY POWER AVAILABILITY EXCEEDS REQUIREMENTS WITH AMPLE MARGIN

TABLE 4-16. LEASAT SOLAR ARRAY DESIGN FACTORS

Factors	Current	Voltage
<b>Cells</b>		
Battery array 1.83 x 2 cm (108 parallel, 47 series)	$I_{sc} = 146 \text{ mA}$ $I_{mp} = 136 \text{ mA}$	$V_{oc} = 582 \text{ mV}$ $V_{mp} = 490 \text{ mV}$
Main array 1.9 x 6.2 cm (376 parallel, 68 series)	$I_{sc} = 489 \text{ mA}$ $I_{mp} = 439 \text{ mA}$	$V_{oc} = 582 \text{ mV}$ $V_{mp} = 490 \text{ mV}$
Diode and harness drop		1.5 V main array 0.8 V battery charge array
Fabrication and process loss	0.97	-
Temperature coefficient	*	*
Seasonal temperatures		
21 June		36°F
21 September		43°F
Seasonal declination/intensity		
21 June	0.8884	
21 September	0.9920	
Effective illumination area	$1/\pi$	
Deviation from cosine	0.97	
Ripple		
Main array	0.99	
Battery arrays	1	
Radiation degradation		
5 yr	0.877	0.907
7 yr	0.868	0.902
Optical transmission loss	0.98	

\* Calculated as function of temperature.

TABLE 4-17. QUALIFIED PRODUCTION SOLAR CELL TYPES COMPARISON

Production Solar Cell Type	Choice to Optimize Design for Given Parameter			
	Area	Weight	Spacecraft Temperature	LEASAT Cost
K-6-1/2			✓	✓
K-7 (K-6-1/2 with sculptured surface)	✓	✓		

cost effective for the LEASAT spacecraft application. Over 100,000 (equivalent 2 X 2 cm) K 6.5 cells are being used on current Hughes programs, including the Solar Maximum Mission arrays and a military spacecraft which are in hardware implementation at the present time.

#### Battery Performance

The 1072 W-hr eclipse load requirement shown in Table 4-14 is supported by a 3387 W-hr battery capability. This capability is provided by three batteries, each having a 28.8 A-hr capacity at an effective discharge voltage of 1.225 V/cell. Each battery contains 32 series cells. This battery sizing results in a 43 percent depth of discharge (DOD) during the longest eclipse. With two of the three batteries, DOD increases to only 49 percent, which is still below the typical 50 to 55 percent DOD design basis for present 7 year geosynchronous satellites. The enhanced battery life resulting from this unusually low depth of discharge assures high confidence in the batteries' ability to support the 5 year LEASAT mission.

The benefit to battery cycle life resulting from control of depth of discharge has been demonstrated over a wide range of Hughes flight and test data. This relationship is illustrated in the experience with earlier battery designs summarized in Figure 4-17, which shows data from programs which have accumulated long flight or test durations to date. The figure demonstrates that the conservatively sized LEASAT batteries can support the full 5 year mission service period even if the prediction is made using the worst case limit of this earlier data. Furthermore, a significant number of refinements in battery design, process control, and on-orbit battery management have been progressively introduced to date through technology developed on IR&D and through accumulation of flight experience with 24 spacecraft over the past 9 years.

Because the pulse width modulated regulator is able to accept battery voltage over a wide range, it has been possible to provide ample voltage margin in the battery above the minimum voltage requirement. With the selected 32 cell design, battery voltage will be above 36.8 volts throughout discharge, and with two of the 32 series cells completely shorted, battery voltage will still remain above 34.5 volts.

#### Power Electronics Performance

The power electronics maintain the bus voltage within the range of 28 to 30 volts dc, whether operating from the solar panel or batteries, which satisfies the voltage regulation limits specified for the GFE as shown earlier (Table 4-14). Test data from the GMS and SDS programs show that typical broadband ripple of 250 mV peak to peak or less will satisfy the FBP 1.5 volt peak to peak ripple requirement. Since the broadband specification is usually found to predominate, this indicates the 1.5 volts peak narrowband CW interference requirement shown will also be met. Review of the similar Anik-C power subsystem design shows that bus limiter response, in conjunction with source capacitance present, will satisfy the positive going transient requirement. Negative transients are normally controlled by the battery at  $\geq 28$  volts,

and severe (nonstandard) transients are limited by a fault clearing tap at the battery at a voltage of about 20 volts. These provisions help ensure that negative going transients do not go below the 0 volt condition specified in Table 4-14, i. e., will not reverse polarity. Any spacecraft bus protection device placed external to the FBP will not disconnect the processor prior to the specified 50 microsecond delay. Furthermore, through the following measures, the spacecraft can survive the 50 microsecond processor short. First, through standard design practice, spacecraft units are designed to survive a 0 volt condition. Secondly, undervoltage trips, where incorporated, will not trip within that time. Finally, battery discharge regulators are protected from the resulting overcurrent by a fault clearing tap that bypasses the regulator under low voltage conditions.

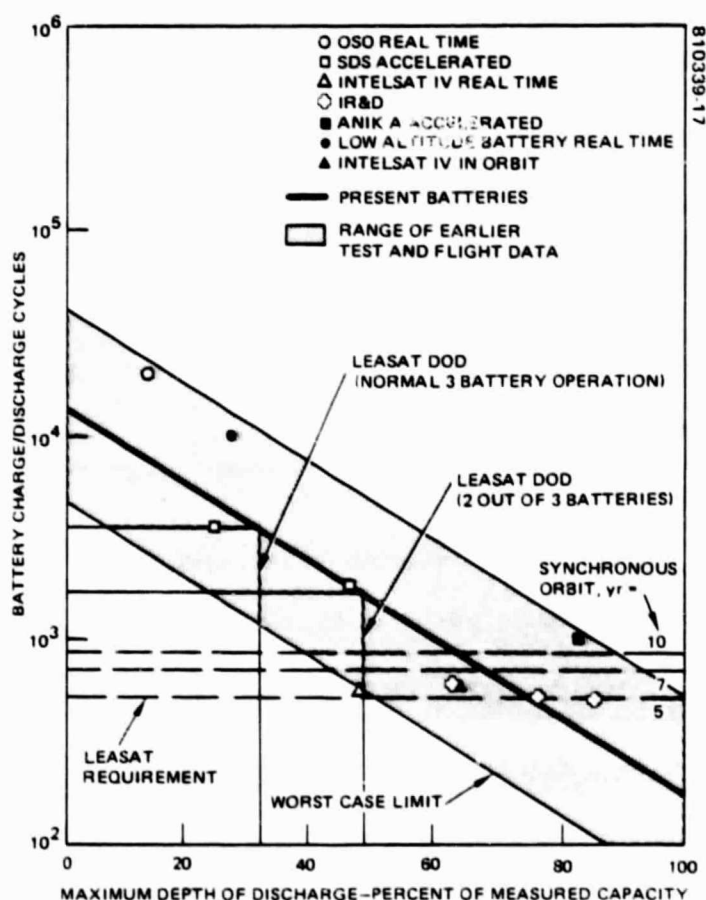


FIGURE 4-17. CYCLE LIFE VERSUS DEPTH OF DISCHARGE

#### 4.1.3.3.3 Equipment Description

Table 4-18 summarizes power subsystem components characteristics. A brief description of these components is also provided.

##### Solar Cell Array

The array consists of four 90° segments with identical solar cell layouts joined to form the 108.2 by 166 inch diameter cylindrical body-mounted array. The Kevlar composite array substrate is a low weight design that provides the required structural stiffness, and thermal expansion characteristics to match that of the silicon solar cells. In the main solar array, a 0.030 cm thick, 1.9 by 6.2 cm size cell is used with a 0.030 cm thick Corning 7940 fused silica cover. The solar cell used in the battery boost charge arrays is identical to that used for the main array, except that it is a smaller (1.83 by 2 cm) size. Totals of 25568 1.9 by 6.2 cm cells and 5076 1.83 by 2 cm cells (2820 in the medium rate array, 752 in each of three trickle charge array) are carried on the spacecraft.

TABLE 4-18. POWER ELECTRONIC COMPONENTS - PHYSICAL CHARACTERISTICS

Unit	Quantity per Spacecraft	Weight, lb		Power, W		Dimensions, in.	Derivation
		Unit	S/C	Unit	S/C		
Solar panel (less substrate)	1	155	155	—	—	108.2 height, 166 diameter	Intelsat IV, SBS
Battery pack	12	22.50	270	—	—	5.5 x 12.8 x 16	
Discharge controller	1	16	16	7.5 stby, 90% effc	7.5 stby, 90% effc	16 x 12 x 3.5	Anik C
Bus limiter	3	2.15	6.5	0.3 stby	2.4 stby	7.8 x 8 x 1.9	Anik C
Charge/reconditioning unit	1	2	2	0.06	0.06	4.5 x 7 x 1.7	Anik C
Battery cell voltage monitor	3	0.6	1.8	0.3 bus 0.48 batt	1.2 bus 1.92 batt	3 x 3.5 x 1.5	SBS, Anik C
Current sensor	1	0.2	0.2	0.2	0.2	3.1 x 1.6 x 1.6	Pioneer Venus
Battery heater controller	3	0.75	2.5	1.5 stby	6 stby	3 x 5 x 1.5	Anik C
Battery heaters	12	0.044	0.53	—	—	on battery	SBS
BAPTA heater switch (spinning)	1	0.2	0.2	0.06	0.06	2.9 x 2.5 x 0.8	Anik C
BAPTA heater switch (despun)	1	0.2	0.2	0.06	0.06	2.9 x 2.5 x 0.8	Anik C
LBS heater switch	2	0.2	0.4	0.03	0.03	2.9 x 2.9 x 1.6	Anik C
SPS heater switch	2	0.2	0.4	0.03	0.03	2.9 x 2.9 x 1.6	Anik C

## Battery

The mechanical packaging of the LEASAT battery has been used on many previous Hughes satellites. Each 32 series cell battery consists of four 8 cell battery packs. Each pack contains cells, thermal shunts, mylar insulators, and machined end plates.

Present Hughes battery cell technology has evolved over recent years as a result of the feedback of extensive in-orbit experience. Key improvements include a revised terminal seal, increased electrolyte volume to extend operating life, increased overcharge protection through control of negative/positive capacity ratio, control of carbonate level to reduce cadmium migration and improve voltage performance, and numerous changes to facilitate battery thermal control to enhance separator life and maintain overcharge protection. The LEASAT battery cell, which is essentially the present SBS cell scale upward one-third in size, reflects that existing hardware technology. Characteristics of the cell are summarized in Table 4-19.

## Power Electronics

Units comprising the power electronics portion of the subsystem are derived from previously flown spacecraft and hardware designs presently being implemented, as discussed in the following paragraphs.

Bus Limiters. Tap bus limiters control the maximum solar cell array voltage to  $29.75 \pm 0.25$  volts dc by shunting tapped portions of the solar array. The limiter elements, consisting basically of power transistors with voltage control circuitry, are essentially the same as those used on MARISAT and other similar spacecraft.

TABLE 4-19. LEASAT BATTERY CELL CHARACTERISTICS

Capacity, A-hr	28.8
Weight, gm	1078
Number of plates	27
Plate current density, mA/cm <sup>2</sup>	2.8
Plate additives	
Positive	Cobalt hydroxide, cadmium
Negative	TFE
Plate thickness, in.	
Positive	0.023
Negative	0.027
Interelectrode space, in.	0.008 to 0.009
KOH concentrate, %	31
KOH volume, cm <sup>3</sup>	114
Soluble carbonates, %	<5
Precharge level	Optimized for operating temperature
Terminal seal	GE built geometry, Ni-Au braze

Battery Discharge Controller. A redundant, three phase, phase width modulated discharge control technique was chosen for LEASAT over other methods because it minimizes bus voltage excursion and thus holds the spacecraft thermal dissipation nearly constant. Also, it can accommodate a wide range of input voltage from the battery, thus permitting conservative battery voltage sizing and reducing battery DOD by efficiently using battery energy over the varying discharge voltage profile. The battery discharge controller is identical to the present Anik C design, except for modification in the output circuits for higher LEASAT power.

Battery Charge/Reconditioning Unit. The battery charge/reconditioning unit provides charging current to the batteries at rates governed by the chosen arrangement of solar cell charge arrays. They also permit discharge reconditioning at either of two rates determined by selection of discharge loads.

Battery Cell Voltage Monitor. Each battery is provided with a cell voltage monitor to sample and serially multiplex individual cell voltages to a dedicated analog telemetry channel. Data from the monitor obtained during discharge and reconditioning ensure that individual cells are not reversed and are not overcharged during charge.

Battery Heater Controller. Two battery heater controllers, in conjunction with strip heaters mounted on the battery packs, limit the minimum battery temperature to one of two selectable set points, 1° or 5°C.

Current Sensor. The current sensor design has been employed on the Hughes Pioneer Venus program. The sensor is of the dc amplifier type which does not use magnetics or switching circuits and, hence, does not generate EMI.

#### Power Subsystem Ground Interfaces

The power subsystem interfaces with ground control through the command and telemetry subsystem.

#### Subsystem Hardware Implementation

During the initial phase of the program, breadboards will be built for the battery discharge controller and battery heater controller. The nickel-cadmium batteries and/or cells will be subjected to thermal cycling, DOD, charge/discharge characterization, and pyro pulse testing under expected LEASAT orbit conditions. All development testing will be completed on cells/batteries prior to flight hardware qualification and acceptance testing completion. Testing will be augmented by a battery cell analysis program, which will ensure the high quality standards required for long life performance. Routine solar array coupon thermal cycling tests to the LEASAT environments are planned.

#### **4.1.3.3.4 Electrical Distribution Harness**

The LEASAT wire harness requirements are met with conventional designs widely used on prior spacecraft. The most significant requirements are those for EMI control, which are met through attention to harness layout to control coupling between wires and through use of existing shield and shield termination techniques.

The harness design employs the flexible, kapton/H-film insulated wire commonly used on Hughes spacecraft. Conductor material is high tensile strength copper. The wire is available in single 19-strand form, and also in preassembled/pretested twisted pair and quad with single or double shield. Minimum wire size will be limited to 24 gauge for power leads and 26 gauge for signal leads.

Connectors will be selected from solderless, circular bayonet and high density, rectangular series presently in use on Hughes spacecraft. The rectangular series accommodates the addition of integral feedthrough filters where required for EMI isolation. This is of particular importance to the LEASAT electromagnetics control design.

Attention is given in the harness implementation to ensuring high reliability of the finished product. Proven wire and connectors are selected for the harness design. Redundant wires and connector pins are provided. Further, a number of steps are taken to assure proper fabrication and to control the effects of handling exposure. For example, all harnesses are preassembled on three-dimensional jigs so that subsequent installation on the spacecraft can be accomplished with a minimum of wire bending. Prior to installation on the spacecraft, assembled harnesses are high-potency tested at voltages (conservatively) well in excess of operating values. The harness layout on the equipment shelves, which on the STS-optimized LEASAT bus provide relatively unconstrained installation area, permits accessibility, and mating/demating with a minimum of harness flexing for unit changeout. Connector savers are used where applicable during test.

The wire harness design supports the system availability with a reliability of 0.997 for 5 years and 0.996 for 7 years. Harness weight, based on the Syncom IV bus harness layout and conductor weights from GMS, is a total of 104 pounds.

#### **4.1.3.3.5 Conclusion**

The power subsystem design meets all specified requirements and Hughes' standards to ensure successful mission operation with a reliability of 0.990 for 5 years. Existing designs used for the electrical distribution harness yield a reliability of 0.997 for 5 years. Limiting the battery DOD to 43 percent, controlling battery temperature, and incorporating sufficient redundancy to accommodate failed cells in each battery as well as the complete loss of one battery ensures full eclipse battery capability for more than



10 years. The solar array margin of 15 percent after 5 years of degradation imposed by a conservative radiation model ensures a large margin for mission life expectancy and load growth.

#### 4.1.3.4 Propulsion

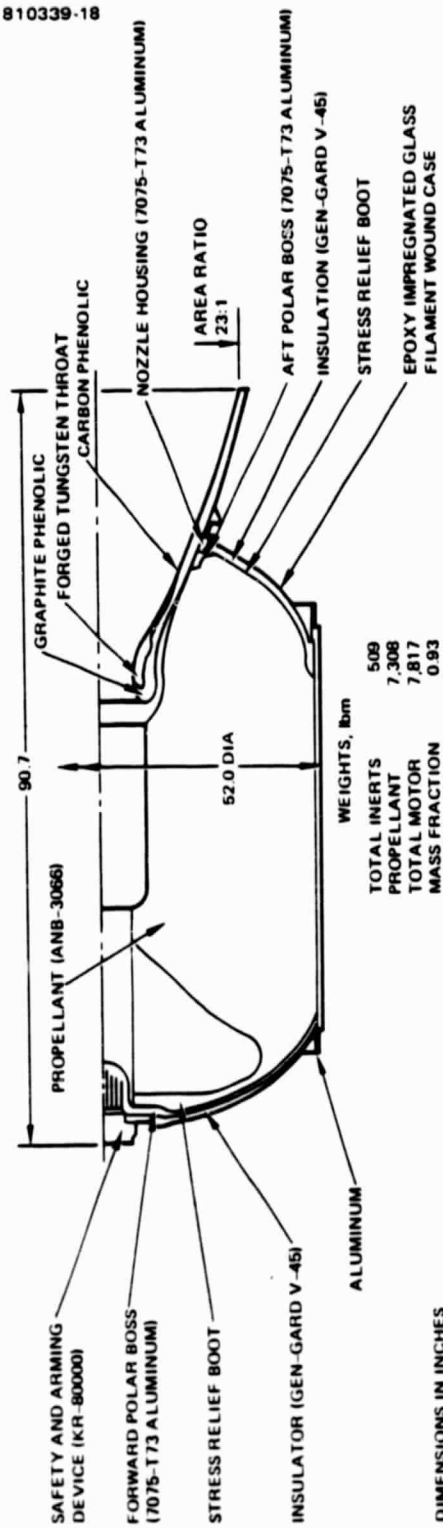
Propulsion is provided by subsystems whose ability to perform the required mission will be demonstrated on the Syncom IV spacecraft. A solid propellant subsystem utilizing the Minuteman III third stage motor injects the spacecraft into an intermediate orbit 45 minutes after separation from the Shuttle. The liquid bipropellant subsystem utilizing 100 lbf thrusters developed for the Apollo project is fired on successive perigee passages to raise the apogee to synchronous altitude. The LBS is subsequently used to inject the spacecraft into synchronous orbit. A redundant reaction control subsystem using equipment developed for the Intelsat IVA/COMSTAR program is used for spin axis attitude and spin rate control, station acquisition, stationkeeping, and station change maneuvers.

The use of the Minuteman III third stage motor for the perigee injection function all but eliminates technical and schedule risk. To date, Thiokol has produced 662 Minuteman III motors at their Wasatch Division. There have been 49 flight tests and 52 static tests without a failure.

The liquid bipropellant thruster assembly was originally qualified for the Apollo program with a 40 to 1 expansion ratio nozzle. The thruster is being modified for the Syncom IV program to incorporate a nozzle having an expansion ratio of 100 to 1 which will improve the LBS performance by 2 percent. Propellants are monomethylhydrazine and nitrogen tetroxide and are carried in four hemispherical tanks. The propellants are settled to the outlet of each tank by the centrifugal force associated with the spinning environment, assuring bubble-free propellant at each tank outlet and precluding any requirement for a mechanical expulsion device. Helium pressurant gas is stored in two high pressure spheres and is isolated from both the pressure reducing system and the propellant tanks by a normally closed squib valve assembly and a latching valve. The latching valve closes the high pressure helium supply between maneuvers.

The reaction control subsystem components are identical to those that have performed without malfunction in the Intelsat IVA/COMSTAR series of spacecraft. The exact Syncom IV configuration, which will be flown a year prior to LEASAT, will be used for the LEASAT.

Monopropellant hydrazine is used in a pressure-blowdown mode, with gaseous helium as the pressurant. Propellant is settled to the tank exit port by the centrifugal force associated with the spinning environment, assuring gas-free propellant at each tank outlet and precluding any requirement for a mechanical expulsion device. The subsystem is separated into two functionally redundant halves, with propellant divided between the two. A cross-connect latching valve allows transfer of propellant, between the halves, making all propellant available to any thruster. Each half contains two con-  
spherical tanks.



DIMENSIONS IN INCHES

FIGURE 4-18. SOLID PROPULSION SUBSYSTEM MOTOR FOR LEASAT (MODIFIED STAGE III MINUTEMAN MOTOR)

There are three hydrazine catalytic decomposition thrusters per half system, one axial and two lateral. The lateral thrusters are mounted at the outer surface of the spacecraft, with their thrust vectors offset from the spinning axis by 45°. The lateral thrusters operate individually for spacecraft spin rate control, and in pairs for spacecraft east-west stationkeeping and station change maneuvers. The axial thrusters provide injection error corrections, attitude trim, and north-south stationkeeping. The lateral and axial thrusters perform their functions in both the pulsed and steady state modes.

The SPS, which provides the main perigee propulsion to raise apogee, is discussed in the first section. It utilizes a simplified version of the Minuteman III third stage motor which has had 101 test firings, all of which have been successful. The LBS, which is described next, utilizes Marquardt R4D thrusters which have been flown on the Apollo spacecraft with complete success. The final section describes the hydrazine monopropellant RCS that is derived from the highly reliable Intelsat IVA and COMSTAR spacecraft programs.

#### 4.1.3.4.1 Solid Propellant Subsystem

##### Introduction

The use of the Minuteman III motor for the perigee injection function all but eliminates technical and schedule risk. To date, Thiokol has produced 662 Minuteman III motors at their Wasatch Division. There have been 49 flight tests and 52 static tests without a failure. This extensive history verifies the motor's applicability to the LEASAT mission. This section describes the motor, the test program, and how Hughes will manage the solid propellant motor program.

##### Description

The SPS design is shown in Figure 4-18. The motor case is an epoxy-impregnated, glass filament-wound case with integral aluminum bosses for attachment of the igniter and nozzle assemblies. A cylindrical attachment skirt with an aluminum thrust ring is an extension of the cylindrical section of the case. The 52.0 inch diameter motor has an overall length of 90.7 inches. The motor case is insulated with Gen-Gard V-45, a silica-loaded nitride rubber. Stress relief boots are used in the fore and aft ends. A case-bonded grain of ANB-3006 propellant is cast in the motor case in a finocyl configuration. A poly-butadiene liner, designated SD-851, is used to bond the propellant-to-insulation interface.

The nozzle assembly has a contoured exit cone with a 23:1 expansion ratio. A tungsten throat and tape-wrapped carbon-phenolic exit cone liner and entrance section comprise the nozzle components exposed to the propellant exhaust products. An aluminum nozzle housing supports the throat and an integral flange is used to attach the nozzle assembly to the chamber.

#### PERFORMANCE SUMMARY

MEOP, psia	700
MAXIMUM THRUST, lbf	42,620
BURN TIME, sec	60.1
AVERAGE EXPANSION RATIO	23.6
TOTAL IMPULSE $\times 10^6$ , lbf-sec	2.083
VACUUM SPECIFIC IMPULSE, sec	282.1

810339-19

#### MATERIALS

CASE	5901 GLASS
NOZZLE	TUNGSTEN/CARBON PHENOLIC
INSULATION	SILICA FILLED NBR
PROPELLANT	ANB-3086 (A1/AP/CTPB)

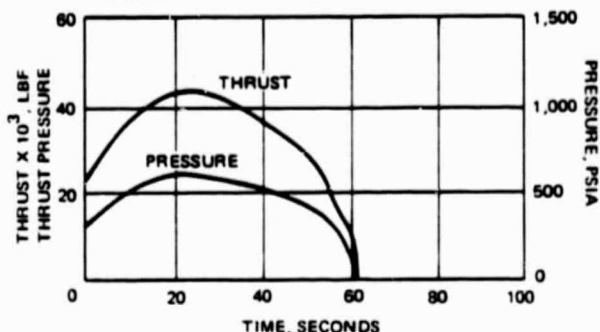


FIGURE 4-19. STAGE III MINUTEMAN PERFORMANCE

The ignition system consists of a KR 80000-9 safe-and-arm device and a one-piece molded epoxy-fiberglass chamber loaded with boron potassium nitrate pellets. The safe-and-arm device is an electromechanical unit which uses dual squibs and is attached to the igniter assembly.

The Stage III Minuteman motor has several design features that are not required for the LEASAT application. These include six mounting brackets on the forward dome that are used to hold linear shaped charges for thrust termination, ports in the nozzle for liquid injection thrust vector control, and an added extension on the forward skirt which is used as a secondary mounting point. These auxiliary devices will be deleted for the LEASAT application. Qualification tests on two motors will verify the use of this modified configuration for LEASAT.

#### Performance

The performance of the Minuteman third stage motor is as well characterized as that of any solid propellant motor (see Figure 4-19). There have been 52 static tests. The vacuum specific impulse is 282.1 seconds. This performance is delivered with an expansion ratio of 23.6. Motor burn time is 60.1 seconds. Maximum thrust of 42,620 pounds occurs one-third of the way through the burn time, so that maximum acceleration imparted to LEASAT is only 3.7 g. The maximum expected operating pressure (MEOP) is 700 psi. All motor cases are proof tested at MEOP.

#### 4.1.3.4.2 Liquid Bipropellant Subsystem

##### Introduction

The LBS will augment the transfer orbit apogee-raising function of the SPS and perform the orbit circularization maneuver at synchronous orbit altitude utilizing highly reliable, flight-qualified thrusters and propellant control equipment. The LBS is described in this section, with emphasis on the key component, the Marquardt R4D rocket motor.

##### Description

The LBS shown schematically in Figure 4-20 is located in the spinning section of the spacecraft. When commanded, the propellant control valves of the two liquid bipropellant thrusters are opened. The oxidizer, nitrogen tetroxide ( $N_2O_4$ ), and the fuel, monomethylhydrazine (MMH), are pressure fed to the thrusters where the propellants ignite spontaneously to produce high temperature gases that are exhausted through a De Laval nozzle to produce thrust.

The propellants are settled to the outlet of each tank by the centrifugal force associated with the spinning spacecraft, assuring bubble-free propellant flow at each tank outlet and avoiding the requirement for mechanical expulsion devices. Helium pressurant gas is stored in two high pressure spheres and is isolated from both the pressure regulator and propellant tanks by a normally closed squib valve assembly and a latching valve during launch. The latching valve closes off the high pressure helium supply between maneuvers.

LBS maneuvers may be performed by a single thruster in the unlikely event that a propellant flow control valve fails. Should the valve fail in a closed position, the subsystem liquid manifold design allows all of the propellant to be available to the redundant thruster. If a propellant valve fails in an open position, or if an excessive leakage condition is detected between LBS burns, the latching valves in the propellant feed lines to that thruster would be closed.

The STS launch vehicle has specific safety design requirements for all spacecraft payloads. They are: 1) two independent valve seats must be used to prevent subsystem propellant leakage, and 2) the design of the subsystem pressure vessels must meet the requirements of either MIL-STD-1522 or the American Society of Mechanical Engineering Boiler and Pressure Vessel Code for unfired pressure vessels. Both of these requirements are satisfied by the design of the LBS. In addition, the LBS complies with the safety requirements outlined in the Range Safety Manual, AFETRM 127-1, and the KSC Safety Program, KMI 1710.1C.

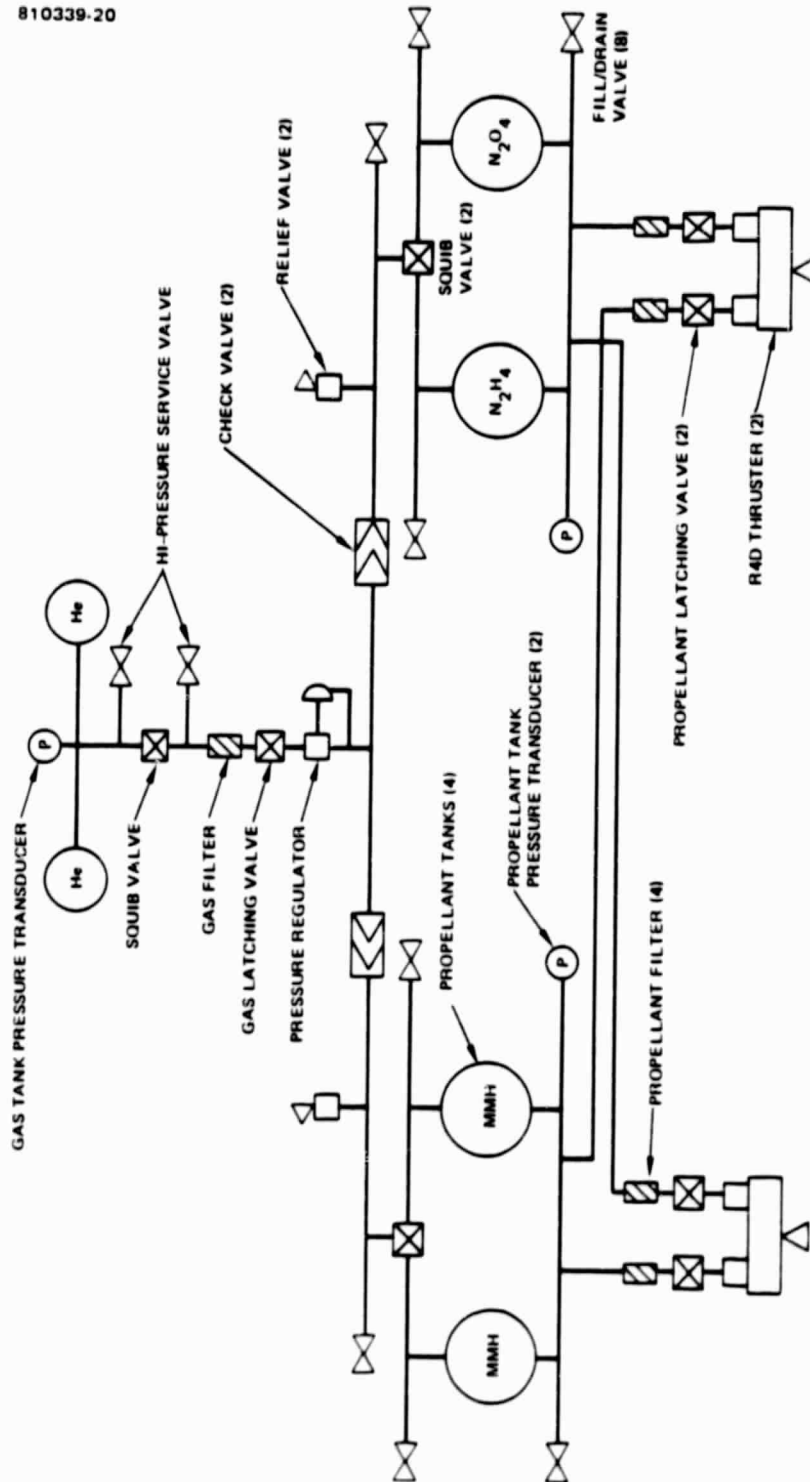


FIGURE 4-20. LIQUID BI-PROPELLANT SUBSYSTEM SCHEMATIC

## Performance

Each of the two R4D engines develops 100 pounds of force at an injector inlet pressure of 189 psia. The specific impulse has been increased from 292 to 297 seconds by increasing the nozzle expansion ratio from 40:1 to 100:1. The total impulse provided by the LBS is approximately 914,048 lb-secs. For a single engine to provide the entire impulse would require its burning for approximately 9000 seconds, whereas the engines are qualified for 32,000 seconds of operation. Also, the multiple start capability of the engine, which will allow distributing the impulse between the apogee-raising and perigee-raising maneuvers, is well within the engine's demonstrated capability for 5000 restarts.

## Equipment Description

**R4D Engine.** The model R4D liquid bipropellant engine manufactured by the Marquardt Corporation, Van Nuys, California, consists of two rapid response integral solenoid operated valves, an injector assembly, a thrust chamber, a two-piece nozzle, and associated clamps and seals, as shown in Figure 4-21. The motor design incorporates the following features:

- 1) Molybdenum combustion chamber and coatings
- 2) Ribbed L-605 exit bell used to minimize weight of the 100:1 expansion bell
- 3) Fuel film cooled combustion chamber
- 4) Preigniter integral with the injector head for ignition spike suppression

The radiation and film-cooled combustion chamber is made of forged molybdenum and is coated with molybdenum disilicide to provide oxidation protection. The nozzle up to an expansion ratio of 6.8 is also made of coated molybdenum. Beyond that point a lightweight L-605 stainless steel expansion bell is attached with an expansion ratio of 100 to 1. Use of the L-605 cobalt base alloy in the bell construction allows for weight reduction in the exit area where gas temperatures and pressures are less severe than in the combustion chamber. The life of the chamber is dependent upon the wall temperature and duty cycle. For the design conditions of this engine, the operating life expectancy is greater than  $10^6$  seconds. The LEASAT mission requires that the engines operate for 9000 seconds. The multiple restart capability of the engines has been thoroughly demonstrated. Seven hundred and ninety-seven R4D engines have been produced, of which 469 have been fired in space 989,441 times, with no failures.

- |  |                             |
|--|-----------------------------|
| 1. PREIGNITER  | 15. DIRECT COIL             |
| 2. INTERMEDIATE MIDDLE RING - EIGHT PREIGNITER FUEL COOLING ORIFICES | 16. OXIDIZER VALVE ASSEMBLY |
| 3. PREIGNITER CHAMBER ORIFICES                                       | 17. SPRING                  |
| 4. INNERMOST RING - EIGHT PRIMARY OXIDIZER ORIFICES                  | 18. AUTOMATIC COIL          |
| 5. MIDDLE RING - EIGHT PRIMARY FUEL ORIFICES                         | 19. FUEL ORIFICE            |
| 6. SPLIT RING  | 20. RETAINING RING          |
| 7. OUTERMOST RING - EIGHT CHAMBER WALL FUEL COOLING ORIFICES         | 21. CAL                     |
| 8. INJECTOR HEAD ASSEMBLY  | 22. FUEL VALVE ASSEMBLY     |
| 9. ANNULUS   | 23. SPACER                  |
| 10. OXIDIZER PREIGNITER TUBE   | 24. FUEL PREIGNITER TUBE    |
| 11. INSERT ASSEMBLY  | 25. COMBUSTION CHAMBER SEAL |
| 12. INSULATOR  | 26. ATTACH RING             |
| 13. SEAT ASSEMBLY  | 27. COMBUSTOR               |
| 14. ARMATURE   | 28. LOCK RING               |
|  | 29. WASHER                  |
|  | 30. ATTACH NUT              |
|  | 31. BELL                    |

810339-21

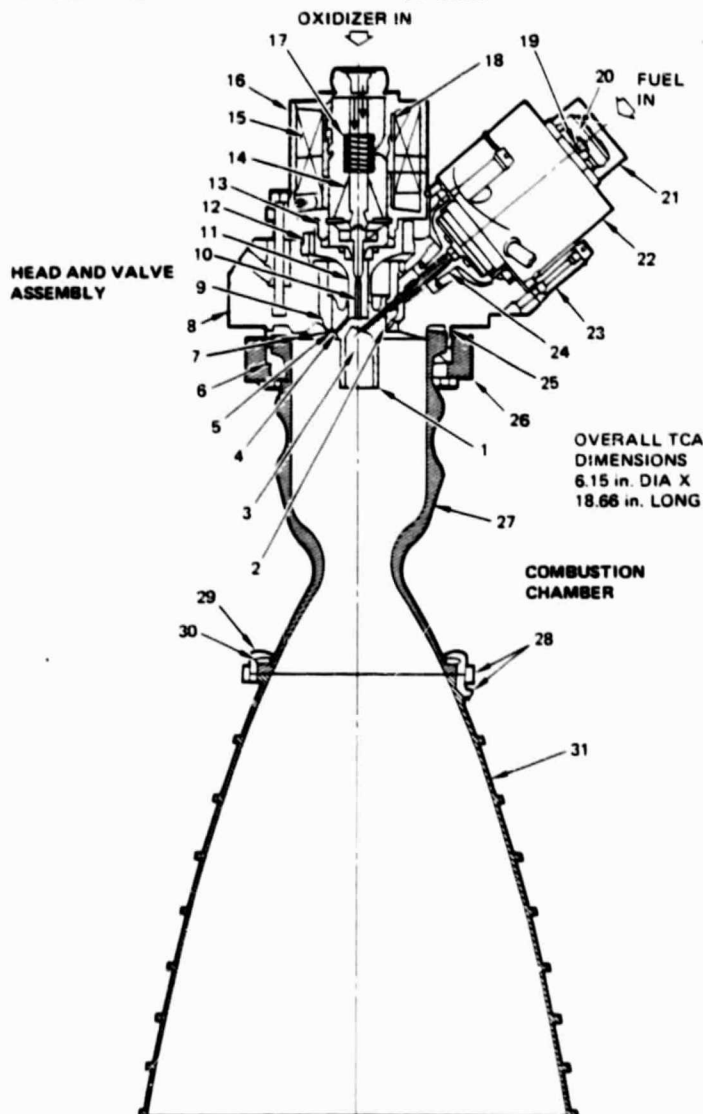


FIGURE 4-21. FLIGHT PROVEN MARQUARDT R40 THRUSTER ASSEMBLY USED IN LBS



Propellant Feed Equipment. The propellant required for the LEASAT mission is contained within four identical conispherical propellant tanks. Two of the tanks contain the oxidizer (1917 pound) and two contain the fuel (1162 pound). The tanks are manufactured from titanium forgings.

Each thruster has independent, solenoid-operated fuel and oxidizer valves to control the flow of the respective propellant into the thruster injector. In addition to these solenoid valves, a latching valve is provided upstream of each solenoid valve as a redundant backup to preclude potential leakage of fuel and/or oxidizer into the thruster combustion chamber during servicing operations or during the launch phase vibration environment.

Ten manually operated service valves are incorporated in selected locations in the subsystem gas and liquid lines. The valves provide access to various points and permit functional testing of subsystem components during spacecraft system tests and prelaunch operations, despite the normally closed squib valves. These 10 valves also provide access to the subsystem for prelaunch of the pressurant and propellant required for the mission.

All joints in both the high and low pressure gas circuits are tungsten inert gas (TIG) welded using procedures and equipment that has been employed on Hughes propulsion systems over the past eight years. All joints on the liquid side of the subsystem are also TIG welded, except for the mechanical connections at the thruster. This welding provides a structurally sound, essentially leak-free subsystem, similar to flight-proven Hughes reaction control subsystem designs. The mechanical connections at the thrusters are downstream from the latching valve in each of the propellant feed lines, and they are only exposed to the full subsystem liquid pressure subsequent to separation from the STS. Nonetheless, leak tests of these connections are made several times during prelaunch spacecraft checkout.

Pressurization Equipment. High pressure helium is regulated to the required operating pressure by means of a single-stage pressure regulator. A high pressure gas filter located upstream of the pressure regulator assembly protects the regulator from any debris that may be entrained in the pressurant as a consequence of the firing of the gas isolation squib valve. Low pressure gas on the outlet side of the regulator assembly is divided into two circuits. One circuit delivers pressurant to the oxidizer tanks and the other delivers pressurant to the fuel tanks. Each pressurant circuit contains a dual check valve assembly to preclude possible comingling of the fuel and oxidizer vapors via the propellant tank pressurizing circuit. For launch safety compatibility with STS, a squib valve that is normally closed is incorporated in each of the pressurizing circuits, in addition to the dual check valve assembly, to prevent liquid fuel or oxidizer leakage into the common pressurant gas circuit. Both the fuel and the oxidizer pressurant circuits have relief valve assemblies to preclude overpressurization of the propellant tank assemblies.

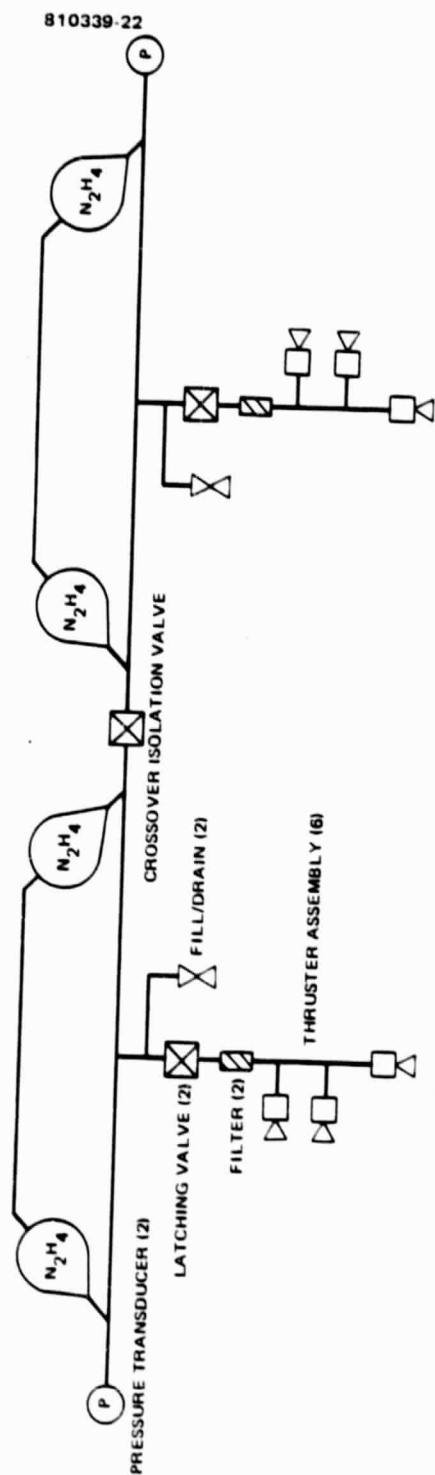


FIGURE 4-22. REACTION CONTROL SUBSYSTEM SCHEMATIC

Conclusion. The liquid bipropellant subsystem utilizes regulated pressurization and is capable of operating in a continuous mode without limitation. Because propellant is stabilized at the outlet of each tank by the centrifugal force produced by the spinning spacecraft, no mechanical propellant expulsion devices (e.g., surface tension or bladder) are required.

Liquid bipropellant subsystems have been reliably and successfully used for many military spacecraft, as well as on the Symphonie and Viking Orbiter programs. This experience, together with Hughes experience with the LBS components on previous programs will provide a background that will ensure the reliability of the LBS.

#### 4.1.3.4.3 Reaction Control Subsystem

##### Introduction

The reaction control subsystem (RCS) is similar to those that have performed without malfunction in seven Intelsat IVA and COMSTAR spacecraft; only the routing of the tubing has been changed. This section provides functional and physical descriptions of the RCS and discusses its performance and its development plan.

##### Description

The RCS shown schematically in Figure 4-22, is located in the spinning section of the spacecraft. It provides all impulses for attitude control and stationkeeping for over a 7 year operational lifetime. Ground commands operate the flow control valve. When the valve is open it allows hydrazine to be pressure-fed to the thruster, where it catalytically decomposes to produce the thrust by expansion of the hot gas through a nozzle.

Monopropellant hydrazine is used in a pressure-blowdown mode, with gaseous helium as the pressurant. Propellant is forced to the tank exit port by the centrifugal force associated with the spinning environment, assuring gas-free propellant at each tank outlet and precluding any requirement for mechanical expulsion devices.

The subsystem is separated into two functionally redundant halves, with propellant divided equally between the two. A cross-connect latching valve allows transfer of propellant between the halves, making all propellant available to any thruster. Each half contains two conispherical tanks. A latching isolation valve is located in the propellant manifold between the two redundant fuel systems. Two additional latching valves provide isolation of either or both of the two thruster branches (normally open). The valves provide the capability to shut off a thruster branch if there is evidence of flow control valve leakage. All joints in the pressurized portion of the subsystem are tungsten inert gas (TIG) welded. This design feature provides a leak-free, structurally sound subsystem similar to all flight-proven Hughes designs.

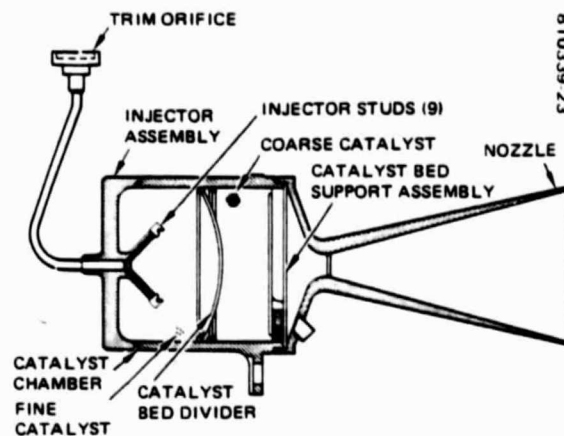
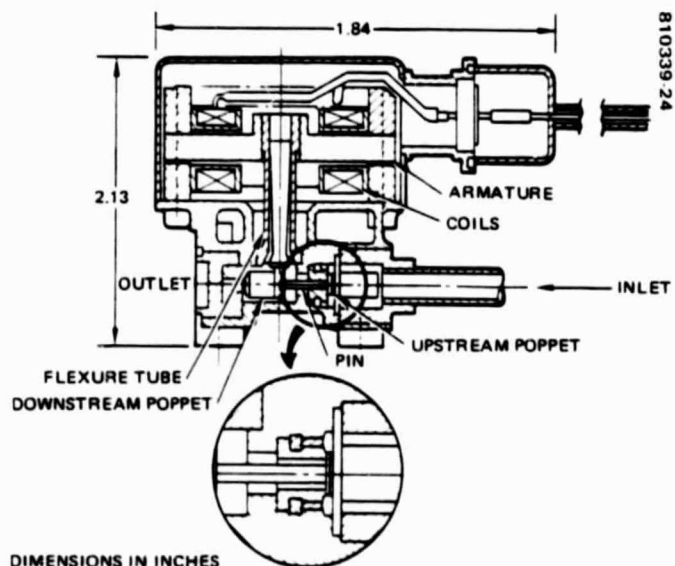


FIGURE 4-23. FLIGHT PROVEN HE-54 THRUSTER PERFORMANCE EASILY SATISFIES LEASAT REQUIREMENTS



DIMENSIONS IN INCHES

FIGURE 4-24. HIGHLY RELIABLE RCS FLOW CONTROL VALVE

There are three thrusters for each half-subsystem, one axial and two lateral. The lateral thrusters are mounted at the outer surface of the spacecraft, with their thrust vectors offset from the spin axis by 45°. These lateral thrusters operate individually for spacecraft spin rate control and in pairs for spacecraft east-west stationkeeping and station change maneuvers. The axial thrusters provide injection error corrections, attitude trim, and north-south stationkeeping. The lateral and axial thrusters perform their functions in both the pulsed and steady state modes.

The same Shuttle-imposed safety design requirements discussed for the LBS apply to the RCS. Both requirements are satisfied by the LEASAT RCS design. In addition to the Shuttle requirements, the propulsion subsystem complies with the safety requirements outlined in the Range Safety Manual, AFETRM 127-1, and in the KSC Safety Program, KMI 1710.1C.

### Performance

The specific impulse of the RCS will vary from 218 to 200 seconds for the pulsed mode over the mission lifetime, and from 228 to 220 seconds for the continuous firing mode. The mass-weighted average value of specific impulse ( $I_{sp}$ ) for all station-keeping operations is 200 seconds. During the 7 year LEASAT mission, the total number of pulses required will be well within the 53,900 pulse capability demonstrated in the qualification program. A continuous firing capability of 2000 seconds has been demonstrated in the qualification program.

The conispherical propellant tanks' initial fractional fill, for the required propellant load of 344 pounds, is approximately 83 percent. A helium pressurant mass of 0.24 pound, is required for the mission.

### Thruster Assembly

The Hughes Model HE-54 thruster, assembly, illustrated in Figure 4-23, consists of an inlet tube, an injector, a catalyst bed chamber, a catalyst bed divider, a bed support, a nozzle, and a flow control valve. With the exception of the inlet tube, catalyst, valve, and screens, all parts are fabricated from a cobalt-nickel alloy that has excellent resistance to pressure and thermal stresses as well as to the nitriding environment of the hot decomposed hydrazine.

The flow control valve qualified with this thruster is manufactured by the Hydraulic Research and Manufacturing Division of Textron, part number 480002000. The valve features redundant seats, poppets, and electrical coils that are the active elements of a direct current torque motor as shown in Figure 4-24. Tungsten carbide poppets and seats ensure high cyclic life without degradation of sealing surfaces. The seats are sealed into the stainless steel body with aluminum crush rings.

Propellant from the flow control valve is routed to the injector through a trim orifice and a single inlet tube. The propellant then is distributed equally through nine injector studs into the catalyst bed. Screens, retained over the outlet of each stud by end caps, prevent migration of the catalyst into the flow passages and control of the streams from the stud. This design feature controls the thermal environment of the injector during firing and soakback, ensuring repeatable pulse performance without the need for catalyst bed heaters.

The HE-54 thruster catalyst bed chamber is loaded with fine (20 to 30 mesh) and coarse (14 to 18 mesh) catalyst. Hughes' proprietary processing produces uniform, spherical granules, resulting in a strong catalyst bed resistant to fracture, compaction, and void formation. The two catalyst sizes are separated by a dome-shaped screen of 40 mesh platinum iridium wires.

The thruster, qualified for Intelsat IVA, SIRIO, and COMSTAR satellites, will be used in both lateral and axial positions. The thruster is qualified over the supply pressure range of 300 to 50 lb/in<sup>2</sup> and successful thruster performance has been demonstrated at temperatures from 40° to 140°F. Seven hot restart firings were interspersed at various points in the qualification test program to demonstrate the restart capabilities and effect on thruster life.

#### Propellant Tank

The propellant tank's conispherical shape permits 100 percent propellant utilization in orbit and complete draining during ground checkout and test. The tank is manufactured from two 6Al-4V titanium alloy forgings machined to form hemispherical and conical segments. The two halves are welded to form the complete tank. The tank volume is 2860 in<sup>3</sup>, and the tank is designed for a maximum operating pressure of 350 lb/in<sup>2</sup> with a 2 to 1 safety factor, consistent with MIL-STD-1522 and compliant with the STS requirements.

#### Filter

The RCS filter used on all Hughes hydrazine subsystems incorporates stacked, etched titanium disks positioned so that the etched passages lie one above the other. Each disk is chem-milled on one face to provide radial flow paths of controlled size. The filter has a capacity for particulates that are contained in 3175 kg of hydrazine.

#### Latching Valve

The latching valve, manufactured by Hydraulic Research Corporation and Manufacturing Division of Textron, Valencia, California, is qualified and flight-proven on Intelsat IVA and COMSTAR. The valve is supplied with a high back pressure relief for the propulsion subsystem interconnect function and with a low back pressure relief for the tank/thruster isolation functions.

### Fill and Drain Valve

The fill and drain valve is a Hughes design that is manually operated and acts directly with the primary seal formed between a tungsten carbide ball and a 6Al-4V titanium seat machined into the valve body. The ball, retained in a stem assembly, is moved on and off the seat without rotation when the locking nut is rotated on the valve body. An O-ring provides a seal against external leakage around the valve stem. The inlet port cover cap also serves as a redundant seal. An aluminum closure cap, using a K-seal at its base, is an additional redundant sealing provision.

### Miscellaneous Components

The pressure and temperature sensors monitor subsystem status. The pressure transducer is a potentiometer device. It produces an analog output 0 to 5 volts dc over a range of 0 to 400 psia (with a 2 percent accuracy). Temperature sensors on each thruster valve cover provide positive indication of thruster firing.

The heaters are similar to those used on Intelsat IVA and COMSTAR with resistance values selected to maintain the subsystem temperatures within acceptable limits. Redundant propellant line heaters and redundant-element molded heaters on all valves, pressure transducers, and filters preclude propellant freezing. The heaters are wired through fuses to the spacecraft buses.

### Conclusion

In addition to benefitting from the use of proven technology and flight-proven components, the LEASAT RCS will realize the advantage of utilizing proven manufacturing, and assembly, techniques. The RCS is a proven hydrazine monopropellant design that takes advantage of the spacecraft's centrifugal force to provide gas-free propellant at each tank outlet, thereby eliminating the need for a mechanical expulsion device. It is identical to the one that has performed flawlessly on orbit on the Intelsat IVA and COMSTAR programs. High subsystem reliability is further ensured by complete hardware redundancy.

#### 4.1.3.5 Thermal Subsystem

A simple, heater-augmented, passive thermal control design is chosen for LEASAT because of its inherent high reliability and low risk. Thermal balance is maintained for the spacecraft internal components by using the spin-averaged solar input to the drum as the dominant stable temperature sink.

The spacecraft forward closure is used as a radiator and as a shield to isolate the spacecraft interior from solstice solar thermal loads. The forward end closure consists of an outboard spun section and an inboard

despun section. The spun element is the primary radiator of heat dissipated on the equipment shelf. The primary function of the despun sun shield is to prevent large temperature swings on the BAPTA. To accomplish this, the despun sun shield is lined with a superinsulation blanket which acts as a near adiabatic boundary. An internal light baffle attached to the despun sun shield keeps solar energy from entering the gap between the spun and despun elements.

The aft end thermal closure prevents spacecraft overheating due to rocket motor exhaust plume convective and radiation heating, and it limits spacecraft interior temperature swings in transfer and synchronous orbits due to seasonally varying solar illumination of the spacecraft aft end. The barriers consist of a single shield constructed of titanium, painted on the outside with a high temperature black paint. The inside, coated with gold, provides radiation decoupling between barrier and spacecraft.

Insulating blankets consisting of ten layers of aluminized Mylar are used to preclude large temperature swings of the RCS tanks during eclipses. Insulation in the SPS cavity provides a near adiabatic aft end boundary. A thermal baffle on the aft side of the despun shelf is employed to direct the heat to the BAPTA.

Heaters are employed for components that have narrow operational temperature ranges. These components include the reaction control subsystem, the BAPTA, and batteries. The heaters are a standard, proven design used on the Intelsat IV, MARISAT, and Telesat Hughes programs. Heaters are installed on the batteries because Hughes has self-imposed constraints on the battery temperature to insure their life for 7 years. The batteries are conductively decoupled from the interior of the spacecraft and their internally generated heat is rejected to the side radiators especially tailored for this purpose. Heaters are used during battery charging operations since there is no internal heat being generated within the battery. This thermal control approach allows the batteries to operate within a narrow temperature range of 41°F and 68°F during eclipse season and 32°F to 68°F during solstices. The mission average temperature is designed to be below 60°F to promote long battery lifetime.

Hughes has used the design successfully for 15 years on 35 spacecraft (seven commercial and two military programs). The subsystem design gives special consideration to minimizing electrostatic charging and intermodulation effects and providing long battery life.

This thermal subsystem achieves simple thermal control through use of materials flight-proven on Hughes spacecraft. This section describes how thermal balance for the spacecraft internal components is achieved by using spin-averaged solar input to the spacecraft spinning section as the dominant stable temperature sink and the forward (north facing) thermal barrier as the principal radiator. In addition, it discusses how heater augmented thermal control maintains the batteries in a narrow temperature range, thus



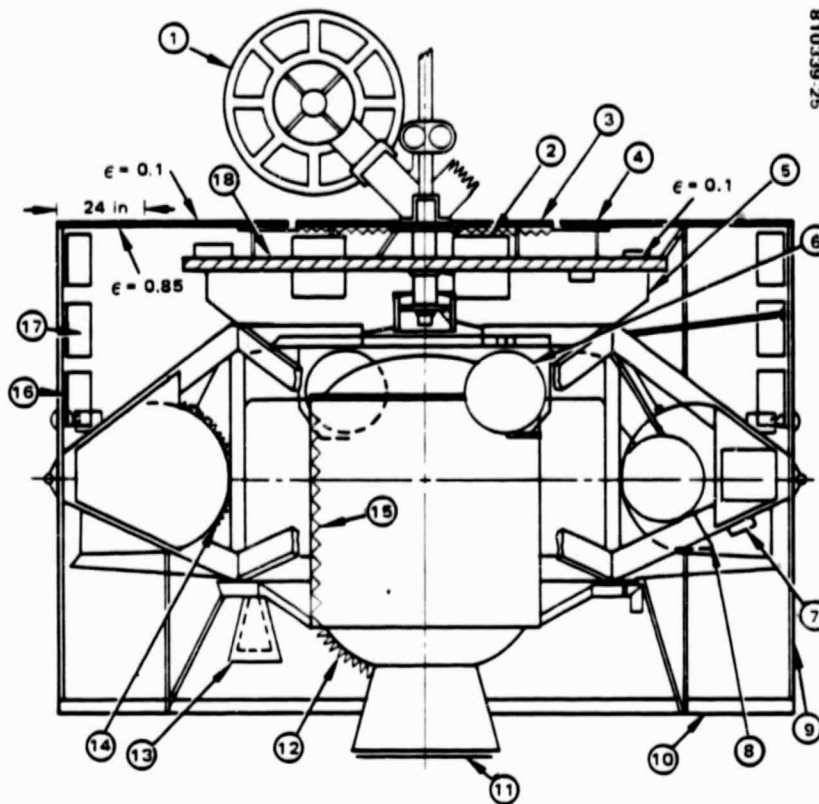
assuring their long life. The performance summary highlights control of spacecraft temperatures within acceptable limits during various mission phases. Discussion of thermal control aspects of STS integration shows that Hughes' approach achieves effective LEASAT thermal control in the severe STS thermal environment.

LEASAT thermal control elements are shown in Figure 4-25. Their functions are identical to similar elements used on other Hughes dual-spin commercial and military spacecraft. Thermal balance is maintained for the spacecraft internal components by using spin-averaged solar input to the spinning section as the dominant stable temperature sink. The spacecraft forward (north facing) thermal barrier is used as a radiator and shield to isolate the spacecraft interior from solstice thermal loads.

The forward end barrier consists of an outboard spun section and inboard despun section. The spun element is the primary radiator of heat dissipated on the equipment shelf. It is a 59.0 inch inner diameter, 166.0 inch outer diameter, and 0.38 inch thickness annular disk that attaches to the forward edge of the solar panel. The structure is an aluminum-faced aluminum honeycomb composite. A 2 mil sheet of teflon is heat bonded to the aluminum outer facesheet prior to assembly of the composite structure. The inward facing surface has a portion painted black ( $\epsilon = 0.85$ ) and a portion of bare aluminum ( $\epsilon = 0.1$ ). These areas are sized to absorb and re-emit approximately 70 percent of the total generated heat on the shelf. The surface is 44 percent black and 56 percent bare aluminum.

The despun forward thermal barrier is supported by the center hub of the despun shelf and by standoffs from the shelf. The barrier is a 0.25 inch thick annular ring, 58.0 inches in diameter, with a 10.0 inch diameter hole in the center. A 12.0 inch wide annular brim, 0.12 inch thick, is added to the aft side of the barrier. The brim is constructed of fiberglass facesheets and aluminum honeycomb core, with a perforated aluminum mesh bonded to the forward surface to form an RF choke between the spinning and despun thermal barriers.

Even though RFI effects are also minimized by locating the antennas away from the forward barrier, the thermal subsystem has been designed to provide additional protection. The outward surface of the forward barrier consists of 2 mil teflon heat bonded on aluminum foil. The composite of teflon and aluminum foil provides necessary RF properties and low solar absorptance ( $\alpha = 0.17$  at the BOL and 0.28 at the EOL) with high surface emittance ( $\epsilon = 0.7$ ) for heat rejection. This composite was developed on two current Hughes programs, SBS and Anik C. Electrostatic discharge effect is minimized by cutting the teflon into separate 2.5 ft<sup>2</sup> patches. Small areas prevent large charge buildup on nonmetallic surfaces. All metallic surfaces are grounded.



- 1) ANTENNA - BARE FIBERGLASS, MARISAT TYPE
- 2) BLANKET - 5 LAYER BLANKET
- 3) SUNSHIELD (DESPUN) - BLACK INSIDE, 2 mil TEFLON OUTSIDE
- 4) SUNSHIELD (SPUN) - 2 mil TEFLON ON 4 mil ALUMINUM, 2 1/2 ft<sup>2</sup> PATCHES ON ALUMINUM HONEYCOMB 44% BLACK, 56% BARE ALUMINUM INSIDE,  $\alpha = 0.17$  BOL,  $\alpha = 0.28$  EOL,  $\epsilon = 0.7$  OUTSIDE
- 5) BAPTA BAFFLE - POLISHED ALUMINUM  $\epsilon = 0.1$
- 6) RCS TANKS - 10 LAYER BLANKET, 3 W HEATER
- 7) SPUN UNITS - BLACK OR LOW  $\epsilon$  AS REQUIRED
- 8) PROPULSION LINES - ALUMINUM KAPTON WRAP, HEATERS 0.2 W/ft
- 9) SOLAR PANEL - K-6% CELLS,  $\epsilon = 0.83$ ,  $\alpha = 0.72$  OPERATING,  $\alpha = 0.79$  OPEN, BARE KEVLAR INSIDE,  $\epsilon = 0.8$
- 10) AFT BARRIER - TITANIUM, GOLD INSIDE, BLACK HI-TEMPERATURE SPEREX PAINT OUTSIDE
- 11) NOZZLE COVER - BARE ALUMINUM
- 12) SPS - 5 LAYER BLANKET, 50 W HEATER
- 13) LBS SHIELD - 10 mil STAINLESS SHIELD, HIGH TEMPERATURE BLACK PAINT, 10 W HEATER
- 14) LBS TANK BLANKET - 5 LAYERS
- 15) SPS CAVITY - 10 LAYER BLANKET
- 16) RADIATOR FOR BATTERIES - ALUMINUMIZED 5 mil TEFLON OUT, SIDE,  $\alpha = 0.17$  0.28,  $\epsilon = 0.78$ , BARE ALUMINUM INSIDE,  $\epsilon = 0.1$
- 17) BATTERIES - BARE/BLACK COMBINATION, 30 W HEATER PER BATTERY
- 18) SHELF - BLACK, LOW  $\epsilon$  OUTBOARD AFT SIDE

FIGURE 4-25. THERMAL CONTROL ELEMENTS

The primary function of the despun sun shield is to prevent large temperature swings on the BAPTA. To accomplish this, the despun sun shield is lined with a super-insulation blanket which acts as a near adiabatic boundary. An internal light baffle attached to the despun sun shield keeps solar energy from entering the gap between the spun and despun elements.

The aft thermal barrier is fabricated from 0.002 inch thick titanium sheets reinforced with welded stiffeners, and is attached to the aft end of the solar panel and aft frame on the structure. Cutouts are provided for the thrusters. The barrier serves the following control functions: 1) prevents spacecraft overheating during SPS firing, 2) provides local protection from LBS thruster exhaust plume convective heating, and 3) limits spacecraft interior temperature swings in transfer and synchronous orbits due to seasonally varying solar illumination of the spacecraft aft end. The barrier consists of a single shield constructed of titanium, painted on the outside with a high temperature black paint. The inside, coated with gold, provides radiation decoupling between the barrier and spacecraft. Insulating blankets consisting of 10 layers of aluminized Mylar are used to prevent large temperature swings of the RCS tanks during eclipses. Insulation in the SPS motor cavity provides a near adiabatic aft end boundary. A thermal baffle on the aft side of the despun shelf is employed to direct the heat to the BAPTA.

Heaters are employed for components that have narrow operational temperature ranges. These components include the RCS, BAPTA, and batteries. The heater is a standard, proven design used on Hughes' Intelsat IV, MARISAT, and, TELESAT programs. Heaters are installed on the batteries because Hughes has self-imposed battery temperature constraints to ensure 7 year life. The batteries are conductively decoupled from the spacecraft interior, and their internally generated heat is rejected to side radiators especially designed for this purpose. Heaters are used during battery charging operations since no internal heat is generated within the battery during this time. This thermal control approach allows the batteries to operate within a narrow temperature range of 41° and 59°F during eclipse season, with brief temperature excursions to 68°F during discharge and overcharge modes. The heaters are not used during solstices when the batteries are in trickle charge. Battery temperatures are between 32° and 59°F during solstices. A similar design approach is employed on all current Hughes programs.

Key features implemented in unit thermal designs are: 1) separation of battery packs from the despun shelf, 2) conduction isolation and thermal finish on the receivers and low power dissipators, and 3) a radiation baffle that reflects heat from the high power dissipators on the outer perimeter of the shelf to the BAPTA in the center of the shelf.

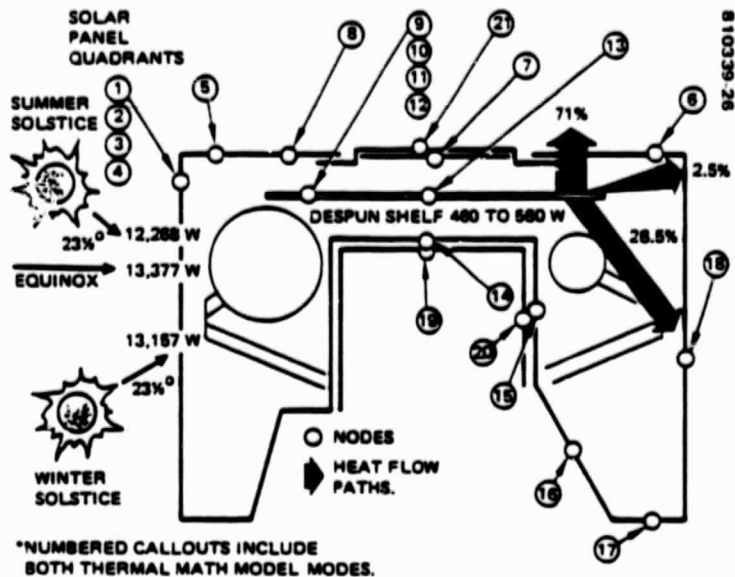


FIGURE 4-26. BULK THERMAL MATHEMATICAL MODEL

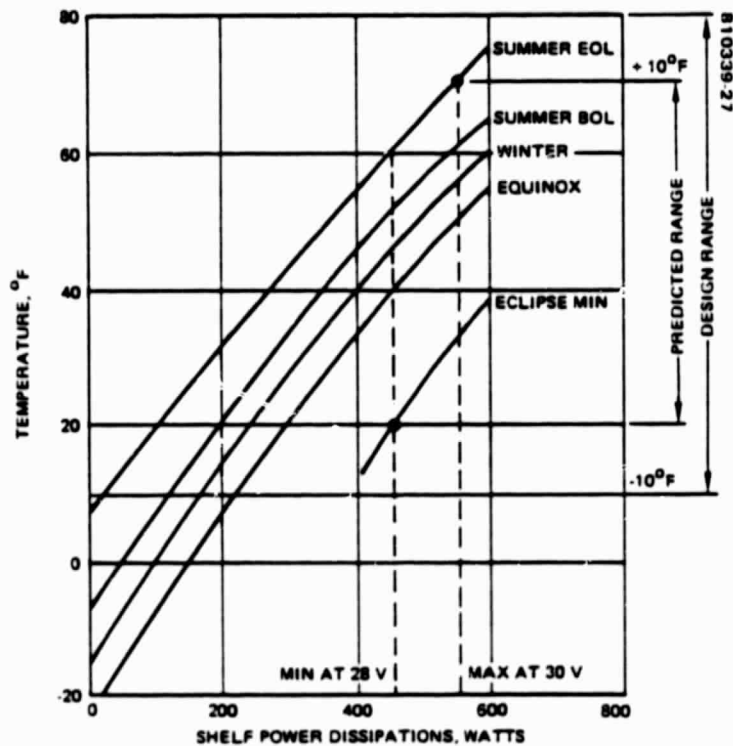


FIGURE 4-27. REASONABLE DESIGN RANGE ACHIEVED FOR ALL SEASONS WITH LEASAT PASSIVE DESIGN

Hughes' selected approach for maintaining the required thermal balance during the transfer orbit phase is to turn on the UHF equipment. This approach has the advantage of allowing the heat to be generated in the units where it is most effective in maintaining their temperatures.

#### 4.1.3.5.1 Performance Summary

Principal heat flow paths from the shelf are shown in Figure 4-26. To determine the flow and overall spacecraft thermal performance, a bulk thermal mathematical model was generated whose nodal subdivisions are also shown in Figure 4-26. The despun shelf nominal thermal performance for synchronous orbit environments at the BOL with maximum voltage of 30 volts and at EOL with minimum voltage of 28 volts is shown in Figure 4-27. The special condition of two failed 25 kHz channels and three failed 5 kHz channels, imposed for establishing lower temperature design limits, corresponds to the "failed satellite" criteria defined in the RFP. Predicted bulk shelf temperature range is between 20° and 71°F. Design range is 10°F above and 10°F below maximum and minimum predicted temperatures. Qualification range is 20°F above and below, respectively.

Bulk structure temperature distribution is shown in Table 4-20 for synchronous orbit environments at BOL and EOL. Transfer orbit temperatures are less critical because SPS firing is initiated at local midnight, thus ensuring eclipses of less than 30 minutes. These bulk temperatures provide boundary conditions for detailed analytical models used to perform unit temperature evaluation. Nominal predicted temperatures for the units are summarized in Table 4-21. Acceptance temperatures are compatible with temperatures used to ensure long life for MARISAT and SDS spacecraft.

#### 4.1.3.5.2 STS Thermal Integration

The most severe sunloading conditions for a deployment attitude are shown in Figure 4-28. The spacecraft can experience solar loading through the gaps between the orbiter bay and spacecraft. Reflections from the radiator are also a thermal consideration. The temperatures of the solar panel would exceed 210°F within 1 hour if it were exposed to the worst solar loading condition without a protective blanket.

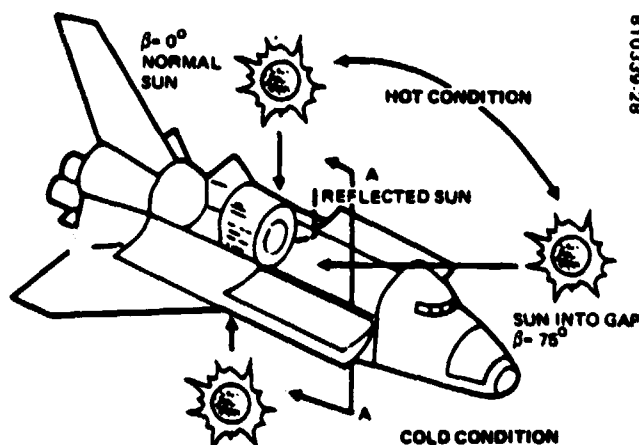
The worst cold design condition is for the cargo bay to be in shadow for 3 hours, after which the STS rotates for 10 hours at five revolutions per hour. This condition is equivalent to a continuous eclipse with a nonoperating spacecraft. Without thermal control provisions the bulk shelf temperature could fall below the minimum design temperature of 20°F within 45 minutes, and RCS lines could reach their 40°F limit within 2 hours.

Hughes' approach to STS thermal integration is to provide an ejectable blanket on the solar panels and axial end plane gap closures. A 1000 watt heater is installed on the solar panels, with power provided through an

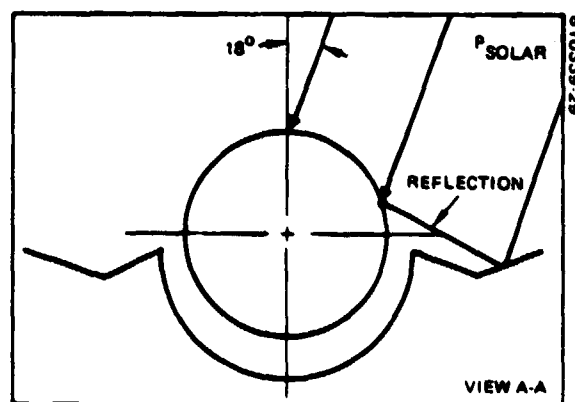
TABLE 4-20. LEASAT BULK SPACECRAFT TEMPERATURE PREDICTIONS USED TO EVALUATE UNIT TEMPERATURES

Node	Location	Winter BOL 30 V	Temperature °F						Five Channel Failed Eclipse 28 V	Transfer Orbit *	
			Summer		Equinox						
			BOL 30 V	EOL 30 V	BOL 30 V	Eclipse Minimum	Minimum	Maximum			
1	Solar panel (forward)	46	38	40	44	-138	-142	-114	66		
2	Solar panel (forward)	46	38	40	44	-138	-142	-114	66		
3	Solar panel (forward)	46	38	40	44	-138	-142	-114	66		
4	Solar panel (forward)	46	38	40	44	-138	-142	-114	66		
5	Sunshield (bare)	-156	-46	-3	-159	-210	-212	-186	40		
6	Sunshield (bare)	-156	-46	-3	-159	-210	-212	-186	40		
7	Despun blanket	23	38	52	18	0	-13	-6	30		
8	Radiator (black)	-39	-7	16	-44	-88	-98	-86	40		
9	Shelf (outboard)	57	61	71	50	33	20	20	50		
10	Shelf (outboard)	57	61	71	50	33	20	20	50		
11	Shelf (outboard)	57	61	71	50	33	20	20	50		
12	Shelf (outboard)	57	61	71	50	33	20	20	50		
13	Shelf (inboard)	46	55	66	41	34	18	20	50		
14	Truss (forward)	47	54	64	42	32	17	25	40		
15	Truss (sides)	53	38	41	44	-2	-4	23	64		
16	Aft barrier	158	-122	-121	-117	-217	-219	-188	60		
17	Aft barrier	-16	-172	-170	-168	-244	-245	-224	50		
18	Solar panel (aft)	51	36	38	46	-138	-140	-112	72		
19	Insulation (aft)	-169	-165	-159	-172	-177	-185	-180	-169		
20	Insulation (aft)	-130	-139	-137	-135	-164	-165	-144	-120		
21	Despun sunshield	-249	-48	4	-251	-256	-262	-257	-48		

\*Minimum shelf power = 340 watts.



a) SUN POSITION DURING HOT AND COLD CONDITIONS



b) SOLAR REFLECTIONS AT 18° TILT

FIGURE 4-28. STS ENVIRONMENT USED TO DETERMINE THERMAL CONTROL REQUIREMENTS

TABLE 4-21. LEASAT COMPUTER PREDICTED UNIT  
TEMPERATURES TO ALLOW REASONABLE UNIT  
DESIGN TEMPERATURES ON ORBIT

Unit	Temperature Range °F	
	Predicted	Design
53 W UHF amp	30 to 85	20 to 95
37 W UHF amp	30 to 80	20 to 95
Multiplexer	25 to 80	15 to 90
UHF receiver	40 to 88	30 to 100
FLTBCST input assembly	20 to 80	10 to 90
Preamp and down converter	30 to 85	20 to 95
Dual bypass	20 to 80	10 to 90
FLBCST processor	25 to 85	15 to 95
X band transmitter	20 to 80	10 to 90
5 kHz receiver	15 to 80	5 to 90
Power amp	40 to 110	30 to 120
Dual converter	15 to 80	5 to 90
Earth sensor	30 to 95	15 to 110
Sun sensor	30 to 70	-45 to 80
BAPTA	40 to 70	30 to 80
Attitude control electronics	-5 to 80	-15 to 100
Batteries (trickle charge)	38 to 58	32 to 68
Discharge regulator	50 to 100	-20 to 140
Bus limiter	-10 to 100	-20 to 170
RCS	50 to 113	40 to 140
LBS	50 to 130	40 to 140
SPS	40 to 80	50 to 90

umbilical connector by the orbiter. The combination of the blankets and heater allows the spacecraft to survive an even more severe environment than NASA's current design condition (Lunney memo PA/GSL-13-78, dated 8 May 1978). Calculated temperature of propellant tanks will be below 100°F even during STS abort descent and landing.

#### 4.1.3.5.3 Conclusion

The heater-augmented passive thermal design selected for LEASAT (a reliable, proven approach in many Hughes spacecraft) contributes to assurance of continuous, satisfactory communication performance.

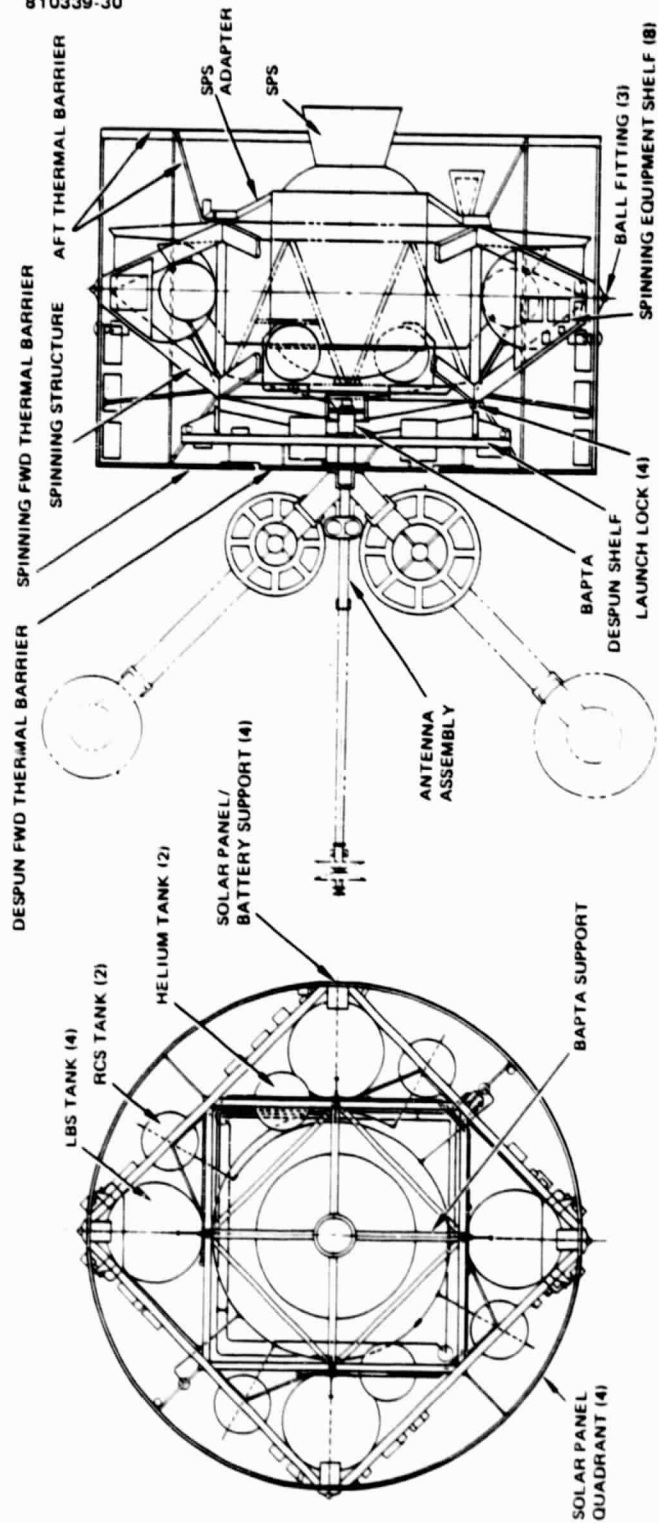


FIGURE 4-29. LEASAT STRUCTURAL ARRANGEMENT



#### 4.1.3.6 Structure

##### 4.1.3.6.1 Introduction

The proposed LEASAT spacecraft structure is sized to accommodate the Stage III Minuteman solid rocket motor, all LEASAT equipment, and propellant supplies. It is designed to support spacecraft equipment internally, thereby minimizing STS payload bay space and launch cost.

The structure subsystem description presented in this section begins with an overview of the arrangement which emphasizes the structural load paths, spacecraft interface to the STS cradle, and the launch lock interface between the spacecraft spinning and despun sections. A discussion of the basic bus structure, the payload support structure, the solid propellant subsystem (SPS) adapter, the solar cell array substrate, and the thermal barriers follows. The next subsection summarizes the trade studies which led to the selection of the graphite fiber reinforced plastic (GFRP) structure, the three-point spacecraft attachment, the structural truss optimization, and the launch lock concept. The structural design criteria and analysis are also presented.

##### 4.1.3.6.2 Description

###### Structural Arrangement

The LEASAT structure subsystem is composed of two major assemblies, the spinning and despun sections. The structural arrangement is shown in Figure 4-29. The spinning structure section supports the majority of the spacecraft associated systems except the communications system and a small portion of the telemetry and command system. The despun structural section supporting the communications payload and TT&C system consists of the despun platform, the antenna support, and despun thermal barrier. The despun platform structural design is similar to the design used on past Hughes programs such as Intelsat IVA, Intelsat IV, and several military programs.

Spinning Structure. The primary (spinning) structure is a square truss that carries spacecraft loads to the five-point cradle supports. The spacecraft is supported in its cradle at five points which lie in a plane passing through the spacecraft center of mass. This support concept avoids a cantilevered spacecraft payload and thereby minimizes the amplification of mass acceleration in response to dynamic Shuttle excitations.

The cradle supports the spacecraft in the Shuttle bay and provides the structural stiffness and mechanical interfaces required. It is attached to the Shuttle at five points, as shown in Figure 4-30, on opposite longerons and at the keel. The five points are capable of taking shear in two directions and provide a statically determinant interface with the Shuttle and thus eliminate the possibility of loads being induced in the spacecraft due to Shuttle distortion.

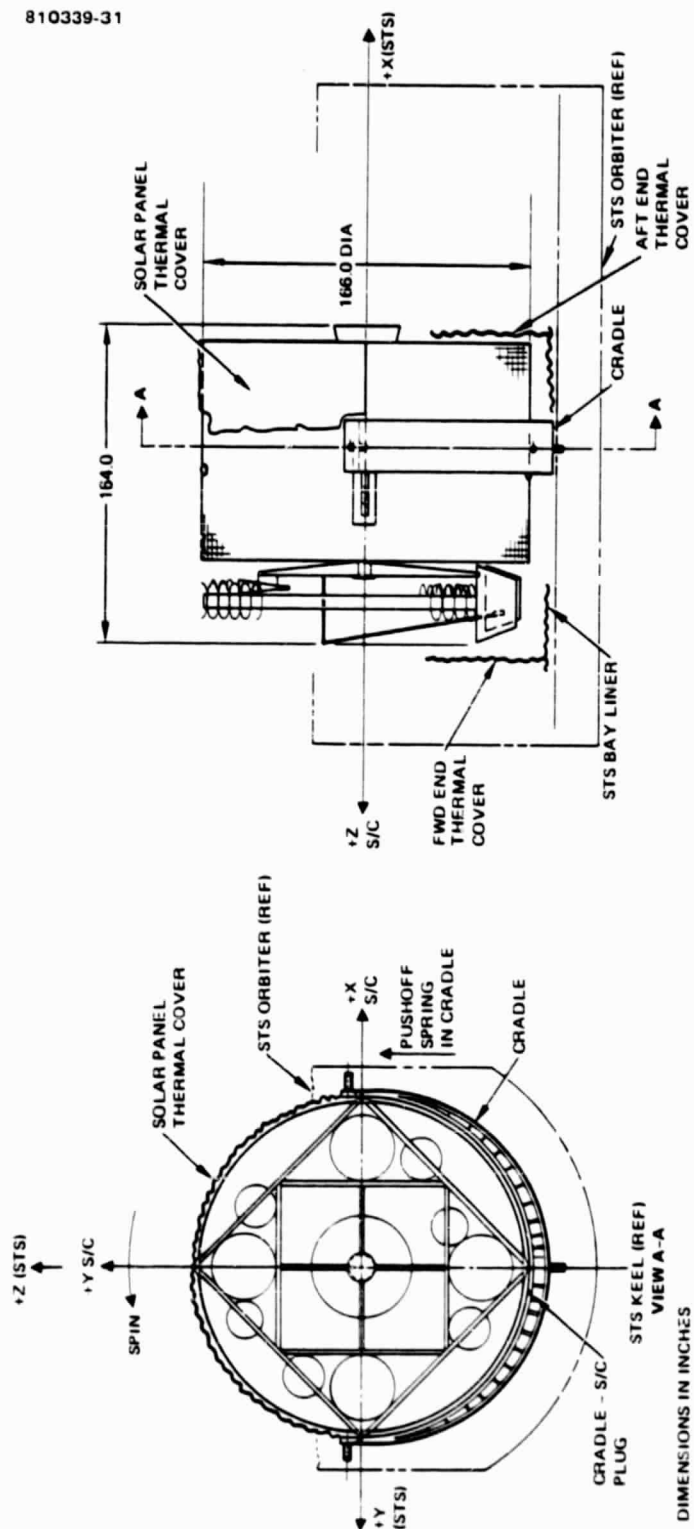


FIGURE 4-30. SPACECRAFT CRADLE ASSEMBLY

Four launch lock mechanisms are located at the midspan of the truss, where they provide normal and shear load transfer from the equipment platform to the truss structure. A redundant load path exists through the bearing assembly, which carries only a minor portion of the flight loads. Once in orbit, the equipment platform is unlocked by activating four pyrotechnic pin pullers, thereby allowing the shelf to be despun.

The truss is a graphite fiber reinforced plastic, aluminum honeycomb composite structure. Truss members are joined by aluminum machined fittings that are fastened together with bolts. Subsystem components located in the spinning section are mounted to eight vertical panels attached to the sides of the quadrapod structure. The panels consist of aluminum facesheets and aluminum honeycomb core. Threaded inserts are bonded in the assembly to provide for component mounting. The panels are thermally isolated from the primary structure by the use of attachment fittings that provide for thermal expansion compensation to eliminate distortions in the main frame.

The structural support for the BAPTA is provided by four beams which tie to the midpoints of the forward truss members and a centrally located BAPTA mounting hub. These beams are also constructed of GFRP facesheets and aluminum honeycomb core.

The liquid bipropellant subsystem (LBS) tanks are nested in the quadrapod of the truss structure and supported by the aft members of the quadrapod through monoball-pillow block devices at two points on the tank equator. A third mounting point on the tank equator is supported from the aft member of the truss by a bipod assembly which allows for free expansion of the tank under pressure.

Each reaction control subsystem (RCS) tank is attached to the lower truss member by a machined aluminum fitting at its aft mounting point; the opposite mounting point of the tank is supported by a bipod strut assembly from the forward truss member. The use of the bipod as a flexure device allows for free expansion of the RCS tanks during pressurization.

Helium tanks are supported by a fixed machined fitting attached to the forward truss member and by a slide mechanism, on the opposite side of the tank, which is attached to the aft truss member. The slide mechanism allows for growth of the tank along its axis while providing lateral restraint of the tank. The solid propellant subsystem (SPS) adapter structure provides the structural transition from the primary truss structure to the SPS and houses the jettison mechanism for the SPS and adapter assembly. The structure is stiffened by a rectangular torque box ring at the interface to the spacecraft structure. The torque ring interfaces with the spacecraft structure through eight separation mechanisms and four jettison assemblies. The release of the adapter is provided by eight squib-actuated separation nuts on the spacecraft primary truss and by bolt catchers on the adapter. Spring-operated

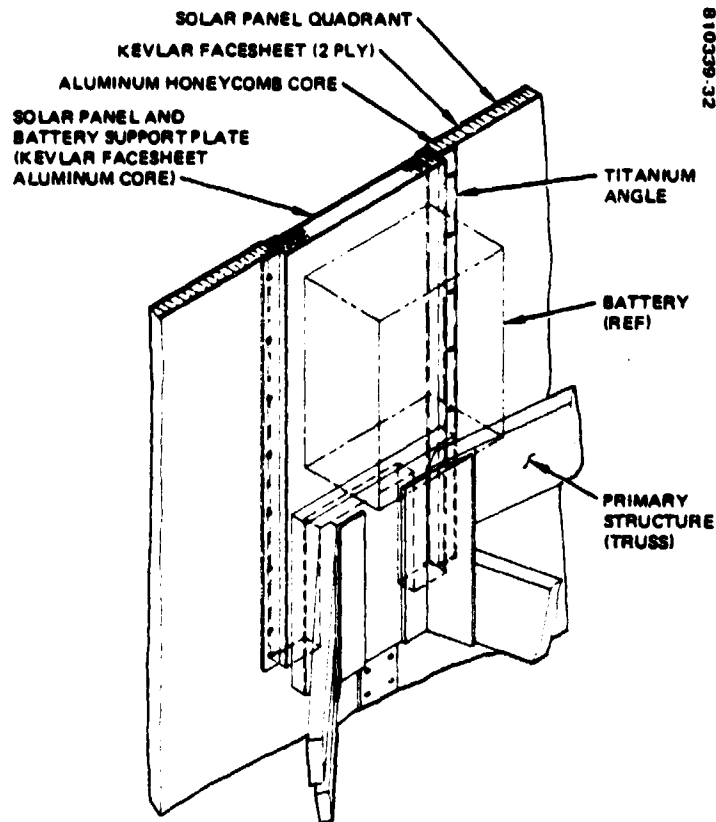


FIGURE 4-31. SOLAR PANEL AND BATTERY SUPPORT

pistons on the SPS adapter approximately 90 degrees apart provide equal jettison forces for the assembly. Prior to SPS jettison, the explosive transfer assemblies for the motor are severed by cable cutters.

Extending forward from the ball fittings to the forward thermal barrier are kevlar and aluminum honey comb core panels, illustrated in Figure 4-31, that provide the mounting base for the batteries. Titanium angles along the longitudinal edges facilitate the installation of solar panel quadrants and isolate the structure thermally from the solar panel. The solar panels are supported with additional struts from the corners of the truss to the midspan of each panel.

#### 4.1.3.6.3 Despun Structure

The despun structure consists of a central hub which interfaces with the despun hub of the BAPTA, eight radial ribs whose ends are connected by eight intercostals, and the circular equipment shelf. The hub, ribs and the intercostals are made of aluminum. A 110.0 inch diameter aluminum faced honeycomb shelf, 2.5 inches thick and stiffened by the rib/hub assembly, is provided for mounting the subsystem components. Four launch lock fittings supported by bipods attached to the shelf intercostals transfer the loads from the despun assembly to the primary spinning structure during launch.

The antenna support structure mounts the communications subsystem UHF helical antennas and the TT&C subsystem biconical horns. Each of the two UHF helical antennas is supported by a two-bar deployment linkage to stow the antennas during launch and transfer orbit and to deploy the antenna to its operating position. The X-band horn antennas are supported by a cantilevered beam that is mounted to the despun side of the BAPTA. The TT&C antenna is stowed during launch and deployed during the transfer orbit.

### Truss Versus Central Thrust Tube

The spacecraft internal structure uses four quadrapod assemblies connected to a central box structure. The alternative approach for primary structure is a conventional semi-monocoque conical shell supported by the quadrapods in a manner similar to that of the baseline design. The shell design requires a more complex set of support fittings for tanks. The truss design permits the quadrapods to be opened sufficiently to enclose the large LBS tanks and to allow them to be mounted directly to primary structure. The small RCS and helium tanks are also conveniently mounted directly to frame members.

### Truss Structure Construction

Aluminum and graphite were evaluated for constructing the truss structure. Graphite has the advantage of substantially higher stiffness and strength-to-weight ratio than aluminum. The aluminum structure considered consists of rectangular extruded tubes; the graphite beam design is an aluminum honeycomb with graphite facesheets. Both approaches utilize machined aluminum fittings to tie the members with bolts.

An analysis made to compare the weights of high strength aluminum and graphite for the required frame structure indicates that the graphite design is approximately 170 pounds lighter than the aluminum design.

Launch Locks Versus Marmon Clamp. The four launch lock configuration was chosen in preference to a clamped BAPTA. The launch locks provide a more direct and efficient load path for transferring the large shear and axial flight loads from the 600 pound despun shelf to the primary truss structure. Hence, they result in a lighter structure configuration.

## 4.1.3.6.4 Structural Design Performance

### Requirements

The LEASAT structure is designed to survive and support, without adverse distortion, all subsystems under all expected environments over the design life of the spacecraft. The spacecraft and cradle ultimate design load factors, shown in Table 4-22, are based on data published in Shuttle Orbiter/Cargo Interfaces, ICD 2-19001, Johnson Space Center, Revision 16, November 1977. The three conditions shown in the table encompass the load factors of all other flight events.

The liftoff and landing cases are events that result in significant elastic response of the spacecraft. Since the accelerations presented in ICD 2-19001 are inputs to the cradle at the STS interface, appropriate amplification and uncertainty factors have been applied to the dynamic loads, as noted in Table 4-22. The liftoff load factors are derived directly from ICD 2-19001 and include a 1.25 amplification factor plus a 1.25 uncertainty factor on the dynamic portion. The landing load factors have been modified to reflect a 6.0 ft/sec sink speed based on recent discussions with NASA/JSC and a review of coupled loads analyses recently performed for similar payloads in the STS cargo bay. The emergency landing loads are taken directly from ICD 2-19001. All load factors include an ultimate-to-limit factor of 1.5.

TABLE 4-22. ULTIMATE DESIGN LOAD FACTORS, g'S

Flight Event	N <sub>Lateral</sub>	N <sub>Vertical</sub>	N <sub>Longitudinal</sub>
Liftoff*	±2.3	±5.9	+1 -6.1
Landing (6 ft/sec)**	±1.7	+2.5 -5.5	±2.5
Emergency landing***	±1.5	+2 -4.5	+4.5 -1.5

\*Includes 1.25 amplification factor, 1.25 uncertainty factor on dynamic portion, and overall ultimate-to-limit factor of 1.5.

\*\*Includes 1.10 uncertainty factor on dynamic portion plus an overall ultimate-to-limit factor.

\*\*\*Load factors operate separately. The longitudinal factors are effective within a cone of 20° half-angle.

TABLE 4-23. STRUCTURAL DESIGN CRITERIA

<b>Stiffness</b>	
•	Deflection limited to avoid contact between spacecraft elements
•	3 Hz spacecraft minimum to avoid in-orbit coupling with control system
•	8 Hz spacecraft minimum frequency to limit spacecraft deflections and dynamic amplification during launch
•	30 Hz minimum equipment shelf frequency to decouple from STS landing resonances
<b>Strength</b>	
•	1.5 ultimate/limit load factor
•	No yield at ultimate load
•	Pressure vessels:
	Ultimate safety factor = 4:1 burst test only
	Ultimate safety factor = 2:1 fracture mechanics plus burst test or waiver by previous flight experience
•	Pressurized lines ultimate SF > 4

The structure is designed to meet both stiffness and strength requirements, as summarized in Table 4-23. Structural stiffness is sufficient to prevent deflections that produce contact between elements of the spacecraft or exceed the STS bay space envelope. In the launch configuration, the minimum spacecraft/cradle frequency will exceed 8 Hz to prevent large load amplifications due to coupling with Shuttle modes. The equipment shelf is designed to maintain a minimum bending frequency of 30 Hz to decouple from fundamental modes observed during STS landing. To avoid control system interactions, a minimum space vehicle frequency of 3 Hz is chosen for the on-orbit satellite configuration.

The structural analysis considers: 1) structural misalignment and dimensional tolerances, 2) structural fatigue due to mechanical and thermal loading, 3) creep deformation, 4) combined mechanical and thermal environments, 5) thermal distortion, 6) stress corrosion, and 7) control/structure coupling. The structural design is such that there is a positive margin of safety between the ultimate applied load and the allowable member yield load. The ultimate design load is obtained by multiplying the maximum expected flight (limit) load by the safety factors.

Material strengths and other physical properties employed in the structural analysis are selected from authorized reference sources MIL-HDBK-5C and 17 and from the Hughes test data bank when appropriate. For single load path structures the minimum guaranteed values ("A" values in MIL-HDBK-5C) are used as allowables; for structures with redundant load paths, 2 $\sigma$  probability values ("B" values in MIL-HDBK-5C) are used.

#### Structure Analysis

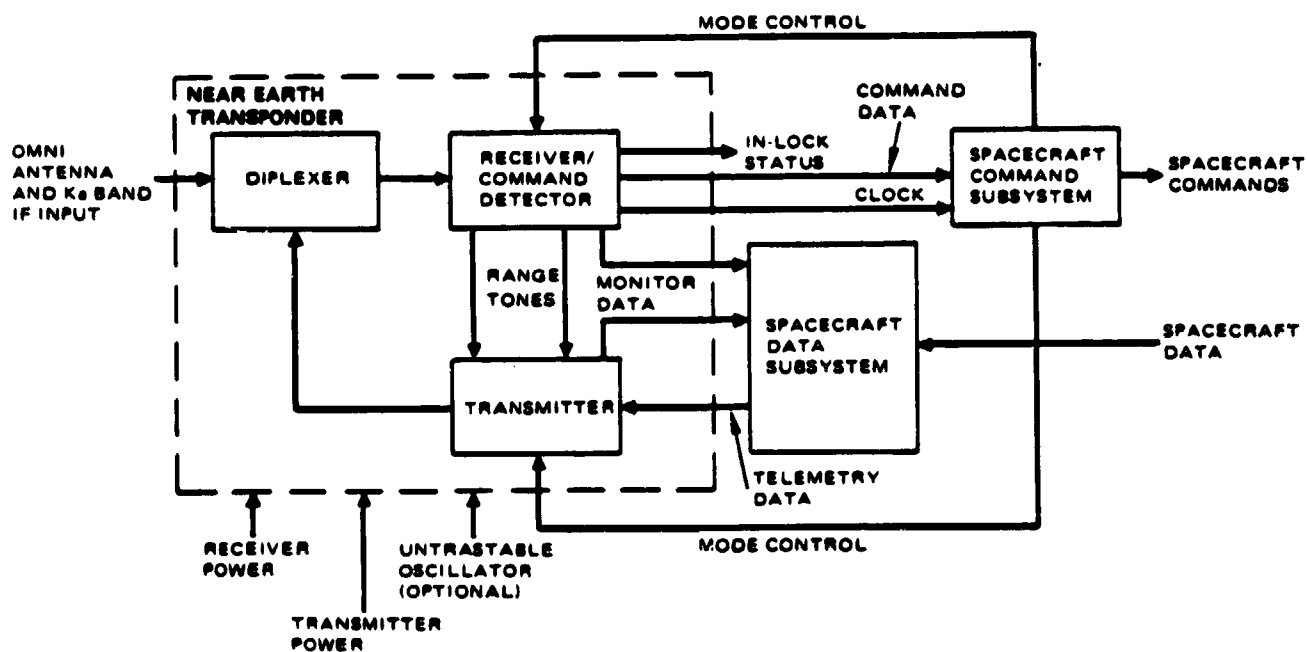
A preliminary structural analysis has been performed to ensure that strength and stiffness requirements have been met and to permit accurate sizing of the primary structural elements. A finite element math model was generated to define internal member loads and evaluate spacecraft resonant frequencies. The math model consists of two segments representing the spinning and despun portions of the spacecraft.

A new math model of the LEASAT despun section was generated to compute internal member loads and spacecraft frequencies for both the stowed and deployed antenna configurations.

#### 4.1.3.6.5 Conclusion

The LEASAT spacecraft is an STS optimized bus to provide a structure that has the flexibility for growth with a minimal amount of new development work. Materials such as graphite and kevlar provide a highly efficient structure which results in maximum payload weight capabilities. Large margins of safety for stress and dynamics requirements, in addition to a development plan that profits directly from Hughes' previous spacecraft programs, provide a risk free structural configuration with respect to design, fabrication, and schedule goals.

810339-117



**FIGURE 4-33. NASA STANDARD NEAR EARTH TRANSPONDER AND INTERFACES**



#### 4.1.4 LEASAT Modifications for 30/20 GHz System

Using the previous LEASAT spacecraft description as a baseline, the following sections present the modifications of the LEASAT required to develop a 30/20 GHz spacecraft design. The telemetry, tracking and command system is modified to provide TT&C service at 30/20 GHz and at an S band rather than at the X band and UHF frequencies associated with LEASAT's defense application. The attitude control system is modified to accept a radio beacon error signal for platform despin, and the liquid apogee motor system is provided to improve off the shelf thrusters for better performance. Also presented are supporting analyses and summary data.

##### 4.1.4.1 Telemetry, Tracking, and Command System

The telemetry, tracking, and command (TT&C) system will operate on two frequency bands. During transfer orbit, the TT&C system will operate at S band in conjunction with the NASA STDN network. Once the satellite is at its orbital station, the TT&C function will operate through the 30/20 GHz payload as discussed below. If the 30/20 GHz TT&C link should become unavailable because of an anomaly or severe rain attenuation the on-station TT&C function can return to the S band mode. The S band TT&C links operate through the NASA standard near earth transponder (NASA/SNET). Operating at S band the system will be completely compatible with planned modifications of STDN to make it compatible with the deep space network (DSN). The use of K band TT&C requires no modification of the spacecraft bus since the payload will downconvert the 30 GHz TT&C signal to the NASA/SNET S band input frequency and upconvert the NASA/SNET S band output to the 20 GHz downlink frequency. The 30/20 GHz TT&C RF link is discussed in Section 2.1, Communications. A functional block diagram of this proposed system is shown in Figure 4-32. The diagram depicts appropriate cross-strapping between the S and K band portions of the system. Interconnection of the K band system to the telemetry and command unit is provided by conversion of the K band signal to an S band IF so that a NASA standard near earth transponder (NASA/SNET) for the mission can be utilized. The LEASAT X band antenna, filters, transmitters, and receivers will be removed.

The NASA/SNET proposed for this mission is fabricated by Motorola and is currently under consideration by Hughes for the next series of GOES spacecraft under negotiation with NASA. The transponder has been developed and qualified to meet the needs of most NASA missions by providing factory installed options for some application variable parameters. The functional block diagram for the NASA/SNET and its interfaces is given in Figure 4-33. Typical performance parameters for the transponder are shown in Table 4-24 for both its transmitter and receiver.

The command unit in SNET interfaces with redundant spacecraft command decoders. It is programmable to operate at a selectable bit rate varying from 125 to 2000 bps. The data is in nonreturn to zero (NRZ) format. The transmitter functions as either a telemetry transmitter or in conjunction with the receiver as a coherent ranging transponder. The downlink modulation indices are selectable by command.

TABLE 4-24. NASA STANDARD NEAR EARTH TRANSPONDER CHARACTERISTICS

<b>Receiver</b>	
Noise figure: (50 ohm source, VSWR 1.1:1.0)	
Into receiver terminal	5.5 dB
Into diplexer antenna port	6.5 dB
Tracking loop bandwidth (threshold)	
$28L_0$	200 Hz $\pm$ 20%
Frequency stability	
+10°C to +40°C	$\pm 7$ parts per $10^6$
Command threshold	
$+P_R = -174 \text{ dBm} + (E_b/N_0)(\text{dB}) + \text{NF dB} + \text{Loss (dB)} + 10 \log R_B$ $- 10 \log [2J_1^2(\theta)]$	
where:	
$E_b/N_0 = (\text{Signal per bit})/(\text{noise density})$ for $10^{-5}$ ber	Nominal - 10.5 dB Worst case - 11.6 dB
NF = noise figure into diplexer 6.5 dB max	
Loss = receiver detection loss 2 dB max	
$R_B$ = command data rate, bps	
$J_1$ = bessel function, first kind, first order	
$\theta$ = peak modulation index, radians	
<b>Transmitter</b>	
Frequency settability, aging and temperature stability	
Combined effect over 1 year, +10°C to +40°C	$\pm 10$ parts per $10^6$
Phase modulation linearity	2% to 1 rad, peak 5% to 2 rad, peak
Transmitter power	2 to 4 watts

The predicted power budgets for all S band data links between the spacecraft and the NASA STDN are summarized in Tables 4-25 through 4-27. All resulting link margins represent the difference between the predicted achievable  $E_b/N_0$  value and the theoretical  $E_b/N_0$  value required for an average bit error rate of  $10^{-5}$ . The command data link margins represent the difference between the received power level and a threshold level required for proper reception of commands by the NASA/SNET.

Table 4-25 contains the link budgets for commanding from the STDN 9 meter and 34 meter antenna subnets. The uplink signal will consist of a ranging and command signal; either or both may be present. The command signal is a 2 Kbs NRZ-L data stream  $\pm 90^\circ$  PSK modulated on a 16 KHz sub-carrier, which is phase modulated on the main carrier ( $f_c = 2034.2$  MHz). The ranging signal is a 125 KHz square wave which phase modulates the main carrier directly. Phase modulation indices are assumed accurate to within  $\pm 10$  percent, based on previous program experience, and adverse tolerances have been considered in compiling the budgets.

TABLE 4-25. SYSTEM COMMAND LINK (S BAND)

Item	Units	9 M Subnet				34 M Subnet			
Ground antenna size	m	9				34			
EIRP	dBm	113				128.3			
Polarization loss	dB	3				3			
Space loss*	dB	193.4				193.4			
Ground antenna track loss	dB	0.5				0.5			
Receive antenna gain	dB	-10.5				-10.5			
Losses between antenna and receiver	dB	5.7				5.7			
Received signal power	dBm	-100.1				-84.8			
Modulation indices									
Command	Radians	0.4	0.36	1.0	0.9	0.4	0.36	1.0	0.9
Ranging	Radians	0.4	0.44	—	—	0.4	0.44	—	—
Command signal mod loss	dB	-11.9	-12.9	-4.1	-4.8	-11.9	-12.9	-4.1	-4.8
Command threshold $P_R$	dBm	-111.1	-110.1	-118.9	-118.2	-111.1	-110.1	-118.9	-118.2
Margin	dB	11.1	10.1	18.8	18.1	26.3	25.3	34.1	33.4

\*Space loss for  $D = 55,000$  km and  $f = 2,034.2$  MHz.

TABLE 4-26. SYSTEM TELEMETRY LINK (S BAND)

Item	Units	9 M Subnet				34 M Subnet			
S/C EIRP	dBm	20				20			
Polarization loss	dB	0.2				0.2			
Space loss*	dB	194.1				194.1			
Ground antenna track loss	dB	0.5				0.5			
G/T, ground station	dB/°K	24.1				34.2			
Received $S/N_0$	dB	47.9				58			
Mod indices									
Telemetry	Radians	1.0	0.9	1.4	1.26	1.0	0.9	1.4	1.26
Command	Radians	0.4	0.44	1.0	1.1	0.4	0.44	1.0	1.1
Ranging	Radians	0.4	0.44	—	—	0.4	0.44	—	—
Mod loss	dB	-2.6	-3.4	-2.4	-3.3	-2.6	-3.4	-2.4	-3.3
Available $S/N_0$	dB	45.3	44.5	45.5	44.6	55.4	54.6	55.6	54.7
Required $E_b/N_0$ **	dB	9.6				9.6			
Implementation loss	dB	1.5				1.5			
Bit rate, Q	dB	33				33			
Margin	dB	1.2	0.4	1.5	0.5	11.3	10.5	11.5	10.6

\*Space loss calculated for  $D = 55,000$  km,  $f = 2,209.086$  MHz.

\*\*Theoretical required  $E_b/N_0$  for  $10^{-5}$  BER.

TABLE 4-27. SYSTEM RANGING LINK (S BAND)

Item	Units	9 M Subunit						34 M Subnet					
Ground station EIRP	dBm	113						128.3					
Space loss	dB	193.4						193.4					
Ground antenna track loss	dB	0.5						0.5					
Polarization loss	dB	3						3					
Spacecraft G/T	dB/°K	-47						-47					
(S/N <sub>0</sub> ) <sub>u</sub> *	dB-Hz	67.7						83					
(S/N <sub>0</sub> ) <sub>d</sub> *	dB-Hz	47.9						58					
(S/N <sub>0</sub> ) <sub>r</sub> *	dB-Hz	47.9						58					
Mod indices													
Telemetry	Radians	-	-	1.0	1.1	1.4	1.54	-	-	1.0	1.1	1.4	1.54
Ranging	Radians	0.4	0.36	0.4	0.36	1.0	0.36	0.4	0.36	0.4	0.36	1.0	0.36
Command	Radians	-	-	0.4	0.44	-	-	-	-	0.4	0.44	-	-
Mod loss	dB	-8.2	-9.1	-13.9	-16.4	-23.6	-39.3	-8.2	-9.1	-13.9	-16.4	-23.6	-39.3
Available S/N <sub>0</sub>	dB-Hz	39.7	38.8	34	31.5	24.3	8.6	49.8	48.9	44.1	41.6	34.4	18.7
Required S/N <sub>0</sub>	dB-Hz	30	30	30	30	30	30	30	30	30	30	30	30
Margin	dB	9.7	8.8	4	1.5	-6.7	-21.4	19.8	18.9	14.1	11.6	4.4	-11.3

\*Ground station equipment requirements.

The EIRP values used for spacecraft and ground station are discussed and summarized in Table 4-28. The modulation loss values are given for both command only and simultaneous commanding and ranging. Losses are computed for nominal and worst case (due to +10 percent tolerance) values of the modulation indices.

The link budgets for telemetry from the spacecraft to the 9 meter and 34 meter DSN subnets are presented in Table 4-26. The telemetry signal is a 2 Kbs Bi-0L (Manchester encoded) data stream phase modulated

TABLE 4-28. EIRP, G/T, AND ANTENNA GAIN VALUES USED IN LINK CALCULATIONS

S/C or Ground Station System	Antenna Transmit	Gains, dB Receive	EIRP, dBm	G/T, dB/°K
DSN 9 m station*	-	-	113	24.1
DSN 34 m station*,**	55.3	56	108.3 to 128.3	34.2
Spacecraft omni***	-	-10.5	20	-47

\*JPL provided all values.

\*\*The EIRP variation is due to specified range in transmitter power of 53-73 dBm; JPL did not comment on the source of these variations.

\*\*\*Derived from EIRP and G/T specifications for GOES G, H, I. The antenna gains were for the GOES D, E, F omni antenna; these gains may be changed to meet the new EIRP and G/T requirements.

directly on the downlink carrier ( $f_c = 2209.086$  MHz). This carrier may also be simultaneously phase-modulated by the command subcarrier which is allowed to leak through the transponder, and ranging squarewave received on the uplink.

For the 9 meter subnet the margins are very small, only a 0.4 dB margin results for simultaneous telemetry, ranging, and commanding when worst case index values are used. Due to the increase in ground station G/T these margins improve by 10.1 dB when the 34 meter subnet is used.

The link budget for the ranging function is presented in Table 4-27.

The ranging signal is a 125 kHz squarewave which directly phase modulates the downlink carrier. It may be present simultaneously with the command and telemetry signals.

For ranging only, adequate margins result for both the 9 meter and 34 meter subnets. For simultaneous ranging, commanding, and telemetry, the margins are adequate for the 34 meter subnet, but are low for the 9 meter subnet.

The maximum prime power requirements for the NASA/SNET transponder are 17.2 and 26.3 watts total for peak RF outputs of 1 and 2.5 watts, respectively. With receiver and CDV unit operational only, this power requirement drops to 7.5 watts dc. The voltage requirement of the input prime power is +28 volts  $\pm 7$  Vdc. The receiver is on at all times with transmitter commanded on/off as long as prime power is available for the transmitter.

The weight of NASA/SNET transponder is 3.3 kg or 7.3 pounds. The size of the envelope that will house the unit including external cabling is 9.05 inches by 8.68 inches by 3.4 inches (22.99 cm by 22.05 cm by 8.64 cm).

The unit will sustain cumulative dose of  $3 \times 10^3$  rad (si) at the component location. Vibration levels of  $0.1 \text{ G}^2/\text{Hz}$  about all three axes of the unit are acceptable over a frequency range of 70 to 1000 Hz with 6 dB/OCT rolloff outside this range.

The other changes required of the LEASAT TT&C subsystem are removal of the encryption/decryption units and modifying the telemetry and command formats via the PROMs that exist in the present subsystem.

There are ample spare telemetry and command channels to accommodate the 30/20 GHz payload. These channels will be implemented as required via the new shelf wiring harness.

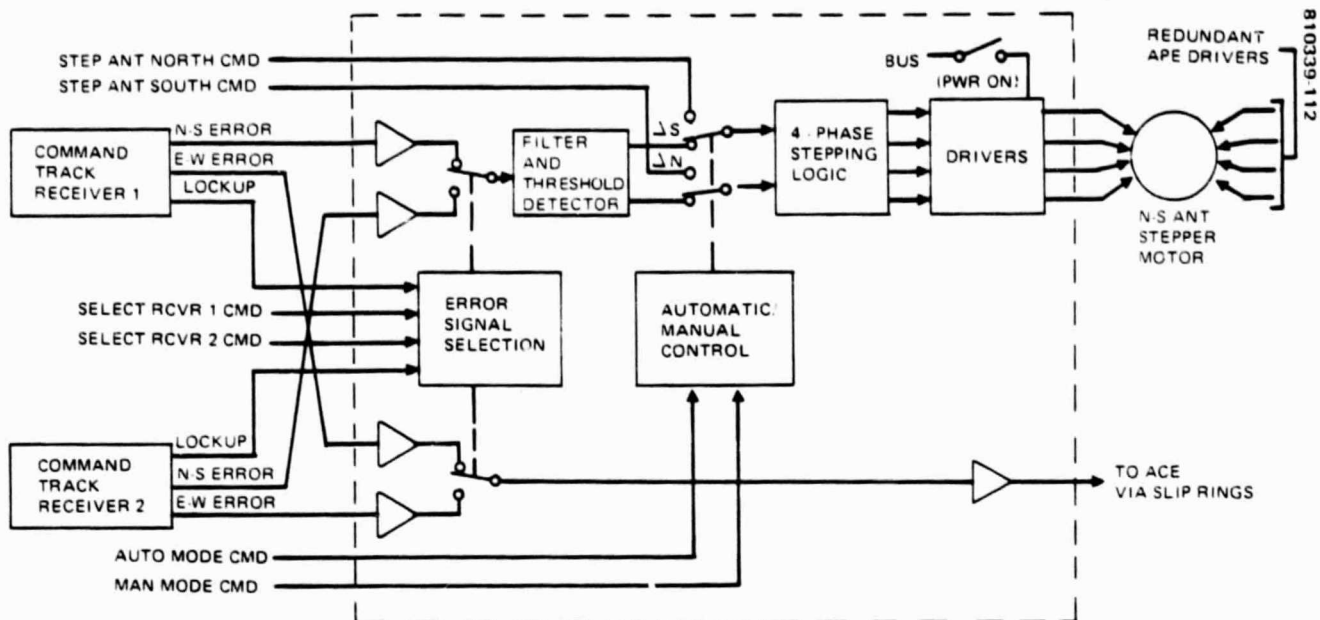
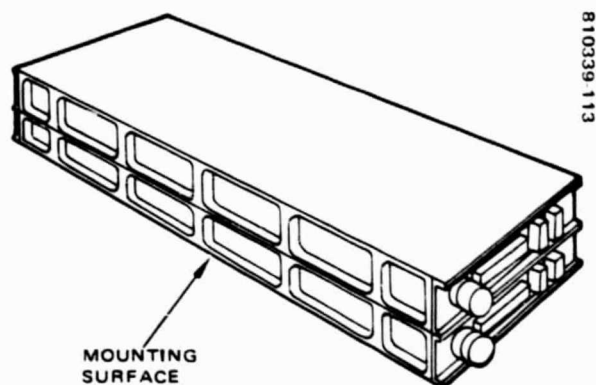


FIGURE 4-34. ANTENNA POSITIONER ELECTRONICS BLOCK DIAGRAM



PHYSICAL CHARACTERISTICS

SIZE = 45.5 x 15.0 x 7.1 cm

WEIGHT = 3.43 kg (7.55 lb)

POWER = 2.5 W

PARTS COUNT

124 I/C + 1036 DISCRETE

UNIT INTERNALLY REDUNDANT

FIGURE 4-35. ANTENNA POSITIONER ELECTRONICS

#### 4.1.4.2 Attitude Control

The 30/20 GHz system requires that the multibeam antenna be pointed to within an accuracy of less than  $0.05^\circ$  to satisfy communication link performance. The LEASAT antenna is pointed with an accuracy of  $0.7^\circ$  by controlling the attitude of the spin axis and the angular position of the despun platform in response to error signals from an earth sensor. The ordered magnitude improvement required of the 30/20 GHz spacecraft is achieved by reorienting the antenna main reflector in elevation relative to the spacecraft body in response to an error signal from a 30 GHz earth based beacon. The azimuth orientation is still controlled by platform despun but also in response to a beacon error signal. The use of the elevation axis circumvents the problem of maintaining constant spin-axis attitude in the face of solar torques. This approach is identical to that used on the operational Hughes SBS design, wherein the received beacon signal is resolved into east-west and north-south components, and then processed by the antenna positioning electronics (APE) and attitude control electronics (ACE) to drive the north-south antenna positioning mechanism (APM) and east-west despun platform motor. Since the present LEASAT design does not include an APE or APM, they will be added and almost identical to those of the SBS design. Also the LEASAT ACE will receive minor modifications to accept the APE east-west signal as primary drive for the azimuth positioning of the antenna. The use of a spinning spacecraft with a despun platform results in a yaw gyroscopically stabilized vehicle requiring only a single beacon station and a single elevation control mechanism on the spacecraft antenna. The use of the earth sensors on the 30/20 GHz design will be relegated to transfer orbit and on-orbit attitude determination, initial on-orbit antenna despun and acquisition, and as a backup to the primary beacon mode.

Typical antenna pointing error budgets applicable to the 30/20 GHz system are listed in Tables 4-29 through 4-31. All results satisfy the  $0.05^\circ$  requirement.

Figure 4-34 shows the block diagram of the APE, APM, and command track receivers. The communications and track receivers are part of the microwave subsystem. Figure 4-35 and Table 4-32 give further details on the APE and APM.

#### 4.1.4.3 Propulsion

The LAM subsystem will use the Ford qualified thrusters rather than the Marquart thrusters to obtain an increase in specific impulse ( $\approx 308$  sec). This improvement plus targeting the orbit for  $0^\circ$  inclination results in additional RCS propellant (no pre-on-orbit burns) being made available to satisfy a 4 year stationkeeping requirement of  $\pm 0.02^\circ$  in inclination.

#### 4.1.4.4 Configuration and Structural Modifications

The LEASAT despun shelf modifications necessary to accommodate the 30/20 GHz payload are illustrated in Figures 4-36 through 4-38. Figure 4-36 shows the forward and aft (dashed) layout of the payload, TT&C,

TABLE 4-29. EAST-WEST BEAM POINTING ERROR BUDGET

<u>Error Types and Sources</u>	<u>Error, deg (3<math>\sigma</math>)</u>
<u>Constant</u>	
Tracking boresight calibration	0.0064
Omni antenna interference offset	0.0056
Command bias granularity	0.0016
Servo electronics null offset	0.0010
RSS subtotal	0.0089
<u>Long term variations</u>	
Track receiver	0.0104
Servo electronics	0.0010
RSS subtotal	0.0104
<u>Diurnal variations</u>	
Track receiver	0.0108
Track filter network	0.0058
BAPTA friction torque variation	0.0040
RSS subtotal	0.0129
<u>Short term variations</u>	
Track receiver noise	0.0013
Beacon signal random variation	0.0042
Dynamic coupling of wobble into E-W	0.0006
BAPTA friction torque disturbances	0.0050
Response to accelerometer noise	0.0003
RSS subtotal	0.0067
<u>Total error in steady state operation</u>	0.0389
<u>Maneuver transient errors</u>	
E-W velocity maneuver	0.0055
N-S velocity maneuver	0.0021
Attitude trim maneuver	0.0060
<u>Worst case pointing error</u>	
Sum of steady state and worst case maneuver transient errors	0.0449

and APE units on the despun shelf. The high power RF units are on the forward side and couple easily to the antenna. They are located radially outward to couple thermally to the forward spinning thermal barriers for heat removal. The low power RF units and digital units are shielded from high power units by locating them on the aft side of the shelf.

All units have been located with a concern for minimizing waveguide lengths, digital cable lengths, mass properties, and thermal control. Figure 4-37 shows a side view of the shelf with the associated despun and spinning thermal barriers. Both barriers will be modified LEASAT designs. The shelf dimensions and design are identical to those of the LEASAT, only the unit mounting bolt holes and attachment features need changes. The extensive shelf area leaves ample margin for repositioning and growth of the payload if required.



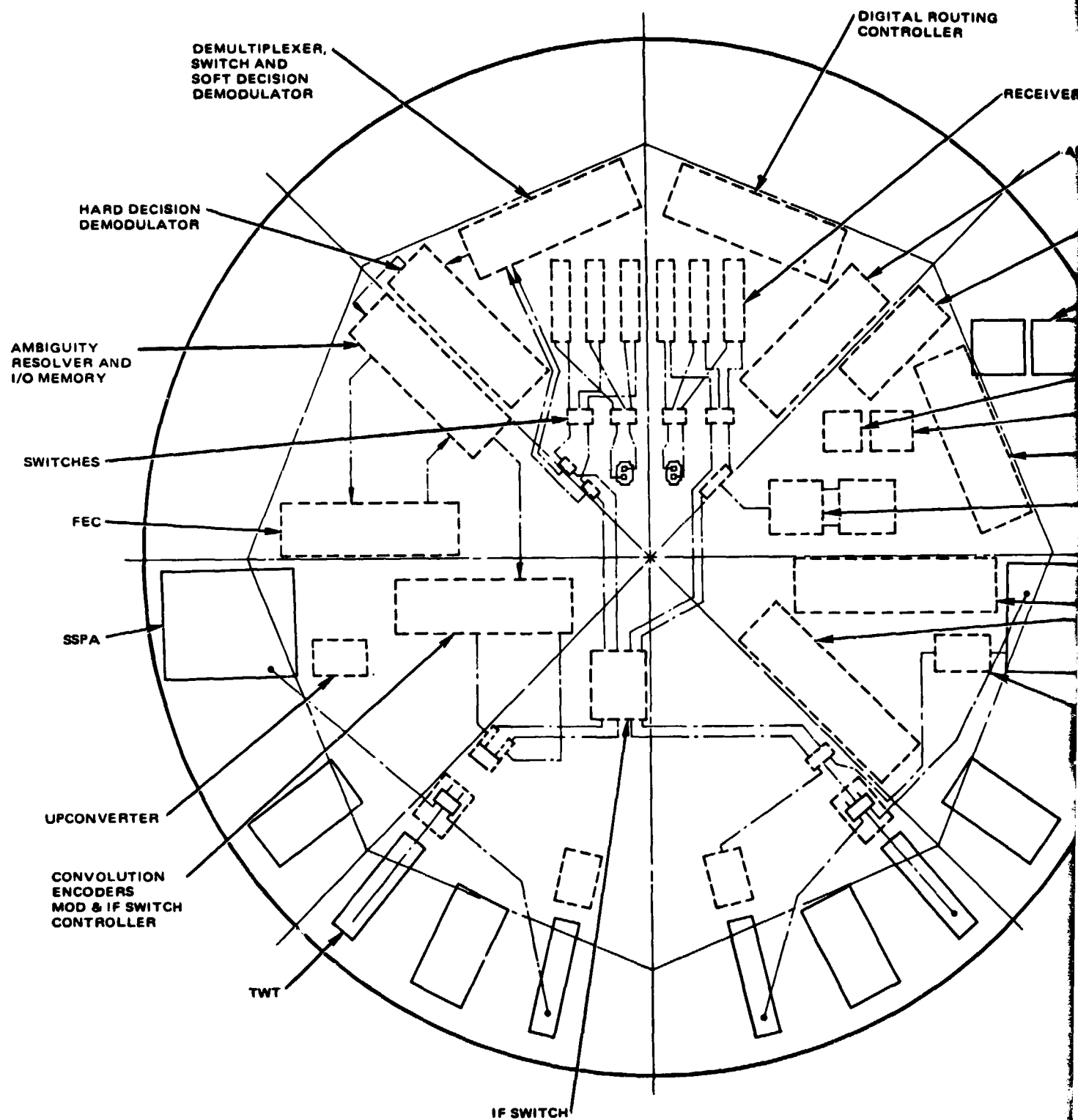
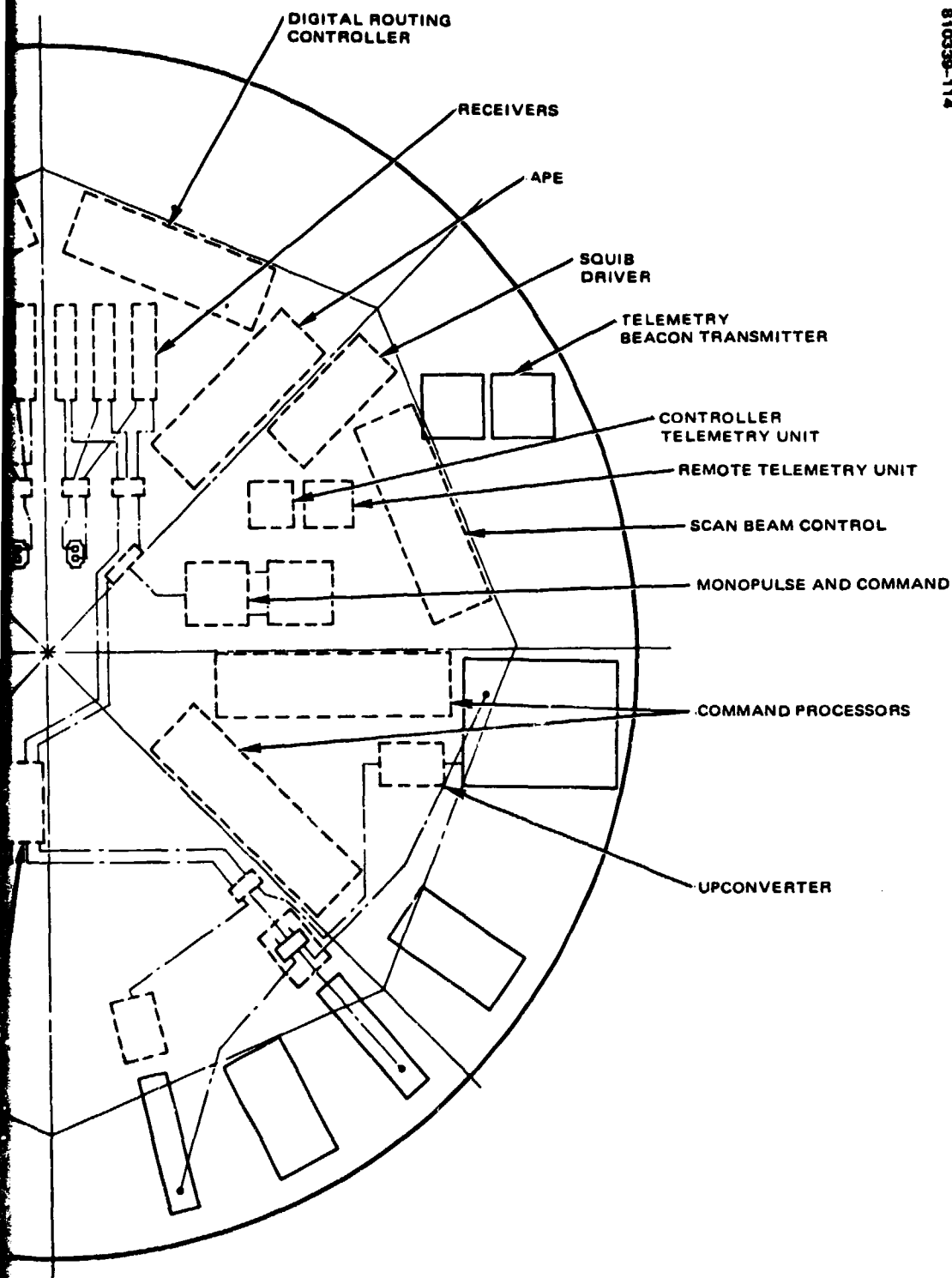


FIGURE 4-36. 30/20 GHZ PAYLOAD LAYOUT

810339-114



LAYOUT

OLDOUT FRAME 2

TABLE 4-30. NORTH-SOUTH BEAM POINTING ERROR BUDGET

<u>Error Types and Sources</u>	<u>Error, deg (3<math>\sigma</math>)</u>
<u>Constant</u>	
Tracking boresight calibration	0.0052
Omni antenna interference offset	0.0056
Command bias granularity	0.0016
Servo electronics null offset	0.0010
RSS subtotal	0.0077
<u>Long term variations</u>	
Track receiver	0.0041
Servo electronics	0.0010
RSS subtotal	0.0042
<u>Diurnal variations</u>	
Track receiver	0.0040
Track filter network	0.0030
RSS subtotal	0.0050
<u>Short term variations</u>	
Beacon signal random variation	0.0028
Wobble and bearing runout	0.0025
Stepper servo deadband	0.0035
Nutation induced by antenna stepping	0.0002
Dynamic coupling of E-W jitter to N-S	0.0004
RSS subtotal	0.0052
<u>Total error in steady state operation</u>	0.0221
<u>Maneuver transient errors</u>	
E-W velocity maneuver	0.0029
N-S velocity maneuver	0.0035
Attitude trim maneuver	0.0100
<u>Worst case pointing error</u>	
Sum of steady state and worst case maneuver transient errors	0.0321

TABLE 4-31. BEAM ROTATION ERROR BUDGET

<u>Error Types and Sources</u>	<u>Error, deg (3<math>\sigma</math>)</u>
<u>Constant</u>	
Antenna rotation misalignment	<u>0.0050</u>
RSS subtotal	<u>0.0050</u>
<u>Long term variations</u>	
No identified errors	
<u>Diurnal variations</u>	
Spin axis attitude drift	0.1600
Attitude trim correction error	0.0620
Attitude measurement uncertainty	<u>0.0200</u>
RSS subtotal	<u>0.1728</u>
<u>Short term variations</u>	
Wobble and bearing runout	0.0025
Nutation induced by antenna stepping	0.0002
Dynamic coupling of E-W jitter to rotation	<u>0.0004</u>
RSS subtotal	<u>0.0025</u>
<u>Total error in steady state operation</u>	<u>0.1803</u>
<u>Maneuver transient errors</u>	
E-W velocity maneuver	0.0024
N-S velocity maneuver	0.0062
Attitude trim maneuver	<u>0.0100</u>
<u>Worst case pointing error (rotation)</u>	<u>0.1903</u>
Sum of steady state and worst case maneuver transient errors	
<u>Equivalent pointing error</u>	<u>0.017</u>

TABLE 4-32. ANTENNA POSITIONER MECHANISM CHARACTERISTICS

Drive system	Redundant
Motor	Size 15, PM, 45 deg stepper
Torque output	16 ft-lb
Output shaft stiffness	1025 ft-lb/deg
Positioning increment	0.0025 deg/step
Travel range	70 deg
Backlash	Zero
Potentiometer	42 k $\Omega$ , conductive plastic
Motor power	Approx 15 W (during step)
Weight	3.44 kg (7.57 lb)
Temperature range	-51 $^{\circ}$ to 65.6 $^{\circ}$ C (-60 $^{\circ}$ to 150 $^{\circ}$ F)

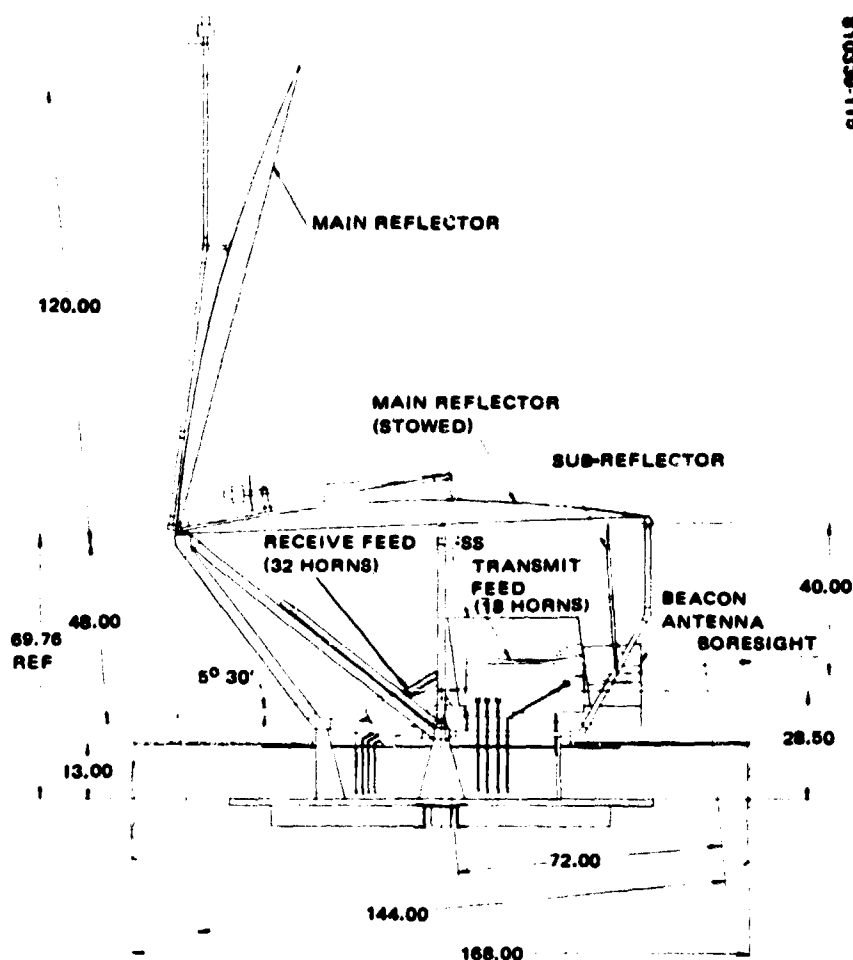


FIGURE 4-37. SIDE VIEW OF SHELF WITH ASSOCIATED DESPUN AND SPINNING THERMAL BARRIERS

The antenna layout is shown in Figures 4-37 (side and top views) and 4-38 (reflector axis view). The main reflector and omni antennas are shown both stowed and deployed. All antenna elements, beacon antennas, waveguides that connect to the shelf units and structural support elements are shown.

A spacecraft isometric is shown in Figure 4-39.

#### 4.1.4.5 Analysis and Summaries

##### 4.1.4.5.1 Thermal Analysis

Basic LEASAT thermal control elements are unchanged with the 30/20 GHz transponder integrated in the spacecraft. The power dissipation of the 30/20 GHz payload on the despun shelf is less than on the LEASAT (LEASAT 606 watts, 30/20 GHz 568 watts). Therefore, the black portion of the forward radiator is reduced from 44 percent to 40 percent. The bare aluminum portion is increased from 56 percent to 60 percent.

810339-116

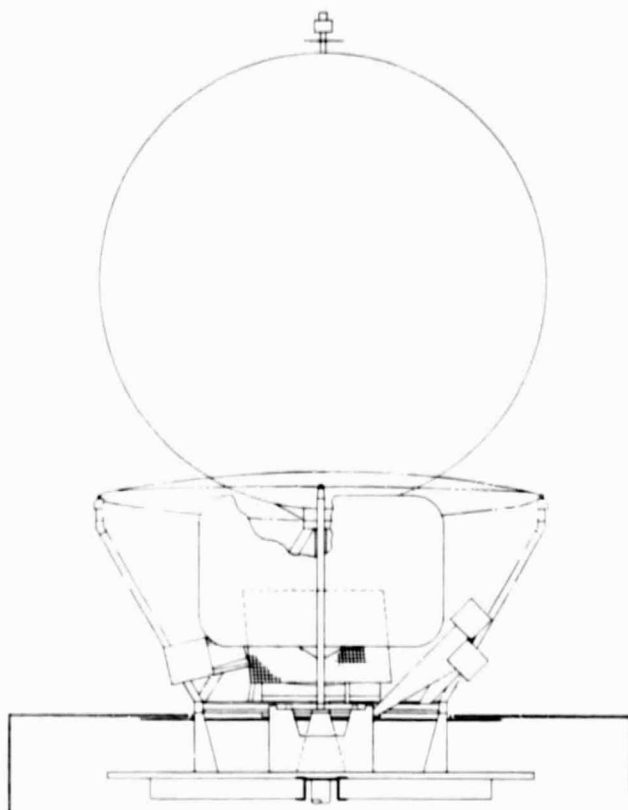


FIGURE 4-38. REFLECTOR AXIS VIEW OF SHELF

810339-118

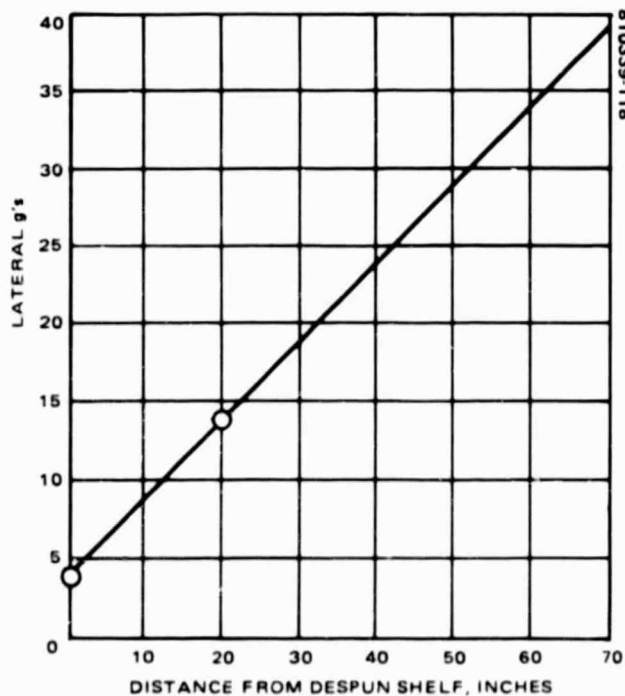


FIGURE 4-40. LATERAL G's LIMIT LEASAT DISTANCE FROM DESPUN SHELF

810339-117

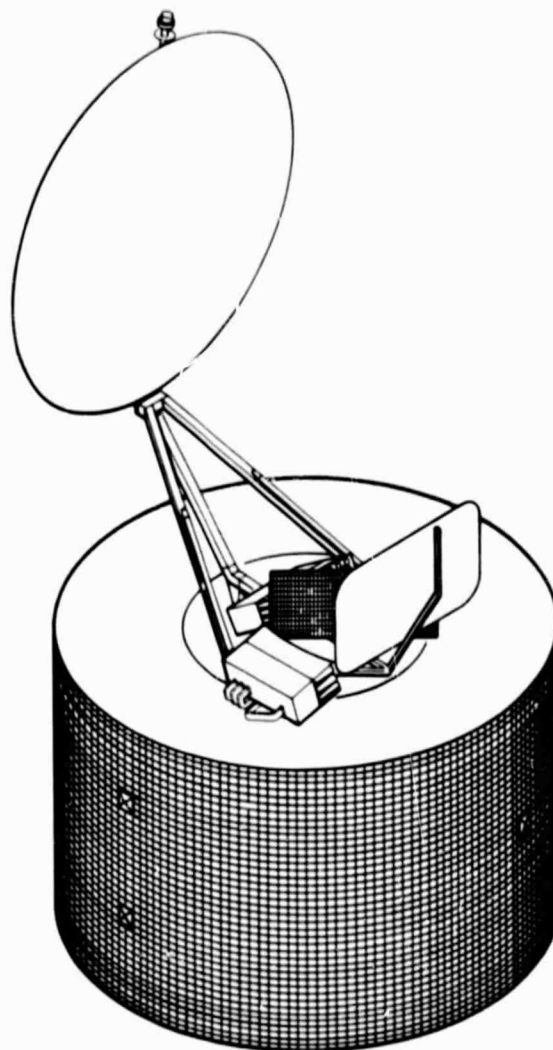


FIGURE 4-39. LEASAT SPACECRAFT ISOMETRIC

The TWTs and solid state amplifiers, the highest power dissipators, are located on the outboard portion of the shelf where the heat rejection is the most efficient. All receiver units are located on the aft side of the shelf to minimize the RFI effects and to stabilize the temperatures during eclipses. The heat concentration on the shelf is approximately 12 to 15 w/ft<sup>2</sup>. The design temperature ranges for the 30/20 GHz transponder remain similar to those shown in Table 4-21 for the LEASAT units, TWTs <140°F, SSPA <110°F.

The antenna subsystem for the 30/20 GHz transponder is different; therefore, the thermal design is different. The feeds and the antenna support structures are wrapped in a multilayer blanket to minimize thermal distortion. The maximum calculated temperature gradient in a thermally wrapped boom is less than 20°F. The active switches behind the feeds are provided with a blanket that radiatively couples it to the interior of the spacecraft.

NASA's current design constrains the STS to earth facing orientation with 30 minute sun facing and 90 minute space facing maneuvers. These constraints allow the spacecraft to survive with an 1800 watt heater installed on the solar panels and power provided through an umbilical connector by the orbiter.

#### 4.1.4.5.2 Structural Analysis

##### Loads Analysis

The LEASAT bus is used to mount the 30/20 GHz antenna system with the basic LEASAT despun shelf unchanged. The LEASAT lateral and axial loads are used which were derived from LEASAT/STS coupled loads analysis. The lateral g loads on the LEASAT antenna which is approximately 20 inches from the despun shelf are extrapolated linearly for the 30/20 GHz antenna which is approximately 65 inches from the despun shelf in the stowed position (see Table 4-33).

The above load factors are maximum, not condition nor time dependent. Therefore, using combinations of these load factors is conservative for preliminary design analyses. Figure 4-40 presents lateral g's limit versus distance from the despun shelf for the Z axis.

TABLE 4-33. LEASAT MAXIMUM LIMIT COMPONENT  
"G" LEVELS

	X	Y	Z
Despun shelf	5.97	1.83	3.73
Antenna	12.52	14.21	14.27

Two design load conditions are defined for preliminary design:

Condition I: Z and X loads acting simultaneously

Condition II: Z and Y loads acting simultaneously

The lateral Z and Y loads are taken from Figure 4-40. The CG of the stowed antenna is taken as 65 inches from the despun shelf.

Antenna load factors 30/20 GHz are as follows:

Condition I: Z = 37 g's limit

X = 12.5 g's limit

Condition II: Y = 37 g's limit

X = 12.5 g's limit

#### Antenna Tripod Support Analysis

The antenna weight of 50 pounds is distributed 50 percent to the tripod support and 50 percent to the inboard stowed support structure.

The loads on the tripod apex are then as follows:

#### Condition I

$$Z = (50)(0.5)(37) = 925 \text{ lb (limit)}$$

$$Z = 925 \times 1.4 = 1295 \text{ lb ultimate (ULT)}$$

$$X = (12.5)(0.5)(50)(1.4) = 438 \text{ lb (ULT)}$$

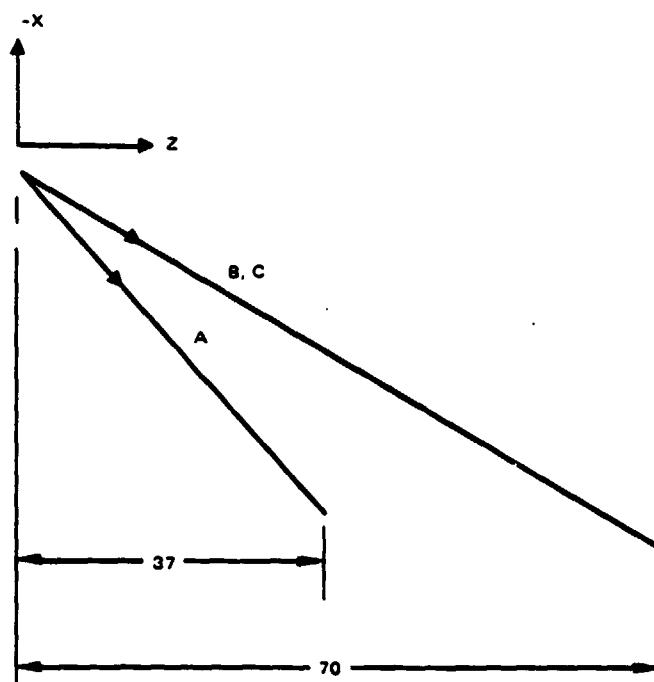
#### Condition II

$$Y = (50)(0.5)(37)(1.4) = 1295 \text{ lb (ULT)}$$

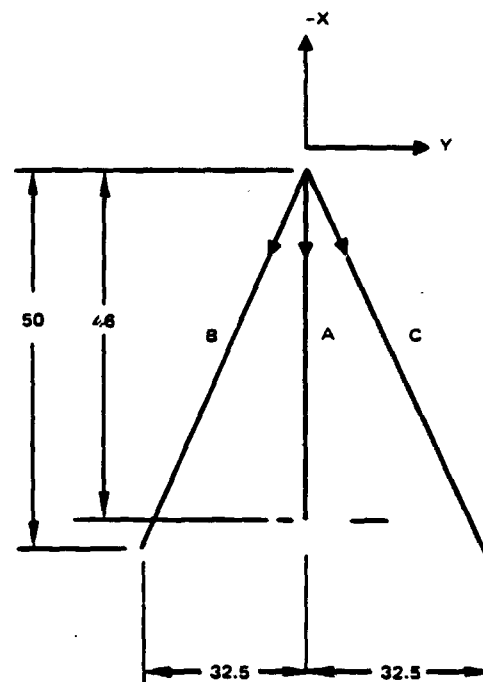
$$X = 438 \text{ lb (ULT)}$$

<u>Member</u>	<u>X</u>	<u>Y</u>	<u>Z</u>	$\frac{L}{\sqrt{X^2+Y^2+Z^2}}$	$\frac{X}{L}$	$\frac{Y}{L}$	$\frac{Z}{L}$
A	46	0	37	59.0	0.78	0	0.627
B	50	-32.5	70	92.0	0.54	-0.353	0.761
C	50	32.5	70	92.0	0.54	0.353	0.761





DIMENSIONS IN INCHES



1) X Load

$$\Sigma F_X = 0$$

$$0.78A + 0.54B + 0.54C + X = 0$$

2) Y Load

$$\Sigma F_Y = 0$$

$$= 0.353B + 0.353C + Y = 0$$

3) Z Load

$$\Sigma F_Z = 0$$

$$0.627A + 0.761B + 0.761C + Z = 0$$

Solving equations simultaneously we have,

$$A = -2.985 X + 2.12 Z$$

$$B = 1.28 X + 1.41 Y - 1.53 Z$$

$$C = 1.28 X - 1.41 Y - 1.53 Z$$

Taking X, Y, and Z loads as either plus or minus from STS/SC coupled analyses, the maximum tripod member compression loads are:

$$A = -2.985 (438) + 2.12 (-1295)$$

$$A = -4053 \text{ lb (ULT)}$$

$$B = 1.28 (-438) - 1.53 (1295)$$

$$B = -2542 \text{ lb (ULT)}$$

$$C = -2542 \text{ lb (ULT)}$$

Graphite/epoxy square tubes are used for the tripod of T300/5208.

Member A 3 inch square tube

$$t = 0.077 \text{ in.} - 14 \text{ plies of } 0.0055 \text{ in.}$$

$$(0_4, \pm 45, 0_2, \mp 45, 0_4)$$

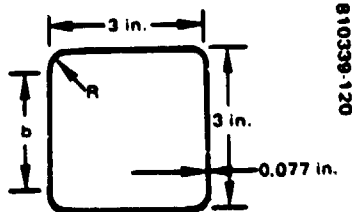
$$I = (2) (3) (0.077) (1.4615)^2 + \frac{2(0.077) (3)^3}{12}$$

$$I = 1.33 \text{ in}^4$$

$$A = 0.924 \text{ in}^2$$

$$b/t = \frac{3 - 2r}{0.077} = 31$$

$$f_c = \frac{4053}{0.924} = 4400 \text{ psi (ULT)}$$



Crippling allowable is taken from Reference for  $b/t = 38.2$

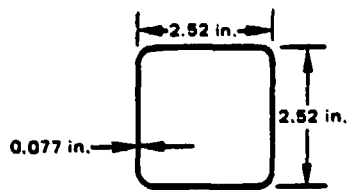
$$F_{cc} = 17320 \text{ psi}$$

$$\text{Margin of safety (MS)} = \frac{17,370}{4,400} - 1 = + \underline{\underline{2.9}}$$

Column buckling is not critical.

#### Members B and C

2.52 in. square tube  $t = 0.077$



T 300/5208 graphite epoxy

$$I = 0.714 \text{ in.}^4$$

$$A = 0.725 \text{ in.}^2$$

$$B = C = 2542 \text{ lb (ULT)}$$

$$P_{CR} = \frac{\pi^2 E I}{L^2} = \frac{(3.14)^2 (18 \times 10^6) (0.714)}{(92)^2}$$

$$P_{CR} = 14,900 \text{ lb}$$

$$F_{cc} = 17,370 \text{ psi}$$

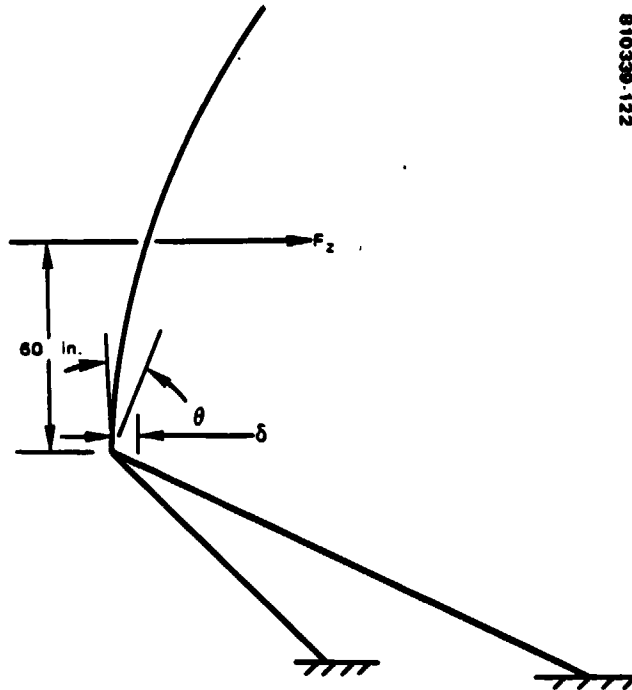
$$f_c = \frac{2542}{0.725} = 3500 \text{ psi}$$

$$MS = \frac{17,370}{3,500} - 1 = \underline{\underline{3.96}}$$

### Primary Antenna Deployed Structural Frequency\*

The deployed Z direction (normal to plane of disk) frequency is calculated.

A 1 g load at the deployed dish CG is imposed



810330-122

The deflection and rotation at the apex fitting is,

$$\delta = \sum \frac{S U L}{AE}$$

$$\theta = \int \frac{M m dS}{EI}$$

$S$  = Member axial load due to 1 g in Z direction

---

\*"SBS Antenna Subsystem Stress Analysis HS-376B Program," Vol II, HS 376A/B-09115, 30 November 1979

U = Virtual member load due to 1 unit load in Z direction

M = Member bending moment due to 1 g load in Z direction

m = Virtual member bending moment due to 1 in.-lb unit moment in Z direction

Member	S	U	L	A	E
A	106	2.12	59	0.925	18 by $10^6$
B	-76.5	-1.53	92	0.725	18 by $10^6$
C	-76.5	-1.53	92	0.725	18 by $10^6$

Distributing the moment according to the relative stiffness of the tripod members results in the following moment distribution factors;

$$D.F_A = 0.438$$

$$D.F_B = D.F_C = 0.281$$

$$\text{Evaluating the } \sum \frac{S U L}{A E} \text{ and } \int \frac{M m dS}{E I}$$

we have

$$\delta = 2.45 \times 10^{-3}$$

$$\theta = \sum \frac{M m dS}{E I} = \frac{1}{(E I)_A} (33,956)$$

$$+ \frac{1}{E I_B} (21,793) + \frac{1}{(E I)_C} (21,793)$$

$$\theta = \frac{1}{2.4 \times 10^7} (33,956) + \frac{1}{1.29 \times 10^7} (43,586)$$

$$\theta = 4.79 \times 10^{-3} \text{ radians}$$

At reflector center of gravity

$$\delta_{\text{Total}} = 2.45 \times 10^{-3} + 4.79 (60)10^{-3} = 0.29 \text{ in.}$$

$$f = \frac{3.13}{\sqrt{\delta_{\text{Total}}}}$$

$$f = 5.8 \text{ Hz}$$

Feasibility of the design has been established. In future analyses, a NASTRAN math model and analysis will be performed including the tripod, mounting brackets, and despun shelf. Since 3 to 4 Hz is a goal for the total spacecraft in the deployed configuration, a frequency of 5.8 Hz for the major contributing structure is of the correct magnitude since the despun shelf and attachments will add flexibility and drop the frequency several Hz.

The LEASAT despun shelf is used without major structural changes for the 30/20 GHz configuration. The structural adequacy of the shelf is based on a comparison of the total shelf weight of the antenna and equipment mounted to the shelf. Table 4-34 indicates that the LEASAT shelf must sustain higher loads than that imposed by the 30/20 GHz, since the LEASAT shelf weight exceeds the 30/20 GHz weight by 51 pounds. Future analyses performed will provide a NASTRAN structural model of the shelf with discrete equipment and antenna loads imposed subjected to STS/SC coupled transient landing and liftoff cases.

TABLE 4-34. COMPARISON OF LEASAT AND 30/20 GHz  
DESPUN SHELF WEIGHTS

Items	LEASAT, lb	30/20 GHz, lb
Antenna and shelf equipment	611.66	549
Thermal control, attitude control, wire harness	68.6	80.3
Shelf structure	181.31	181.31
Total platform stowed	861.57	810.61

#### 4.1.4.5.3 Mass Properties

The spacecraft weight summary is presented in Table 4-35. The communication payloads are detailed in Section 3. The spacecraft bus details are in Table 4-36.

TABLE 4-35. SPACECRAFT WEIGHT SUMMARY

Item	Payload Weight, lb	
<b>Payload</b>		<b>465</b>
Antenna	189	
Microwave	123	
Digital	111	
Margin (10%)	42	
<b>Bus</b>		<b>2,285</b>
TT&C	123	
Controls	75	
Power	541	
Propulsion	323	
Structure	1,100	
Margin (rotor)	114	
Spacecraft (dry)		2,750
Propellant (BOL)		345
RCS (4+ yr)	324	
LAM residual	21	
Spacecraft (BOL)		3,095
Transfer orbit expendables		12,191
Shuttle deployment		15,286
Cradle and ASE		1,785
Shuttle payload		17,071

The on-orbit weight capability is somewhat less than that for the present LEASAT, but there is more RCS propellant available for station-keeping in the 30/20 GHz design. This additional propellant is required to maintain the tight north-south orbital control ( $\pm 0.025^\circ$ ) over a 4 year period. This requirement is driven by the desire to implement low cost nontracking ground station antenna systems.

The total spacecraft weight margin provided by excess propulsion capability is 156 pounds. A 10 percent payload weight margin of 42 pounds was allocated leaving 114 pounds as a rotor margin. Some of the 114 pounds rotor margin can be shared between rotor margin and payload margin. The ultimate limit on the payload weight is the requirement that the spin to transverse inertia ratio ( $I_s/I_t$ ) be greater than 1.05 for spacecraft stability. If one-half of the 114 pounds rotor weight margin (or weight growth) is deployed at the perimeter of the satellite an  $I_s/I_t$  ratio of 1.064 results at the end of 4 years. Of the remaining 57 pounds, a large fraction could be added to the payload if the remainder was distributed at the rotor perimeter. The fraction would depend on whether the weight growth was above the despun platform (e. g., the antenna) or on the platform which is very near the center of gravity.

TABLE 4-36. BUS SUBSYSTEM WEIGHTS (LB)

Subsystems	Bus Total	Plat	Rotor
<b>TT&amp;C</b>			
Rotor	48	84	48
Platform			
Remote decoder (4)	4.4		
Command processor (2)	39.6		
Squib driver	4.4		
Receive + transmit network	2.6		
Remote multiplexer (7)	4.7		
Encoder (2)	13.6		
S band trans (2)	14.6		
Total	123		
<b>Controls</b>			
Rotor	54	21	54
Despun			
BAPTA (SH)	13.9		
APE	7.5		
Total	75.4		
<b>Power</b>			
Rotor	536.2	5	536
Platform	4.6		
Total	540.8		
<b>Propulsion</b>			
RCS	37.2	—	323
LAM	285.4		
Total	322.6		
<b>Structure</b>		236	864
Harness			
Despun	33.6		
Spun	69.9		
Spaceframe			
Despun	181.3		
Spun	661.7		
Thermal			
Despun	21.1		
Spun	121.4		
Balance weight (rotor)	10.7		
Total	1,099.7	346	1,825
Total despun (payload + 346) = 811			



If option 1 was implemented the payload weight would decrease by 49 pounds. Option 1, which is described in 2.1, eliminates one of the scanning beams and reduces the BBP throughout. Option 2, also described in 2.1, adds a frequency division multiple access (FDMA) experiment which weighs 16 pounds. Although this cuts into the 42 pounds (10 percent) weight margin the additional payload weight available from the rotor weight margin could compensate. In any case, if weight growth required a reduction of the payload the entire FDMA experiment could be removed without impact to the basic system.

#### 4.1.4.5.4 Power Summary

All spacecraft designs have ample power margins as shown in Table 4-37. During eclipse operation, the margin on batteries is reduced, but still ample as shown in Table 4-38 for the baseline TS design. The detailed bus loads are given in Table 4-39.

If it were desirable to operate both the TS and CPS system simultaneously, it could be done with approximately 70 watt of margin during eclipse. This would require a change in the despun shelf layout to realize acceptable thermal control.

TABLE 4-37. POWER SUMMARY (WATTS)

Item	Baseline		Option 1		Option 2	
	TS	CPS	TS	CPS	TS	CPS
Payload						
Antenna	1.8	9.8	1.8	6.3	1.8	9.8
Microwave	515.6	285.6	515.6	285.6	518.6	285.6
Digital	41.0	223.2	41.0	88.8	41.0	223.2
Bus	228.0	228.0	228.0	228.0	228.0	228.0
TT&C (48)						
Controls (37)						
Power (92)						
Thermal (51)						
Spacecraft	786.4	746.6	786.4	608.7	789.4	746.6
Capability (4 yr)	1,090	1,090	1,090	1,090	1,090	1,090
Margin	303.6	343.3	303.6	481.3	300.6	343.4

**TABLE 4-38. ECLIPSE POWER SUMMARY  
(WATTS)**

<u>Payload</u>	
Antenna	1.8
Microwave	515.6
Digital	41.0
<u>Bus</u>	313.0
TT&C (48)	
Controls (37)	
Power (177)	
Thermal (51)	
<u>Spacecraft</u>	871.4
<u>Capability</u> (43% DOD)	1,072
Margin	200.6

**TABLE 4-39. BUS SUBSYSTEM POWER**

Bus Subsystem		Power (Watts)	
TT&C			48
Despun		43	
S band transponder	(26)		
Command processor	(11)		
Remote multiplexers	(2)		
Despun encoder	(4)		
Spun		5	
Controls			36.5
Despun			
Antenna positioning electronics		2.5	
Spun		34	
Power			92
Summer solstice	92		
Eclipse	(177)*		
Thermal			51
Total			228
			(313)*

#### 4.1.4.6 Conclusion

The LEASAT spacecraft can be readily adapted to accommodate the 30/20 GHz program. The new 30/20 GHz spacecraft will satisfy all mission objectives, minimize shuttle launch costs, and provide ample payload weight and power margins for future growth.

## 4.2 LAUNCH VEHICLE SYSTEM

### 4.2.1 Introduction

The function of the launch vehicle system (LVS) is to provide an interface between the spacecraft and the shuttle while the spacecraft is in the shuttle; to perform the functions required to separate the spacecraft from the shuttle; and to change the spacecraft's orbit from the shuttle's low altitude orbit to the designated near synchronous drift orbit.

The approach chosen for the LEASAT and for the 30/20 GHz flight experiment system which uses the LEASAT bus is to integrate the LVS into the spacecraft. The spacecraft is injected into transfer orbit by the combination of a perigee kick motor (PKM), which is mounted within the spacecraft structure, and the first burn of a restartable liquid apogee motor (LAM). The spacecraft is then injected into the synchronous orbit by the LAM second burn and the spacecraft reaction control system (RCS). The use of a PKM mounted within the structure of the spacecraft rather than an externally mounted stage, such as the SSUS-A, reduces the length of the shuttle payload. The combination of an integrated PKM, LAM and a widebody satellite (422 cm/14 feet in diameter) results in a shuttle payload which occupies only 17 feet of the shuttle payload bay when the spacecraft antenna is stowed. This short length is a significant advantage because the cost of a shuttle launch and the ability to share a launch with other payloads depends on the ratio of payload length to shuttle bay length or the ratio of payload weight to the shuttle total payload weight capability, whichever is greater. This design approach results in nearly equal ratios for weight and length which is an optimum shuttle payload configuration.

### 4.2.2 Launch Configuration

#### 4.2.2.1 Shuttle Bay Installation

The installation of the payload in the shuttle bay is illustrated in Figure 4-41 and Figure 4-42. The mechanical interface with the shuttle is provided by a reusable cradle, with five contact points between the spacecraft and the cradle, and five contact points between the cradle and the shuttle. The cradle provides mechanical support to the spacecraft during launch; avionics and electrical interfaces between the spacecraft and orbiter; and a means for ejecting the spacecraft from the orbiter.

#### 4.2.2.2 Spacecraft Launch Configuration

Figure 4-43 illustrates the spacecraft launch configuration and the functional operation of the post injection sequences (PES), which will be described later. All switch positions are shown in the launch configuration. Since the battery discharge regulator is off, the spacecraft is unpowered while installed in the shuttle. The spacecraft separation switches are open, hence

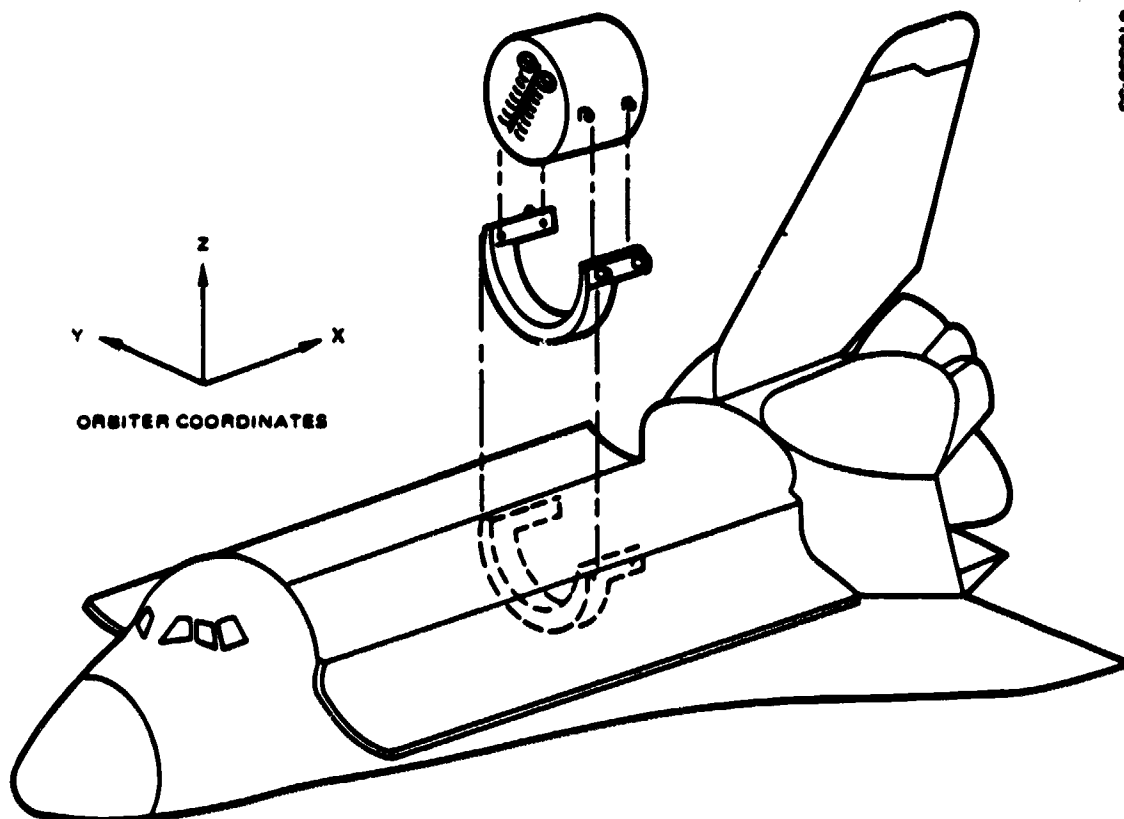


FIGURE 4-41. LAUNCH CONFIGURATION

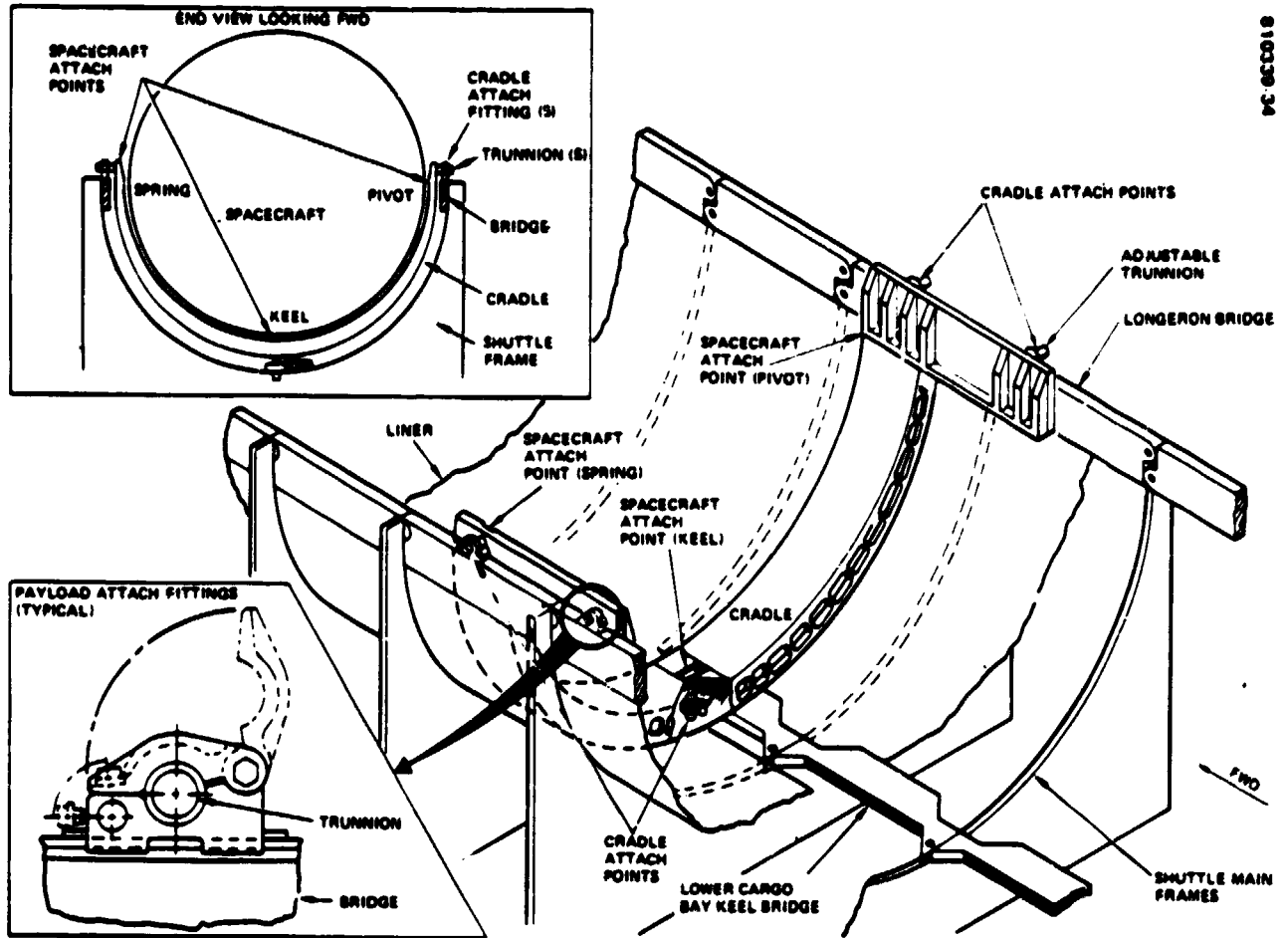
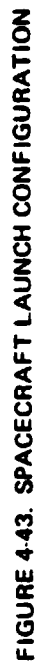


FIGURE 4-42. TYPICAL CRADLE SHUTTLE BAY INSTALLATION



the pyro buses are not powered. There are two umbilical connectors, each of which includes jumpers on the STS side, which inhibit the PES from starting. The g switches are located so that they will change state at a spacecraft spin rate of 30 rpm. They are used to stop spinup and to inhibit certain PES command outputs, as described later. The power disable switches open upon PKM staging and disable the pyro buses. The following describes detailed launch configuration for each subsystem:

- Electrical power subsystem
  - Battery discharge regulator OFF
  - Shunt and tap limiters ENABLED
  - Battery charge/recondition unit OFF
  - Battery cell voltage monitors ON
  - Battery heater controller ENABLED
  - RCS propulsion heaters ENABLED
- Telemetry, tracking and command subsystem

The TT&C units are unpowered at launch but automatically establish the following configuration upon initial application of power

  - Telemetry beacon transmitter 1 OFF (ranging upon PES signal input)
  - Telemetry beacon transmitter 2 OFF (telemetry upon PES signal input)
  - Despun encoder 1 TRANSFER orbit format
  - Despun encoder 2 OFF
  - Spinning encoder 1 and 2 Off
  - Primary remote telemetry units ON
  - Command processor 1 and 2 ON (clear mode)
  - Remote decoders STANDBY (first command to each decoder turns it on, command not executed)
- Communications subsystem
  - All units OFF
- Attitude control subsystem
  - All units OFF
- Propulsion subsystem
  - RCS: 83 percent fraction fill; 352 pounds and 300 psia
  - LAM: 95 percent fraction fill; 4092 pounds; helium at 4200 psia

SPS: Minuteman III; 7308 pounds fuel, 80 pounds additional inerts

All RCS and LAM valves closed at launch.

#### 4.2.3 Launch Operations Description

##### 4.2.3.1 Ascent Operations Overview

This section describes the activities/operations required of the shuttle (STS), the spacecraft, and the ground controllers in order to effect a successful ascent to synchronous orbit. The activities described begin at the time the payload bay doors of the STS are closed for the last time and end with a brief "on-orbit test" description, which is the last activity planned prior to starting service.

The shuttle payload bay doors are closed at nominally L-20 hours. The spacecraft batteries are fully charged, and the spacecraft is completely checked out and reported "ready-for-launch" by this time. Once the payload bay doors are closed, the spacecraft is unpowered (except for special thermal control power later provided by the shuttle) and there will be neither a command nor a telemetry link.

The STS is launched into a 160 nautical mile, 90 minute parking orbit. The STS attitude is controlled such that the payload bay doors are earth facing, and the doors are opened (nominally at L+2 hours). After bay door opening, the payload bay is earth facing, with maximum excursions of 30 minutes sun facing and 90 minutes deep space facing (thermal stabilization between excursions required). Life support systems for the STS are sized for a maximum of 7 days in orbit. The spacecraft will be manifested with at least two other payloads. NASA expects that the first payload will be ejected within 24 hours of launch, and subsequent payloads will be ejected at a rate of one per day.

Spacecraft ejection from the shuttle is nominally 1.5 fps and 2 rpm. The postejection sequencer (PES) starts and automatically turns on the spacecraft, deploys the TT&C antenna, spins up the spacecraft to 35 rpm, fires the perigee kick motor to place the spacecraft into the first elliptical subtransfer orbit, and turns on the required heaters, all at the proper time. In order to achieve the target apogee altitude for injection into synchronous orbit, three augmentations are required using the liquid apogee motor (LAM) bipropellant subsystem (see Figure 4-44). These augmentations are ground controlled and timed to occur at perigee. Once reaching the target apogee, the LAM is used again to inject the spacecraft into synchronous orbit. Upon achieving synchronous orbit, the spacecraft is configured for earth pointing and a comprehensive on-orbit test is performed to verify spacecraft performance. Upon completion of the test, the spacecraft is placed into service.

##### 4.2.3.2 Prelaunch Through Shuttle Ejection Sequence of Events

As shown in Table 4-40, and Figure 4-45, the shuttle payload bay doors are planned to be closed for the last time at launch minus 20 hours.



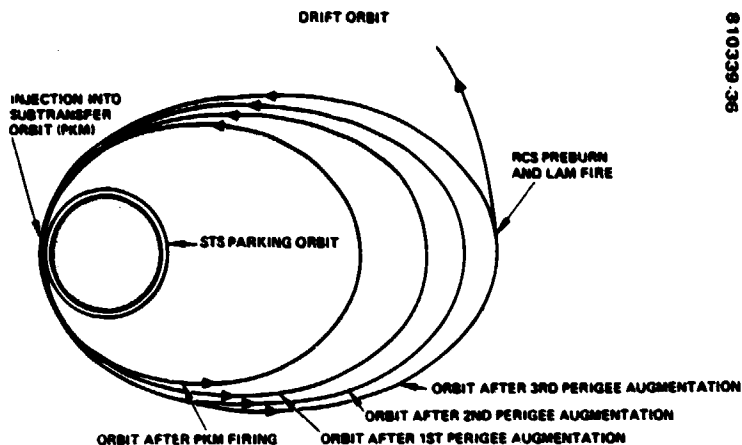


FIGURE 4-44. ASCENT OPERATIONS OVERVIEW

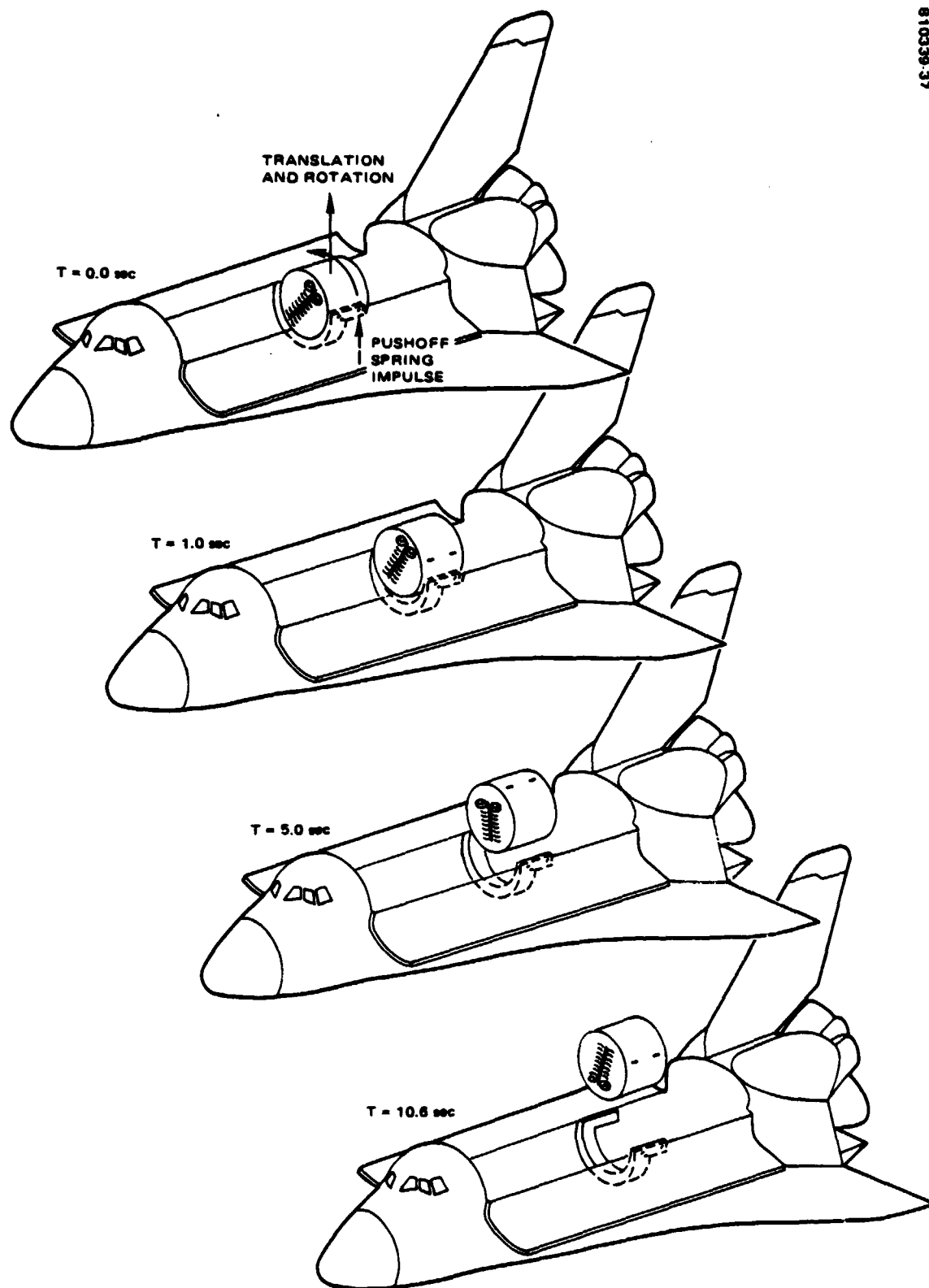
The batteries will be fully charged and the spacecraft will have been completely checked out and reported ready-for-launch prior to door closure. Purge gas temperature in the payload bay following door closure will be  $65 \pm 5^\circ\text{F}$ .

Just prior to launch, the STS SCU and tape recorder will be turned on to monitor engineering data. These data will not be available real time, but will be made available by NASA for postflight analysis. These data could prove to be especially useful, in case of a launch abort, to determine the environmental conditions to which the payloads were subjected. The data will include the following:

- 1) Accelerometer measurements
- 2) Strain gauge measurements
- 3) PKM temperature
- 4) Cradle temperature
- 5) Solar panel temperature
- 6) Propulsion tank temperature

Just prior to opening of the shuttle payload bay doors, the following spacecraft heaters will be enabled. These heaters are thermostatically controlled (on at  $65^\circ\text{F}$  and off at  $70^\circ\text{F}$ ):

- 1) Solar panel substrate
- 2) RCS propulsion
- 3) Perigee kick motor
- 4) TT&C antenna actuator



SPACECRAFT EJECTION

FIGURE 4-45. SPACECRAFT EJECTION

**TABLE 4-40. PRELAUNCH THROUGH SHUTTLE  
EJECTION SEQUENCE OF EVENTS**

L - 20 hr	Close STS bay doors
L - 5 min	Turnon SCU and tape recorder
L = 0	Liftoff
L + 2 hr	Turnon shuttle powered spacecraft heaters
	Open STS bay doors
S-TBD	Enable and activate 4 cradle pin motor drivers
S-TBD	Prepare TV and photographic equipment
S - 5 min	Disable all STS powered spacecraft heaters
S = 0	Fire spacecraft hold-down mechanism squibs
	1) Spacecraft ejection velocity $\approx$ 1.5 fps
	2) Spin rate $\approx$ 2 rpm
S + 5 min	Turnon cradle electronics heater

There are four cradle pins and a spring holddown which must be released in order to effect spacecraft ejection from the shuttle. Control of these mechanisms is via the shuttle SSP. The pins will be sequentially driven (keel pin last) while monitoring their position on the CRT. Once all pins have been released, the circuit to perform spring holddown squib firing will be enabled via the SSP. Time of squib firing will be controlled such that the PKM will fire at the correct orbit location near perigee, 45 minutes after spacecraft ejection from the STS. The separation springs and mechanisms will be sized such that the ejection velocity will nominally be 1.5 fps (1 fps minimum) and the spin rate will nominally be 2 rpm.

Prior to spacecraft ejection, all shuttle powered spacecraft heaters will be turned off via the SSP. Actual separation is planned to be viewed via closed circuit TV at the cockpit, and the event will be photographed using a hand-held high speed movie camera.

Subsequent to spacecraft ejection, the cradle and cradle electronics heaters will be turned on to keep the cradle and electronics above survival temperatures.

#### 4.2.3.3 Post Ejection Sequencer Activities (Coast Phase)

As shown in Table 4-41, upon spacecraft separation from the shuttle, both umbilical connectors will open and the spacecraft separation switches will actuate, resulting in activation of pyro bus 1 and 2 which power the PES and the spun squib and solenoid drivers. Since the inhibit jumpers wired into the umbilical are now removed, both PESs will start, and the preprogrammed sequence specified below will occur. The g-switches have been selected and are located so that they will close upon sensing a 35 rpm spin rate. Signals up to and including the spinup jet fire are logic OR'ed with the inverted g switch signal, hence the timer will only output these signals when the spacecraft is spinning at less than 35 rpm. Spin jet firing will therefore be terminated by the g switch closures at 35 rpm. All signals after spinup jet firing are logic OR'ed with the g-switch signal, hence the spin rate must be greater than 35 rpm for these activities to occur.

TABLE 4-41. POST EJECTION SEQUENCER ACTIVITIES (COAST PHASE)

S = 0	Separation switches activate and both umbilicals disconnect
S + 60 sec	Spacecraft powerup
S + 70 sec	Enable antenna arming relays
S + 75 sec	Enable TT&C antenna deployment
S + 80 sec	Fire TT&C antenna deployment
S + 180 sec	Activate T&C links
S + 190 sec	Open RCS latch valves 1 and 2
S + 195 sec	Open RCS latch valves 1 and 2
S + 200 sec	Fire spinup jets
S + 14 min 0 sec	Close RCS latch valves 1 and 2
S + 44 min 56 sec	Arm PKM
S + 44 min 58 sec	Enable PKM
S + 45 min 00 sec	Fire PKM
S + 45 min 05 sec	Disable PKM squib driver
S + 50 min 00 sec	Despun shelf heaters on and disable antenna arming relay

Sixty seconds after separation, the spacecraft bus will be powered by turning on the battery discharge regulator. The spacecraft will still be in the shuttle shadow at this time, hence the batteries will provide the required load current until the spacecraft is no longer shadowed. The following units will turn on at this time:

- 1) Battery discharge regulator
- 2) Shunt and tap limiters
- 3) Battery strip heaters
- 4) RCS propulsion heaters
- 5) Despun encoder 1
- 6) Primary RTUs
- 7) Command processor 1 and 2
- 8) All squib/solenoid drivers

The next activity is deployment of the omni antenna. To meet NASA safety requirements, there must be a three command sequence. Two independent ENABLE commands followed by FIRE are used.

The spacecraft command and telemetry links will be configured by turning on the following units into their proper configuration:

- 1) Telemetry beacon transmitter 1 (ranging)
- 2) Telemetry beacon transmitter 2 (telemetry)
- 3) Attitude control electronics 1 and 2
- 4) Spinning encoders 1 and 2

Spinup to 35 rpm is the next activity. Both latch valves are opened. The PES wiring to the latch valves will be cross-strapped such that the relative timing between PES 1 and 2 and the proper operation of both PES units can easily be determined during system test by reviewing the current signatures. Spinup jet firing is initiated 200 seconds after spacecraft separation, meeting the NASA safety requirements under worst case assumptions. Both spinup jets will be fired using 19.7 pounds of RCS fuel. Spinup will be terminated upon g switch closure. A backup to termination of spinup is the removal of the PES signal at the time equivalent to twice spinup. Twice spinup time was selected to allow for the possibility of only a single spinup jet working. A third backup is the closure of the RCS latch valves.

Per NASA safety directives, PKM fire is to occur 45 minutes after spacecraft separation and require a three command sequence. The preprogrammed PES sequence of ARM, ENABLE, and FIRE is issued 45 minutes after spacecraft separation, consistent with these requirements. The PKM will fire for 61 seconds, burning 7305 pounds of propellant resulting in a subtransfer orbit period of approximately 6 hours.

Finally, to place the spacecraft in a safe, thermal balance configuration, the despun shelf heaters are turned on and the antenna arming relays are disabled.

#### 4.2.3.4 Transfer Orbit Operations

As shown in Table 4-42, depending on the injection opportunity selected, ground acquisition is expected approximately 10 minutes after PKM burn. Spacecraft status, including orbit and attitude determination, is monitored and should corrective action be required, ground commands will be used. Planned spacecraft command sequences for battery charge management, LAM heater turnon and LAM pressurization are issued.

The PKM is released during the first subtransfer orbit, near apogee. The PKM wire cutter and release nut squibs (8 release nuts) are fired in a sequence such that no more than four squibs fire simultaneously. Upon PKM separation, the power disable switches open, disconnecting the pyro buses. Attitude and orbit determination take place for the remainder of the orbit in preparation for the first perigee augmentation activity.

**TABLE 4-42. TRANSFER ORBIT  
OPERATIONS**

- Ground acquisition
- Spacecraft health verification
- Battery charge management
- LAM heater turnon and pressurization
- PKM staging
- Attitude and orbit determination
- Configure PACE and ENABLE
- LAM fire at perigee
- Attitude and orbit determination
- Reorientation for apogee boost
- LAM burn and spin rate control

The perigee assist control electronics (PACE) is turned on and configured for the first LAM augmentation. Nominally, PACE measures the earth chord width as determined by the selected reference sensor and fires the LAM at the appropriate point in the orbit based on a detected  $45^\circ$  chord width and a programmed time delay. The LAM firing duration is also programmed into the firing timer. A backup mode exists within the PACE such that a time delay to LAM fire can be programmed. This technique would be used should the Earth chord mode fail to function properly, requiring ground determination of perigee time for firing based on accurate orbit determination.

The required delta V for perigee augmentation to achieve a 450 nautical mile biased apogee is 2040 fps. This requires an expenditure of 1378.3 pounds of fuel and a total fire duration of 34.7 minutes, based on worst case assumptions. Actual LAM unit performance data is used during the mission to predict the firing durations. For 98 percent efficiency, the burn time should not exceed approximately 10 minutes. Therefore, it is expected that three augmentations will be performed, two burns would result in a fuel penalty of approximately 26 pounds. Detailed attitude and orbit determination will, of course, be performed after each maneuver.

Upon achieving the desired transfer orbit, the spacecraft is reoriented for the apogee boost attitude. Using the LAM subsystem results in a total reorientation time of approximately 45 minutes, requiring the expenditure of 28.4 pounds of LAM fuel.

It is expected that two LAM burns will be required for AMF, the first being the coarse maneuver and the second a trim. The LAM burns require 2600 pounds of fuel and take 67 minutes. To correct for any spin changes resulting from uncertainties of LAM cant angles, RCS jets are fired in parallel with LAM fire, as required. A total of 12.9 pounds of RCS fuel is budgeted for spin rate control.

TABLE 4-43. EARLY ON-ORBIT OPERATIONS

<u>Drift orbit</u>
Orbit trim
Reorientation to orbit normal
Battery management
Master oscillator turnon
Station acquisition
<u>Earth acquisition</u>
Fire squibs to unlock despun shelf
Despin and acquire earth on selected sensor reference
Deploy UHF antennas
<u>On-orbit test</u>
Spacecraft functional checkout
Payload functional checkout and performance test

#### 4.2.3.5 Early On-Orbit Operations

Once the spacecraft has been injected into near-synchronous orbit, the RCS is used to reduce orbit eccentricity and remove any other orbit variations introduced (see Table 4-43). A delta V of 150 fps with RCS fuel requirements of 47.4 pounds is budgeted for this activity. The spin axis is reoriented to orbit normal to establish the final operational attitude. A maximum 118.5° reorientation requires 13.3 pounds of LAM fuel and takes 66 minutes. Minor delta V and attitude trim corrections complete the station acquisition activities.

The drift orbit is expected to last less than 30 days. In addition to the usual orbital attitude determination, tracking, and telemetry data evaluation performed throughout, predictions of solar eclipse times are used to begin a battery charge management strategy for all batteries. The master oscillator will be turned on during the drift orbit prior to its use, to provide a maximum "on-time" (bake-out).

Synchronous orbit operations begin with release of the despun platform locks, despinning of the despun shelf by turning on a BAPTA motor, and deploying the antenna. Upon successful earth pointing of the antenna, the spacecraft units are functionally checked out, including switching to redundant units.

Payload functional checkout is designed to verify proper operation of each channel. Upon completion of the "on-orbit test", the satellite is placed in service.

### 4.3 SPACE SEGMENT RELIABILITY

Estimates of the reliability of the 30/20 GHz flight experiment's space segment are given in Tables 44 and 45. The reliability shown, which is calculated from the number and type of parts, is relatively high compared to that of current communication satellites. This is due to the shorter life (2 and 4 years compared with 7 to 10 years) and the smaller number of traveling wave tube amplifiers (TWTAs) required for success. Of course, this analysis does not account for the immaturity of much of the technology involved and the lack of experience in designing, building, and operating such a system.

TABLE 44. 30/20 GHz RELIABILITY FOR VARIOUS SUCCESS CRITERIA  
MISSION DURATION: 2 YEARS

Items	Full Capacity	Full Trunk Capacity	Full CPS Capacity	Partial Capacity		
				Loss of ≤1 Trunk Beam ≤2 Scan Beam Spots	Loss of ≤1 Trunk Beam	Loss of ≤2 CPS Spots
Antenna subsystem	0.8494	0.9981	0.8499	0.9795	0.9882	0.9832
Microwave subsystem	0.9732	0.9732	0.9861	0.9851	0.9952	0.9861
BBP	0.9842	0.9999	0.9842	0.9842	0.9999	0.9842
Payload	0.8136	0.9713	0.8249	0.9503	0.9834	0.9543
Bus	0.9744	0.9744	0.9744	0.9744	0.9744	0.9744
Boost	0.991	0.991	0.991	0.991	0.991	0.991
System reliability	0.7857	0.9379	0.7965	0.9176	0.9496	0.9216

\*This allows one spot failure in each beam.

TABLE 45. 30/20 GHz RELIABILITY FOR VARIOUS SUCCESS CRITERIA  
MISSION DURATION: 4 YEARS

Items	Full Capacity	Full Trunk Capacity	Full CPS Capacity	Partial Capacity		
				Loss of ≤1 Trunk Beam ≤2 Scan Beam Spots	Loss of ≤1 Trunk Beam	Loss of ≤2 CPS Spots
Antenna subsystem	0.7537	0.9867	0.7398	0.9568	0.9872	0.9609
Microwave subsystem	0.9025	0.9025	0.9481	0.9462	0.9906	0.9481
BBP	0.9534	0.9999	0.9534	0.9534	0.9999	0.9534
Payload reliability	0.6485	0.8904	0.6814	0.8335	0.9778	0.868
Bus	0.9232	0.9232	0.9232	0.9232	0.9232	0.9232
Boost	0.991	0.991	0.991	0.991	0.991	0.991
System reliability	0.5933	0.8146	0.6228	0.7625	0.8946	0.7947

\*This allows one spot failure in each beam.



The estimate shows a very high probability (0.92) that at least partial experiments in both trunk and CPS modes can be carried on for a minimum of 2 years and a high probability (0.76) that this capability will be available for 4 years. This partial capability is quite adequate. Since there are 16 spots in the uplink and 10 spots in the downlink for each scan beam, the loss of a single spot in each beam is easily tolerated. The three trunk nodes remaining if one trunk transponder is lost are adequate to meet the objectives of trunk experiments.

The reason for the lower reliability of the CPS relative to the trunking service is the complexity of the beam forming networks which generate the scanning beams. Although the BBP is the most complex part of the payload, its reliability is high because of the extensive use of large scale integrated circuits.

The model used for the calculations is shown in Figure 4.3-1. The models for each of the payload major elements are shown in Figures 4.3-2 through 4.3-5. The bus reliability shown is the result of detailed calculations made as part of the LEASAT program. The probability of successful boost and orbit insertion (0.991) is based on historical data. This reliability may be different for shuttle launch but the difference will have a negligible effect on overall reliability. The payload model shown in Figures 4.3-1 through 4.3-3 is for complete success. The model is modified for the partial success case. Other characteristics of the model are as follows:

- 1) Basic electronic failure rates as given in MIL-HDBK-217C
- 2) Mission duration:

2 years	(17,520 hours)
4 years	(35,040 hours)
- 3) Electrical stress ratio is assumed to be equal to 20 percent; the exception, tantalum capacitors, is equal to 50 percent.
- 4) Dormant failure rate is assumed to be 10 percent of operating failure rate
- 5) All components' useful life, time to wearout, is significantly greater than the proposed mission duration.



FIGURE 4.3-1. 30/20 GHZ PAYLOAD RELIABILITY BLOCK DIAGRAM

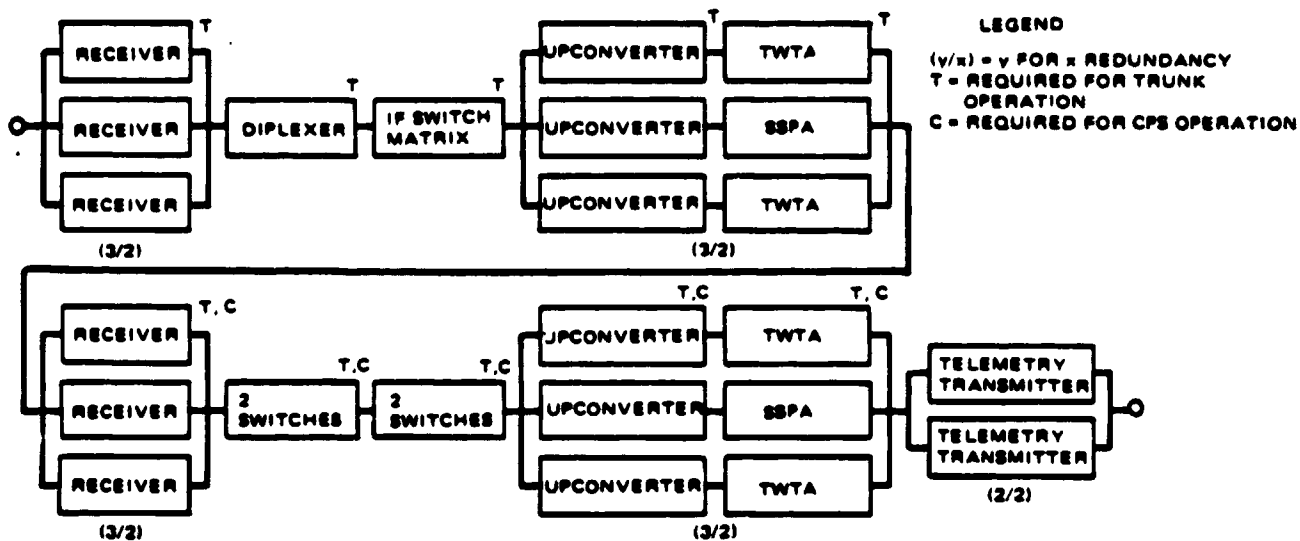


FIGURE 4.3-2. MICROWAVE SUBSYSTEM RELIABILITY BLOCK DIAGRAM

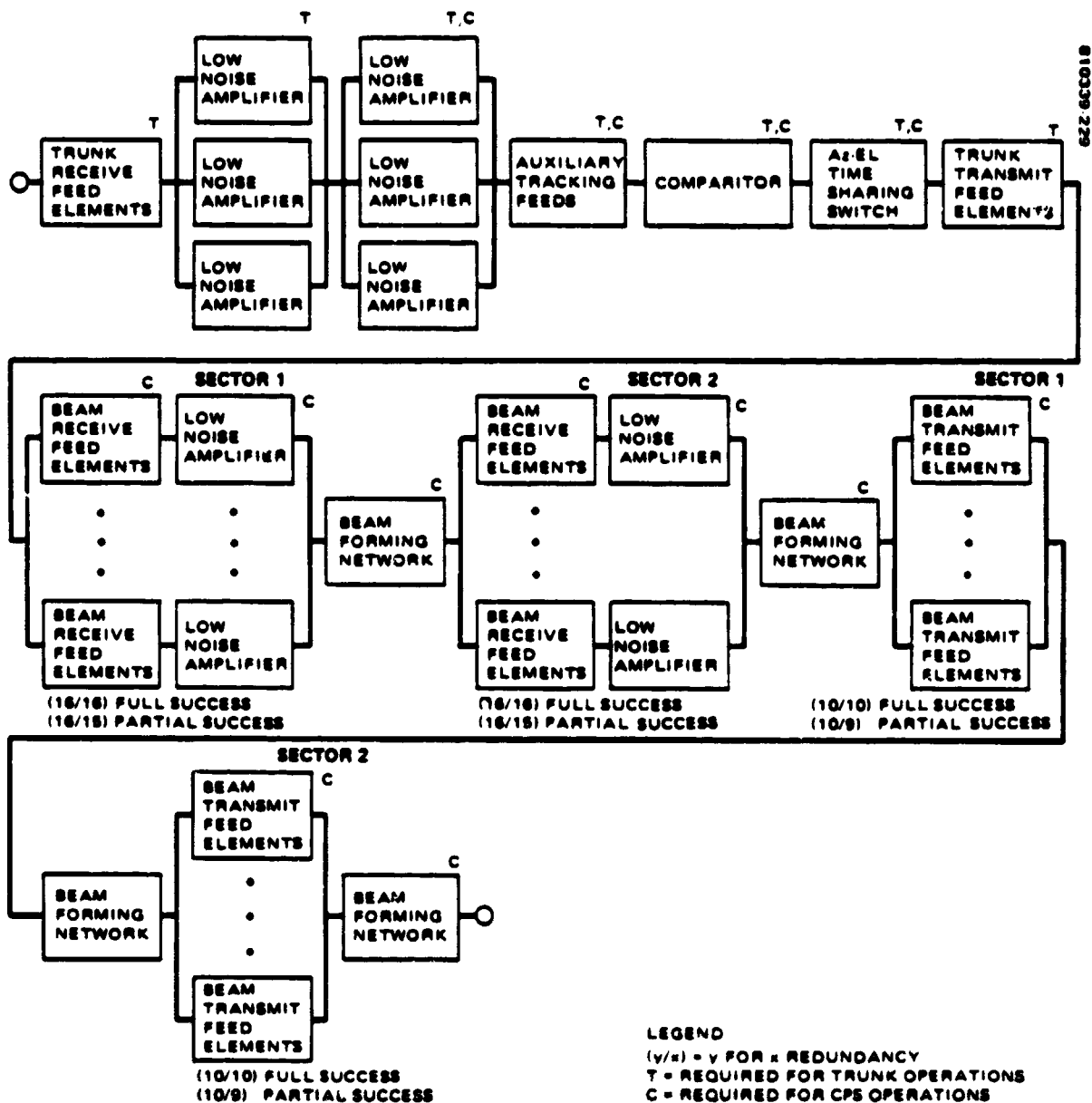


FIGURE 4.3-3. COMMUNICATION ANTENNA SUBSYSTEM RELIABILITY BLOCK DIAGRAM

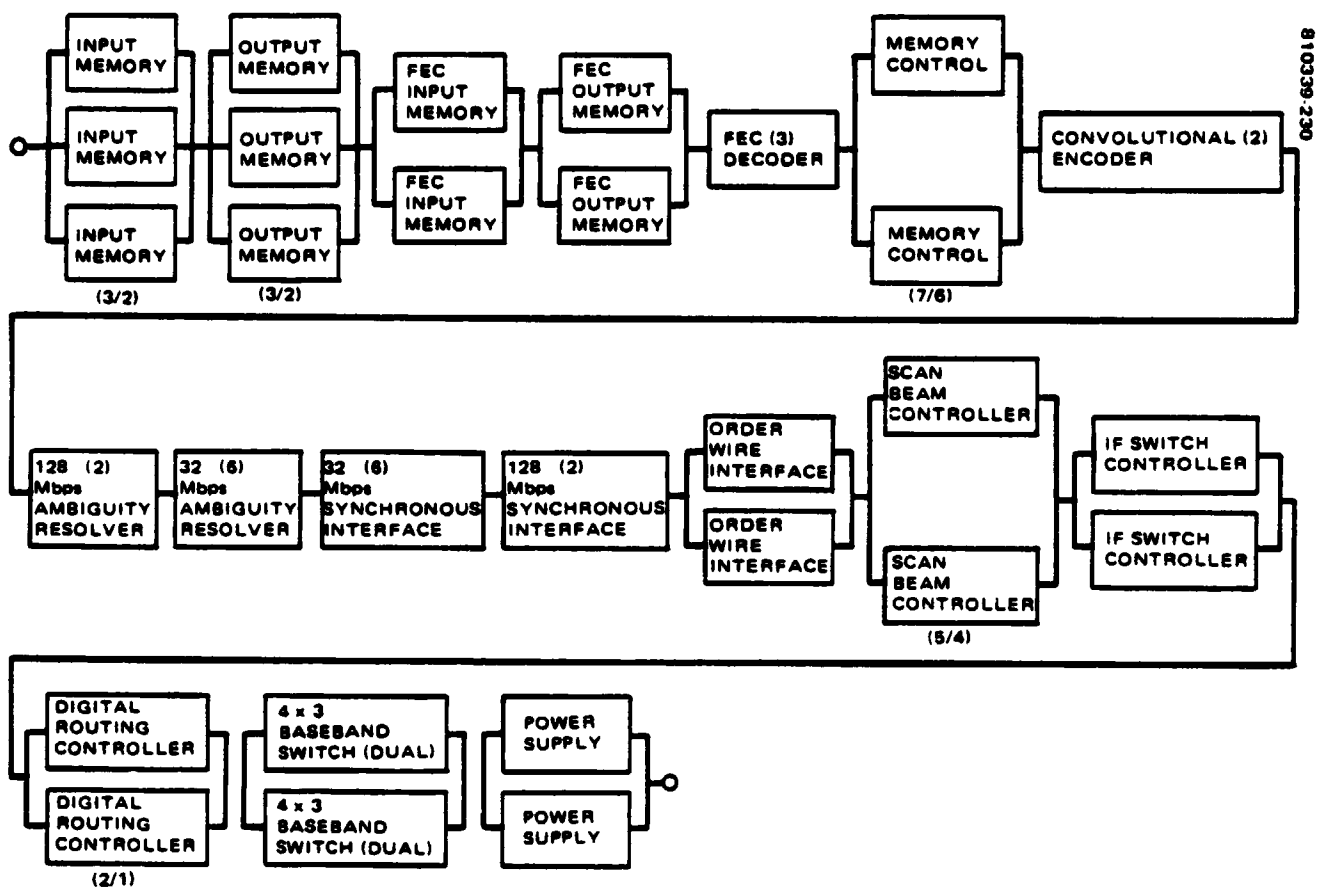


FIGURE 4.3-4. DIGITAL ELECTRONICS RELIABILITY BLOCK DIAGRAM

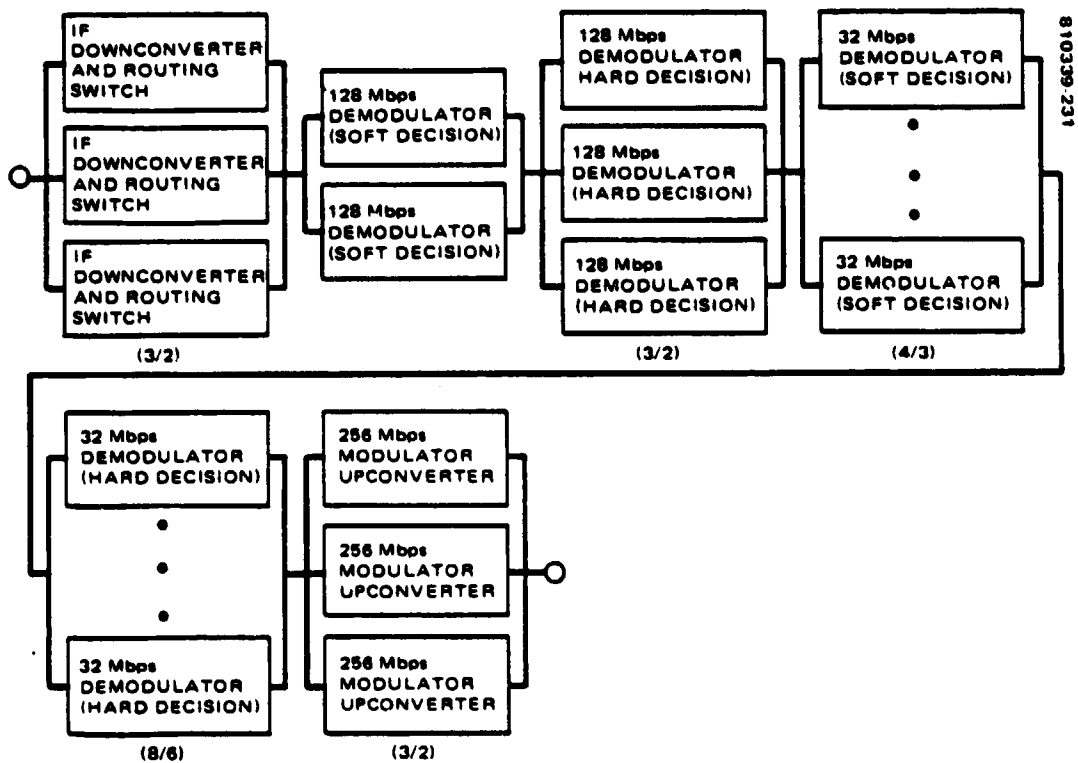


FIGURE 4.3-5. ANALOG ELECTRONICS RELIABILITY BLOCK DIAGRAM

## 5. TERRESTRIAL SEGMENT

The terrestrial segment configuration is illustrated in Figure 5-1. The NASA portion of the system consists of a master control terminal (MCT) and a customer premise service (CPS) station, both in Cleveland. The CPS station is transportable. Other trunk and CPS terminals are to be supplied by experimenters and installed within the satellite antenna coverage pattern.

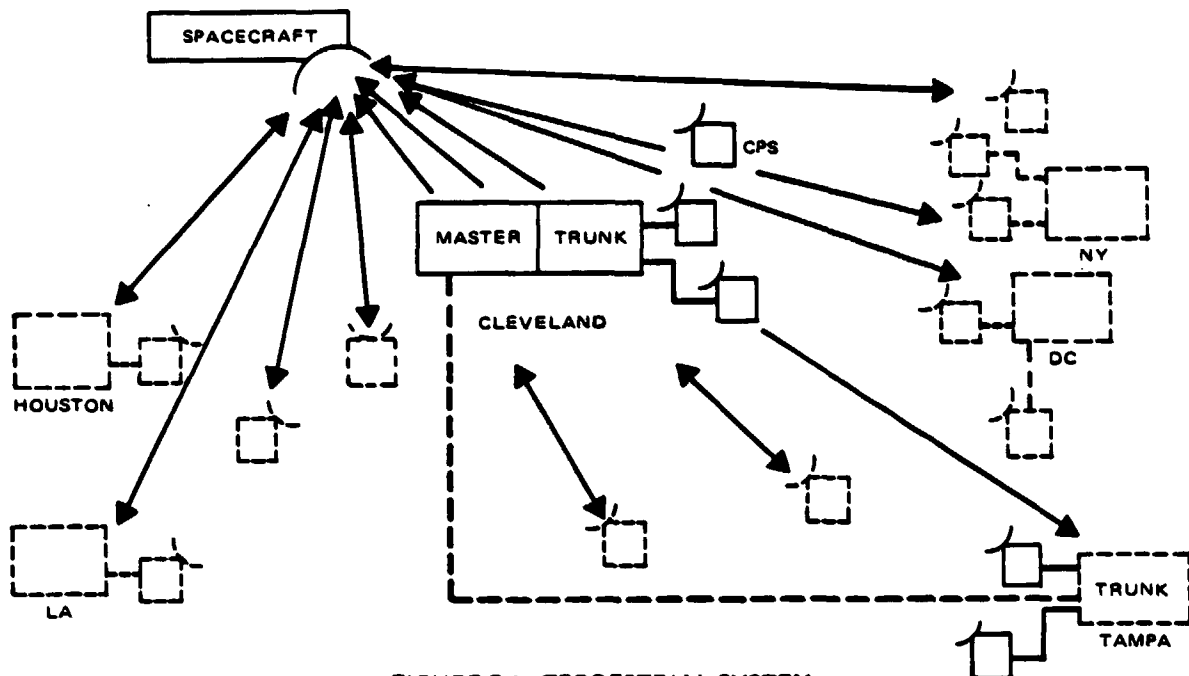
The MCT configuration is shown in Figure 5-2. The central control station (CCS) is the processing and control facility for the entire 30/20 GHz flight experiment. It communicates with the satellite and with other terminals through the MCT trunk station and its associated antenna sites. Two antenna sites are provided to improve trunking service propagation reliability by site diversity. The sites will be separated by a distance, 10 to 20 km, determined by the sites selected by NASA. A diversity switch connects the antenna site which is most suitable at any time to the trunk station. The diversity site selection process is described in 5.2.

In addition to providing TS, the MCT, at NASA's direction, also contains a high rate CPS capability. By making use of the 5 meter antenna at the MCT for the high rate CPS the need for an additional 5 meter antenna is eliminated. The low rate CPS uses a 3 meter antenna.

The functional requirements on the terrestrial segment are listed in Table 5-1. The Mission Operations function and its implementation are discussed in 5.3 below. The implementation of the experiment plan is discussed in 5.4.

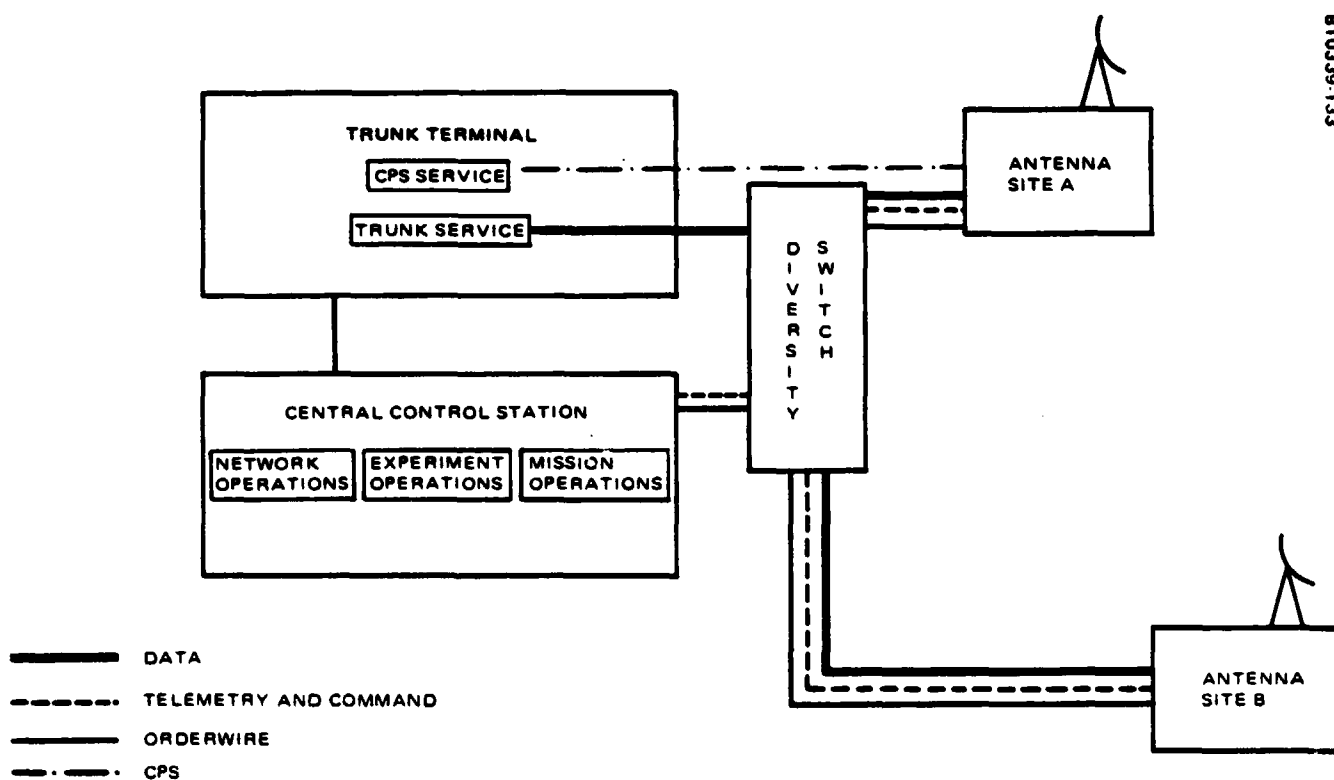
TABLE 5-1. TERRESTRIAL SEGMENT FUNCTIONS

Mission Operations	Communications Operations	Experiment Operations
Launch/transfer orbit Subsystem control Stationkeeping Attitude control	Transmission Payload control Synchronization Station control Link control Channel assignment	Service Technology



810339-132

FIGURE 5-1. TERRESTRIAL SYSTEM



810339-133

FIGURE 5-2. MASTER CONTROL TERMINAL

The communications operation function is divided in two parts. The transmission function, which involves the communication link, was discussed in 2.1. Its implementation is discussed in the following section, 5.1. The requirements for control of the communication link were defined in 2.2. The implementation of these requirements is discussed in 5.2.

## 5.1 IMPLEMENTATION OF COMMUNICATIONS LINKS

The baseband and RF equipment for the ground segment are shown in Figures 5-3 (TS), 5-4 and 5-5 (MCT), and 5-6 (CPS). This section presents a discussion of the RF equipment that consists of the following key components: narrow beam, high gain antennas (3 meter CPS, 5 meter TS); high power TWTAs (200 watts TS, 20 watts CPS); up/downconverters; and low noise amplifiers. The baseband or TDMA equipment is described in 5.2.

### 5.1.1 Antennas

The design of the 5 meter antennas required for the TS stations is based on available equipment with the exception of a new 30/20 GHz feed. The Scientific-Atlanta (SA) antennas are representative of those available. The 5.5 and 7.7 meter versions (Model 8101) are being used on the operational Hughes SBS system. These antennas operate in the transmit frequency range of 14.0 to 14.5 GHz and receive frequency range of 11.7 to 12.2 GHz. The antenna required for the 30/20 GHz will be based on the available SA 5 meter antenna (Model 8008).

The antenna utilizes 24 panels for the precision die-stamped paraboloidal main reflector and has a shaped subreflector to implement a highly efficient Cassegrain feed design. The reflectors, feed, antenna hub, and support and structure form an integral part designed for ease of installation, main-terrace, and optimum transmission. The elevation-over-azimuth mount provides for ample azimuth ( $110^\circ$ ) and elevation ( $45^\circ$ ) adjustments. The antenna can be either fixed or command pointed. Deicing, rain deviator, and a variety of base mounts are available.

A new antenna feed is required to accommodate the 30/20 GHz frequencies. Preliminary concepts and development estimates have been generated based on Hughes' experience with ground radars operating in this band.

The surface loss due to 0.025 inch errors are estimated to be 2 dB at 30 GHz and 0.7 dB at 20 GHz for the 0.36 F/D of this antenna. The presently available accuracies are 0.22 inch (ambient) and 0.035 inch (operating); environmental conditions are listed in Table 5-2.

It is anticipated that with structural design modifications an 0.025 inch surface accuracy can be achieved for the 30/20 GHz main reflector at a reasonable cost.



TABLE 5-2. ANTENNA PERFORMANCE

Parameter	5 m	3 m
Operating frequency, GHz		
Receive	17.7 to	20.2
Transmit	27.5 to	30.0
Feed type	Diagonal horn	Corrugated horn
Gain at midband, dB		
Receive	57.6	53.1
Transmit	60.2	55.8
VSWR	1.3:1	
Polarization	Linear	
Axial ratio, dB	> 35	
Isolation between ports, dB	> 35	> 30
Beamwidth (3 dB), deg		
Receive	0.23	0.36
Transmit	0.14	0.23
Polarization adjustment, deg	360	
Pointing increment, deg	0.007	
Pointing accuracy, deg	0.03	
[ 48 km/hr (30 mph) wind gusting to 72 km/hr (45 mph) ]		
Environmental		
Temperature, °C (°F)	-30 to 50 (-22 to 122)	
Wind: operate/survive, km/hr (mph)	75 (46.5) mph/200 (126)	
Humidity, %	0 to 100	
Solar radiation, mW/cm <sup>2</sup> (Btu/hr-ft <sup>2</sup> )	110 (350)	

Based on the SBS wind environment limit of 75 km/hr, the antenna can be pointed to within an accuracy of 0.03°. This is well within the 30/20 GHz requirement of 0.05°. This performance, plus a tight spacecraft stationkeeping tolerance ( $\pm 0.020^\circ$ ), allows for the use of a fixed pointed antenna during nominal on-orbit operation.

Table 5-2 summarizes the 50 meter antenna data.

The CPS stations will use 3 meter antennas based on an available SA design (Model 8006). A new 30/20 GHz feed will be developed and used with the main reflector in a prime focus quasi-buttonhook arrangement. The reflector consists of six panels, and the antenna pointing is manual. The surface accuracy and pointing accuracy satisfy requirements, i. e., 0.025 inch and 0.03°. Table 5-2 lists the pertinent 3 meter antenna data.

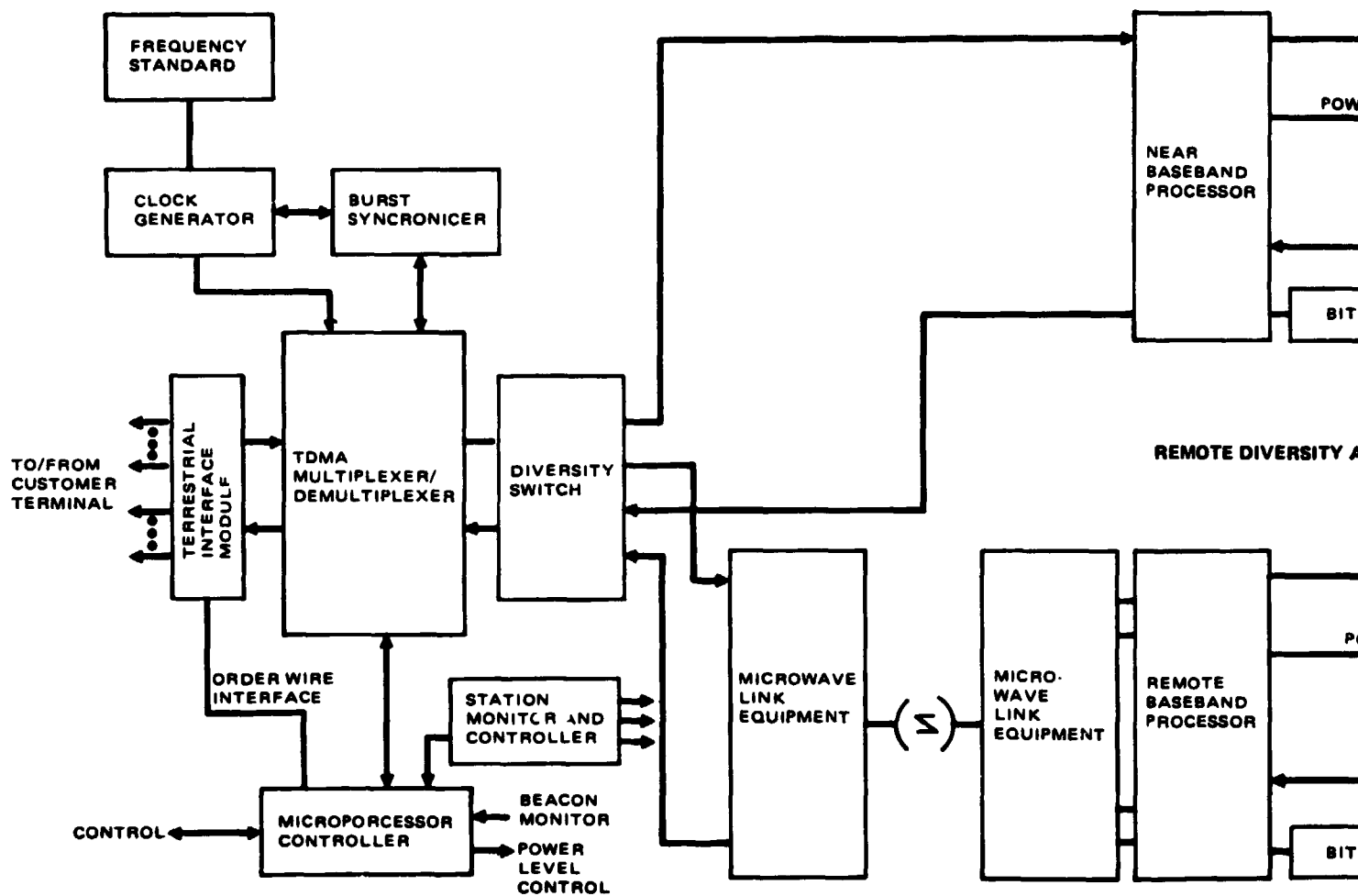
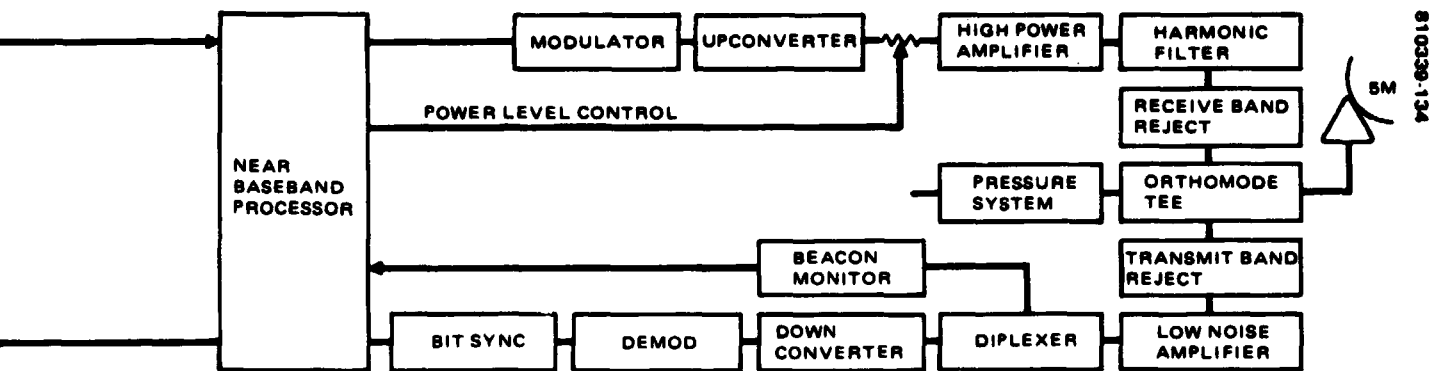
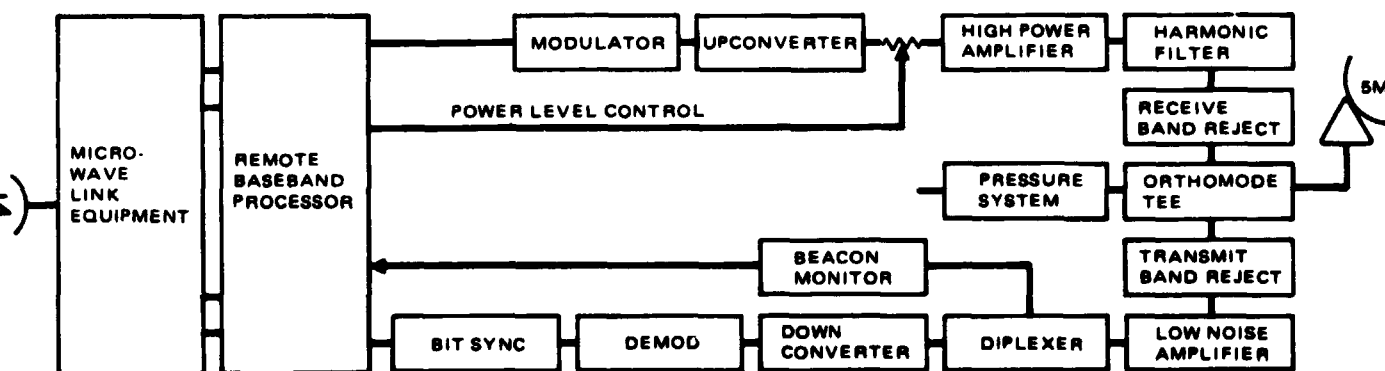


FIGURE 5-3. STANDARD TRUNK STATION HARDWARE CONFIGURATION

**OLDOUT FRAME**



#### REMOTE DIVERSITY ANTENNA SITE



2  
FOLDOUT FRAME

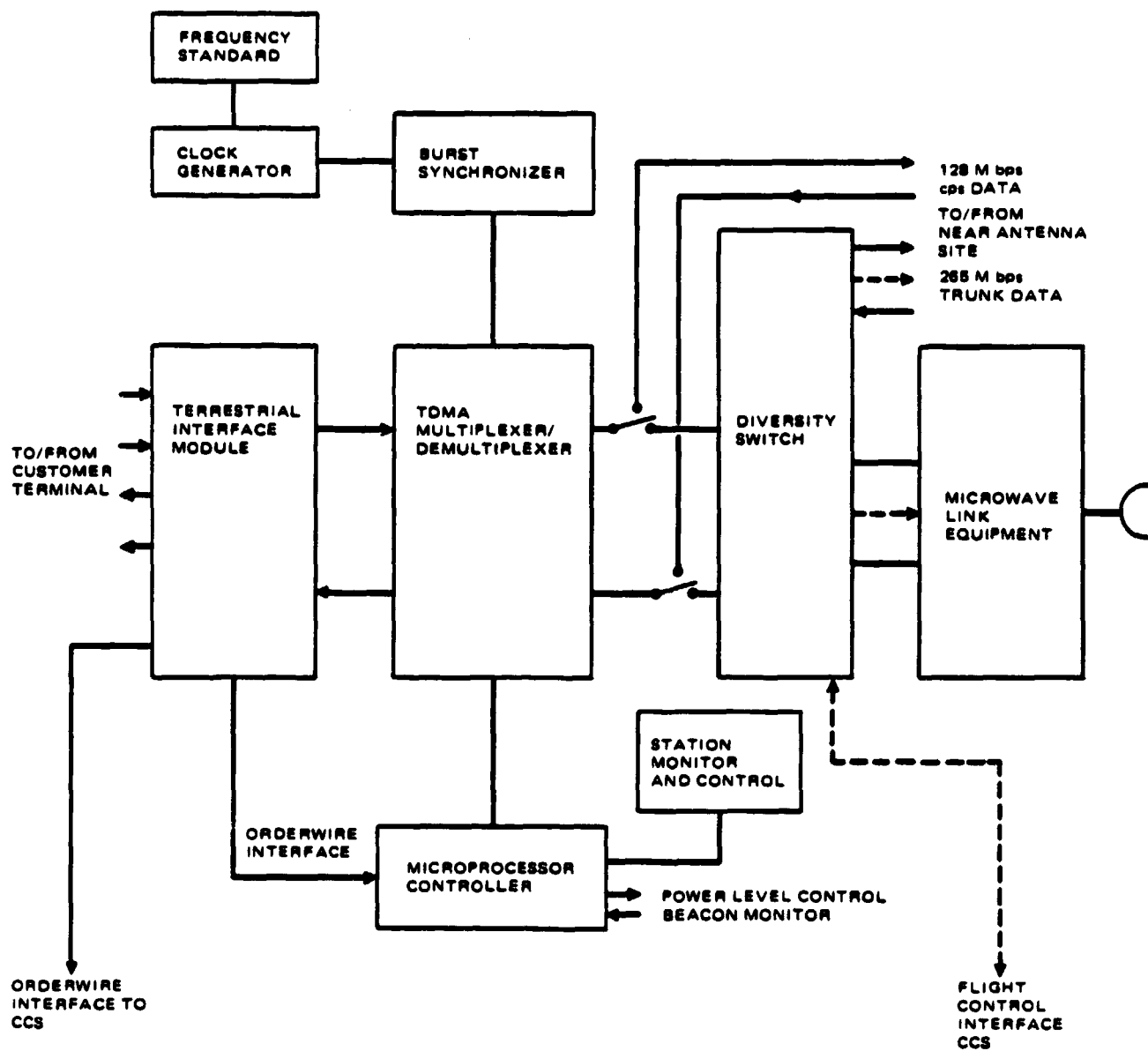
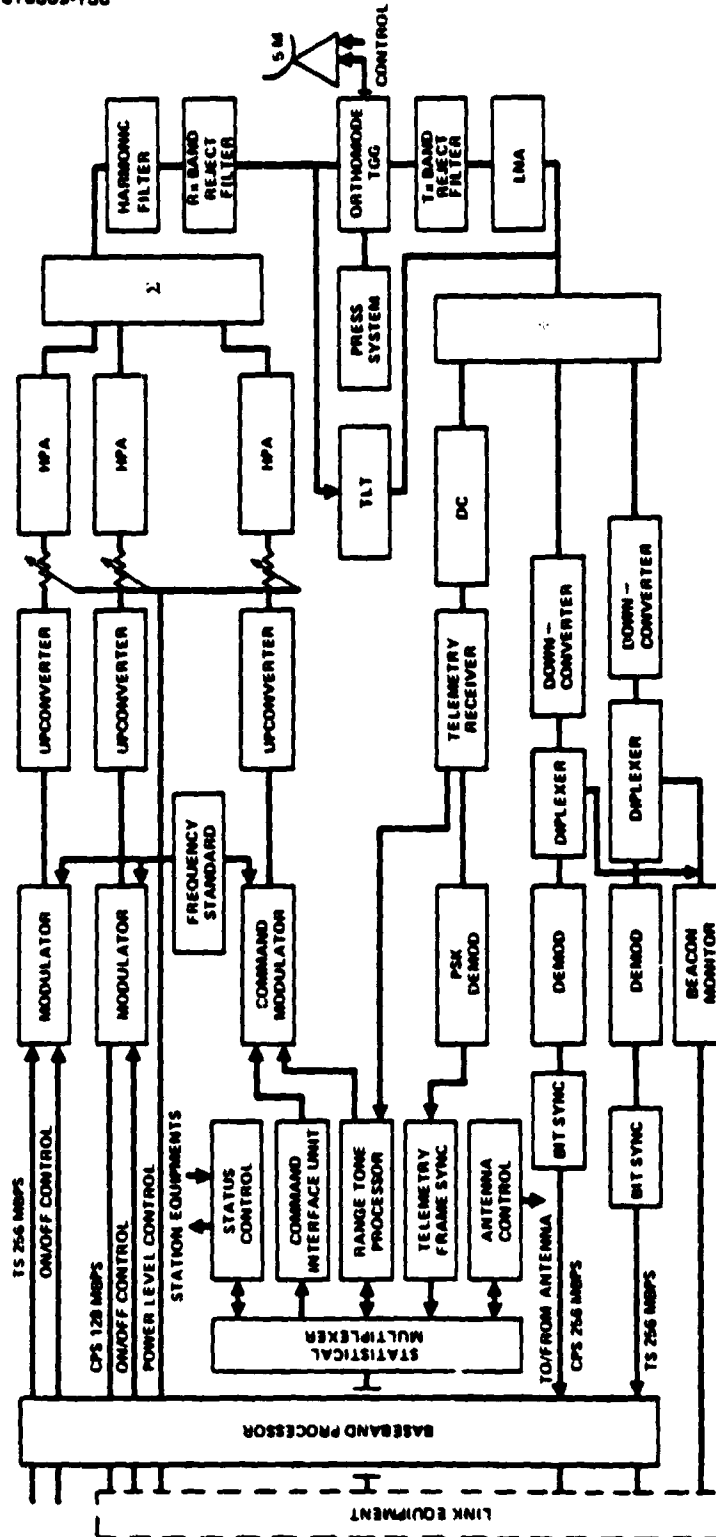


FIGURE 5-4. MASTER CONTROL TERMINAL TRUNK STATION BASEBAND PROCESSING



**FIGURE 5-5. MCT ANTENNA SITE**

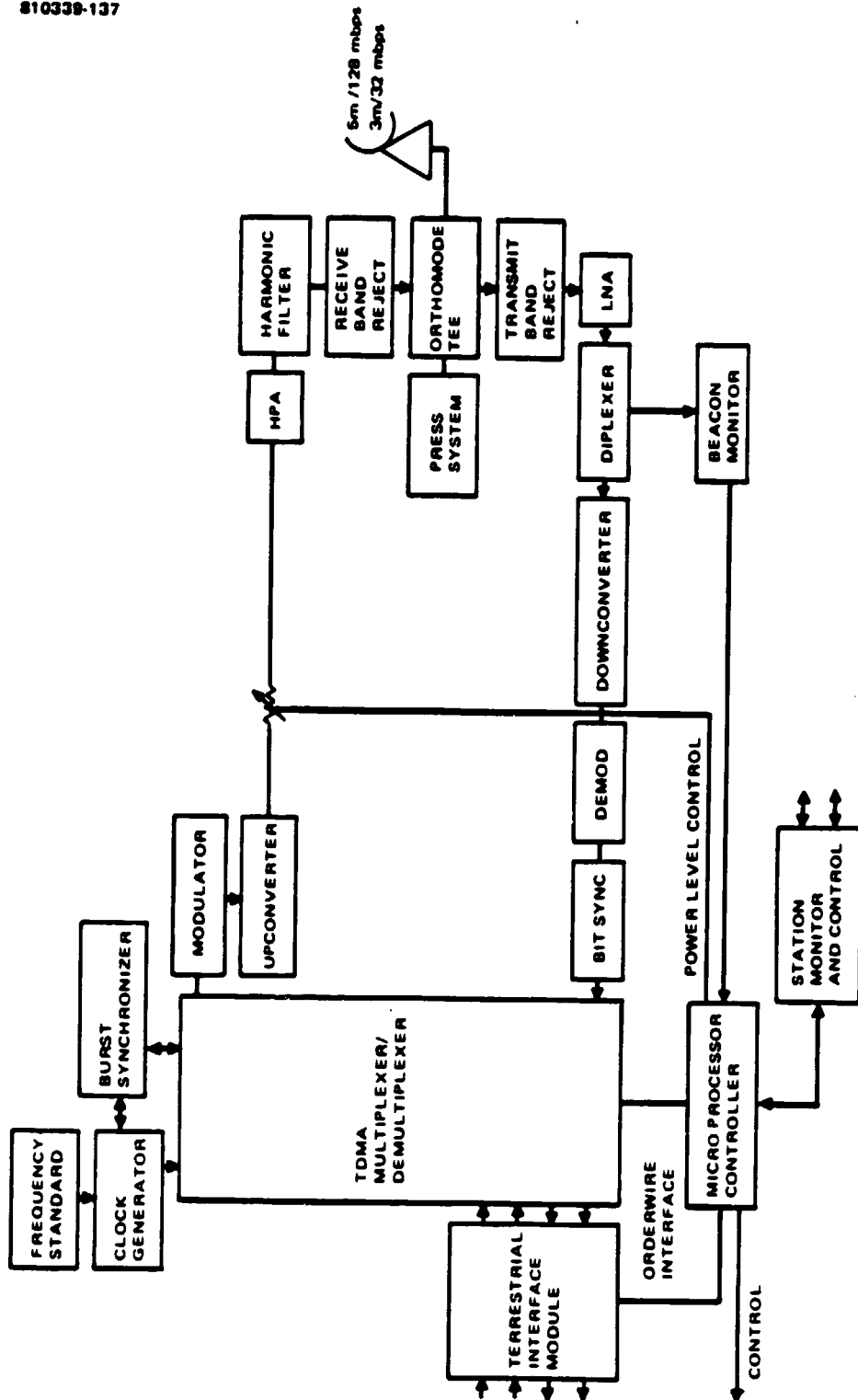


FIGURE 5-6. CUSTOMER PREMISE SERVICE STATION

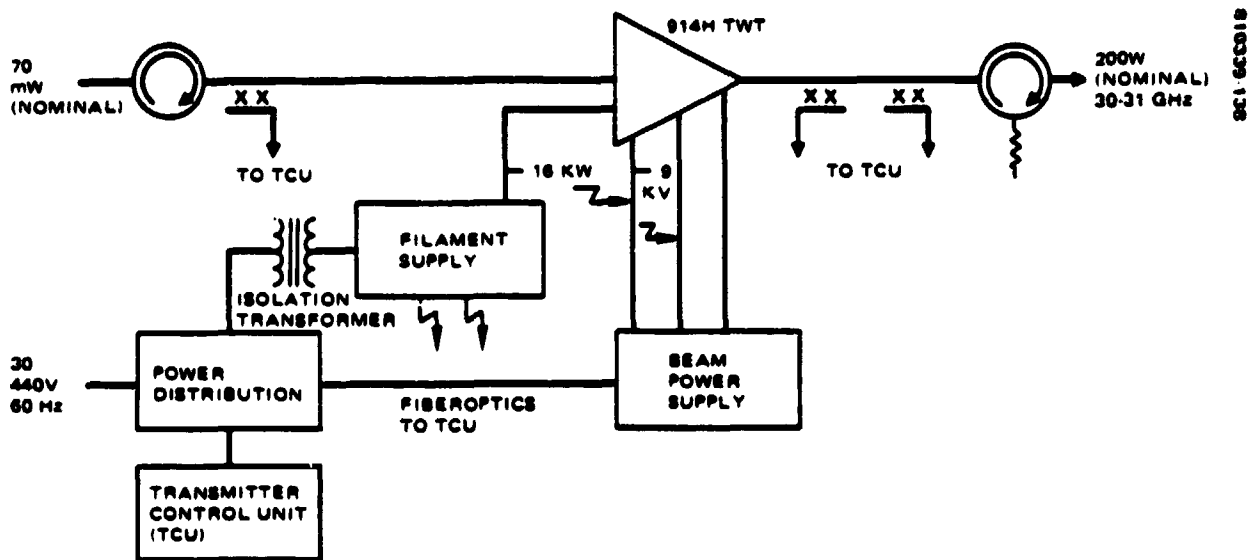


FIGURE 5-7. MM WAVE HPA BLOCK DIAGRAM

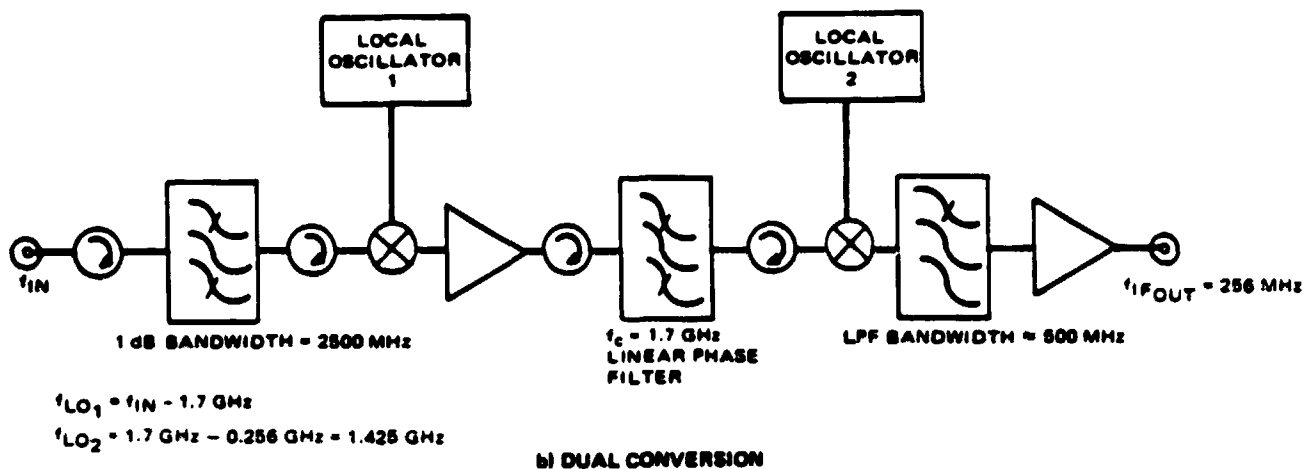
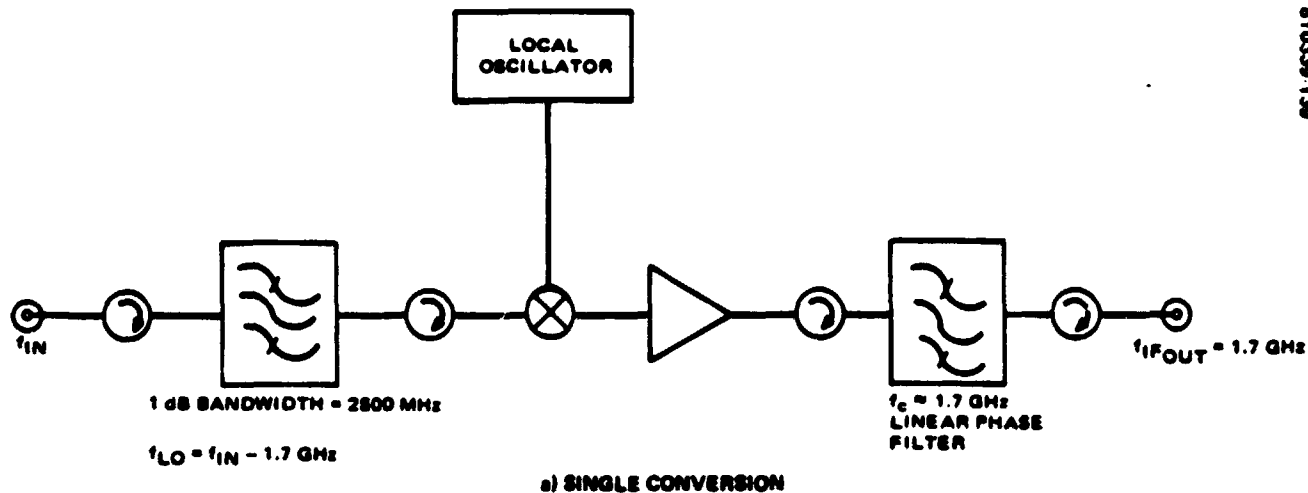


FIGURE 5-8. DOWNCONVERTERS

### **5.1.2 TWT Power Amplifiers**

The 125 watts RF power requirement and 256 MHz bandwidth needed for the TS has resulted in the selection of a TWT. Hughes has developed, tested, and delivered two TWTs (914H) that produced >160 watts from 30 to 31 GHz based on a PPM focused coupled cavity design. The TWT needed for the 30/20 GHz program will be based on this design.

Power for the TWT beam is provided by a modified version of an SCR inverter supply used in a production radar transmitter. This type of supply has proven to be highly reliable in field use under a variety of environmental conditions. Other supplies required for the TWT filament and the logic and controls will be off the shelf standard equipment (see Figure 5-7).

The development of a 20 watt TWT for the CPS will be based on the Hughes 950H, 30 watts at 28 GHz. The tasks required for this effort are to redesign the 950H for higher frequency operation and to generate tooling necessary to produce the tube. Tentative design parameters are shown in Table 5-3.

The tracking and command transmitter in the MCT requires less than 1 watt of RF power output and therefore presents no significant development problem.

### **5.1.3 Downconverter**

Two types of downconverters are shown in Figure 5-8. A dual conversion mode is recommended because of the simplicity of changing channels for a channelized 2.5 GHz bandwidth: only the second local oscillator frequency will need to be changed, while the single conversion scheme will require a filter and local oscillator frequency change. The major cost contribution items derive from the critical requirements of the filters. If the peak-to-peak group delay variation over the band is 3 ns or less, there will be no more than 1 dB degradation in bit error rate (BER). Furthermore, a self-equalized (linear phase) microwave filter can be realized with a -25 dB bandwidth equal to 1.6 times the linear phase bandwidth. While there are tradeoffs to be made, the BER and bandwidth criteria are good guidelines.

The preceding discussion applies to the TS and CPS communications channels. The telemetry channel downconverter (Figure 5-8) can be of a single conversion design feeding standard S band receiver, demodulator, and range tone equipment.

Hughes is one of the few companies that have built converters in the 20 to 40 GHz range. Consideration will be given to adapting these designs to 30/20 GHz usage.

### **5.1.4 Upconverters**

The problems associated with converting intermediate frequencies to 30 GHz are nearly identical to those of downconverting from 20 GHz. Dual



TABLE 5-3. DESIGN PARAMETERS

Frequency	30 GHz
Bandwidth	32/128 MHz
Power output	20 W
Cathode voltage	-7 kV
Cathode current	30 mA
Anode voltage	+200 V
Helix and body current	1 mA
Saturation gain	40 dB
Overall efficiency	25%
Dimensions	
Length	14 in. max
Width	3 in. nom
Height	3 in. nom
Weight	3 lb nom
Cooling	Conduction

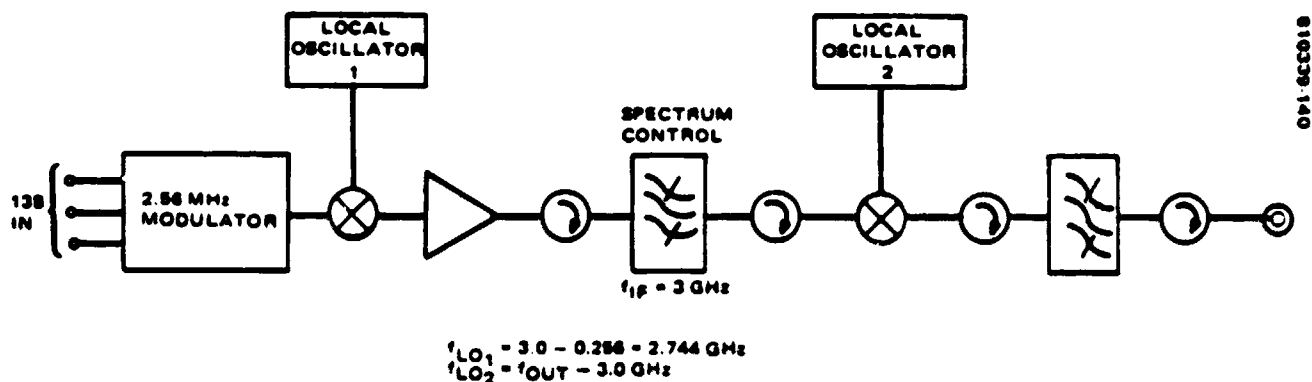


FIGURE 5-9. UPCONVERTERS

conversion is recommended not only for simplicity of changing channels by changing the second local oscillator frequency but also for permitting the spectrum control bandpass filter characteristics to remain unchanged with carrier frequency changes. Figure 5-9 shows a typical configuration for dual conversion. Presently available equipment could be used for the first stage of conversion for the CPS communication channels, i.e., 70 MHz (IF up) to 6 GHz. This would allow operation with available modems.

#### 5.1.5 Low Noise Amplifiers

Based on expected costs, GaAs FET rather than parametric amplifiers will be used for the 30/20 GHz system. GaAs FET devices constitute a new and rapidly expanding technology. Worldwide FET research and development is vigorous and dynamic and can be expected to continue the improving FET

performance trend in the immediate years ahead. Hughes has recently achieved 1.9 dB noise figure in the 20 GHz region. By the mid-1980's such devices could be readily available.

## 5.2 IMPLEMENTATION OF COMMUNICATIONS OPERATIONS

### 5.2.1 Requirements and Design Approach

#### 5.2.1.1 Requirements Allocation

A straightforward systems engineering approach was used to identify the requirements for system elements to satisfy the mission objectives. The approach involved careful allocation of each technical requirement of the system elements to the subsystem level; the investigation of the most promising concepts each element could use to satisfy its allocated requirements; and the selection of design features which are most attractive from the standpoint of performance, cost effectiveness, low risk, and flexibility.

The key requirements which are the major drivers in the system synthesis and the allocation of these requirements are given in Table 5-4.

#### 5.2.1.2 Terrestrial Segment Design Approach

The terrestrial system design uses methods based upon experience in development and operation of satellite communications ground systems such as Palapa, SBS, LEASAT, and Western Union. These methods are designed specifically to provide low life cycle system costs with high system reliability and operability.

The terrestrial system design stresses:

- 1) Automation of routine operations to reduce operations costs and improve operability
- 2) Use of proven design and off the shelf hardware/software to minimize risk and development costs
- 3) Flexibility in function operation to adapt to a variety of experiments
- 4) High reliability and availability of communications links for experiment operations

System availability is provided both by a design that is inherently reliable and easily maintained and by appropriate spares of critical equipment. Flexibility is provided by implementing many station functions in software rather than hardware. The proposed applications software system is of modular structure and data driven through a structured central data base. Thus, the software is readily and reliably modifiable and can be adapted to changing experiment requirements.

TABLE 5-4. TERRESTRIAL SEGMENT REQUIREMENTS ALLOCATION

Requirement	Central Control Station	Trunk Station	CPS Station
Provide communication services at 30/20 GHz	Central control of communication services	Trunk service	CPS service
Provide synchronization of station and spacecraft	Orbit determination Estimated burst transmission time determination	Hierarchy of user services Burst synchronization hardware Position error measurement	Hierarchy of user services Burst synchronization hardware Position error correction
Provide rain margin for link control	Central monitor of station performance and link control	Power level control Diversity switching	Power level control FEC coding
Network operation			
Effective control and scheduling of all system elements	Communications scheduling and planning function Experiment operations system	Responsive to CCS  Orderwire control Terrestrial backup	Responsive to CCS  Orderwire control Terrestrial backup
Alert control personnel to dangerous conditions	Displays and operator controls	Displays and operator controls	Displays and operator controls
Data processing for communication control	Minicomputer system Network control — orderwire operations, assignment algorithm Payload control — data routing, SS-TDM interconnects, beam scanning TDMA synchronization control Satellite oscillator control Station monitor and display Archive processor System data table	Microcomputer system Network and user interface control — orderwire, signaling, multiplexing Link control — power level control, diversity switch control  Status monitor and display	Microcomputer system Station startup and signal acquisition Network and user interface control — orderwire, signaling, multiplexing  Link control — power level control, FEC coding control Status monitor and display
Minimize lifetime cost for hardware and software procurements and development; operations, and maintenance subject to satisfying all other requirements	Optimized manual versus automated implementations Flexible, reliable design Maximum use of available software Central control facility	Maximum use of proven hardware and software	Low cost terminal equipment where possible Minimum equipment complement
Reliability/availability	Standby multiuse processors	Critical equipment spares Reliable design	Critical equipment spares Reliable design
System control shall be designed for rapid recovery from single equipment failures			

Table 5-5 summarizes the terrestrial system design features.

### 5.2.2 Central Control Station

The CCS is a key element in the system, controlling all terrestrial and spacecraft functions. Mission operations, experiment operations, and network operations are centered here. The CCS will be located at the Cleveland trunk site. This combined site is designated the master control

TABLE 5-5. TERRESTRIAL SEGMENT - SUMMARY OF KEY FEATURES

Flexibility	Ease of Operation	Backup Capabilities	Failure-Mode Recovery	Maintainability/Reliability	Existing/Proven
<p>Data driven system</p> <p>Modular system design allows easy upgrade</p> <p>Data base management concept allows operator/analyst access to any archived data</p> <p>Growth capacity in resources</p>	<p>Automation of routine operations</p> <p>Display interactive</p> <p>Automatic flight segment fault detection and alarming</p> <p>Minimal personnel on second and third shift</p>	<p>Three computers, each capable of being configured to support real time operations</p> <p>Resident disk contains software for each subsystem</p>	<p>No single point failures inhibit commanding or telemetry status monitoring</p> <p>Capable of graceful degradation and recovery</p>	<p>Modular design</p> <p>Structured data base</p> <p>Critical spares</p>	<p>Equipment from leading minicomputer manufacturer</p> <p>Off-shelf operating system</p> <p>Command and telemetry processing based on similar Hughes programs</p>

terminal. It will transmit and receive at least one TDMA trunk; it will transmit the spacecraft commands and receive the spacecraft telemetry and beacon signals. Primary payload control functions include baseband processor control, data routing, SS-TDMA interconnects, and CPS beam scanning patterns. Terrestrial control involves network synchronization, link margin control, order wire control, and monitoring of trunk and CPS station operational modes.

The CCS requirements are shown in Table 5-6.

#### 5.2.2.1 CCS Configuration

The CCS is the center for controlling all system operation functions including mission, experiment, and network operations. The functions of mission operations are discussed in 4.2. The facilities and functions of experiment operations are discussed in 2.3. The functions of network operations are discussed in 2.2. The CCS provides personnel, hardware, and software facilities for performing these functions. The configuration of the CCS is shown in Figure 5-10. Figure 5-11 shows a potential layout for the CCS.

The heart of the CCS is the data processing facility. Three identically configured minicomputers are interconnected so that any computer may perform any function. One computer is dedicated to network control, the second to spacecraft control, and the third, primarily a backup for the dedicated computers, may be used for the experiment evaluation and software development.

The CCS controls network stations by orderwire messages. Access to the trunk and CPS orderwire is provided through the communications

TABLE 5-6. CENTRAL CONTROL STATION REQUIREMENTS

<u>General</u>
Focal point for all mission activities. Plan, schedule, and operate flight system and communications network
Provide central data processing facility for computing, storage, and display capacity for all systems activities
<u>Mission Operations</u>
Support prelaunch, launch, and in-orbit operations, including commanding, telemetry analysis, and stationkeeping
<u>Experiment Operations</u>
Support all operations required to conduct communications experiments
<u>Network Operations</u>
Perform network planning to effectively use network resources
Manage and allocate all channel assignments for trunk and CPS station TDMA
Provide nonreal time allocation of trunk channels and reconfiguration of IF switch
Provide nonreal time allocation of CPS scan beam dwell periods and reconfiguration of scan beam format
Provide demand assignment of individual message channels (64 kbps) for CPS service
Provide demand assignment access via orderwire on reservation basis
<u>Data Processing</u>
Provide computing, storage, and display capacity for system operations
Provide computer mainframes and peripheral equipment to allow execution of system control software
Provide disk storage for programs, data base, and files
Provide data base management
Provide capability to interface with communications interface and switching hardware
Provide analyst and operations displays to support systems control
Provide compilers, assemblies, and configuration management tools to support software development and maintenance
Provide software to perform system control functions

station interface panel to the master control terminal communication station. A statistical multiplexer connects the spacecraft control equipment, located at the MCT antenna site, to the CCS mission operations computer. A cesium time standard provides precise timing for synchronization control, terrestrial system/TDMA terminal interface clock matching, and spacecraft oscillator control. The spacecraft control equipment is described in 5.3.

Most of the CCS network control functions are implemented in software. This software is described in 5.2.2.4.

## 5.2.2.2 Data Processing Subsystem

### 5.2.2.2.1 Design Approach

The data processing subsystem design approach is to maximize the use of standard vendor hardware and existing software to satisfy the operations requirements and minimize life cycle cost.

### 5.2.2.2.2 Top Level Architecture

A multitude of options exist for the CCS computer configuration. The basic options include: 1) a large single mainframe, 2) two medium size machines, 3) three or more small machines coupled together in network fashion, 4) combinations of the above. The first option of a single large computer is not desirable based on cost and unreliability of a single point failure. The second option is the next simplest and eliminates the single point failure. Graceful degradation can be provided in this configuration with an appropriate priority driven operating system. The third and fourth methods also meet CCS requirements; however, these are more complex and can reduce the overall system reliability.

Based on these criteria and previous Hughes experience, the approach selected for the CCS is a two machine configuration with a backup. Important considerations in this choice include: 1) two machine configurations of hardware and system software are available from computer vendors (e.g., a dual VAX 1100 series with dual access mass storage supported by the VMS operating system); 2) the mission operations functions and communications management functions are largely separable; and, 3) significant capability

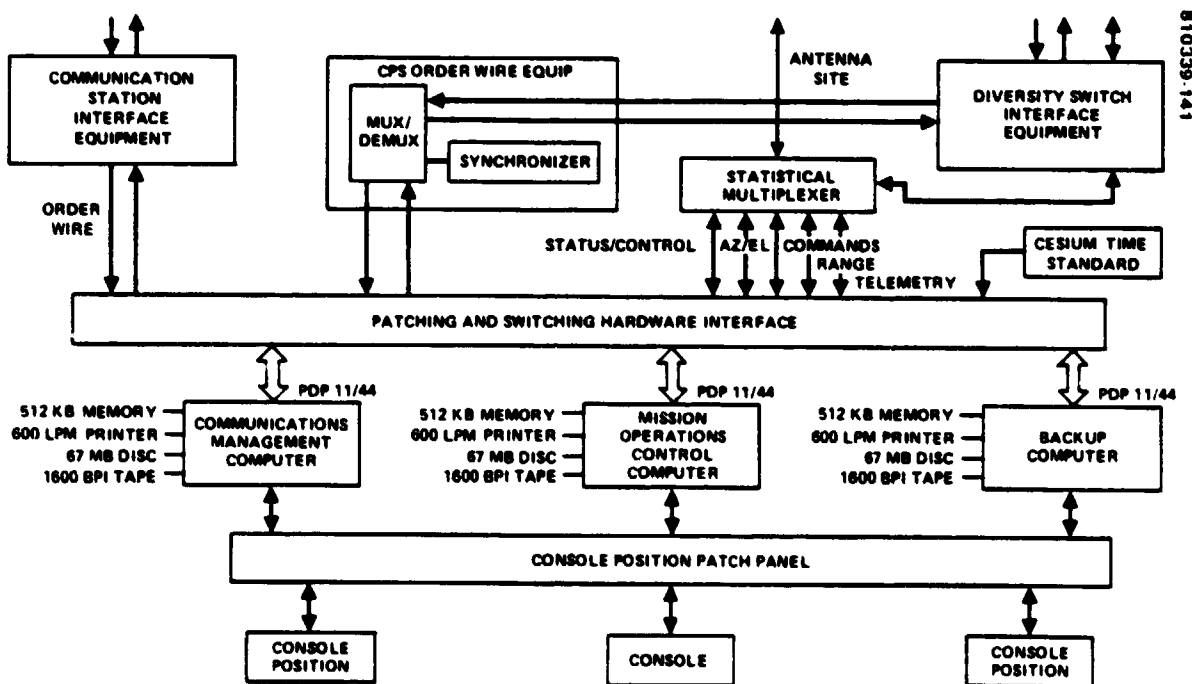


FIGURE 5-10. CENTRAL CONTROL STATION

was available from the LEASAT design. A backup machine is provided to reduce the impact on experiment operations in event of equipment malfunction and to provide significant off-line processing capability for software development and experiment evaluation when the two primary computers are functioning. A patching and switching hardware interface and a console position patch panel are provided to enable rapid reconfiguration of the assigned computer functions. Data storage is provided on movable disk packs to aid system reconfiguration.

#### 5.2.2.2.3 Data Processing Subsystem Configuration

The data processing subsystem is organized to provide central computer resources and interfaces to other CCS subsystems. The data processing subsystem organization is shown in Figure 5-12.

Both the hardware and software of the data processing subsystem derive from the LEASAT baseline. The operating system and support software are resident in each computer and provide management, executive functions, user interfaces, input/output capabilities, and data base access. The applications software functions are allocated such that mission operations functions reside in one computer and communications management functions reside in the other. The off-line functions may reside in background of the respective computers or may be placed in the backup computer. The division of the two major functions into two computers allows for separation of tasks as well as ease of computer switching in the presence of a computer failure.

#### 5.2.2.3 Computer Hardware Group

The computer hardware group consists of three identically configured PDP 11/44 minicomputers. Table 5-7 lists the computer and peripherals for each processor. The central data processing subsystem configuration is shown in Figure 5-13. The peripheral equipment is interfaced to the computer through a standard vendor supplied UNIBUS. The control consoles and CRTs with keyboards interface with the computers through the console position patch panel. All input and output lines go through the switching and patching hardware interface as any processor may perform any function.

The display hardware performs a variety of functions and is configured for optimum use by shift operators and analysts. The configuration includes two identical multipurpose consoles. This provides a station for a spacecraft controller and communications system controller. In addition, alphanumeric and graphic displays are provided for the off-line positions such as planning and analysis.

#### 5.2.2.4 Operating System and Support Software Group

The operating system and support software is standard vendor supplied software or software available from the LEASAT system. It provides the software interface between the computer system (central processor, memory, peripheral equipment), applications software, and the users. The

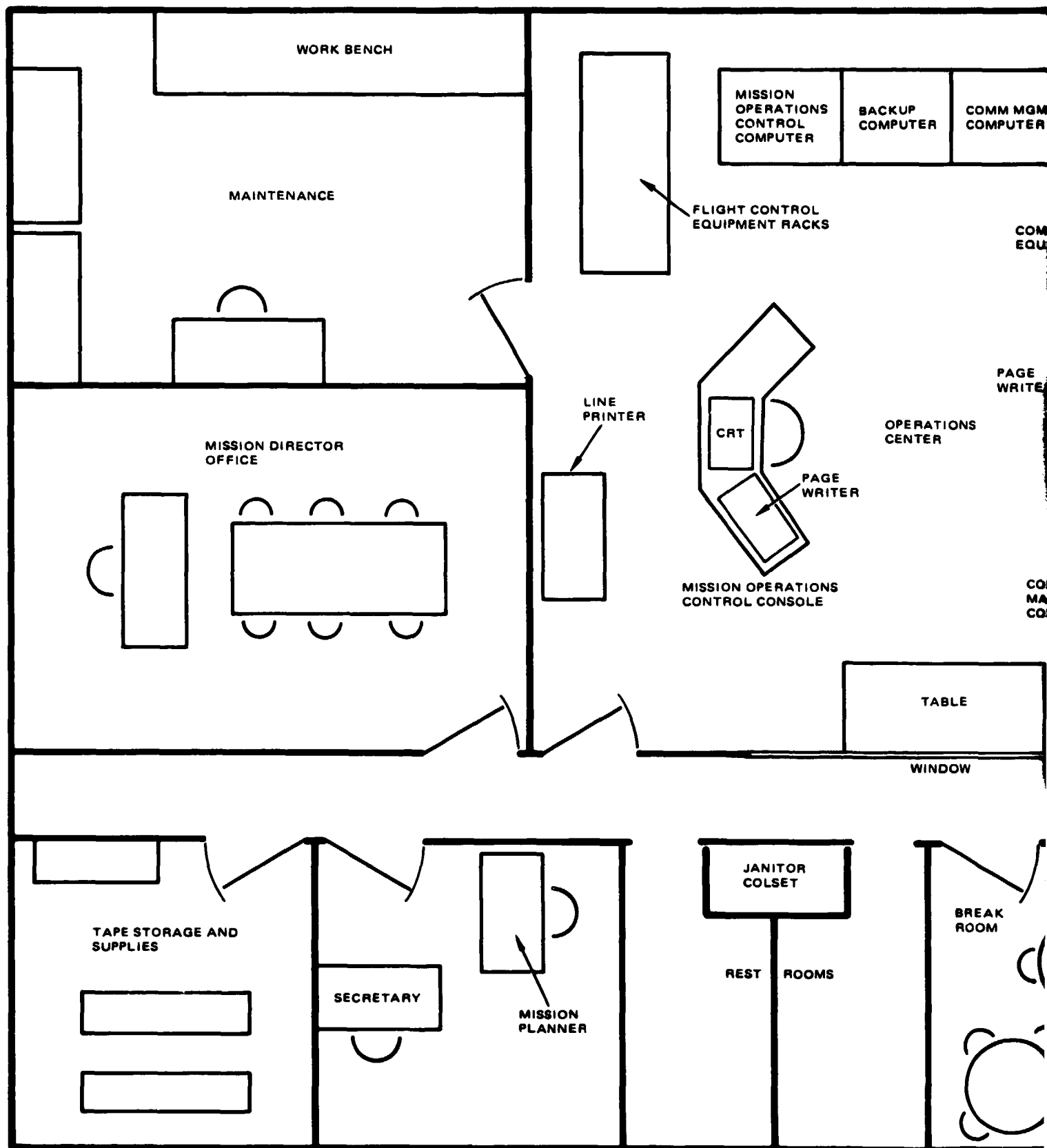
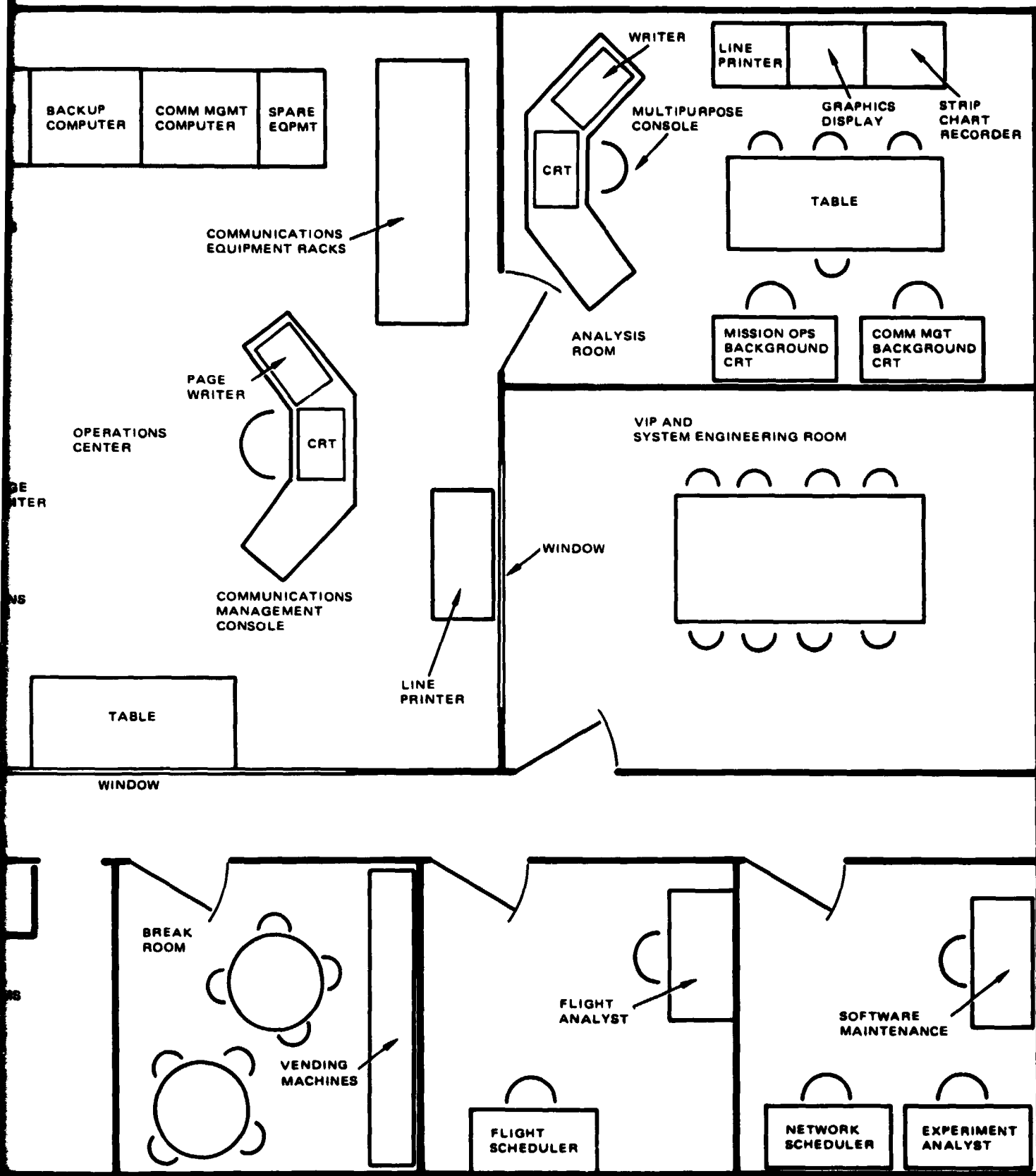


FIGURE 5-11. CENTRAL CONTROL STATION





operating system has the capacity to handle many diverse tasks simultaneously, with dynamic allocation of resources necessary to meet the requirements of the real time environment.

The general architecture of the ground segment software derives from the LEASAT baseline. The peculiar applications tasks for mission operations and communications management are integrated into the structure shown in Figure 5-14. Thus, many software capabilities are inherent to both functions. The software system is built around the control line interpreter to provide operator/system interface and the system data table for storage of system and software variables and control parameters.

#### 5.2.2.4.1 Control Line Interpreter

The key to the support software capability is the experiment command interactive language (ECIL) used by the command line interpreter. ECIL provides highly interactive control through direct execution control statements. This provides the capability to write user defined procedures (PROC's). A PROC is an executable program written in a high level, mission-oriented language. The PROC's may run in scale from simple numeric input programs to highly complex analysis routines. The mission operator can define a sequence of instructions which may be executed in real time as they are defined, or stored on a disk and executed later at will.

#### 5.2.2.4.2 System Data Manager Task

The system data manager (SDM) task processes incoming system data such as spacecraft telemetry, communications control parameters, station telemetry, and tracking data. It manages data for the system data table for use by other processors and generates entries for the archive processor. Other processors or the operator can change items in the system data table via the message processor.

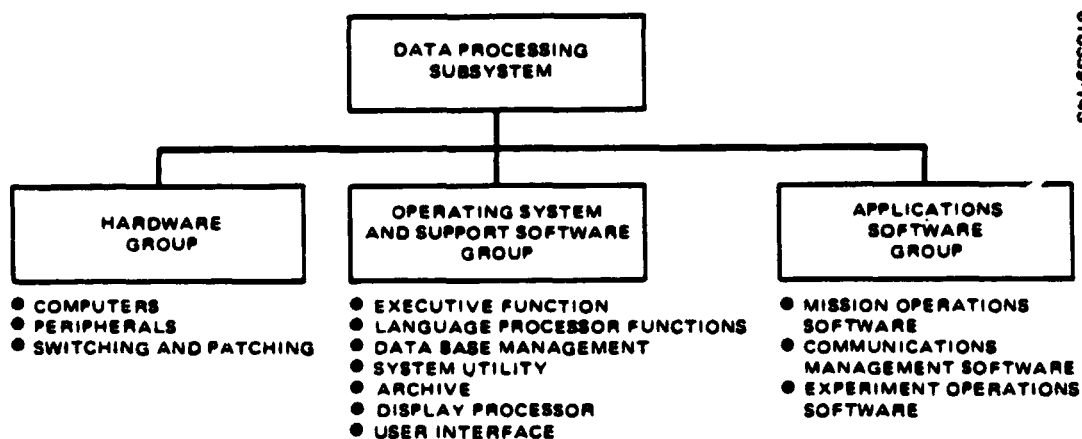
The system data table manager task acquires raw data values, checks for validity, processes the data values for the SDT, limit checks the data, sends alarms to the display processor, generates "derived data points," converts quantities to engineering units, and compresses the data for the archive processor.

#### 5.2.2.4.3 System Data Table

The system data table is under control of the system data table manager task. The basic concept is that all data processed by the system, including spacecraft data, communication control data, ground equipment status, and software control parameters are stored in the system data table for general use. Most data base items necessary for processing a quantity are stored in the entry block associated with the quantity. These quantities, designated as last recorded values (LRVs) include digital values, analog values, and special format values. The data for each LRV includes items such as conversion coefficients, LRV name, alarm limits, control flags, display flags, etc.

**TABLE 5-7. COMPUTER AND PERIPHERAL  
PARTS LIST FOR DEC PDP 11/44 (11 TOTAL)**

Quantity	Description
1	DEC 11/44 computer; includes:
1	11/44 central processor
1	512 kb memory
1	RSX11-M software license
1	Memory management
1	Extended instruction set
1	Automatic bootstrap loader
1	Serial line interface
1	Real time clock
1	KWMOS 67 Mb disk driver
1	A960 cabinet
1	Disk drive 67 Mb
1	Tape drive 9 track 45 ips
1	Line printer (240 lpm)
2	CRT terminal
1	8 line asynchronous multiplexer
1	Floating point processor
1	Tektronics graphic display
1	Gould electrostatic printer/plotter
1	Synchronous line out
1	1 Line asynchronous I/O



**FIGURE 5-12. DATA PROCESSING SUBSYSTEM ORGANIZATION**

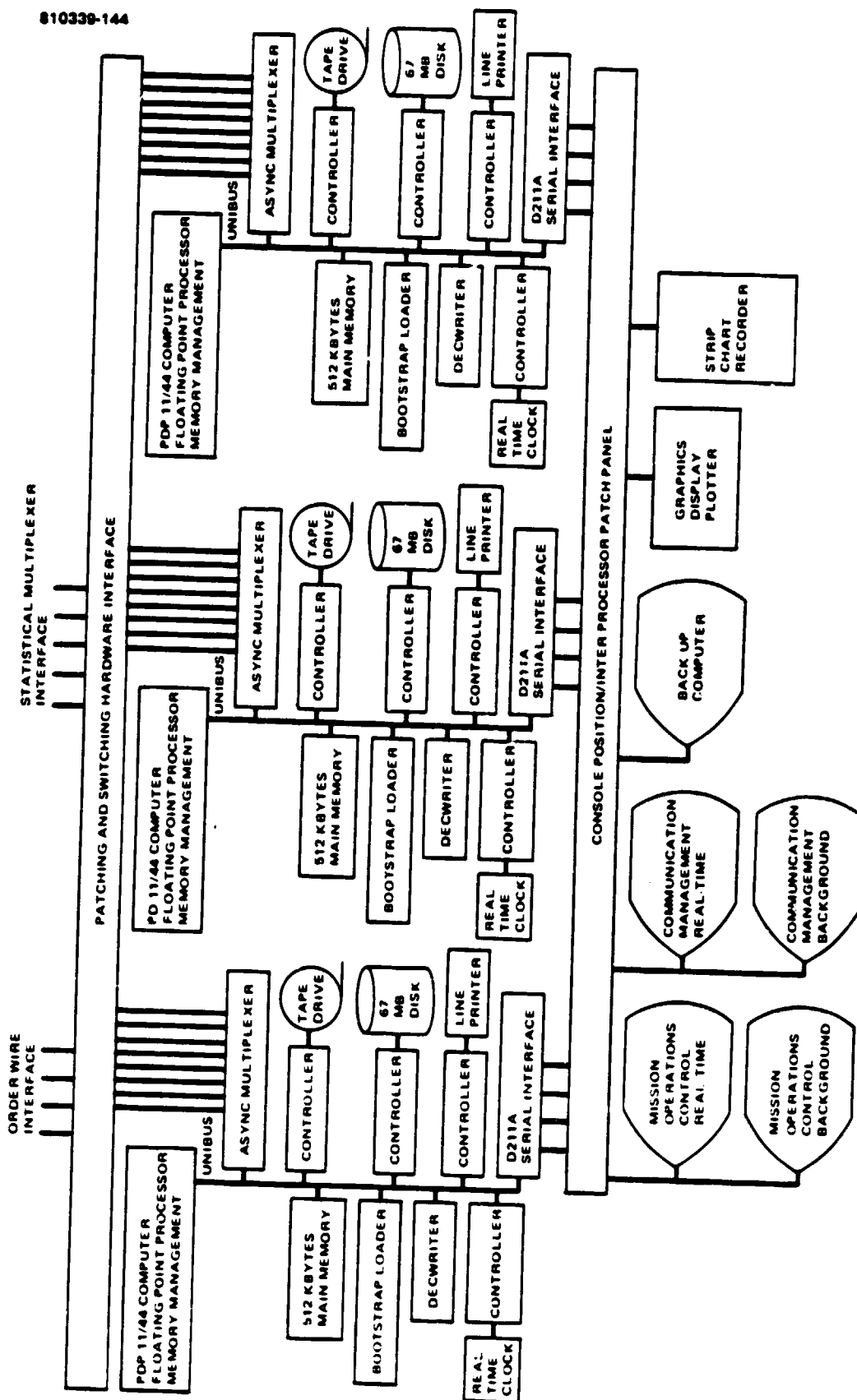


FIGURE 5-13. CENTRAL DATA PROCESSING SUBSYSTEM CONFIGURATION

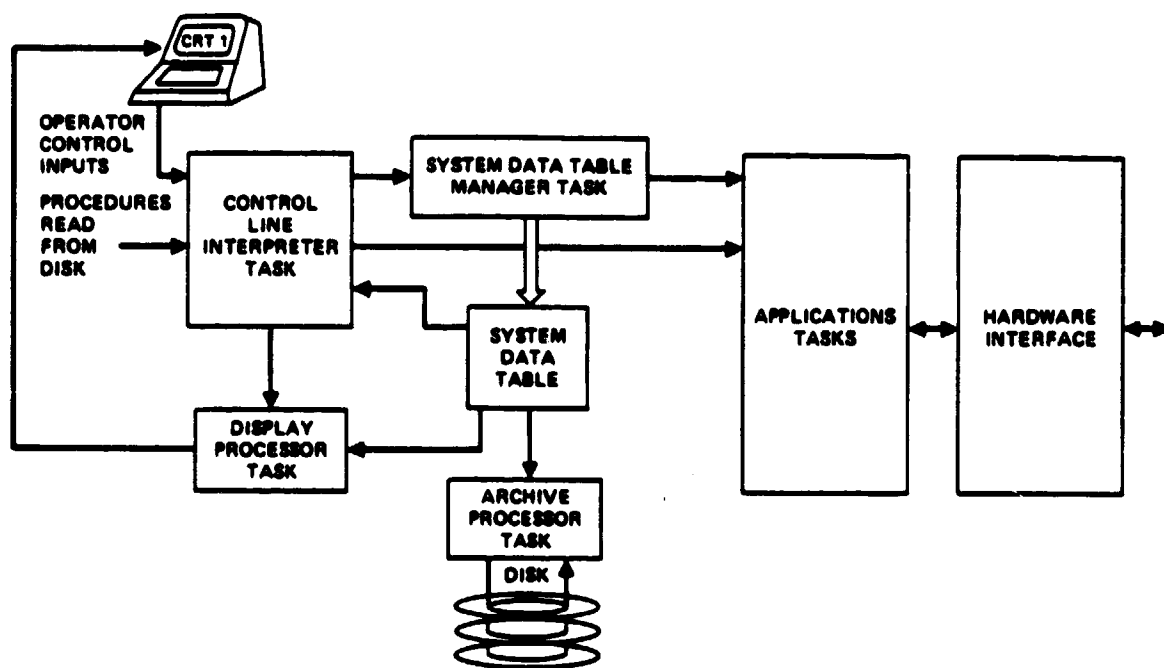


FIGURE 5-14. BASIC SOFTWARE STRUCTURE

#### 5.2.2.4.4 Data Archiving Task

The data archiving task collects spacecraft telemetry, communications control data, attitude, and tracking data for history files for off-line processing. The data archiving task is responsible for transferring data records from the system data table to history files at the request of the SDM, maintaining priority of different types of data, and queuing data to disk during peak loads and when the archive tape is not available.

#### 5.2.2.4.5 Display Processor

The display processor is composed of several independent tasks which are designed to manage the use of CRT and pagewriter display devices for monitoring the spacecraft and terrestrial system activities.

The display processor responds to CLI-interpreted requests and other processors to:

- 1) Display selected LRV pages on the CRT (the LRV number, name, raw or engineering value, units, and alarm limit are displayed)
- 2) Print a snapshot of displayed LRVs on the pagewriter
- 3) Automatically dump selected raw telemetry words in a minor frame on the pagewriter
- 4) Display or print SDT items, including alarm limits, engineering coefficient, print on change deltas, and archiving deltas for selecting LRVs
- 5) Display messages from other tasks

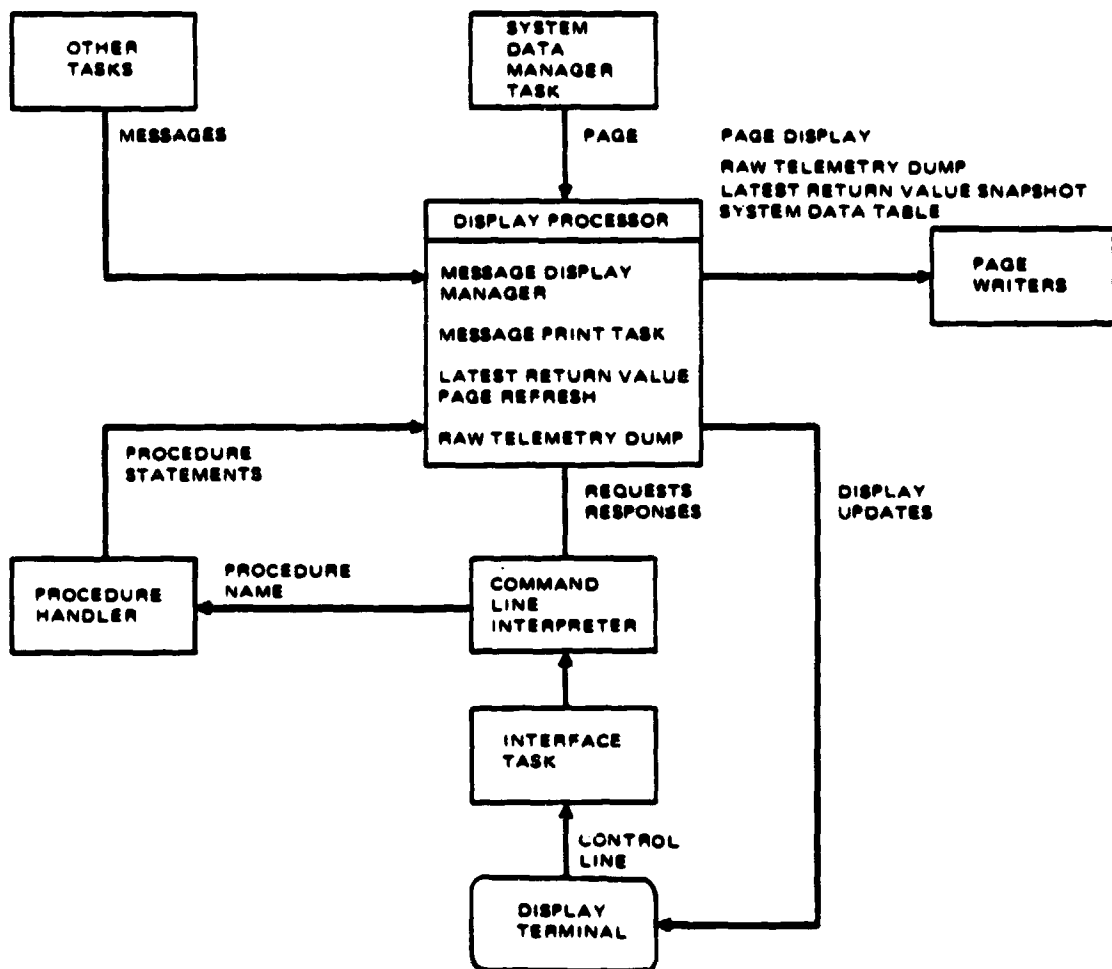


FIGURE 5-15. DISPLAY PROCESSOR DATA PATHS

Other processors communicate with the display processor via dynamically allocated data buffers in the SDT. The display processor data paths are shown in Figure 5-15.

#### 5.2.2.5 Applications Software Group

The terrestrial segment applications software is divided into realtime processing tasks and off-line processing tasks.

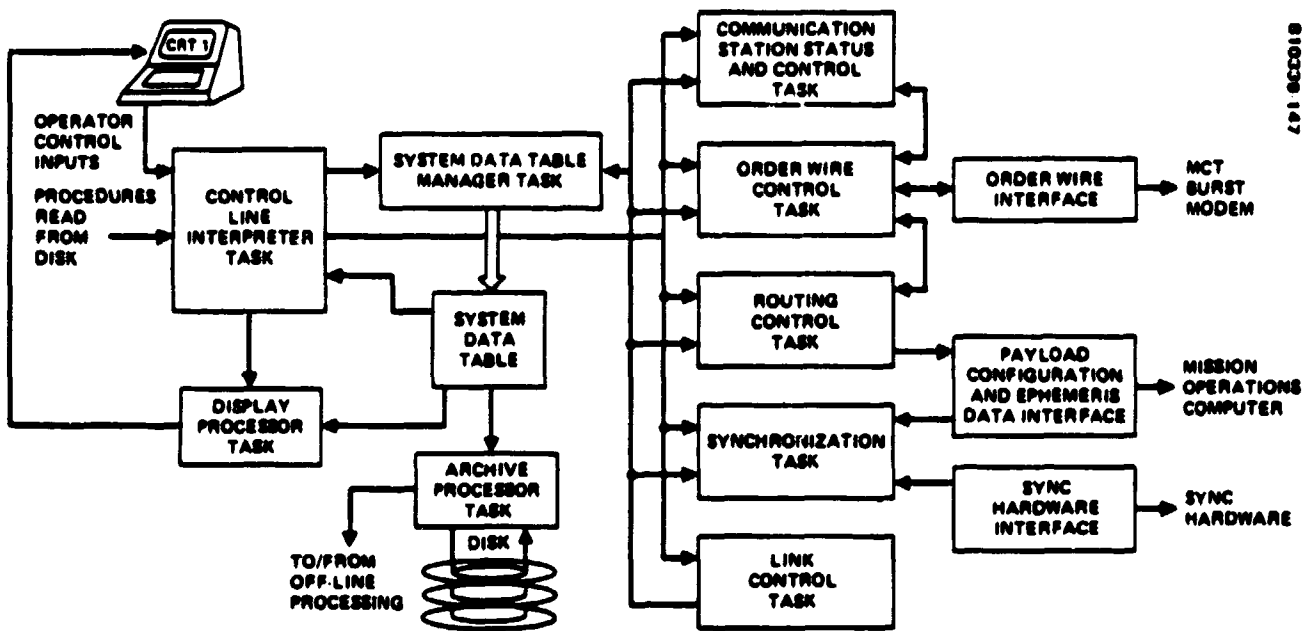


FIGURE 5-16. COMMUNICATIONS MANAGEMENT SOFTWARE, CCS  
REAL TIME PROCESSING

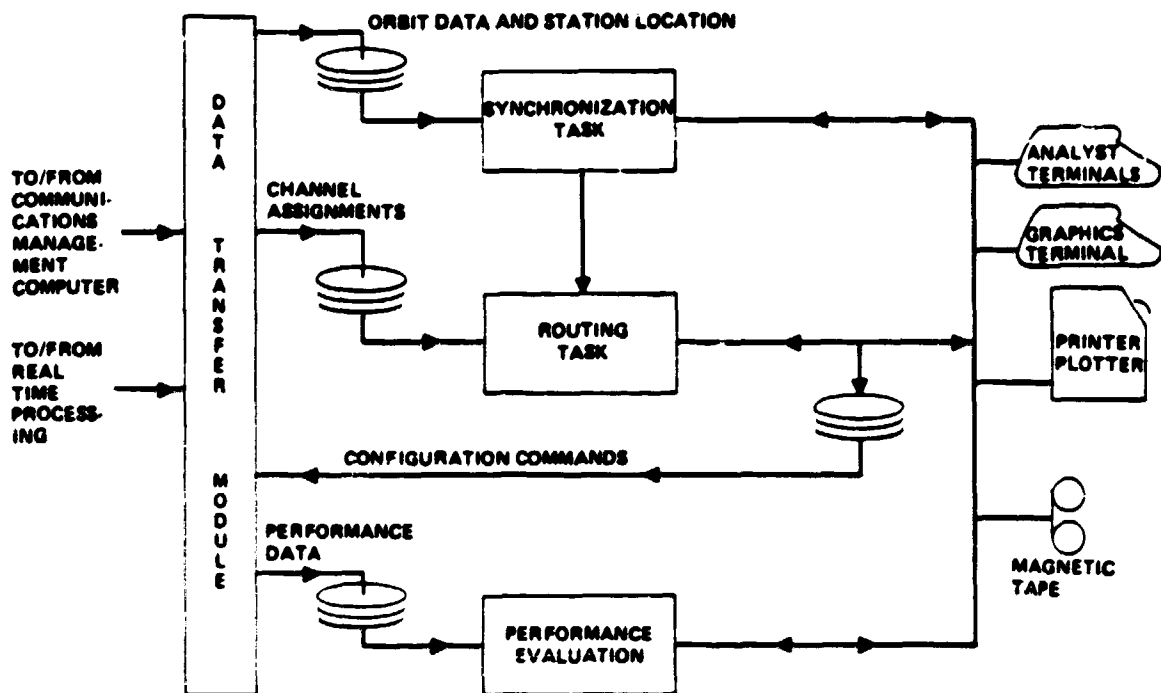


FIGURE 5-17. COMMUNICATIONS MANAGEMENT SOFTWARE,  
CCS OFF-LINE PROCESSING

The real time communications management software provides network and payload control functions which must be performed in real time to communicate through the 30/20 GHz system. Figure 5-16 shows the real time tasks integrated into the LEASAT baseline architecture. The major tasks and their functions are:

- 1) The station status and control task provides an interface with the order wire or terrestrial links for remote control of CPS and trunk stations and remote data gathering.
- 2) The order wire control task provides the communication channel for exchanging system control information. Its interconnection with other processing tasks is primarily through the system data table.
- 3) Network control is the major task of the routing processor. This processor provides controls for the baseband processor, station multiplexers, beam forming network, and IF switch.
- 4) Synchronization provides system timing data for real time operations.
- 5) Link control manages the rain attenuation strategy for diversity switching and CPS data encoding.

The communications management off-line processing software is also derived from LEASAT architecture. It performs the communications management tasks which do not require real time processing. These tasks are as follows:

- 1) Synchronization which uses channel assignments, predicted spacecraft ephemeris, and station location data to produce estimated transmission burst time for each station in the network
- 2) Routing which uses channel assignments to produce the IF switch state matrix and baseband processor controls
- 3) Performance evaluation which makes it possible to analyze the communication system data collected in real time

Data transfer is provided to the real time processors for network and payload control. The architecture of the off-line processing is shown in Figure 5-17.

#### 5.2.2.5.1 Applications Tasks

The following discussion provides details of the tasks required for communications management. The concepts for each task result from an assumed control strategy. The control strategy and concept were developed to determine the effort required for each task.



These tasks may either be performed manually or automated via software. These details address the concept development which is applicable to either manual or automated implementation. The degree of automation in the system is determined by the relative weighting of development cost versus life cycle costs, operational necessity, and experiment objectives.

#### 5.2.2.5.2 Channel Allocation

Channel allocation is the procedure for assigning channel capacity to stations according to the traffic model or station needs. In the baseline concept channel allocation is a manual operation. Figure 5-18 shows the details of channel allocation for the CPS frame. Trunk channel allocation is similar but less detailed as capacity is allocated in larger segments.

The channel allocation process not only allocates communication slots but must also allocate all preamble, order wire, and beam switch times. In a manual channel allocation system, spare capacity is distributed between station contacts to reduce impact on the frame format when additional channels are assigned a station. A demand assignment allocation algorithm would arrange the channels and spare space to optimize use of the channel. When a channel must be encoded for rain margin, two nonencoded channel spaces

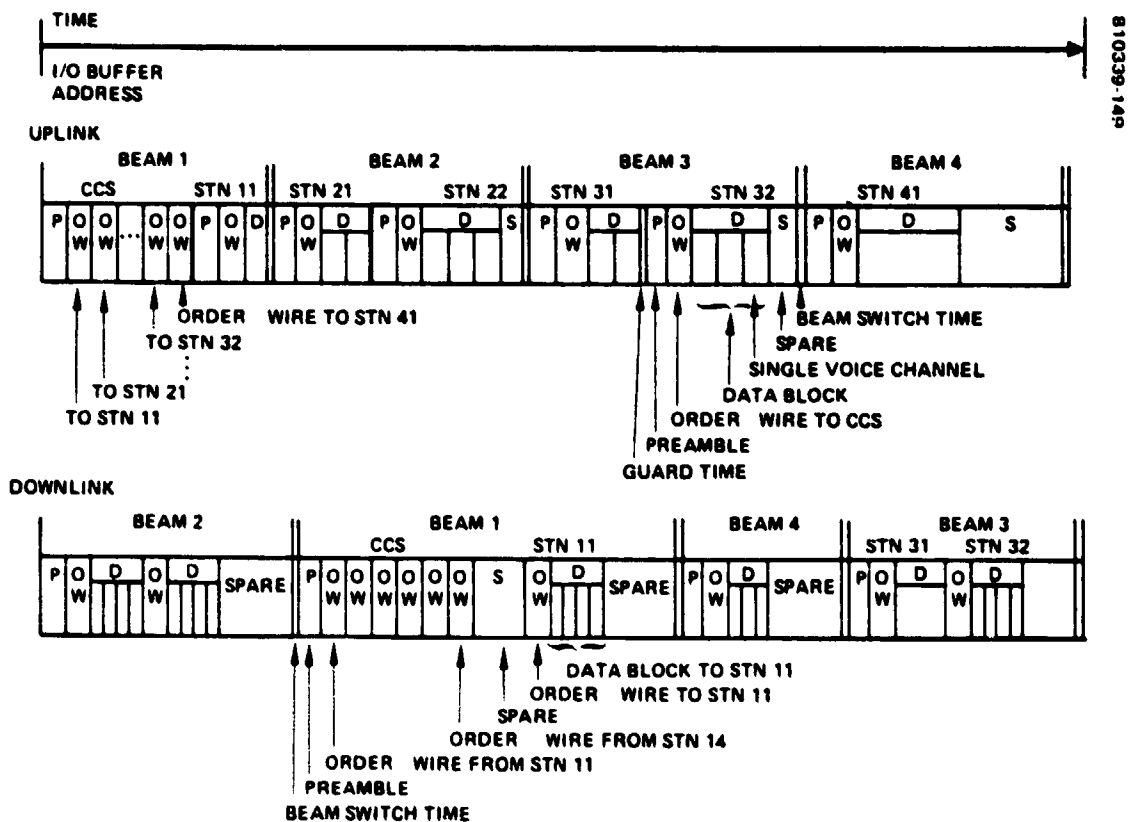


FIGURE 5-18. CHANNEL ALLOCATION

CHANNEL ROUTING TABLE

SLOT	SOURCE	DESTINAT	SLOT
1	CCS	STN 11	87
2	CCS	STN 21	2
3	CCS	STN 22	15
...	...	...	...
15	STN 11	CCS	56
16	STN 11	STN 41	110

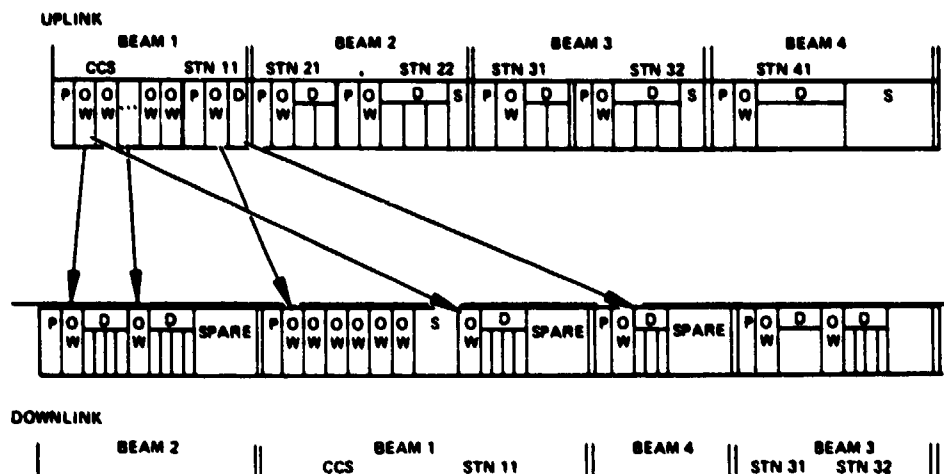


FIGURE 5-19. CHANNEL ALLOCATION ROUTING

must be assigned. As each channel is assigned, a table must be built to show where its corresponding channel was placed in the downlink (Figure 5-19). When full duplex service is requested from a station, the corresponding uplink and downlink slots from the destination station must also be allocated. The channel routing table is required to properly route data through the base-band processor.

#### 5.2.2.5.3 IF Switch Control

After the trunk channels are allocated, the IF switch control matrix may be constructed. This is also a manual process. The IF switch provides "bent pipe" interconnects between source destination trunk pairs according to a preplanned schedule. The switch is controlled by a matrix which is developed at the CCS and sent to the spacecraft via the command uplink. The switch state matrix is stored in a double buffer control memory in the spacecraft. One buffer is used for active control of the switch while the other buffer is available for updating. The switch state matrix is developed from the channel assignments (Figure 5-20). A peculiar code defines the particular on/off states of the switches in the IF switch crossbar and is assigned for each station for an uplink state (source code) and a downlink state (destination code). Codes are then extracted from this source destination pair table according to the sequence of channel assignments. The IF switch control word for any given switch time consists of the source destination pair codes for the interconnects required during that switch time. The IF switch control matrix for a given frame consists of the sequence of all control words for switch times within the frame.

# CHANNEL ASSIGNMENTS

FROM	TO				
CLEVELAND	C	NEW YORK CITY	LOS ANGELES	WASHINGTON, DC	
NEW YORK CITY	N	WASHINGTON, DC	CLEVELAND	LOS ANGELES	
WASHINGTON, DC	W	LOS ANGELES	NEW YORK CITY	CLEVELAND	
LOS ANGELES	L	CLEVELAND	WASHINGTON, DC	NEW YORK CITY	

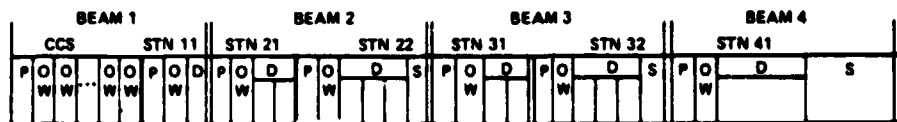
STATION	SOURCE CODE	DESTINATION CODE
CLE	0001 1	1110 E
NYC	0010 2	1101 D
WDC	0011 3	1100 C
LA	0100 4	1011 B
HOU	0010 2	1101 D
TPA	0011 3	1100 C

SOURCE-DESTINATION PAIR TABLE

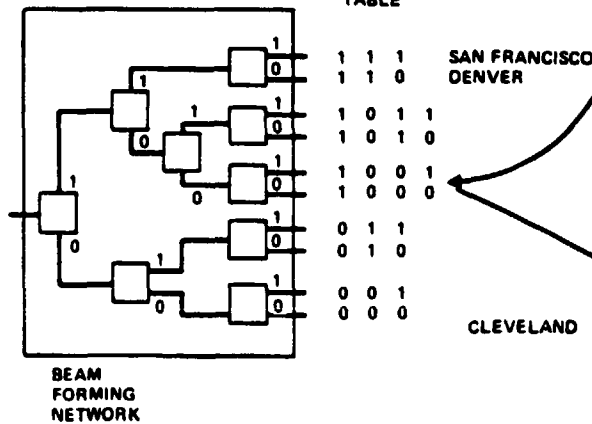
SWITCH STATE MATRIX

TIME	STATE
1	1E 2D 3C 4B
2	1D 2C 3B 4E
3	1B 2E 3D 4C
4	1C 2B 3E 4D

FIGURE 5-20. IF SWITCH CONTROL



BEAM STATE TABLE



FROM CHANNEL ASSIGNMENTS SEQUENTIALLY SELECT BEAM STATE ACCORDING TO SOURCE OR DESTINATION

BEAM CONTROL MATRIX

SWITCH TIME	STATE
1	000
2	1001
3	010

FIGURE 5-21. SCAN BEAM CONTROL MATRIX

#### 5.2.2.5.4 Scanning Beam Antenna Control

The scanning beam antenna control matrix is manually developed from the CPS channel allocations as shown in Figure 5-21. The beam forming network switch array is shown at the left of the figure. The switch positions are labeled 1 if the signal follows the path at the top of the switch, and 0 if the signal follows the path at the bottom of the switch. Thus, for each destination station a code may be developed for the signal path through the switch.

The scan beam control matrix is constructed by selecting codes from the beam state table according to the sequence of the frame allocation. A control matrix is produced for each uplink and downlink scan beam.

#### 5.2.2.5.5 Routing Control Task

The routing control task is the major element of the communications control software. It develops the contents of the baseband processor control memories which are programmed to direct message traffic and provide message data switching on a 64 bit word basis (64 bits equals one telephone voice channel per frame). The digital routing controller receives the control memory update information through the order wire interface and distributes the data to corresponding control memories. Control memories are used to direct the demodulators, input data memories, digital routing switch, order wire interface, and output data memories (Figure 5-22). Control memories for the demodulator provide sync gate enable, sync gate select, and on/off control signals. They also direct the hard/soft demodulator IF switch. The control memory for the input memory, output memory, and order wire provides random read addresses to route data traffic. The modulator control memory provides on/off control for the modulators. The baseband routing switch directs the random transfer of input memory data to the output memory on a word basis.

Figure 5-23 shows the algorithm for building the input memory control memory. The control memory for the input memory contains the sequential list of addresses for reading the data memory into the baseband routing switch. Since data from the uplink is read sequentially into the data memory, the position of data in the uplink frames determines its address in the input memory. By using the channel routing table built during the channel allocation process, a destination table can be constructed that contains data input memory addresses for each station. The control memory contents are built by selecting addresses in the destination table according to the scheme used to control the baseband routing switch.

The routing switch directs the random transfer of input memory data to the output memory on a word basis. It interconnects four inputs (hard decision demodulators 1 and 2, the soft decision demodulator, and the order wire input) with three outputs (beam forming network 1 and 2 and the order wire output) as shown in Figure 5-24. Figure 5-25 depicts the routing switch control memory algorithm. A switch strategy having the interconnects shown

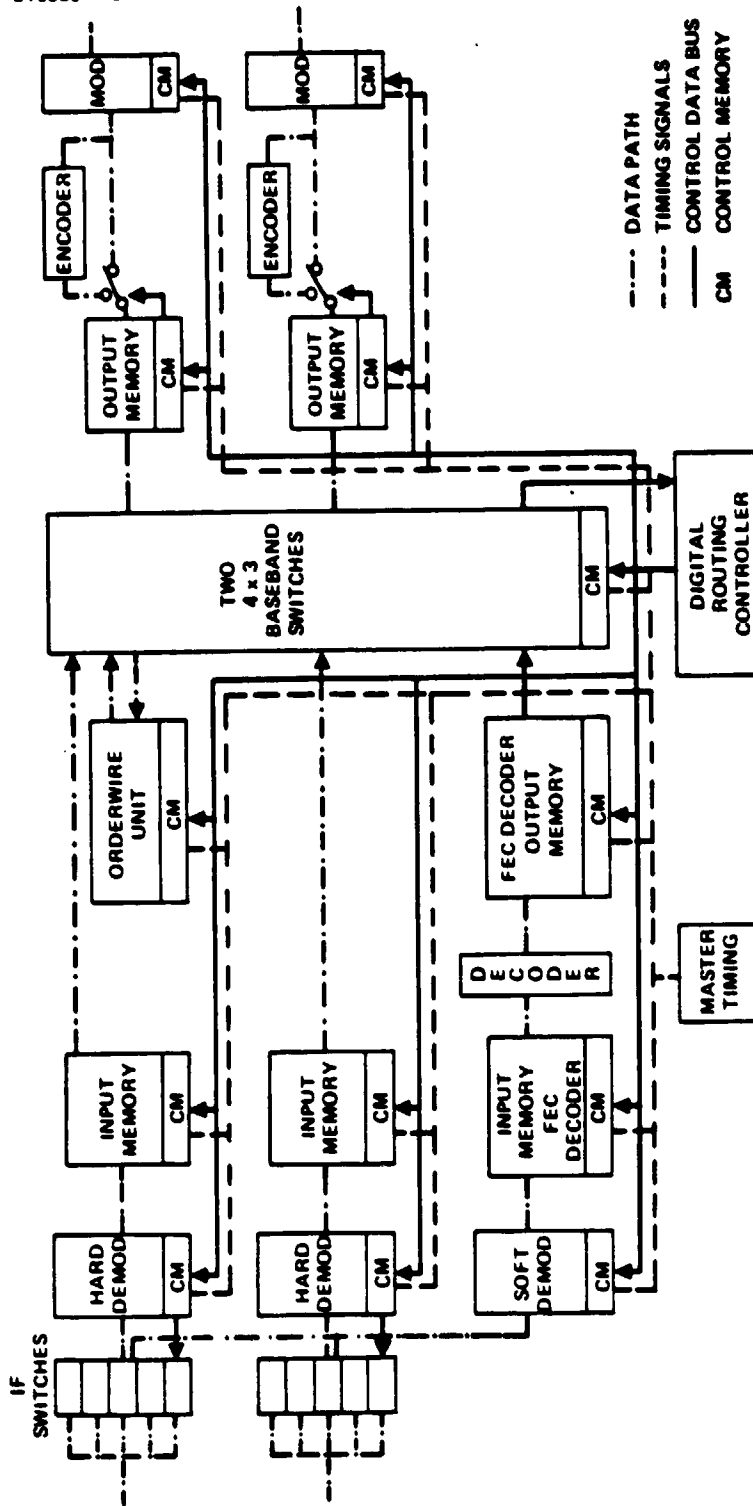


FIGURE 5-22. BASEBAND PROCESSING CONTROL

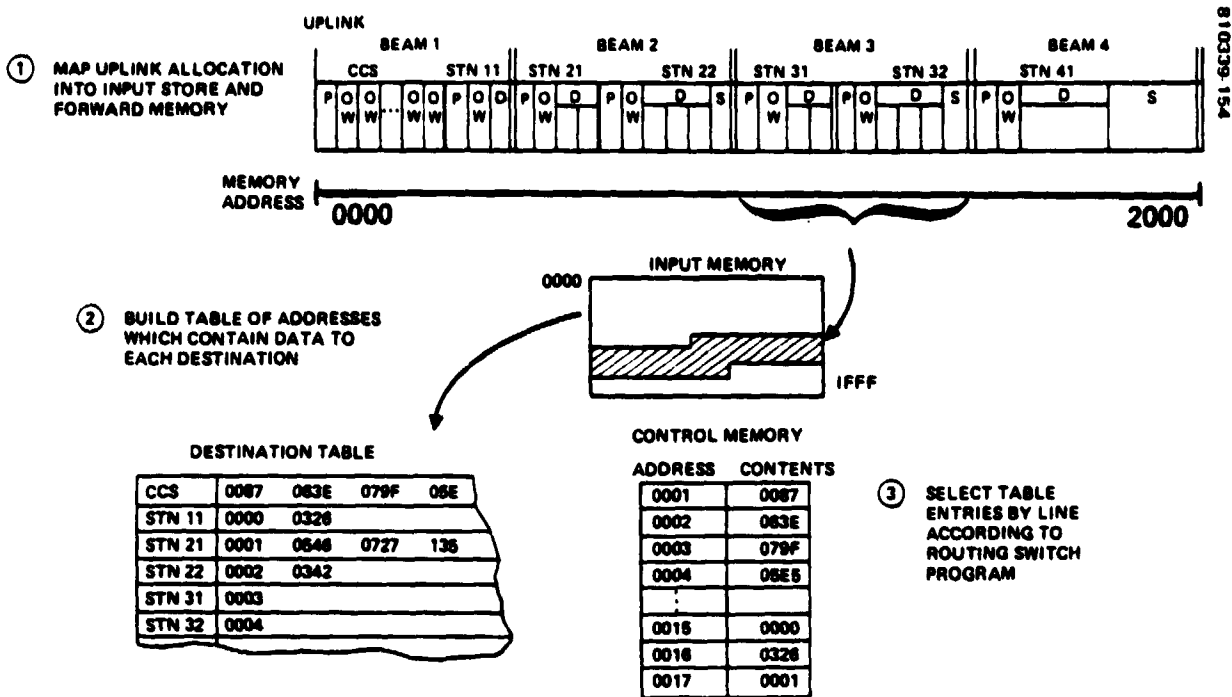


FIGURE 5-23. INPUT MEMORY CONTROL PROGRAMMING

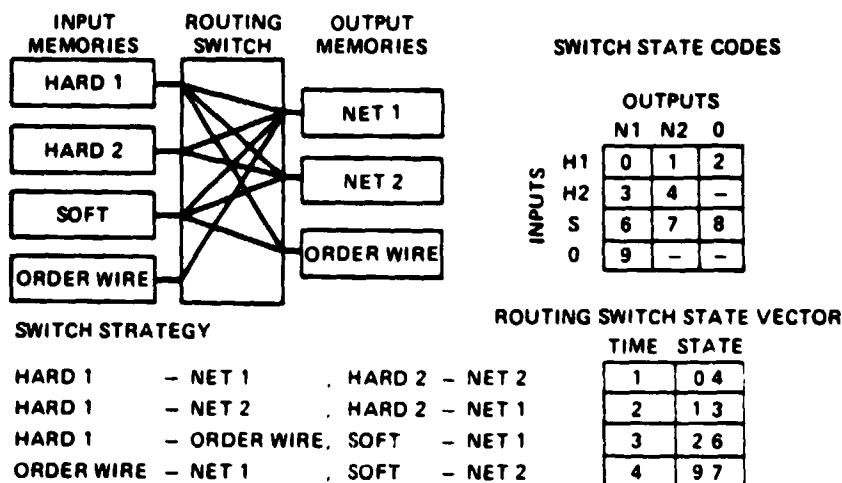


FIGURE 5-24. BBP ROUTING SWITCH INTERCONNECTS

# SWITCH STRATEGY

TIME	1	HARD 1	-	NET 1	, HARD 2	-	NET 2
	2	HARD 1	-	NET 2	, HARD 2	-	NET 1
	3	HARD 1	-	ORDER WIRE	, SOFT	-	NET 1
	4	ORDER WIRE	-	NET 1	, SOFT	-	NET 2

810339-156

## SWITCH STATE CODES

OUTPUTS			
	N1	N2	Q
H1	0	1	2
H2	3	4	-
S	6	7	8
O	9	-	-

## ROUTING SWITCH STATE VECTOR

TIME	STATE
1	0 4
2	1 3
3	2 6
4	9 7

FIGURE 5-25. ROUTING SWITCH CONTROL MEMORY PROGRAMMING

## OUTPUT MEMORY MAP

ADDRESS	DSTN	SLOT
0001	CCS	56
0002	CCS	57
0003	CCS	58
...		
0137	STN 21	1
0138	STN 21	3
0139	STN 21	2

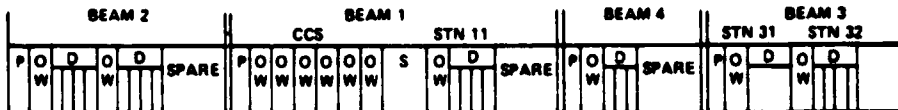
① BUILD OUTPUT MEMORY MAP FROM SEQUENCE WRITTEN THROUGH ROUTING SWITCH AND DOWNLINK CHANNEL ALLOCATION

810339-157

## OUTPUT CONTROL MEMORY

ADDRESS	CONTENTS
0001	0137
0002	0138
0003	0139
...	
0126	0056
0127	0057
0128	0058
0129	0059

DOWNLINK



② SELECT ADDRESSES FROM OUTPUT MEMORY MAP ACCORDING TO DOWNLINK FRAME SEQUENCE

FIGURE 5-26. OUTPUT MEMORY CONTROL PROGRAMMING

is assumed. The horizontal lines are simultaneous interconnects and the vertical rows are sequential interconnects. A code table, which specified the on/off state of the individual switch elements, contains a code for all required interconnects. Since it is assumed that the CCS is in scan beam network 1, interconnects between the order wire interface and network 2 are not required. The switch state control vector is constructed by extracting codes from the switch state code table according to the switch strategy.

Figure 5-26 shows the output memory control memory programming algorithm. The output control memory provides a sequential list of addresses for reading the data memory for output through the modulator. It also contains codes for controlling the FEC encoder switches. Data are written to the output memory sequentially as they are passed through the routing switch. It is necessary to build an output memory map which charts the final destination of each word in the input memory. This map is built from the channel routing table, the input control memory, and the routing switch control memory that was prepared in prior steps. The contents of the output control memory are developed by extracting entries from the output control memory map in the sequence specified by the output frame format.

#### 5.2.2.5.6 Synchronization Task

The synchronization control software has a CCS function and a communications station function. In the CCS the software uses the predicted spacecraft ephemeris, station location, and channel allocation to calculate estimated burst transmission times for each station. The estimated transmit time of a burst signal is given by

$$T_b = \frac{R_e}{c} + n T_b + \gamma$$

where

$R_e$  = estimated slant range calculated from the ephemeris and station location

$c$  = speed of propagation

$nT_b$  = time allotted to other station bursts in the frame

$\gamma$  = one-half the allocated channel time

At the CCS, the synchronization control software also calculates the control parameters for a frame format change. These include the time required for station notification, time of first changed frame at the spacecraft, and time to transmit a frame marker for advanced notice to the stations.



# POWER LEVEL CONTROL

SIGNAL STRENGTH  
OR BER MEASUREMENTS

SIGNAL  
QUALITY

POWER  
LEVEL

POWER  
LEVEL  
CONTROL  
SIGNALS

810039-158

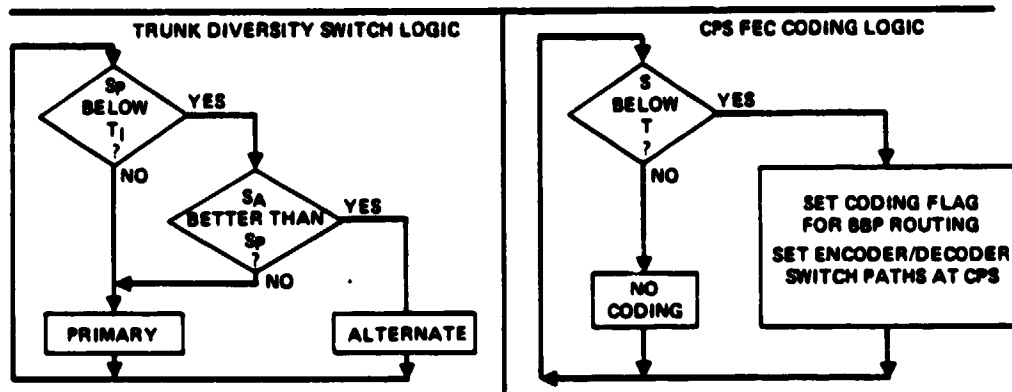


FIGURE 5-27. LINK CONTROL SOFTWARE

At the trunk and CPS stations, the synchronization control software filters the error measurement received on the downlink to determine a correction for the burst synchronizer.

## 5.2.2.5.7 Link Control Task

The Link Control task is depicted in Figure 5-27. The link control software will detect signal fading by comparing the signal strength to clear weather values. When fading is detected an algorithm relating signal strength to increased transmitter power will be used to compensate for fading.

When the rain margin capacity of power level control is exceeded, an additional link margin is provided by a diversity site at the trunk station or FEC coding at the CPS station. The diversity switching algorithm uses primary and alternate logic. Only when the signal quality at the primary site is degraded below a threshold level, and the path has a better signal quality, is the backup selected. This logic is preferred for the following reasons:

- 1) Since the alternate site is distant, the link to this site contains more equipment. This reduces the reliability of the link and increases the frequency of switching due to equipment failure.
- 2) In clear weather the primary site signal quality should be better.
- 3) Diversity switch control is simplified because only one command "Connect the primary site" is sufficient when the signal quality on both routes is better than threshold.

The CPS logic employs a simple threshold test and sets flags to invoke a coded path by the routing processor and to set encoder/decoder switches at the CPS.

#### 5.2.2.5.8 Orderwire Control Task

Network control information is exchanged between the network stations and the CCS via the order wire channel. The order wire channel is a time slot in the uplink and downlink TDMA frame format. The order wire processing task receives data from other software tasks, places the data into standard message formats, buffers these messages into the uplink frame, receives messages from network stations, and transfers message information to other software tasks. Message transmission sequences are buffered into the transmission frame using information from the channel allocation task. Messages are generated for channel allocation requests, channel allocation assignments, stations status reporting, rain margin control commands, and periodic burst timing updates.

#### 5.2.2.5.9 Station Status and Control Task

The station status and control software for the communications management function is adapted from that for the mission operations function. At each CPS or trunk site the station status and control software contains a routine to commutate performance and status data for transmission via order wire, land line, or recording. It also contains an order wire interface routine, and a routine to accept, decode, and route station commands received from the CCS. At the CCS, the station status and control software decommutates the messages received from the stations and routes the data to the data base manager. It also generates station reconfiguration commands. This function is illustrated in Figure 5-28.

#### 5.2.3 Trunk Station

Trunk stations will provide four simultaneously active fixed beams to six cities. The six cities served are: Los Angeles, Cleveland, New York, Washington, Tampa, and Houston. User access is via satellite switched, time division multiple access (SS-TDMA) through fixed beam spot antennas. The trunk station provides communication access for bulk data transmission, synchronization of burst transmissions, link margin for rain attenuation, and remote control and operation of the terrestrial terminal. The trunk station is under direct control by the CCS.

The trunk station requirements are shown in Table 5-8.

The trunk station RF subsystem design is based upon satellite ground station designs that have evolved from many years of successful performance on commercial and NASA programs. The design derives from proven hardware configured for flexibility and availability based upon the LEASAT, SBS, Palapa, and INTELSAT ground systems. The RF subsystem design is discussed in 6.1. The trunk station digital equipment design derives from Hughes involvement in state of the art TDMA systems such as Satellite Business Systems and ARCO communications upgrade.

TABLE 5-8. TRUNK STATION REQUIREMENTS

Communication access	<p>TDMA at 256 Mbps burst rate</p> <p>Up to 5 DS3 (44.736 Mbps) digitally multiplexed carriers</p> <p>Interconnect any trunk station with any other</p> <p>Simultaneous interconnection of four station pairs</p> <p>Minimum burst is 1000 bits</p> <p>Data quality BER = <math>10^{-6}</math></p>
Link margin	<p>18 dB Uplink, 8 dB downlink</p> <p>Variable power control</p> <p>Site diversity with error free switch</p>
Synchronization	Burst times synchronized to within 60 ns of system time
Configuration	Antenna 5M
Other	Remote control and monitor

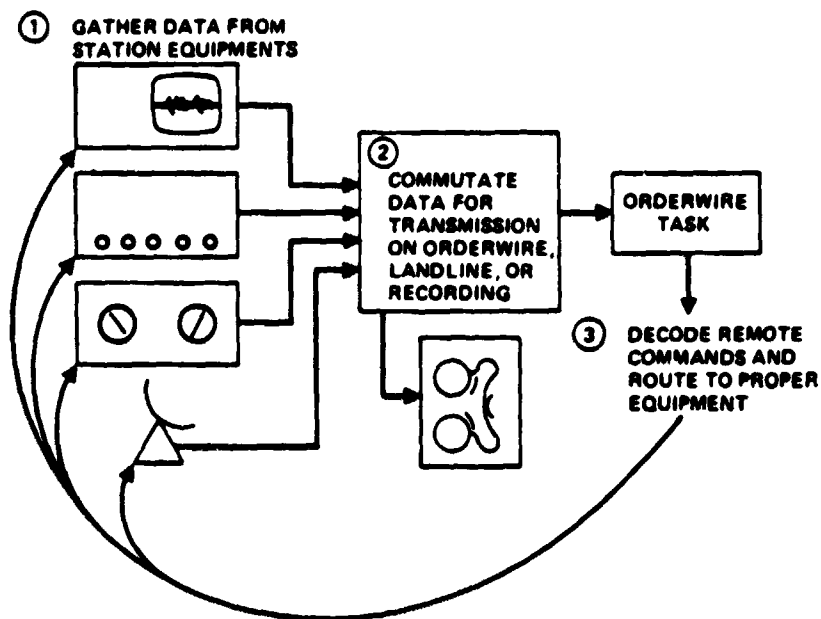


FIGURE 5-28. STATION STATUS AND CONTROL SOFTWARE

### 5.2.3.1 Trunk Station TDMA Hardware Definition

The hardware configuration of a standard trunk station (not the master control terminal trunk station) is shown in Figure 5-3. The TDMA terminal equipment in this station is common to all trunk and CPS stations. The basic functions of the TDMA terminal equipment are:

- 1) To interface with the terrestrial network and perform coding and multiplexing functions on the information signals
- 2) To provide modulation and demodulation functions using QPSK
- 3) To implement all of the TDMA system control functions including synchronization, acquisition, automatic switching, and other housekeeping functions

The principal hardware elements of the trunk station and their functions are described in 5.2.3.1.1 to 5.2.3.1.14.

#### 5.2.3.1.1 Terrestrial Interface Module

The terrestrial interface module (TIM) connects the terrestrial network with the TDMA terminal. Compression and expansion memories are provided to convert continuous low speed terminal input data to the high rate (256 Mbps) burst data for TDMA transmission, and to reconvert the received TDMA burst data to low rate continuous data at the terminal output interface. The data channel buffers are sized for the maximum data rate of the network. The terrestrial interface module also contain word stuffing/destuffing circuits to match the input clock rate to the TDMA system clock rate. Different TIM configurations are provided for each service offered, e. g., multiplex telephony, facsimile, video teleconferencing, and direct digital channels.

#### 5.2.3.1.2 Multiplexer/Demultiplexer

The multiplexer (Figure 5-29) systematically sequences on- frame of the buffered bits from the appropriate TIM buffer into the assigned TDMA frame format. The burst format is implemented by storing the structure of these formats in control memory within the multiplexer. The TIM buffer addresses are read in the sequence stored in the control memory. In addition, the multiplexer sends gating signals to the preamble generator, scrambler, and modulator so that they function at the proper time. The demultiplexer performs the inverse function. It controls the receive timing and sends appropriate data to the expansion buffers.

#### 5.2.3.1.3 Scrambler/Descrambler

The purpose of the scrambler/descrambler is to reduce the transmitted power flux density when the information transmitted contains fixed patterns. Energy dispersal is achieved by modifying all information from the compression buffer by a pseudorandom bit sequence. The pseudorandom

code is introduced by modulo 2 addition of the sequence and data portion of the burst. The pseudorandom codes are reset at the beginning of each burst. On receive, modulo 2 addition of the same pseudorandom sequence to incoming data bursts recovers the data in original form.

#### 5.2.3.1.4 Preamble Generator

The preamble generator, under control of the multiplexer, produces the TDMA frame preamble. Since the preamble is constant from frame to frame, it may be generated via a fixed register memory unit. The preamble generator produces a predetermined bit pattern for carrier and bit timing recovery and the synchronization unique word. The length of each of these fields is given in 5.1.

#### 5.2.3.1.5 Burst Synchronizer

Synchronization of the above equipment is carried out by the burst synchronizer. At the transmit side, the various units run off the clock generator which is pulse locked to the master oscillator in the spacecraft. At the receive side, the equipment runs off the burst clock which is provided by the QPSK demodulator. The operation of the burst synchronizer is discussed in 5.2.3.3.

#### 5.2.3.1.6 Frequency Standard and Clock Generator

These provide synchronized timing signals to all station equipment. The clock generator counts pulses from the frequency standard to provide precise time interval pulses. It is phase locked to the master oscillator.

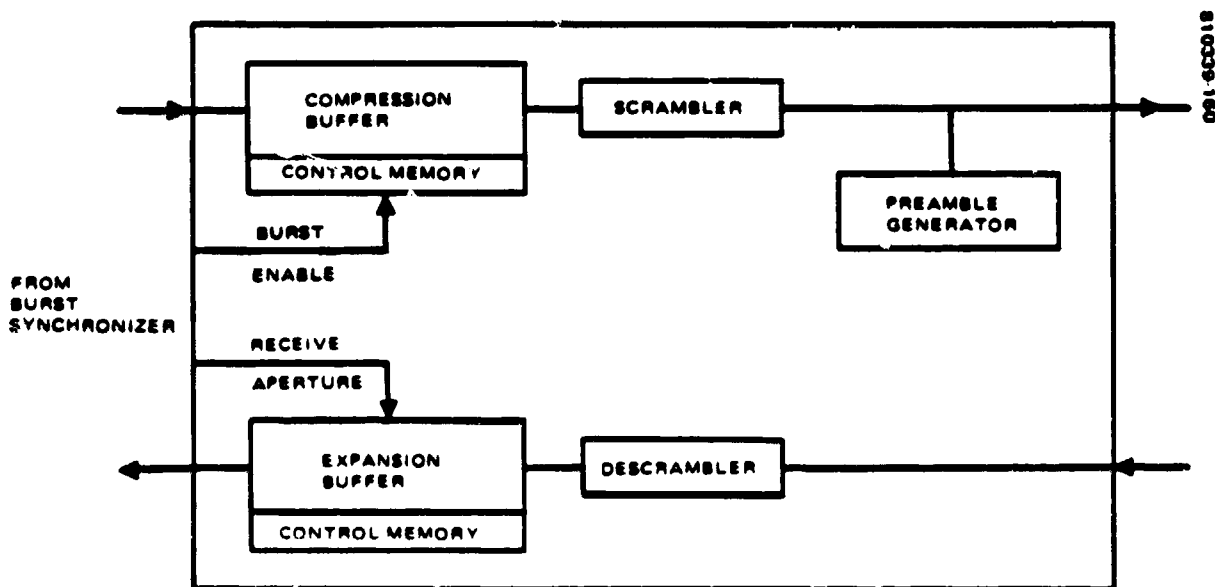


FIGURE 5-29. TDMA MULTIPLEXER/DEMULTIPLEXER

#### 5.2.3.1.7 Microprocessor Controller

The microprocessor controller supports the following operational functions: order wire control, acquisition and synchronization, and link control. Details of each function are given in 5.2.3.5.

#### 5.2.3.1.8 Station Monitor and Controller

A station monitor and controller is recommended for all trunk stations. Its purpose is to provide an interface for unmanned station operation and remote data collection.

#### 5.2.3.1.9 Diversity Switch

The diversity switch routes traffic to the near antenna site or the remote diversity antenna site. The operation of the diversity switch is described below in 5.2.3.4.

#### 5.2.3.1.10 Remote Baseband Processor

The baseband processors in the antenna sites are part of the diversity switch and microwave link implementation. The microwave link transmits the 256 Mbps burst data stream on three 90 Mbps carriers. The baseband processor assembles the three carriers to reconstruct the 256 Mbps data stream. It performs rate matching buffering between the diversity link and the satellite signal. This equipment also implements the clock recovery and carrier on/off signals discussed under diversity switch implementation.

#### 5.2.3.1.11 Modulator/Demodulator

A quadrature phase shift keyed (QPSK) modulator/demodulator is used. It operates at a nominal symbol rate of 128 megabauds per second (256 Mbps), where the bit-to-baud ratio is 2:1. The modulator accepts two parallel data channels (P and Q) in synchronism with the symbol clock and carrier on/off signal. The demodulator accepts these bursts of modulated carriers, recovers a reference carrier and symbol timing from each independently transmitted burst and demodulates them.

#### 5.2.3.1.12 Master Control Terminal

The master control terminal trunk station baseband processing is shown in Figure 5-4 and one of the two identical antenna sites is shown in Figure 5-5. The MCT differs from a standard trunk station in that it contains equipment for 256 Mbps trunk service and 128 Mbps CPS service. It also contains the flight operations control equipment. The CCS is provided orderwire access to network stations through the MCT. The flight operations control equipment is discussed in 5.3.

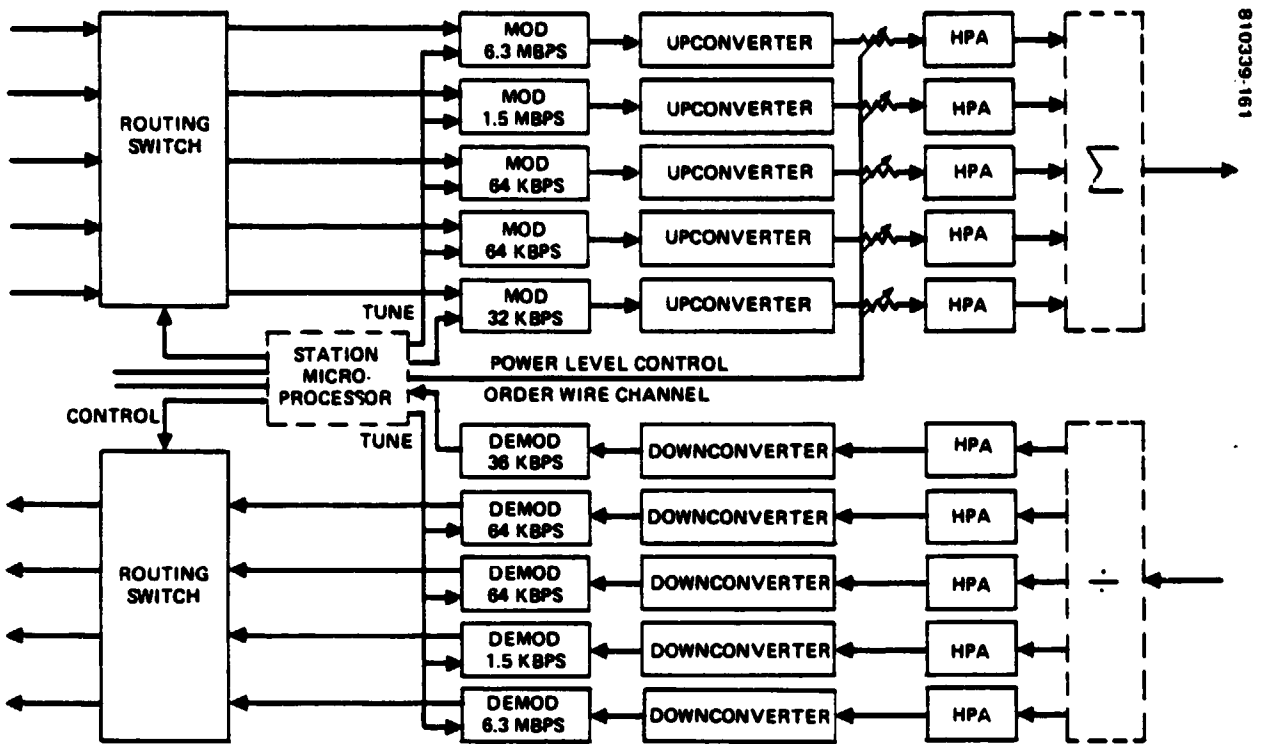


FIGURE 5-30. OPTION 2, FDMA SYSTEM

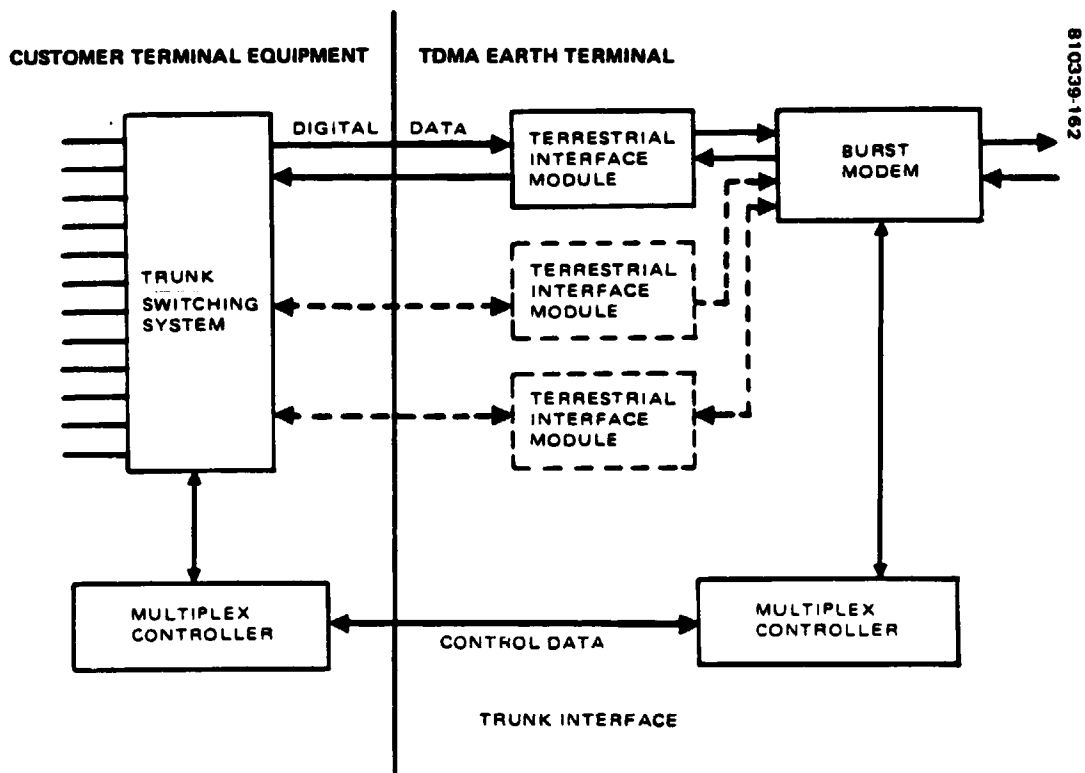


FIGURE 5-31. TRUNK INTERFACE

#### 5.2.3.1.13 Option 2 FDMA System

The additional hardware required at the trunk station to implement the FDMA system is shown in Figure 5-30.

#### 5.2.3.1.14 Hardware Availability

All the baseband equipment can be obtained from that presently available from various suppliers, or from existing equipment that can be readily modified to satisfy 30/20 GHz program needs.

#### 5.2.3.2 User Access

The trunk terminal provides interoffice circuit switching for bulk transmission of data at high transmission rates. Individual circuits and services for a specific destination are multiplexed to form the bulk transmission carriers. The customer terminal equipment includes switching, multiplexing, control equipment, and circuit terminating equipment for interfacing the customer terminal equipment to the TDMA earth terminal. The general interface is shown in Figure 5-31. The trunk switching system provides one or more, up to 5, DS3 (44.736 Mbps) digitally multiplexed data streams to the terrestrial interface module. Control data specifying the type of data, destination, and position in the multiplexed data stream is provided to the TDMA earth station multiplex controller by the trunk switch multiplex controller. The line interface is RS232 or IEEE 488 standard. The earth terminal TDMA equipment is capable of demultiplexing the incoming data stream from the terrestrial side and multiplexing it again to meet the formats required by the satellite side. Another demultiplexing, multiplexing may be performed in passing the received data stream to the customer facility. A detailed interface specification must be prepared for each trunk station where existing equipment may be used. For the experiment program, the primary data source is expected to be a tape recorder with recorded data sets which simulate a variety of trunk services.

Modern telephone equipment employing computerized switching and multiplexing, such as the Bell System's No. 4 Electronic Switching System (ESS 1) can be readily integrated into this system. The basic elements of the ESS 4 are shown in Figure 5-32. The subscriber lines and trunks enter a switching network (1) in which interconnection paths between lines or between lines and trunks are set up. Figure 5-33 is such a time division switching network. The controls for setting up different paths through the switching network are operated by the computer (2). The computer knows the status of the lines and trunks by means of a continuing scanning operation carried out by the activity scanner (3). The scanner detects when a handset is picked up, reads the number dialed, and detects when the receiver is replaced after a call. It also detects and interprets the signals from other switching offices received on the trunks. The signaling equipment (4) provides signals for "busy", ring signals, and on-hook/off-hook signals.

#### 5.2.3.3 Trunk Station Synchronization Implementation

Trunk station synchronization is implemented via the hardware burst synchronizer. Figure 5-34 is a functional diagram of the burst synchronizer. The burst synchronizer essentially measures the time difference between the



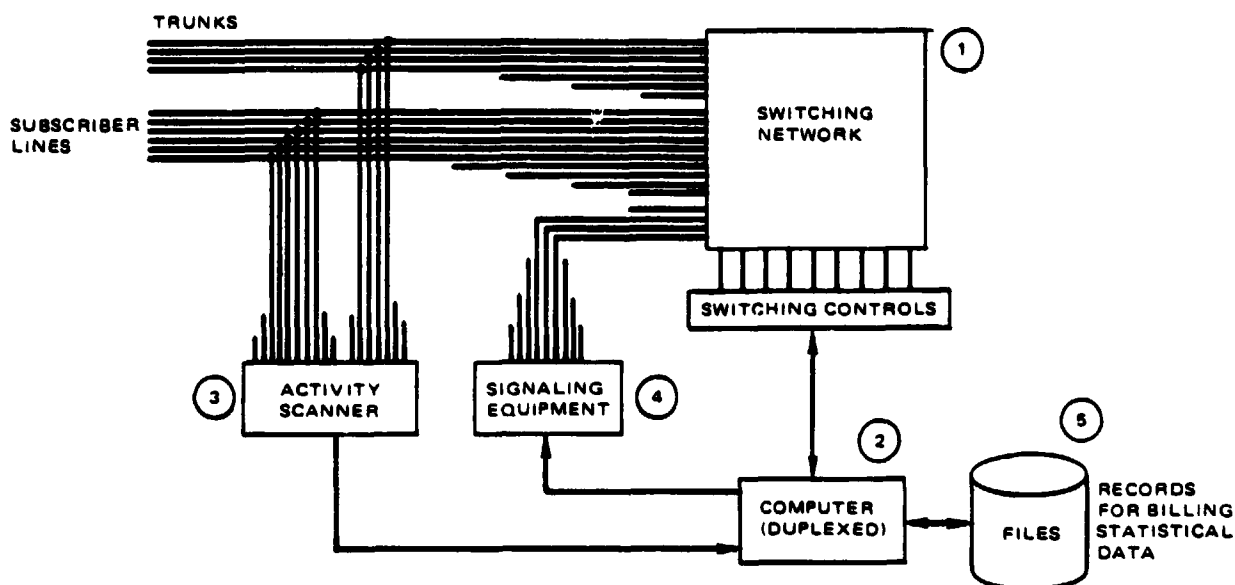


FIGURE 5-32. ESS 4 SWITCHING SYSTEM

received synchronization unique word and the start transmit output of a control counter decoder. A high resolution time interval meter is used to measure the time difference.

The preamble detector processes the received data stream to isolate the synchronization unique word. The unique word consists of a recognizable, specific bit pattern. Its purposes are:

- 1) To designate each burst position in the TDMA frame,
- 2) To designate the first information bit of each burst, and
- 3) To designate the significant instant of a frame start.

The unique word error rate from either misdetected or falsely detected words must be less than  $1 \times 10^{-8}$ .

To provide the desired performance with a minimum length unique word, an aperture technique is used. The time of reception of the unique word for all bursts to be received by an earth station is predicted. The unique word detector is enabled for a time period which is centered at this predicted time and extends for only plus or minus three symbols on either side of this time period. Figure 5-35 shows a typical circuit for unique word processing. The circuit allows a trunk station to lock onto a periodic sequence in a unique word by use of a gated N bit correlator.

The preamble detector provides frame start to the burst enable circuit and a received aperture to the demultiplexer. The burst position error measure processes the received metric code word and determines advance and retard timing for the burst enable circuit. The burst enable clocks the time delay from the frame start mark provided by the preamble detector to

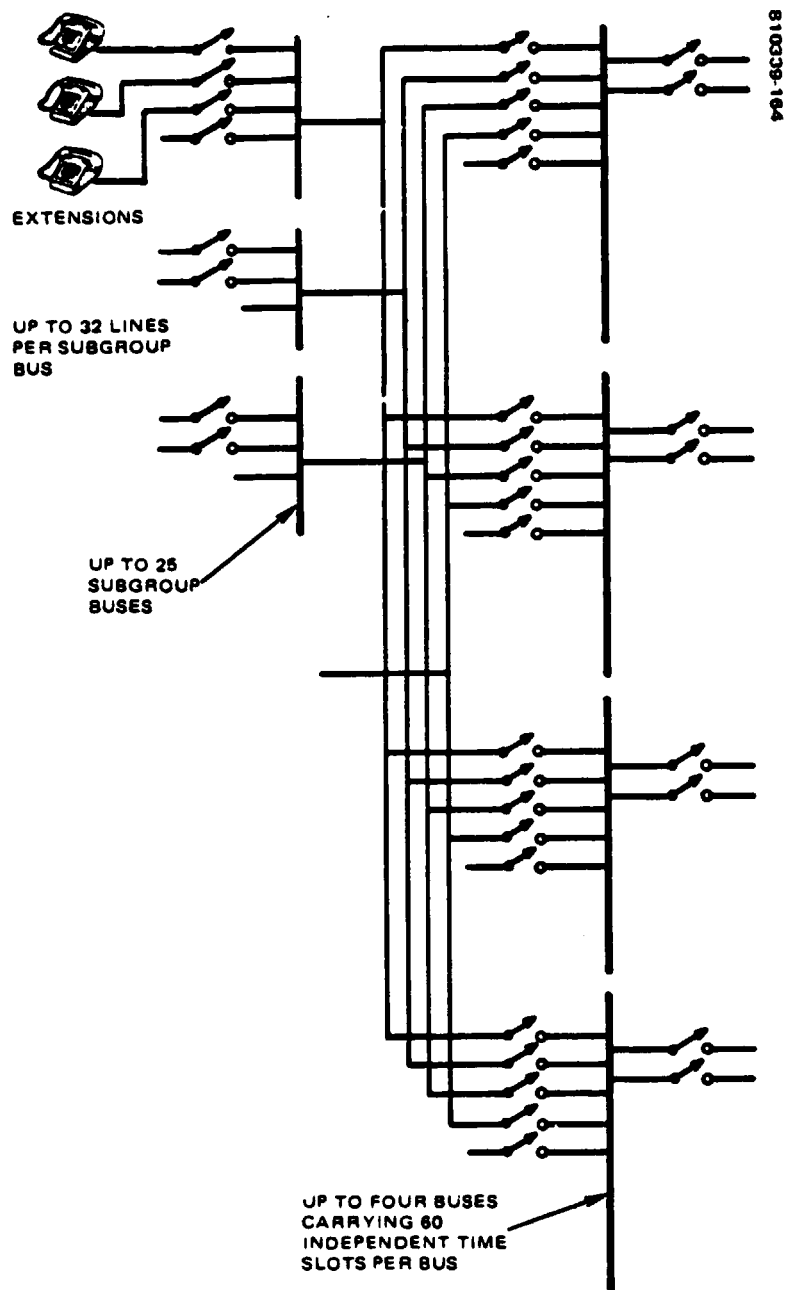


FIGURE 5-33. TIME DIVISION SWITCHING NETWORK

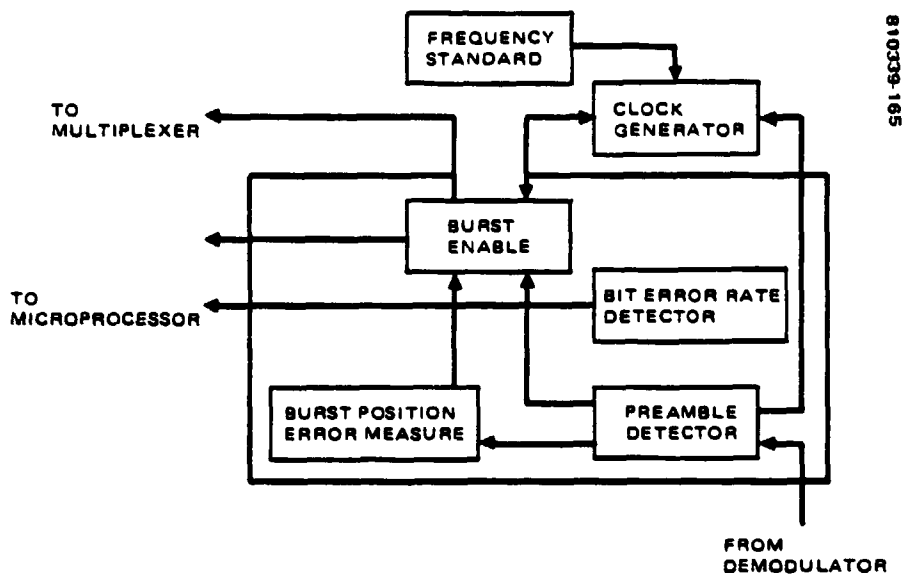


FIGURE 5-34. BURST SYNCHRONIZER FUNCTIONAL DIAGRAM

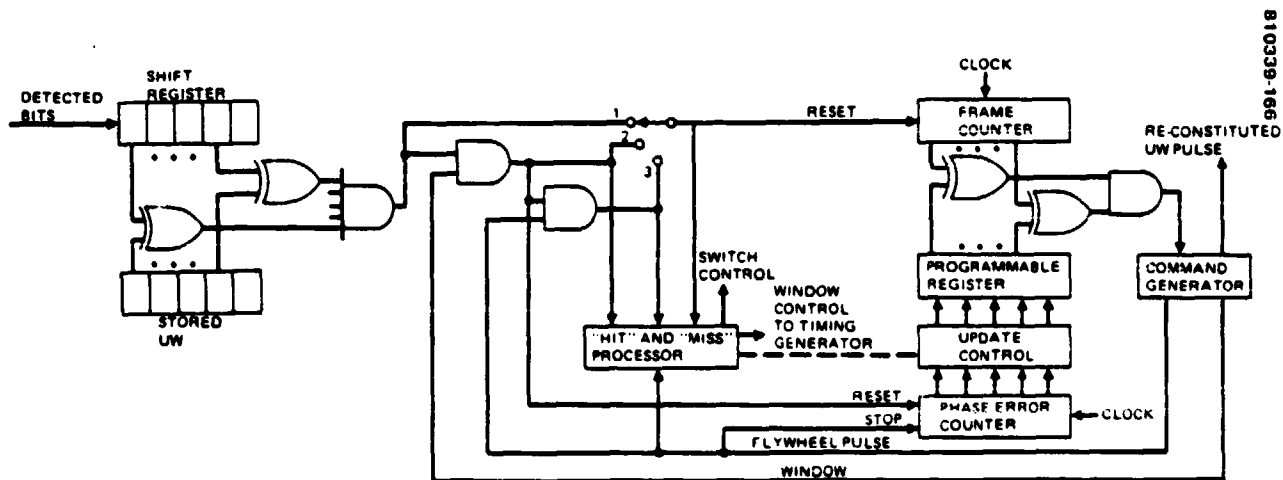


FIGURE 5-35. TYPICAL CIRCUIT FOR UNIQUE WORD PROCESSING

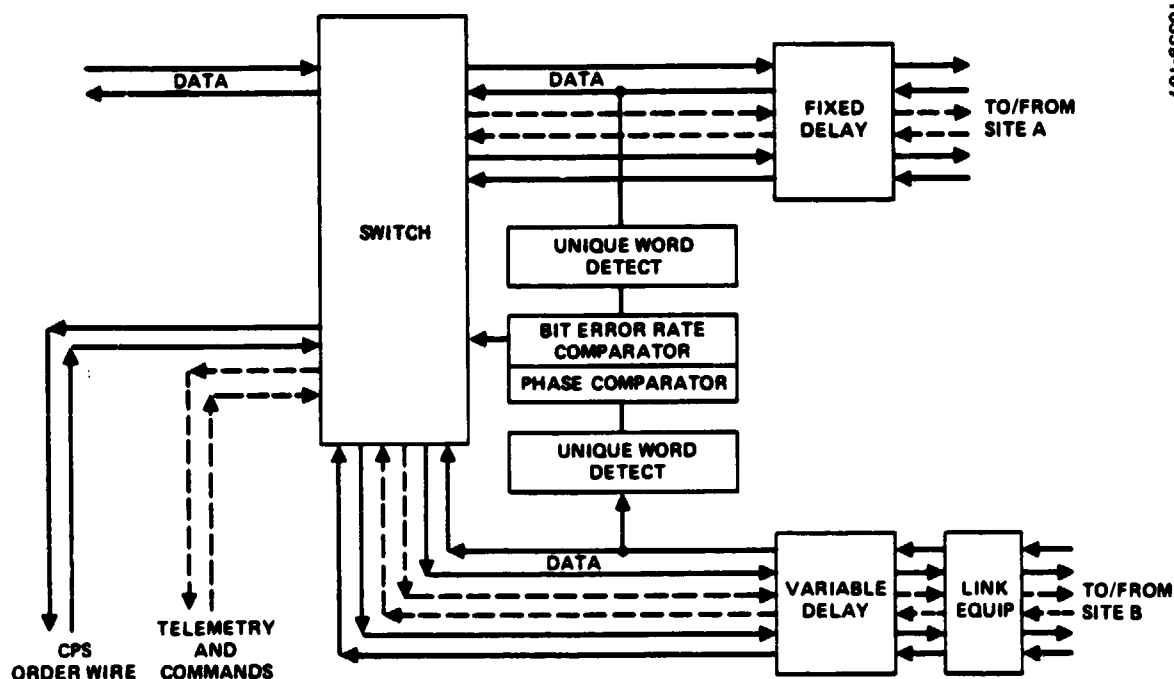
the transmit start mark. Transmit start is determined by the CCS from the channel assignments and corrected using information from the burst position error measure. It provides the burst enable signal to the TDMA multiplexer.

The clock generator is phase locked to the master oscillator in the spacecraft via the frame start word and burst position error measurements. The bit error rate detector monitors communications channel quality by testing for bit errors in the unique word sequence and its special fixed pattern code sequences. The bit error rate is used for analysis of communication service quality and a secondary measure for link control.

#### 5.2.3.4 Spatial Diversity Implementation

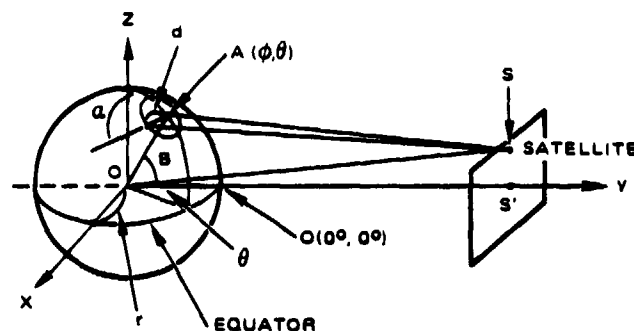
The diversity switch implementation is drawn in Figure 5-36. There are three problems in implementing a space diversity TDMA system:

- 1) diversity synchronization,
- 2) diversity switching control, and
- 3) interconnection of two diversity site antennas.

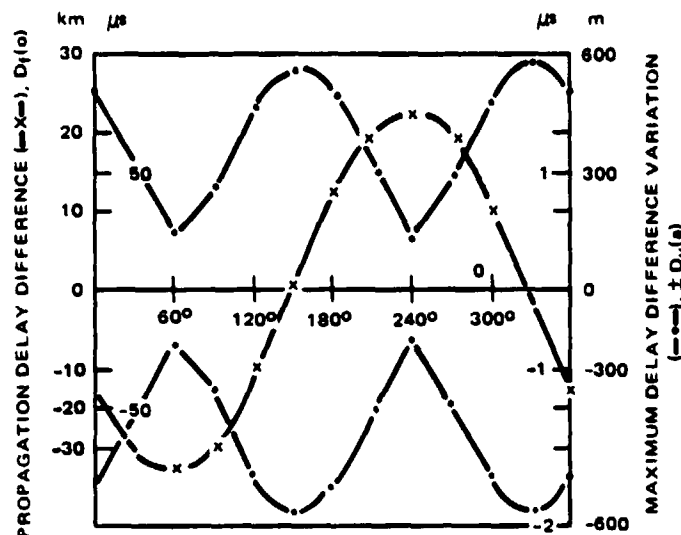


810339-167

FIGURE 5-36. DIVERSITY SWITCH IMPLEMENTATION



810339-168



PROPAGATION DELAY DIFFERENCE =  $S'A - S'B$   
 MAXIMUM DELAY DIFFERENCE VARIATION =  $\text{MAX. } (S'A - S'B) - (S'A - S'B)$

LOCATION OF SITE A:  $\phi$  (LONGITUDE) =  $40^\circ$ ,  $\theta$  (LATITUDE) =  $50^\circ$   
 DISTANCE BETWEEN SITES:  $d = 30 \text{ km}$

SATELLITE MOVEMENT RANGE:  $\begin{cases} \pm 0.5^\circ \text{ FOR NORTH-SOUTH DRIFT} \\ \pm 1.0^\circ \text{ FOR EAST-WEST DRIFT} \end{cases}$

FIGURE 5-37. PROPAGATION DELAY DIFFERENCE

#### 5.2.3.4.1 Diversity Synchronization

The distance between two diversity sites will cause considerable delay difference between the two diversity paths. Further this delay difference will vary as the satellite moves. In order to effect a diversity switch without loss of transmitted data, the transmission delays on the two paths must be measured and equalized. The delay time difference is absorbed by a delay device inserted in the path between the satellite and the burst synchronizer. Since the delay device is in the burst synchronizer loop both data continuity and uninterrupted burst synchronization are provided simultaneously. Measurement errors are absorbed by executing the diversity switch within a time slot, such as guard time, in which there is no significant information.

The delay capacity required for time delay equalization is strongly dependent on the satellite stationkeeping accuracy as well as the spacing and geographical location of diversity sites. Figure 5-37\* gives the propagation delay difference and its maximum variation as a function of the angle between the longitude of site A and the straight line connecting sites A and B. The maximum delay capacity for stations separated by 30 km and transmitting at 256 Mbps is 176.5  $\mu$ sec which is 45.2 kbits. The maximum delay variability is 3.8  $\mu$ sec which is 973 bits. Digital delay devices such as shift registers and random access memories are preferable for time delay equalization because of the ease of variable delay control, stability, and capability of high speed transmission.

To equalize the time delays in the downlink detection timings for the unique word of the sync burst from both antennas are compared at the phase comparator. A variable digital delay circuit at the receive side of diversity path B is adjusted to minimize the delay difference.

To obtain the precise delay difference in the uplinks, a standby burst consisting of a preamble is transmitted from the remote site in an assigned TDMA frame. The position error of the preamble burst is supplied by the TDMA terminal by means of the synchronization loopback. The delay circuit is adjusted according to this position error. As a backup technique, the delay circuit is adjusted according to delay differences measured on the receive side.

#### 5.2.3.4.2 Diversity Switching

The diversity switch controller measures and adjusts the delay difference on the two paths, and executes diversity switching according to signal quality measurements made on the two paths. Signal quality is primarily determined by measuring carrier to noise ratio of the beacon signal. Bit error rate measured in the unique word portion of the preamble may be used as a secondary measure. Switch control uses prime and backup logic. That is, site A will be selected as long as the signal quality on this path is not below that on the other path nor below threshold. The advantages of this logic are discussed in 5.2.2.4. Both up- and downlinks are switched from the same control decision.

#### 5.2.3.4.3 Diversity Interconnection

Interconnection of the diversity terminals by cable, microwave radio, waveguide, and fiber optic techniques were studied. The microwave link provides the most economic link with no technical difficulty. Two antenna sites 30 km apart can be connected without a repeater. Since the microwave link is implemented with three 90 Mbps carriers, the burst data stream must be constructed at the antenna site and the PSK modem is located at the remote

---

\*From Watanabe, et al., "Space Diversity System for TOMA Satellite Links," IEEE 4th International Conference on Digital Satellite Communications, October 1978, pp.319-326.

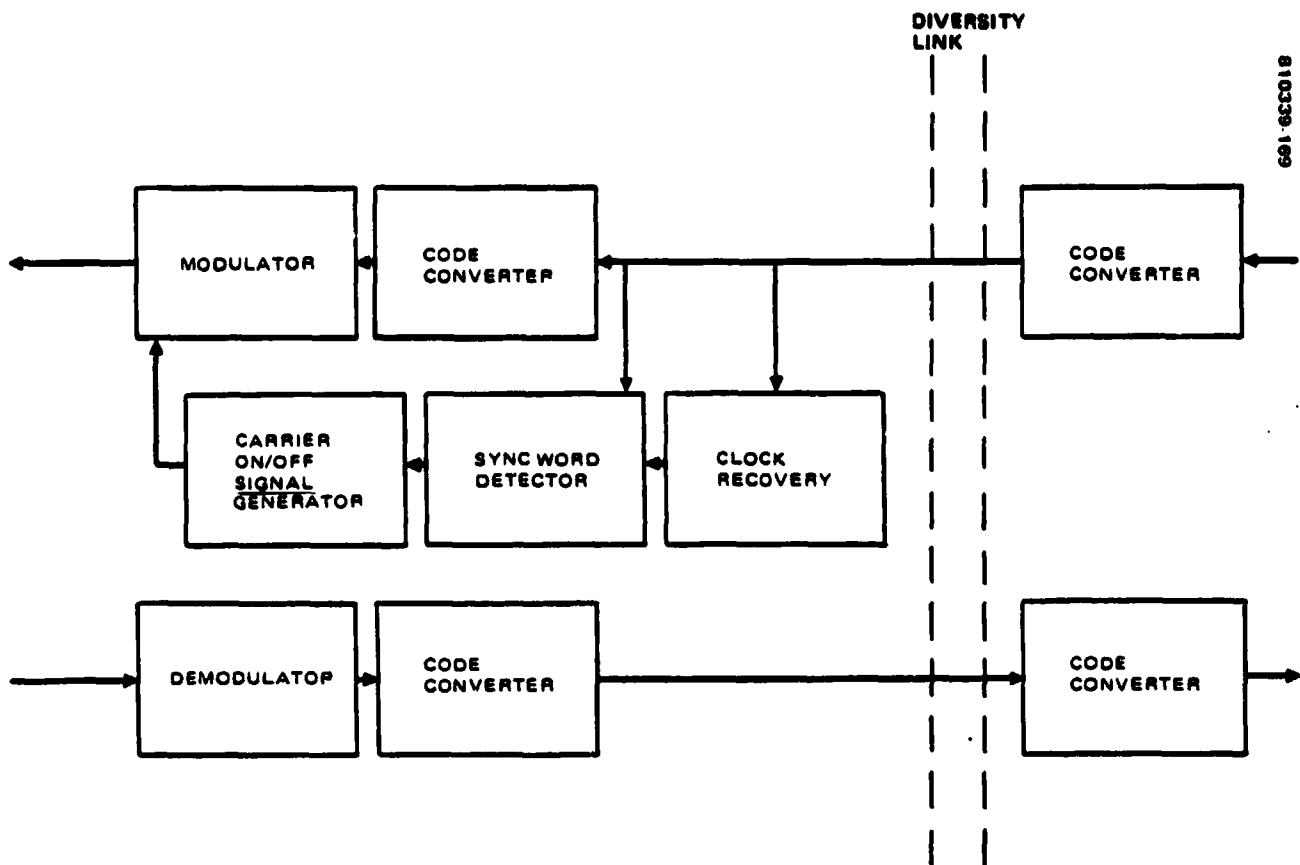


FIGURE 5-38. REMOTE SITE CLOCK RECOVERY AND MODULATOR ON/OFF SIGNAL GENERATION

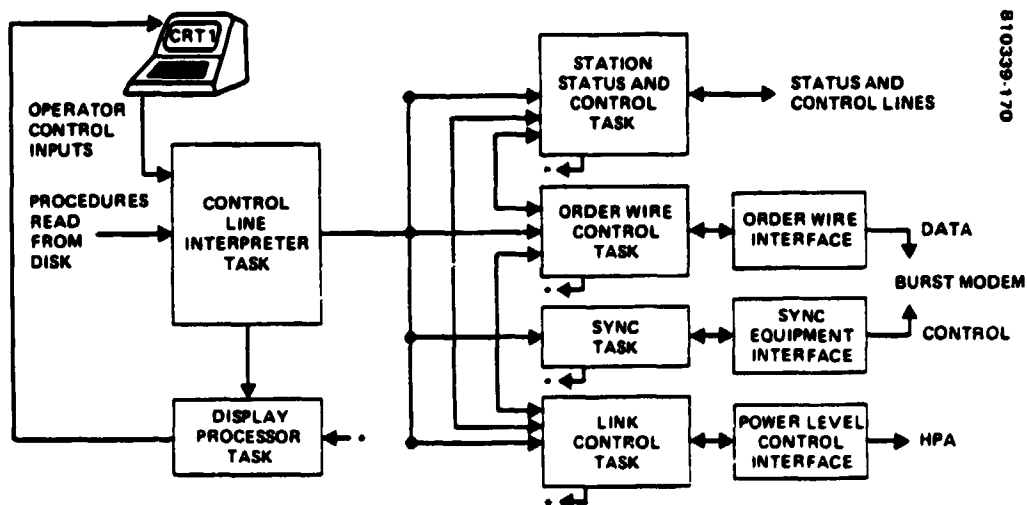


FIGURE 5-39. TRUNK STATION SOFTWARE

antenna site. Carrier on/off signals and station clock signals must be provided at the remote site. This problem is solved by assigning a synchronization word to a burst to be transmitted. This word, which has a unique pattern of several bits, is placed just before the burst and detected by a sync word detector to form the carrier on/off signal (Figure 5-38). A clock recovery circuit extracts the clock from the signal in the uplink to supply the station clock to devices at site B.

#### 5.2.3.5 Trunk Station Data Processing

The trunk station data processing is implemented in a Digital Equipment Corp. LSI-11 microprocessor. The real time software for trunk stations is taken from the CCS real time software architecture. The trunk station software architecture is shown in Figure 5-39. Operator interfaces from the basic architecture are retained; however, the system data table is not needed because data volume is much smaller. Interprocess communication is via common pool memory. The real time tasks, shown in the figures, reflect those of the CCS. There are no off-line tasks. The major tasks and their functions are:

- 1) Station status and control: collect status data from station equipment, format data for transmission to the CCS or local recording, accept reconfiguration commands from the CCS, pass the commands to the proper equipment.
- 2) Orderwire control task: controls the exchange of control messages between the CCS and the trunk station
- 3) Synchronization task: processes burst error measurements and controls the burst synchronizer for initial acquisition
- 4) Link control task: processes beacon data to determine power level control signal for HPA. Request FEC coding initiation by CCS.

#### 5.2.3.6 CCS Staffing

Based upon experience with other orbital mission operations, the CCS staffing is recommended as follows.

##### 5.2.3.6.1 Operations Group

Provides 24 hour per day, 7 day per week operation. Each shift consists of the following:

- 1) Flight segment controller: responsible for the health, safety, and operation of the flight segment
- 2) Communications controller: responsible for the real time operation and management of the communications network



#### **5.2.3.6.2 Planning and Analysis Group**

The group provides for planning and performance analysis function. This is normally on a single shift 5 days per week basis. Weekend planning is performed in advance during normal work week. This group consists of the following positions:

- 1) Planning and Operations Director: responsible for overall operation of the CCS
- 2) Mission Planner: responsible for translation of user requests and system requirements into overall system schedule
- 3) Network Scheduler: responsible for planning communications, resources, and experiments to support user requirements.
- 4) Flight Segment Planner: responsible for planning use of flight segment resources in response to user needs and flight segment housekeeping requirements
- 5) Flight Segment Analyst: responsible for detailed analysis of flight segment including trend analysis, power analysis, expendable management, orbit analysis, and anomaly investigation
- 6) Experiment System Analyst: responsible for detailed analysis of communications network including service acceptability, diversity switch performance, synchronization performance, network control, and anomaly analysis
- 7) Hardware Maintenance: responsible for daily maintenance of all station hardware
- 8) Software Maintenance: responsible for problem analysis and correction of software problems

#### **5.2.4 Customer Premise Service Stations**

The customer premise service (CPS) stations will be placed primarily in the eastern United States. User access is via TDMA through the satellite scanning beam antenna and baseband processor. The CPS station provides telephone digital data and video conference service tailored to the user traffic density. Rain attenuation will be compensated for by forward error correction codes and link power level control. Control of the CPS is provided by order-wire from the CCS. The CPS station requirements are shown in Table 5-9.

**TABLE 5-9. CPS STATION REQUIREMENTS**

Communication access	TDMA burst rate	32 Mbps uplink 256 Mbps downlink	128 Mbps uplink 256 Mbps downlink
	Digitally multiplexed carriers	1 DS-2 (6.3 Mbps)	7 DS-1C (22.06 Mbps)
	Minimum burst	128 bits	512 bits
	Interconnect any CPS stations		
	Data quality	BER $5 \cdot 10^{-6}$	
	Simulate demand access		
	Reservation access orderwire		
Link margin	15 dB uplink	6 dB downlink	
	FEC coding applied to individual link		
	FEC code up to 25 Mbps data in any frame		
Synchronization	Burst times synchronized to within 60 ns of system time		
Configuration	Antennas: 3m and 5m		
Other	Remote control and monitoring		

#### 5.2.4.1 CPS Station Hardware Definition

The hardware configuration of a CPS station is shown in Figure 5-6. The TDMA terminal equipment for the CPS station is the same as that described for the trunk station in 5.2.3.1 with the following exceptions:

- 1) Data rates are lower thus smaller buffers are required in the terrestrial interface module and multiplexer/demultiplexer.
- 2) FEC coding is implemented within the multiplexer/demultiplexer (shown in Figure 5-42).
- 3) CPS burst synchronization error measurements are made by the baseband processor. These error measurements are returned to the CPS station for processing by the burst position error measurement in the burst synchronizer.

The RF equipment for the CPS station is discussed in 5.1.

#### 5.2.4.2 User Access

The CPS terminal provides communications facilities tailored to customer needs. The customer equipment ranges from the familiar telephone set to sophisticated data terminal equipment, including computer terminals and video conferencing equipment. A large variety of equipment is expected to be located at customer facilities, depending on the needs of the individual customer. The general interface is shown in Figure 5-40. The multiplexing switch provides one or more DS-1, DS-1C, or DS-2 digitally multiplexed data streams to the terrestrial interface module. Control data

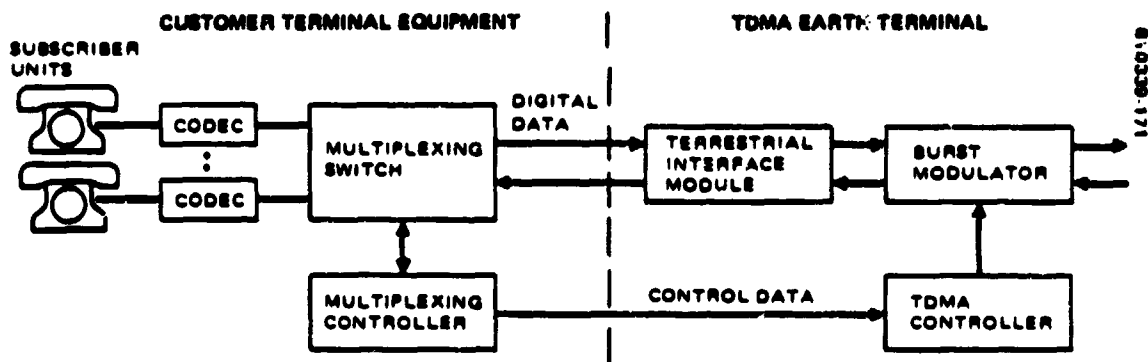


FIGURE 5-40. CPS STATION INTERFACE

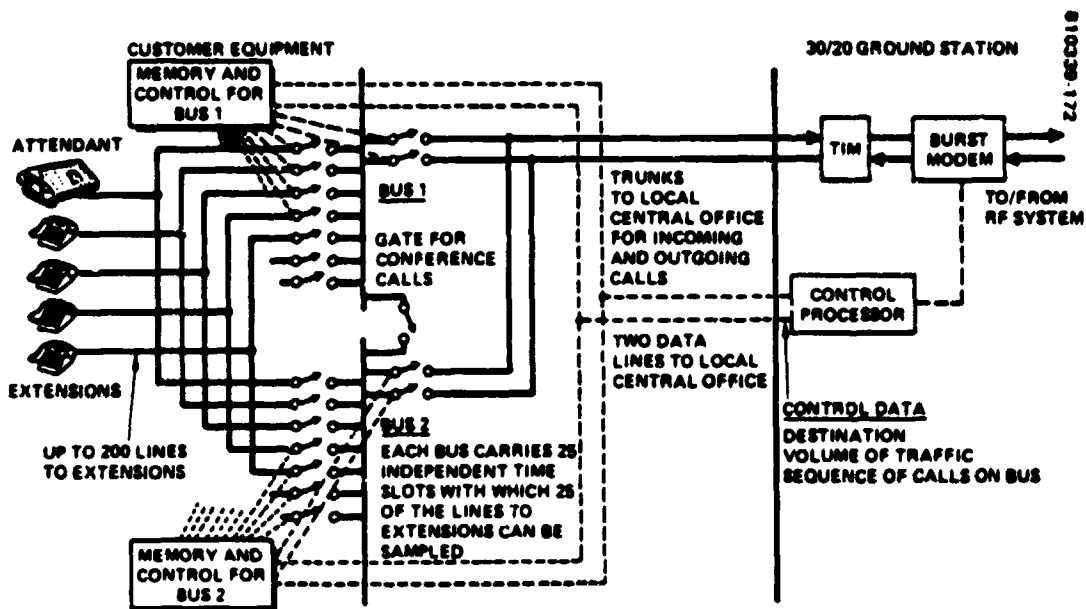


FIGURE 5-41. BELL SYSTEM NO. 101 ELECTRONIC SWITCHING SYSTEM

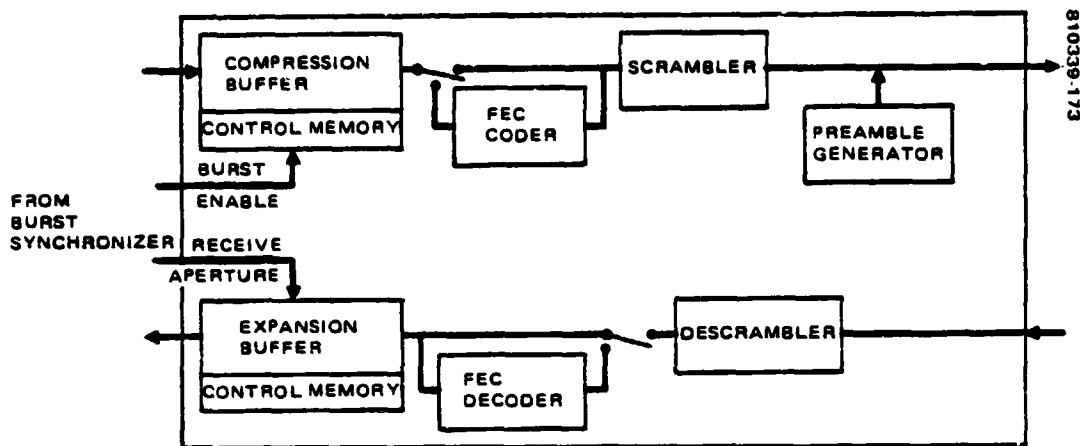


FIGURE 5-42. CPS TDMA MULTIPLEXER/DEMULPLEXER

specifying the type of data, destination, and position in the multiplexed data stream is provided to the TDMA controller via the customer terminal equipment multiplexing controller. The line interface uses the RS232 or IEEE 488 standard. The earth terminal TDMA equipment is capable of demultiplexing the incoming data stream from the terrestrial side and multiplexing it again to meet the frame format on the satellite side. Similarly, data received from the satellite may be demultiplexed and multiplexed for relay to the customer terminal. A detailed interface specification must be prepared for each station where existing equipment may be used. The general interface has sufficient flexibility to accept signals from many types of equipment. For the experiment program, the primary data source is assumed to be a tape recorder with recorded data sets to simulate a variety of multiplexed data services.

Modern telephone equipment employing computerized switching and multiplexing, such as the Bell System No. 101 electronic switching system (ESS 101) can be readily integrated into this system. Figure 5-41 shows the ESS 101 system. The ESS 101's memory and controller assigns the sequence of connecting the individual subscriber lines to the bus and collects dialed digits and signaling data for relay on the control bus. The ESS 101 control processor is connected to the CPS control processor. The signaling data and sequence of calls on the bus are passed to the CPS processor via these control lines. The telephone traffic is sequentially stored in the terrestrial interface module (TIM) memory as it is received on the bus. The burst modem randomly reads telephone traffic from the TIM in the sequence required for the uplink frame format. This sequence is determined by the routing task of the CCS software and sent to the CPS control processor via the order wire.

#### 5.2.4.3 FEC Coding Implementation

The FEC coding approach adopts sub-burst encoding in which the individual sub-bursts between the satellite baseband processor and the CPS station, or vice versa, are encoded. FEC coding is applied to all data bursts transmitted or received by a CPS station when coding is invoked by direction of the CCS. The FEC codec is installed in the multiplexer/demultiplexer as shown in Figure 5-42. FEC coding is not applied to the sync burst or preamble. The preferred point of FEC application is between the compression/expansion buffer and the scrambler/descrambler. In operating the FEC codec two major problems regarding the clock are encountered.

- 1) The difference in data rate between the input and output of the FEC
- 2) The need to maintain the received clock until decoding is completed

To cope with the first problem intermittent clocking is employed. Here the uncoded data stream at the terrestrial side of the FEC codec is operated with an intermittent clock while at the satellite side, the codec data are processed with a continuous terminal clock. The intermittent clock is obtained from the terminal clock by leaving gaps for insertion of the check bits.

The second problem is handled by the elastic buffer in the demultiplexer. The elastic buffer converts the received burst data to a continuous bit stream which is synchronous with the customer terminal equipment clock.

#### 5.2.4.4 CPS Station Data Processing

The CPS station data processing is implemented in a Digital Equipment Corp LSI-11 microprocessor. The software architecture and implementation is the same as for the trunk station which is discussed in 5.2.3.

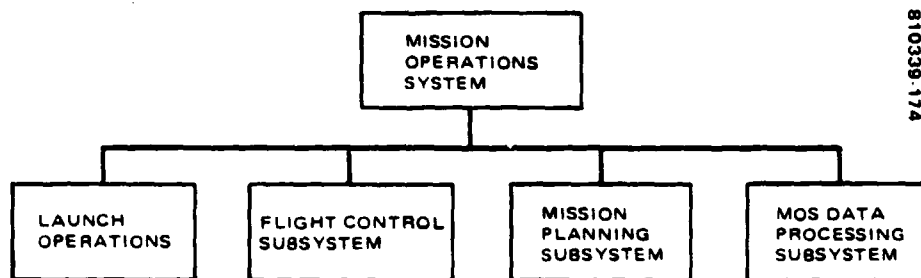


FIGURE 5-43. MISSION OPERATION SYSTEM ORGANIZATION

### 5.3 IMPLEMENTATION OF MISSION OPERATIONS

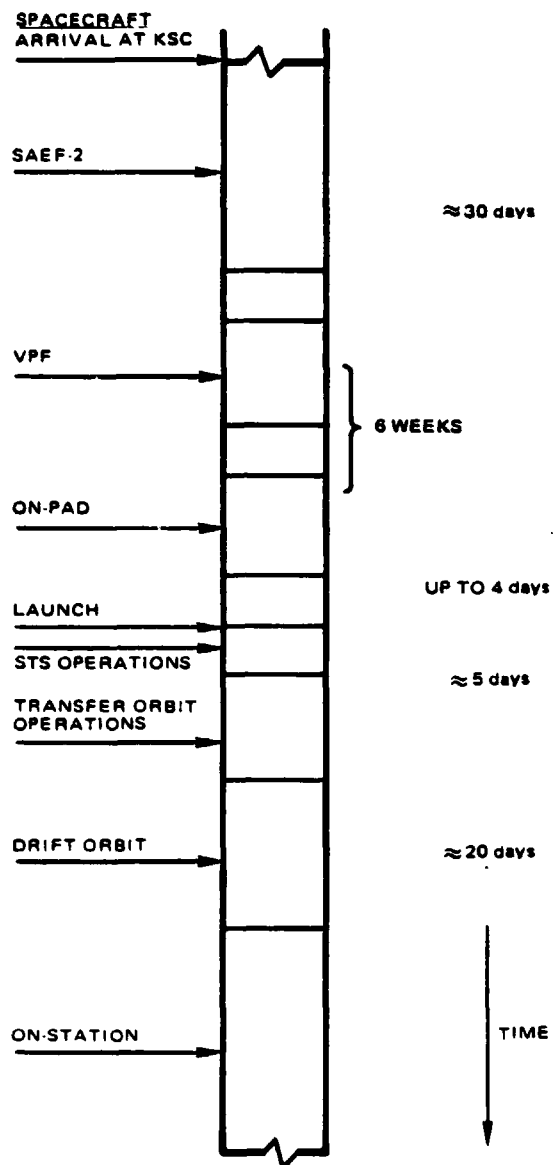
The mission operations system (MOS) encompasses the hardware, software, and functions necessary for control of the spacecraft bus, the communications payload, and attitude determination and orbit control, as well as launch support related activities required to put the satellite on-station and execute the on-orbit test to ensure proper operations of the spacecraft payload. The MOS is organized into four subsystems as shown in Figure 5-43. The launch operations subsystem provides all facilities for control of launch activities. The flight control subsystem performs on-line command and control functions, the mission planning subsystem performs all off-line operations, and the data processing subsystem supplies the computational resources required by the other subsystems.

The MOS shall be capable of supporting all operations required to put the satellite on orbit and to operate the spacecraft and the payload for the two year experiment period. The allocation of the key requirements which are major drivers in the MOS design is given in Table 5-10. These requirements are developed from the functions presented in Section 4.2, Launch Vehicle System.

The mission operations system design was developed by applying methods and design features that have resulted in other successful control centers, including Palapa, GMS, LEASAT, and advanced DOD systems. Subsystem requirements were allocated based on common functional characteristics. The spacecraft command center is combined with the communications network control center to simplify the software and person-to-person interfaces.

TABLE 5-10. MISSION OPERATIONS SYSTEM REQUIREMENTS ALLOCATION

Launch Operations	Flight Control	Mission Planning	Data Processing
Provide spacecraft handling and prelaunch integration and test at Kennedy Space Center.	Perform command generation, transmission, management, and verification of all spacecraft bus and payload commands.	Perform mission planning to effectively control spacecraft resources. Coordinate mission operations with experiment operations.	Provide engineering unit conversion, limit checking, alarm processing, and archiving for housekeeping telemetry.
Provide capability to process telemetry and send commands through remote control station compatible with STS launch.	Perform real time monitoring of spacecraft health and payload operation.	Perform attitude and orbit determination.	Provide data archiving.
Provide capability to direct launch operations from CCS.	Provide capability to send commands and process telemetry from CCS. Provide capability to generate and send manual command sequences in real time, provide manual and automatic command transmission capability, provide special handling for critical and hazardous commands.	Perform maneuver analysis and stationkeeping. Perform spacecraft health and performance evaluation for all spacecraft subsystems.	Provide computing, storage, and display capacity for spacecraft control.



810339-175

FIGURE 5-44. TIMELINE

The design implementation provides cost-effective overall system flexibility, efficiency, reliability, and growth capacity. The design is a low risk data processing development which is based on the following:

- 1) Proven hardware configured for flexibility and availability based largely upon the LEASAT ground system
- 2) Proven and demonstrated software designs that have evolved with experience with many command and control systems
- 3) Proven operations concepts using a cost-effective degree of automation and consideration of flight system health and safety

### 5.3.1 Launch Operations

The launch operations phase of mission operations concerns all activities required to place the spacecraft at its orbital station. It begins with shipment of the spacecraft to Kennedy Space Center and ends when the spacecraft is declared operational for experiments. The launch operations time line is shown in Figure 5-44.

The major operations of the prelaunch activity are shown in Figure 5-45. Launch Operations Flow. Upon receipt by air shipment, the spacecraft is taken to the Safe Arm and Encapsulation Facility (SAFE2) for mechanical operations and spacecraft functional tests. These include filling the propulsion system, PKM installation, STS cargo integration tests, and shuttle compatibility tests. The payload is then transported to the launch complex payload changeout room (PCR). The PCR affords the final opportunity to functionally test the spacecraft in its operating modes. This is also where final cleaning and wipedown is to be performed and the nonflight protective covers removed.

While the spacecraft is installed in the shuttle, it is unpowered. The battery enable plugs are installed; however, the only loads that are connected to the batteries are the battery cell multiplexers, which only draw a total of 22 mA. During those brief times when the STS payload bay is sun facing, the solar panel is illuminated and the spacecraft bus powered. The bus limiters limit the voltage to 42.5 volts dc maximum.

To meet the thermal constraints previously described, special heaters are attached to the spacecraft while it is inside the shuttle through the cradle heater controller which is powered from the STS payload power. These heaters are thermostatically controlled to turn on at 65 and off at 70°F. Their dissipation is:

- 1) Solar panel substrate: 1750 watts
- 2) RCS propulsion: 20 watts
- 3) Perigee kick motor: 60 watts



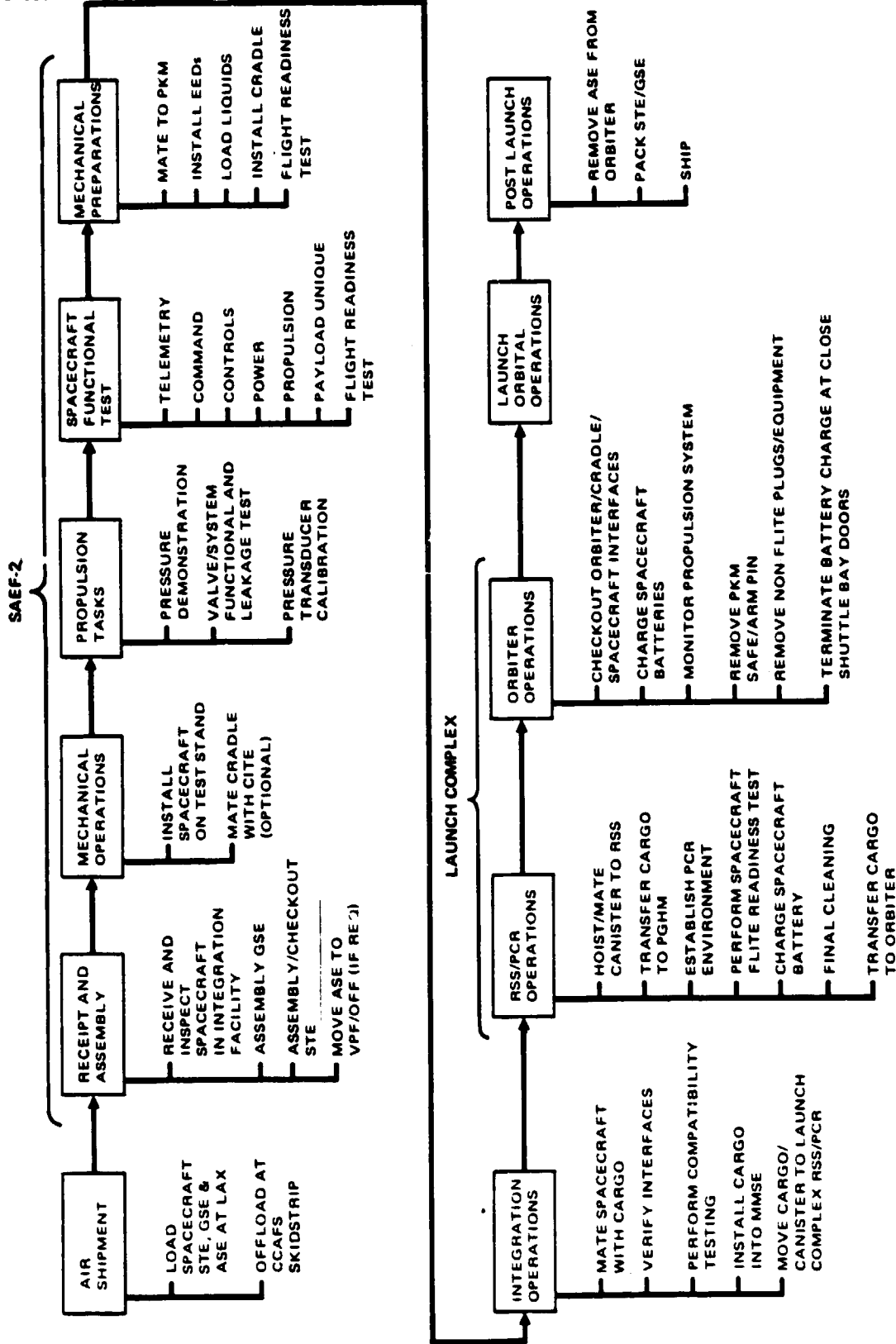


FIGURE 5-45. LAUNCH OPERATIONS FLOW CHART

- 4) TT&C antenna actuator: 10 watts
- 5) Cradle and cradle electronics: 230 watts (turned on after spacecraft ejection)

Since the spacecraft is not turned on while in the shuttle, there is not a great deal of spacecraft data that needs to be monitored. However, for the purposes of postflight analysis, the STS signal conditioning unit (SCU), which is connected to the STS payload tape recorder, is used to monitor engineering data. These data include the following:

- 1) Accelerometer measurements
- 2) Strain gauge measurements
- 3) PKM temperature
- 4) Cradle temperature
- 5) Solar panel temperature
- 6) Propulsion tank temperature

Spacecraft status is monitored in real time at the standard switch panel (SSP) display, and by the astronaut on his CRT via the STS provided multiplexer-demultiplexer (MDM) system. The following functions will be monitored:

<u>SSP</u>	<u>MDM</u>
Payload power on/off status	Cradle pins position (all four)
SCU on/off status	Solar panel temperature
Payload heaters on/off status	PKM temperature
Cradle pins lock/unlock status	Propulsion tank temperature
Spring holddown lock/unlock status	Cradle temperature
Enable squib fire status	

The launch sequence of events, shuttle ejection procedure, and post ejection sequencer operation are discussed in 4.2.

The spacecraft design and all transfer orbit operations are compatible with the loss of a single ground station (12 hours, maximum, before second

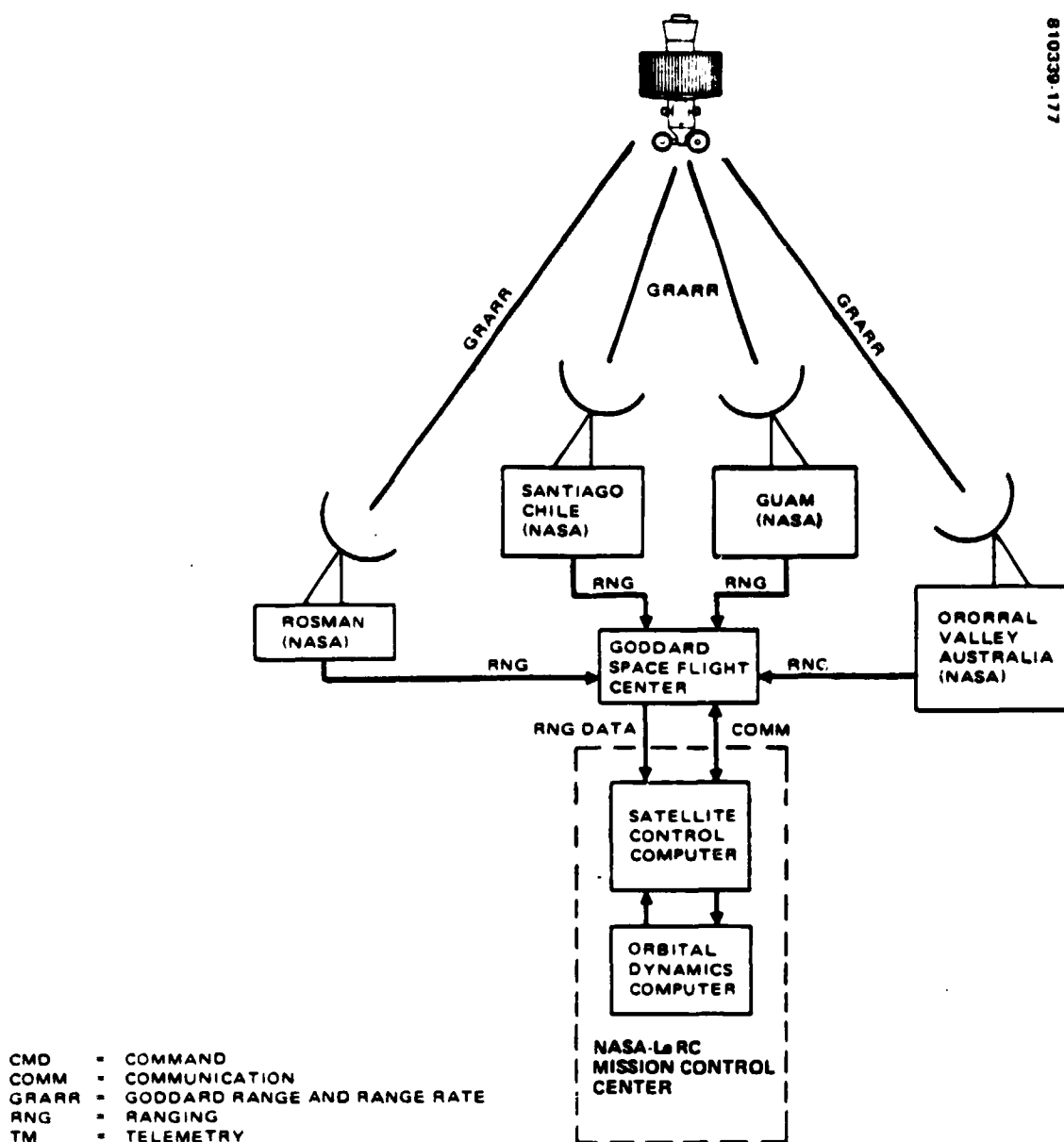


FIGURE 5-46. ASCENT OPERATIONS GROUND CONTROL SYSTEM BLOCK DIAGRAM

ground station visibility). The spacecraft automatically turns itself on post-ST<sub>S</sub> ejection and configures itself into a safe configuration, including initialization of the telemetry and command subsystems. Approximately sized spacecraft heaters automatically turn on at the right time in order to maintain thermal balance. Battery charge management is not required until the fourth subtransfer orbit during eclipse season. Six eclipses result in a maximum battery depth of discharge (DOD) of 45 percent.

#### 5.3.1.1 Ground Control System

Figure 5-46 is a system block diagram that presents an overview of the ground control system for ascent operations. Two telemetry and command stations (TACS), one located in Guam and the other at Rosman, North Carolina, provide command and telemetry visibility of the spacecraft on every apogee during the transfer orbit phase. A Mission Control Center, to be established at NASA-LERC, Cleveland, provides central direction of launch operations. Ranging measurements for orbit determination are performed by coordination between the MCC and NASA Goddard (GSFC). GSFC controls a network of ranging stations (Rosman, North Carolina; Santiago, Chile; and Orroval Valley, Australia) that measure the slant range to the spacecraft.

The two remote tracking stations, operated by NASA will act as relay stations between the spacecraft and the MCC during the transfer orbit phase of the mission. Figure 5-47 is a simplified block diagram of a TACS. The RF equipment (antennas, transmitters, receivers, etc.) is provided by NASA - GSFC. The baseband equipment used to control the spacecraft during transfer orbit will be provided by Hughes to the MCT. It consists of the command, telemetry, computer, communication and timing subsystems and related test equipment. Telemetry and ranging data received at the TACS are transferred to the MCC via communications links.

The MCC located within the MCT in Cleveland, is the central location for all decision making activities associated with the transfer orbit, synchronous orbit injection and initial on-station control of the 30/20 GHz Experiment System Spacecraft.

As shown in Figure 5-48 the MCC facility consists of a spacecraft control computer, an orbital dynamics computer plus additional control, display and communication equipment. The spacecraft control computer monitors and initiates all activities associated with the mission. The orbital dynamics computer performs the analyses and determines orbital parameters and maneuver commands. Operational control instructions for the ground control system and commands for the in-orbit spacecraft originate from the MCC and are routed in the form of computer requests to either TACS.

#### 5.3.2 Flight Control Subsystem

The flight control subsystem is illustrated in Figure 5-49. The design goal is to provide efficiency and flexibility in response to real time requirements. Nonautomated operations allow for manual process control, manual

TABLE 5-11. FLIGHT CONTROL FUNCTIONS

<u>Ranging</u>	<u>Command Processing</u>
Range tone measurements	Timed command processing
Spacecraft position file	Command formatting
<u>Oscillator Control</u>	Command transmission
Determine long term drift	Command verification
Update oscillator	<u>Telemetry Analysis</u>
<u>Ground Segment Status</u>	Spacecraft health and performance analysis
Monitor status of network stations	Telemetry limit checks
Alarm generation	Alarm generation
	Trend analysis

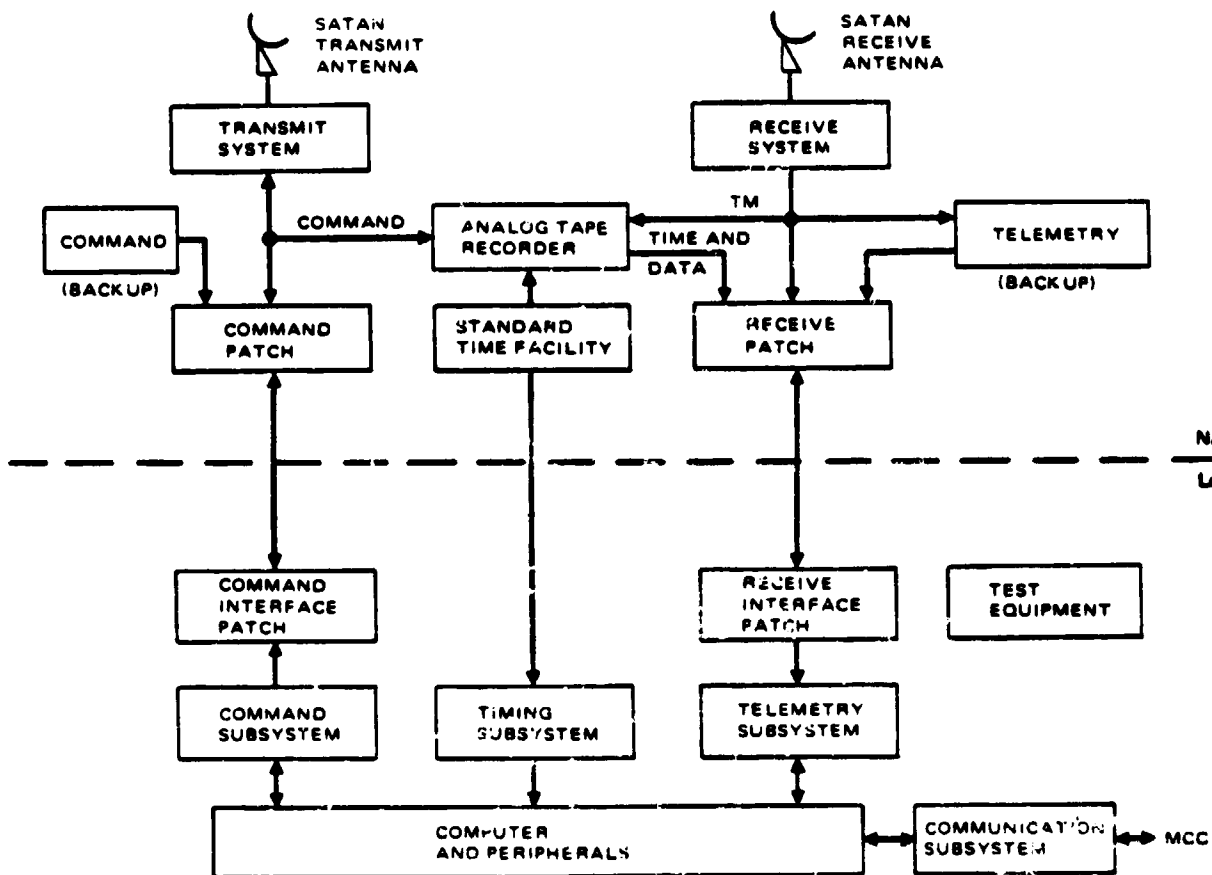
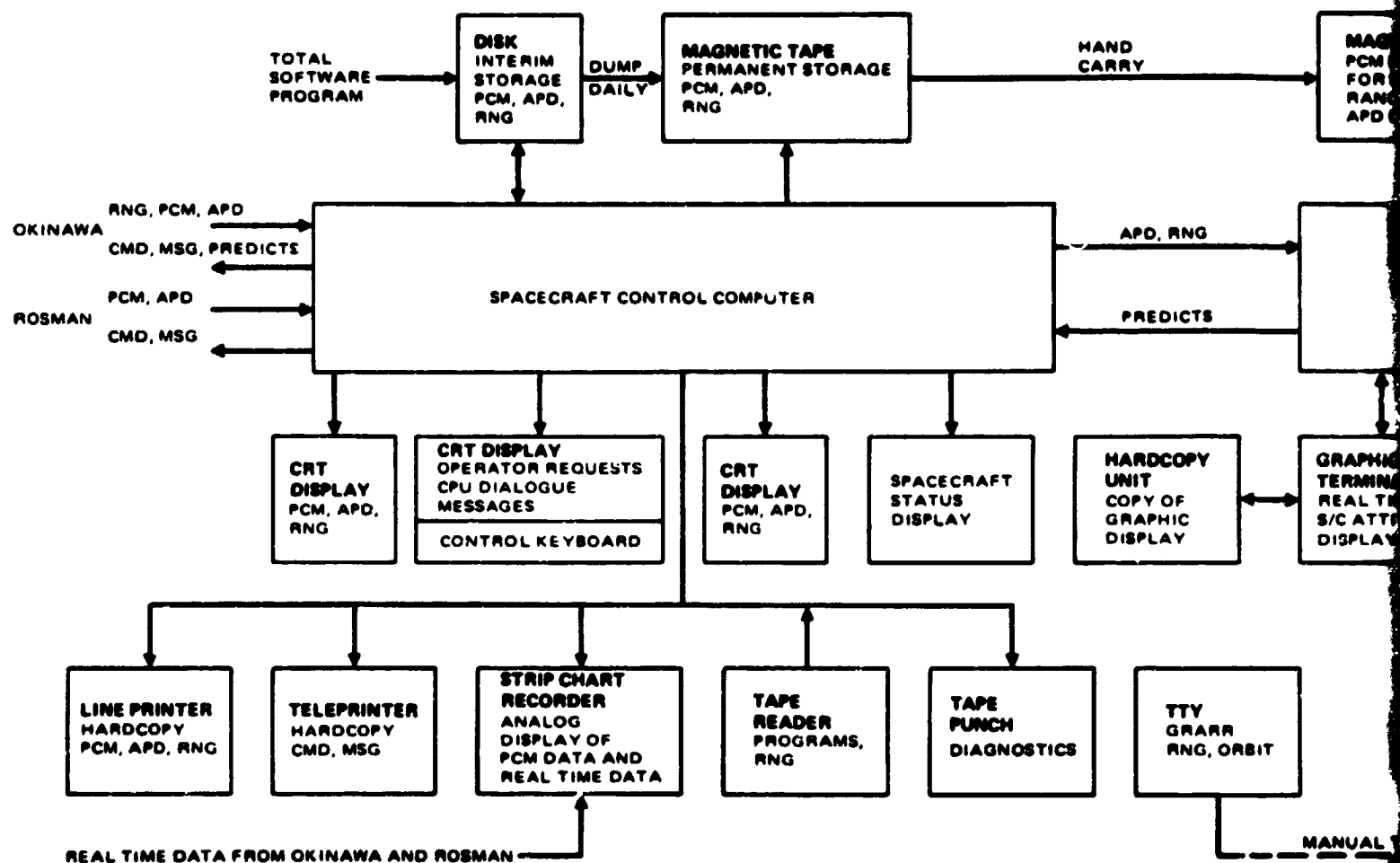
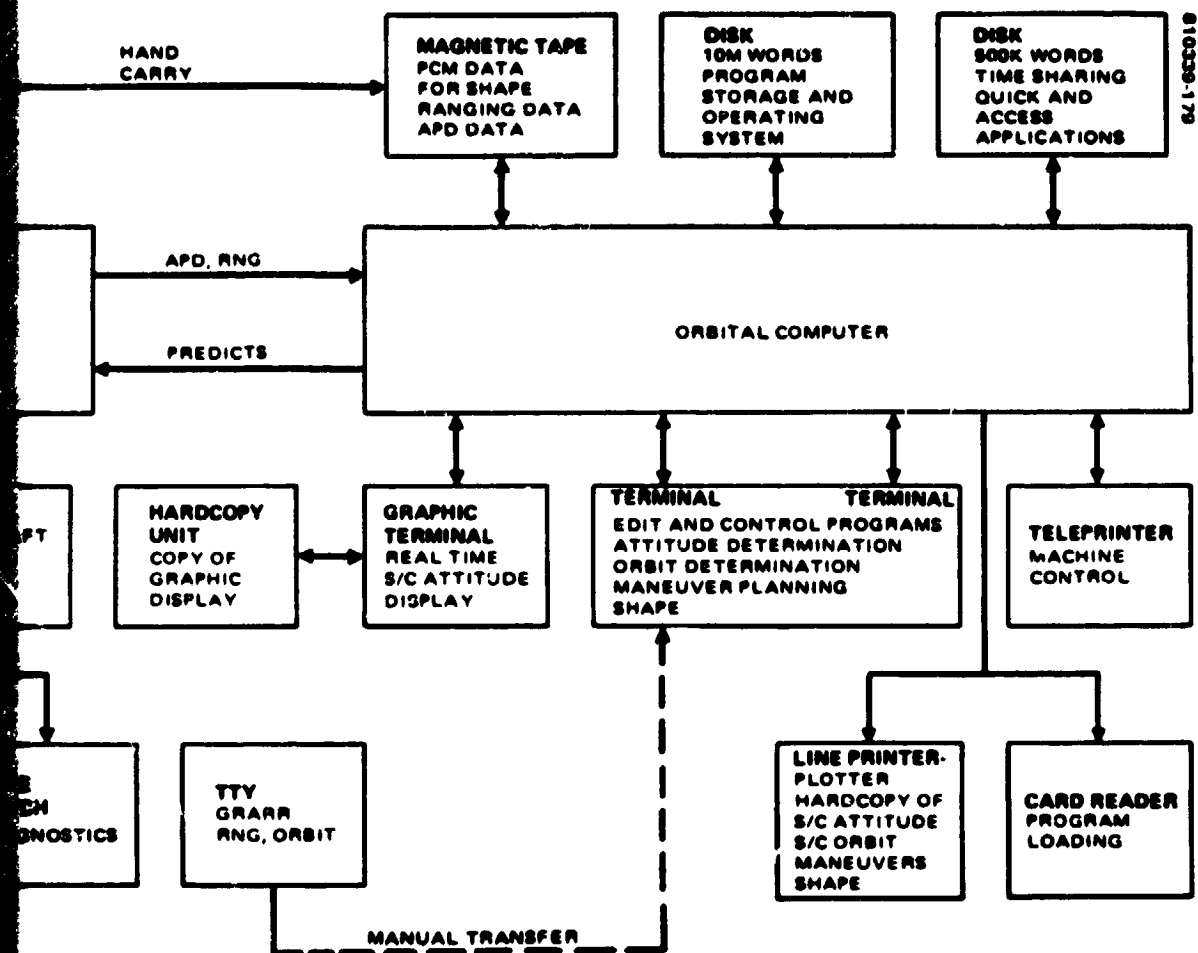


FIGURE 5-47. TACS SIMPLIFIED BLOCK DIAGRAM



APD - ATTITUDE PULSE DIGITIZER  
 CMD - COMMAND  
 CPU - CENTRAL PROCESSOR UNIT  
 CRT - CATHODE RAY TUBE  
 MSG - MESSAGE  
 PCM - PULSE CODE MODULATION  
 RNG - RANGING

FIGURE 5-42. MISSION CONTROL CENTER FUNCTIONAL BLOCK DIAGRAM



2  
FOLDOUT FRAME

intervention in critical, unusual or infrequent event and functional support capabilities (see Table 5-11).

The flight control subsystem consists of a combination of commercial units, and Hughes developed equipment. Maximum use is made of commercial units in order to minimize cost while maintaining a high degree of reliability through selection of proven equipment.

The principal hardware elements of the flight control subsystem are:

- 1) PDP 11/44 computer: provides computing capability for command and telemetry processing. Generates alarm messages and warnings to the spacecraft controller
- 2) Command interface unit (CIU): receives the spacecraft command bits from the computer and passes the command to the command modulator
- 3) Command modulator: accepts a digital command string from the CIU, provides FSK modulation, and FM modulates the 55 MHz I/F carrier with the FSK tones. The FM modulator portion of the command modulator is also capable of accepting the range tones instead of FSK tones as the modulation source for ranging.
- 4) Frame sync: locates the TM sync pattern and properly "frames" the data which is then sent to the computer
- 5) Telemetry receiver: selects, under computer control, the desired telemetry channel and performs phase demodulation of the received signal
- 6) Bit sync: receives the output of the telemetry receiver and outputs a clocked digital signal to the frame sync
- 7) Range tone processor: operates under computer control through the command and telemetry groups to establish range to the spacecraft
- 8) Selectable telemetry display: displays selected telemetry data directly from the frame synchronizer prior to processing by the PDP 11/44 or from the computer
- 9) Telemetry tape recorder: records the raw telemetry as supplied by bit synchronizer outputs
- 10) Asynchronous serial formatter: collects azimuth, elevation, and station status information from various point in the antenna site. It receives station control data from the asynchronous multiplexer.



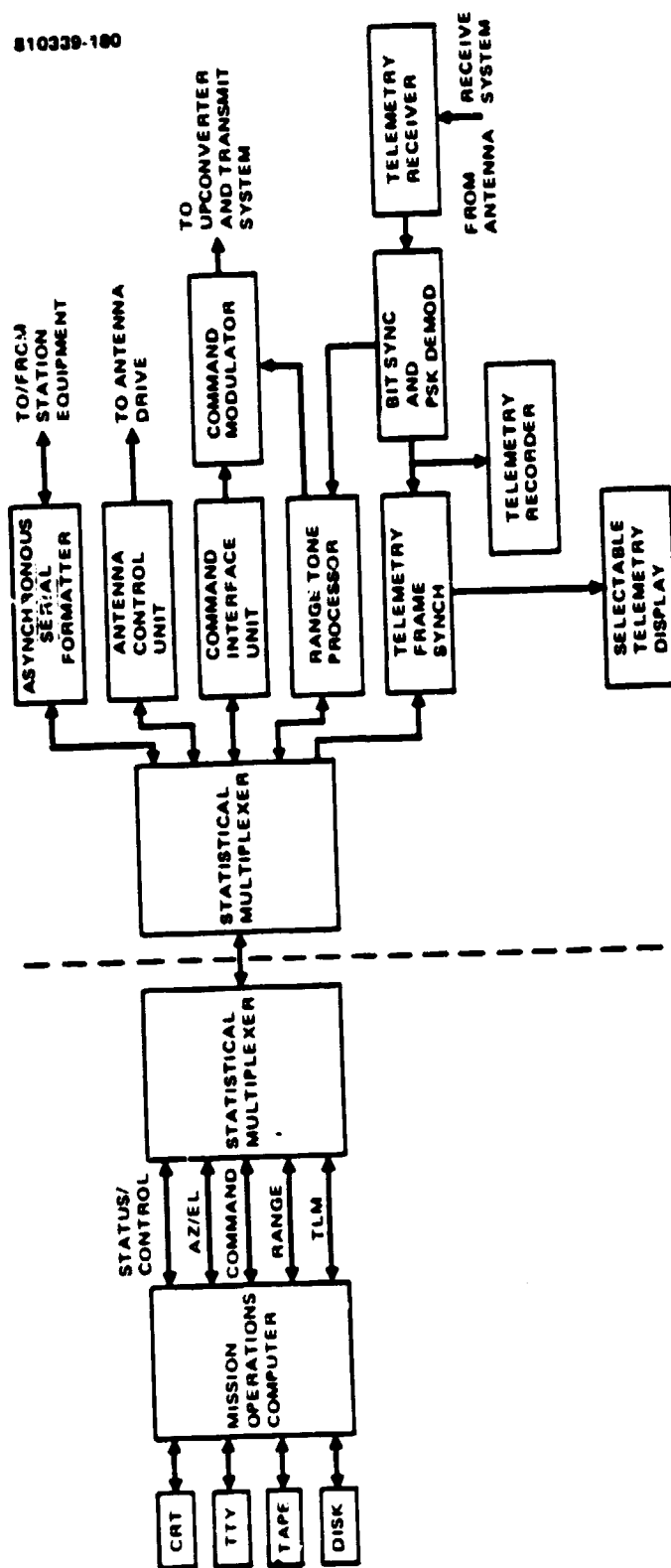


FIGURE 5-49. FLIGHT OPERATIONS CONTROL SUBSYSTEM

The CRT display/keyboards are used for controlling the spacecraft. The TTY hardcopy unit provides printouts of alarms, messages and selected data. A single synchronous, serial data link over a four wire line provides the link between the Central Control Station and the RF Antenna site. Statistical multiplexers are used at each end to multiplex five asynchronous serial channels over the synchronous channel. Switching capability is provided at the CCS to connect any of the PDP 11/44s to the signal processing equipment.

#### 5.3.2.1 Command Processing Data Flow

The processing of spacecraft commands in the PDP 11/44 is performed by the ECIL command line interpreter (CLI) and spacecraft command task. The CLI software receives the command request as typed by the spacecraft controller and converts the English-like request into one or more command strings, then transmits the strings to the command interface unit (CIU). Commands may also be entered from prestored disk sequences. The CIU generates the actual command bits. Commands are sent by the CIU to the command modulator for appropriate signal modulation. After upconversion of the signal the command goes over an S band or 30 GHz link to the spacecraft.

#### 5.3.2.2 Telemetry Processing Data Flow

The telemetry stream is received on an S band or 20 GHz link. The telemetry processing group includes a receiver to convert the IF telemetry to baseband, a PSK demodulator which recovers the 1 Kbps telemetry stream from the 32 KHz subcarrier, a bit synchronizer to reconstruct a clock corresponding to the telemetry stream, and a frame synchronizer to extract telemetry minor frames for display on the selectable telemetry display and processing on the PDP 11/44 computer. Real time PDP 11/44 processing includes display, alarms, limit checking and archiving, and selecting data sets for spacecraft attitude and tracking data.

A four channel tape recorder is available for recording raw telemetry. Two channels are used for telemetry, one channel is for IRIGB serial time code, and one channel for voice annotation.

#### 5.3.2.3 Ranging System

The ranging system provides precise measurement of the spacecraft range from the MCT. This data is used with ground antenna pointing data for orbit determination, stationkeeping, and network synchronization. The ranging system is illustrated in Figure 5-50.

The range tone processor, RTP, sends square wave ranging signals to the command modulator and receives ranging signals from the telemetry receiver. The phase delay between the transmitted and received tones is measured with an accuracy of  $1/1024 \times 360$  degrees. Phase measurements are made periodically by selecting one of four tone frequencies. The results of these measurements sent to the computer and displayed on the RTP front panel.

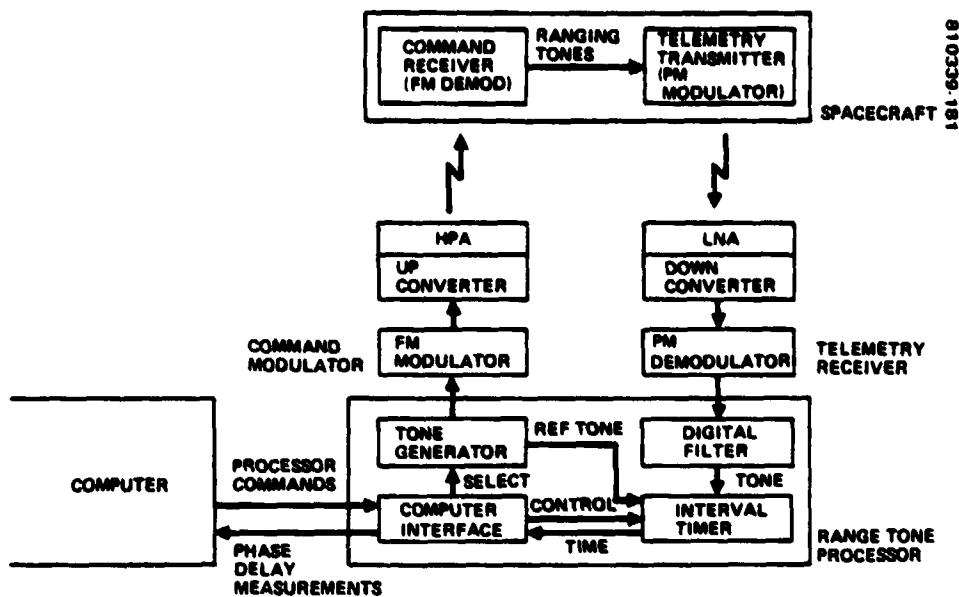


FIGURE 5-50. RANGING SYSTEM

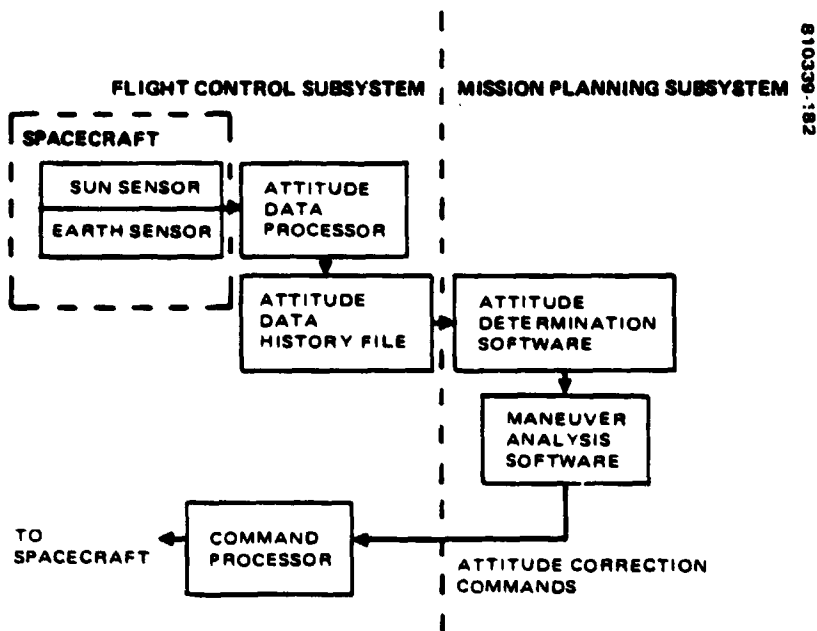


FIGURE 5-51. ATTITUDE DETERMINATION FUNCTION

#### 5.3.2.4 Controller's Console

The principal element of the controller's station is the CRT display/keyboard. A DECwriter hard copy printer is located nearby with the computer. The selectable telemetry display and a strip chart recorder are also located near the controller's console.

The DECwriter provides a permanent record of spacecraft commands, alarms and error messages, CRT LRV snaps, raw TM dumps, LRV data base parameters, and other software messages.

The CRT displays provide full visibility to all significant spacecraft data and ground status.

#### 5.3.3 Mission Planning Subsystem

The mission planning subsystem provides capability to efficiently plan and schedule all off-line mission control functions. The primary functions of the mission planning subsystem are attitude determination, orbit determination and prediction, stationkeeping, spacecraft health and performance evaluation, and flight operations planning. The mission planning functions are primarily manual operations which are supported by applications software.

##### 5.3.3.1 Spin Axis Attitude Determination

The attitude determination function is illustrated in Figure 5-51. The earth and sun provide convenient targets for spin axis attitude determination. Sun and earth sensor data are placed in the spacecraft telemetry stream, and relayed to the ground for attitude determination processing. These data are collected into attitude data sets by the real time flight control subsystem. These data sets are accessed by the attitude determination software which determines spin axis declination and right ascension. Attitude correction maneuvers are periodically determined by the maneuver planning software. This task produces thruster firing commands which are sent to the spacecraft by the flight control subsystem.

##### 5.3.3.2 Orbit Determination

The orbit determination function is illustrated in Figure 5-52. Flight system tracking is provided by the flight control subsystem. The ranging task history file is accepted by the orbit determination software. This task integrates range rate and antenna position data to determine spacecraft position and the spacecraft orbit. A predicted flight segment ephemeris is produced for mission scheduling and network synchronization. The spacecraft orbit is used by the maneuver planning software for stationkeeping maneuvers.

### 5.3.3.3 Stationkeeping

Gravitational anomalies, solar and lunar gravitational effects, and solar radiation pressure will continually perturb the spacecraft orbit and attitude. Thus periodic orbit and attitude determinations, and stationkeeping and attitude correction maneuvers will be required throughout the spacecraft operational lifetime.

Periodic north-south velocity change maneuvers are required to prevent a steady increase in orbit inclination due to solar and lunar tidal effects on the satellite orbit. The increase averages  $0.84^\circ$  per year, which corresponds to a velocity change of 148.5 fps/year. To keep the orbit inclination (latitude) within the range of  $\pm 0.02$  degrees, the maximum allowable time between velocity maneuvers is 23 days.

Periodic east-west maneuvers are required to keep the satellite at its desired orbital station. The disturbing force is due to longitudinal variation in the earth's gravitational field. The maximum east-west acceleration is about 0.0019 degrees per day, and the corresponding AV is 6 fps/year. The optimum control strategy is a single sided limit cycle so that fuel is expended in only one direction (see Figure 5-53). For a  $\pm 0.02$  degree dead-band limit at worst orbital position, the maximum allowable time between maneuvers is 16 days. The maneuver analysis software uses data from the orbit determination software and the attitude determination software to determine stationkeeping maneuver commands.

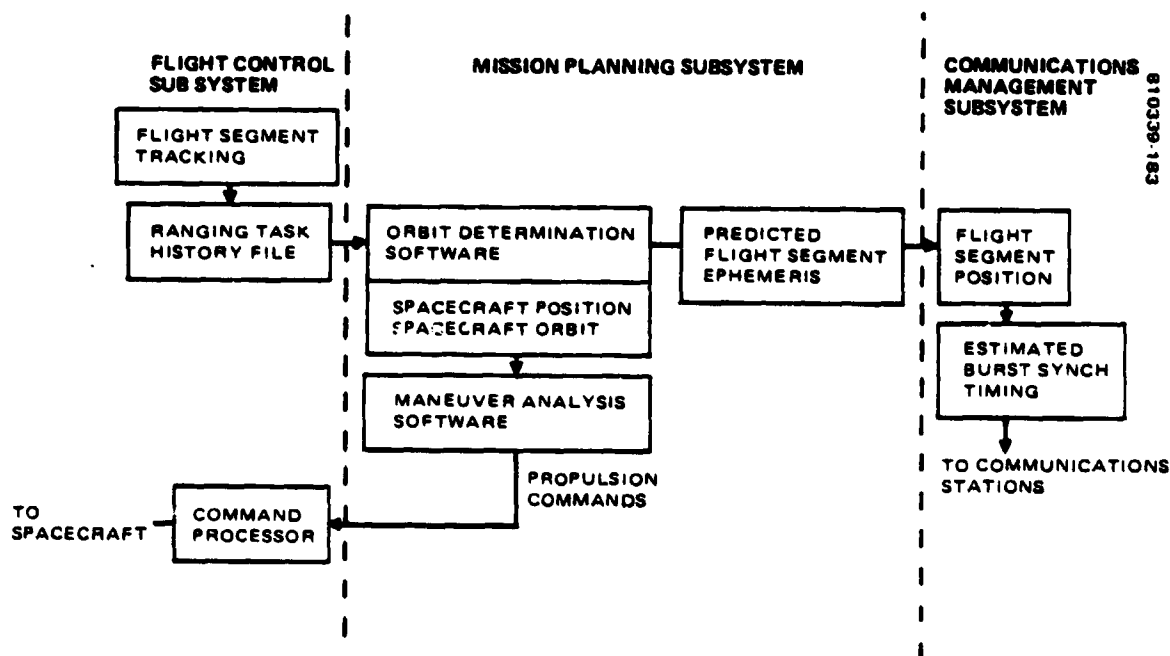


FIGURE 5-52. ORBIT DETERMINATION FUNCTION

The operational stationkeeping accuracies achieved on the Anik program are shown in Figure 5-53. The Anik I orbit determination was based on two station tone ranging, while that for Anik II was based on one station range, azimuth and elevation data. These data indicate that 0.02 degree stationkeeping accuracies are generally achievable (see Figure 5-54).

#### 5.3.3.4 Spacecraft Health and Performance Analysis

In order to monitor and control subsystem performance the analyst must monitor all flight segment telemetry and review the alarm history. Comprehensive reports and plots of the telemetry and alarm data will aid troubleshooting and fault isolation techniques. Long term performance is also evaluated. Software is provided for attitude control system performance monitoring, maneuver command evaluation, antenna pointing calibration, and power and thermal management.

#### 5.3.3.5 Flight Operations Planning

The mission planning subsystem provides the capability to efficiently plan, schedule, and generate commands for flight segment operations. This function in conjunction with experiment operations scheduling and planning produces a schedule that is conflict free among flight segment users. This schedule identifies the time of day and orbit number for each experiment and spacecraft housekeeping operation.

The mission plan resulting from this coordinated activity is translated into:

- 1) Time ordered command data sets
- 2) Timelines describing the sequence of operations
- 3) Orbit plans defining the detailed procedures and sequences to be performed by all operations personnel in support of mission plans.
- 4) Data management reporting that describes the plans, modifications, and summary of data collection

Operating system and support software that provide data and support the mission planning analyst include: plotting and display, report generation, experiment command interactive language (ECIL), and data base manager. The analyst uses the mission plan, mission event translation tables in the data base, and supporting data from disk files to generate a composite command data file. This data file is available to the flight control subsystem for commanding the spacecraft.

#### 5.3.4 MOS Data Processing Subsystem

The MOS data processing subsystem was derived from the LEASAT baseline. It is an integral element of the CCS. The general features of this subsystem are the same as those of the CCS data processing subsystem and

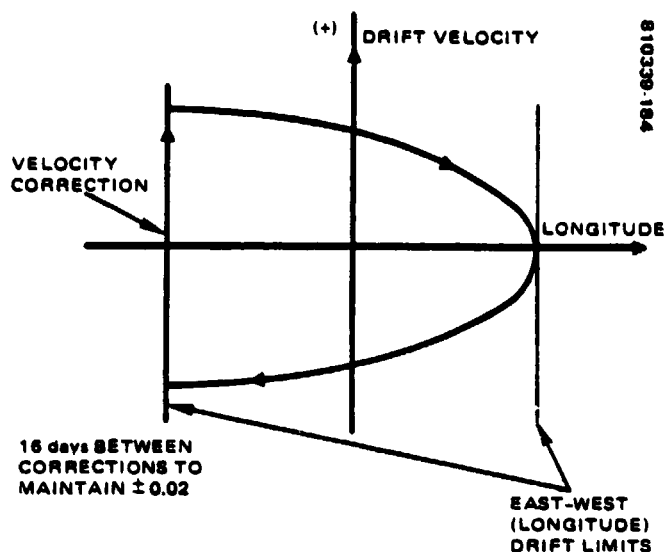


FIGURE 5-53. EAST-WEST STATIONKEEPING PROFILE

	STATIONKEEPING EXPERIENCE*						810330-194
	ANIK I (LONGITUDE = 114°W)			ANIK II (LONGITUDE = 109°W)			
	POSITION**		ATTITUDE†	POSITION**		ATTITUDE†	
	LONGITUDE	LATITUDE		LONGITUDE	LATITUDE		
NOMINAL CONTROL BAND	± 0.035°	± 0.035°	± 0.14°	± 0.075°	± 0.025°	± 0.07°	
UNCERTAINTY (3σ) CONTROL BAND ††	± 0.015°		± 0.045°	± 0.025°		± 0.03°	
CORRECTION FREQUENCY	ONCE EACH 4 wk		ONCE EACH 4 wk	ONCE EACH 8 wk	ONCE EACH 2 wk	ONCE EACH 2 wk	

- \* ANIK I DATA SPAN ~ 9 mo; ANIK II DATA SPAN ~ 4 mo
- \*\* ORBIT DETERMINATION FOR F 1 BASED ON TWO STATION RANGING. ORBIT DETERMINATION FOR F 2 BASED ON ONE STATION RANGE, AZIMUTH, AND ELEVATION DATA
- † ATTITUDE CONTROL BAND FOR ANIK II IS 1/2 THAT FOR ANIK I DUE TO INCREASED GAIN-SLOP FOR U.S. USERS
- †† UNCERTAINTY DUE TO ORBIT DETERMINATION, PREDICTION, THRUSTER REPEATABILITY AND OPERATIONAL QUANTIZATION DELAYS. REFERS TO SATELLITE POSITION OR ATTITUDE INCLUSIVE OF ONE CYCLE, i.e., FROM DETERMINATION JUST PRIOR TO MANEUVER

FIGURE 5-54. ANIK STATIONKEEPING EXPERIENCE

are described in 5.2.3.2. The features specific to mission operations processing are described below. Refer to Table 5-7 for the MOS data processing hardware configuration.

#### 5.3.4.1 Flight Control Software

The real time mission operations software organization is shown in Figure 5-55. This software provides status monitoring, telemetry processing, command generation and verification, and other tasks required for real time control of the spacecraft.

##### 5.3.4.1.1 Station Status and Control

Various hardware elements of the ground station are controlled by the station status and control task in response to instructions entered by the operator, or status data received from the hardware elements. This processor is part of the basic software configuration described in 5.2.3.

##### 5.3.4.1.2 Telemetry Processing

Telemetry data processing logic is shown in Figure 5-56. Telemetry data are accepted through the PCM decommutation task. The telemetry values are maintained in the system data table. Limit checks and alarms are displayed to the operator via the display processor task.

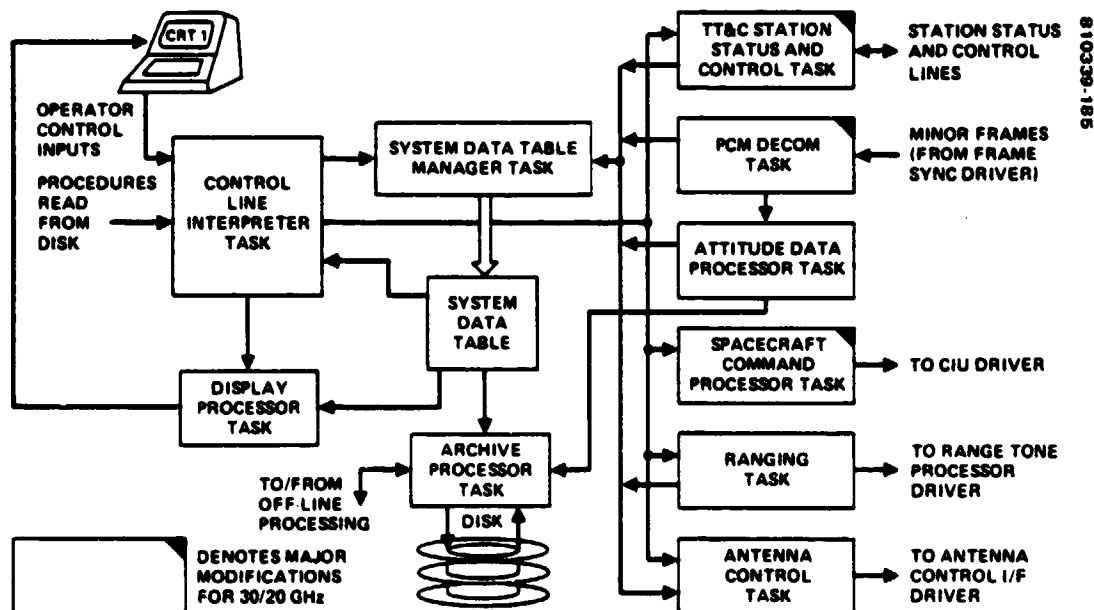


FIGURE 5-55. MISSION OPERATIONS SOFTWARE REAL TIME PROCESSING



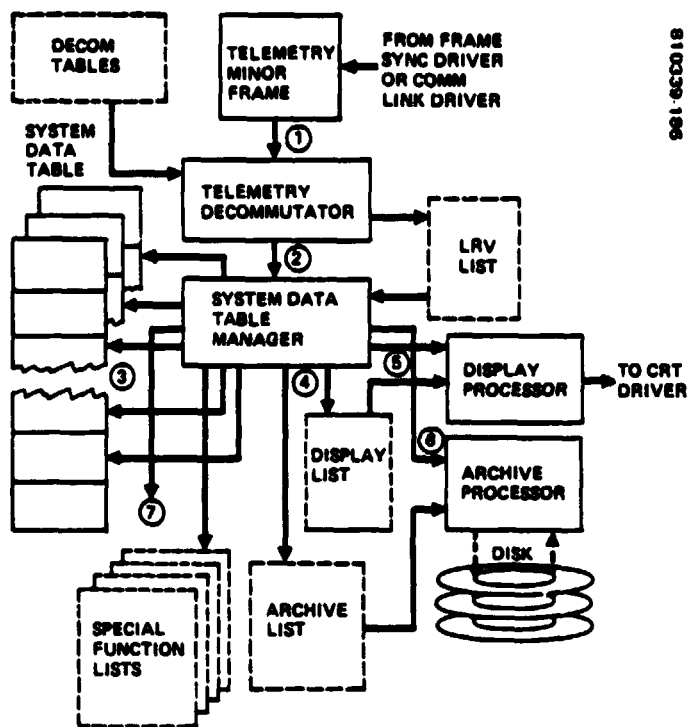


FIGURE 5-56. TELEMETRY DATA PROCESSING LOGIC

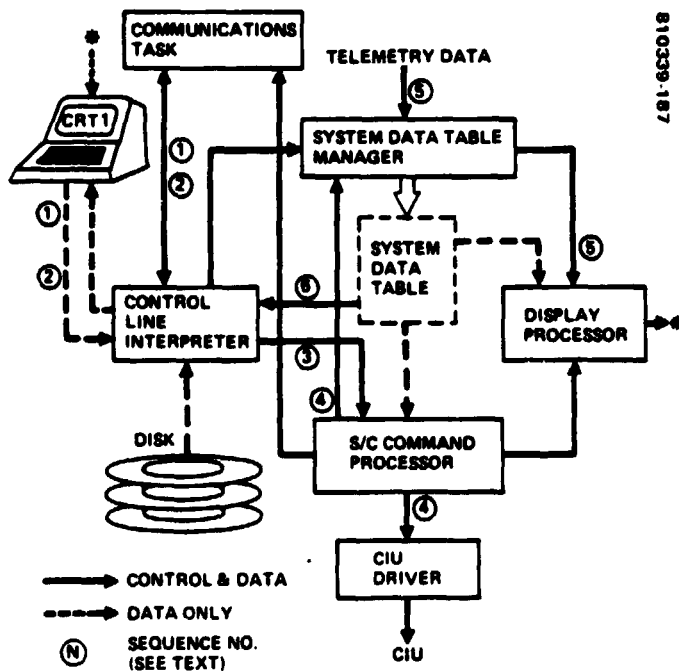


FIGURE 5-57. COMMAND PROCESSING LOGIC

#### 5.3.4.1.3 Attitude Data Processor

The spacecraft attitude processor accepts a time-consistent set of attitude data from the telemetry processor and formats the values for later off-line processing.

#### 5.3.4.1.4 Spacecraft Command Processing

Command processing logic is shown in Figure 5-57. The spacecraft commands may be input on a individual basis via the keyboard or called from disk as a sequence of commands. The spacecraft command processor function is to accept command data from CLI, build an uplink and spacecraft compatible command bit string, and output it to the command interface unit. The system data manager task is invoked to set command verification indicators requested by the command processor, perform command verification for the LRVs whose indicators are set, and update command status upon receipt of station telemetry. The display processor is invoked to display command echo messages to be printed, and error messages to be displayed and printed. The system data table provides commanding parameters and the critical command list.

#### 5.3.4.1.5 Ranging Task

Ranging task data flow is shown in Figure 5-58. The ranging task provides range and antenna angle data sets from the ranging equipment. A separate calibration mode is provided to measure ground delays introduced in the Hughes ranging scheme. The communications processor assumes much of the burden of the ranging task by reading range data from the range tone processor and antenna angles from the antenna servo. The ranging task activates the range tone processor and reads phase measurement approximately 20 times on 100 ms centers. From these readings it estimates the range and range rate. The first estimates are used to estimate phase delay that will be achieved at the next highest frequency. Once the highest frequency is attained, range and range rate samples are scaled, time tagged, and passed to the communications task along with antenna azimuth and elevation angles.

#### 5.3.4.1.6 Antenna Control Task

The antenna control task logic is shown in Figure 5-59. The antenna control task calculates the azimuth (AZ) and elevation (EL) angles for pointing the steerable antenna. The program can be operated in a program track mode with AZ/EL angles determined from supplied coefficient or in a search pattern mode that superimposes a scan pattern on the basic tracking profile. The antenna can also be operated in an autotrack mode where pointing angles are determined by received beacon signals.

#### 5.3.4.2 Mission Planning Software

The off-line mission operations software organization is shown in Figure 5-60. This software provides functions which are performed routinely but do not require real time processing. The basic off-line software architec-

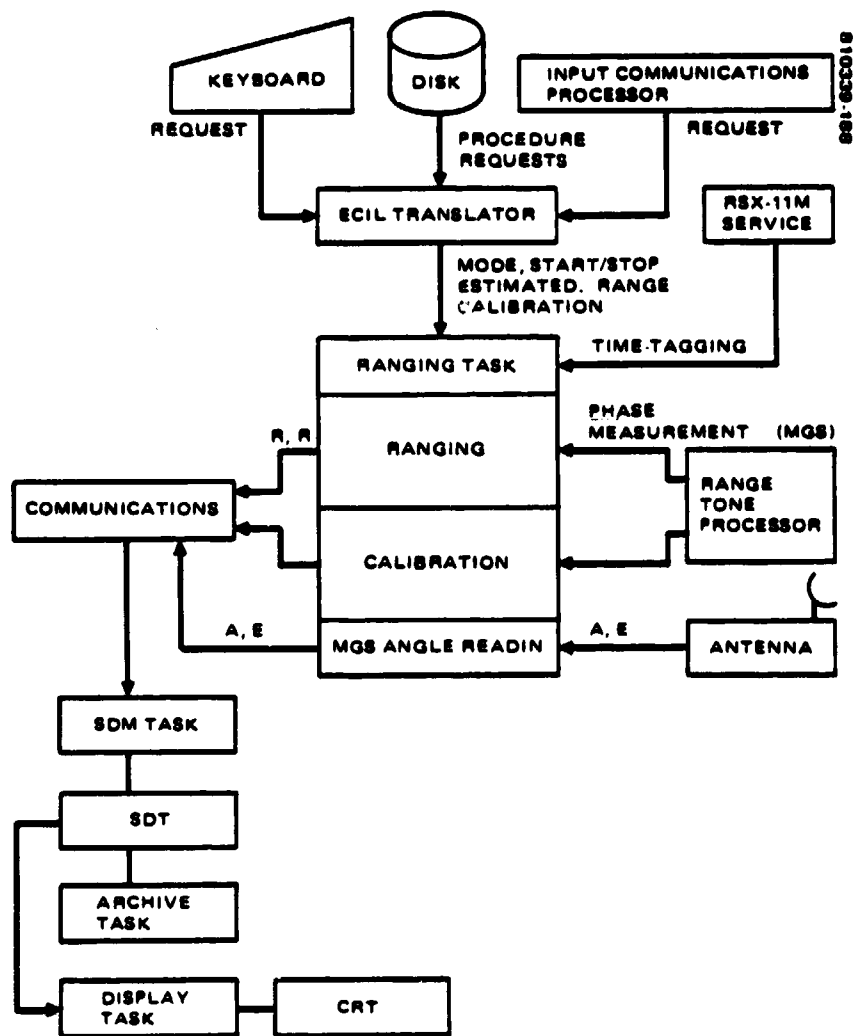


FIGURE 5-58. RANGING TASK DATA FLOW

ture provides applications tasks access to the real time processors, historical data files, and control terminals. Specific tasks of the off-line software are discussed below.

#### 5.3.4.2.1 Launch Window Generation

The launch window is calculated principally with the aid of the computer program WINDOW. For a given input day and liftoff time (incremented by an amount specified in the input), 24 variables that could affect the launch window are calculated. The program is run for the different orbit and attitude configurations:

- 1) Transfer orbit, injection attitude, first perigee to first apogee
- 2) Transfer orbit, liquid apogee motor firing attitude, first apogee to twelfth apogee

Mission analysts can determine the launch window by examining the following variables output:

- 1) Right ascension of spin axis
- 2) Right ascension of ascending node
- 3) Angle between sunline and spin axis
- 4) Angle between sunline and orbit plane
- 5) Duration of transfer orbit shadow

The factor of primary importance in establishing the window is the thermal constraint or sun angle.

#### 5.3.4.2.2 Shadowing Predictions

Predictions for the shadowing of the spacecraft in the transfer, drift, or geostationary orbits are made with the aid of the SHADOW computer program. Predictions are made within the time interval defined by the input starting and ending dates for a spacecraft in an arbitrary earth orbit. The program can also be used to calculate the time of earth-moon conjunctions. Near the time of conjunctions, data from either the north or south earth sensors may be ignored since the earth pulse will be modified by the presence of a moon pulse.

#### 5.3.4.2.3 Acquisition Table and Ephemeris Generation

The computer program ACQTBL performs two important functions during the transfer and drift orbit mission: 1) prediction of orbit and attitude data, and 2) prediction of other data for the earth stations and the mission analysts.

Earth station output data include items such as spacecraft acquisition tables, antenna drive tapes, polarization angle predictions, and signal level predictions of the telemetry command antennas.

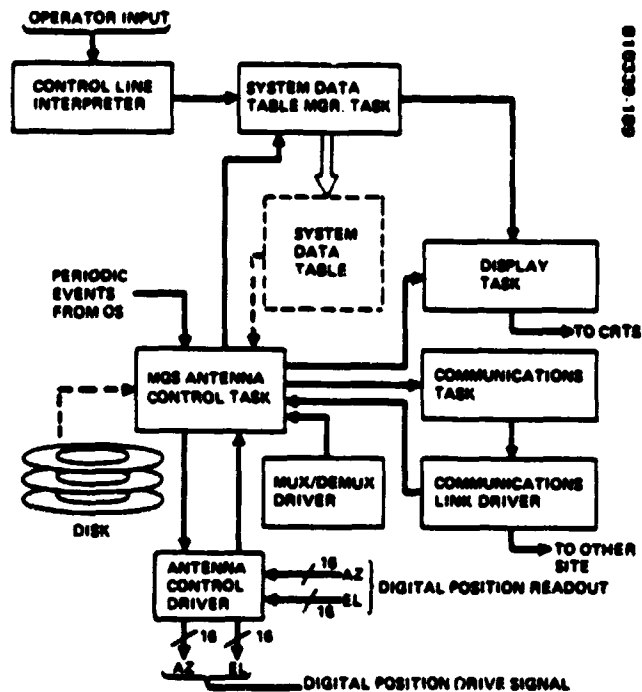


FIGURE 5-59. ANTENNA CONTROL LOGIC

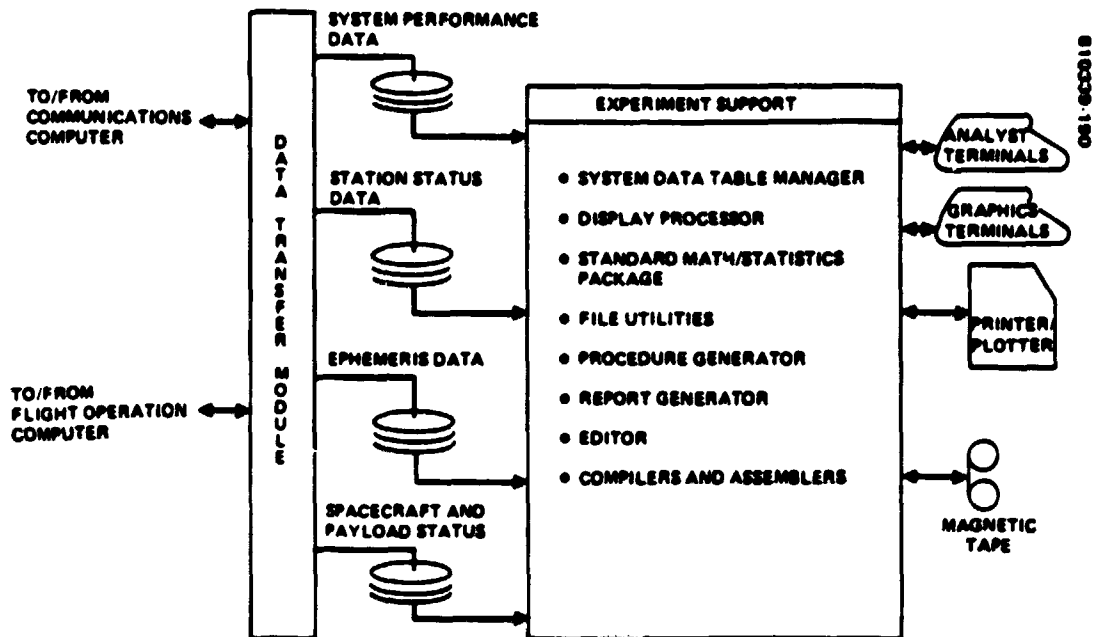


FIGURE 5-60. MISSION OPERATIONS SOFTWARE OFF-LINE PROCESSING

Orbit and attitude output data to be used by mission analysts will include predictions of spacecraft inertial position and velocity vectors, orbital elements, attitude t-times, range measurements, sun angle ( $\phi$ ), and sun interference data.

Prior to liftoff, a set of nominal orbital elements and a nominal spin axis attitude is used as an input to synthesize the nominal mission. This assists mission personnel in realistically analyzing and rehearsing the transfer orbit mission. The above parameters are also employed in the generation of antenna drive tapes used for initial search and acquisition of the spacecraft at the TACS.

After liftoff, the orbit and attitude input parameters based on STS performance are provided by NASA. These data will be used to generate initial acquisition data for the TACS. This will be in the form of an antenna drive tape forwarded to the TACS. Other input data after acquisition are derived from spacecraft telemetry (e.g., spin speed) or from mission analysis (e.g., signal threshold levels, earth sensor biases).

#### 5.3.4.2.4 Orbit Determination

The orbit determination system consists of three principal software programs: 1) PREPRO, 2) WCRSB, and 3) ORBDET. Characteristics of each are given below.

PREPRO is a data preprocessor. Its functions are to eliminate spurious data (caused by measurement and transmission noise, etc ) and to compress data.

WCRSB is a least squares orbit determination algorithm using numerical iteration to converge on a solution. Given an epoch, an initial estimate of the orbit (obtained from either the nominal orbit or the STS parameters) and a suitable time arc of azimuth, elevation, and/or range, WCRSB will converge on the orbit solution. To meet accuracy and storage requirements, WCRSB uses preedited data (culled and compressed data). WCRSB is employed as a prime orbit determination program during the transfer and drift orbit mission.

ORBDET uses numerical integration of the orbital equations of motion to differentially correct an estimate of the orbital elements. It includes the perturbations required in the stationkeeping phase.

#### 5.3.4.2.5 Attitude Determination (SPINAX, ATTDET)

The attitude sensor telemetry pulse train is transmitted to the attitude pulse digitizer, which outputs the spin period, solar aspect angle, earth chord widths, and sun-earth separation measured in the equatorial plane of the spacecraft. These four types of data are smoothed and used in the program SPINAX to obtain an initial spacecraft attitude, which is also useful for

input to the ATTDET program. The filtering equations built into the ATTDET program reduce the noise and permit the estimation of biases on the above data types. This estimation may require collection of data over a full orbit.

A limited amount of data may be selected by the analyst and input to the ATTDET program to obtain a quick attitude determination. This determination can be improved as more data are chosen by the analyst and input to the program. Prior to each successive ATTDET run, an updated covariance matrix from the previous determination is input to optimize the attitude determination process. On the basis of analysis of rms and mean residuals output by ATTDET, weighting criteria can be assessed for the data and the biases can be estimated.

Prior to any reorientation maneuver, the ATTDET program will be run to determine spacecraft attitude. Subsequent to any reorientation, the attitude resulting from the maneuver must be determined to evaluate that maneuver.

In stationkeeping phase, perhaps three or four groups of data are taken over a period of 2 weeks to permit an estimation of the effect of solar torque on the spacecraft attitude. This effect is then incorporated into the ATTDET program by the analyst. Periodically, biases and seasonal effects on attitude determination will be determined.

#### 5.3.4.2.6 Reorientation Maneuvers

The fundamental computer program used for a reorientation maneuver is BATMAN. The program provides information for the reaction control system calibration program and for monitoring the maneuver when it is in progress. The reorientation maneuver is divided into three phases: 1) the mission analysis and maneuver computation phase, 2) the command preparation and initiation phase, and 3) the maneuver execution, observation, and evaluation phase.

#### 5.3.4.2.7 Mission Analysis and Maneuver Computation Phase

Before the BATMAN program is run, orbit and attitude data must be collected and smoothed, and programs WCRSB and ATTDET utilized to enable the analysts to establish the current orbit and attitude. Subsequently, other computer programs such as FUSIT, which is used for determining apogee motor firing attitude and time will be used to assist in the selection of a desired new attitude. ACQTBL will also be run to permit scheduling the maneuver by taking into consideration station elevation angle, telemetry and command signal strengths, proximity of the spacecraft line of sight to the direction of the sun, rate of change of range to the spacecraft, etc. The BATMAN program is then run to determine the magnitude of the maneuver and the phase angle (the angle between the plane defined by the spin axis and the sunline of sight, and the plane defined by the direction of reorientation) for input to the RCS calibration program. BATMAN also generates information for the construction of a Mercator chart and other plots that are used to

monitor the progress of the maneuver. Finally, it determines several parameters for the command message (command number, pulse duration, start angle, and number of pulses).

#### 5.3.4.2.8 Command Preparation and Initiation Phase

During this phase, the MCC is set up to execute and monitor the maneuver. Software involvement is limited to the preparation of the Mercator chart and other plots using the information generated by BATMAN.

#### 5.3.4.2.9 Maneuver Execution, Observation, and Evaluation Phase

As the reorientation progresses, data consisting of sun sensor and earth sensor are processed and transmitted to MCC, El Segundo. The data are then plotted on the charts prepared in advance and are used together with an evaluation of PCM telemetry data to monitor the progress of the maneuver. If the reorientation is not following the desired path, the jet start angle is adjusted on the basis of information derived from the plots on the Mercator chart. In parallel with this manual monitoring, the real time attitude determination (RTAD) program automatically follows the maneuver and computes course correction. At the completion of the maneuver, the orbit, current attitude, and desired attitude are again determined and compared to either verify that the desired attitude has been achieved or to provide a starting point for the next reorientation maneuver.

#### 5.3.4.2.10 Canted Jet Maneuvers (CANJET)

CANJET assists mission analysts in determining the canted jet boost needed to achieve a desired drift rate (that is, it is used mainly as a prediction program).

Inputs to the program are the orbital elements, current spacecraft attitude, the desired drift rate, time interval during which canted jet firings are to be simulated, and time increment between successive firings. The program only considers boost directions that are in the plane defined by the spin axis vector and the velocity vector. Thus, at a given time, there are two possible boost directions. At each time increment, CANJET determines the canted jet boost and the resulting orbit.

Before CANJET is run, orbit and attitude data must be collected and programs WCRSB and ATTDET utilized to enable the analysts to establish the current orbit and attitude. If the desired change in drift rate is large, the canted jet maneuver must be performed in segments. The reason for this is that the PSIFV angle, which is defined as the angle between the plane containing the spin axis and the sun line of sight, and the plane containing the spin axis and the velocity vector, will change appreciably during the maneuver. The PSIFV angle, calculated by CANJET, determines the delay input to the synchronous controller to determine when the canted jets are



actuated relative to the reference  $\psi$  or IP pulse. The delay angle on the synchronous controller must therefore be readjusted periodically when the maneuver is of long duration.

The mission analysts assess the results of the CANJET run to determine the optimum time for the maneuver on the basis of the effects on the orbit, amount of fuel used, command and telemetry visibility, etc. Subsequent to this exercise, CALIB (the RCS calibration program) is used to determine the canted jet firing parameters for the command message (e. g., delay angle and number of pulses).

#### 5.3.4.2.11 Axial Jet Maneuvers (AXJET)

AXJET is used to determine the axial jet boost needed to achieve a desired drift rate.

Inputs to the program are the orbital elements from the orbit determination system, the spacecraft attitude determined by ATTDDET, the desired drift rate, the time interval during which axial jet firings are to be simulated, and the time increment between successive firings. At each time increment, AXJET determines the axial jet boost required and the resulting orbit.

Before AXJET is run, orbit and attitude data will be collected and programs WCRSB and ATTDDET utilized to enable the analysts to establish the current orbit and attitude. AXJET is then run, and the analysts determine the best time to perform the maneuver based on parameters similar to those evaluated for canted jet maneuvers. CALIB is used to determine the axial jet firing parameters for the command message, e. g., delay angle and duration of axial jet burn.

#### 5.3.4.2.12 Reaction Control System Calibration (CALIB)

After determining the required magnitude and direction of an attitude or orbit maneuver, the parameters necessary for firing the reaction control subsystem must be determined. The program CALIB accepts as an input, the current spacecraft configuration, e. g., roll moment of inertial, fuel pressures, and temperatures, etc., and maneuver parameters and calibration factors based on bookkeeping during previous maneuvers. The program generates output necessary for putting together the maneuver command message. The program also predicts the spacecraft mass properties, fuel pressures, etc. at the end of a maneuver, thus permitting bookkeeping of spacecraft parameters on a continuing basis during experiment operations. Calibration factors are determined and adjusted by measuring the pre-maneuver and the postmaneuver orbit and attitude status and comparing these with the change in status predicted by the maneuver programs.

#### 5.3.4.2.13 Apogee Motor Firing

Computer program FUSIT6 assists the analysts in the calculation of the apogee motor firing (AMF) attitudes and times to achieve specified drift

rates with minimum RCS fuel usage, based on certain drift orbit maneuver sequences. FUSIT6 also aids in the determination of the AMF attitude for minimum fuel usage for the same time as above but unconstrained by the specified drift rate. By analyzing the various attitudes and by evaluating the effects of these attitudes on all aspects of the drift orbit mission, the attitude required to arrive on station can be determined. This best attitude can then be input into the FUSIT2 program to further examine the effects of various firing times.

Nonnominal situations involving both excess and deficient energies, in which certain mission constraints may need to be violated, are also resolved by using FUSIT6.

#### 5.3.4.2.14 Velocity Increment Evaluation

The VINCEV program assists analysts in determining the actual  $\Delta V$  applied during an orbital change as well as the direction of firing when the orbital elements before and after a maneuver are known. Data obtained are used to obtain the RCS calibration data and the spacecraft parameters.

The program input uses the orbit before and after the maneuver from the orbit determination system, maneuver information, e.g., targeted  $\Delta V$ , burn duration, and spacecraft attitude from ATTDDET. The output is velocity increment magnitude and direction, and the difference between the actual and targeted  $\Delta V$  vectors.

#### 5.3.4.2.15 Stationkeeping

The three programs uniquely applicable to stationkeeping maneuvers planning are MEAN, PREDCT, and KEEP.

##### MEAN

Program MEAN accepts osculating orbital elements at a given epoch from the orbit determination program ORBDDET and generates mean elements free from periodic terms that are of short period relative to the time between orbit corrections. The remaining motion due to perturbations resulting from the gravitational effects of the sun and moon, the earth's oblateness and triaxiality, and the solar radiation pressure will alter these mean elements as a function of time. The manner in which the mean elements change is also generated and together with the mean elements are outputted for use by programs PREDCT and KEEP.

##### PREDCT

PREDCT is a predictor program that allows analysts to see the evolution of mean orbital elements of interest in stationkeeping. The latitude, longitude, and radius of the spacecraft are also predicted. The effect of a maneuver can be included at any point in the period over which predictions have been requested.

## KEEP

Program KEEP is designed to determine the corrections needed to counter the orbital motions produced by the perturbations. Using vector representation, the program determines the magnitude, direction in space, and time of application of impulsive corrections to minimize the relative spacecraft motion from nominal stationarity. A targeting strategy is developed to accomplish this minimization. The vector element changes required to go from the initial vector state provided by MEAN to the state dictated by the targeting strategy are then determined as the difference between two vectors, thus providing the component velocity increments and their point of application.

KEEP is used also to determine the spin axis attitude correction needed to counter the motion produced by solar radiation torques. The program determines the required magnitude and spatial direction of the precession maneuver that will minimize the relative spin axis motion. The initial vector state is provided by ATTDET. The final state dictated by the targeting strategy requires knowledge of the manner in which the solar radiation torque precesses the spin axis. The latter is computed within KEEP. The difference between the initial and final vector representing the initial and final attitudes provides the magnitude and direction of the required torque.

### 5.3.4.2.16 Spacecraft Health (SHAPE)

The spacecraft health and performance evaluation (SHAPE) program is used to periodically summarize the health of the spacecraft subsystems (e.g., temperatures, motor current, bus voltage, RCS pressure, etc.). The PCM data provided by the LCS data system, which flags out-of-tolerance values, are periodically sampled to form trends for further analysis and/or cross-correlation if desired. The output of SHAPE is summarized in a report.

## 5.4 IMPLEMENTATION OF EXPERIMENT OPERATIONS

The experiment operations system provides the resources necessary to coordinate and conduct service and technology experiments and to distribute data and analysis for experiments using the 30/20 GHz communications system. Experiment operations functions are conducted at the central control station in conjunction with mission operations and network operations. The design provides a minimum cost approach which satisfies the experiment planning and analysis requirements.

### 5.4.1 Experiment Operations Requirements

The experiment operations system shall be capable of supporting all operations required to conduct the experiments in the experiment plan,

gather experiment data and analyze the results of the experiments conducted. The primary requirements are:

- 1) Perform experiment planning to effectively use network resources and meet the objectives of the experiment program
- 2) Coordinate experiment plans with mission operations and network operations to produce a conflict-free system schedule
- 3) Collect experiment data to form comprehensive data sets for analysis
- 4) Analyze experiment data to determine communication system performance and develop new experiments
- 5) Distribute data sets and analysis results to the carrier experimenters
- 6) Coordinate the efforts of all carrier and NASA experimenters.

#### 5.4.2 Experiment Operations Design Approach

The primary consideration of the experiment operations system design is to provide a capability to effectively plan and conduct experiments within the constraints of a minimum cost approach. This was accomplished by collecting the existing elements of the mission operations system and the terrestrial system that would contribute to the functions of this system. The result is a semi-automatic system that is efficient, adaptive and low cost. As in the other terrestrial system elements, the design stresses flexibility, reliability and operability.

#### 5.4.3 Experiment Operations Description

The operations performed by the experiment operations system fall into two general categories: 1) experiment planning and scheduling, and 2) experiment performance and evaluation. The experiment operations system interfaces are shown in Figure 5-61.

##### 5.4.3.1 Experiment Scheduling and Mission Planning

The experiment scheduling function will receive requests from NASA and communications carrier experimenters, and generate mission plans which will be translated into command data for further processing by mission operations software. The resultant output will consist of mission plans, alternate plans, and network configuration/reconfiguration messages that coordinate ground and spacecraft support activities. Actual spacecraft commands will be generated and transmitted by the mission operations system.

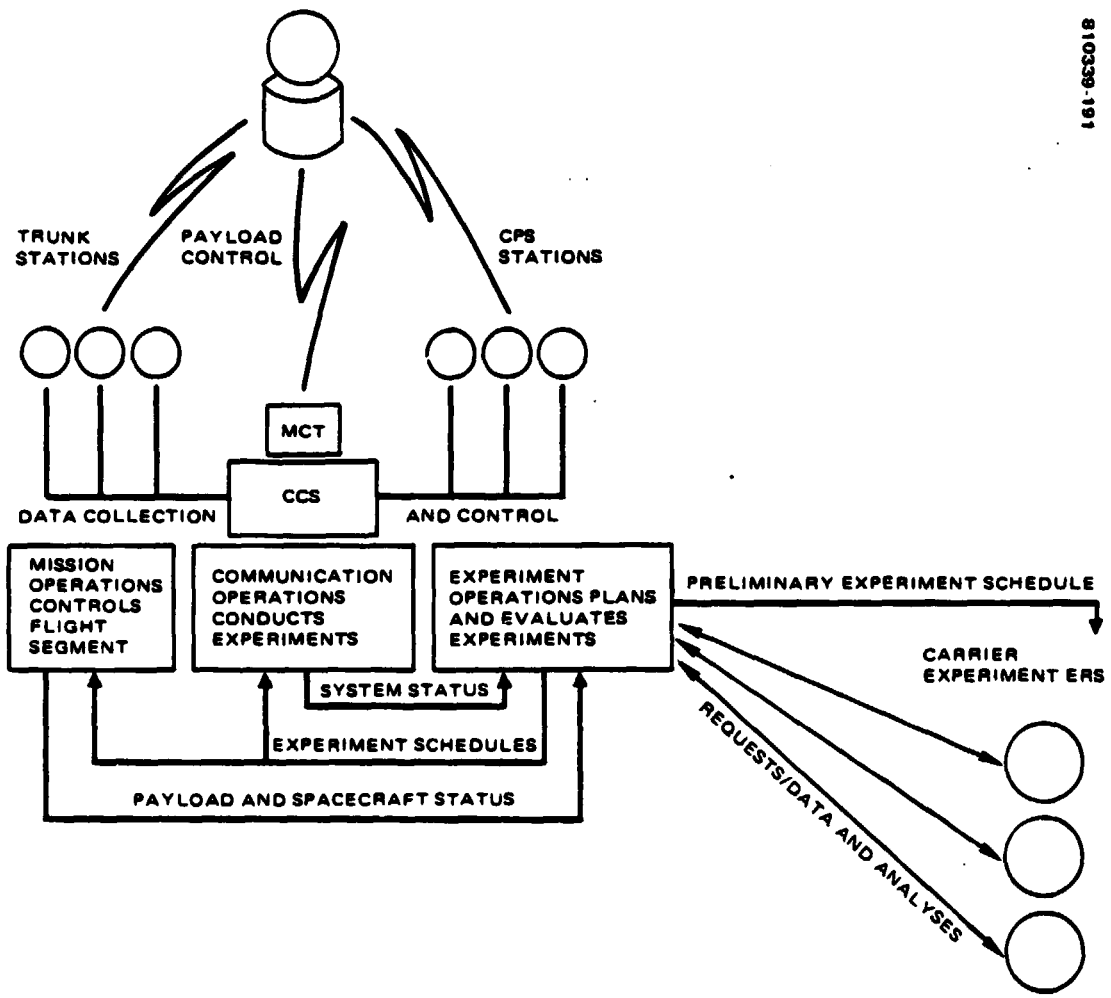


FIGURE 5-61. EXPERIMENT OPERATIONS INTERFACES

Experiment scheduling will be a manual function which performs the following tasks:

- 1) Accept and translate daily operational requirements and priorities into operational schedules
- 2) Produce monthly preliminary activity plans consisting of experiments to be conducted, spacecraft housekeeping events, maneuvers, and link schedules
- 3) Coordinate with mission operations and experimenters and produce weekly updated schedules
- 4) Produce daily station schedules showing all experiment activities, including instrument data collections, and appropriate operations personnel activities
- 5) Produce alternate mission plans and network reconfiguration messages as required to accommodate changes in weather, spacecraft, or personnel

Due to the nature of the service experiments, experiment operations will be very repetitive. Many experiments will measure the same elements under different traffic or weather conditions. Therefore, nominal mission plans and network schedules can be developed through an iterative approach over an extended period of time, eliminating the need for sophisticated optimization techniques. Experiment operation functional flow is shown in Figure 5-62.

#### 5.4.3.2 Experiment Performance and Evaluation

The design of the terrestrial segment stresses flexibility and adaptability to maximize its potential for performing a variety of experiments. The operations concepts are primarily implemented in software for ease of modification and experimentation. From prior operational experience, Hughes has learned that in order to be responsive to changes in system operation, software should be data base driven. Data base changes versus software coding changes are much faster and less costly to implement. The LEASAT software baseline, which is used in all 30/20 GHz operations functions provides total system control through data base values, and strong data base management capability. The data base architecture will enhance adaptive experimental techniques to determine the best implementation of the major communication functions: channel assignment, synchronization, link control, and orderwire control.

The experiments are physically performed by the communications operations function of the CCS. Many of the functions required for experiment performance and evaluation are inherent in the CCS communications and mission operations systems. The software architecture of the central data processing system provides processing support for experiment perfor-

mance and evaluation. The off-line experiment support software architecture is shown in Figure 5-63. No special software development is required. All the capability shown in the figure is available in the mission operations, communications management, and operating system software. The real time software provides data collection, data base management, and archiving functions which can collect the experiment data for evaluation. The data base manager task can be used to access the history tapes built by the archive processors. Remote data collection can be supported by the station status and control equipment and the telemetry ingest function of the mission operations software. The alarm monitor can be used for experiment analysis and to flag experiment opportunity conditions such as precipitation. The experiment command interactive language (ECIL) coupled with the display processor provides an interactive data analysis and display capability which experimenters can use for experiment evaluation. Direct executing procedures can be developed and the results displayed in interactive sessions. These software capabilities are assembled and installed in the backup computer to provide significant experiment analysis capability. Experiment evaluation may also be performed in the background of the mission operations and communications management computer.

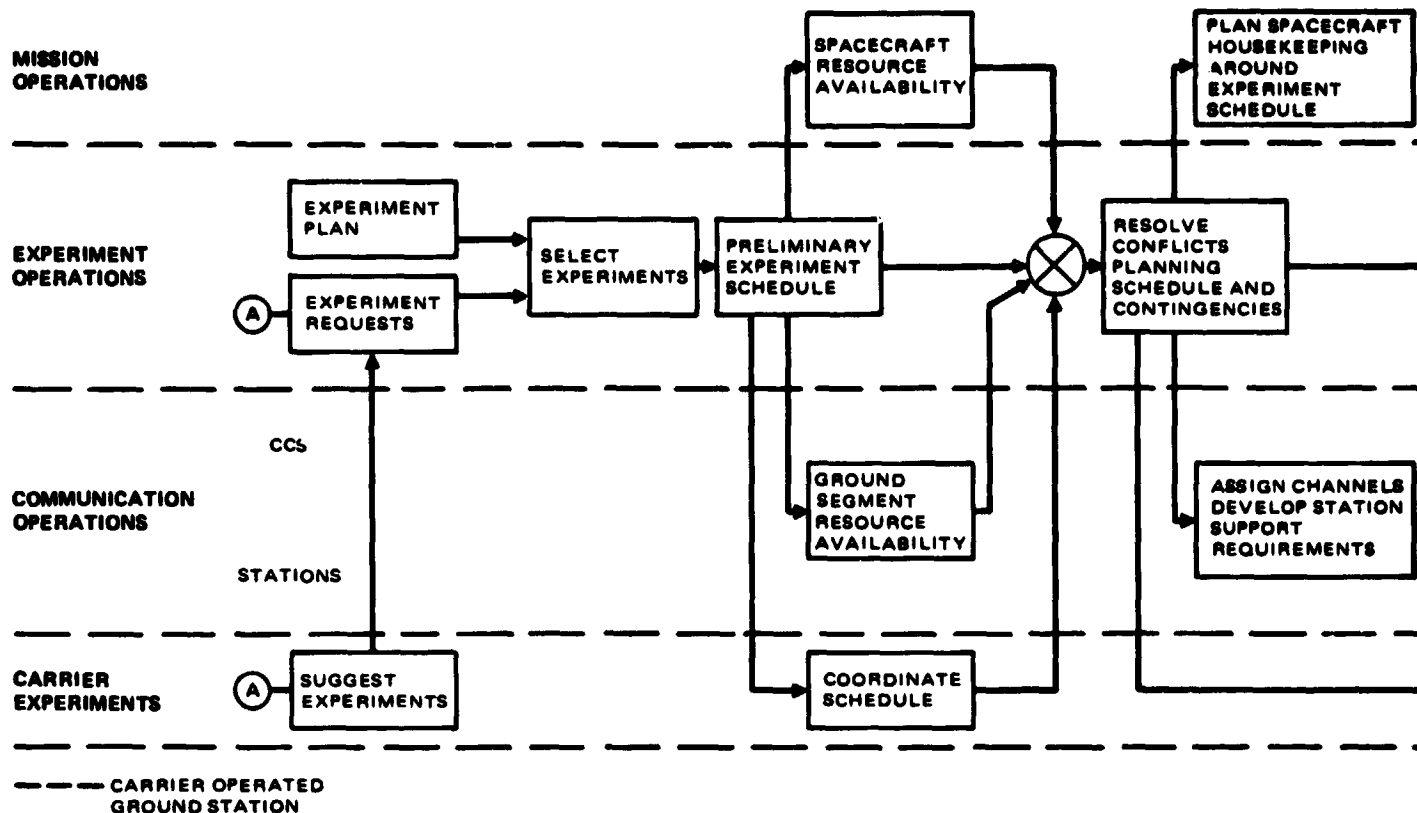


FIGURE 5-62. EXPERIMENT OPERATION FUNCTIONAL FLOW

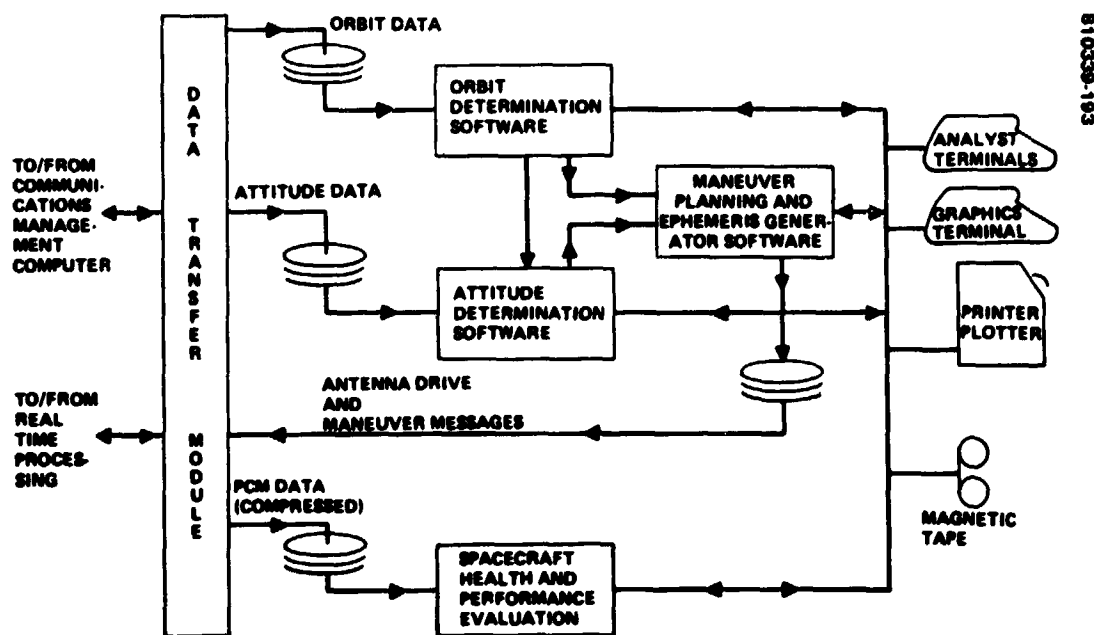
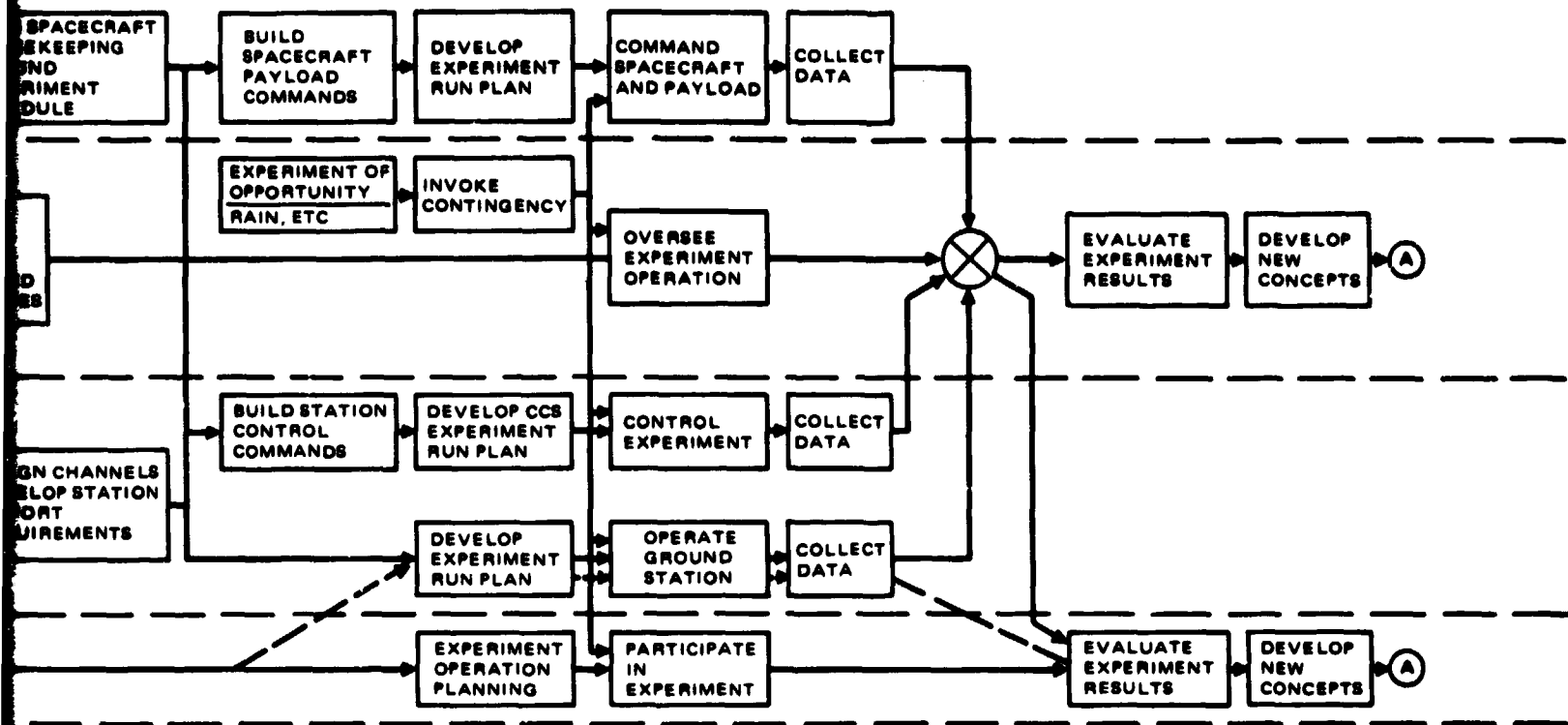


FIGURE 5-63. EXPERIMENT SUPPORT SOFTWARE OFF-LINE PROCESSING





2  
BOLDOUT FRAME